SHIP LONGITUDINAL STRENGTH MODELLING

A Thesis Submitted for
the Degree of Doctor of Philosophy
in the Faculty of Engineering
of the University of Glasgow

by

Ying-Tsair LIN, BSc, MSc

Department of Naval Architecture and Ocean Engineering
University of Glasgow

March, 1985

ProQuest LLC.
789 East Eisenhower Parkway
P.O. Box 1346
Ann Arbor, MI 48106 – 1346

To my late Grandmother,

my Parents and my Wife

SUMMARY

The aims of the research work presented in this thesis are to assess the effects of weld-induced residual stresses and initial imperfections on the collapse behaviour of a ship's hull girder, and to demonstrate the close correlation that exists between the hull's ultimate longitudinal strength and the maximum load-carrying capacity of its components under compressive loads.

A theoretical method for evaluating the ultimate longitudinal strength of a ship's hull girder under vertical bending is described. The hull's midship cross-section is discretised into structural elements such as stiffened panels, plate elements and hard corners. Effects of buckling of compressive components are allowed for by incorporating the load-end shortening curves of unstiffened and stiffened plates into the hull strength analysis. An incremental approach is employed to derive the moment-curvature relationship and hence the peak moment for the hull girder. Curvature, rather than bending moment, increments are imposed on the hull girder to enable the post-collapse behaviour to be followed. Comparisons with tests on welded steel box girder models and other analytical methods show that the agreement is satisfactory.

Prior to determining the vertical moment-curvature relationship for a hull, the load-end shortening curves need to be established for each stiffened panel forming the hull's mid-ship cross-section. An analytical method is developed to examine the large deflection elasto-plastic behaviour of stiffened panels under uniaxial compression. The method is based on a beam-column approach in which the

longitudinally stiffened plating is treated as a series of beam-columns formed by the stiffeners and an associated width of plates. The beam-column model is continuous over three supports provided by transverse frames to take effect of interaction between adjacent spans into account. Dynamic Relaxation is employed to numerically solve the non-linear equilibrium equations. The strength contribution from the plating, allowing for buckling effects, is accounted for by using the plate average stress-strain curves. The load is applied through end displacements such that both the pre- and post-collapse behaviour can be traced. It is shown by comparisons with test results and other analytical methods that the present one satisfactorily predicts the behaviour of stiffened compression panels.

A numerical method to generate the plate average stress-strain curves for the stiffened panel analysis is proposed. The results from an existing parametric study on the large deflection elasto-plastic behaviour of practical plates in compression with constrained edges are used as basic data. A simplified procedure is followed to interpolate the average stress-strain curve for the plate with parameters different from the standard cases.

An analytical study on the ultimate strength behaviour of longitudinally framed frigate-type hulls is presented. Five naval frigates designed in the 1950's and 1960's are analysed by the present incremental approach. The derived load-end shortening curves for the stiffened panels and moment-curvature curves for the hull girders are presented. It is shown that the ultimate strength of longitudinally framed hulls is strongly influenced by the full-range behaviour of components under compressive loads in association with bending. In particular, the ultimate hull strengths are closely correlated with

the maximum load-carrying capacities of the critical stiffened panels which are located in deck structures in the sagging condition and in bottom structures in the hogging condition.

Two simple expressions for predicting the ultimate moment capacity of longitudinally stiffened hulls in the sagging and hogging conditions are proposed. They are based on the results of the numerical analysis for appropriate initial imperfections in the plate and stiffened panels. The ultimate bending moments of a variety of hull and box girders predicted by the strength formulae are compared with the numerical and experimental results. Satisfactory agreement is obtained which suggests that the proposed formulations could form the basis of an improved design method.

ACKNOWLEDGEMENTS

The author wishes to express his sincere gratitude to the following:

Dr. P.A. Frieze, for his helpful guidance and expert advice throughout the duration of the research, and for his generous assistance in providing the original computer program developed by Drymakis;

Prof. D. Faulkner, for his valuable help in providing the structural mid-ship sections of the warships, and for his constructive recommendations regarding the modified mid-ship sections of the transversely framed ships;

Ministry of Education, Taiwan, Republic of China, for providing financial support during this work;

Prof. C.C. Liao, National Taiwan University, Republic of China, for his recommendation and encouragement to study in this University;

Computing Service consultants in the University of Glasgow, for their useful advice with technical aspects of programming;

Mrs. M.C. Frieze, for her typing of this thesis expertly and with great patience;

Mrs. R. Young, for her help in tracing some of the diagrams; and

His wife, Kuei-Hua, for her support, extreme patience and understanding during the course of the study.

CONTENTS

NOTATION

Chapter 2:

b	Plate width
E	Elastic modulus
E_o^*	Initial tangential modulus of stress free plate
t	Plate thickness
β	Non-dimensional plate slenderness ratio $\left(= \frac{b}{t}\sqrt{\frac{\sigma_Y}{E}}\right)$
δ_o	Amplitude of initial plate deflection
δ_o'	Initial plate deflection ratio $(= \delta_o/t)$
ε	Applied uniform strain at end of plate
ε_Y	Yield strain
ε'	Average non-dimensional strain $(= \varepsilon/\varepsilon_Y)$
ε_r'	Non-dimensional residual compressive strain
σ	Mean compressive stress
σ_Y	Yield stress
σ'	Average non-dimensional stress $(= \sigma/\sigma_Y)$
σ_r	Residual compressive stress
σ_r'	Non-dimensional residual compressive stress $(= \sigma_r/\sigma_Y)$
η	Tension yield zone ratio

Notes on subscripts:

C	denotes pre-compression zone
E	denotes yielding tension blocks at edges of plate
F	denotes stress free plate

Chapters 3 and 4:

A	Cross-sectional area
	A_p - fully effective plate
	A_s - stiffener
	A_t - stiffener with fully effective plate
b	Width of plate between longitudinal stiffeners
C^*	Generalised stiffened plate elasto-plastic in-plane tangential rigidity
$C_{u,w}$	Viscous damping coefficients
D^*	Generalised stiffened plate elasto-plastic flexural rigidity
E	Modulus of elasticity
E_p^*	Elasto-plastic equivalent to E for plate
E_s^*	Elasto-plastic equivalent to E for stiffener
G^*	Generalised stiffened plate elasto-plastic interaction tangential rigidity
I	Moment of inertia for the cross-section of the plate-stiffener combination
$K_{u,w}$	Non-dimensional viscous damping coefficients
L_1, L_2	Length of one stiffener span between transverse girders
M	Bending moment (increment ΔM)
P	Axial force (increment ΔP)
r	Radius of gyration for the cross-section of the plate-stiffener combination
t_p	Plate thickness
u	In-plane displacement in x-direction
u_A	Applied end displacement
w	Out-of-plane deflection in y-direction
δ_o	Amplitude of initial plate deflection
$\overline{y_p}$	Distance of centroid of plate-stiffener combination from mid-plane of the plate

α Ratio of stiffener area to plate area ($= A_s/A_p$)

β Non-dimensional plate slenderness ($=\left(b/t_p\right)\sqrt{\sigma_{Yp}/E}$)

Δ Amplitude of initial stiffener deflection

ε_a Direct axial strain at centroid of plate-stiffener combination (increment $\Delta\varepsilon_a$)

ε_t Total axial strain at a cross-section subdivision (increment $\Delta\varepsilon_t$)

λ Non-dimensional column slenderness ($=\left(L/\pi r\right)\sqrt{\sigma_Y/E}$)

$\rho_{u,w}$ Fictitious densities

ϕ Curvature (increment $\Delta\phi$)

σ_Y Average yield stress of the plate-stiffener combination

σ_{Yp} Plate yield stress

σ_{Ys} Stiffener yield stress

σ_r Average compressive residual stress in plate

σ_u Ultimate stress of stiffened panel

Chapters 5 and 6:

A_j Cross-sectional area of j^{th} structural element

b Plate width in transverse direction

E Young's modulus

E_j Young's modulus of material of j^{th} structural element

E_Q Young's modulus of material at outermost fibre

F_C Sum of yielding axial forces carried by structural elements in compressive region

F_ℓ Total axial force acting on lower part of mid-section divided by an assumed neutral axis

F_u Total axial force acting on upper part of mid-section divided by an assumed neutral axis

F_T Sum of yielding axial forces carried by structural elements in tensile region

h Distance between outermost fibre and elastic neutral axis of mid-section

I_E Moment of inertia of midship cross-section about its elastic neutral axis

M_{i-1}, M_i $(i-1)^{th}$ and i^{th} cumulative bending moments

ΔM_i i^{th} incremental bending moment $(= M_i - M_{i-1})$

M_p Fully plastic moment

M_u Ultimate bending moment

M'_u $= M_u/M_p$

M_Y First yield bending moment

S Initial stiffness of plate in tension

t Plate thickness

$\overline{Y_E}$ Height of elastic neutral axis of midship cross-section above base line

Y_i Convergent location of effective neutral axis corresponding to i^{th} curvature increment

$Y_{k-1}, Y_k, Y_{k+1}, Y_{k+2}$ $(k-1)^{th}$, k^{th}, $(k+1)^{th}$ and $(k+2)^{th}$ try locations for determining effective neutral axis

$\overline{Y_p}$ Height of plastic neutral axis of midship cross-section above base line

Y_1 First try location for determinining effective neutral axis

y_j Distance between centroid of j^{th} structural element and base line

ε Convergence criterion ratio

ε' Non-dimensional strain

$\varepsilon_{i-1,j}, \varepsilon_{ij}$ Strains at j^{th} structural element after imposition of $(i-1)^{th}$ and i^{th} curvature increments

$\Delta\varepsilon_{ij}$ $= \varepsilon_{ij} - \varepsilon_{i-1,j}$

ε'_{ij} $= \varepsilon_{ij}/\varepsilon_{Yj}$

ε'_m Non-dimensional strain at which yielding occurs in pre-compression zone

ε_Y $= \sigma_Y/E$

ε_{Yj} $= \sigma_{Yj}/E_j$

ε_{YQ} $= \sigma_{YQ}/E_Q$

σ' Non-dimensional stress

$\sigma_{i-1,j}, \sigma_{ij}$ stresses at j^{th} structural element after imposition of $(i-1)^{th}$ and i^{th} curvature increments

$\Delta\sigma_{ij}$ $= \sigma_{ij} - \sigma_{i-1,j}$

σ'_{ij} $= \sigma_{ij}/\sigma_{Yi}$

σ_r Average compressive residual stress

σ'_r $= \sigma_r/\sigma_Y$

σ_Y Yield stress

σ_{Yj} Yield stress of material of j^{th} structural element

σ_{YQ} Yield stress of material at outermost fibre

ϕ_C Critical curvature at which virtually linear response ends

ϕ_{i-1}, ϕ_i $(i-1)^{th}$ and i^{th} cumulative curvatures

$\Delta\phi_i$ i^{th} curvature increment $(= \phi_i - \phi_{i-1})$

$\Delta\phi'_i$ $= \Delta\phi_i/\phi_Y$

ϕ_u Curvature corresponding to ultimate bending moment

ϕ'_u $= \phi_u/\phi_Y$

ϕ_Y Curvature corresponding to first yield bending moment

η Width of residual stress tension zone as proportion of plate thickness

Chapter 7:

A Total cross-sectional area $(= A_D + 2A_S + A_B)$

A_B Cross-sectional area of the bottom structure

A_D Cross-sectional area of the deck

A_S Cross-sectional area of one side-shell

a,b,c Distances as indicated in Fig. 7-5

D	Depth of the midship section
g	Distance of the neutral axis below the centre of the deck
M_p	Fully plastic moment
M_u	Ultimate bending moment
M_Y	First yield bending moment
S_F	Fully plastic shape factor
Z	Elastic section modulus
Z_e	Effective section modulus
α_B	$= A_B/A$
α_D	$= A_D/A$
α_S	$= A_S/A$
γ	$= g/D$
γ_a	$= a/D$
γ_b	$= b/D$
γ_c	$= c/D$
σ_u	Average ultimate compression strength of the critical stiffened panel
σ_{uD}	Average ultimate compressive stress in the deck
σ_{uS}	Average ultimate stress in the compressed portions of the side-shells
ϕ	$= \sigma_u/\sigma_Y$
ϕ_D	$= \sigma_{uD}/\sigma_Y$
ϕ_S	$= \sigma_{uS}/\sigma_Y$
ζ	Load shedding factor for the deck and side-shells
ζ_D	Load shedding factor for the deck
ζ_S	Load shedding factor for the side-shells

Chapter 1

INTRODUCTION AND LITERATURE REVIEW

1.1 INTRODUCTION

The design philosophy inherent in most of the Rules and Regulations of Classification Societies all over the world has traditionally been based on elastic structural analysis. Namely, the longitudinal strength calculation deals with the elastic response of a ship's hull girder to a condition of static and nominally assumed wave-induced loadings. The section modulus is calculated using linear bending theory and the design criteria is then that the maximum bending stress is limited to some prescribed fraction of the material yield strength. As the section modulus is proportional to the bending moment imposed on the ship, it is regarded as an expedient measure of longitudinal bending strength of the hull girder. This approach is commonly used together with some semi-empirical formulae concerning the allowable maximum bending stress, and may be applied to ship hulls of conventional type with a certain validity.

However, with no explicit consideration being given to complex structural processes such as elasto-plastic buckling and post-buckling behaviour in association with hull collapse, the elastic section modulus by itself may hardly be an accurate indication of the true bending strength of the hull girder. For two hulls having identical section modulii and made of the same material, one may have stronger resistance to buckling of the compressed parts and

hence can sustain a greater bending moment than the other. Thus, it is essential to incorporate structural instability analyses in a hull strength assessment.

Faced with the deficiencies of the section modulus approach, naval architects have generally recognised a need for more accurate design methods, applicable to ship hulls of a new type, involving the utilisation of ultimate hull strength in ship structural design. The development of limit state design methods is a logical outcome of these approaches. By concentrating on the limiting conditions beyond which a hull girder will fail to perform its function, the limit state design method can properly determine the true longitudinal hull strength, with effects of yielding and buckling of the structural elements being taken into account. This will undoubtedly be helpful in assessing the real margin of safety between the load-carrying capacity of the hull girder as a beam and the maximum bending moment acting on the ship.

Some methods have recently been developed concerned with the evaluation of the ultimate longitudinal strength of a ship's hull girder. Since the evaluated ultimate capacity depends largely on the conditions at final failure of the hull girder, it is necessary to identify its possible modes of failure. From the point of view of structural analysis, the failure of a hull girder subjected to vertical bending moment may be due to brittle fracture, fatigue fracture, yielding or instability, or a combination of these. It may fail gradually as in the case of a lengthening fatigue crack or spreading plasticity, or suddenly, as through plastic instability or propagation of a brittle crack[1-1]. In view of the fact that both brittle fracture and fatigue demand careful attention to local design

and proper selection of materials, they are not considered in the present study. That is, only overall ductile failure of the hull as a girder is dealt with.

As pointed out by Caldwell [1-2], the main obstacle to accurate determination of the peak moment, which defines the true ultimate longitudinal strength of a ship's hull girder, has been the uncertainty regarding the effects of local buckling of plates and stiffened panels forming those parts of the hull cross-section which experience compressive load. Results from full-scale structural tests on ships [1-3] have also shown that there is a close correlation between the ultimate bending strength of the hull and the buckling strength of compressive components of the hull. Recent research concerned with the strength of ship deck and bottom structures and steel box girder bridge decks has led to a much improved understanding of the collapse behaviour of plates and stiffened panels under uniaxial compression. This will, of course, be helpful in estimating the ultimate bending moment at which all members have exhausted their strength, and collapse is iminent. Since the strain levels existing at members differ from one location to the other when the ultimate bending moment is reached, it is apparent that not only the maximum load-carrying capacity but also the post-buckling strength of structural elements is required for the determination of ultimate hull strength. A computer program [1-4], in which the Dynamic Relaxation approach was employed to analyse the large deflection elasto-plastic behaviour of double-span stiffened panels under compressive loads, was therefore developed to generate the load-shortening curves over the pre- and post-collapse ranges for stiffened panels.

When dealing with the full range behaviour of structural elements forming a mid-ship cross-section, it is convenient to focus on strain rather than the familiar concept of stress. With the help of strain, the predictions of individual element responses can be readily combined into a hull girder response prediction model. Thus, in deriving the bending moment-curvature relationship for a hull girder, incremental curvatures are imposed on it to compute the corresponding bending moments. Following these lines, a computer program HULLG, which will be described in Chapter 5, was developed to compute hull bending moment-curvature curves and from these to identify the hull's ultimate bending strength.

1.2 LITERATURE REVIEW

1.2.1 Unstiffened Plates

1.2.1.1 Theory: It is necessary to use the large deflection elasto-plastic equations for predicting the elastic and inelastic buckling, collapse and post-buckling behaviour of plates subjected to in-plane compressive loads. Von Karman derived the large-deflection plate equations and Marguerre modified them to take initial deformations into account. An exact solution of the large deflection elasto-plastic equations encounters great difficulty. However, with the advent of high-speed and large-capacity computers, it has been possible to generate numerical solutions to these equations.

Moxham[1-5] and Little[1-6] obtained elasto-plastic load-end shortening curves for plates under uniaxial compression using energy principle methods. The former used current strain values to minimise the energy whereas the latter used previously known stress values with strain changes, to calculate stress changes. Crisfield[1-7]

presented a finite element solution to the problem, including single-layer and multi-layer approaches. Frieze[1-8] and Harding[1-9], using the single-layer and multi-layer approaches respectively, solved the finite difference formulations of the governing equations by the dynamic relaxation technique.

In representing residual stresses, Moxham[1-5,1-10], Little and Crisfield used an idealised stress distribution in which the average stress actually arising in the compression zone was assumed to be balanced by yield tension blocks at the base of welded stiffener attachments. Frieze and Harding modified the shape of the tension block to suit their finite-difference mesh.

Parametric studies[1-9,1-11,1-12,1-13] have been carried out and yielded valuable design data for the case of square and rectangular plates under uniaxial compression using the afore-mentioned computer programs. In ref. [1-11], for example, the effects of initial deformations and residual stresses on the behaviour of plates with various longitudinal edge restraints have comprehensively been examined. The results were presented in the form of average stress-strain curves over the entire loading history for a range of practical plate slendernesses and imperfections.

Comparison between the load-end shortening curves from the energy principle method, the finite element method and the finite difference method shows that the agreement is satisfactory up to peak load but with a little difference in unloading characteristics. However, only a limited number of cases could be analysed to generate the basic results using one of the large deflection elasto-plastic computer programs for economic reasons. Interpolation, such as in ref. [1-14], may therefore be employed to generate load-end shortening

curves for plates with slendernesses and levels of imperfections different from the cases examined.

1.2.1.2 Tests: Testing plates under uniaxial compression requires a test rig to load the ends of plate specimens. The main problem encountered in testing is to simulate realistic boundary conditions at the unloaded edges. Even though a lot of work has been devoted to tests on plates, much of the early work failed in providing the correct boundary conditions, as observed by Davidson[1-15].

Tests by compressing square box columns[1-16] avoid some support problems at the unloaded edges, but the box corners may provide a small amount of in-plane restraint. Tests on isolated plates require particular care over the support of unloaded edges. Ractliffe[1-17] used a finger system which allowed for both simply supported and clamped edges and which were free to pull-in, but required considerable preparation of the plate edges. Moxham[1-18] set up an improved system allowing plates of uniform thickness, without edge preparation, to be tested. Bradfield[1-19] used Moxham's rig which enabled plates of varying thicknesses to be tested. The load-end shortening curves obtained from these tests on isolated plates have provided a sound basis for correlation with the results from large-deflection elasto-plastic numerical analyses.

1.2.2 Stiffened Plates

1.2.2.1 Beam-column approach: In the beam-column approach the longitudinally stiffened panels between transversals are treated as a series of beam-columns formed by the stiffeners with some associated width of plates. One of these approaches is to assume that the plate width is equal to the stiffener spacing, and allow for plate buckling

effects by considering the limiting stresses in the plate as those predicted by a buckling analysis of the plate panel. The alternative approach is to assume an effective plate width, either derived from theoretical analyses or by using semi-empirical formulae, and to limit the stress to yield.

Ostapenko[1-20] did the pioneering work in this approach concerning the stiffened panels of the type used in ship's hulls. Dwight[1-21] suggested a design method, based on the full width approach, in which a modified version of the Perry-Robertson formula was employed. Moolani[1-22] also adopted the full width approach in studies of single- and multi-span panels. His method applied stress loading increments and did not examine the post-buckling behaviour of the stiffened panels. Drymakis[1-23] used a similar method except that the load was applied through end displacement increments so that the post-collapse path could be traced.

Murray[1-24] adopted the Perry-Robertson formula, as Dwight, but used the alternative method of assuming an effective plate width. Horne and Narayanan[1-25] used the effective width approach based on elastic large-deflection analyses of plates. However, unlike Murray, they allowed for the reduction in plate stiffness irrespective of the column slenderness. Crisfield[1-12] examined panels as an assemblage of beam-columns using finite element formulations for idealising the structures. Smith[1-26] conducted single- and double-span analyses of stiffened panels of the types found in ship structures.

1.2.2.2 Tests: Several tests[1-24,1-26,1-27,1-28] have been conducted on stiffened panels subjected to uniaxial compression. Dorman and Dwight[1-27] tested twelve stiffened compression panels in isolation. The investigation involved failures initiated by the plate as well as

the stiffener. Horne and Narayanan[1-28] tested thirty-four isolated stiffened panels under uniaxial compression. Both the loading and unloading characteristics of the panels were recorded. Murray[1-24] tested thirteen stiffened panels, comprising nine loaded axially and four with combined axial-lateral loadings. Smith[1-26] conducted tests on twelve full-scale grillages representing typical warship deck and single bottom structures under compressive load combined in some cases with lateral pressure.

1.2.3 *Hull Girders*

1.2.3.1 Analytical work: Some methods have recently been developed concerning the evaluation of ultimate longitudinal strength of a ship's hull girder. One of the pioneering works in this field was due to Caldwell[1-2] in which a simplified analysis procedure was presented for calculating the ultimate longitudinal strength for a single-deck ship in a sagging condition from the scantlings and material properties of its cross-section. In his solution it is necessary to define a structural instability factor to enable the maximum strength of a box girder cross-section equivalent to the ship's mid-ship cross-section to be predicted. Although this factor was not developed in the paper, Faulkner[1-29] suggested a design method for taking this buckling effect into account, basically through a reduction factor. Betts and Attwell[1-30] provided numerical solutions on several limiting bending moments of two naval ships using Caldwell's method. In the report[1-31] of the International Ship Structure Congress in Tokyo, the buckling and plastic behaviour of structural elements in ships and the ultimate longitudinal strength of ships were extensively discussed. Reference [1-32] includes several chapters concerned with hull girder failure modes, margins of safety, and hull girder reliability. A Ship

Structure Committee report[1-33] has developed a procedure for estimating the fully plastic moment and the shakedown moment allowing for the buckling and instability effects of the stiffened panels and with the objective of determining the ultimate strength of a ship's hull girder.

Smith has made some significant contributions[1-34,1-35,1-36,1-37] on determining the ultimate moment behaviour of a ship's hull girder. He was the first to advocate the incremental moment-curvature approach[1-34], in which the hull's mid-ship cross-section was subdivided in plate and stiffened panel units, for evaluating the ultimate hull strength. He has discussed the alternative failure modes of components under compressive loads and examined the influence of local compressive failure on ultimate longitudinal strength of a ship's hull. In ref. [1-35], he considered the whipping response of a ship's hull to impulsive loads, in addition to behaviour under quasi-static loads. His approach was based on approximate characterisation of the strength of elements of hull cross-sections under tensile and compressive loads associated with hull-girder bending together with lateral pressure loads. In examining the factors influencing the ultimate strength of a ship's hull under combined loads[1-36], he has considered the influence of imperfections resulting from the fabrication process and the consequences of damage due to collisions, grounding, hydrodynamic overload or weapon effects. Furthermore he, together with some other researchers[1-37], have made hull strength assessments on two transversely framed torpedo-boat destroyers for ship structural reliability analysis.

Billingsley[1-38] described an engineering approach for evaluating the impact of buckling of individual structural elements on

the capability of the hull girder to withstand bending moments. The method is based on simple models of plate element response and stiffener element response, and assumed average conditions of edge fixity and average quality of construction in terms of plating fairness, residual stress and alignment. Adamchak[1-39,1-40] has developed a computer program to estimate the ductile collapse strength of conventional surface ship hulls under vertical longitudinal bending. In his formulation, failure modes of yielding, beam-column buckling and tripping instability were included, and the effects of lateral pressure loadings, fabrication-induced distortion and initial prestrain were accounted for. Ostapenko[1-41] proposed a method for the determination of the ultimate strength of longitudinally stiffened ship hull girder segments of rectangular single-cell cross-section, subjected to bending, shear and torsion. The method considered the overall non-linear behaviour by taking into account the compatibility of deformations between the individual components. Comparison of the method with the results of three tests on a small hull girder specimen has shown that it was acceptably accurate for the loading case of moment and shear.

1.2.3.2 Tests: With regard to full-scale structural tests, three ship hulls including one British destroyer *ALBUERA*[1-42] and two American destroyers *PRESTON* and *BRUCE*[1-43,1-44], all of which were riveted, have been tested to destruction. The *ALBUERA* was longitudinally framed while the others were transversely framed. The experimental data available on the structural behaviour up to collapse of hulls subjected to longitudinal vertical bending are limited to these three cases. Although the present analysis technique is capable of dealing with both longitudinal and transverse framing systems, it takes no account of rivet slip. Thus, comparisons

between the present method and experimental data are to be focused on welded steel box girder models.

A huge experimental programme[1-45,1-46] has been conducted at Imperial College of Science and Technology, London, to investigate the behaviour of steel box girders and their components. Ten quarter-scale model box girders with components of varying proportions were tested up to collapse to obtain data on the various aspects of box girder behaviour. From these models, two box girders Model 2 and Model 4 loaded in pure bending are chosen for comparisons of theory and experiment.

Test on a series of seven stiffened box girders similar to ship hulls[1-47] have been carried out under conditions of pure bending by Reckling at the Institute of Mechanics of the Technical University, Berlin. Dimensions of the box girders were designed to cover the failure modes such as premature collapse by the buckling of side walls, delayed collapse by the restraining effect of the side walls, and collapse by nearly simultaneous buckling of single fields between the stiffeners and of the whole deck. The ultimate load behaviour of Model 23 and Model 31 is analysed by the present approach for comparisons with the experimental results.

1.3 AIM OF THESIS

The aims of the research work presented in this thesis are to assess the effects of weld-induced residual stresses and initial imperfections on the collapse behaviour of ship's hull girders, and to establish the relationship, if any, between the hull's ultimate longitudinal strength and the maximum load-carrying capacity of its components under compressive loads. To achieve these ends, a

numerical procedure is established to derive the bending moment-curvature relationship for the hull girder, and from which to identify its peak moment. The results of tests on box girders subjected to pure bending are compared with those obtained numerically to substantiate the procedure. In particular, it is hoped to propose simple expressions which can be used in design to estimate the ultimate moment capacity of hull girders.

1.4 SCOPE OF THESIS

Chapter 2 describes a simplified method to generate the average stress-strain curves for plates under uniaxial compression. The numerical results from the large deflection elasto-plastic analysis [1-11] of plates are used as basic data in the method, allowing for effects of residual stresses and initial plate deflections.

In Chapter 3, a beam-column approach using the Dynamic Relaxation method to examine the large deflection elasto-plastic behaviour of stiffened panels in compression is described. The effect of interaction between adjacent spans of the stiffened panels is considered by adopting a double-span model.

In Chapter 4, results obtained by the method developed in Chapter 3 are compared with existing experimental and numerical results, in the form of ultimate strengths or load-shortening curves of stiffened panels. Differences between the results based on one-span and double-span models are discussed.

In Chapter 5, a numerical procedure for determining the bending moment-curvature relationship for a ship's hull girder under vertical bending is presented. The hull's mid-ship cross-section is

subdivided into structural elements such as stiffened panels, plate elements and hard corners. The methods in Chapter 2 and Chapter 3 are applied to generating the average stress-strain curves for the structural elements. These individual element responses are then combined into an overall response for the hull girder.

Chapter 6 describes applications of the method developed in Chapter 5 to the ultimate strength prediction of box girder models, transversely framed torpedo-boat destroyers and longitudinally framed frigates. Comparisons between the numerical and experimental results for the box girders are made. Effects of compressive residual stresses, initial imperfections, residual stresses in tension flange and behaviour of hard corners on the ultimate strength behaviour of the box girders are examined. From the point of view of structural efficiency, comparisons between transverse and longitudinal framing systems are made. The close correlation between the hull's ultimate strength and the maximum load-carrying capacity of its components under compressive loads are demonstrated.

In Chapter 7, simple expressions for the ultimate bending moment capacity of a ship's hull girder under vertical bending are proposed. The new formulations, which are deduced from the numerical results of the previous chapters, are used to predict the ultimate moment capacities of longitudinally framed hull and box girders. Satisfactory agreement with the numerical and experimental results is demonstrated.

Chapter 8 contains the conslusions of the research programme and recommendations for future work.

Chapter 2

PLATE MODEL - A SIMPLIFIED APPROACH

2.1 INTRODUCTION

Plating plays an important role in ship structures. Deck, side shell and bottom plating of a ship's hull constitute a watertight envelope to provide the buoyancy for keeping the ship afloat. In addition, the platings act together as a box girder in resisting bending and other loads imposed on the structure. It is commonly found[1-35] that between 60% and 80% of a hull girder is formed by deck, side shell, bottom and longitudinal bulkhead plating. Loss of stiffness in the plating due to buckling accelerates elasto-plastic buckling of stiffened panels which leads directly to a reduction in effective section modulus of a hull's mid-ship cross-section. Thus, the ultimate hull strength is strongly influenced by the compressive stiffness and strength of plate elements.

Recently some numerical techniques[1-8,1-12,2-1] have been developed which are capable of examining the complex large deflection elasto-plastic behaviour of plates under compressive loads. A parametric study[1-11] carried out by using the computer program[1-8], for example, has provided valuable design data for practical compression plates covering a range of realistic levels of initial deformation and residual stress. The results of this study were presented in the form of average stress-strain curves which had the merit of defining not only ultimate strength but also plate stiffness

at any point in the strain range. These curves were derived for plate panels in which simple supports were fixed against out-of-plane movement, unloaded edges were constrained in-plane to remain straight but free to pull-in, and loaded edges were held straight and displaced uniformly. These boundary conditions closely represent that pertaining to a typical internal panel of a multi-stiffened flange plate, and hence are considered suitable for both the stiffened panel and hull girder analyses.

However, it is impractical to directly incorporate these methods into the overall analysis of stiffened panels or hull girders. An approximate method is therefore proposed to generate the average stress-strain curves for the plates in uniaxial compression with constrained edges. Results of the parametric study[1-11] are adopted as basic data from which the average stress-strain curves are interpolated for the residual stress-free plates with parameters different from the standard cases by using cubic splines. A simplified procedure is then followed to generate the average stress-strain curves, i.e. the load-end shortening curves for the plates with residual stresses.

2.2 SIMPLIFIED PLATE MODEL

2.2.1 Shape of Load-End Shortening Curves

The strength and stiffness of square or rectangular plates under uniaxial compression may appropriately be presented in the form of load-end shortening curves. Both theoretical and experimental studies have clearly shown the important influence of initial deformations and weld-induced residual stresses, in addition to plate slenderness, on the load-end shortening relationship.

Although δ_o/t, where δ_o is the maximum initial deformation and t the plate thickness, has proved to be the non-dimensional form for initial bow, it has been found[1-11,1-26,2-2] to relate approximately to β^2 and lie typically in the range 0.05 β^2 to 0.15 β^2 with values of up to 0.40 β^2 in heavily-welded plates. It can be seen in the curves of the parametric study[1-11] that the effect of initial deformation is generally to reduce the compressive strength of plates and to change the mode of failure to a more gradual process. This effect is most marked in plates with moderate slenderness.

The intensity of residual stresses depends strongly on the adopted sequence and type of welding, such as manual, mig, CO_2, fusarc, submerged arc, etc. Measurements carried out during hull construction[2-3], where welding was performed manually following a two-pass, step-back procedure, have indicated values of average compressive residual stress σ_r in the range 0.1 to 0.25 σ_y. Moxham[1-10] and Faulkner[2-4] have presented approximate methods for relating residual stresses to sizes of welds.

The presence of residual stresses causes some reduction of compressive strength and stiffness over a range of strain from $(\varepsilon_y - \sigma_r/E)$ to $2\varepsilon_y$, where ε_y is yield strain in uniaxial compression and E Young's modulus. It hastens the onset of yielding, shifts the peak load to a greater shortening and removes the sharp drop in load beyond the peak. It thus allows for more load redistribution between components of a complete structure, such as the ship's hull girder or box girder bridge, before maximum load is reached.

2.2.2 *Basic Considerations*

2.2.2.1 Parameters: The parameters which influence the behaviour of plates in compression and hence the shape of the plate average stress-strain curves may be classified as follows:

(a) Primary parameters:

- plate slenderness
- maximum initial deformation
- weld-induced residual stress

(b) Secondary:

- aspect ratio of the plate.

A long plate, as commonly found in longitudinally framed hulls, buckles in half-waves, the lengths of which approach the plate width. That is, a buckled plate subdivides approximately into squares. The critical aspect ratio into which the plate buckles depends on the magnitude of the initial deformation as well as the plate slenderness[1-8]. However, since the results for aspect ratios close to unity only vary within 1 or 2%[1-12], the aspect ratio of unity was adopted in the parametric study[1-11], and hence is implied in the present simplified method.

The plate average stress-strain curves in ref. [1-11] were obtained using a Young's modulus of 205,000 N/mm^2 and a yield strength of 245 N/mm^2. It was found[1-11] that unique values of β, δ_o' ($\equiv \delta_o/t$) and σ_r' (σ_r/σ_Y) produced unique average stress-strain curves, provided stresses were expressed relative to yield strength. However, Faulkner[2-5] found that the best fit to data of δ_o' varied with β^2. It was then concluded[1-11] that presenting δ_o' as a function of β^2 would be the most appropriate way of incorporating the initial deformations into a plate study. Thus, the shape of the plate average stress-strain curves is

considered to be function of the parameters β, δ_o'/β^2 and σ_r' in the present method.

2.2.2.2 Basic data: As mentioned previously, the average stress-strain curves in ref. [1-11] derived for residual stress-free plates with the parameters varied in a systematic way are to be used as basic data. The standard values to be used for β and δ_o'/β^2 are listed in Tables 2-1 and 2-2 respectively. All of the twenty basic curves, reproduced in Figs 2-1 to 2-5 for β = 0.691, 1.037, 1.383, 2.074 and 2.766 respectively were numerically stored in the computer program. Each curve was represented by 151 values of non-dimensional average stress which corresponded to 151 values of non-dimensional average strain varying from 0.00 to 3.00 in increments of 0.02.

2.2.3 *Interpolation*

An interpolation scheme using cubic splines[2-6] was adopted to derive the average stress-strain curves for the residual stress-free plates with slendernesses and initial deformations different from the standard values for β and δ_o'/β^2. The stress ratio corresponding to each strain ratio is determined in two steps. First of all, the stress ratio for the plate with the specific initial deformation is calculated by using the cubic spline which is fitted to the data for the four basic levels of imperfections. This calculation is repeatedly performed for each of the five standard plate slendernesses. Secondly, the stress ratio for a plate of a particular slenderness is determined from the cubic spline which is fitted to the five stress ratios found in the first step.

Table 2-1

Basic Slenderness Ratios

(σ_Y = 245 N/mm^2)

Plate Code	1	2	3	4	5
β	0.691	1.037	1.383	2.074	2.766
b/t	20	30	40	60	80

Table 2-2

Basic Initial Deflection Ratios

Imperfection Code	1	2	3	4
δ_o'/β^2	0.04358	0.08716	0.17432	0.34864

2.2.4 Effects of Residual Stresses

The average stress-strain curves were derived in ref. [1-11] for residual stress-free plates as well as the plates with three levels of residual stress. However, the strain range over which the plate behaviour is influenced by residual stress changes with this level of stress. A simplified procedure, rather than direct interpolation, is therefore used to take the effect of residual stresses into account.

The residual stress distribution in a plate is assumed to take the idealised pattern as shown in Fig. 2-6, in which the average stress actually arising in the pre-compression zone (σ_r) is balanced by yielding tension blocks of width ηt at the edges given by:

$$\sigma_r = \frac{2\eta t}{b - 2\eta t}\sigma_Y \qquad \ldots \quad (2.1)$$

Let the average stress-strain curve for the residual stress-free plate of slenderness β with initial deformation δ_o'/β^2 be given by:

$$\sigma_F' = f(\varepsilon_F') \qquad \ldots \quad (2.2)$$

as shown in Fig. 2-7. This relationship is assumed to hold in the central region of a welded plate having the same β and δ_o'/β^2 as the unwelded plate but with a pre-compression stress σ_r. Thus, the stress σ_C' corresponding to the applied strain ε_C' (Fig. 2-8) can be expressed by the following function:

$$\begin{aligned}\sigma_C' &= f_C(\varepsilon_C') \\ &= f(\varepsilon_C' + \varepsilon_r') - \sigma_r' \qquad \ldots \quad (2.3)\end{aligned}$$

where σ_r' is the non-dimensionalised pre-compression stress and ε_r' is the strain corresponding to σ_r', i.e. $\sigma_r' = f(\varepsilon_r')$ as shown in Fig. 2-7.

As a consequence of initial tensile yielding, the edge portions are assumed to remain linearly elastic up to the strain $\varepsilon'_E = 1/E^*_o$ with tangential modulus E^*_o, and to behave according to eqn (2.2) afterwards. Thus, the stress applied to the edge portions relates to ε'_E (Fig. 2-9) as follows:

$$\sigma'_E = f_E(\varepsilon'_E) = \begin{cases} E^*_o \cdot \varepsilon'_E & , \quad \varepsilon'_E \leq \dfrac{1}{E^*_o} \\ f\left(\varepsilon'_E - \dfrac{1}{E^*_o}\right) + 1 & , \quad \varepsilon'_E > \dfrac{1}{E^*_o} \end{cases} \qquad \ldots \quad (2.4)$$

where E^*_o is the initial tangential modulus of the unwelded plate, i.e.

$$E^*_o = \left.\frac{d\sigma'_F}{d\varepsilon'_F}\right|_{\varepsilon'_F = 0}$$

Since the strain is applied uniformly and simultaneously to the end of the welded plate, i.e. to both the central region and to the edge portions, there is no difference between ε'_C and ε'_E, i.e. $\varepsilon' = \varepsilon'_C = \varepsilon'_E$. Based on equilibrium, the average stress σ' applied to the whole plate can be obtained as follows:

$$\sigma' = \frac{\{\sigma'_C \cdot (bt - 2\eta t^2) + \sigma'_E \cdot 2\eta t^2\}}{bt}$$

$$= f_C(\varepsilon') \cdot \left(1 - \frac{2\eta t}{b}\right) + f_E(\varepsilon') \cdot \frac{2\eta t}{b} \qquad \ldots \quad (2.5)$$

Following this procedure, it is straight-forward to derive the average stress-strain curve (Fig. 2-10) for a welded plate from that for the residual stress-free plate.

2.2.5 Manual of Computer Program

Following the simplified procedure described above, the computer program PLATSS was developed and coded in FORTRAN IV. A list of the input variables and their definitions is presented in Appendix A.

2.3 COMPARISONS

2.3.1 Comparisons with Crisfield's Method

Crisfield's approximate procedure[1-14] is similar to the present method in taking account of the effect of residual stresses except that the edge portions are assumed to remain linearly elastic up to $\varepsilon'_E = 2$ as a result of initial tensile yielding, unlike eqn (2.4) in the present method. That is, the following relationship was adopted in ref. [1-14] to represent the behaviour of the tension yielding blocks:

$$\sigma'_E = \begin{cases} \varepsilon'_E \ , & \varepsilon'_E \leq 2 \\ 2 \ , & \varepsilon'_E > 2 \end{cases} \qquad \ldots \quad (2.6)$$

The present method is compared with Crisfield's method in Figs 2-11 to 2-13 for $\sigma'_r = 0.1$, 0.2 and 0.3 respectively. In deriving these curves for welded plates, the average stress-strain curve shown in Fig. 2-7 for an unwelded plate was used in both methods. The agreement is quite satisfactory in the range $\varepsilon' < 2$. However, beyond this range the difference is significant, particularly in the cases of high residual stresses.

Crisfield's results in Figs 2-11 to 2-13 are rearranged in Fig. 2-14 from which it can be clearly seen that the average stress-

strain curves for welded plates lie above the residual stress-free curve over the range $\varepsilon' > 2$. This is in contradiction to the results of his numerical method[1-12] from which it is concluded that the present procedure is probably more appropriate in dealing with the effect of residual stresses.

2.3.2 *Comparisons with Frieze's Results*

The average stress-strain curves for welded plates derived by the present simplified method are compared with those obtained by Frieze's more rigorous analysis technique[1-8] in Figs 2-15 to 2-20. Comparisons are made for plates having the parameters: $\beta = 0.691$, 1.037, 1.383, 2.074 and 2.766, $\delta_o'/\beta^2 = 0.08716$ and $\sigma_r' = 0.033$, 0.102 and 0.327. From the figures, it can be seen that the results of the simplified approach correlate closely with those derived numerically in ref. [1-11].

Chapter 3

STIFFENED PANEL MODEL

3.1 INTRODUCTION

The skin of steel plated structures is essentially composed of stiffened plate elements often with longitudinal and trasnverse stiffeners as shown in Fig. 3-1. Stiffeners are welded onto plates as a means of creating more efficient structures, and to strengthen unsupported areas of plate. This form of construction is commonly found in many types of structures. In a ship, for example stiffened plates are found everywhere, from the bottom structure, to the side shells, to the decks, and to the super-structure.

The stiffening system that had been adopted in the early days of steel hull construction was based mainly on the use of transverse members. However, most present-day ships have a longitudinal framing system[3-1] since this is far more effective in resisting longitudinal compressive loads. The plates which are thus predominantly stiffened in the longitudinal direction are transversely supported at larger distances by web frames or cross-girders. The main function of these members is to resist the transverse loads that are induced by the water pressure on the side shell and bottom structures. In addition, they provide support for the longitudinal stiffeners to ensure collapse occurs in an interframe mode rather than an overall grillage mode.

Interframe collapse involves lateral-torsional buckling or flexural buckling of stiffeners. Lateral-torsional instability occurs in panels with torsionally weak stiffeners. These tend to be rarely used in ship structures so this form of buckling is encountered only very infrequently[1-34]. The most common mode of failure therefore is interframe flexural buckling which involves collapse of the longitudinal stiffeners and associated plating with the transverse frames remaining basically in their original positions. It has been shown[1-22,1-26,1-34] that failure of a stiffened panel may be sensitive to the direction of buckling leading to important interactions between adjacent stiffener spans. It is therefore important to account for the continuous double-span nature of such panels.

Buckling analysis of stiffened panels in compression has received considerable attention by researchers during the last decade. The beam-column approach, which is a popular simplified approach, treats the longitudinally stiffened panel as a series of beam-columns formed by the stiffeners with some associated width of plate as shown in Fig. 3-2. This approach has been studied numerically either by solving the equilibrium equations using the effective moment-curvature-thrust relationships of the beam section[3-2,3-3], or by incremental finite element or finite difference methods[1-12,1-26,3-4,3-5,1-23]. Loss of stiffness due to plate buckling is accounted for by using load-end shortening curves derived from separate studies on plates in compression. Large deflection elasto-plastic analysis of plates has provided realistic load-end shortening curves of plate panels[1-8,1-9 1-12,1-26,2-1,3-6,3-7] which have been used in stiffened plate analysis[1-12,1-23,1-26,3-5].

The present method is based on the beam-column approach to examine the large deflection elasto-plastic behaviour of stiffened

panels under uniaxial compression. The adopted beam-column model is effectively continuous over many supports provided by transverse frames to take the effect of interaction between adjacent spans into account. Dynamic Relaxation is employed to numerically solve the non-linear equilibrium equations. The strength contribution from the plating, allowing for buckling effects, is accounted for by using the plate average stress-strain curves which were derived separately by the computer program[1-8,3-8]. The stiffeners may be of flat-bar section, angle section, T-section and any other combination of rectangular sections and are assumed to follow the material stress-strain relationship. The load is applied through end displacements such that both the pre- and post-collapse behaviour can be traced. Therefore, load-end shortening curves can be derived for each stiffened panel forming a mid-ship cross-section from which the vertical moment-curvature relationship for the section may be determined incrementally[1-34,1-35, 1-36,3-9].

3.2 THEORY

3.2.1 Basis

When orthogonally stiffened panels are subjected to compression in the longitudinal direction, the continuous stiffeners buckle alternatively upwards and downwards in adjacent spans. It is therefore apparent that symmetry about the centre-line of each span can be assumed, and a beam-column may be analysed by a model ranging from the centre-line of one span to the centre-line of the next span (Fig. 3-3).

The Dynamic Relaxation method using finite difference formulae to express the derivatives is employed to solve the large deflection stiffened plate equations for elastic-perfectly plastic materials.

The effect of initial deflections and residual stresses is included in the analysis. The mode of failure caused by interaction between overall column buckling and plate buckling is examined. Both the plate-induced (PI) and stiffener-induced (SI) modes, which are defined by initial compressive yielding at the plate and at the tip of the stiffener respectively, are considered.

3.2.2 *Dynamic Relaxation (DR)*

The finite difference method is one of the more versatile methods for solving plate problems. When the equations governing the deflection of plate structures together with the boundary conditions are written in finite difference form a set of simultaneous equations is obtained. These simultaneous equations can be solved by various methods such as matrix methods[3-10], relaxation[3-11], electrical analogues[3-12], or Dynamic Relaxation.

DR was originally developed by Day and Otter and has been used to analyse a variety of problems including portal frames[3-13], pressure vessels[3-14], plates[1-9,3-15,3-16], stiffened plates[1-23], short thin-walled beams and columns[3-17], shells[3-18,3-19], cylinders[3-20] and box sections[3-21].

An equivalent dynamic problem is considered in DR instead of solving the simultaneous equations directly. This dynamic problem can be solved by a finite difference approach which involves an iterative procedure and avoids the solution of simultaneous equations.

An interlacing finite difference mesh is used to discretise the system so as to obtain better accuracy for a given number of degrees of freedom[3-13,3-16]. The equations of motion of the equivalent dynamic problem are formed by equating the sum of the viscous

and mass-acceleration forces at any node to the out-of-balance forces arising from the lack of equilibrium found from the equilibrium equations. If the damping and inertia forces are also expressed in finite difference form as functions of velocities and time increments, the equations of motion can be rearranged to give an explicit expression for the velocities at any node in terms of the previous velocities and current out-of-balance forces. Displacements can then be obtained by using a first-order expression to integrate the velocities.

Steps in the iteration loop may be summarised as follows[1-23, 3-16,3-18,3-21].

Step 1. Calculate stress resultants in terms of strain resultants using the elasto-plastic rigidities;

Step 2. Apply stress boundary conditions;

Step 3. Calculate new velocities from the equations of motion;

Step 4. Integrate velocities to give new displacements;

Step 5. Apply displacement boundary conditions;

Step 6. Calculate strain resultants from displacements;

Step 7. Return to Step 1.

The iterative procedure is repeated until the velocities everywhere reach an acceptably low level and the oscillations of the dynamic problem die out. The achievement of this convergence is subject to a suitable systematic choice of iteration parameters such as fictitious densities and damping factors. The concept of fictitious densities was introduced to improve computational efficiency[3-16,3-18,3-22], and as a general guide a value for the damping factor slightly less than critical should result in the fastest convergence[3-15].

3.2.3 Plate Behaviour

The plate is examined separately using the large deflection elasto-plastic plate program[1-8], and its behaviour is then represented in the form of load-shortening curves. These curves were derived for plate panels having the features as discussed in Chapter 2 and which can be summarised as follows:

(a) all edges are simply supported and fixed against out-of-plane deflection,

(b) the loaded edges are held straight and displaced uniformly in-plane,

(c) the unloaded edges are constrained in-plane to remain straight but free to pull-in,

(d) an elastic-perfectly plastic stress-strain relationship is assumed for the material behaviour,

(e) initial out-of-plane deformations are considered as doubly-sinusoidal in shape, and

(f) weld-induced residual stress distributions are represented by the idealised pattern shown in Fig. 2-6.

In the beam-column approach the plate is considered as one unit, and strain, stress and other parameters are calculated at the heart of the plate. The strength contribution by the plate including the effect of plate buckling is accounted for by using the load-shortening curves derived from numerical analyses such as those of Frieze[1-8] and Carlsen[3-23].

3.2.4 Beam-Column Model

3.2.4.1 Discretisation: The coordinate system adopted for the analysis of the stiffened plates is shown in Figs 3-4 and 3-5. The x-axis coincides with the longitudinal direction, the y-axis over the depth of the cross-section and the z-axis across the width of the plate. The beam-column is divided into several segments in the x-direction (Fig. 3-5), and the stiffener is also subdivided into layers over its depth (Fig. 3-4) so as to account for the development of plastic zones. Each layer is assumed to have elastic-perfectly plastic material properties. Since in the calculation of the elasto-plastic tangential rigidities Simpson's first rule is used to integrate over the depth of the cross-section, any odd number of sub-divisions can be adopted to define the stiffener.

The sign convention is such that the tensile strains and stresses are positive and the compressive ones negative. Central finite differences are used in the representation of partial differential equations, and interlacing meshes are adopted as shown in Fig. 3-5, i.e. w-nodes and u-nodes are located at the ends and centres of each segment of the beam-column respectively.

3.2.4.2 Assumptions: The beam-column is analysed on the basis of the following assumptions:

1. The stiffener is so stocky that it does not buckle locally.
2. Plane sections of the stiffener remain plane and perpendicular to the neutral axis, i.e. the strain distribution over the depth of a cross-section is linear.
3. The strength contribution of the plate to the beam-column is accounted for by appropriate plate load-shortening curves. These curves apply to any segment of the beam-column.

4. Strain hardening is neglected, so the material stress-strain curve is assumed to be of the elastic-perfectly plastic form.
5. Shear deformations and the effects of shear stresses on yielding are neglected.
6. The slope of the beam-column everywhere is small.
7. Residual stresses in the stiffener are usually smaller than those in the plate[3-24] and are too variable to quantify[3-25]: they are therefore ignored in the analysis.

3.2.4.3 Governing equations: The equilibrium equations in the case of a beam-column take the form[3-26]:

$$\frac{d^2M}{dx^2} + P\left(\frac{d^2w}{dx^2} + \frac{d^2w_o}{dx^2}\right) = 0 \qquad \ldots \quad (3.1)$$

$$\frac{dP}{dx} = 0 \qquad \ldots \quad (3.2)$$

The equations will not be satisfied at every station of the beam-column until an equilibrium deflected form is achieved. Out-of-balance forces thus arise during the iteration process and can be equated to the simulated equations of motion as follows:

$$\rho_w \frac{d\dot{w}}{dt} + C_w\dot{w} = \frac{d^2M}{dx^2} + P\left(\frac{d^2w}{dx^2} + \frac{d^2w_o}{dx^2}\right) \qquad \ldots \quad (3.3)$$

$$\rho_u \frac{d\dot{u}}{dt} + C_u\dot{u} = \frac{dP}{dx} \qquad \ldots \quad (3.4)$$

Taking central finite differences with respect to time, where velocities are calculated at times $\Delta t/2$ before and after time t, and out-of-balance forces at time t, eqs (3.3) and (3.4) give:

$$\dot{w}_a = \frac{1 - K_w/2}{1 + K_w/2}\dot{w}_b + \frac{\Delta t}{\rho_w(1 + K_w/2)}\left[\frac{d^2M}{dx^2} + P\left(\frac{d^2w}{dx^2} + \frac{d^2w_o}{dx^2}\right)\right] \qquad \ldots \quad (3.5)$$

$$\dot{u}_a = \frac{1 - K_u/2}{1 + K_u/2}\,\dot{u}_b + \frac{\Delta t}{\rho_u(1 + K_u/2)}\,\frac{dP}{dx} \qquad \ldots \quad (3.6)$$

where K_w ($= C_w\,\Delta t/\rho_w$) and K_u ($= C_u\,\Delta t/\rho_u$) are non-dimensionalised viscous damping coefficients in the w- and u-directions respectively.

The displacements at time t + Δt can then be found by integrating the velocities:

$$w_a = w_b + \dot{w}_a\,\Delta t \qquad \ldots \quad (3.7)$$

$$u_a = u_b + \dot{u}_a\,\Delta t \qquad \ldots \quad (3.8)$$

and are used in the next cycle of calculations to obtain the new stress resultants. The procedure is continued until equilibrium is reached.

3.2.4.4 Incremental procedure: Since plasticity spreads gradually over the depth and along the length of the beam-column with increasing loading, it is very difficult to derive analytical solutions. A numerical procedure, where the loads are applied incrementally through the end displacements, is thus adopted to deal with the problem.

The incremental form of the large deflection direct strains and curvatures are as follows[1-23,3-21]:

$$\Delta\varepsilon_a = \frac{du_t}{dx} - \frac{du_p}{dx} + \frac{1}{2}\left(\frac{dw_t}{dx} - \frac{dw_p}{dx}\right)\left(\frac{dw_t}{dx} + \frac{dw_p}{dx} + 2\,\frac{dw_o}{dx}\right) \qquad \ldots \quad (3.9)$$

$$\Delta\phi = -\left(\frac{d^2w_t}{dx^2} - \frac{d^2w_p}{dx^2}\right) \qquad \ldots \quad (3.10)$$

where subscripts t and p indicate current and previous values of total displacements respectively.

Based on the assumption that after bending plane sections remain plane, the total strain at any location of the cross-section is given by:

$$\Delta\varepsilon_t = \Delta\varepsilon_a + y\Delta\phi \qquad \ldots \quad (3.11)$$

where y is the distance from that location to the line of action of the external force.

The incremental stress resultants corresponding to the increments in axial strains and curvatures can be found through numerical integration over the area of the cross-section. The increment in axial force, for example is given by:

$$\begin{aligned}
\Delta P &= \int_{A_p} E_p^* \, (\Delta\varepsilon_a + y\Delta\phi) \, dA + \int_{A_s} E_s^* \, (\Delta\varepsilon_a + y\Delta\phi) \, dA \\
&= E_p^* \, (A_p \, \Delta\varepsilon_a - A_p \, \bar{y}_p \, \Delta\phi) \\
&\quad + \Delta\varepsilon_a \int_{A_s} E_s^* \, dA + \Delta\phi \int_{A_s} E_s^* \, y \, dA \\
&= \{E_p^* \, A_p + \int_{A_s} E_s^* \, dA\} \, \Delta\varepsilon_a + \{- E_p^* \, A_p \, \bar{y}_p + \int_{A_s} E_s^* \, y \, dA\} \, \Delta\phi \\
&= C^* \, \Delta\varepsilon_a + G^* \, \Delta\phi \qquad \ldots \quad (3.12)
\end{aligned}$$

Similarly, the increment in bending moment is given by:

$$\begin{aligned}
\Delta M &= \int_{A_p} E_p^* \, (\Delta\varepsilon_a + y\Delta\phi) \, y \, dA + \int_{A_s} E_s^* \, (\Delta\varepsilon_a + y\Delta\phi) \, y \, dA \\
&= E_p^* \, (- \Delta\varepsilon_a \, A_p \, \bar{y}_p + \Delta\phi \, A_p \, \bar{y}_p^2) \\
&\quad + \Delta\varepsilon_a \int_{A_s} E_s^* \, y \, dA + \Delta\phi \int_{A_s} E_s^* \, y^2 \, dA \\
&= \{- E_p^* \, A_p \, \bar{y}_p + \int_{A_s} E_s^* \, y \, dA\} \, \Delta\varepsilon_a + \{E_p^* \, A_p \, \bar{y}_p^2 + \int_{A_s} E_s^* \, y^2 \, dA\} \, \Delta\phi \\
&= G^* \, \Delta\varepsilon_a + D^* \, \Delta\phi \qquad \ldots \quad (3.13)
\end{aligned}$$

where $$C^* = E_p^* A_p + \int_{A_s} E_s^* \, dA \qquad \ldots \quad (3.14)$$

$$D^* = E_p^* A_p \bar{y}_p^2 + \int_{A_s} E_s^* y^2 \, dA \qquad \ldots \quad (3.15)$$

$$G^* = - E_p^* A_p \bar{y}_p + \int_{A_s} E_s^* y \, dA \qquad \ldots \quad (3.16)$$

and subscripts p and s indicate plate and stiffener respectively.

The tangential modulus for the stiffener E_s^* is obtained from the material stress-strain curve, whereas that for the plate E_p^* is calculated as the slope of its load-shortening curve at the value of strain corresponding to the previous load. The elastic value is assumed for E_p^* or E_s^* at those nodes where unloading occurs after the peak load is reached.

3.2.4.5 Boundary conditions: The boundary conditions can be included in the Dynamic Relaxation procedure in a systematic manner. For inter-frame flexural buckling, the transverse frames remain basically at their original positions. Thus the deflections are specified as zero at those locations. Continuity over supports is considered in the present study by assuming no rotational restraint at the transverse frames. Due to symmetry about the centre-line of each span of the beam-column, the values of the slopes at mid-spans are zero.

In summary, the boundary conditions are as follows:

1. $w = 0$, at point B (Fig. 3-5);
2. $dw/dx = 0$, at point A, i.e. $w_1 = w_2$;
3. $dw/dx = 0$, at point C, i.e. $w_{12} = w_{13}$.

3.2.4.6 Initial imperfections: In the beam-column approach, residual stresses in the cross-section are incorporated in the following way:

1. For the plate, the residual stresses have been considered in the separate study of the plate, and their effect is allowed for by using the plate load-shortening curves.

2. For the stiffener, residual stresses are not considered due to the fact that the effect of residual stresses on the stiffener is generally small compared with that on the plate, and that no pattern has yet been found which reliably represents residual stresses in stiffeners[1-22,3-25].

When simply supported beam-columns buckle the sinusoidal form is the most usual mode of buckling. Thus half-sinusoidal waves were used in each span to account for the initial stiffener deflections found in practice. The amplitude of the initial stiffener deflections in each span of the beam-column could be different both in magnitude and direction. A positive or negative value of amplitude indicates an initial stiffener deflection towards or away from the stiffener outstand respectively (Fig. 3-6).

3.3 NUMERICAL ANALYSIS

3.3.1 Application of Load

As the effect of plasticity spreads slowly over the structure, loading is applied incrementally through end displacements so that the pre- and post-buckling behaviour can be followed. The calculation of elasto-plastic rigidities, which is performed at the end of each load increment, is outside the Dynamic Relaxation iterative loop. It is also appropriate since yield has to be determined for the static configuration Once the rigidities are calculated, they apply throughout the next increment without modification. Consequently, only small increments in applied end displacements are permitted, especially when significant changes in the rigidities occur such as in the region shortly before and after peak load, and in the case of slender beam-columns early in the load cycle. However, it is unnecessary to use very small increments

in places where there are no sharp changes in the rigidities since the results obtained would be the same as those obtained using larger increments.

For the convenience of data preparation, the end displacements are non-dimensionalised by the displacement required to cause yield:

$$u_a = \frac{(L_1 + L_2)}{2} \frac{\sigma_Y}{E} \qquad \ldots \quad (3.17)$$

A preliminary run in which increments of 0.05 to 0.10 are used, is performed to determine the approximate value of strain corresponding to the ultimate load. The size of increments can then be determined for the final run.

The load history can appropriately be divided into four stages where different increment sizes are adopted:

1. Initially elastic values are assumed for the rigidities E^*, therefore a small increment of 0.001 is required.
2. Increments of 0.05 ~ 0.10 can be used between 0.001 and $u_p - 0.1$ where u_p is the estimated non-dimensionalised end displacement corresponding to peak load.
3. Typical increments of 0.005 ~ 0.01 are suitable for the range between $u_p - 0.1$ and $u_p + 0.1$.
4. The increments can be increased to 0.10 after $u_p + 0.1$ has been passed.

3.3.2 *Iteration Parameters*

3.3.2.1 Time increments and densities: The time increment Δt must be less than a critical value for numerical stability. In ref. [3-27]

semi-empirical stability criteria are used to establish the bounds for time increments which are functions of mass densities and mesh sizes. However, it has been shown[3-28] that time increments can be conveniently set to unity, and that the convergence of DR is further enhanced if the calculation is normalised by using fictitious densities ρ_{w_i}, ρ_{u_i} which are found from the individual row-sums of the stiffness matrices:

$$\rho_{w_i} = \frac{1}{4} \sum_j |C_{w_{ij}}| \qquad \ldots \quad (3.18)$$

$$\rho_{u_i} = \frac{1}{4} \sum_j |C_{u_{ij}}| \qquad \ldots \quad (3.19)$$

where $C_{w_{ij}}$ and $C_{u_{ij}}$ are the elements of the stiffness matrix implicit in the finite difference formulation of the structure for w- and u-directions respectively.

From eqs (3.5) and (3.18), the fictitious densities at w-node i of the beam-column can be determined as follows:

$$\rho_{w_i} = \frac{1}{4}\left\{\overline{\frac{d^2M}{dx^2}} + |P|\left(\overline{\frac{d^2w}{dx^2}} + \overline{\frac{d^2w_o}{dx^2}}\right) + \bar{P}\left(\left|\frac{d^2w}{dx^2}\right| + \left|\frac{d^2w_o}{dx^2}\right|\right)\right\}$$

$$= \frac{4EI}{(\Delta x)^4} + \frac{|P|}{(\Delta x)^2} + \frac{EA}{4\Delta x}\left(2 + \left|\frac{dw}{dx}\right| + \left|\frac{dw_o}{dx}\right|\right) \times \left(\left|\frac{d^2w}{dx^2}\right| + \left|\frac{d^2w_o}{dx^2}\right|\right)$$

$$\ldots \quad (3.20)$$

Similarly, the fictitious densities at u-node i of the beam-column are obtained from eqs (3.6) and (3.19):

$$\rho_{u_i} = \frac{1}{4}\overline{\frac{dP}{dx}} = \frac{1}{4(\Delta x)}\left\{\overline{P_{i+1}} + |-1|\,\overline{P_i}\right\}$$

$$= \frac{EA}{4(\Delta x)^2}\left\{\left(2 + \left|\frac{dw}{dx}\right| + \left|\frac{dw_o}{dx}\right|\right)_{i+1} + \left(2 + \left|\frac{dw}{dx}\right| + \left|\frac{dw_o}{dx}\right|\right)_i\right\}$$

$$\ldots \quad (3.21)$$

where the finite difference coefficients of the displacements are:

$$\overline{\frac{dw}{dx}} = \frac{2}{2\Delta x} = \frac{1}{\Delta x} \qquad \overline{\frac{du}{dx}} = \frac{2}{\Delta x}$$

$$\overline{\left(\frac{dw}{dx}\right)^2} = \frac{2}{\Delta x}\left|\frac{dw}{dx}\right|$$

Although the derivation of eqs (3.20) and (3.21) is based on the elastic expressions of stress resultants, only a few cases have been encountered which indicate an under- or an over-estimate of the fictitious densities has been made.

3.3.2.2 Damping factors: An essential requirement of DR is that the damped oscillations should quickly reduce to zero. The oscillations usually consist of an unknown combination of the different modes of vibration. Thus the damping factors must be chosen so that the vibration due to each mode will become effectively zero. A vibrating system with critical viscous damping converges most rapidly to its equilibrium position. However, a value for the damping factor just less than critical is preferred since it will result in a solution that oscillates slightly about its equilibrium position rather than converges from one side[3-16,3-29].

It has been concluded[3-15,3-30] that once the natural frequency of a structure in respect to each displacement is known, the critical damping factors can be calculated. The natural frequency can be determined either by tracing displacements or by following the variation in kinetic energy calculated as the sum of the squares of the velocity components. However, it is unnecessary to calculate the damping factors for every beam-column since damping factors are not greatly influenced by slight variations in beam-column parameters and a visual check is usually sufficient to ensure that the damping is slightly less than critical.

In order to accelerate convergence, trial values of displacements are obtained prior to the application of the load increment by extrapolation using the previous values of displacements and the ratio of the new to the previous load increments:

$$w_{i,n+1} = w_{i,n} + (w_{i,n} - w_{i,n-1}) \times \frac{d_{n+1} - d_n}{d_n - d_{n-1}} \quad \ldots \quad (3.22)$$

$$u_{i,n+1} = u_{i,n} + (u_{i,n} - u_{i,n-1}) \times \frac{d_{n+1} - d_n}{d_n - d_{n-1}} \quad \ldots \quad (3.23)$$

where w, u are the displacements in w- and u-directions respectively, d is the applied end displacement, subscript n indicates the values at the n^{th} load level, and subscript i the node number.

3.3.3 *Numerical Procedure*

The steps included in the beam-column analysis can be summarised as follows:

1. Initialise the strain resultants, stress resultants, displacements, velocities and elastic rigidities.
2. Input data concerning the dimensions of the cross-section, the length of the spans of the beam-column, Young's Modulii and yield stresses of the plate and stiffener, the load-shortening curve of the plate, the amplitudes of the initial deflections, the number of iterations, the damping factors and load increments.
3. Generate initial deflected form.
4. Calculate the geometric particulars and centroids of the cross-section.
5. Determine the fictitious densities.
6. Apply the load increment in terms of the end displacement.

7. Obtain the trial displacements by using the displacements at the previous load level except for the first load increment.
8. Enter Dynamic Relaxation iterative loop.
9. Calculate the slopes, curvatures and incremental strain resultants.
10. Calculate incremental stress resultants.
11. Calculate fictitious densities and hence velocities.
12. Calculate displacements and apply displacement boundary conditions.
13. End Dynamic Relaxation cycle.
14. Determine the elasto-plastic rigidities for the plate from the load-shortening curve of the plate and for the stiffener from the material stress-strain curve.
15. Integrate the rigidities over the cross-section to obtain the total rigidities.
16. Calculate total strains for every layer of the cross-section.
17. Store the current values of the displacements and strains. Return to Step 6.

3.3.4 *Numerical Stability*

The iterations are repeated until the oscillations of the simulated dynamic problem have died out, i.e. the velocities everywhere reach a suitably low level. The main factors affecting the achievement of this equilibrium state are discussed in this section.

The plate is considered as a single layer by using the load-shortening curve of the plate to account for its local instability and yielding. By virtue of Simpson's first rule, any odd number of subdivisions over the depth of the stiffener can be used in the

analysis. There is no limitation on the number of segments along the length of the beam-column.

Variation of the ultimate strength of a beam-column with the number of subdivisions over the depth of the stiffeners is shown in Figs 3-7, 3-9, 3-11 and 3-13, while variation of the ultimate strength with the number of segments along the length of the beam-column is shown in Figs 3-8, 3-10, 3-12 and 3-14 for λ = 0.3, 0.5, 1.0 and 1.5 respectively. Details of the stiffened panels used in the convergence study are listed in Table 3-1. From these figures, it can be concluded that a model with 11 subdivisions and 15 segments is adequate for obtaining a good degree of accuracy.

The plate load-shortening curve is represented numerically as a multi-linear curve. There is no need to use Lagrangian interpolation or cubic splines if the points on the curve are closely spaced.

Correct selection of the damping factors is required to achieve fast convergence. The recommended values are 0.030 ~ 0.060 for K_w and 0.300 ~ 0.500 for K_u respectively. In some cases, however, numerical instability was encountered at a certain level of loading even though a wide range of the damping factors had been used. This difficulty was solved by increasing the fictitious densities gradually after each load application.

Table 3-1

Details of Stiffened Panels used in Convergence Study

Reference No.	F1	F2	F3	F4
Length between Transverse Girders (mm)	914.4	1524.0	3047.9	4571.9
Plate Thickness (mm)	7.55	7.55	7.55	7.55
Web Dimension	105 × 5.1	105 × 5.1	105 × 5.1	105 × 5.1
Table Dimension	44.5 × 9.1	44.5 × 9.1	44.5 × 9.1	44.5 × 9.1
b/t_p	55	55	55	55
β	2.173	2.173	2.173	2.172
λ	0.3	0.5	1.0	1.5
Tensile Yield Strength of Plate (N/mm^2)	320.0	320.0	320.0	320.0
Tensile Yield Strength of Stiffener (N/mm^2)	320.0	320.0	320.0	320.0
Compression Residual Stress (N/mm^2)	64.0	64.0	64.0	64.0
Initial Plate Imperfection (mm)	b/200	b/200	b/200	b/200
Initial Stiffener Imperfection (mm)	+0.0015 L -0.0015 L	+0.0015 L -0.0015 L	+0.0015 L -0.0015 L	+0.0015 L -0.0015 L

Chapter 4

A STUDY ON STIFFENED PANELS

4.1 INTRODUCTION

In this chapter the analytical method described in Chapter 3 is used to examine the behaviour of stiffened panels. The method is based on the beam-column approach in which the longitudinally stiffened panels supported by the relatively stronger transverse girders are treated as a series of beam-columns formed by the stiffeners with the associated width of plate equal to the stiffener spacing. A continuous double-span model is adopted to account for interaction between adjacent stiffener fields. Plate buckling effects are allowed for by using plate average stress-strain curves which were derived separately.

The predicted strengths using the present method are compared with test results and those obtained by other numerical methods. Differences between the analytical results for one-span and double-span beam-columns are discussed. A parametric study on the behaviour of double-span stiffened panels is then carried out covering a range of practical geometric parameters and realistic levels of initial imperfections.

To initially check the validity of the computer program based on the present method, a confirmation run was performed for the squash condition. A very stocky stiffened panel ($\lambda = 0.1$, $\beta = 0.691$) without

residual stress present was chosen for this purpose. The result obtained, presented in the form of a load-end shortening curve as shown in Fig. 4-1, is exactly the same as the elastic-perfectly plastic curve.

4.2 COMPARISONS WITH EXPERIMENTAL RESULTS

The computer program DSTPL based on the numerical formulation in Chapter 3 is to be applied to examine the collapse behaviour of stiffened panels which have been tested by other researchers. The original specimen reference numbers given to the test panels are retained in the present study. Some of the specimens available for study are intermittently welded. Since their behaviour is possibly influenced by the lack of continuity of welding, continuously welded panels are preferred in selecting specimens for comparisons. The measured values of component dimensions, yield strength of the material, weld-induced residual stresses and initial imperfections are used in the numerical analysis. Comparisons are made in a non-dimensional form, in which both the experimental collapse loads and the predicted ultimate strengths of stiffened panels are expressed as fractions of their squash loads.

4.2.1 *Horne and Narayanan*

Tests were carried out by Horne, et al.[4-1] on 33 stiffened panels which were formed into three groups intended to investigate the effects of plate slenderness, type of welding and torsional buckling of the stiffeners on the collapse behaviour of stiffened panels. Two panels, PF5 and PF11, were chosen for study from the first group, and one panel, SW5, from the second group. All of the panels were stiffened by flat-bars using continuous welding. The measured values of

specimen dimensions, material properties, residual stresses and initial imperfections are tabulated in Table 4-1. The ultimate strengths predicted by the present method are compared with the collapse strengths observed in the tests[4-1] in the same table. It can be seen that the predicted strengths lie within 4% of the collapse loads for all specimens. That is, the theory correlates very satisfactorily with these particular results.

Since the panels considered were tested under pin-ended conditions[4-1] while a continuous beam-column model was used in the present method, their results are compared with those of the single-span analysis[1-23] in Table 4-2. It is of interest to note that although the single-span analysis[1-23] theoretically simulates the specimens more closely than the present method, the latter predicts the test results more accurately than the former, which underestimates the ultimate strength values by about 10%. This could be due to the introduction of a degree of constraint by the end plates of the specimens which has resulted in an increase in panel strength.

4.2.2 *Dorman and Dwight*

Twelve tests on stiffened plate panels were conducted by Dorman and Dwight[1-27] to examine the influence of weld-induced residual stresses and initial imperfections on the behaviour of such panels under uniaxial compressive loads. Each panel was divided by four transverse girders into five stiffened sections of equal span to minimise the effect of local end restraint. Four panels TPA3, TPA4, TPB3 and TPB4, all of which were longitudinally stiffened by flat-bars were selected for comparison. The shape of the initial stiffener deflections was specified to be alternately upwards and downwards in adjacent spans. Details of the test panels, including

the specified magnitudes of initial stiffener deflections, the measured values of specimen dimensions, material properties and weld-induced residual stresses are summarised in Table 4-3. Both the experimental collapse loads and the predicted ultimate strengths are listed in the same table from which it can be clearly seen that the agreement is satisfactory and the differences are less than 6% in all cases.

4.2.3 *Smith*

Results of a series of tests on full-scale welded steel grillages under compressive load combined in some cases with lateral pressure were presented by Smith in ref. [1-26]. The grillages were constructed following as far as possible normal shipyard practices. All stiffeners were standard Admiralty tee bars and were continuously welded to the plating. Two grillages 2b and 3b representing possible ship-bottom configurations, which were tested under compressive load alone and collapsed by interframe flexural buckling of the longitudinal stiffeners associated with inelastic buckling of plate panels[1-26], were chosen for comparison with the analytical method. The average measured values of plate thicknesses, stiffener dimensions and tensile yield strength of the plating and stiffeners are summarised in Table 4-4 together with the maximum average applied compressive stresses observed in the tests and as determined by the analysis. It is seen that the predicted strengths for the grillages are 97.7% and 93.8% of the corresponding test values.

TABLE 4-1 COMPARISON BETWEEN EXPERIMENTAL TESTS BY HORNE AND NARAYARAN AND PRESENT NUMERICAL METHOD

SPECIMEN REFERENCE NO.	PF5	PF11	SW5
LENGTH OF STIFFENED PANELS (MM)	2700	2700	2700
PLATE THICKNESS (MM)	10.0	9.8	9.9
STIFFENER DIMENSION	150X15.15	150X15.15	150X15.10
B / T	30	35	48
L / R	55	56	60
TENSILE YIELD STRENGTH OF PLATE (N/MM^2)	413.3	378.8	408.4
TENSILE YIELD STRENGTH OF STIFFENER (N/MM^2)	415.6	410.1	408.8
MEASURED COMPRESSIVE RESIDUAL STRESS (N/MM^2)	136.0	83.0	110.0
INITIAL PLATE IMPERFECTION (MM)	+1.4	+1.6	+2.0
INITIAL STIFFENER IMPERFECTION (MM)	+3.5	+3.3	+2.1
NON-DIMENSIONAL COLLAPSE STRESS (EXPERIMENT)	0.790	0.720	0.640
NON-DIMENSIONAL ULTIMATE STRESS (NUMERICAL)	0.761	0.749	0.641

TABLE 4-2 COMPARISONS OF EXPERIMENTAL RESULTS WITH THOSE PREDICTED BY USING THE NUMERICAL SINGLE-SPAN AND DOUBLE-SPAN MODELS

SPECIMEN REFERENCE NO.	ULTIMATE STRENGTH (σ_u/σ_Y)			RATIOS	
	EXPERIMENTAL	NUMERICAL			
	PIN-ENDED	SINGLE-SPAN	DOUBLE-SPAN	(2)/(1)	(3)/(1)
	REF. (4-1)	REF. (1-23)	PRESENT		
	(1)	(2)	(3)		
PF5	0.790	0.700	0.761	0.886	0.963
PF11	0.720	0.660	0.749	0.917	1.040
SW5	0.640	-	0.641	-	1.002

TABLE 4-3 COMPARISON BETWEEN EXPERIMENTAL TESTS BY DORMAN AND DWIGHT AND PRESENT NUMERICAL METHOD

SPECIMEN REFERENCE NO.	TPA3	TPA4	TPB3	TPB4
LENGTH BETWEEN TRANSVERSE GIRDERS (MM)	1143	1143	1143	1143
PLATE THICKNESS (MM)	6.32	6.68	6.40	6.30
STIFFENER DIMENSION	127X9.53	127X9.53	127X9.53	127X9.53
B / T	40	50	40	50
L / R	27.9	29.5	28.0	28.9
TENSILE YIELD STRENGTH OF PLATE (N/MM^2)	291	285	313	298
MEASURED COMPRESSIVE RESIDUAL STRESS (N/MM^2)	31.3	16.5	38.1	40.7
INITIAL PLATE IMPERFECTION (MM)	B/200	B/200	B/200	B/200
INITIAL STIFFENER IMPERFECTION (MM)	+3.18 -2.12	+3.18 -2.12	+2.12 -3.18	+2.12 -3.18
NON-DIMENSIONAL COLLAPSE STRESS (EXPERIMENT)	0.841	0.730	0.793	0.726
NON-DIMENSIONAL ULTIMATE STRESS (NUMERICAL)	0.825	0.769	0.809	0.753

TABLE 4-4 COMPARISON BETWEEN EXPERIMENTAL TESTS BY SMITH AND PRESENT NUMERICAL METHOD

GRILLAGE REFERENCE NO.	2B	3B
LENGTH BETWEEN TRANSVERSE GIRDERS (IN)	60	60
PLATE THICKNESS (IN)	0.290	0.252
WEB DIMENSION	4.125 X 0.212	2.790 X 0.183
TABLE DIMENSION	1.760 X 0.375	1.100 X 0.250
B / T	41.4	47.6
L / R	36.0	66.0
TENSILE YIELD STRENGTH OF PLATE (TSI)	17.1	16.6
TENSILE YIELD STRENGTH OF STIFFENER (TSI)	18.1	14.7
MEASURED COMPRESSIVE RESIDUAL STRESS (TSI)	8.5	10.7
INITIAL PLATE IMPERFECTION (IN)	0.0060 X B	0.0150 X B
INITIAL STIFFENER IMPERFECTION (IN)	+0.0010 X L -0.0006 X L	+0.0019 X L -0.0030 X L
NON-DIMENSIONAL COLLAPSE STRESS (EXPERIMENT)	0.830	0.610
NON-DIMENSIONAL ULTIMATE STRESS (NUMERICAL)	0.811	0.572

4.3 COMPARISONS WITH NUMERICAL RESULTS

In this section, the results of the present method are compared with those of three other numerical methods, all of which are based on the beam-column approach to examining the behaviour of stiffened panels under compressive loads. Comparisons are made in a non-dimensional form, as in the previous section. That is, the stresses and strains are non-dimensionalised with respect to yield strength and yield strain of the material respectively.

4.3.1 Moolani

Both the single-span and multi-span beam-column approaches were employed by Moolani [1-22] to analyse the behaviour of stiffened compression panels. In the single-span approach, the collapse strengths of the stiffened sections between transverse girders were determined ignoring any interaction between adjacent spans. The results from this approach will be compared with those of the present method in section 4.3.3. In the multi-span approach, the stiffened panels were considered as continuous members supported by springs at the transverse girder positions. The results from Moolani's two-span approach are compared with those of the present method in this section.

The plate of the stiffened panels has b/t_p ratios of 20 with no residual stress, and hence the material elasto-plastic stress-strain relationship can be used as the average stress-strain curve for the plate. A flat-bar is used to stiffen the plate, and both have the same cross-sectional area. The lengths of the stiffened panels were adjusted so that L/r ratios of 40, 70, 100 and 130 were generated. Two types of initial imperfections are considered in the comparison. The first type (Type A) relates to the preferred buckling mode, i.e. the

stiffener deflects towards its outstand in one span and away from the outstand in the adjacent span. The second type (Type B) corresponds to the stiffener deflecting towards the outstand in one span only.

The load-end shortening curves as derived for the stiffened panels of L/r = 40, 70, 100 and 130 are shown in Fig. 4-2 for the Type A initial imperfection and in Fig. 4-3 for the Type B initial imperfection. From these curves, the ultimate strengths of the stiffened panels with these two types of initial imperfections can be identified. The results are compared with those obtained from Moolani's method in Table 4-5 and Fig. 4-4. The agreement is very satisfactory. Although the present method predicts higher values than Moolani's method in all cases, the difference on average is only 1.5%.

4.3.2 *Carlsen*

The strength of stiffened plates in compression has been analysed using the finite difference computer program STAGS by Carlsen[3-6] covering a range of plate and column slendernesses. The stiffened panels adopted for comparison were stiffened by T-section stiffeners and have the following parameters:

column slenderness	λ = 0.1, 0.3, 0.5, 1.0, 1.5
plate slenderness	b/t_p = 30, 55, 80
stiffener to plate area ratio	α = 0.3
yield strength	σ_Y = 320 N/mm^2

The plate average stress-strain curves used for the analysis were taken directly from ref. [3-6] and are reproduced in Fig. 4-5. These curves were derived for plates with initial plate deformations of δ_o = b/200 and weld-induced residual stresses σ_r' = 0.20. The initial stiffener deflections specified in the two spans are of the same magnitude Δ = L/750 but in opposite directions.

TABLE 4-5 COMPARISON BETWEEN NUMERICAL RESULTS BY MOOLANI'S AND PRESENT METHOD

L/R	B/T	IMPERFECTION TYPE	MOOLANI'S RESULT	PRESENT METHOD	RATIO
40	20	A	0.920	0.939	0.980
		B	0.963	0.972	0.991
70	20	A	0.774	0.788	0.982
		B	0.888	0.892	0.996
100	20	A	0.552	0.565	0.977
		B	0.636	0.646	0.985
130	20	A	-	0.383	-
		B	-	0.428	-

♦♦♦ IMPERFECTION TYPE ♦♦♦

1. TYPE A : + L/750 IN FIRST SPAN
   - L/750 IN SECOND SPAN

2. TYPE B : + L/750 IN FIRST SPAN
   0 IN SECOND SPAN

The load-end shortening curves derived for the stiffened panels of varying column slenderness are shown in Figs 4-6 to 4-8 for plate slendernesses of b/t_p = 30, 55 and 80 respectively. Some of these curves are compared with Carlsen's results in Figs 4-9 to 4-12. The ultimate strengths of the panels computed by the present and Carlsen's methods are listed in Table 4-6 and compared in the forms of ultimate strength-column slenderness curves (Fig. 4-13) and ultimate strength-plate slenderness curves (Fig. 4-14). The agreement is good both from the point of view of ultimate strength and of the critical strain at which the stiffened panels reach their maximum loads (Figs 4.9 to 4.12). The present analysis is also seen to be capable of penetrating much farther into the post-buckling range than the STAGS solution.

The load-end shortening curves presented in Figs 4-6 to 4-8 are shown rearranged in Figs 4-15 to 4-19 such that the variation in the ultimate strength of the stiffened panels with plate slenderness can be clearly seen.

4.3.3 *Drymakis*

A parametric study of stiffened panels using the beam-column approach was presented by Drymakis in ref. [1-23] to investigate the pre- and post-buckling behaviour of stiffened panels subjected to compressive axial loading. In his formulation, the stiffened plates between transverse frames were treated as a series of simply supported columns over a single stiffener span, neglecting the effect of continuity of spans. The stiffened panels were reanalysed using the present double-span model, covering the following parameters:

column slenderness λ = 0.330, 0.572, 0.770, 0.990, 1.266, 1.871, 2.531

plate slenderness b/t_p = 60

stiffener to plate area ratio $\alpha = 0.40$

yield strength $\sigma_Y = 245\ N/mm^2$

initial stiffener deflection $\Delta/L = 1/500,\ 1/750,\ 1/1000$

The average stress-strain curves for the plate with an initial plate deformation magnitude of $\delta_o/b = 1/250$ and weld-induced residual stress $\sigma_r' = 0.25$ were derived using the computer program[1-8] and are shown in Fig. 4-20.

The ultimate strengths of stiffened panels obtained by the present method are compared with Drymakis' results in Table 4-7 and Figs 4-21 and 4-22. Moolani's results using his single-span model are also listed in Table 4-7 for comparison. In the range of low and high slendernesses the agreement is satisfactory with the strengths predicted by the present method lying between those obtained by the other two methods. In the region of intermediate column slenderness $0.770 < \lambda < 1.266$, however, a significant difference between the present results and those of the other two methods is observed. Since the present method is the only one in which a double-span model is formulated, it seems to follow that this difference is attributable to the effects of continuity.

TABLE 4-6 COMPARISONS OF ULTIMATE STRENGTH OF STIFFENED PANELS BETWEEN THE PRESENT METHOD AND CARLSEN'S NUMERICAL RESULTS

PLATE SLENDERNESS	COLUMN SLENDERNESS	ULTIMATE STRENGTH (σ_u / σ_Y)		RATIO
b/t_p	λ	CARLSEN (1)	PRESENT (2)	(1) (2)
30	SQUASH*	-	0.926	-
	0.1	-	0.928	-
	0.3	0.872	0.879	0.992
	0.5	0.807	0.821	0.983
	1.0	0.575	0.574	1.002
	1.5	0.325	0.334	0.973
55	SQUASH*	-	0.756	-
	0.1	-	0.757	-
	0.3	0.667	0.690	0.967
	0.5	0.618	0.629	0.982
	1.0	0.479	0.487	0.984
	1.5	0.323	0.320	1.009
80	SQUASH*	-	0.628	-
	0.1	-	0.633	-
	0.3	0.540	0.575	0.939
	0.5	0.516	0.533	0.968
	1.0	0.393	0.416	0.945
	1.5	0.264	0.279	0.946

μ = 0.974

COV = 2.3 %

* SQUASH LOAD - $\sigma_u = (\sigma_{PM} + \sigma_{SM} * \alpha) / (1+\alpha)$

$\sigma_r' = 0.20$ $\delta_0 = b/200$

$\alpha = 0.30$ $\sigma_{YS} = \sigma_{YS} = 320\ N/mm^2$ $\Delta = 0.0015L$

TABLE 4-7 COMPARISON OF ULTIMATE STRENGTHS OF STIFFENED PANELS BETWEEN MOOLANI'S, DRYMAKIS' AND THE PRESENT METHOD

COLUMN SLENDERNESS	INITIAL STFFENER DEFLECTION	ULTIMATE STRENGTH (σ_u / σ_Y)			RATIO	
		MOOLANI	DRYMAKIS	PRESENT	(1)	(2)
λ	L/Δ	(1)	(2)	(3)	(3)	(3)
0.330	1000	-	-	0.691	-	-
	750	0.681	0.698	0.689	0.988	1.013
	500	0.677	0.698	0.685	0.988	1.019
0.572	1000	-	-	0.656	-	-
	750	0.641	0.678	0.651	0.985	1.041
	500	0.615	0.620	0.644	0.955	0.963
0.770	1000	-	-	0.613	-	-
	750	0.545	0.584	0.602	0.905	0.970
	500	0.530	0.551	0.585	0.906	0.942
0.990	1000	-	-	0.549	-	-
	750	0.489	0.495	0.535	0.914	0.925
	500	0.465	0.471	0.511	0.910	0.922
1.266	1000	-	-	0.440	-	-
	750	0.412	0.417	0.425	0.969	0.981
	500	0.387	0.393	0.404	0.958	0.973
1.871	1000	-	-	0.238	-	-
	750	0.230	0.237	0.232	0.991	1.022
	500	0.217	0.227	0.222	0.977	1.022
2.531	1000	-	-	0.136	-	-
	750	0.131	0.136	0.134	0.978	1.015
	500	0.125	0.133	0.129	0.969	1.031

$b/t_p = 60$ $\quad \delta_0 = b/250$ $\quad \sigma_r/\sigma_Y = 0.25$

$\alpha = 0.40$ $\quad d/t_s = 10$ $\quad \sigma_Y = 245\ N/mm^2$

4.4 PARAMETRIC STUDY

4.4.1 General

In this section a parametric study on the behaviour of double-span stiffened panels in compression is described. A range of practical geometric parameters and realistic levels of initial imperfections and residual stresses is covered. The purpose is to examine the influence of column slenderness, plate slenderness, stiffener to plate area ratio and initial stiffener deflection on the strength of stiffened panels.

The numerical results are presented mainly in the form of load-end shortening curves, including the pre- and post-collapse behaviour of stiffened panels. Additionally, ultimate strength-slenderness curves are produced to investigate the variation of the strength of stiffened panels with column slenderness.

4.4.2 Stiffened Panel Parameters

4.4.2.1 Geometric parameters: The plate is assumed to be stiffened by flat-bars with a depth to thickness ratio $d/t_s = 10$ to ensure they are outside the tripping range for stiffeners. The stiffened panels adopted for the study are classified into the following groups:

Group A - $\beta = 2.074$ ($b/t_p = 60$), $\alpha = 0.4$

Group B - $\beta = 1.037$ ($b/t_p = 30$), $\alpha = 0.4$

Group C - $\beta = 1.037$ ($b/t_p = 30$), $\alpha = 0.2$

The values of b/t_p are computed for mild steel with a yield stress of 245 N/mm^2 and a Young's modulus of 205,000 N/mm^2. To enable complete ultimate strength-slenderness curves can be obtained, each group contains seven column slendernesses $\lambda = 0.330$, 0.572, 0.770, 0.990, 1.260, 1.871 and 2.531, corresponding to $L/r = 30$, 52, 70, 90, 115, 170 and 230 for mild steel.

4.4.2.2 Initial imperfections: Selection of initial stiffener deflection magnitudes is based on the permissible out-of-plane deflections contained in various Codes. A value of Δ = L/1000 is chosen from the Merrison Rules [4-2] in which the values of Δ = - L/1200 or + L/900 were specified. In BS5400 [4-3], a value of Δ = L/750 was specified and hence is adopted for the present study. Further, the value of Δ = L/500 used in the European Recommendations for Steel Construction [4-4] and proposed by Massonnet [4-5] is considered as a third value. Stiffener distortions of this magnitude are used to account in part of residual stresses in the stiffener since measured distortions are usually less than L/1000.

4.4.2.3 Residual stresses: To take the effect of plate residual stresses into account, the plate average stress-strain curves corresponding to σ_r' = 0.25 as shown in Fig. 4-20 are used. This value corresponds to a moderate level of residual stress and is associated with the behaviour of plates throughout this study.

4.4.3 Continuous Double-Span Beam-Columns

4.4.3.1 Effects of column slenderness: As indicated above, three levels of initial stiffener deflections are assumed for each of the seven stiffened panels in a group. That is, 21 load-end shortening curves are derived for each group. These curves are shown in Figs 4-23 to 4-28 for Group A, Figs 4-29 to 4-34 for Group B and in Figs 4-35 to 4-40 for Group C. The ultimate strengths identified from these figures are plotted as ultimate strength-slenderness curves for stiffened panels with Δ = L/1000, L/750 and L/500 in Figs 4-44 to 4-46 for Groups A, B and C respectively. It can be clearly seen that the behaviour of stiffened panels is strongly affected by column slenderness in all cases. Increasing λ leads to a reduction in the

ultimate strength of stiffened panels. For values of intermediate column slenderness $0.770 < \lambda < 1.266$, in which interaction occurs between yielding and flexural buckling of the stiffened panels, the drop in strength after peak load is most pronounced (see for example, Fig. 4-39).

4.4.3.2 Effects of initial stiffener deflections: Some of the load-end shortening curves presented in the previous section are re-presented in Figs 4-41 to 4-43 to highlight the effect of initial stiffener deflection. From these curves along with the ultimate strength-slenderness curves in Figs 4-44 to 4-46, it is found that initial bows mainly influence the behaviour of stiffened panels in the range of moderate column slenderness and that the effect is most pronounced in the region close to peak load.

4.4.3.3 Effects of plate slenderness: The load-end shortening curves for stiffened panels in Group A ($b/t_p = 60$, $\alpha = 0.4$), together with those in Group B ($b/t_p = 30$, $\alpha = 0.4$), are re-presented in Figs 4-47 to 4-49 to demonstrate the effect of plate slenderness on the behaviour of stiffened panels. The corresponding ultimate strength-slenderness curves are also shown in Figs 4-50 to 4-52 for the three levels of initial stiffener deflection considered. In the range of low column slenderness, stiffened panel collapse is mainly due to yielding of the material or buckling of the plate. Thus for a particular λ, increasing β generally results in a significant drop in the stiffened panel load-carrying capacity. Increasing λ changes the dominant mode of failure from one of yielding or plate buckling to one of overall column buckling and hence reduces the effect of β on the collapse behaviour of stiffened panels.

4.4.3.4 Effects of stiffener to plate area ratio: To appreciate the effect of varying stiffener to plate area ratio on the behaviour of stiffened panels, the load-end shortening curves for Group B ($b/t_p = 30$, $\alpha = 0.4$) are compared with those for Group C ($b/t_p = 30$, $\alpha = 0.2$) in Figs 4-53 to 4-55. Comparisons between the ultimate strength-slenderness curves for the two groups are made in Figs 4-56 to 4-58. It is seen that increasing the ratio of stiffener area to plate area from $\alpha = 0.2$ to $\alpha = 0.4$ slightly improves the load-carrying capacity and post-peak behaviour of the stiffened panels.

Chapter 5

HULL GIRDER MODEL

5.1 FAILURE MODES

The evaluation of peak moment, which defines the true ultimate longitudinal strength of a ship's hull girder, will help in assessing the margin of safety between the hull's ultimate moment capacity and the extreme bending moment acting on the ship. The ultimate capacity is connected with the limiting condition beyond which a hull girder can no longer fulfil its function. Thus, before the estimation of peak moment can be made, the possible modes of failure of a hull girder subjected to vertical bending moment have to be discussed.

From the point of view of structural analysis, the failure of a ship's hull girder subjected to vertical bending moment may be due to brittle fracture, fatigue fracture, yielding, spreading of plasticity, instability, or a combination of these events. It may fail gradually as in the case of a lengthening fatigue crack or spreading plasticity, or suddenly, through plastic instability or propagation of a brittle crack[1-1].

Brittle fractures, which occur usually at low temperatures, usually start from a point of stress concentration either inherent in the original design or arising from material defects, or resulting from poor workmanship. They propagate rapidly through the structure. This form of failure resulted in the loss of ships built of mild

steel which were expected to be ductile. Intensive research in the 1950's led to the conclusion that since the behaviour of steels under impact, was found to change suddenly around its 'transition temperature', structures which performed satisfactorily at one temperature could fail suddenly as the temperature was reduced. The likelihood of brittle fracture can now be reduced by the use of materials which are notch-tough down to sufficiently low temperatures.

In general, the fatigue life of unflawed materials used in shipbuilding exceeds the demands made upon the materials in a ship's life. However, a ship's structure inevitably contains many points of stress concentration caused by discontinuities which are built into the ship unintentionally by the method of construction or deliberately for reasons of architecture. Thus a relatively small number of load reversals can lead to low-cycle fatigue fractures which may be exaggerated by the effects of corrosion[5-1]. In fact, with the effective prevention of brittle fracture since the 1950's, almost all macroscopic cracks can now be attributed to low-cycle fatigue. Fortunately, these cracks propagate with such a low speed that they can generally be detected and repaired before damage becomes serious[5-2]. Both brittle and fatigue cracks, which demand careful attention to local design and proper selection of materials, are not considered in the present study.

Although initial yield, which occurs at some points in a structure, does not necessarily cause direct failure, the spreading of plastic deformation over a substantial portion of a structure may lead to structural failure. In the case of a hull girder, yielding commences in the deck or bottom structure and spreads towards side shells as the applied vertical bending moment is increased. Ultimately, a

fully plastic moment is reached when the yield stress has been developed at every point throughout the depth of the girder [1-2]. This moment represents an upper limit of a girder's longitudinal strength, but will rarely be attained due to the adverse effects of buckling of the longitudinal structure between frames, of weld-induced residual stresses or of initial deformations resulting from fabrication. In the practical case, failure is influenced by buckling or yielding of the compression flange and yielding of the tension flange.

When a structural member is subjected to compression, buckling may occur at stress levels well below the yield strength. This type of instability failure is characterised by a relatively rapid increase in deflection for a small increase in load as the compressive stress approaches a critical value. For a hull girder under vertical bending moment, buckling does not immediately result in complete collapse of the girder. The post-buckling behaviour depends on the detailed structural arrangement. In transversely framed ships, the plating buckles and wrinkles between frames so the reserve strength after buckling may be small. In longitudinally framed ships, however, the plating after buckling between longitudinals, shirks its load to the attached stiffeners and the plate-stiffener combination can carry further loading until it buckles between transverse supporting members. As a result, the maximum load-carrying capacity of longitudinally framed vessels may be significantly greater than the load at which buckling commences.

The possible collapse modes for a stiffened panel under axial compression are:

(a) Flexural buckling induced by plate failure: this mode involves buckling towards the stiffener outstand and is precipitated by loss of compressive strength and stiffness of the plate.

(b) Flexural buckling induced by stiffener failure: in this case collapse occurs away from the stiffener outstand.

(c) Torsional tripping of the stiffener: this mode can occur in panels with torsionally weak stiffeners.

(d) Overall grillage buckling: this involves buckling of the longitudinal as well as transverse stiffeners.

Torsional buckling is usually avoided by providing sufficiently stocky stiffeners, and suppression of overall buckling can be achieved by the use of stiff transverse supporting members. The major problem facing a designer is interframe flexural buckling in modes as shown in Fig. 5-1, in particular, Mode a, induced either by plate failure or stiffener failure.

5.2 *DISCRETISATION*

As mentioned previously, failure of an individual structural element, either precipitated by yielding or buckling, does not necessarily imply failure of the entire girder. Failure of a number of structural elements, however, do result in collapse of the hull. This may occur in two different ways: (1) collapse caused by a series of failures of structural elements, and (2) simultaneous overall instability of the complete cross-section. Although the finite element method can be used to deal with the latter problem, the complexity of the mathematical model needed to idealise the complete hull girder still presents a practical obstacle as far as computer time and cost are concerned. Fortunately, except for the overall grillage buckling, the ductile collapse of a ship's hull girder is most probably due to a sequence rather than a coincidence of failures of structural elements. With the simultaneous failure being excluded, it seems

reasonable to assume that failure of an element is not directly influenced by the other elements of the cross-section. This enables one to divide the midship section into structural elements, which respond to the imposed loads independently, and to concentrate on their collapse behaviour. The types of structural elements considered in the present study include the stiffened panel, the plate element and the hard corner.

5.2.1 *Stiffened Panel*

This type of structural element, which is typically found in longitudinally framed structures, is composed of a stiffener and attached plate. The plate ranges from the midpoint of a plate panel between two longitudinal stiffeners to the midpoint of the adjacent plate panel. The choice of edge 1 versus edge 2 of the plate is made in the counterclockwise direction (Fig. 5-2). The stiffener may be a flat-bar, a T-section or a angle bar, to which a code number is assigned respectively (Fig. 5-3).

The behaviour of stiffened panels under compression can conveniently be represented by load-end shortening curves, i.e. average stress-strain curves. The computer program DSTPL described in Chapter 3 is used to generate the load-end shortening curves for stiffened panels which make up the cross-section of a hull girder or a box girder.

The parameters which affect the compressive behaviour of stiffened panels include plate slenderness, weld-induced residual stress in the plate, maximum initial deformation in the plate, column slenderness of the stiffened panel and initial stiffener bow. The effects of all these parameters are accounted for by the use of load-end shortening curves. In a longitudinally framed hull girder, the

midship section usually comprises fifty or more stiffened panels, which may differ in geometry, material property or location in the cross-section. Since part of these panels exhibit virtually the same collapse behaviour, it is uneconomical to generate the average compressive stress-strain curve for every stiffened panel forming the cross-section. Stiffened panels are divided into groups of panels with nearly identical parameters. A representative panel within each group is selected, based on engineering judgment, for generating the load-shortening curve.

5.2.2 *Plate Element*

This kind of structural element comprises a single plate only and is defined by its thickness and the coordinates of the plate edges. There are two possible ways in which plate panels may be found in box girders or hull girders. Firstly, 'wide plate' elements are created in transversely framed panels. Secondly, 'long plate' elements are identified in longitudinally framed structures where a plate-stiffener combination is so stocky that interframe flexural buckling is precluded and only the effect of plate buckling has to be allowed for.

Behaviour of wide plate elements under longitudinal compression is basically equivalent to the behaviour of long plates under transverse compression which can be appropriately covered by average stress-strain curves. Recent numerical studies[5-3,5-4] provide a useful basis for the evaluation of the stiffness and strength of long plates in transverse compression, which are strongly influenced by plate slenderness, aspect ratio and level of weld-induced imperfection. Typical average stress-strain curves derived from ref. [5-3] are illustrated in Figs 5-4 and 5-5.

5.2.3 *Hard Corner*

At certain locations of a hull cross-section, the local structure is strengthened by the connecting members in such a rigid way that it is reasonable to assume that the structure can sustain the imposed compressive load up to the yield point and beyond without suffering any form of instability. That is, it effectively follows the material stress-strain curve over the full loading range. These regions, called 'hard corners'[1-34], include deck stringers, shear strakes, intersections of deck plating with deep girders and longitudinal bulkheads, intersections of shell plating with superstructure, bilge keels, deep girders, longitudinal bulkheads and keel, etc.

The geometry of hard corners can be described in two different ways. In the first approach, a hard corner composed of several interconnecting plates is treated as a group of plate elements and defined by thicknesses and locations of the plate elements. Secondly, the area, centroid and moment of inertia of the cross-section of a hard corner are calculated manually and input directly. This format allows a number of interconnecting plates to be described as a single hard corner element.

5.3 *PLATES IN TENSION*

The tensile behaviour of plates is mainly influenced by the magnitude of weld-induced residual stress. For stress-free plates it is appropriate to suppose that the plates follow the material stress-strain curve. Reference code '0' is used to represent this case as shown in Fig. 5-6. For plates with weld-induced residual stress (Fig. 2-6), however, initial stiffness is reduced due to the yielding tension blocks by the amount:

$$S = \frac{b - 2\eta t}{b} = 1 - \frac{2\eta t}{b}$$

$$= 1 - \frac{\sigma_r'}{1 + \sigma_r'} = \frac{1}{1 + \sigma_r'} \qquad \ldots \quad (5.1)$$

If a linear relationship is assumed up to the point where yielding occurs in the pre-compression zone, the non-dimensional strain corresponding to this point is:

$$\varepsilon_m' = \frac{1}{S} = 1 + \sigma_r' \qquad \ldots \quad (5.2)$$

Reference code '1' is assigned to this case.

If a parabola is assumed to represent the response over the strain range $1 \leq \varepsilon' < 1 + 2\sigma_r'$, it can be expressed by:

$$\sigma' = \frac{1}{4\sigma_r' (1 + \sigma_r')}[- \varepsilon'^2 + (2 + 4\sigma_r') \varepsilon' - 1] \qquad \ldots \quad (5.3)$$

and is connected to the neighbouring linear sections with the appropriate slopes. Reference code '2' is assigned to this case. This form of representation is to account for the adverse effects due to initial deformation and residual stress.

5.4 ASSUMPTIONS

The assumptions made in predicting the hull girder response to extreme vertical bending moment is described in the following:

1. Plane cross-sections of the hull girder before bending remain plane after any load application, thus the distribution of strain over the cross-section is linear (Fig. 5-7).

2. The midship section of the hull girder is discretised into a set of structural elements of which the height is sufficiently small compared with the ships depth that a uniform strain

distribution can be assumed to act over the cross-section of each element. The uniform strain acting on the cross-section of a structural element is taken as the value of the linearly distributed strain at the centroid of the cross-section (Fig. (Fig. 5.8).

3. The stress-strain relationship for either long or wide plate elements in compression is appropriately represented by average stress-strain curves derived from the large deflection elasto-plastic analysis of the isolated plate panels simplified as described in Chapter 2.

4. The elasto-plastic behaviour of stiffened panels in compression is described by load-end shortening curves which are derived separately.

5. The hard corner behaviour is adequately defined by the material stres-strain curve.

6. Since shear forces are generally small at the midship section, the effect of shear stress on yielding is considered to be small enough so that it can be neglected.

7. Neither fatigue nor ductile fracture modes of failure are considered.

8. Since ultimate hull girder collapse occurs in most cases before outer-fibre strains reach two times yield strain, and for shipbuilding steels strain hardening does not occur until strain exceeds yield strain by eight to ten times, it can be assumed that the material itself is elastic-perfectly plastic in tension and compression.

5.5 NUMERICAL PROCEDURE

5.5.1 Application of Load Increments

In the present study, the loading is applied to the hull girder in the form of curvature (Fig. 5-9) instead of bending moment. Since a linear strain distribution over the mid-section is assumed, the strain at the centroids of structural elements caused by the imposed curvature can be determined on the basis of the mid-section's effective neutral axis. The corresponding stress acting on each structural element is then calculated from its average stress-strain curve using interpolation if necessary. Although strain is assumed to be distributed linearly over the section, stress varies non-linearly due to the effects of fabrication-induced distortions, weld-induced residual stress and structural instability. Finally, the bending moment acting on the hull girder is computed for the applied curvature by summing the contributions from all of the structural elements. After this procedure has been repeated for increasing levels of curvature, pairs of data of bending moments and curvatures can be obtained to plot the bending moment-curvature curve which includes the maximum bending moment and the pre- and post-collapse behaviour of the hull girder.

Since the curvature at which collapse of a girder occurs varies to a high degree with the magnitude of the ships height, it is appropriate to express the curvature increments in a form non-dimensionalised with respect to ϕ_Y:

$$\phi_Y = \frac{\varepsilon_{YQ}}{h} = \frac{\sigma_{YQ}}{E_Q \cdot h} \qquad \ldots \quad (5.4)$$

where ϕ_Y is the curvature at which first yield occurs at the extreme

fibre which is located at the deck or bottom of the structure, and h is the distance between this outermost fibre and the elastic neutral axis of the mid-section.

5.5.2 *Location of Effective Neutral Axis*

The location of the plane of zero strain, which will be referred to as the 'effective neutral axis', for an applied curvature is determined by the state of stress existing in the structural elements forming the midship section. As the applied loading is increased, the effective neutral axis shifts towards the tension flange due to loss of stiffness of the structural elements in the compression zone. At each value of curvature, location of the effective neutral axis is determined on the condition that the sum of the axial forces carried by all of the structural elements equals zero.

The state of stress of a structural element is connected with a particular value of strain through the element's average stress-strain curve, while the strain itself is proportional to the distance between the centroid of the structural element and the effective neutral axis. Therefore, the location of the effective neutral axis must be determined in an iterative way from the condition of equilibrium.

The algorithm employed is schematically illustrated in Fig. 5-10 and summarised as follows:

1. The first guess of the location of the elastic neutral axis for the first curvature increment Y_1 is determined assuming a fully effective mid-section. For subsequent curvature increments, their first tries are based on the convergent results of the previous increments.

2. The axial forces F_u and F_ℓ, carried by the structural elements above and below the assumed neutral axis respectively are calculated according to the following procedures:

(i) Since the strain distribution is assumed linear over the depth of the mid-section, the incremental strain $\Delta\varepsilon_{ij}$ induced by the i^{th} curvature increment $(\Delta\phi_i' \times \phi_Y)$ at the j^{th} element is given by:

$$\Delta\varepsilon_{ij} = (\Delta\phi_i' \times \phi_Y) \times (y_j - Y_1)$$

where y_j is the distance between the centroid of the j^{th} element and the base line. The cumulative strain ε_{ij} is obtained by adding the previous value $\varepsilon_{i-1,j}$ to $\Delta\varepsilon_{ij}$:

$$\varepsilon_{ij} = \varepsilon_{i-1,j} + \Delta\varepsilon_{ij}$$

The non-dimensional strain ε'_{ij} is then given by:

$$\varepsilon'_{ij} = \frac{\varepsilon_{ij}}{\varepsilon_{Yj}} = \frac{\varepsilon_{ij} \times E_j}{\sigma_{Yj}}$$

where ε_{Yj}, σ_{Yj} and E_j are yield strain, yield stress and Young's modulus for the material of the j^{th} element respectively.

(ii) The corresponding non-dimensional stress σ'_{ij} carried by the j^{th} structural element is derived from its average stress-strain curve, which is represented as a multi-linear curve in the computer program HULLG, by using linear interpolation. The cumulative stress σ_{ij} and incremental stress $\Delta\sigma_{ij}$ are then given by:

$$\sigma_{ij} = \sigma'_{ij} \times \sigma_{Yj}$$

$$\Delta\sigma_{ij} = \sigma_{ij} - \sigma_{i-1,j}$$

(iii) The axial force F_u acting on the upper part of the mid-section is the sum of the axial loads carried by the structural elements located above the assumed neutral axis:

$$F_u = \sum_{\text{(Upper Part)}} (A_j \times \Delta\sigma_{ij})$$

where A_j is the cross-sectional area of the j^{th} structural element. Similarly, the axial force F_ℓ acting on the lower part of the mid-section is given by:

$$F_\ell = \sum_{\text{(Lower Part)}} (A_j \times \Delta\sigma_{ij})$$

3. In the sagging condition the upper and lower parts are subjected to compressive and tensile loads respectively, and vice versa in the hogging condition. Therefore, the condition of equilibrium that the net axial force acting on the whole mid-section must be equal to zero can be re-stated as the condition that F_u and F_ℓ are equal in magnitude. In the iterative process, iterations are performed until a convergent solution is reached. Convergence is assumed in the present study to have been achieved when the condition

$$\frac{\left||F_u| - |F_\ell|\right|}{|F_u| + |F_\ell|} < \varepsilon \qquad \ldots \quad (5.5)$$

is satisfied, where ε is a pre-selected small positive number.

4. If eqn (5.5) is not satisfied, further iterations on neutral axis location are required for the current curvature increment. The next trial value is determined by the relative magnitudes of the axial forces F_u and F_ℓ. If F_u is greater than F_ℓ, the trial neutral axis is shifted upwards:

$$Y_{k+1} = Y_k + \frac{\overline{Y_E}}{50}$$

where Y_{k+1} and Y_k are the next and current trial values, respectively, and $\overline{Y_E}$ is the height of the elastic neutral axis above the base line of the mid-section. If F_ℓ is greater than F_u, the trial neutral axis is shifted downwards:

$$Y_{k+1} = Y_k - \frac{\overline{Y_E}}{50}$$

This sequence of trial values is used repeatedly until the relative magnitudes of the axial forces F_u and F_ℓ are reversed, i.e. the effective neutral axis is located somewhere between the previous (Y_{k-1}) and current (Y_k) neutral axis locations. Afterwards, a scheme of interval-halving is employed to search more accurately for the location of the effective neutral axis.

5. In the process of interval-halving, the next try (Y_{k+1}) is given by:

$$Y_{k+1} = \frac{Y_k + Y_{k-1}}{2}$$

If the result derived by assuming Y_{k+1} as the neutral axis location does not yet satisfy the convergence criteria, the trial value for the $(k+2)^{th}$ iteration is computed according to the range in which the effective neutral axis is situated. When the following inequality

$$(|F_u| - |F_\ell|)_{k+1} \times (|F_u| - |F_\ell|)_{k-1} < 0$$

is satisfied, the effective neutral axis is located between Y_{k+1} and Y_{k-1}, and therefore Y_{k+2} for a further try is given by:

$$Y_{k+2} = \frac{Y_{k+1} + Y_{k-1}}{2}$$

Otherwise, the effective neutral axis is located between Y_{k+1} and Y_k, and Y_{k+2} is given by:

$$Y_{k+2} = \frac{Y_{k+1} + Y_k}{2}$$

6. As a safeguard against an infinite number of iterations arising caused by the input of incorrect data, the number of iterations in each curvature increment is restricted by an upper limit ITMAX at which point the program will stop iterating and print out a warning message.

5.5.3 *Evaluation of Bending Moment*

After the location of the effective neutral axis $\bar{Y}_i$ of the mid-section is determined for a particular curvature increment $(\Delta\phi_i' \times \phi_Y)$, the corresponding incremental bending moment ΔM_i can then be evaluated. The values of stress on each structural element are computed as described in the previous section. The bending moment increment is then obtained by summing the contributions from all the structural elements that make up the mid-section:

$$\Delta M_i = \sum_{\text{(Whole Section)}} (A_j \times \Delta\sigma_{ij}) \times (y_j - \bar{Y}_i) \qquad \ldots \quad (5.6)$$

and the cumulative bending moment M_i is given by:

$$M_i = \sum_{n=1}^{i} (\Delta M_n)$$

$$= \sum_{n=1}^{i-1} (\Delta M_n) + \Delta M_i$$

$$= M_{i-1} + \Delta M_i \qquad \ldots \quad (5.7)$$

This moment corresponds to the cumulative curvature up to curvature increment $(\Delta\phi_i' \times \phi_Y)$:

$$\phi_i = \sum_{n=1}^{i} (\Delta\phi_n' \times \phi_Y)$$

$$= \sum_{n=1}^{i-1} (\Delta\phi_n' \times \phi_Y) + (\Delta\phi_i' \times \phi_Y)$$

$$= \phi_{i-1} + (\Delta\phi_i' \times \phi_Y) \qquad \ldots \quad (5.8)$$

M_i and ϕ_i are non-dimensionalised with respect to the fully plastic moment M_P and the first yield curvature ϕ_Y.

The fully plastic moment of a ship girder, which represents an upper limit of its load-carrying capacity as a beam, is readily calculable based on the plastic hinge concept[1-2]. Following the method of classical plasticity, the ultimate limit condition is reached when yield occurs at every point of the cross-section. In this case, the 'plastic neutral axis' coincides with the interface which divides the cross-section into two regions with equal 'squash' loads in tension and compression. This condition of equilibrium requires that the equation:

$$F_T = F_C \qquad \ldots \quad (5.9)$$

must be satisfied, where F_T is the sum of yield loads carried by the structural elements of the region in tension:

$$F_T = \sum_{\text{(Region in Tension)}} (A_j \times \sigma_{Yj})$$

and similarly F_C is given by:

$$F_C = \sum_{\text{(Region in Compression)}} (A_j \times \sigma_{Yj})$$

Consequently, the fully plastic moment M_P can be computed for the limit condition as follows:

$$M_P = \sum_{\text{(Whole Section)}} (A_j \times \sigma_{Yj}) \times (y_j - \bar{Y}_P)$$

where $\bar{Y}_P$ is the height of the plastic neutral axis above base line.

The first yield curvature ϕ_Y and the corresponding bending moment M_Y of a ships girder can be determined by the standard section modulus calculation. First of all, the location of the 'elastic neutral axis' $\bar{Y}_E$ must be determined for the fully effective mid-section. Then ϕ_Y is given by the eqn (5.4), and M_Y can be evaluated as follows:

$$M_Y = \frac{\sigma_{YQ} \cdot I_E}{h} \qquad \ldots \quad (5.10)$$

where h is the distance between the elastic neutral axis and the outermost structural element, σ_{YQ} is yield stress of its material, and I_E is moment of inertia of the cross-section about this axis.

5.5.4 *Flow Chart*

Flow charts for the computer program HULLG are illustrated in Figs 5-11 to 5-13. Calculation of the geometric properties of structural elements, i.e. stiffened panels, plate elements and hard corners, determination of the location of the elastic neutral axis, first yield curvature, and first yield bending moment for the fully effective cross-section, and determination of the plastic neutral axis, the corresponding bending moment for the fully plastic cross-section are shown in Fig. 5-11. Application of the load increment in curvature terms, calculation of the values of strain and stress increments at centroids of all the structural elements, and evaluation of the corresponding incremental bending moment for the mid-section are shown in Fig. 5-12. The algorithm used to determine the location of the

effective neutral axis for each curvature increment is shown in Fig. 5-13.

5.5.5 *Summary of Computation Procedure*

The steps involved in the computer program to obtain the bending moment-curvature relationship for ship hull girders can be summarised as follows:

(1) Input the data concerning:

(i) title for print-out and general information of the girder,

(ii) profile of structural midship section,

(iii) stiffener geometry,

(iv) configuration and material properties of the combined plate-stiffener elements,

(v) average compressive stress-strain curves for the stiffened panels,

(vi) initial imperfections,

(vii) convergence criteria and maximum allowable number of iterations,

(viii) load increments.

(2) Calculate area, geometric centroid, and moment of inertia of the cross-section of each structural element, and calculate its area-weighted material properties.

(3) Plot profile of structural midship section, if required.

(4) Determine the average tensile stress-strain relationship for each structural element according to its weld-induced residual stress.

(5) Print out the preliminary results for data verification, if required.

(6) Determine the location of the elastic neutral axis for the fully effective mid-section, and calculate the moment of inertia of the cross-section about this axis, the first yield curvature, and the corresponding bending moment.

(7) Determine the location of the plastic neutral axis and the corresponding bending moment for the fully plastic midship section.

(8) Enter the loop of load increments. Apply load increment in curvature terms.

(9) Enter iteration loop to determine the location of the effective neutral axis of the cross-section.

(i) Assume the neutral axis to be located at the same position as for the previous load increment.

(ii) Calculate the net axial force acting on the whole cross-section. If this force is less than a pre-defined value, jump to Step (10).

(iii) Shift the assume neutral axis to a new position on a fixed interval basis until the net axial force reverses sign. Afterwards, use the method of interval-halving to search for the effective neutral axis.

(10) Determine the distribution of strain and stress increments over the section, and calculate the corresponding bending moment increment.

(11) Return to Step (8) for the next load increment.

5.6 BENDING MOMENT - CURVATURE CURVE

5.6.1 Sign Convention

The sign convention for vertical bending of hull girders as adopted in the present study is shown in Fig. 5-14. Curvature of the hull girder axis is considered to be positive when the hull girder is bent concave upwards and negative when concave downwards, i.e. positive in the sagging condition and negative in the hogging condition. Also the bending moment is positive when it produces compression in the deck structure and tension in the bottom structure. Therefore, a positive bending moment produces positive curvature while a negative bending moment produces negative curvature.

5.6.2 Moment-Curvature Relationship

Using the numerical procedure described above, it is therefore possible to obtain a particular bending moment increment for any curvature increment imposed on a box girder or a hull girder. If this procedure is repeatedly carried out for accumulating levels of curvature, pairs of corresponding data of bending moment and curvature are generated from which to plot the non-dimensional bending moment-curvature curve. Separate runs are performed for the hull girder in the sagging and in the hogging conditions to provide the complete history of the girder under vertical bending.

The full range of behaviour in either the sagging or the hogging condition can be divided into three zones of behaviour. Typical curves are shown in Fig. 5-15. The first zone depicts stable behaviour in which the curvature imposed on the hull girder is less than a critical value ϕ_c, which is the smaller of the curvatures to first yield or to the buckling of some major components. If the

effects of neither buckling nor yielding are significant, the curve in this region is virtually linear. The slope of the bending moment-curvature curve, however, commences to decrease noticeably from the curvature ϕ_c and decreases until it eventually approaches zero at ϕ_u the curvature at which peak moment occurs. The second zone, i.e. the transition zone, ranges from ϕ_c to ϕ_u. The third zone occurs beyond ϕ_u and is characterised by negative slopes, i.e. the load-carrying capacity of the hull girder as a beam drops with increasing curvature.

Collapse behaviour of hull girders mainly differs in the last two zones and is influenced by such factors as material properties, geometric configurations, initial imperfections, degree of structural redundancy, etc. For a girder with little redundancy, collapse is usually precipitated by failure of a significant portion of the structure, leading to a sudden drop in bending moment capacity after reaching the critical curvature. The second zone, therefore, lasts for a relatively short range in this case. In contrast, for a girder with greater redundancy, collapse occurs gradually as a result of the successive failure of smaller portions of the structure. That is, the load shirked by some components due to their failure can be carried by the reserve load-carrying capacity of neighbouring elements. Thus, final collapse of the whole mid-section is delayed by this load redistribution, which results in a longer transition zone.

5.6.3 *Fully Effective Curve*

When all the structural elements forming the mid-section of a hull girder are assumed to follow the material stress-strain curve both in tension and compression, a bending moment-curvature curve can be provided for the fully effective cross-section (Fig. 5-15). Since effects of structural instability are excluded in this idealised case,

bending failure can occur through material yielding only. As the accumulative curvature is increased, yielding begins at the outermost fibre of the deck or bottom structure, and then spreads gradually down or up the side shells. The curve thus approaches asymptotically a horizontal line determined by the fully plastic moment. Comparing this fully effective curve with the realistic bending moment-curvature curve, the difference that is attributable to buckling effects can clearly be identified.

5.7 *MAIN FEATURES OF COMPUTER PROGRAM*

The computer program HULLG consists of a main program and 16 subroutines, and programming was undertaken in standard FORTRAN IV. Comment cards have been extensively used to assist in the understanding of the program. The computer core required to run the program is about 75,000 bytes (or 52,000 bytes if the subroutine used to plot the mid-section profile is excluded) on an ICL 2988 computer.

The number of allowable structural elements, average compressive stress-strain curves and load increments are 250, 20 and 200 respectively as presently dimensioned in the program. The capacity of the program is in most cases sufficient to accommodate the ultimate strength analysis of a hull girder and can readily be enlarged by redimensioning the arrays in the program as required.

A manual of the input data is presented in Appendix B.

Chapter 6

ANALYTICAL STUDY ON HULL GIRDERS

6.1 INTRODUCTION

In Chapter 5 of this thesis, a mathematical model for analysing the ultimate strength behaviour of hull girders was described. The present chapter deals with applications of the computer program HULLG based on that model.

The ultimate strengths of box girders Model 2 and Model 4, which were tested at Imperial College under pure bending conditions and failed by buckling of the stiffened compression flange panels [1-45, 1-46], are evaluated by the present method for comparisons with the experimental results in section 6.2. The effects of initial stiffener deflections, behaviour of hard corners and residual stresses contained in the tension flange on the behaviour of box girders are examined.

In section 6.3, two box girders Model 23 and Model 31 tested by Reckling [1-47] are analysed using the present method to be compared with the test results. Variation of the ultimate strengths of box girders with welding residual stresses and initial imperfections are also presented.

In section 6.4, ultimate strength analyses are performed on two hypothetical ships HULL A and HULL B. Results are compared with those obtained by Adamchak [1-39].

In section 6.5, hull strength assessments are made on two transversely framed warships, *T.B.D. COBRA* and *T.B.D. WOLF*. Results are compared with those obtained by Faulkner, et al.[1-37]. Considering the low efficiency of transversely framed hulls, three versions with mixed framing or longitudinal framing are derived from *COBRA's* hull and are examined by the present approach.

In section 6.6, the ultimate strength behaviour of five longitudinally framed frigates, *TYPE 14*, *WHITBY*, *ROTHESAY*, *TYPE 81* and *LEANDER* classes is investigated. The results will be used in the derivation of simple expressions for the ultimate moment capacity of hull girders in Chapter 7.

6.2 *COMPARISONS WITH EXPERIMENTAL RESULTS - DOWLING, et al.*[1-45,1-46]

Two of the steel box girder models, Model 2 and Model 4, tested by Dowling, et al. at Imperial College, were selected for comparison with the present numerical approach. Both models were subjected to pure bending and failed by buckling of the stiffened compression flange panels. Model 8 of the same series was also tested in pure bending. It suffered orthotropic buckling of the compression flange, however, so was 'not amenable' for comparison with the present approach.

6.2.1 *Model 2*

The cross-section of box girder Model 2[6-1,6-2] was discretised into structural elements, i.e. stiffened panels, plate elements and hard corners, as shown in Fig. 6-1. The component dimensions and material properties of this model are as listed in Table 6-1. The hard corners were assumed to have an elastic-perfectly plastic relationship in both tension and compression.

TABLE 6-1 COMPONENT DIMENSIONS AND MATERIAL PROPERTIES OF STEEL BOX GIRDER MODEL 2 AND MODEL 4

(DOWLING et al [1-45, 1-46])

	MODEL 2	MODEL 4
1. COMPRESSION FLANGE PLATE		
STIFFENER SPACING	241.30	120.65
THICKNESS	4.8641	5.0165
YIELD STRESS	297.3	221.0
YOUNG'S MODULUS	208,500	207,000
2. TENSION FLANGE PLATE		
STIFFENER SPACING	241.30	120.65
THICKNESS	4.8641	4.9428
YIELD STRESS	297.3	215.6
YOUNG'S MODULUS	208,500	208,700
3. WEB PLATE		
STIFFENER SPACING	273.05	98.425
	-	114.300
	-	111.125
THICKNESS	3.3655	4.9428
YIELD STRESS	211.9	280.6
YOUNG'S MODULUS	216,200	214,100
4. STIFFENER (ANGLE)		
TOTAL DEPTH	50.800	50.800
TABLE WIDTH	15.875	15.875
THICKNESS	4.7625	4.7625
YIELD STRESS	276.2	287.9
YOUNG'S MODULUS	191,500	199,200
5. STIFFENER (FLAT)		
DEPTH	-	50.800
THICKNESS	-	6.3500
YIELD STRESS	-	303.8
YOUNG'S MODULUS	-	206,200

UNITS - LENGTH IN MM
STRESS IN N / MM^2

In the first test on Model 2, collapse was precipitated by plate buckling at one end of the box probably due to the high transverse residual stress near the diaphragm[6-2]. After stiffening of the end bays the box was tested again and collapse occurred in an internal section, but the sustained jack load after reaching its maximum load was exactly the same as in the first test. Residual stresses and initial imperfections measured before each of these two tests, and therefore after the first test in the case of the second test, which are listed in Table 6-2, were used in the present study to analyse the overall behaviour of the box girder. The average stress-strain curves for plate panels in the compression flange and webs were derived by the simplified method and are as shown in Fig. 6-2 for Test 2A and in Fig. 6-3 for Test 2B. These curves were used in the large deflection elasto-plastic analysis of the double-span stiffened panels with residual stresses and initial imperfections as listed in Table 6-2. The computed load-shortening curves for the stiffened panels in the compression flange and the webs are as shown in Fig. 6-4 for Test 2A and in Fig. 6-5 for Test 2B.

The pure bending tests on Model 2 were carried out in the sagging condition. Therefore, the bending moment-curvature relationships were computed using the present method for the sagging condition only. They are plotted in Fig. 6-6, together with the experimental result[6-3] and the fully plastic result in both sagging and hogging. Comparisons between the predicted and experimental results are also presented in Table 6-2. The agreement is seen to be satisfactory with the predicted maximum bending moment being 4.9% higher than the collapse moment in Test 2A and 4.6% lower than in Test 2B.

TABLE 6-2 INITIAL IMPERFECTIONS AND COMPARISONS BETWEEN NUMERICAL AND TEST RESULTS OF STEEL BOX GIRDER MODEL 2 (DOWLING et al [1-45, 1-46])

	TEST 2A	TEST 2B
1. WELD-INDUCED RESIDUAL STRESS / YIELD STRESS	0.176	0.176
2. INITIAL PLATE DEFLECTION / PLATE WIDTH	1/400	1/100
3. INITIAL STIFFENER DEFLECTION / SPAN LENGTH	-1/1450 +1/2280	+1/ 580 -1/1430
4. MID-SECTION PARTICULARS		
TOTAL AREA (MM^2)	21554	21554
MOMENT OF INERTIA (M^2-MM^2)	3411.8	3411.8
ELASTIC NEUTRAL AXIS ABOVE BASE LINE (MM)	465.10	465.10
FULLY PLASTIC BENDING MOMENT (KN-M)	2243.3	2243.3
5. NUMERICAL RESULTS		
PEAK BENDING MOMENT (KN-M)	1619.6	1471.4
NON-DIMENSIONAL	0.7220	0.6560
6. EXPERIMENTAL RESULTS		
COLLAPSE BENDING MOMENT (KN-M)	1542.7	1542.7
NON-DIMENSIONAL	0.6877	0.6877

NOTE -

1. CORNER BEHAVIOUR IS REPRESENTED BY MATERIAL STRESS-STRAIN CURVE

2. EFFECTS OF RESIDUAL STRESSES IN TENSION FLANGE ARE NOT CONSIDERED

6.2.2 Model 4

Box girder Model 4[6-4,6-5] had the same overall dimensions as Model 2, but its stiffeners were more closely spaced than those in Model 2. The cross-section of Model 4 was discretised into structural elements including stiffened panels, plate elements and hard corners, as shown in Fig. 6-7. The component dimensions and material properties of this model are listed in Table 6-1 together with those of Model 2.

6.2.2.1 Effects of initial imperfections: As demonstrated in the previous chapters, stiffness and load-carrying capacity of stiffened panels are dependent to a certain extent on the magnitudes of the weld-induced residual stress and initial imperfections, in addition to such parameters as plate slenderness and column slenderness. Consequently, maximum bending moment and collapse behaviour of box girders incorporating such members are similarly influenced. Therefore, where initial imperfections and residual stresses in panels vary, it is necessary in trying to use one stiffened panel stress-strain curve to represent the panel behaviour that this should be representative for the entire panel, and not just the maximum, for example. Thus three combinations of initial imperfection data were selected from the measurements[6-5]: they are listed in Table 6-3. One average residual stress in the plate and one maximum initial plate deflection were used throughout, while three different levels of maximum initial stiffener deflection in two consecutive spans were adopted for the three cases. The deflections correspond to the most severely deformed condition and to two slightly deformed shapes. The load-shortening curves for the stiffened panels in both the compression flange and the webs with the three combinations of initial imperfections were computed using the Dynamic Relaxation approach and are as shown in Fig. 6-8. By incorporating these load-

TABLE 6-3 INITIAL IMPERFECTIONS AND COMPARISONS BETWEEN NUMERICAL AND TEST RESULTS OF STEEL BOX GIRDER MODEL 4

(DOWLING et al [1-45, 1-46])

	MODE 1	MODE 2	MODE 3
1. WELD-INDUCED RESIDUAL STRESS / YIELD STRESS	0.562	0.562	0.562
2. INITIAL PLATE DEFLECTION / PLATE WIDTH	1/800	1/800	1/800
3. INITIAL STIFFENER DEFLECTION / SPAN LENGTH	-1/1050 +1/1950	-1/ 660 +1/4920	-1/ 510 +1/ 510
4. MID-SECTION PARTICULARS			
TOTAL AREA (MM^2)	29144	29144	29144
MOMENT OF INERTIA (M^2-MM^2)	4331.6	4331.6	4331.6
ELASTIC NEUTRAL AXIS ABOVE BASE LINE (MM)	468.82	468.82	468.82
FULLY PLASTIC BENDING MOMENT (KN-M)	2626.9	2626.9	2626.9
5. NUMERICAL RESULTS			
PEAK BENDING MOMENT (KN-M)	2420.5	2417.6	2343.5
NON-DIMENSIONAL	0.9214	0.9203	0.8921
6. EXPERIMENTAL RESULTS			
COLLAPSE BENDING MOMENT (KN-M)	2212.4	2212.4	2212.4
NON-DIMENSIONAL	0.8422	0.8422	0.8422

NOTE -

1. CORNER BEHAVIOUR IS REPRESENTED BY MATERIAL STRESS-STRAIN CURVE
2. EFFECTS OF RESIDUAL STRESSES IN TENSION FLANGE ARE NOT CONSIDERED

shortening curves as the effective stress-strain curves in the present incremental moment-curvature analysis, the sagging bending moment-curvature relationships were obtained for box girder Model 4: the results are shown in Fig. 6-9.

Mode 3 represented the largest measured values of the initial stiffener deflections towards and away from the stiffener outstand - this represents a severely deformed condition. Comparing the predicted peak bending moment in this case with the experimental result[6-6] shows that the present method overestimates the collapse bending moment by 5.9% which is reasonable.

Modes 1 and 2 represented two slightly deformed shapes. The bending moment-curvature curves for these two cases almost coincided as shown in Fig. 6-9. The computed peak bending moments for Modes 1 and 2 were 9.4% and 9.3% higher than the collapse bending moment.

The peak bending moments computed for these three modes of initial imperfections and the experimental collapse bending moment of Model 4 are summarised in Table 6-3. Changing the initial stiffener deflection mode from (- 1/1050, + 1/1950) to (- 1/510, 1/510) results in 3.3% decrease in maximum bending moment.

6.2.2.2 Effects of hard corners: The bending moment-curvature relationship of a box girder is also influenced by the behaviour of its hard corners which are assumed in the present study to be elastic-perfectly plastic in both tension and compression. To examine the effects of hard corners on the collapse behaviour of a box girder, hard corners were introduced with the following characteristics (Fig. 6-10):

Type A - the load-shortening curve of the stiffened panel adjacent to the hard corner;

Type B - the average compressive stress-strain curve for plate panel alone;

Type C - the material stress-strain relationship.

Based on these assumptions, the corresponding sagging bending moment-curvature curves for the box girder were computed: they are as shown in Fig. 6-11. In the determination of these relationships, the load-shortening curve for the stiffened panel with the Mode 3 initial imperfections was used to represent the compressive behaviour of the stiffened panels in the compression flange and the webs. The predicted maximum bending moments corresponding to these three types of corners are listed in Table 6-4.

Since both the stiffness and the maximum load-carrying capacity of the Type C corner are greater than those of the Type A corner, the peak bending moment computed for the box girder incorporating Type C is consequently greater than that for Type A. However, the difference between the two is very small (0.9%) due to the fact that the plates and the stiffeners in the compression flange and webs are very stocky ($\beta = 0.786$, $\lambda = 0.490$). Behaviour of the model incorporating the Type B corner lies between the other two as shown in Fig. 6-11 and Table 6-4.

6.2.2.3 Effects of residual stresses in tension flange: In most cases examined in the present study, behaviour of the tension elements making up the cross-section of a box girder or a hull girder were assumed to be elastic-perfectly plastic. However, a structural element in tension does not necessarily follow the elastic-perfectly plastic behaviour if the effects of weld-induced residual stresses are accounted for in the analysis.

TABLE 6-4 INITIAL IMPERFECTIONS AND COMPARISONS BETWEEN NUMERICAL AND TEST RESULTS OF STEEL BOX GIRDER MODEL 4 (DOWLING et al [1-45, 1-46])

	TYPE A	TYPE B	TYPE C
1. WELD-INDUCED RESIDUAL STRESS / YIELD STRESS	0.562	0.562	0.562
2. INITIAL PLATE DEFLECTION / PLATE WIDTH	1/800	1/800	1/800
3. INITIAL STIFFENER DEFLECTION / SPAN LENGTH	-1/510 +1/510	-1/510 +1/510	-1/510 +1/510
4. MID-SECTION PARTICULARS			
TOTAL AREA (MM^2)	29144	29144	29144
MOMENT OF INERTIA (M^2-MM^2)	4331.6	4331.6	4331.6
ELASTIC NEUTRAL AXIS ABOVE BASE LINE (MM)	468.82	468.82	468.82
FULLY PLASTIC BENDING MOMENT (KN-M)	2626.9	2626.9	2626.9
5. NUMERICAL RESULTS			
PEAK BENDING MOMENT (KN-M)	2321.6	2324.2	2343.5
NON-DIMENSIONAL	0.8838	0.8848	0.8921
6. EXPERIMENTAL RESULTS			
COLLAPSE BENDING MOMENT (KN-M)	2212.4	2212.4	2212.4
NON-DIMENSIONAL	0.8422	0.8422	0.8422

NOTE -

1. CORNER BEHAVIOUR IS REPRESENTED BY
   LOAD-SHORTENING CURVE OF STIFFENED PANEL (TYPE A)
   OR AVERAGE STRESS-STRAIN CURVE OF PLATE (TYPE B)
   OR MATERIAL STRESS-STRAIN CURVE (TYPE C)
2. EFFECTS OF RESIDUAL STRESSES IN TENSION FLANGE ARE NOT CONSIDERED

In order to study the effects of different tensile behaviour of structural elements on the bending moment-curvature relationship of a box girder, the elements in the tension flange were assumed to have one of the following types of behaviour:

Type 1 - the same as the material, i.e. the elastic-perfectly plastic behaviour;

Type 2 - the initial stiffness is reduced due to tension yielding blocks induced by welding and remains constant up to yield after which it follows the perfect plastic curve.

The bending moment-curvature relationships for box girder Model 4 with these two types of tension behaviours are as shown in Fig. 6-12, from which the peak bending moments were identified and are as listed in Table 6-5. From Fig. 6-12 it can be seen that the effect of residual stresses in the tension flange are to decrease the initial stiffness of the girder. However, it makes little difference (1.2%) as far as the maximum bending moments are concerned (Table 6-5).

6.3 *COMPARISONS WITH EXPERIMENTAL RESULTS - RECKLING*[1-47]

A series of seven fabricated steel box girders subjected to pure bending has been tested at the Technical University of Berlin by Reckling[1-47]. These girders were orthogonally stiffened in a similar way to ship's hulls. Among these box girders, Model 23 and Model 31 were chosen and analysed by the present numerical approach to be compared with the experimental results.

Tests on Model 31 showed that the collapse was delayed by the restraining effect of the side walls, the 'box girder effect' as described by Reckling, in spite of earlier buckling of deck panels.

TABLE 6-5 INITIAL IMPERFECTIONS AND COMPARISONS BETWEEN NUMERICAL AND TEST RESULTS OF STEEL BOX GIRDER MODEL 4 (DOWLING et al [1-45, 1-46])

	TYPE 1	TYPE 2
1. WELD-INDUCED RESIDUAL STRESS / YIELD STRESS	0.562	0.562
2. INITIAL PLATE DEFLECTION / PLATE WIDTH	1/800	1/800
3. INITIAL STIFFENER DEFLECTION / SPAN LENGTH	-1/510 +1/510	-1/510 +1/510
4. MID-SECTION PARTICULARS		
TOTAL AREA (MM^2)	29144	29144
MOMENT OF INERTIA (M^2-MM^2)	4331.6	4331.6
ELASTIC NEUTRAL AXIS ABOVE BASE LINE (MM)	468.82	468.82
FULLY PLASTIC BENDING MOMENT (KN-M)	2626.9	2626.9
5. NUMERICAL RESULTS		
PEAK BENDING MOMENT (KN-M)	2343.5	2316.0
NON-DIMENSIONAL	0.8921	0.8816
6. EXPERIMENTAL RESULTS		
COLLAPSE BENDING MOMENT (KN-M)	2212.4	2212.4
NON-DIMENSIONAL	0.8422	0.8422

NOTE -

1. CORNER BEHAVIOUR IS REPRESENTED BY MATERIAL STRESS-STRAIN CURVE
2. EFFECTS OF RESIDUAL STRESSES IN TENSION FLANGE ARE EXCLUDED (TYPE 1) OR INCLUDED (TYPE 2)

Model 23 had the same overall dimension as Model 31 but had more longitudinal stiffeners in the deck and side walls. As observed in tests, collapse of Model 23 occurred by buckling of the plate panels between longitudinal stiffeners in the deck coinciding with failure of the whole deck.

6.3.1 *Model 23*

Component dimensions and material properties for Model 23 are given in Table 6-6, and its cross-section was discretised into structural elements, as shown in Fig. 6-13, according to the procedures described previously. Since a single value of yield stress was given for the whole box girder in ref. [1-47], this value is assumed for both the plates and the stiffeners.

The average compressive stress-strain curves for the plate panels in the deck and side walls of Model 23 were derived using the simplified method described in Chapter 2 and are shown in Fig. 6-14. Using these curves in the large deflection elasto-plastic analysis of stiffened panels, the load-shortening curves were computed for the isolated stiffened panels taken from the deck and the side walls and are as shown in Fig. 6-15. Welding residual stresses and initial imperfections used in the derivation of the load-shortening curves are listed in Table 6-7. The stiffened panels in tension were assumed to follow the material stress-strain curve, as were the hard corners in both tension and compression.

These effective stress-strain curves of the structural elements were then used in the computer program HULLG to generate the bending moment-curvature curves for the box girder under the following conditions:

TABLE 6-6 COMPONENT DIMENSIONS AND MATERIAL PROPERTIES OF STEEL BOX GIRDER MODEL 23 AND MODEL 31 (RECKLING)

	MODEL 23	MODEL 31
1. COMPRESSION FLANGE PLATE		
STIFFENER SPACING	85.71	120.00
THICKNESS	2.50	2.50
2. TENSION FLANGE PLATE		
STIFFENER SPACING	85.71	120.00
THICKNESS	2.50	2.50
3. WEB PLATE		
STIFFENER SPACING	100.00	133.33
THICKNESS	2.50	2.50
4. STIFFENER (ANGLE)		
TOTAL DEPTH	30.00	30.00
TABLE WIDTH	20.00	20.00
THICKNESS	2.50	2.50
5. STIFFENER (FLAT)		
DEPTH	30.00	30.00
THICKNESS	2.50	2.50
6. YIELD STRESS	246.0	255.0
YOUNG'S MODULUS	210,000	210,000

UNITS - LENGTH IN MM
STRESS IN N /MM^2

TABLE 6-7 INITIAL IMPERFECTIONS AND COMPARISONS BETWEEN NUMERICAL AND TEST RESULTS OF BOX GIRDER MODEL 23 (RECKLING)

1. WELD-INDUCED RESIDUAL STRESS / YIELD STRESS	= 0.20
2. INITIAL PLATE DEFLECTION / PLATE THICKNESS	= 0.25
3. INITIAL STIFFENER DEFLECTION / SPAN LENGTH	= +1/1000 = -1/1000
4. MID-SECTION PARTICULARS	
TOTAL AREA (MM)	= 6875.0
MOMENT OF INERTIA (M -MM)	= 197.44
ELASTIC NEUTRAL AXIS ABOVE BASE LINE (MM)	= 200.00
FULLY PLASTIC BENDING MOMENT (KN-M)	= 268.20
5. EXPERIMENTAL RESULTS	
COLLAPSE BENDING MOMENT (KN-M)	= 249.37
NON-DIMENSIONAL	= 0.9298

6. NUMERICAL RESULTS	CASE 1	CASE 2	CASE 5	CASE 6
NUMBER OF STIFFENED PANELS INCLUDED IN HARD CORNER	1	2	1	2
RESIDUAL STRESSES ARE INCLUDED IN TENSION FLANGE	NO	NO	YES	YES
PEAK BENDING MOMENT (KN-M)	237.85	239.93	232.80	234.61
NON-DIMENSIONAL	0.8868	0.8946	0.8680	0.8747

1. the plate panels in the deck neighbouring the deck-side wall intersections were treated as hard corners;

2. the plate panels in the side walls adjacent to the deck-side wall intersections were treated as hard corners in addition to the requirements of condition 1.

The derived bending moment-curvature relationships are shown in Fig. 6-16 together with the following curves:

3. Numerically computed fully effective response, i.e. all the structural elements follow the material stress-strain relationship to give M_p at infinite curvature;

4. Experimentally obtained (by Reckling).

The predicted peak bending moments, fully palstic bending moment and test collapse bending moment are listed in Table 6-7. It can be seen in this table that correlation between the numerical and experimental results is satisfactory as far as the maximum bending moments are concerned. The difference in the maximum values is 4.6% between the Case 1 and test results, and 3.8% between the Case 2 and test results.

Although both predicted peak bending moments agree quite well with the test result, the computed bending moment-curvature curves stray from the experimental curve (Fig. 6-16) over the loading range. That is, the predicted initial stiffness of the box girder differs significantly from the measured stiffness. Since including welding residual stresses in the tension flange usually leads to a decrease in the initial stiffness of a box girder, two other conditions were examined, viz.

5. the same as Case 1 except that residual stresses in structural elements in tension were considered; and

6. the same as Case 2 except that residual stresses in structural elements in tension were considered.

The bending moment-curvature curves derived for the box girder under these conditions are compared with the experimental results in Fig. 6-17, while the peak predicted bending moments are listed in Table 6-7. The difference in maximum bending moment between the numerical and experimental results is 6.6% for Case 5 and 5.9% for Case 6, slightly greater than those for Cases 1 and 2, but the predicted initial stiffness in Cases 5 and 6 correlate significantly better with the experimental results.

In Fig. 6-18, the bending moment-curvature curve for Case 2 is compared with that for Case 6. This tends to confirm the result reported in the previous section that the effect of residual stresses on structural elements in tension is mainly to decrease the initial stiffness of a box girder but to have little influence on its maximum value.

6.3.2 *Model 31*

Component dimensions and material properties for Model 31 are given in Table 6-6 together with those of Model 23. The cross-section of Model 31 was discretised into structural elements as shown in Fig. 6-19.

The stiffened panel load-shortening curves were computed using the present Dynamic Relaxation approach for the deck and side walls having the residual stresses and intial imperfections listed in Table 6-8 for Case 2: they are shown in Fig. 6-20. These curves were then

input to the computer program HULLG to perform the ultimate strength analysis of the girder cross-section in which hard corners are assumed to follow the material stress-strain relationship. The derived bending moment-curvature relationship is compared with the experimental result in Fig. 6-21 while the peak values are compared in Table 6-8. The agreement is seen to be satisfactory with a 6.0% difference existing between the predicted and observed ultimate bending moments.

6.3.2.1 Effects of initial stiffener deflections: Model 31 was also used to analyse the effects of initial stiffener deflections, weld-induced residual stress and initial plate deformation on the collapse behaviour of a box girder. First the effects of initial stiffener deflection are considered. For this, in addition to Case 2 ($\Delta/L = 1/1000$, $\delta_o/t = 0.55$, $\sigma'_r = 0.20$), ultimate strength analyses are performed on the box girder for the following cases:

Case 1 - $\Delta/L = 1/2000$, $\delta_o/t = 0.55$, $\sigma'_r = 0.20$;

Case 3 - $\Delta/L = 1/500$, $\delta_o/t = 0.55$, $\sigma'_r = 0.20$.

It can be seen that these two cases correspond to changes in the initial stiffener deflections while the remaining parameters are kept constant.

The load-shortening curves for these cases are shown in Figs 6-22 and 6-23. The load-shortening curves for the deck stiffened panels with different levels of initial stiffener deflection are shown together in Fig. 6-24, and those for the side wall stiffened panels are presented in Fig. 6-25. The web stiffened panels are seen to be more sensitive to initial stiffener distortion than the flange panels.

The resulting curves for the cross-section are shown in Fig. 6-26 while the maximum bending moments are listed in Table 6-8 and are

TABLE 6-8 INITIAL IMPERFECTIONS AND COMPARISONS BETWEEN NUMERICAL AND TEST RESULTS OF BOX GIRDER MODEL 31 (RECKLING)

1. WELD-INDUCED RESIDUAL STRESS / YIELD STRESS = 0.20			
2. INITIAL PLATE DEFLECTION / PLATE THICKNESS = 0.55			
3. MID-SECTION PARTICULARS TOTAL AREA (MM^2) = 6250.0 MOMENT OF INERTIA (M^2-MM^2) = 180.35 ELASTIC NEUTRAL AXIS ABOVE BASE LINE (MM) = 200.00 FULLY PLASTIC BENDING MOMENT (KN-M) = 253.65			
4. EXPERIMENTAL RESULTS COLLAPSE BENDING MOMENT (KN-M) = 215.88 NON-DIMENSIONAL = 0.8511			
5. NUMERICAL RESULTS	CASE 1	CASE 2	CASE 3
INITIAL STIFFENER DEFLECTION / SPAN LENGTH	+1/2000 -1/2000	+1/1000 -1/1000	+1/ 500 -1/ 500
PEAK BENDING MOMENT (KN-M)	204.32	202.96	199.74
NON-DIMENSIONAL	0.8055	0.8002	0.7875

plotted in Fig. 6-27. Not unexpectedly, the ultimate strength of Model 31 is seen to decrease with increasing initial stiffener deflection magnitude, the decrease however, as the initial stiffener deflection varies from $\Delta/L = 1/2000$ to $\Delta/L = 1/500$ is only 2.2%.

6.3.2.2 Effects of residual stresses: Second, the influence of weld-induced residual stresses was examined by analysing the following cases:

Case 4 - $\Delta/L = 1/1000$, $\delta_o/t = 0.55$, $\sigma_r' = 0.05$;

Case 5 - $\Delta/L = 1/1000$, $\delta_o/t = 0.55$, $\sigma_r' = 0.35$;

and comparing the results with those of Case 2.

The load-shortening curves obtained for the stiffened panels in Cases 4 and 5 are shown in Figs 6-28 and 6-29 respectively. The curves in Figs 6-20, 6-28 and 6-29 are then re-presented in Fig. 6-30 to highlight the effect of residual stresses on the response of the deck stiffened panel and similarly in Fig. 6-31 for the side wall stiffened panel. The effect on stiffness and strength is here seen to be significant. The corresponding curves from program HULLG are shown in Fig. 6-32 while the predicted peak bending moments are listed in Table 6-9 and plotted in Fig. 6-33. From these results it can be seen that an increase in residual stresses from $\sigma_r' = 0.05$ to $\sigma_r' = 0.20$ results in a 1.4% increase in peak bending moment. This can probably be attributed to the fact that the post-buckling strengths of stiffened panels with $\sigma_r' = 0.20$ are greater than those of stiffened panels with $\sigma_r' = 0.05$, as demonstrated in Figs 6-30 and 6-31, although the ultimate strengths of the former are lower than those of the latter. A further increase in residual stresses from $\sigma_r' = 0.20$ to $\sigma_r' = 0.35$ makes practically no difference to the load-carrying capacity of the box girder.

TABLE 6-9 INITIAL IMPERFECTIONS AND COMPARISONS BETWEEN NUMERICAL AND TEST RESULTS OF BOX GIRDER MODEL 31 (RECKLING)

1. INITIAL PLATE DEFLECTION / PLATE THICKNESS	= 0.55
2. INITIAL STIFFENER DEFLECTION / SPAN LENGTH	= +1/1000 = -1/1000
3. MID-SECTION PARTICULARS	
TOTAL AREA (MM^2)	= 6250.0
MOMENT OF INERTIA (M^2-MM^2)	= 180.35
ELASTIC NEUTRAL AXIS ABOVE BASE LINE (MM)	= 200.00
FULLY PLASTIC BENDING MOMENT (KN-M)	= 253.65
4. EXPERIMENTAL RESULTS	
COLLAPSE BENDING MOMENT (KN-M)	= 215.88
NON-DIMENSIONAL	= 0.8511

5. NUMERICAL RESULTS	CASE 4	CASE 2	CASE 5
WELD-INDUCED RESIDUAL STRESS / YIELD STRESS	0.05	0.20	0.35
PEAK BENDING MOMENT (KN-M)	200.09	202.96	203.02
NON-DIMENSIONAL	0.7889	0.8002	0.8004

6.3.2.3 Effects of initial plate deflections: Finally, Model 31 was analysed for the following cases:

Case 6 - $\Delta/L = 1/1000$, $\delta_o/t = 0.22$, $\sigma'_r = 0.20$;

Case 7 - $\Delta/L = 1/1000$, $\delta_o/t = 0.88$, $\sigma'_r = 0.20$;

to illustrate the effect of initial plate deflections.

The stiffened panel load-shortening curves corresponding to Cases 6 and 7 are shown in Figs 6-34 and 6-35. These curves and those of Case 2 are rearranged in Figs 6-36 and 6-37 to demonstrate the effect of initial plate distortions on the response of the deck and the side wall stiffened panels respectively. The corresponding bending moment-curvature curves as derived by the present analysis are shown in Fig. 6-38. The maximum predicted bending moments are set out in Table 6-10 and plotted in Fig. 6-39 from which it is clearly seen that the ultimate strength of the box girder decreases with increases in the initial plate deflection magnitude. In particular, when the initial plate deflection varies from $\delta_o/t = 0.22$ to $\delta_o/t = 0.88$, the computed maximum bending moment drops by 2.7%.

Of all the cases examined above, Case 6 corresponds most closely to the tested girder, i.e. the present procedure underestimates the experimental result by 4.6%.

TABLE 6-10 INITIAL IMPERFECTIONS AND COMPARISONS BETWEEN NUMERICAL AND TEST RESULTS OF BOX GIRDER MODEL 31 (RECKLING)

1. WELD-INDUCED RESIDUAL STRESS / YIELD STRESS = 0.20			
2. INITIAL STIFFENER DEFLECTION / SPAN LENGTH = +1/1000 = -1/1000			
3. MID-SECTION PARTICULARS TOTAL AREA (MM^2) = 6250.0 MOMENT OF INERTIA (M^2-MM^2) = 180.35 ELASTIC NEUTRAL AXIS ABOVE BASE LINE (MM) = 200.00 FULLY PLASTIC BENDING MOMENT (KN-M) = 253.65			
4. EXPERIMENTAL RESULTS COLLAPSE BENDING MOMENT (KN-M) = 215.88 NON-DIMENSIONAL = 0.8511			
5. NUMERICAL RESULTS	CASE 6	CASE 2	CASE 7
INITIAL PLATE DEFLECTION / PLATE THICKNESS	0.22	0.55	0.88
PEAK BENDING MOMENT (KN-M)	205.85	202.96	200.33
NON-DIMENSIONAL	0.8116	0.8002	0.7898

6.4 COMPARISONS WITH ADAMCHAK'S NUMERICAL RESULTS

A computer program ULTSTR was developed at DTNSRDC[1-39] to estimate the ductile longitudinal strength of conventional ship hulls. Based on a variety of empirical solutions for components of plated structures, the bending moment-curvature relationship was determined incrementally for the hull girder. The collapse bending moment can readily be identified from this relationship. The ductile failure modes considered in ULTSTR included yielding, interframe flexural buckling and tripping instability. Two illustrative examples incorporating various degrees of complexity were reported in ref. [1-39] in relation to HULL A and HULL B. Ultimate strength analyses were carried out on these hull girders using the present method for comparison with Adamchak's results.

6.4.1 HULL A

The midship cross-section of HULL A was discretised into structural elements as shown in Fig. 6-40. The hard corners were assumed, as usual, to follow the elastic-perfectly plastic behaviour in both tension and compression. Seven typical stiffened panels were chosen from the cross-section to be analysed by the Dynamic Relaxation approach with the residual stress and initial imperfections listed in Table 6-11. The derived load-shortening curves for the stiffened panels are shown in Figs 6-41 and 6-42. Using these curves in the ultimate strength analysis of the hull girder, the sagging and hogging bending moment-curvature relationships were generated and are compared with Adamchak's numerical results in Fig. 6-43. The calculated mid-section particulars, first yield bending moments and ultimate bending moments in the sagging and hogging conditions are listed in Table 6-12.

TABLE 6-11 INITIAL IMPERFECTIONS AND WELD-INDUCED RESIDUAL STRESS USED IN HULL STRENGTH ASSESSMENTS

1. WELD-INDUCED RESIDUAL STRESS / YIELD STRESS	= 0.20
2. INITIAL PLATE DEFLECTION / PLATE THICKNESS	= $0.15 * \beta^2$
3. INITIAL STIFFENER DEFLECTION / SPAN	= +1/1000 , -1/1000

TABLE 6-12 COMPARISONS OF THE STRENGTH OF "HULL A" BY ADAMCHAK'S AND THE PRESENT METHOD

1. METHOD	ADAMCHAK	PRESENT	RATIO
2. FRAME SPACING (IN)	96.0	96.0	-
3. TOTAL SECTIONAL AREA (IN^2)	978.62	978.62	1.0000
4. ELASTIC NEUTRAL AXIS ABOVE BASE LINE (IN)	163.43	163.61	0.9989
5. MOMENT OF INERTIA ABOUT ELASTIC N.A. (FT^2-IN^2)	119062	118297	1.0065
6. YIELD STRESS OF THE MATERIAL (PSI)	45000.0	45000.0	-
7. PLASTIC NEUTRAL AXIS ABOVE BASE LINE (IN)	-	172.53	-
8. FULLY PLASTIC BENDING MOMENT (TONF-FT)	-	205150	-
9. SAGGING CONDITION			
FIRST YIELD BENDING MOMENT (TONF-FT)	-	188146	-
SHAPE FACTOR	-	1.090	-
COMPUTED ULTIMATE BENDING MOMENT (TONF-FT)	126964	139594	0.9095
M_U / M_P	-	0.680	-
10. HOGGING CONDITION			
FIRST YIELD BENDING MOMENT (TONF-FT)	-	174167	-
SHAPE FACTOR	-	1.178	-
COMPUTED ULTIMATE BENDING MOMENT (TONF-FT)	122321	138372	0.8840
M_U / M_P	-	0.674	-

The cross-sectional area, location of the elastic neutral axis and moment of inertia of the cross-section computed by the present method are almost the same as those obtained by Adamchak. However, differences in the ultimate bending moments predicted by the two methods are 9% in the sagging condition and 12% in the hogging condition. As reported in ref. [1-39], the collapse of HULL A was precipitated by tripping instability in both the sagging and hogging conditions. Since tripping instability is not considered as a possible failure mode in the present method, it is thought that the significant differences in ultimate bending moments are in part attributable to this factor.

6.4.2 HULL B

The midship cross-section of HULL B was discretised into structural elements including hard corners and stiffened panels as shown in Fig. 6-44. Eight typical stiffened panels were taken from the cross-section and were analysed by the present method with the residual stresses and initial imperfections specified in Table 6-11. The generated load-shortening curves for these panels are shown in Figs 6-45 and 6-46 and were used in the ultimate strength analysis of the hull girder. The derived sagging and hogging bending moment-curvature relationships are compared with Adamchak's results in Fig. 6-47, while the mid-section particulars, first yield bending moments and ultimate bending moments are compared in Table 6-13. The cross-sectional area, location of the elastic neutral axis and moment of inertia of the cross-section computed by the present method agree very satisfactorily with Adamchak's results. However, significant differences in ultimate bending moments (25% for the sagging condition and 29% for the hogging condition) are observed between the results obtained by the two methods. This can be attributed to the same reason as that for HULL A.

TABLE 6-13 COMPARISONS OF THE STRENGTH OF "HULL B" BY ADAMCHAK'S AND THE PRESENT METHOD

1. METHOD	ADAMCHAK	PRESENT	RATIO
2. FRAME SPACING (IN)	96.0	96.0	-
3. TOTAL SECTIONAL AREA (IN^2)	1604.48	1604.48	1.0000
4. ELASTIC NEUTRAL AXIS ABOVE BASE LINE (IN)	174.52	174.51	1.0001
5. MOMENT OF INERTIA ABOUT ELASTIC N.A. (FT^2-IN^2)	225028	224535	1.0022
6. YIELD STRESS (PSI)			
SHELL	80000.0	80000.0	-
INNER BOTTOM	45000.0	45000.0	-
INNER DECKS	33000.0	33000.0	-
KEEL PLATE	11000.0	11000.0	-
7. PLASTIC NEUTRAL AXIS ABOVE BASE LINE (IN)	-	165.15	-
8. FULLY PLASTIC BENDING MOMENT (TONF-FT)	-	563301	-
9. SAGGING CONDITION			
FIRST YIELD BENDING MOMENT (TONF-FT)	-	494152	-
SHAPE FACTOR	-	1.140	-
COMPUTED ULTIMATE BENDING MOMENT (TONF-FT)	199189	267162	0.7456
M_U / M_P	-	0.474	-
10. HOGGING CONDITION			
FIRST YIELD BENDING MOMENT (TONF-FT)	-	550426	-
SHAPE FACTOR	-	1.023	-
COMPUTED ULTIMATE BENDING MOMENT (TONF-FT)	322121	456629	0.7054
M_U / M_P	-	0.811	-

6.5 COMPARISONS WITH SMITH's NUMERICAL RESULTS

The Torpedo-Boat Destroyer *COBRA* collapsed by breaking her back and sank in rough seas on her first journey in 1901. The disaster was re-examined in the light of 1980's technology[1-37], leading to the conclusion that since *COBRA's* hull was transversely framed and was structurally too weak even to withstand the moderate sea conditions, the *COBRA* may have been lost due to buckling not being properly considered in her design. Hull strength assessments were made of T.B.D. *COBRA* and a similarly constructed vessel T.B.D. *WOLF* in ref. [1-37] in the sagging and hogging conditions using the analysis procedures reported in ref. [1-36]. The results are compared below with those obtained by the present incremental moment-curvature approach.

6.5.1 T.B.D. COBRA

The midship cross-section of *COBRA* was obtained from ref. [1-37] and was discretised into structural elements as shown in Fig. 6-48, the label number against each plate element representing the corresponding average stress-strain curve shown in Fig. 6-49. These effective stress-strain curves for wide plates under compressive load were also taken from ref. [1-37]. The ultimate strength of *COBRA's* hull was then evaluated using the computer program HULLG.

Results in the form of bending moment-curvature curves are shown in Fig. 6-50 for the sagging and hogging conditions. The computed mid-section particulars, fully plastic moment, first yield bending moments and maximum bending moments are listed in Table 6-14, together with the results from ref. [1-37]. As might be expected, the agreement is very satisfactory as far as maximum bending moments are concerned (1.3% difference for the sagging condition and 2.0% difference for the hogging condition).

TABLE 6-14 COMPARISONS BETWEEN ULTIMATE STRENGTH OF TRANSVERSELY FRAMED T.B.D. "COBRA" BY SMITH'S AND THE PRESENT METHOD

1. METHOD	SMITH	PRESENT	RATIO
2. TOTAL SECTIONAL AREA (M^2)	-	0.1106	-
3. ELASTIC NEUTRAL AXIS ABOVE BASE LINE (M)	-	2.091	-
4. YIELD STRESS OF THE MATERIAL (N/MM^2)	-	247	-
5. PLASTIC NEUTRAL AXIS ABOVE BASE LINE (M)	-	1.549	-
6. FULLY PLASTIC BENDING MOMENT (MN-M)	-	40.90	-
7. SAGGING CONDITION			
FIRST YIELD BENDING MOMENT (MN-M)	-	33.25	-
SHAPE FACTOR	-	1.230	-
COMPUTED ULTIMATE BENDING MOMENT (MN-M)	16.70	16.49	1.013
M_U / M_P	-	0.403	-
8. HOGGING CONDITION			
FIRST YIELD BENDING MOMENT (MN-M)	-	35.30	-
SHAPE FACTOR	-	1.159	-
COMPUTED ULTIMATE BENDING MOMENT (MN-M)	21.40	20.98	1.020
M_U / M_P	-	0.484	-

6.5.2 T.B.D. WOLF

The midship cross-section of *WOLF* obtained from ref. [1-37] was subdivided into structural elements as shown in Fig. 6-51. Ultimate strength analyses were then performed on the hull girder using the curves in Fig. 6-49 as the effective stress-strain relationships for the structural elements. The derived bending moment-curvature curves are shown in Fig. 6-52. Results of mid-section particulars, fully plastic moment, first yield bending moments and maximum bending moments are compared with those of ref. [1-37] in Table 6-15. The difference obtained by the two methods is 3.6% in maximum sagging bending moment and 1.0% in maximum hogging bending moment. Again the similarity of the results is to be expected.

6.5.3 Effects of Framing Systems

In view of the general structural weakness inherent in transversely framed ships, *COBRA's* hull was converted into a longitudinally stiffened girder using three different arrangements as follows:

Type 1 - frame space is 533.4 mm, 4 stiffeners are attached to the deck plating and 6 stiffeners to the bottom plating.

Type 2 - frame space is 1600.2 mm, 6 stiffeners are attached to the deck plating and 18 stiffeners to the bottom plating.

Type 3 - frame space is 1600.2 mm, the numbers of stiffeners attached to the deck, shell and bottom plating are 6, 20 and 18 respectively.

TABLE 6-15 COMPARISONS BETWEEN ULTIMATE STRENGTH OF TRANSVERSELY FRAMED T.B.D. "WOLF" BY SMITH'S AND THE PRESENT METHOD

1. METHOD	SMITH	PRESENT	RATIO
2. TOTAL SECTIONAL AREA (M^2)	-	0.1054	-
3. ELASTIC NEUTRAL AXIS ABOVE BASE LINE (M)	-	2.159	-
4. YIELD STRESS OF THE MATERIAL (N/MM^2)	-	247	-
5. PLASTIC NEUTRAL AXIS ABOVE BASE LINE (M)	-	1.887	-
6. FULLY PLASTIC BENDING MOMENT (MN-M)	-	37.93	-
7. SAGGING CONDITION			
FIRST YIELD BENDING MOMENT (MN-M)	-	30.82	-
SHAPE FACTOR	-	1.231	-
COMPUTED ULTIMATE BENDING MOMENT (MN-M)	18.00	17.38	1.036
M_U / M_P	-	0.458	-
8. HOGGING CONDITION			
FIRST YIELD BENDING MOMENT (MN-M)	-	29.89	-
SHAPE FACTOR	-	1.269	-
COMPUTED ULTIMATE BENDING MOMENT (MN-M)	15.80	15.96	0.990
M_U / M_P	-	0.421	-

The midship cross-sections of the hulls were subdivided into structural elements as shown in Figs 6-53, 6-56 and 6-59 for Type 1, Type 2 and Type 3 hulls respectively. Before evaluating the ultimate strengths of the hulls, it is necessary to obtain the load-shortening curves for the stiffened panels forming their cross-sections. Typical stiffened panels chosen from the cross-sections were analysed by the Dynamic Relaxation approach, and the generated load-shortening curves are plotted in Figs 6-54, 6-57 and 6-60 for the stiffened panels of Type 1, Type 2 and Type 3 hulls respectively. Incorporating these curves into ultimate hull strength assessments, bending moment-curvature curves were derived as shown in Figs 6-55, 6-58 and 6-61 for the Type 1, Type 2 and Type 3 hulls. The moment-curvature relationship for the original transversely framed hull is shown in each of these figures for comparison. Results of mid-section particulars, first yield bending moments, fully plastic moments and maximum bending moments of the hulls are summarised in Table 6-16.

Comparisons between the results for the Type 1 hull and the original one show that attaching 10 longitudinal stiffeners to a transversely framed hull with frame spacing unchanged results in increases in its ultimate strength of 29.6% in the sagging condition and 21.7% in the hogging condition. For the Type 2 hull, the frame space is enlarged three times but 24 stiffeners are now attached to the plating. This conversion leads to a 33.3% increase in the sagging ultimate strength and a 51.7% increase in the hogging ultimate strength. The Type 3 hull has the same frame space as the Type 2 hull, but has 44 stiffeners. The increases in maximum bending moments in these cases are 65.2% and 65.1% under the sagging and hogging conditions respectively. From the above comparisons, the efficiency of longitudinally framed hulls is clearly demonstrated.

TABLE 6-16 *COMPARISONS BETWEEN THE STRENGTH OF TRANSVERSELY AND LONGITUDINALLY FRAMED HULL GIRDERS OF T.B.D. "COBRA"*

1. TYPE OF FRAMING	TRANS. ORIGINAL	LONGL. TYPE 1	LONGL. TYPE 2	LONGL. TYPE 3
2. FRAME SPACING (M)	0.5334	0.5334	1.6002	1.6002
3. NUMBER OF STIFFENERS	-	10	24	44
4. TOTAL SECTIONAL AREA (M^2)	0.1106	0.1153	0.1172	0.1266
5. ELASTIC NEUTRAL AXIS ABOVE BASE LINE (M)	2.091	2.082	1.989	2.010
6. YIELD STRESS OF THE MATERIAL (N/MM^2)	247	247	247	247
7. PLASTIC NEUTRAL AXIS ABOVE BASE LINE (M)	1.549	1.517	1.293	1.468
8. FULLY PLASTIC BENDING MOMENT (MN-M)	40.90	42.97	43.60	46.11
9. SAGGING CONDITION				
FIRST YIELD BENDING MOMENT (MN-M)	33.25	34.99	35.05	36.27
SHAPE FACTOR	1.230	1.228	1.244	1.271
COMPUTED ULTIMATE BENDING MOMENT (MN-M)	16.49	21.37	21.98	27.24
M_U / M_P	0.403	0.497	0.504	0.591
10. HOGGING CONDITION				
FIRST YIELD BENDING MOMENT (MN-M)	35.30	37.49	40.97	41.55
SHAPE FACTOR	1.159	1.146	1.064	1.110
COMPUTED ULTIMATE BENDING MOMENT (MN-M)	20.98	25.53	31.82	34.63
M_U / M_P	0.513	0.594	0.730	0.751

6.6 HULL STRENGTH ASSESSMENTS ON FRIGATES

Ultimate strength analyses of the longitudinally framed hulls of five frigates, *TYPE 14*, *WHITBY*, *ROTHESAY*, *TYPE 81* and *LEANDER* classes, were carried out by the present method. The midship cross-section particulars and material properties of the hull girders are summarised in Table 6-17 for *TYPE 14*, *WHITBY* and *ROTHESAY* classes, and in Table 6-18 for the other two classes. According to the procedures described previously, the midship cross-sections were subdivided into structural elements including stiffened panels, plate elements and hard corners as shown in Figs 6-62 (*TYPE 14* class), 6-65 (*WHITBY* class), 6-69 (*ROTHESAY* class), 6-73 (*TYPE 81* class) and 6-78 (*LEANDER* class). Members such as keel plates, bilge keels, deep girders and the deck stringer-sheer strake junctions, in which buckling is suppressed by the rigid inter-connected structures, were treated as hard corners. The number labelled against each stiffened panel in the aforementioned figures corresponds to a particular load-shortening curve contained in Fig. 6-63 for the *TYPE 14* class, in Figs 6-66 and 6-67 for the *WHITBY* class, in Figs 6-70 and 6-71 for the *ROTHESAY* class, in Figs 6-74, 6-75 and 6-76 for the *TYPE 81* class, or in Figs 6-79 and 6-80 for the *LEANDER* class frigate. These curves were generated separately by using the computer program DSTPL for the elasto-plastic analysis of the double-span stiffened panels with weld-induced stresses and initial imperfections as listed in Table 6-11.

Results in the form of bending moment-curvature relationships are presented in Figs 6-64, 6-68, 6-72, 6-77 and 6-81 for the five frigates both in the sagging and hogging conditions. The computed first yield bending moments, shape factors, fully plastic moments and peak bending moments are set out in Table 6-17 for the *TYPE 14*,

WHITBY and *ROTHESAY* classes, and in Table 6-18 for the *TYPE 81* and *LEANDER* classes. From these tables, it can be seen that the shape factors for the frigates concerned range from 1.20 to 1.41 in the sagging condition, and from 1.16 to 1.23 in the hogging condition. Furthermore, the ratios of maximum bending moments to fully plastic moments of the hulls varies from 0.51 to 0.69 in the sagging condition, and from 0.75 to 0.87 in the hogging condition. That is, the strengths of the hulls as required to resist sagging loads are significantly smaller than those to resist hogging loads.

TABLE 6-17 LIST OF THE STRENGTH OF LONGITUDINALLY FRAMED HULL GIRDERS "TYPE 14", "WHITBY" AND "ROTHESAY" CLASS FRIGATES

1. CLASS	TYPE 14	WHITBY	ROTHESAY
2. FRAME SPACING (M)	1.3716	1.3716	1.3716
3. TOTAL SECTIONAL AREA (M^2)	0.2949	0.4329	0.4704
4. ELASTIC NEUTRAL AXIS ABOVE BASE LINE (M)	2.933	4.246	4.194
5. YIELD STRESS OF THE MATERIAL (N/MM^2)	314.6	314.6	314.6
6. PLASTIC NEUTRAL AXIS ABOVE BASE LINE (M)	2.199	4.078	3.963
7. FULLY PLASTIC BENDING MOMENT (MN-M)	205.3	425.2	464.4
8. SAGGING CONDITION			
FIRST YIELD BENDING MOMENT (MN-M)	171.4	338.7	368.5
SHAPE FACTOR	1.198	1.255	1.260
COMPUTED ULTIMATE BENDING MOMENT (MN-M)	141.4	218.7	243.2
M_U / M_P	0.689	0.514	0.524
9. HOGGING CONDITION			
FIRST YIELD BENDING MOMENT (MN-M)	177.4	361.4	396.6
SHAPE FACTOR	1.157	1.177	1.171
COMPUTED ULTIMATE BENDING MOMENT (MN-M)	169.3	366.8	403.9
M_U / M_P	0.825	0.863	0.870

TABLE 6-18 LIST OF THE STRENGTH OF LONGITUDINALLY FRAMED HULL GIRDERS "TYPE 81" AND "LEANDER" CLASS FRIGATES

1. CLASS	TYPE 81	LEANDER
2. FRAME SPACING (M)	1.9812	1.3716
3. TOTAL SECTIONAL AREA (M^2)	0.6471	0.5790
4. ELASTIC NEUTRAL AXIS ABOVE BASE LINE (M)	4.735	5.242
5. YIELD STRESS OF THE MATERIAL (N/MM^2)	255.2	339.9
6. PLASTIC NEUTRAL AXIS ABOVE BASE LINE (M)	5.333	6.259
7. FULLY PLASTIC BENDING MOMENT (MN-M)	541.8	688.9
8. SAGGING CONDITION		
FIRST YIELD BENDING MOMENT (MN-M)	385.1	504.9
SHAPE FACTOR	1.407	1.364
COMPUTED ULTIMATE BENDING MOMENT (MN-M)	308.3	425.1
M_U / M_P	0.569	0.617
9. HOGGING CONDITION		
FIRST YIELD BENDING MOMENT (MN-M)	469.1	561.1
SHAPE FACTOR	1.155	1.228
COMPUTED ULTIMATE BENDING MOMENT (MN-M)	406.4	576.2
M_U / M_P	0.750	0.836

Chapter 7

SIMPLIFIED SHIP BENDING DESIGN MODEL

7.1 INTRODUCTION

The conventional approach to the longitudinal strength calculation of a ship has been based on the linear bending theory. Since this makes no distinction between the tension and compression flanges of the hull girder, it is valid only when the compression flange is adequately stiffened to resist buckling. To allow for buckling effects, attempts have been made to modify the elementary beam theory for improving the prediction technique. As ultimate strength theory can properly determine the true longitudinal hull strength, the philosophy of utilising hull strength in ship structural design has become a topic of great interest in the ship research and design community.

As demonstrated in Chapter 5, the present method, which is similar to the ultimate strength analysis approach developed by Smith[1-34,1-35,1-36,1-37], is capable of accurately predicting the ultimate longitudinal strength of a ship's hull girder. However, it is impractical to perform such an ultimate strength analysis on a ship, particularly at the stage of preliminary design. From the point of view of design, a simple expression for the ultimate moment capacity seems more helpful in assessing the real margin of safety between the load-carrying capacity of the hull girder as a beam and the maximum bending moment acting on the ship.

This chapter is therefore devoted to the derivation of formulae for predicting the ultimate bending moment capacity of a ship's hull girder. In section 7.2, existing ultimate strength approaches are briefly discussed. In section 7.3, simple expressions for the ultimate moment capacity are obtained from the data relating to the maximum load-carrying capacity of stiffened panels (Chapter 4) and the ultimate bending moment strength of hull girders (Chapter 6) by using the least-squares method. A design prediction procedure is then suggested and the strength formulae compared with the numerical results.

7.2 EXISTING STRENGTH FORMULAE

7.2.1 Excluding Buckling

7.2.1.1 First yield moment: It has been proposed[7-1] that, once the yield stress is exceeded in either flange, the resulting excessive strain will overload the adjacent structure and hence trigger ultimate failure of the hull girder. Based on this limiting condition and the linear bending stress distribution, the utlimate bending moment M_u is given by:

$$M_u = M_Y = Z\,\sigma_Y = \frac{M_p}{S_F} \qquad \ldots \quad (7.1)$$

where Z is the section modulus and S_F the shape factor: the other terms are as defined previously. For the purposes of deriving explicit expressions for the ultimate moment capacity, it is convenient to represent the midship cross-section by an equivalent lumped area form as shown in Fig. 7-1. Assuming the linear stress distribution with a maximum value of σ_Y in the deck for this simple box girder, M_u is expressed by the following equation[7-1]:

$$M_u = M_Y = \sigma_Y\, AD \left[\alpha_D\gamma + 2\alpha_S\left(\frac{1}{3\gamma} - 1 + \gamma\right) + \alpha_B\left(\frac{1}{\gamma} - 2 + \gamma\right)\right]$$

$$\ldots \quad (7.2)$$

where $\gamma = g/D$, $\alpha_D = A_D/A$, $\alpha_S = A_S/A$ and $\alpha_B = A_B/A$. Here, g is the distance of the elastic neutral axis below the deck, D the ship depth, A the total cross-sectional area, and A_D, A_S and A_B are the cross-sectional areas of the deck, one side-shell and the bottom respectively.

7.2.1.2 Fully plastic moment: Following the method of classical plasticity, a fully plastic condition is reached when yield stress has developed at every point throughout the depth of a ship's hull girder[1-2] Using the lumped area approach (Fig. 7-1), the ultimate bending moment corresponding to this limiting condition, i.e. fully plastic moment is given by ref. [1-2]:

$$M_u = M_p = \sigma_Y AD \left[\alpha_D\gamma + 2\alpha_S \left(\frac{1}{2} - \gamma + \gamma^2\right) + \alpha_B (1-\gamma)\right] \quad \ldots \quad (7.3)$$

As has been shown in Chapters 5 and 6, this moment represents an upper limit of a girder's longitudinal strength, but is rarely obtained due to the adverse effects of buckling and initial imperfections.

7.2.2 *Including Buckling*

7.2.2.1 Vasta and ISSC: In discussing the experimental results relating to full-scale ship structural tests, Vasta[1-3] suggested that the limiting bending moment for a longitudinally framed hull can be approximated by the product of its elastic section modulus and its critical panel strength. That is, the ultimate bending moment can be taken as:

$$M_u = Z\sigma_u = (Z\sigma_Y)\left(\frac{\sigma_u}{\sigma_Y}\right) = M_Y \phi$$

$$= M_p \frac{\phi}{S_F} \quad \ldots \quad (7.4)$$

where σ_u is the panel ultimate strength. Although the use of this simple expression was supported by the ISSC[1-31], it has been criticised as being pessimistic in regard to predicting ultimate strength[7-2] by ignoring plastic hinge capacity, and as being

optimistic in girder stiffness since it ignores the loss of stiffness which arises due to buckling of plates and stiffened panels. Dwight[7-3] has suggested that eqn (7.4) can be used as a lower limit for ultimate moment capacity. This will be discussed later in this chapter.

The bending stress distribution corresponding to the limiting condition suggested by Vasta[1-3] is shown in Fig. 7-2, from which the ultimate bending moment for a simple box girder can be obtained:

$$M_u = \sigma_u \, AD \left[\alpha_D \gamma + 2\alpha_S \left(\frac{1}{3\gamma} - 1 + \gamma\right) + \alpha_B \left(\frac{1}{\gamma} - 2 + \gamma\right)\right] \quad \ldots \quad (7.5)$$

7.2.2.2 Caldwell: To take buckling effects into account, Caldwell[1-2] considered the following limiting condition existed when the girder had reached its ultimate bending moment. In the bottom structure and the side-shells below the neutral axis, the position of which was determined by equating tension and compression zone areas, yield stress in tension was assumed to have fully developed. On the compression side, structural instability factors ϕ_D and ϕ_S were introduced for the deck and the side-shells above the neutral axis to make allowance for buckling. The bending stress distribution corresponding to this limiting condition is shown in Fig. 7-3. By using the lumped area representation of the mid-ship cross-section, the resulting ultimate bending moment is:

$$M_u = \sigma_Y \, AD \left\{\phi_D \, \alpha_D \gamma + 2\alpha_S \left[\frac{1}{2} - \gamma + \gamma^2 \frac{(1+\phi_S)}{2}\right] + \alpha_B \, (1-\gamma)\right\}$$

$$\ldots \quad (7.6)$$

As indicated in ref. [1-29], it was implicit in Caldwell's approach that once an element reached its maximum load, it continued to carry that load under increasing strain. As has been seen, this is rarely the case in practice. It therefore appears to follow that eqn (7.6) will produce optimistic predictions of the ultimate bending moment.

7.2.2.3 Oakley: In considering the buckling of plate panels under compressive loads, Oakley[7-4] suggested a practical approach by using the concept of an effective width of plating associated with each longitudinal stiffener. Since the effective width varies with the applied stress, this approach requires an iterative process to calculate the effective section modulus. Two or three iterations are usually needed to reach a convergent solution[7-4], which gives an effective longitudinal stress distribution as shown in Fig. 7-4. The resulting ultimate bending moment is given by:

$$M_u = Z_e \sigma_Y \qquad \ldots \quad (7.7)$$

where Z_e is the effective section modulus of the midship cross-section. This equation satisfies both the equilibrium condition, and the deformation condition associated with the basic assumption that plane sections remain plane, but does not allow for residual strength after the buckling of plate panels.

7.2.2.4 Mansour and Faulkner: For a complex section, eqn (7.7) involves tedious iterations in determining the effective section modulus. An alternative expression has been suggested for longitudinally framed ships in the sagging condition by Mansour and Faulkner[7-2]:

$$M_u = Z \sigma_u (1+k\nu) = (Z \sigma_Y) \left(\frac{\sigma_u}{\sigma_Y} \right) (1+k\nu)$$

$$= M_Y \phi (1+k\nu) = M_p \frac{\phi (1+k\nu)}{S_F} \qquad \ldots \quad (7.8)$$

where $k\nu$ is a function of the ratio of one side-shell area to the deck area. The term $1+k\nu$ was taken as 1.1 for a frigate cross-section in ref. [7-5].

7.2.2.5 Wong: It is apparent that the ultimate bending strength of a ship's hull girder is influenced by the post-peak behaviour of its compressed members, in addition to their maximum load-carrying capacity. To include the effect of load-shedding, Wong[7-6] proposed two patterns of bending stress distribution. These were termed Type 1 and Type 2 and are shown in Figs 7-5 and 7-6 respectively. The resulting ultimate bending moments are given by:

$$M_u = \sigma_Y \, AD \left\{ \alpha_D \phi_D (\gamma_a + \gamma_b) + \alpha_S \phi_S \left[\frac{\gamma_a^2}{3} (1+2\zeta) + \gamma_a \gamma_b (1+\zeta) + \frac{2}{3} \gamma_b^2 \right] + \frac{2}{3} \alpha_S \gamma_c^2 + \alpha_B \gamma_c \right\} \quad \ldots \quad (7.9)$$

for Type 1, and

$$M_u = \sigma_Y \, AD \left\{ \alpha_S \left(\frac{\phi_S}{3} + \frac{2}{3} \phi_S \zeta_S + 1 \right) \gamma^2 + \gamma(\alpha_D \zeta_D \phi_D - 2\alpha_S - \alpha_B) + \alpha_S + \alpha_B \right\} \quad \ldots \quad (7.10)$$

for Type 2, where $\gamma_a = a/D$, $\gamma_b = b/D$ and $\gamma_c = c/D$, and a, b and c are the distances as indicated in Fig. 7-5. For these solutions, it is necessary to determine the load-shedding factors (ζ, ζ_D, ζ_S) to enable the ultimate strength for a ship's hull girder to be calculated. It was suggested by Wong[7-6] that a value of 0.2 σ_u load shedding, i.e. $\zeta = 0.8$, might be used on the safe side in connection with the limit state design approach.

7.2.2.6 Faulkner and Sadden: The ships strength model chosen for the mean ultimate moment by Faulkner and Sadden[7-5] was:

$$\overline{M_u} = \sigma_Y \, Z \, [(1 - \alpha_Y + \alpha_Y \alpha_c \phi) \, \alpha_Y] \, \alpha_S = \overline{\sigma_Y} \, Z (1 - \alpha_Y + \alpha_Y \alpha_c \phi) \, \alpha_S \quad \ldots \quad (7.11)$$

where α = 1 + systematic errors, i.e. $\alpha_Y = 1 + \zeta_Y = \overline{\sigma_Y}/\sigma_Y$, $\alpha_c = 1 + \zeta_c$ and $\alpha_S = 1 + \zeta_S$. Here, ζ_Y is the systematic error in yield strength,

ζ_c the systematic error which may arise in using idealised design codes to evaluate σ_u, and ζ_S represents the margin between the moment at which compression collapse occurs in the weakest portion of the hull and the ultimate bending moment. By using the systematic errors assumed in ref. [7-5], viz. $\zeta_Y = 0.1$, $\zeta_c = 0.15\ (1-\phi)(2+\zeta_Y)$ and $\zeta_S = 0.15$, eqn (7.11) becomes:

$$\overline{M_u} = \overline{\sigma_Y}\, Z(-\ 0.1 + 1.4465\ \phi - 0.3465\ \phi^2) \times 1.15$$

$$= \overline{M_p}\, \frac{1.15(-\ 0.1 + 1.4465\ \phi - 0.3465\ \phi^2)}{S_F} \qquad \ldots \quad (7.12)$$

7.3 ULTIMATE MOMENT EXPRESSION

7.3.1 *Background*

It can be seen from the existing strength formulae, eqs (7.4), (7.6), (7.8), (7.9), (7.10) and (7.12) that the ultimate moment capacity of a hull under vertical bending is considered to be dominated by the strength ($\sigma_u = \phi\ \sigma_Y$) of the compression flange. Regarding this strength, Vasta[1-3] suggested the use of the average representative panel strength of the compression flange. This was supported by Caldwell[1-2] in considering the effect of structural instability. In Oakley's effective width approach[7-4], the strength factor ϕ is associated with plate effectiveness but makes no allowance for the strength of longitudinal stiffeners. Faulkner and Sadden[7-5] used the average ultimate compression strength of the critical stiffened panel.

As has been shown in Chapter 6, the ultimate bending strength of longitudinally framed hulls predicted by the numerical analysis (Chapter 5) closely correlates with the maximum load-carrying capacity of their critical stiffened panels. Therefore, it is proposed to

adopt Faulkner and Sadden's definition of σ_u in the derivation of a simple expression for ultimate hull strength.

7.3.2 *Strength Formula for Stiffened Panels*

7.3.2.1 Least-squares method: The ultimate strength of a stiffened panel is primarily a function of column slenderness (λ), plate slenderness (β), initial plate deformation (δ_o), initial stiffener deflection (Δ) and weld-induced residual stress (σ_r). However, by selecting for design, suitable values for δ_o, Δ and σ_r, the number of independent variables reduces to two. From Table 4-6, appropriate values for the initial imperfections seem to be $\delta_o = b/200$, $\Delta = 0.0015\ L$ and $\sigma_r = 0.2\ \sigma_Y$. Therefore, the ultimate strength can be expressed as:

$$\phi = \frac{\sigma_u}{\sigma_Y} = f(\lambda,\beta) \qquad \ldots \quad (7.13)$$

To fit a function to the numerical data contained in Table 4-6, the least-squares method[2-6] is employed. Equation (7.13) is assumed to take the following form:

$$\phi = \frac{1}{\sqrt{C_1 + C_2\,\lambda^2 + C_3\,\beta^2 + C_4\,\lambda^2\beta^2 + C_5\,\lambda^4}} \qquad \ldots \quad (7.14)$$

Let Φ_i represent a numerical value, and let ϕ_i be the corresponding value from eqn (7.14), i.e.

$$\phi_i = \frac{1}{\sqrt{C_1 + C_2\,\lambda_i^2 + C_3\,\beta_i^2 + C_4\,\lambda_i^2\beta_i^2 + C_5\,\lambda_i^4}} \qquad \ldots \quad (7.15)$$

where λ_i and β_i are the values of column slenderness and plate slenderness in Table 4-6.

Before determining the values for the parameters C_1, C_2, C_3, C_4 and C_5, eqn (7.14) is transformed to the following polynomial by

taking inverses and squares:

$$y = \frac{1}{\phi^2} = C_1 + C_2 \lambda^2 + C_3 \beta^2 + C_4 \lambda^2\beta^2 + C_5 \lambda^4 \quad \ldots \quad (7.16)$$

Similarly, eqn (7.15) becomes:

$$y_i = \frac{1}{\phi_i^2} = C_1 + C_2 \lambda_i^2 + C_3 \beta_i^2 + C_4 \lambda_i^2\beta_i^2 + C_5 \lambda_i^4 \quad \ldots \quad (7.17)$$

The least-squares method seeks to minimise the sum of squares of the deviations of Y_i $(= 1/\Phi_i^2)$ from the predictions of eqn (7.17), rather than the deviations of Φ_i from the use of eqn (7.15). That is, it requires that:

$$S = \sum_{i=1}^{N} (Y_i - y_i)^2$$

$$= \sum_{i=1}^{N} (Y_i - C_1 - C_2 \lambda_i^2 - C_3 \beta_i^2 - C_4 \lambda_i^2\beta_i^2 - C_5 \lambda_i^4)^2 \quad \ldots \quad (7.18)$$

be a minimum. N is the number of data points $(\lambda_i, \beta_i, Y_i)$. At the minimum, all the partial derivatives $\partial S/\partial C_1$, $\partial S/\partial C_2$, $\partial S/\partial C_3$, $\partial S/\partial C_4$ and $\partial S/\partial C_5$ vanish, thus:

$$\frac{\partial S}{\partial C_1} = 0 = \sum_{i=1}^{N} 2(Y_i - C_1 - C_2 \lambda_i^2 - C_3 \beta_i^2 - C_4 \lambda_i^2\beta_i^2 - C_5 \lambda_i^4)(-1)$$

$$\frac{\partial S}{\partial C_2} = 0 = \sum_{i=1}^{N} 2(Y_i - C_1 - C_2 \lambda_i^2 - C_3 \beta_i^2 - C_4 \lambda_i^2\beta_i^2 - C_5 \lambda_i^4)(-\lambda_i^2)$$

$$\frac{\partial S}{\partial C_3} = 0 = \sum_{i=1}^{N} 2(Y_i - C_1 - C_2 \lambda_i^2 - C_3 \beta_i^2 - C_4 \lambda_i^2\beta_i^2 - C_5 \lambda_i^4)(-\beta_i^2)$$

$$\frac{\partial S}{\partial C_4} = 0 = \sum_{i=1}^{N} 2(Y_i - C_1 - C_2 \lambda_i^2 - C_3 \beta_i^2 - C_4 \lambda_i^2\beta_i^2 - C_5 \lambda_i^4)(-\lambda_i^2\beta_i^2)$$

$$\frac{\partial S}{\partial C_5} = 0 = \sum_{i=1}^{N} 2(Y_i - C_1 - C_2 \lambda_i^2 - C_3 \beta_i^2 - C_4 \lambda_i^2\beta_i^2 - C_5 \lambda_i^4)(-\lambda_i^4)$$

$$\ldots \quad (7.19)$$

Dividing each by -2 and rearranging leads to five linear equations to be solved simultaneously:

$$
\begin{aligned}
C_1 N &+ C_2\Sigma\lambda_i^2 + C_3\Sigma\beta_i^2 + C_4\Sigma\lambda_i^2\beta_i^2 + C_5\Sigma\lambda_i^4 = \Sigma Y_i \\
C_1\Sigma\lambda_i^2 &+ C_2\Sigma\lambda_i^4 + C_3\Sigma\lambda_i^2\beta_i^2 + C_4\Sigma\lambda_i^4\beta_i^2 + C_5\Sigma\lambda_i^6 = \Sigma Y_i\lambda_i^2 \\
C_1\Sigma\beta_i^2 &+ C_2\Sigma\lambda_i^2\beta_i^2 + C_3\Sigma\beta_i^4 + C_4\Sigma\lambda_i^2\beta_i^4 + C_5\Sigma\lambda_i^4\beta_i^2 = \Sigma Y_i\beta_i^2 \\
C_1\Sigma\lambda_i^2\beta_i^2 &+ C_2\Sigma\lambda_i^4\beta_i^2 + C_3\Sigma\lambda_i^2\beta_i^4 + C_4\Sigma\lambda_i^4\beta_i^4 + C_5\Sigma\lambda_i^6\beta_i^2 = \Sigma Y_i\lambda_i^2\beta_i^2 \\
C_1\Sigma\lambda_i^4 &+ C_2\Sigma\lambda_i^6 + C_3\Sigma\lambda_i^4\beta_i^2 + C_4\Sigma\lambda_i^6\beta_i^2 + C_5\Sigma\lambda_i^8 = \Sigma Y_i\lambda_i^4
\end{aligned}
\qquad \ldots \quad (7.20)
$$

All the summations in the above equations run from 1 to N.

The values of λ_i, β_i and Y_i ($= 1/\Phi_i^2$) are substituted into eqn (7.20) to set up the simultaneous linear equations. By solving these equations, the result is $C_1 = 0.960$, $C_2 = 0.765$, $C_3 = 0.176$, $C_4 = 0.131$ and $C_5 = 1.046$, so the least-squares method gives:

$$
y = \frac{1}{\phi^2} = 0.960 + 0.765\,\lambda^2 + 0.176\,\beta^2 + 0.131\,\lambda^2\beta^2 + 1.046\,\lambda^4 \qquad \ldots \quad (7.21)
$$

or

$$
\phi = \frac{\sigma_u}{\sigma_Y} = \frac{1}{\sqrt{0.960 + 0.765\,\lambda^2 + 0.176\,\beta^2 + 0.131\,\lambda^2\beta^2 + 1.046\,\lambda^4}} \qquad \ldots \quad (7.22)
$$

7.3.2.2 Comparisons with numerical results: It is of interest to assess the accuracy of the predictions of eqn (7.22) with the numerical results in Table 4-6. Thus, the values of ultimate strength predicted by this simple expression are compared with the numerical results in Fig. 7-7 and Table 7-1. It can be clearly seen that the agreement is good, with a mean ratio of 1.004 and COV = 2.9% being obtained for the ratio of the simple prediction to the numerical result.

TABLE 7-1 COMPARISONS OF THE ULTIMATE STRENGTH OF STIFFENED PANELS BETWEEN NUMERICAL RESULTS AND STRENGTH FORMULA

PLATE SLENDERNESS	COLUMN SLENDERNESS	ULTIMATE STRENGTH ($\phi = \sigma_u / \sigma_Y$)		RATIO
β	λ	NUMERICAL RESULTS	EQ. (7-22)	$\frac{\phi_F}{\phi_N}$
		ϕ_N	ϕ_F	
1.185	0.1	0.926	0.907	0.979
	0.3	0.879	0.877	0.998
	0.5	0.821	0.814	0.991
	1.0	0.574	0.559	0.974
	1.5	0.334	0.340	1.018
2.173	0.1	0.756	0.744	0.984
	0.3	0.690	0.721	1.045
	0.5	0.629	0.674	1.072
	1.0	0.487	0.487	1.000
	1.5	0.320	0.313	0.978
3.161	0.1	0.628	0.604	0.962
	0.3	0.575	0.586	1.019
	0.5	0.533	0.550	1.032
	1.0	0.416	0.414	0.995
	1.5	0.279	0.281	1.007

MEAN = 1.004

COV = 2.9%

Equation (7.22) is plotted in the form of ϕ-λ curves for β = 0, 1, 2, 3, 4 and 5 as shown in Fig. 7-8, and in the form of ϕ-β curves for λ = 0.0, 0.2, 0.4, 0.6, 0.8, 1.0, 1.2 and 1.4 as shown in Fig. 7-9. It is demonstrated in these figures that eqn (7.22) gives 1.021 when λ and β equal zero. It should theoretically be 1.0, but if one were to make some allowance for the difference between tensile and compressive yield, this would be the form of modification required. Therefore, since eqn (7.22) provides a good estimate for all other λ and β, it seems reasonable to retain the equation as derived since it makes a small concession to the extra strength demonstrated by compressive yielding.

7.3.3 *Strength Formulae for Hull Girders*

7.3.3.1 Proposed formulations: The ultimate moment capacity (M_u) of longitudinally framed hulls under vertical bending is closely correlated with the ultimate strength (ϕ) of the critical compression panels, as demonstrated in Fig. 7-10 and Table 7-2 for girders in the sagging condition and in Fig. 7-11 and Table 7-3 for girders in the hogging condition. Since many hard corners are provided by the keel plates, deep girders and bilge keels which exist in the compressed part of a vessel in hogging, it is necessary to consider sagging and hogging conditions separately in deriving simple expressions for the ultimate moment capacity.

In the sagging condition, all of the longitudinally framed girders analysed in Chapter 6 were included in Fig. 7-10 and Table 7-2 except for HULL B (composite girder), Type 1 *COBRA* (mixed framing), Type 2 *COBRA* (mixed framing) and *TYPE 14* Class (relatively small deck area). The numerical results for the *TYPE 81* Class and the *LEANDER* Class were derived for the hulls without superstructures.

TABLE 7-2 COMPARISONS OF THE ULTIMATE SAGGING MOMENT OF HULL GIRDERS PREDICTED BY USING EQ. (7-24) WITH NUMERICAL AND EXPERIMENTAL RESULTS

SHIP OR BOX GIRDER	CRITICAL STIFFENED PANEL			ULTIMATE BENDING MOMENT M_u/M_P			RATIOS	
	λ	β	ϕ EQ. (7-22)	NUMERICAL	EXPERIMENTAL	EQ. (7-24)	(6)/(4)	(6)/(5)
	(1)	(2)	(3)	(4)	(5)	(6)		
S.B.G. MODEL 2	0.644	1.873	0.664	0.722	0.689	0.694	0.961	1.007
S.B.G. MODEL 4	0.490	0.786	0.866	0.892	0.842	0.893	1.001	1.060
S.B.G. MODEL 23	0.465	1.173	0.829	0.887	0.930	0.859	0.968	0.924
S.B.G. MODEL 31	0.396	1.673	0.777	0.800	0.851	0.809	1.011	0.951
HULL A	0.598	2.204	0.639	0.680	-	0.667	0.981	-
COBRA - TYPE 3	0.769	2.073	0.590	0.591	-	0.613	1.037	-
WHITBY CLASS	0.466	3.666	0.505	0.514	-	0.516	1.004	-
ROTHESAY CLASS	0.466	3.666	0.505	0.524	-	0.516	0.985	-
TYPE 81 CLASS	0.509	2.376	0.643	0.619	-	0.671	1.084	-
LEANDES CLASS	0.765	1.925	0.532	0.564	-	0.547	0.971	-

MEAN = 1.000

COV = 3.7%

TABLE 7-3 COMPARISONS OF THE ULTIMATE HOGGING MOMENT OF HULL GIRDERS PREDICTED BY USING EQ. (7-25) WITH NUMERICAL RESULTS

SHIP GIRDER	CRITICAL STIFFENED PANEL			ULTIMATE BENDING MOMENT M_u/M_p		RATIO
	λ	β	ϕ			
			EQ. (7-22)	NUMERICAL	EQ. (7-25)	(5)
	(1)	(2)	(3)	(4)	(5)	(4)
COBRA - TYPE 3	0.650	2.073	0.637	0.751	0.745	0.992
TYPE 14 CLASS	0.548	1.582	0.741	0.825	0.831	1.007
WHITBY CLASS	0.408	1.633	0.780	0.863	0.860	0.996
ROTHESAY CLASS	0.408	1.633	0.780	0.870	0.860	0.988
TYPE 81 CLASS	0.385	2.232	0.695	0.784	0.788	1.005
LEANDES CLASS	0.413	1.481	0.802	0.875	0.877	1.002

MEAN = 0.998

COV = 0.8%

The relationship between M_u/M_p and ϕ is assumed to take the following form:

$$\frac{M_u}{M_p} = d_1 + d_2 \phi + d_3 \phi^2 \quad \ldots \quad (7.23)$$

By using the least-squares method as described in section 7.3.2.1, the parameters in eqn (7.23) were determined: $d_1 = -0.172$, $d_2 = 1.548$ and $d_3 = -0.368$. Thus, eqn (7.23) becomes:

$$\frac{M_u}{M_p} = -0.172 + 1.548 \phi - 0.368 \phi^2 \quad \ldots \quad (7.24)$$

This equation applies to vessels in the sagging condition and is used in connection with eqn (7.22).

In the hogging condition, all box girder models, HULL A (relatively weak bottom structure) and HULL B (composite girder) were excluded from the derivation and hence are not included in Fig. 7-11 or Table 7-3. *TYPE 81* Class and *LEANDER* Class were also treated as hulls without superstructure in deriving the numerical results.

Similarly, by using the least-squares method, the following expression was obtained:

$$\frac{M_u}{M_p} = +0.003 + 1.459 \phi - 0.461 \phi^2 \quad \ldots \quad (7.25)$$

which applies to vessels in the hogging condition and is used in connection with eqn (7.22).

7.3.3.2 Application to design: It can be clearly seen in eqs (7.24) and (7.25) that the ultimate bending moment (M_u) is a function of the fully plastic moment (M_p) and the ultimate strength (ϕ) of the critical stiffened panel. Thus, to predict the ultimate longitudinal strength

for a hull girder or box girder, the following procedure is suggested:

1. Determine the plastic neutral axis position, i.e. the interface that divides the cross-section into two regions with equal squash loads in compression and tension.

2. Calculate the fully plastic moment M_p for the fully effective midship section.

3. Identify the critical stiffened panel. This will generally be the panel appearing most frequently in the compression flange of the girder in either the sagging or hogging condition.

4. Compute the values of the column slenderness λ and the plate slenderness β for the critical panel.

5. Calculate the ultimate strength (ϕ) of the critical panel by using eqn (7.22).

6. Calculate the ultimate bending moment for the girder by using eqn (7.24) or (7.25).

7.3.4 *Comparisons with Numerical Results*

7.3.4.1 Present formulae: The strength formulae proposed in section 7.3.3.1 are now applied to predicting the ultimate bending moment for the hulls and box girders considered in Chapter 6. The results are compared with those obtained numerically in Fig. 7-10 and Table 7-2 for the hulls in the sagging condition, and in Fig. 7-11 and Table 7-3 for the hulls in the hogging condition. The agreement is seen to be satisfactory, with a mean ratio of 1.000 and COV = 3.7% in the sagging condition and a mean ratio of 0.998 and COV = 0.8% in the hogging condition being obtained for the ratio of the simple prediction to the numerical result. Even the predictions of the experimental results

are good as shown in Table 7-2. It would appear therefore that eqs (7.24) and (7.25) can be used with confidence for the preliminary design of ships hulls and probably even for the final design check.

7.3.4.2 Existing formulae: The existing strength formulae for ultimate moment capacity reviewed in section 7.2.2 are compared with the numerical results in Table 7-4 for the hulls in the sagging condition and in Table 7-5 for the hulls in the hogging condition. Since the effective width approach requires an iterative process to calculate the effective section modulus, it is excluded from the comparisons. In view of the uncertainty concerning the load-shedding factor, Wong's formulae are also excluded.

It was suggested in section 7.2.2.1 that Vasta's expression[1-3], i.e. eqn (7-4), would be pessimistic when predicting ultimate hull strength since it ignored plastic hinge capacity. This seems to be confirmed in Tables 7-4 and 7-5 where it is seen that a mean value of 0.815 and a COV = 5.7% for the hulls in the sagging condition and a mean value of 0.776 and a COV = 1.7% for the hulls in the hogging condition are obtained for the ratio of Vasta's prediction to the numerical result.

It was predicted in section 7.2.2.2, since the effect of load-shedding is not allowed for in Caldwell's approach[1-2], that eqn (7-6) is likely to produce optimistic predictions of the ultimate bending moment. This is clearly demonstrated in Tables 7-4 and 7-5 in which it is seen that a mean ratio of 1.186 and a COV = 8.7% are obtained for the ratio of Caldwell's prediction to the numerical result for the hulls in the sagging condition, and a mean ratio of 1.072 and COV = 2.8% for the hulls in the hogging condition.

Since Mansour and Faulkner's expression[7-2] gives a mean ratio compared with the numerical result of 0.897 and COV = 5.7% (Table 7-4, sagging condition) and a mean ratio of 0.854 and COV = 1.7% (Table 7-5, hogging condition), eqn (7.8) achieves an improvement of the prediction over Vasta's approach[1-3] but with the same COV.

Faulkner and Sadden's expression (eqn (7-12), ref. [7-5]) is seen to improve both the mean ratio (0.995) and the COV (5.2%) in the sagging condition and to improve the mean ratio (0.941) with a small COV (2.0%) in the hogging condition, and clearly is the best of the existing formulae. Compared with the present approach, it still generates larger values of COV (5.2% and 2.0% compared with 3.7% and 0.8% for the hulls in the sagging and hogging conditions respectively) and needs more calculations including some estimates of systematic errors.

TABLE 7-4 COMPARISONS OF THE ULTIMATE SAGGING MOMENT OF HULL GIRDERS PREDICTED BY USING EXISTING FORMULAE WITH NUMERICAL RESULTS

SHIP OR BOX GIRDER	CRITICAL STIFFENED PANEL ϕ EQ. (7-22) (1)	ULTIMATE BENDING MOMENT M_u/M_P NUMERICAL PRESENT (2)	VASTA [1-3] (3)	CALDWELL [1-2] (4)	MANSOUR [7-2] (5)	FAULKNER [7-5] (6)	RATIOS (3)/(2)	(4)/(2)	(5)/(2)	(6)/(2)
S.B.G. MODEL 2	0.664	0.722	0.626	0.840	0.689	0.768	0.867	1.163	0.954	1.064
S.B.G. MODEL 4	0.866	0.892	0.722	0.924	0.794	0.856	0.809	1.036	0.890	0.960
S.B.G. MODEL 23	0.829	0.887	0.747	0.940	0.822	0.892	0.842	1.060	0.927	1.006
S.B.G. MODEL 31	0.777	0.800	0.700	0.880	0.770	0.844	0.875	1.100	0.963	1.055
HULL A	0.639	0.680	0.586	0.758	0.645	0.720	0.862	1.115	0.949	1.059
COBRA - TYPE 3	0.590	0.591	0.464	0.760	0.511	0.573	0.785	1.286	0.865	0.970
WHITBY CLASS	0.505	0.514	0.402	0.666	0.443	0.497	0.782	1.296	0.862	0.967
ROTHESAY CLASS	0.505	0.524	0.401	0.670	0.441	0.495	0.765	1.279	0.842	0.945
TYPE 81 CLASS	0.643	0.619	0.510	0.768	0.560	0.626	0.824	1.241	0.905	1.011
LEANDES CLASS	0.532	0.564	0.418	0.727	0.459	0.516	0.741	1.289	0.814	0.915
						MEAN =	0.815	1.186	0.897	0.995
						COV =	5.7%	8.7%	5.7%	5.2%

TABLE 7-5 COMPARISONS OF THE ULTIMATE HOGGING MOMENT OF HULL GIRDERS PREDICTED BY USING EXISTING FORMULAE WITH NUMERICAL RESULTS

SHIP OR BOX GIRDER	CRITICAL STIFFENED PANEL ϕ EQ. (7-22) (1)	ULTIMATE BENDING MOMENT M_u/M_P NUMERICAL PRESENT (2)	VASTA [1-3] (3)	CALDWELL [1-2] (4)	MANSOUR [7-2] (5)	FAULKNER [7-5] (6)	RATIOS (3)/(2)	(4)/(2)	(5)/(2)	(6)/(2)
COBRA - TYPE 3	0.637	0.751	0.574	0.850	0.631	0.705	0.764	1.132	0.840	0.939
TYPE 14 CLASS	0.741	0.825	0.640	0.877	0.704	0.777	0.776	1.063	0.853	0.942
WHITBY CLASS	0.780	0.863	0.663	0.914	0.729	0.799	0.768	1.059	0.845	0.926
ROTHESAY CLASS	0.780	0.870	0.666	0.920	0.733	0.803	0.766	1.057	0.842	0.923
TYPE 81 CLASS	0.695	0.784	0.626	0.827	0.689	0.765	0.798	1.055	0.879	0.976
LEANDES CLASS	0.802	0.875	0.685	0.933	0.754	0.823	0.783	1.066	0.862	0.941
							MEAN = 0.776	1.072	0.854	0.941
							COV = 1.7%	2.8%	1.7%	2.0%

Chapter 8

CONCLUSIONS and FUTURE WORK

CONCLUSIONS

The aim of this work has been to produce simplified design formulae for predicting the ultimate vertical bending moment capacity of ship and similar box-like cross-sections. This has been done following the development of a suite of computer programs capable of predicting the load-shortening behaviour of plates and stiffened panels which constitute such cross-sections and the moment-curvature response of the entire section using the plate and stiffened panel load-shortening behaviour to simulate individual panel behaviour.

Each phase of the work was done independently and proven before being used in the next stage. Achievements and conclusions concerning each of these stages were as follows:

8.1 Plate Model

1. A procedure for generating load-end shortening curves for plates in compression was developed using a curve-fitting approach to data generated by a previous parametric study of such elements. For residual stress-free plates with slendernesses and initial deflections different from the standard cases, the load-end shortening curves were interpolated from the basic data using cubic splines. A simplified method was followed to derive the load-end shortening curves for plates with residual stresses.

2. Comparisons with more rigorous analysis techniques showed that the results of the simplified approach correlate closely with those derived numerically.

8.2 *Stiffened Panel Model*

1. A numerical procedure was developed for predicting the axial load-shortening response of stiffened panels. It was based on the beam-column approach in which the longitudinally stiffened plating was treated as a series of beam-columns composed of stiffeners and attached plating. The model assumed continuity over supports provided by transverse frames. It used large deflection beam-column equations which included plasticity on a layered basis, the response of the plating being derived using the simplified plate model. The procedure was capable of tracing the pre- and post-collapse behaviour.

2. Comparisons with a variety of test results showed that the agreement was satisfactory as differences were less than 4% in most cases and always within 6%. It was found important to examine the correct mode of failure and to use the measured values of weld-induced residual stresses and initial imperfections in analysing test specimens, since the maximum load-carrying capacities of stiffened panels were strongly affected by these factors. Close correlation with test results demonstrated that the present method could be used with confidence.

3. The present method also showed satisfactory agreement with other numerical solutions of double-span models: the average difference of less than 3%. Close correlation was demonstrated both from the points of view of ultimate strength and of the critical strain at which the stiffened panel reached its maximum load.

4. Comparisons with other numerical solutions of single-span models showed that the agreement was good in the range of low and high slenderness, but a significant difference was observed in the range of intermediate column slenderness. Since the difference was attributable to the effects of continuity, it could be concluded that interaction between adjacent spans occurred in the intermediate range, and its effects usually resulted in an increase in maximum load-carrying capacity of a stiffened panel.

5. Following a parametric study on stiffened panel response, it was found that stiffened panel strength depended primarily on two parameters, the column slenderness λ and the plate slenderness β. For low values of λ, stiffened panel collapse occurred due to buckling of the plate or yielding of the material. Thus, increasing β generally resulted in a reduction in the maximum load-carrying capacity of stiffened panels due to the loss of plate effectiveness. Increasing λ changed the dominant mode of failure from one of local plate buckling to one of overall column buckling and hence reduced the influence of β on stiffened panel collapse behaviour.

6. Concerning secondary parameters, the following aspects of stiffened panel behaviour were noted.

(a) Increasing the ratio of stiffener area to plate area from $\alpha = 0.2$ to $\alpha = 0.4$ slightly improved the load-carrying capacity and post-peak behaviour of stiffened panels.

(b) Initial stiffener deflection Δ affected the behaviour of stiffened panels mainly in the range of moderate column slenderness, and the influence was most pronounced

in the peak load region. For low and high values of λ, the influence was less pronounced.

(c) The effect of increasing initial plate deflection δ_o was to decrease the initial stiffness and the ultimate strength of stiffened panels.

(d) Increasing weld-induced residual stress σ_r resulted in a drop in stiffened panel strength but an improvement in post-collapse behaviour.

7. By selecting appropriate magnitudes of δ_o, Δ and σ_r for design, a simple expression was proposed for the ultimate strength of stiffened panels (section 7.3.2), which was considered as a function of column slenderness λ and plate slenderness β. Comparisons of this formula with numerical results showed that the agreement was satisfactory, with a mean ratio of 1.004 and a COV = 2.9% being obtained for the ratio of the simple prediction to the numerical result, covering wide ranges of column slenderness and plate slenderness.

8.3 *Hull Girder Model*

1. The formulation of a numerical method for evaluating the ultimate strength of a ship's hull girder under vertical bending has been presented. The hull's midship cross-section was subdivided into structural elements such as stiffened panels, plate elements and hard corners. The effects of plate and stiffener buckling were allowed for by using the load-shortening responses derived from the plate and stiffened panel models. The moment-curvature relationships and hence peak moments of hull girders were then found by an incremental approach.

2. The hull girder model was correlated against existing test results on four welded steel box girders, denoted Model 2, Model 4,

Model 23 and Model 31. Agreement between the results was satisfactory with the following particular lessons being learnt.

3. The peak moment of Model 2 predicted by the present method with residual stress and initial imperfections measured prior to Test 2A was 4.9% higher than the experimental collapse bending moment, but it was 4.6% lower than the collapse moment for Test 2B.

4. In connection with Model 4, the following aspects were noted.

(a) The present method overestimated the collapse bending moment by 5.9%.

(b) When initial stiffener deflection was changed from the average measured value to the maximum one, the girder's ultimate strength dropped 3.3%.

(c) As a result of the stocky plates and stiffeners used in the compression flange and webs of Model 4, its ultimate strength was only slightly influenced by whether the behaviour of the hard corners was assumed to follow the material stress-strain curve or the load-shortening curves of the adjacent stiffened panels.

(d) Including residual stresses in the tension flange mainly had the effect of decreasing the initial stiffness of the girder, but made little difference in the predicted peak moment.

5. For Model 23, the following aspects were noted.

(a) When residual stresses were excluded from the tension flange, agreement between the computed and experimental

ultimate strengths was satisfactory, although the predicted initial stiffness was higher than demonstrated in the test.

(b) When residual stresses were included in the tension flange, the agreement between the numerical and experimental results was satisfactory both in the sense of ultimate strength and initial stiffness.

6. In relation to Model 31, the following aspects were noted.

(a) The present method underestimated the collapse bending moment by 6.0% when measured maximum initial imperfections were used.

(b) As a result of increasing the initial stiffener deflection from $\Delta = L/2000$ to $\Delta = L/500$, the predicted peak moment decreased by 2.2%.

(c) Contrary to expectation, an increase in residual stresses from $\sigma_r' = 0.05$ to $\sigma_r' = 0.20$ resulted in a 1.4% increase in the predicted peak moment. This was due to the fact that the post-buckling strength of stiffened panels with $\sigma_r' = 0.20$ was greater than that of the same panels with $\sigma_r' = 0.05$. A further increase from $\sigma_r' = 0.20$ to $\sigma_r' = 0.35$ made almost no difference to the predicted peak moment.

(d) When initial plate deflections were increased from $\delta_o/t = 0.22$ to $\delta_o/t = 0.88$, the predicted peak moment dropped by 2.7%.

7. The following conclusions were drawn in relation to the transversely framed hulls of torpedo-boat destroyers *COBRA* and *WOLF*.

(a) The predicted results were in agreement with other numerical solutions.

(b) The values of M_u/M_p for transversely framed hulls were exceptionally low: 0.403 (sagging) and 0.484 (hogging) for *COBRA* and 0.458 (sagging) and 0.421 (hogging) for *WOLF*.

(c) Hard corners contributed significantly to the hulls' strength, otherwise the predicted peak moments would be much lower due to the weakness of transverse framing.

8. In view of low structural efficiency inherent in transversely framed ships, *COBRA's* hull was converted into three types of hulls using mixed or longitudinal framing. The predicted sagging M_u/M_p for these three hulls ranged from 0.497, to 0.504, and to 0.591 as compared with 0.403 for *COBRA*. The corresponding values in the hogging condition were 0.594, 0.730, 0.751 as compared with 0.484. These examples demonstrated the superiority of mixed and longitudinal framings to transverse framing from the point of view of ultimate hull strength.

9. A comprehensive theoretical study on the ultimate strength behaviour of longitudinal framed frigates under vertical bending has been carried out. Five naval frigates designed in the 1950's and 1960's were analysed by the present method. The following conclusions were drawn from this study.

(a) The M_u/M_p values for frigate-type hulls were much smaller than unity as a result of buckling of deck,

shell and bottom panels under compressive loads. This was the case particularly in the sagging condition as the deck structures of the frigates were considerably more slender than the bottom structures, and hence more susceptible to instability.

(b) The M_u/M_p ratios for the five frigates varied from 0.51 to 0.69 in the sagging condition and from 0.75 to 0.87 in the hogging condition.

(c) The ultimate strengths of longitudinally framed hulls were strongly influenced by the full-range behaviour of their components under compressive loads arising from overall bending. Thus, the shape of the compressive load-end shortening curves, which included pre-collapse stiffness, maximum load-carrying capacity and post-collapse strength of the stiffened panels, played a very important role in determining the ultimate strength of a ship's hull.

(d) The shape factors (M_p/M_Y) for the five frigate-type hulls ranged from 1.20 to 1.41 in the sagging condition and from 1.16 to 1.23 in the hogging condition.

(e) For all of the frigate-type hulls both in the sagging and hogging conditions, the peak moments were reached at curvatures much less than $2\phi_Y$, i.e. hull girders collapsed before outermost-fibre strains exceeded $2\varepsilon_Y$. Since shipbuilding steels began to strain harden at $3 \sim 10\ \varepsilon_Y$, it was reasonable to assume that strain hardening effects could be neglected.

10. The following conclusions were drawn in relation to simple expressions derived for determining the ultimate moment capacity of hull girders and box girders.

(a) On the basis of the close correlation demonstrated between the ultimate bending moment of longitudinally framed girders and the maximum load-carrying capacity of the critical compression panels, strength formulae were proposed for the ultimate moment capacity of the girders in the sagging and hogging conditions.

(b) Comparisons of the proposed formulae with numerical results showed that the agreement was satisfactory, as a mean ratio of 1.000 and a COV = 3.7% in the sagging and a mean ratio of 0.998 and a COV = 0.8% in the hogging condition were obtained for the ratio of the simple prediction to the numerical result. Even comparisons with the experimental results of box girders were also seen to be good. It appeared to follow that the proposed formulae could be used with confidence for the preliminary design of ships hulls and probably even for the final design check.

(c) Vasta's expression[1-3] was pessimistic in predicting ultimate hull strength (on average 18.5% and 22.4% underestimates in the sagging and hogging conditions respectively) since it ignored plastic hinge capacity. On the other hand, Caldwell's approach[1-2] produced optimistic predictions (on average 18.6% and 8.7% overestimates in the sagging and hogging conditions respectively) due to the neglecting of load-shedding.

(d) Mansour and Faulkner's expression[7-2] demonstrated an improvement in mean ratio (0.897 and 0.854 in the sagging and hogging conditions respectively) upon Vasta's approach but produced the same COV (5.7% and 1.7% in the sagging and hogging conditions respectively).

(e) Faulkner and Sadden's expression showed an improvement in predicting both the mean ratio (0.995) and the COV (5.2%) in the sagging condition and improved the mean ratio (0.941) with a small COV (2.0%) in the hogging condition, and clearly was the best of the existing formulae. Compared with the present approach, it still generated larger values of COV and needed more calculations including some estimates of systematic errors.

FUTURE WORK

In view of the lack of experimental data concerning the collapse behaviour of welded ship hulls under vertical bending, a need for large-scale structural tests on welded ship hull models up to collapse obviously exists. As the test data becomes available, it would be useful to compare the results with those predicted by the present method. Additionally, it will provide a measure for determining the relative reliability of the various theoretical formulations. To be beneficial, the scale of the models should be large enough so that the possible failure modes can be investigated, the corresponding collapse loads can be extrapolated to full-scale, and the influence of residual stresses and initial imperfections on the ultimate strength can be realistically examined.

Although some of failure modes of a ship's hull can be analysed by the present method to a certain degree of accuracy, others are far from being well established. As a basis for more rigorous assessments of ultimate hull strength, further analytical work is required in addition to the experimental programs. Some recommendations are made as follows:

1. The interaction between failure modes of a hull girder, e.g. plate buckling occurring simultaneously with instability of stiffeners and yielding, should be investigated further.

2. The possibility of hull failure resulting from tripping, i.e. lateral-torsional buckling of the stiffeners, should be examined for some ship structures, where stiffeners of high ratios of depth to thickness are used. The influence of elasto-plastic tripping of stiffeners on post-collapse behaviour of stiffened panels should be considered in the examination.

3. Further attention should be given to hull failure due to brittle or fatigue fracture with a view to incorporating both failure modes in a general analysis procedure together with the other failure modes included in the present study. In particular, stress concentrations caused by structural discontinuities should be examined.

4. As the collapse moment of a ship's hull is strongly affected by hard corners in the cases of transversely framed hulls and slender longitudinally framed hulls, the behaviour of hard corners in hull cross-sections requires further examination.

5. The statistics of initial stiffener distortions relative to adjacent elements of stiffened panels and the associated imperfection effects on the collapse behaviour of a ship's hull need further research.

REFERENCES

Chapter 1:

1-1 'Report of Committee 10', Proc., Vol. 2, International Ship Structures Congress, Oslo, 1967.

1-2 Caldwell, J.B. 'Ultimate Longitudinal Strength', Trans RINA, Vol. 107, 1965.

1-3 Vasta, J. 'Lessons Learned from Full Scale Structural Tests', Trans SNAME, Vol. 66, 1958.

1-4 Lin, Y.T. and Frieze, P.A. 'The Large Deflection Elasto-Plastic Analysis of Double-Span Stiffened Panels under Uniaxial Compression', Department Report, Dept NAOE, Univ. of Glasgow, June 1984.

1-5 Moxham, K.E. 'Compression in Welded Web Plates', PhD Thesis, Univ. of Cambridge, June 1970.

1-6 Little, G.H. 'Rapid Analysis of Plate Collapse by Live-Energy Minimisation', Jnl of Mech. Sci., Vol. 19, 1977.

1-7 Crisfield, M.A. 'Large-Deflection Elasto-Plastic Buckling Analysis of Plates using Finite Elements', TRRL Report LR593, 1973.

1-8 Frieze, P.A. 'Ultimate Load Behaviour of Steel Box Girders and their Components', PhD Thesis, Univ. of London, 1975.

1-9 Harding, J.E., Hobbs, R.E. and Neal B.G. 'The Elasto-Plastic Analysis of Imperfect Square Plates under In-Plane Loading', Proc. Instn Civ. Engrs, Part 2, Vol. 63, March 1977.

1-10 Dwight, J.B. and Moxham, K.E. 'Welded Steel Plates in Compression', The Structural Engineer, Vol. 47, No. 2, 1969.

1-11 Frieze, P.A., Dowling, P.J. and Hobbs, R.E. 'Parametric Study on Plates in Compression', Engg Structures Lab., Civil Engg Dept, Imperial College, London, CESLIC Report BG39, Jan. 1975.

1-12 Crisfield, M.A. 'Full Range Analysis of Steel Plates and Stiffened Plating under Uniaxial Compression', Proc. Instn Civ. Engrs, Part 2, Vol. 59, 1975.

1-13 Harding, J.E., Hobbs, R.E. and Neal, B.G. 'Ultimate Load Behaviour of Plates under Combined Direct and Shear In-Plane Loading', Proc. International Conference on Steel Plated Structures, Imperial College, London, 1976.

1-14 Crisfield, M.A. 'A Computer Program to Generate Load/Shortening Relationships for Simply Supported Steel Plates', TRRL Report LR683, 1975.

1-15 Davidson, H.L. 'Post-Buckling of Long Rectangular Plates', Fritz Engg Lab. Report No. 248.15, Lehigh University, June 1965.

1-16 Becker, H. 'Compressive Strength of Ship Hull Girders', Part I, Unstiffened Panels, Ship Structures Committee Report SSC-217, 1970.

1-17 Dwight, J.B. and Ractliffe, A.T. 'The Strength of Thin Plates in Compression', Proc. Symposium on Thin-Walled Steel Structures, Swansea, 1967.

1-18 Moxham, K.E. 'Buckling Tests on Individual Welded Steel Plates in Compression', Univ. of Cambridge, Dept of Engg, Report CUED/C-Struct/TR.3, 1971.

1-19 Bradfield, C.D. 'Tests on Plates Loaded in In-Plane Compression', Jnl of Constructional Steel Research, Vol. 1, No. 1, Sept. 1980.

1-20 Ostapenko, A. and Lee, T. 'Tests on Longitudinally Stiffened Plate Panels subjected to Lateral and Axial Loading', Fritz Engg Lab. Report No. 248.4, Lehigh University, Aug. 1960.

1-21 Dwight, J.B. 'A Possible Design Procedure for Stiffened Compression Panels', Jnl of Australian Inst. of Steel Construction, Vol. 9, No. 3, 1975.

1-22 Moolani, F.M. 'Ultimate Load Behaviour of Steel Box Girder Stiffened Compression Flanges', PhD Thesis, Univ. of London, 1976.

1-23 Drymakis, E. 'A Numerical Elasto-Plastic Buckling Analysis for Stiffened Plates', MSc Thesis, Univ. of Glasgow, 1981.

1-24 Murray, N.W. 'Analysis and Design of Stiffened Plates for Collapse Load', The Structural Engineer, Vol. 53, No. 3, March 1975.

1-25 Horne, M.R. and Narayanan, R. 'An Approximate Method for the Design of Stiffened Steel Compression Panels', Proc. Instn Civ. Engrs, Part 2, Vol. 59, Sept. 1975.

1-26 Smith, C.S. 'Compressive Strength of Welded Steel Ship Grillages', Trans RINA, Vol. 117, 1975.

1-27 Dorman, A.P. and Dwight, J.B. 'Tests on Stiffened Compression Panels and Plate Panels', Proc. International Conference on Steel Box Girder Bridges, The Instn of Civ. Engrs, London, Feb. 1973.

1-28 Horne, M.R. and Narayanan, R. 'Ultimate Capacity of Longitudinally Stiffened Plates used in Box Girders', Proc. Instn Civ. Engrs, Part 2, Vol. 61, June 1976.

1-29 Faulkner, D. Contribution to Discussion of Reference [1-2].

1-30 Betts, C.V. and Attwell, D.M. 'The Ultimate Longitudinal Strength of Ships', Shipbuilding and Shipping Record, Dec. 1965.

1-31 'Report of Committee on Plastic and Limit Analysis', International Ship Structures Congress, Tokyo, 1970.

1-32 Evans, J.H.(Editor). 'Ship Structural Design Concepts', Ship Structures Committee Project SR-200, US Coast Guard, Washington, D.C., 1974.

1-33 Mansour, A.E. and Thayamballi, A. 'Ultimate Strength of a Ship's Hull Girder Plastic and Buckling Modes', Ship Structures Committee Report SSC-299, 1980.

1-34 Smith, C.S. 'Influence of Local Compressive Failure on Ultimate Longitudinal Strength of a Ship's Hull', International Symposium on Practical Design in Shipbuilding, Tokyo, Oct. 1977.

1-35 Dow, R.S., Hugill, R.C., Clark, J.D. and Smith, C.S. 'Evaluation of Ultimate Ship Hull Strength', Proc. Symposium on Extreme Loads Response, Arlington, USA, 1981.

1-36 Smith, C.S. 'Structural Redundancy and Damage Tolerance in Relation to Ultimate Ship Hull Strength', Proc. Symposium on Design, Inspection, Redundancy, Williamsburg, USA, 1983.

1-37 Faulkner, J.A., Clarke, J.D., Smith, C.S. and Faulkner, D. 'The Loss of HMS COBRA - A Reassessment', RINA Paper for Spring Meetings, 1984.

1-38 Billingsley, D.W. 'Hull Girder Response to Extreme Bending Moments', Proc. 5th Ship Tech. and Research Symposium, Coronado, USA, 1980.

1-39 Adamchak, J.C. 'ULTSTR: A Program for Estimating the Collapse Moment of a Ship's Hull under Longitudinal Bending', DTNSRDC Rep. 82/076, 1982.

1-40 Adamchak, J.C. 'An Approximate Method for Estimating the Collapse of a Ship's Hull in Preliminary Design', Ship Structures Symposium '84, Arlington, USA, 1984.

1-41 Ostapenko, A. 'Strength of Ship Hull Girders under Moment, Shear and Torque', Proc. Symposium on Extreme Loads Response, Arlington, USA, 1981.

1-42 Lang, D.W. and Warren, W.G. 'Structural Strength Investigations on the Destroyer ALBUERA', Trans RINA, Vol. 94, 1952.

1-43 Kell, C.O. 'Investigation of Structural Characteristics of Destroyers PRESTON and BRUCE, Part 1 - Description', Trans SNAME, Vol. 39, 1931.

1-44 Kell, C.O. 'Investigation of Structural Characteristics of Destroyers PRESTON and BRUCE, Part 2 - Analysis of Data and Results', Trans SNAME, Vol. 48, 1940.

1-45 Dowling, P.J., Chatterjee, S., Frieze, P.A. and Moolani, F.M. 'Experimental and Predicted Collapse Behaviour of Rectangular Steel Box Girders', Proc. International Conference on Steel Box Girder Bridges, The Instn of Civ. Engrs, London, Feb. 1973.

1-46 Dowling, P.J., Moolani, F.M. and Frieze, P.A. 'The Effect of Shear Lag on the Ultimate Strength of Box Girders', International Conference on Steel Plated Structures, Imperial College, London, 1976.

1-47 'Report on Committee II.2 on Non-Linear Structural Response', Proc. 7th International Ship Structures Congress, Paris, 1979.

Chapter 2:

2-1 Moxham, K.E. 'Theoretical Prediction of the Strength of Welded Steel Plates in Compression', University of Cambridge, Dept of Engg, Report CUED/C-Struct/TR.2, 1971.

2-2 Faulkner, D. 'Compression Tests on Welded Eccentrically Stiffened Plate Panels', Proc. International Conference on Steel Plated Structures, Imperial College, London, 1976.

2-3 Somerville, W.L., Swan, J.W. and Clarke, J.D. 'Measurement of Residual Stresses and Distortion in Ship Structures', Proc. Conference on the Influence of Residual Stresses and Distortions on Performance of Steel Structures, Inst. Mech. Engrs, London, 1976.

2-4 Faulkner, D. 'Compression Strength of Welded Grillages', Chapter 21 of Reference [1-32].

2-5 Faulkner, D. 'A Review of Effective Plating for use in the Analysis of Stiffened Plating in Bending and Compression', Jnl of Ship Research, Vol. 19, 1975.

2-6 Gerald, C.F. 'Applied Numerical Analysis', 2nd Ed., Addison-Wesley, Massachusetts, USA, 1978.

Chapter 3:

3-1 Taggart, R.(Editor). 'Ship Design and Construction', SNAME, New York, USA, 1980.

3-2 Dowling, P.J. 'Some Approaches to the Non-Linear Analysis of Plated Structures', Proc. Symposium on Non-Linear Techniques and Behaviour in Structural Analysis, TRRL, Crowthorne, UK, Dec. 1974.

3-3 Little, G.H. 'Stiffened Steel Compression Panels - Theoretical Failure Analysis', The Structural Engineer, Vol. 54, No. 12, Dec. 1976.

3-4 Søreide, T.H., Moan, T. and Nordsve, N.T. 'On the Behaviour and Design of Stiffened Plates in Ultimate Limit State', Jnl of Ship Research, Vol. 22, Dec. 1978.

3-5 Carlsen, C.A. 'A Parametric Study of Collapse of Stiffened Plates in Compression', The Structural Engineer, Vol. 58, No. 2, June 1980.

3-6 Carlsen, C.A. 'Simplified Collapse Analysis of Stiffened Plates', Norwegian Maritime Research, No. 4, 1977.

3-7 Ueda, Y., Yasukawa, W., Yao, T., Ikegami, H. and Ohminami, R. 'Effects of Welding Residual Stress and Initial Deformation on Rigidity and Strength of Square Plates subjected to Compression', Trans JWRI, Vol. 4, No. 2, 1975.

3-8 Lin, Y.T. and Frieze, P.A. 'A Simplified Method to Generate the Average Stress-Strain Curves for Plates in Compression', Dept of Naval Architecture & Ocean Engg, Univ. of Glasgow, Report, 1984.

3-9 Lin, Y.T. and Frieze, P.A. 'Ultimate Longitudinal Strength of the Ship's Hull Girder', Dept of Naval Architecture & Ocean Engg, Univ. of Glasgow, Report No. NAOE-82-34, 1982.

3-10 Livesly, R.K. and Birchall, P.C. 'Analysis of a Loaded Cantilever Plate by Finite Difference Methods', R.A.E. Technical Note M.S. 26, 1956.

3-11 Allen, D.N. de G. and Severn, R.T. 'The Stresses in Foundation Rafts', Proc. Instn Civ. Engrs, Vol. 15, 1960.

3-12 Redshaw, S.C. and Rushton, K.R. 'Study of Various Boundary Conditions for Electrical Analogue Solutions of the Extension and Flexure of Flat Plates', Aeronaut. Quarterly, Vol. 12, 1961.

3-13 Day, A.S. 'An Introduction to Dynamic Relaxation', Engineer, Vol. 219, 1965.

3-14 Otter, J.R.H. 'Computations for Prestressed Concrete Reactor Pressure Vessels using Dynamic Relaxation', Nucl. Struct. Engg, Vol. 1, 1965.

3-15 Rushton, K.R. 'Dynamic Relaxation Solutions of Elastic-Plastic Problems', Jnl of Strain Analysis, Vol. 3, No. 1, 1968.

3-16 Frieze, P.A., Hobbs, R.E. and Dowling, P.J. 'Application of Dynamic Relaxation to the Large-Deflection Elasto-Plastic Analysis of Plates', Computers and Structures, Vol. 8, 1978.

3-17 Frieze, P.A. 'Elasto-Plastic Buckling in Short Thin-Walled Beams and Columns', Proc. Instn Civ. Engrs, Part 2, Vol. 65, 1978.

3-18 Cassell, A.C. 'Shells of Revolution under Arbitrary Loading and the use of Fictitious Densities in Dynamic Relaxation', Proc. Instn Civ. Engrs, Part 2, Vol. 45, 1970.

3-19 Frieze, P.A. and Sachinis, A. 'Buckling Analysis of Singly- and Doubly-Curved Shells using Dynamic Relaxation', 1st International Numerical Methods Conference, Univ. of Swansea, Sept. 1980.

3-20 Sachinis, A. 'Ultimate Strength of Unstiffened and Ring Stiffened Circular Cylinders', PhD Thesis, Univ. of Glasgow, 1982.

3-21 Frieze, P.A. 'Interactive Buckling Analysis of Box Sections using Dynamic Relaxation', Computers and Structures, Vol. 9, 1978.

3-22 Cassell, A.C. and Hobbs, R.E. 'Numerical Stability of Dynamic Relaxation Analysis of Non-Linear Structures', International Jnl of Numerical Methods in Engg, Vol. 10, 1976.

3-23 Carlsen, C.A. 'Collapse of Stiffened Panels in Compression. Report I: Plate between Stiffeners', Det norske Veritas, Report No. 76-306, 1976.

3-24 Ostapenko, A. 'Ultimate Strength Design of Wide Stiffened Panels Loaded Axially and Normally', Proc. Symposium on Non-Linear Techniques and Behaviour in Structural Analysis, TRRL, Crowthorne, UK, Dec. 1974.

3-25 Dowling, P.J. and Frieze, P.A. 'Residual Stresses in Welded Steel Box Girder Flanges', Proc. of International Conference on Residual Stresses in Welded Construction and Their Effects, London, Nov. 1977.

3-26 Timoshenko, S.P. and Gere, J.M. 'Theory of Elastic Stability', Second Ed., McGraw-Hill Book Company, New York, 1961.

3-27 Rushton, K.R. 'Large Deflection of Variable Thickness Plates', International Jnl of Mech. Sci., Vol. 10, 1968.

3-28 Cassell, A.C. and Hobbs, R.E. 'Dynamic Relaxation', Proc. Symposium IUTAM, Liège, Publ. Univ. of Liège, 1971.

3-29 Wood, W.L. 'Comparison of Dynamic Relaxation with Three Other Iterative Methods', The Engineer, Vol. 221, 1967.

3-30 Basu, A.K. and Dawson, J.M. 'Orthotropic Sandwich Plates', Proc. Instn Civ. Engrs, Vol. 45, 1970.

Chapter 4:

4-1 Horne, M.R., Montague, P. and Narayanan, R. 'Influence on Strength of Compression Panels of Stiffener Section, Spacing and Welded Connection', Proc. Instn Civ. Engrs, Part 2, Vol. 63, 1977.

4-2 'Merrison Rules: Part IV: Materials and Workmanship', UK, 1973.

4-3 'BS5400 Steel, Concrete and Composite Bridges - Draft', UK, 1979.

4-4 'European Recommendations for Steel Construction', ECCS, 1978.

4-5 Massonnet, Ch. and Janss, J. 'A State of Art Report on Tolerances in Steel Plated Structures', The Design of Steel Bridges, Editors Rockey, K.C. and Evans, H.R., Granada Publishing, 1980.

Chapter 5:

5-1 Nibbering, J.J.W. 'Fatigue of Ship Structures', International Shipbuilding Progress, Sept. 1963.

5-2 Lewis, E.V. and Zubaly, R.B. 'Predicting Hull Bending Moments for Design', Proc. Symposium on Extreme Loads Response, Arlington, USA, 1981.

5-3 Valsgård, S. 'Ultimate Capacity of Plates in Transverse Compression', Det norske Veritas Report No. 79-0104, 1979.

5-4 Dier, A.F. and Dowling, P.J. 'The Strength of Plates subjected to Biaxial Forces', Proc. Conference on Behaviour of Thin-Walled Structures, Glasgow, 1983.

Chapter 6:

6-1 Guile, P.J.D. and Dowling, P.J. 'Steel Box Girders, Model 2 - Progress Report 1', Engg Structure Lab., Imperial College, London, Nov. 1971.

6-2 Frieze, P.A. and Dowling, P.J. 'Steel Box Girders, Model 2 - Progress Report 2', Engg Structures Lab., Imperial College, London, June 1972.

6-3 Chatterjee, S. and Dowling, P.J. 'Steel Box Girders, Model 2 - Progress Report 3', Engg Structures Lab., Imperial College, London, May 1972.

6-4 Guile, P.J.D. and Dowling, P.J. 'Steel Box Girders, Model 4 - Progress Report 1', Engg Structures Lab., Imperial College, London, Feb. 1972.

6-5 Moolani, F.M. and Dowling, P.J. 'Steel Box Girders, Model 4 - Progress Report 2', Engg Structures Lab., Imperial College, London, March 1972.

6-6 Chatterjee, S. and Dowling, P.J. 'Steel Box Girders, Model 4 - Progress Report 3', Engg Structures Lab., Imperial College, London, June 1972.

Chapter 7:

7-1 Evans, J.H. Contribution to Discussion of ref. [1-2].

7-2 Mansour, A.E. and Faulkner, D. 'On Applying the Statistical Approach to Extreme Sea Loads and Ship Hull Strength', Trans RINA, Vol. 115, 1973.

7-3 Dwight, J.B. 'Collapse of Steel Compression Panels', in 'Developments in Bridge Design and Construction', Crosby Lockwood, London, 1971.

7-4 Oakley, O.H. Contribution to Discussion of ref. [1-3].

7-5 Faulkner, D. and Sadden, J.A. 'Toward a Unified Approach to Ship Structural Safety', Trans RINA, Vol. 121, 1979.

7-6 Wong, Y.L. 'Some Considerations in the Ultimate Strength of Ships', MSc Thesis, Univ. of Glasgow, 1977.

Appendix A

Manual of Computer Program PLATSS

Card A XMAX, DELX, YMAX, DELY (4F10.0)

XMAX = Plotting range to which X-coordinate (strain) is limited

DELX = Interval of annotation along X-axis

YMAX = Plotting range to which Y-coordinate (stress) is limited

DELY = Interval of annotation along Y-axis

Default values for these variables are 3.10, 0.20, 1.05, 0.10 respectively.

Card B IEND, IOUT,INCR (3I2)

IEND = Index for end conditions of the interpolating cubic splines [2-6]

= 1 the splines approach linearity at their extremities

= 2 the splines approach parabolas at their extremities

= 3 the end curvatures are found from linear extrapolation from two internal points

IOUT = Index to control output of the generated average stress-strain curves

= 1 output all values of stresses first, and then of strains

= 2 output values of stress and corresponding strain simultaneously

INCR = Interval of data points to be output

Default values for these variables are 1, 1, 1 respectively.

Card C BETA, WZERO, SIGMR (3F10.0)

BETA = Non-dimensional plate slenderness ratio (β)

WZERO = Initial deflection ratio of the plate (δ_o'/β^2)

SIGMR = Residual compressive stress non-dimensionalised with the yield stress (σ_r')

Since one Card C is needed for each case, there will be as many Cards C as the number of plates being generated sequentially in a same run.

Card D A card with '9999' appearing in columns 6-9 is always the last entry in the data deck.

Appendix B

Manual of Computer Program HULLG

Card A TITLE (A80)

TITLE = Alphanumeric parameter to provide the title on the program output.

Card B NOINS, NOMAT, NOSTPL, ISYSM, IPRNT, IPLOT, CONVX, CONVY

(6I5, 2F10.0)

NOINS = Number of different stiffeners included in the cross-section. Two stiffeners with either different geometries or of different materials are considered different

NOMAT = Number of different materials considered in the cross-section. A material is defined by its yield stress (YDST) and Young's modulus (YGMD)

NOSTPL = Number of the average compressive stress-strain curves of the virtually identical stiffened panels included in the cross-section

ISYSM = Index to control input of the cross-section

= 0 the whole cross-section is input, and plotted if IPLOT $\neq$ 0

= 1 half the cross-section is input, and plotted if IPLOT $\neq$ 0

= 2 half the cross-section is input, but the whole cross-section will be plotted if IPLOT $\neq$ 0

IPRNT = Index to control the program output

= 0 final result is output only

= 1 both intermediate and final results will be printed out

IPLOT = Index for plotting the cross-section

= 0 no plot at all

= 1 the cross-section profile is plotted only

= 2 the cross-section profile is plotted, and discretised into plate elements, stiffened panels, or hard corners

= 3 in addition to the above case, the discretised elemental members will be annotated

CONVX = Factor of converting the digitised horizontal coordinates of the cross-section to the real values

CONVY = Conversion factor for vertical coordinates

Card C One such card is required for each elemental member.

DUMMY, ITYPE, NUMBR, NOSTT, NOPMM, NOSPP, ITNSS,

X1, Y1, X2, Y2, PLTHH, ETAA (A4, 6I2, 4X, 6F10.0)

DUMMY = Alphanumeric parameter to provide the name of elemental members on the program output and/or plot

ITYPE = Index to control the intput mode of elemental members

= 1 the elemental member is defined by its dimension and location. Coordinates of both edge 1 and edge 2 of the elemental member are input

= 0 only coordinates of edge 2 of the elemental member are input. Coordinates of edge 1 are assumed to be the same as the coordinates of edge 2 of the previous member

= - 1 the elemental member is defined by its area, the vertical coordinate of its centroid, and the moment of inertia about its horizontal centroidal axis of the cross-section

= 99 after the last elemental member is input

NUMBR = Number of longitudinal stiffeners attached to the plate

NOSTT = Stiffener reference number of longitudinal attached to the plate

NOPMM = Material reference number for the plate of the elemental member

NOSPP = Reference number to identify the average compressive stress-strain curve for the elemental member

ITNSS = Index to specify the type of tensile behaviour of the plate as indicated in Fig. 5-6

= 0 elastic-perfectly plastic material

= 1 the tensile stiffness of the plate is reduced due to the tension yielding blocks caused by welding. A linear relationship between stress and strain is assumed

= 2 the reduced stiffness is accounted for by a parabolic relationship between stress and strain

when ITYPE = 1;

X1, Y1, X2, Y2 = Horizontal and vertical coordinates of edge 1 and edge 2 respectively of the elemental member. The edges for each elemental member are located at the points such that the longitudinal stiffeners attached to the plate are equally spaced. Edge 1 and edge 2 are chosen in a counter-clockwise sequence around the cross-section as shown in Fig. 5-2

when ITYPE = 0;

X1, Y1, X2, Y2 = Same definition as in the case of ITYPE = 1. However, only the values of X2 and Y2 need to be input. The coordinates of edge 1 are taken to be identical to those of edge 2 of the previous elemental member. Usually, this mode is employed when elemental members are continuously input around the midship section.

when ITYPE = - 1;

X1 = Area of the cross-section

Y1 = Vertical coordinate of the centroid of the cross-section

X2 = Moment of inertia of the cross-section about the horizontal centroidal axis

Y2 = Undefined

PLTHH = Plate thickness when ITYPE = 1 or 0

= Undefined when ITYPE = - 1

ETAA = Ratio of the width of tension yielding blocks induced by welding to the plate thickness

The set of Cards C is terminated by a card with '99' appearing in columns 5-6.

Card D (NFTA(NS), NOSM(NS), WBDE(NS), WBTH(NS), FLDE(NS), FLTH(NS), NS = 1, NOINS)(2I5, 6F10.0)

NFTA(NS) = Index to define the NSth stiffener type (Fig. 5-3)

= 1 flat bar

= 2 T-section

= 3 angle with flange oriented in the clockwise direction

= 4 angle with flange oriented in the counter-clockwise direction

NOSM(NS) = Material reference number for the NSth stiffener

WBDE(NS) = Web depth of the NSth stiffener

WBTH(NS) = Web thickness of the NSth stiffener

when NFTA(NS) = 1;

FLDE(NS) = Undefined

FLTH(NS) = Undefined

when NFTA(NS) = 2, 3, 4;

FLDE(NS) = Flange width of the NSth stiffener

FLTH(NS) = Flange thickness of the NSth stiffener

Since one Card D is needed for each stiffener, there will be NOINS Cards D included in the data deck.

Card E (YDST(NM), YGMD(NM), NM = 1, NOMAT)(2F10.0)

YDST(NM) = Yield stress of the NMth material

YGMD(NM) = Young's modulus of the NMth material

There are NOMAT Cards E in the data deck.

Card F NDATA(JS), NDTYPE, NREV

NDATA(JS) = Number of data points representing the JSth average compressive stress-strain curve for a stiffened panel

NDTYPE = Index to control input format for values of average stresses and strains

= 2 Card G is employed

= 1 Card H and Card I are employed

NREV = Parameter indicating the order of data points

= 0 data points are input in increasing order

= 1 data points are input in decreasing order.

Card G (STRS(ID,JS), STRN(ID,JS), ID = 1, NDATA(JS))(2F10.0)

STRS(ID,JS) = Stress at the IDth data point of the JSth average compressive stress-strain curve for a stiffened panel

STRN(ID,JS) = The corresponding value of strain

One Card G is required for each data point.

Card H (STRS(ID,JS), ID = 1, NDATA(JS))(8F10.0)

STRS(ID,JS) = Same definition as for Card G.

Card I (STRN(ID,JS), ID = 1, NDATA(JS))(8F10.0)

STRN(ID,JS) = Same definition as for Card G.

One Card F and a set of Cards G (when NDTYPE = 2) or a set of Cards H and Cards I (when NDTYPE = 1) are needed for each average compressive stress-strain curve for a stiffened panel.

Card J ALLOW, ITMAX, IPHI (F10.0, 2I10)

ALLOW = Convergence criterion parameter. In the process of determining the effective neutral axis location of the midship section, convergence is assumed to have been achieved when the following equation is satisfied

$$\left| \frac{|AFT - AFC|}{|AFT + AFC|} \right| < ALLOW$$

where AFT and AFC are computed tensile and compressive axial forces respectively acting on the two parts of the midship section separated by the assumed neutral axis. The default value of this parameter is 10^{-6}

ITMAX = Maximum number of iteration cycles allowed in determining the effective neutral axis location of the

midship section. When iterations are being performed, the program will continue until either the convergence is achieved or the number of cycles reaches ITMAX. A value of 100 is used as the default value of ITMAX

IPHI = Index for input of curvature increments

= 0 non-dimensional curvature increments are input

= 1 real curvature increments are input.

Card K PHIA(1) (F10.0)

PHIA(1) = Initial non-dimensional curvature when IPHI = 0 or initial real curvature when IPHI = 1.

Card L PH, NOPHI (F10.0, I10)

PH = Total non-dimensional curvature at the end of the next load range when IPHI = 0 or total real curvature at the end of the next load range when IPHI = 1

NOPHI = Number of increments in the next load range

One Card L is needed for each load range. A set of Cards L is terminated by a card with '99999' appearing in columns 16 - 20.

Note = when a parameter is undefined, the field is left blank.

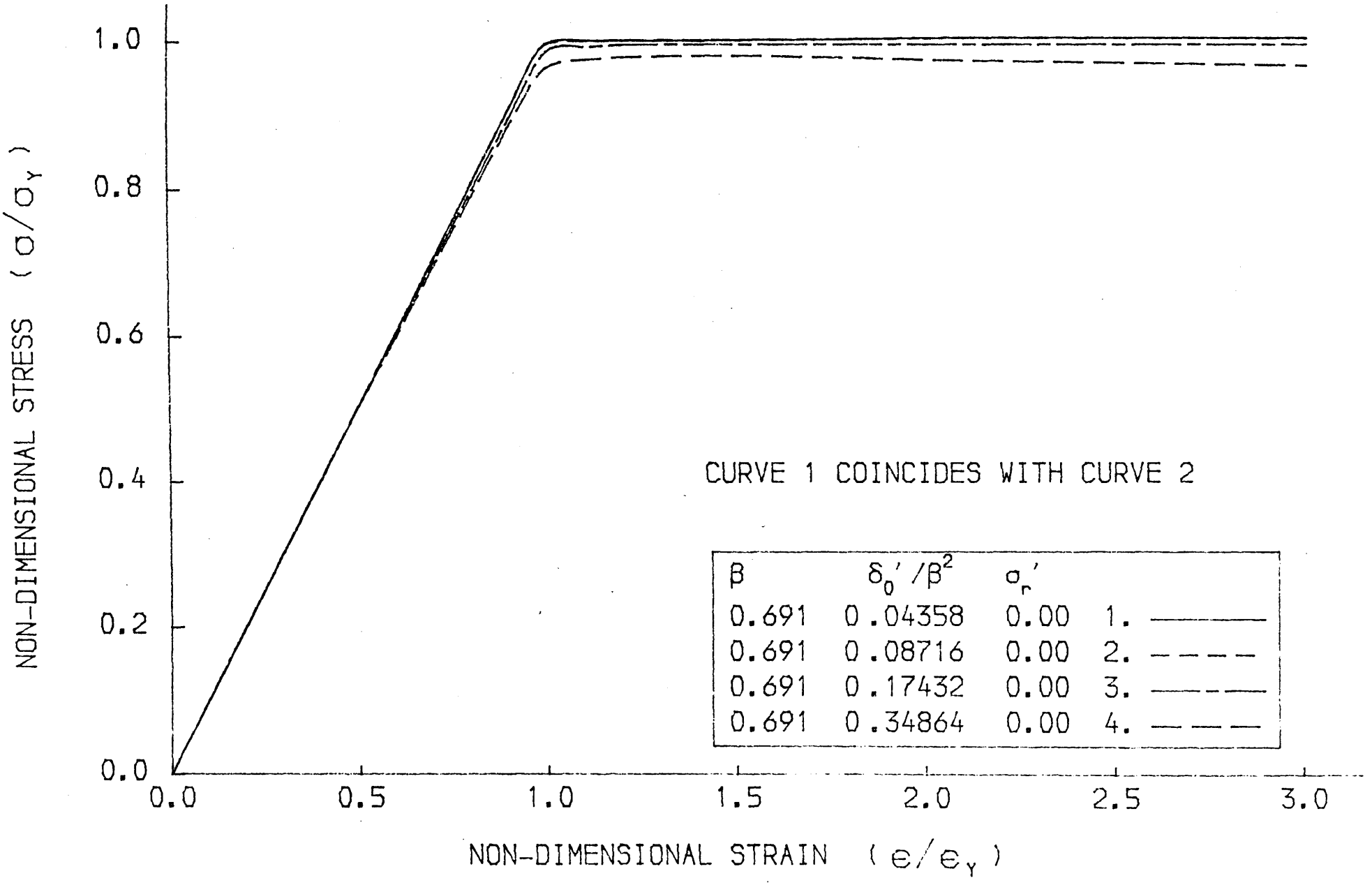

FIG.2-1 AVERAGE STRESS-STRAIN CURVE FOR THE PLATE

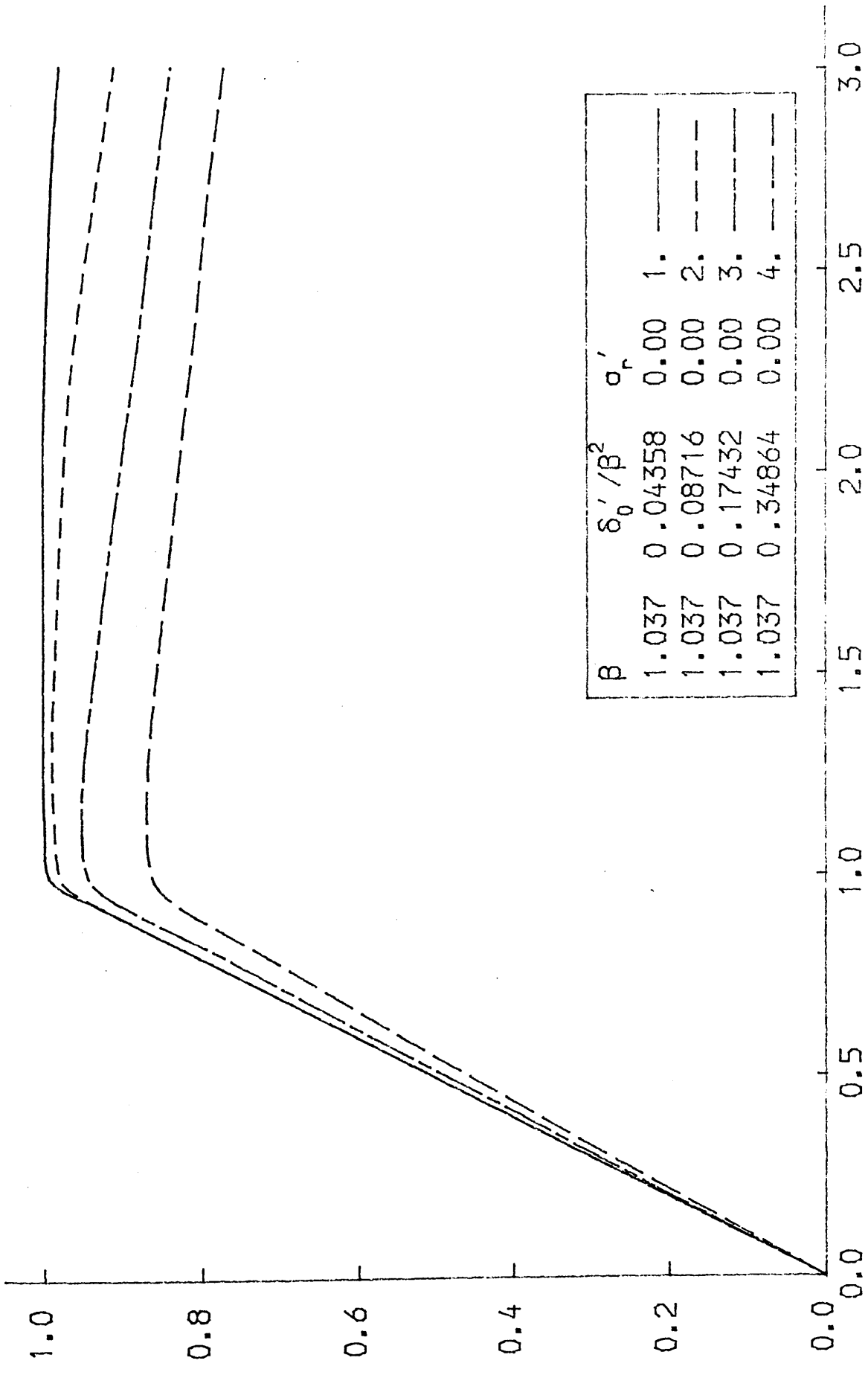

FIG.2-2 AVERAGE STRESS-STRAIN CURVE FOR THE PLATE

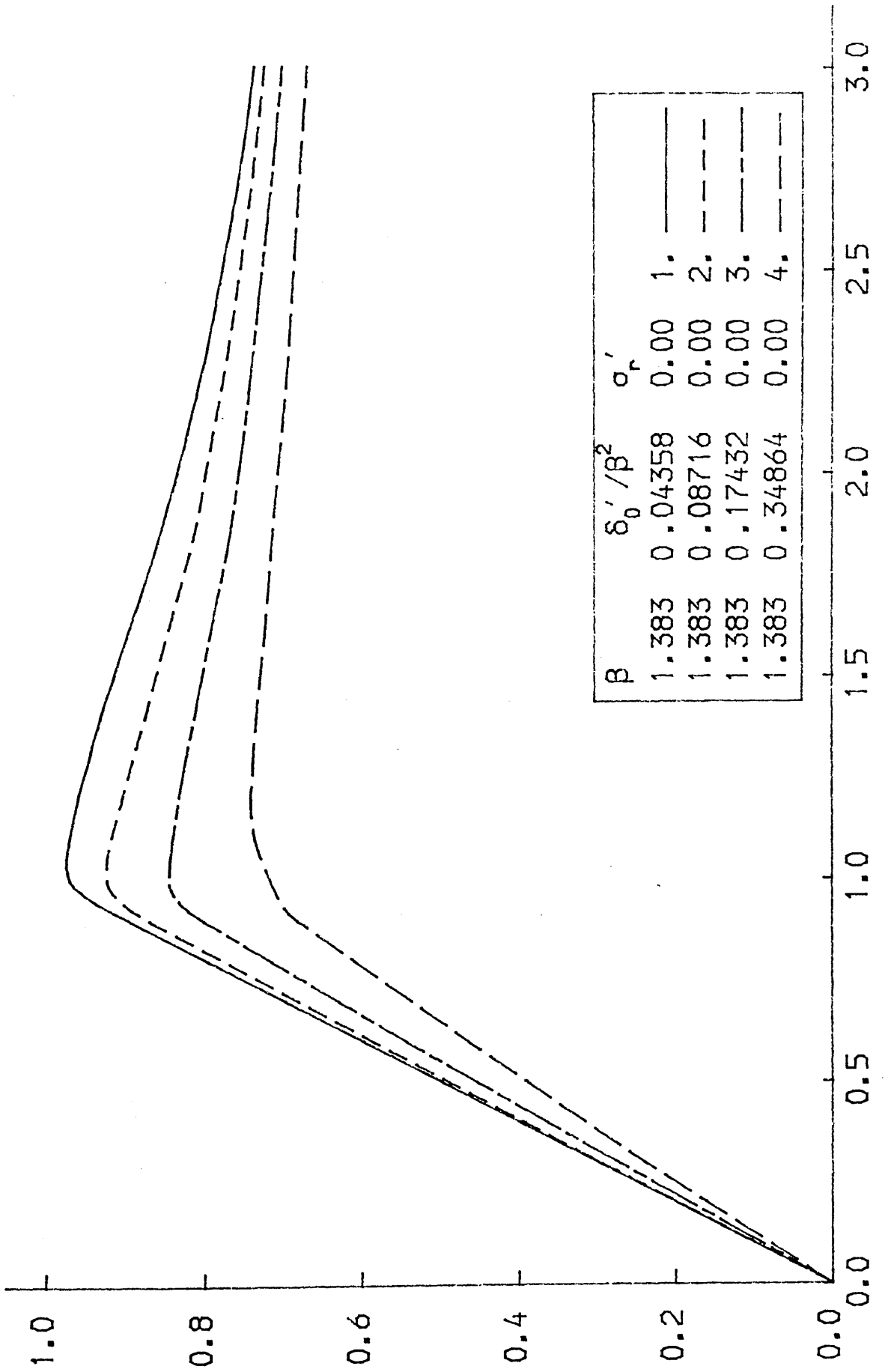

FIG.2-3 AVERAGE STRESS-STRAIN CURVE FOR THE PLATE

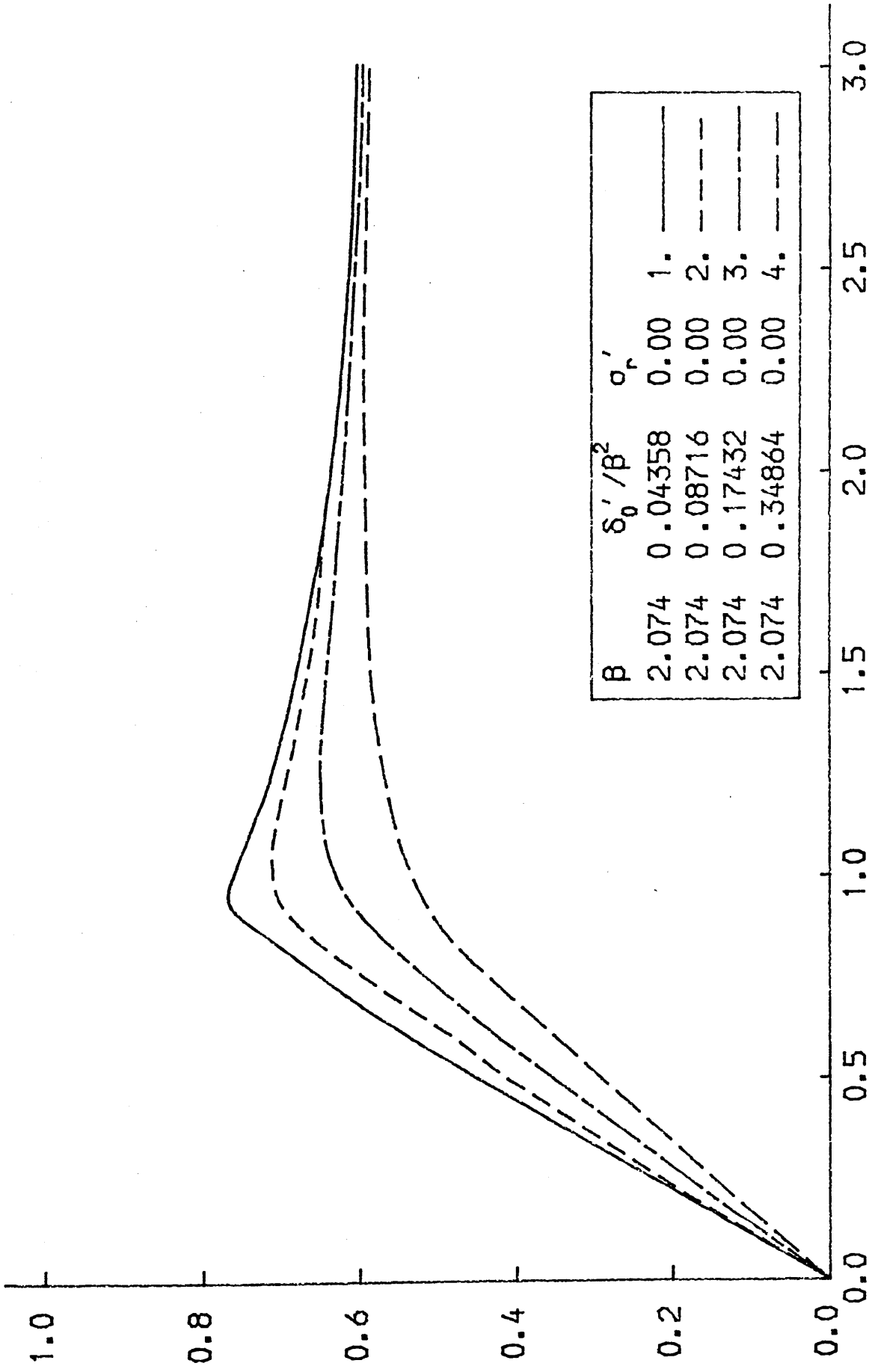

FIG.2-4 AVERAGE STRESS-STRAIN CURVE FOR THE PLATE

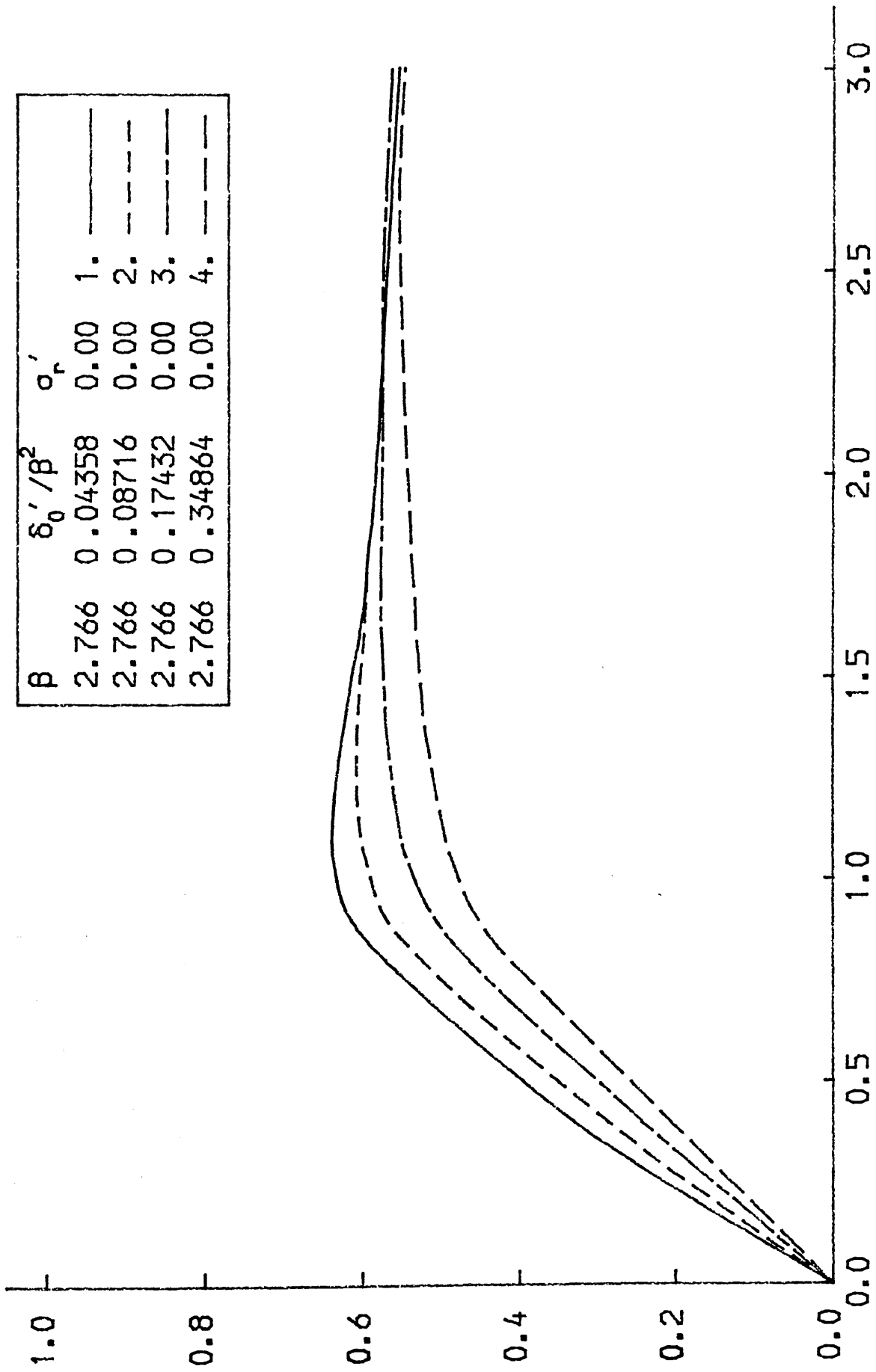

FIG.2-5 AVERAGE STRESS-STRAIN CURVE FOR THE PLATE

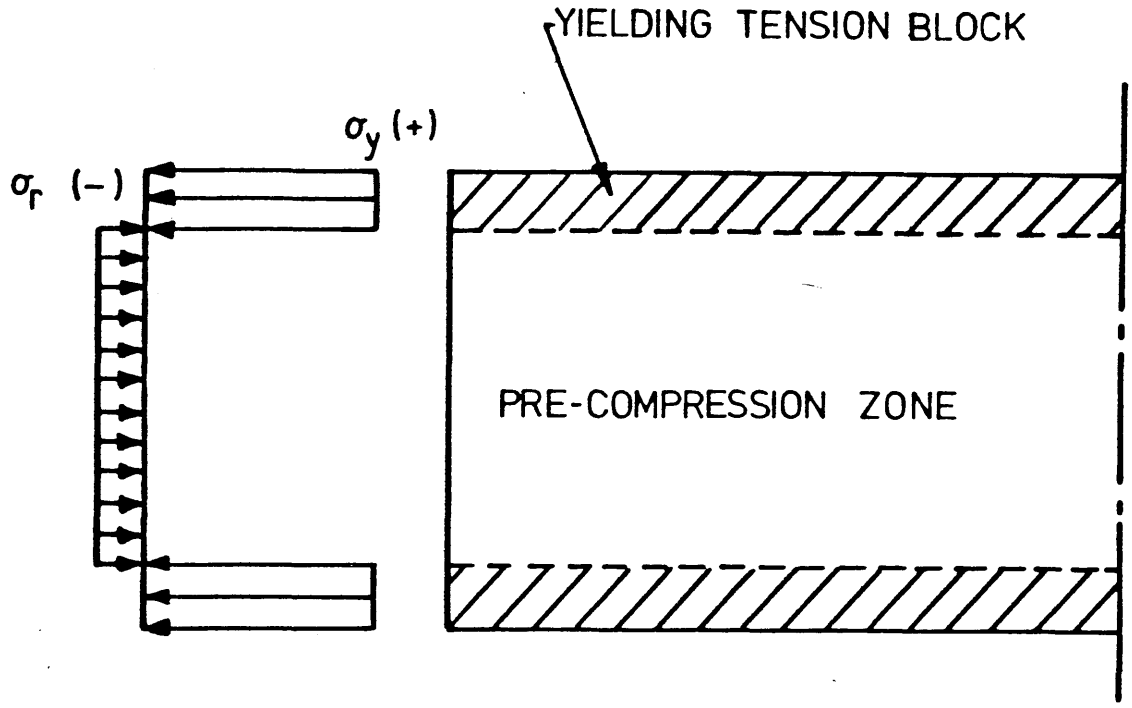

FIG. 2-6 IDEALIZED MODEL FOR WELDING RESIDUAL STRESSES IN PLATE.

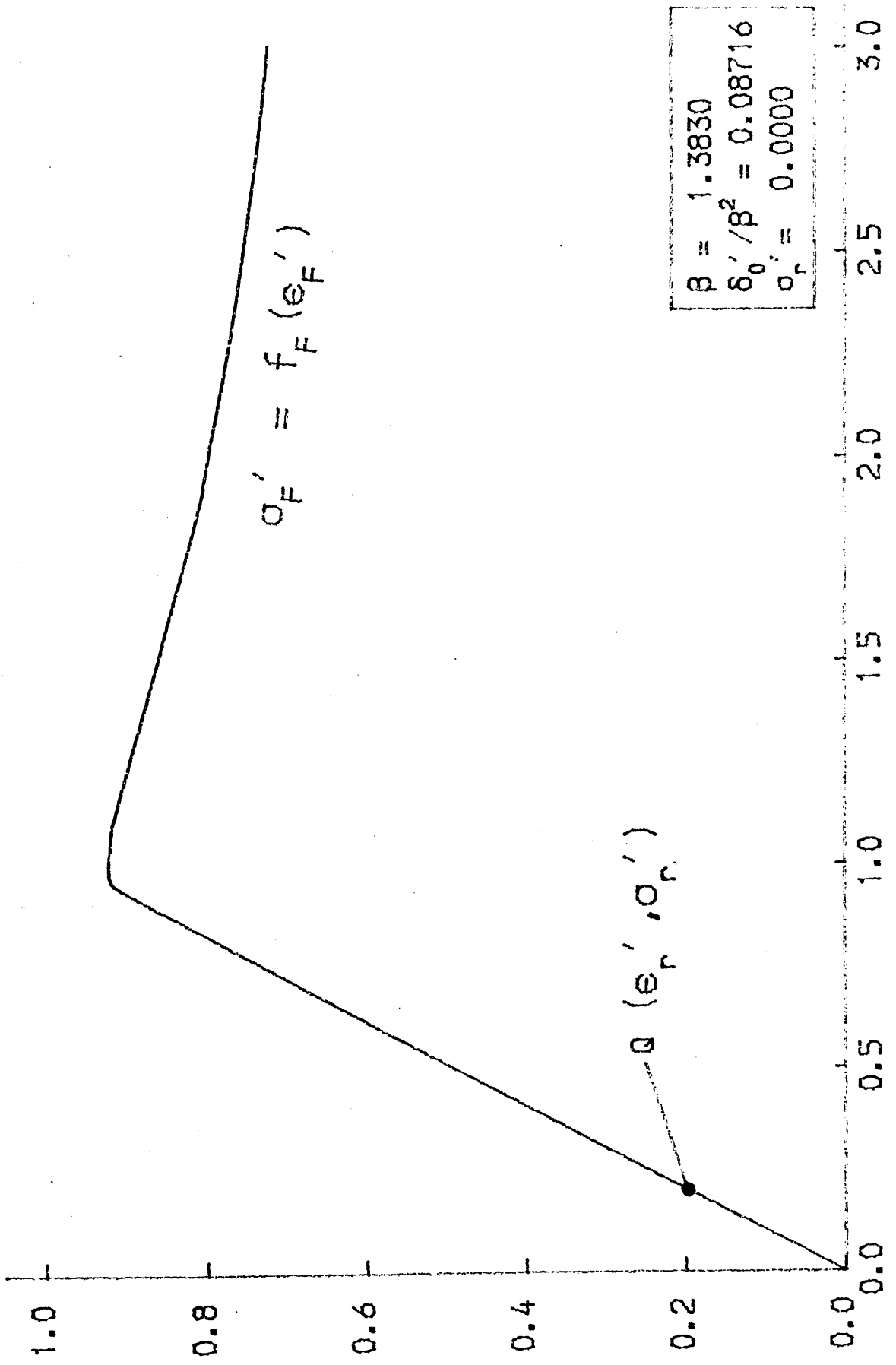

FIG.2-7 AVERAGE STRESS-STRAIN CURVE FOR STRESS FREE PLATE

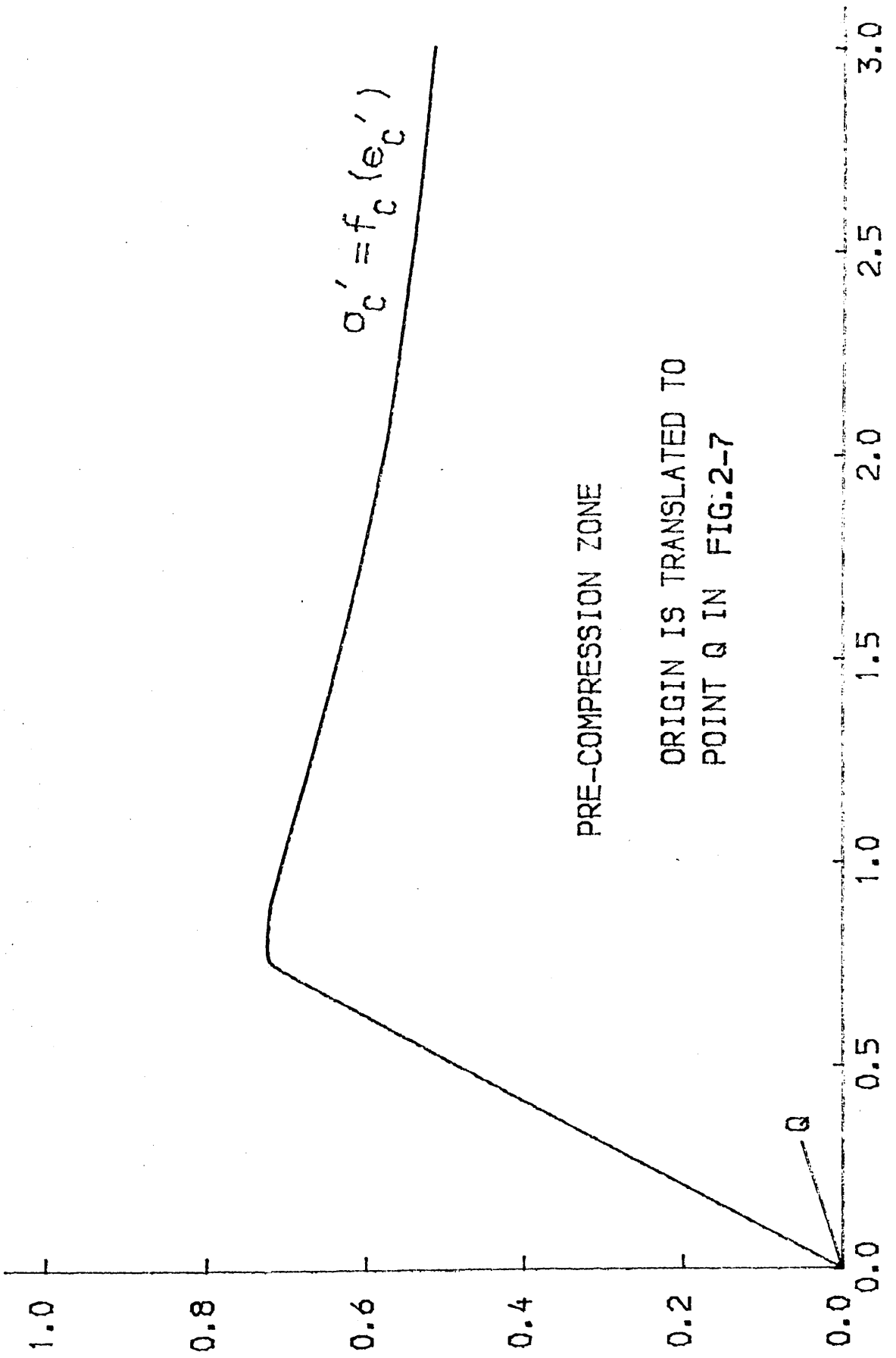

FIG.2-8 AVERAGE STRESS-STRAIN CURVE FOR WELDED PLATE

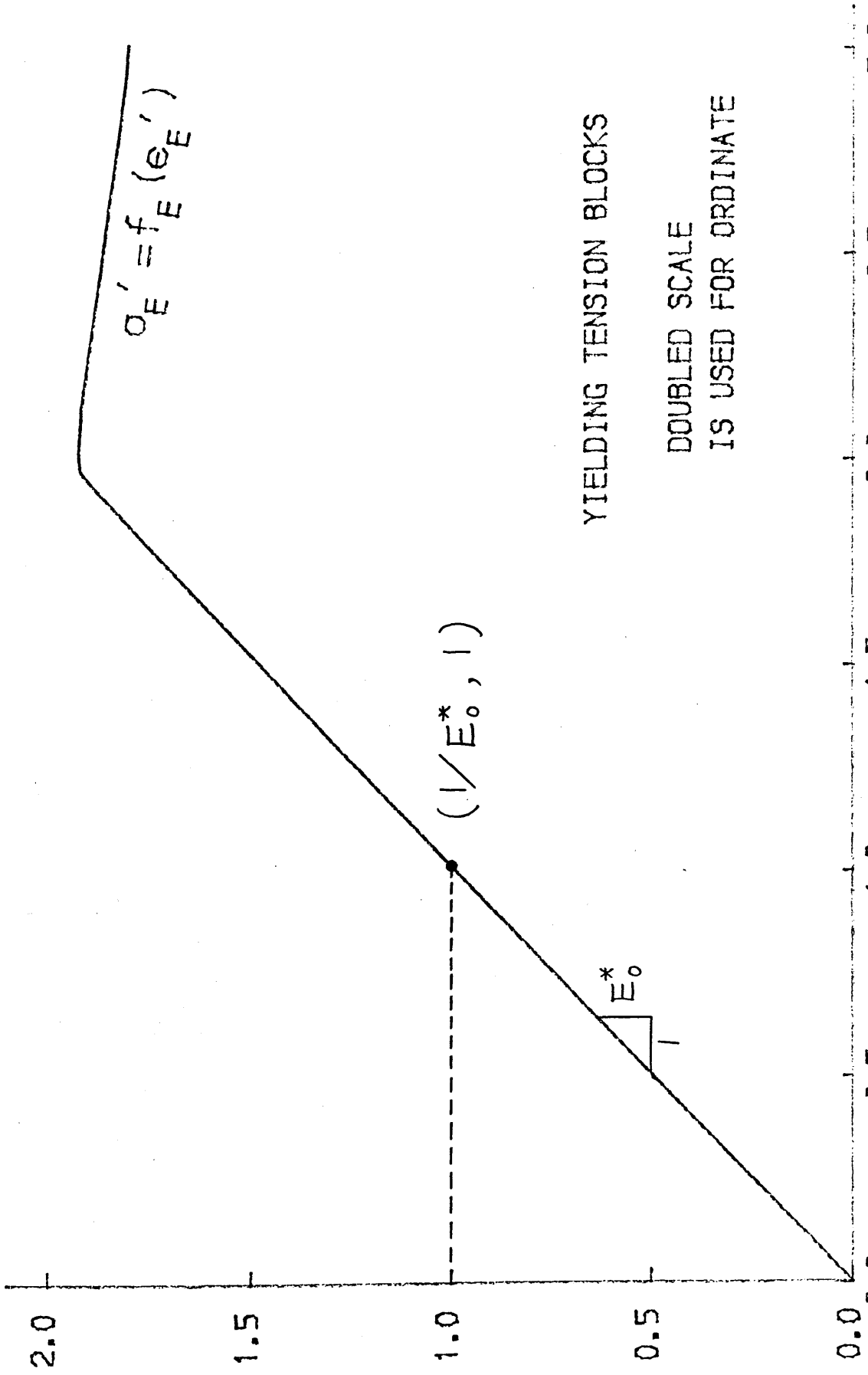

FIG.2-9 AVERAGE STRESS-STRAIN CURVE FOR WELDED PLATE

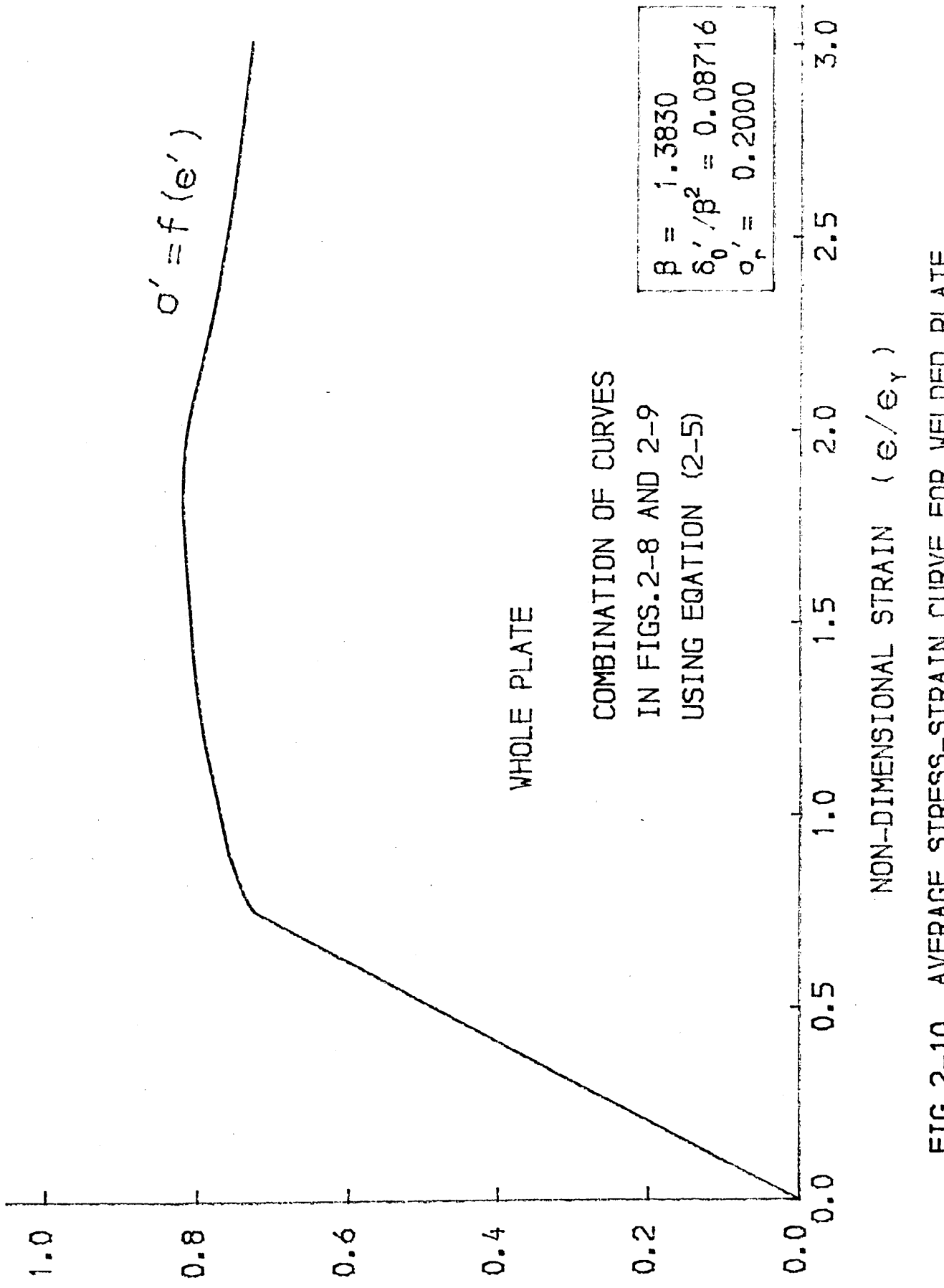

FIG.2-10 AVERAGE STRESS-STRAIN CURVE FOR WELDED PLATE

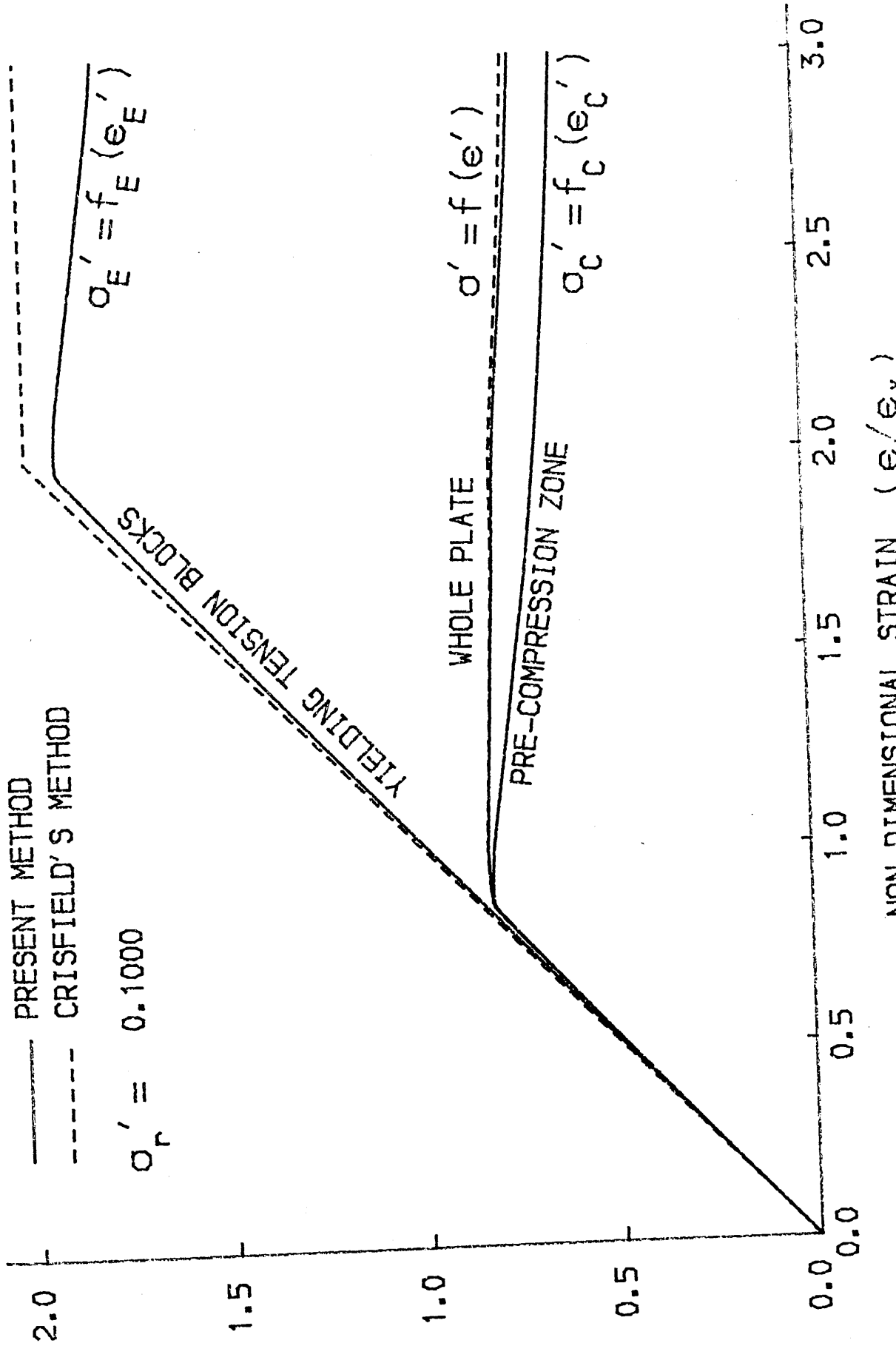

FIG.2-11 AVERAGE STRESS-STRAIN CURVE FOR WELDED PLATE

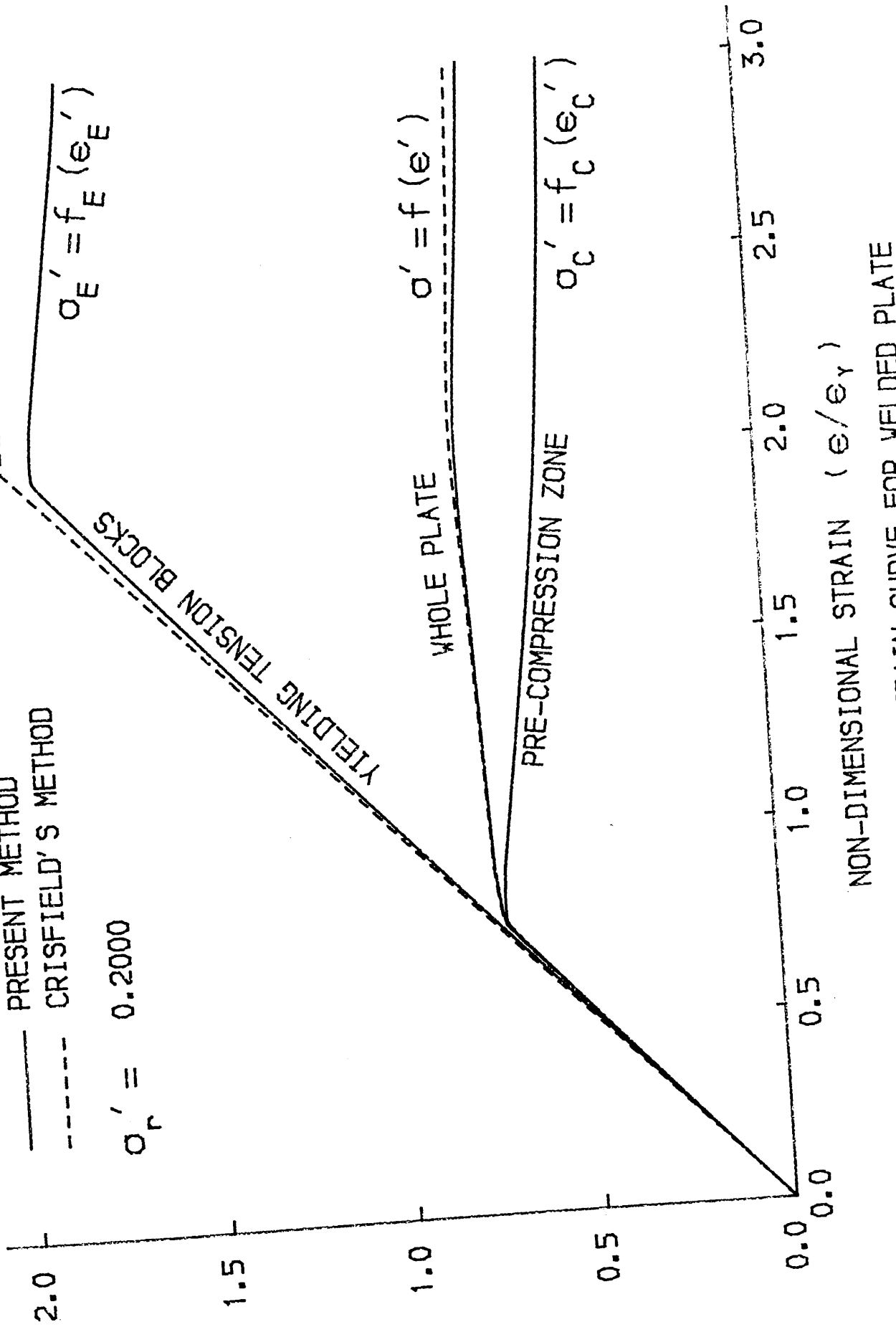

FIG.2-12 AVERAGE STRESS-STRAIN CURVE FOR WELDED PLATE

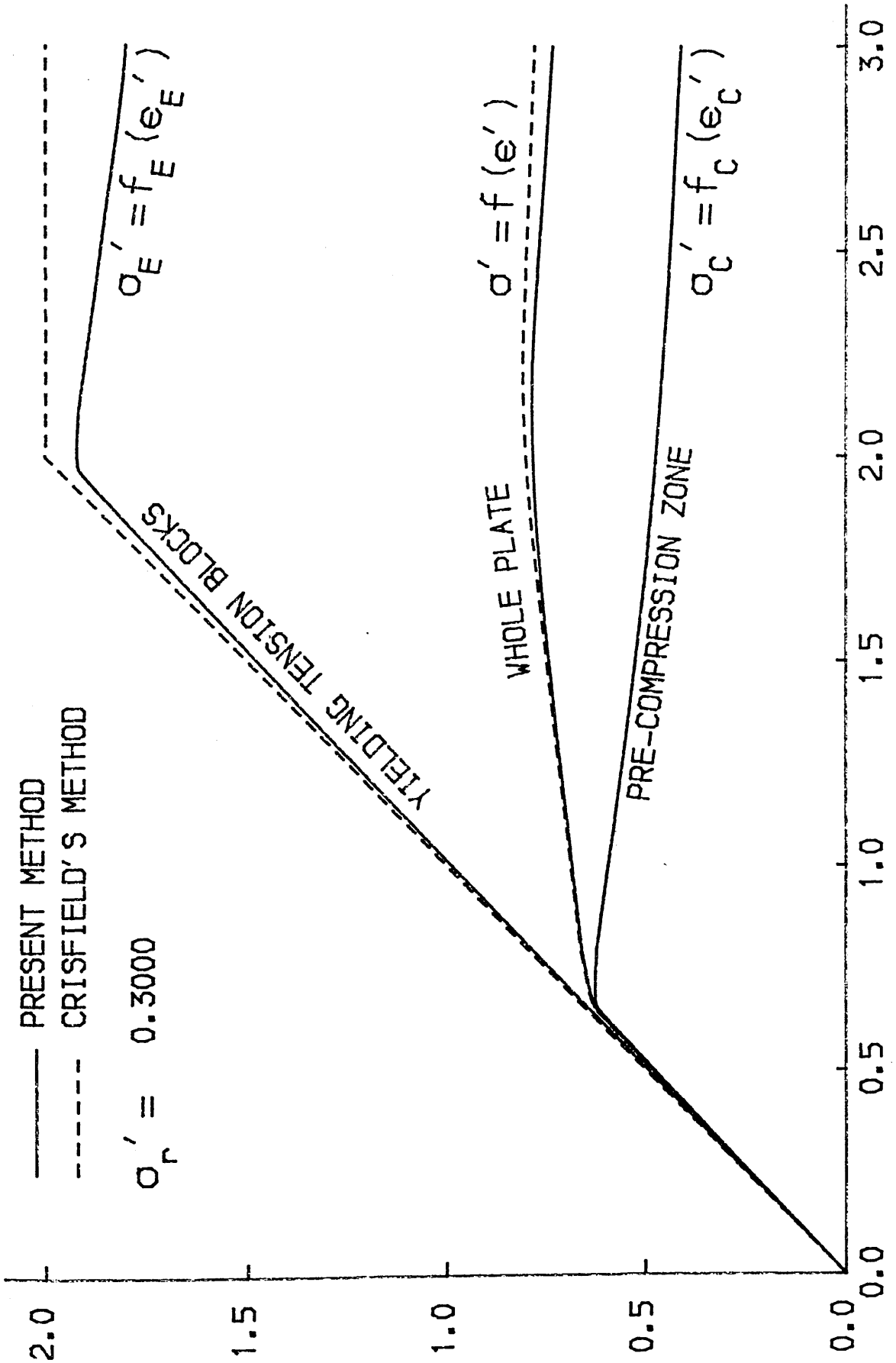

FIG.2-13 AVERAGE STRESS-STRAIN CURVE FOR WELDED PLATE

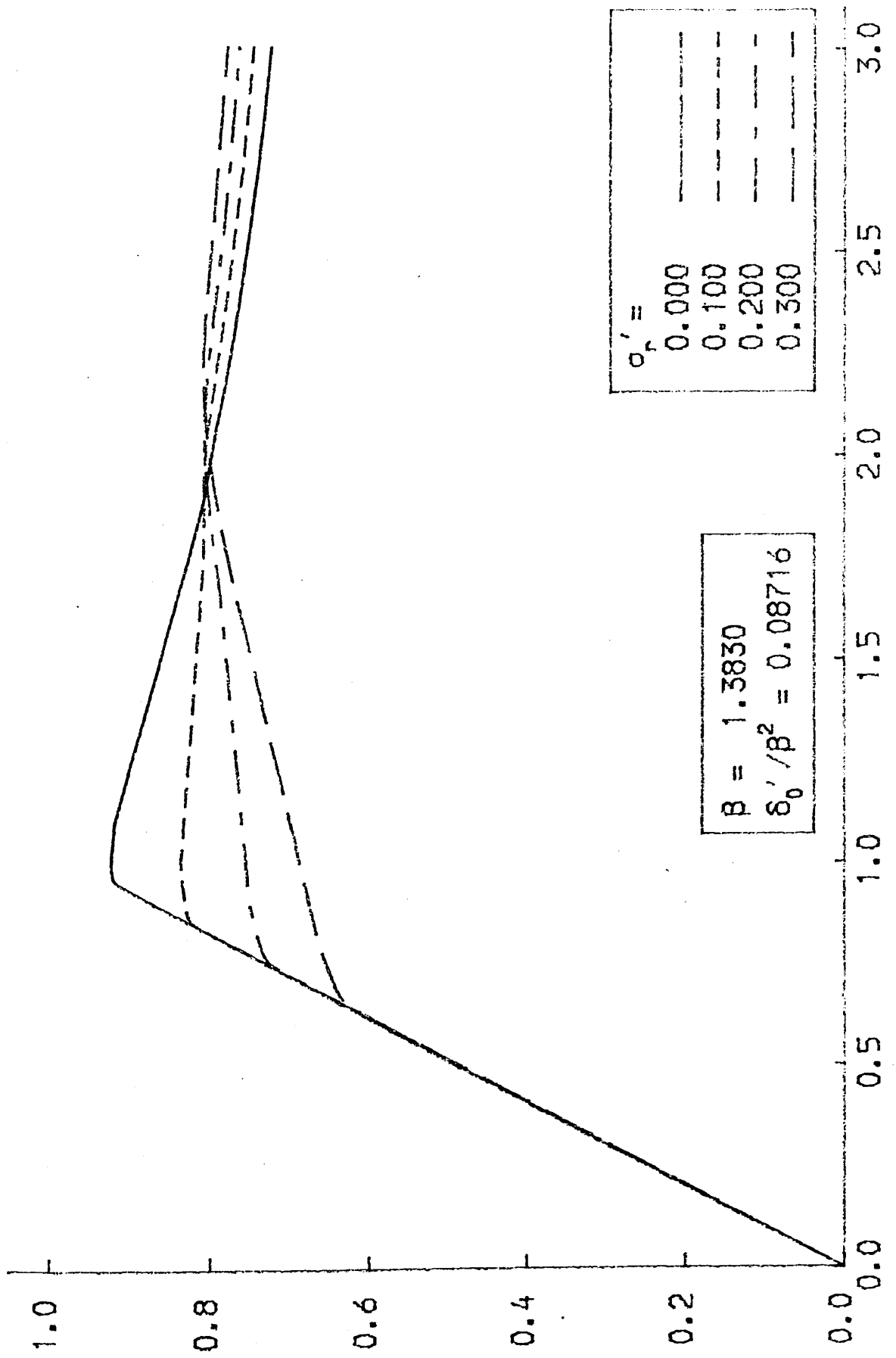

FIG.2-14 AVERAGE STRESS-STRAIN CURVE FOR THE PLATE

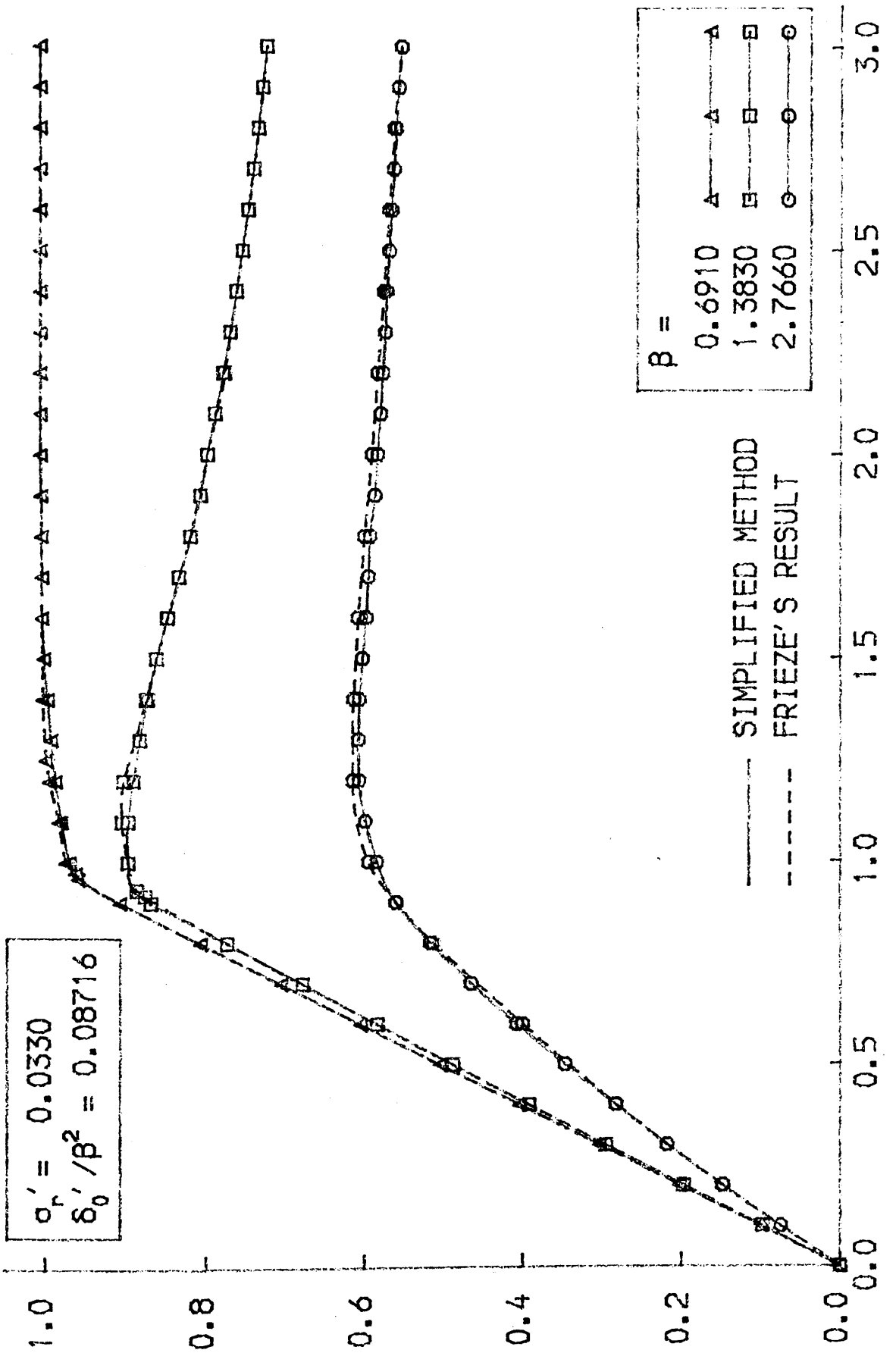

FIG.2-15 AVERAGE STRESS-STRAIN CURVE FOR THE PLATE

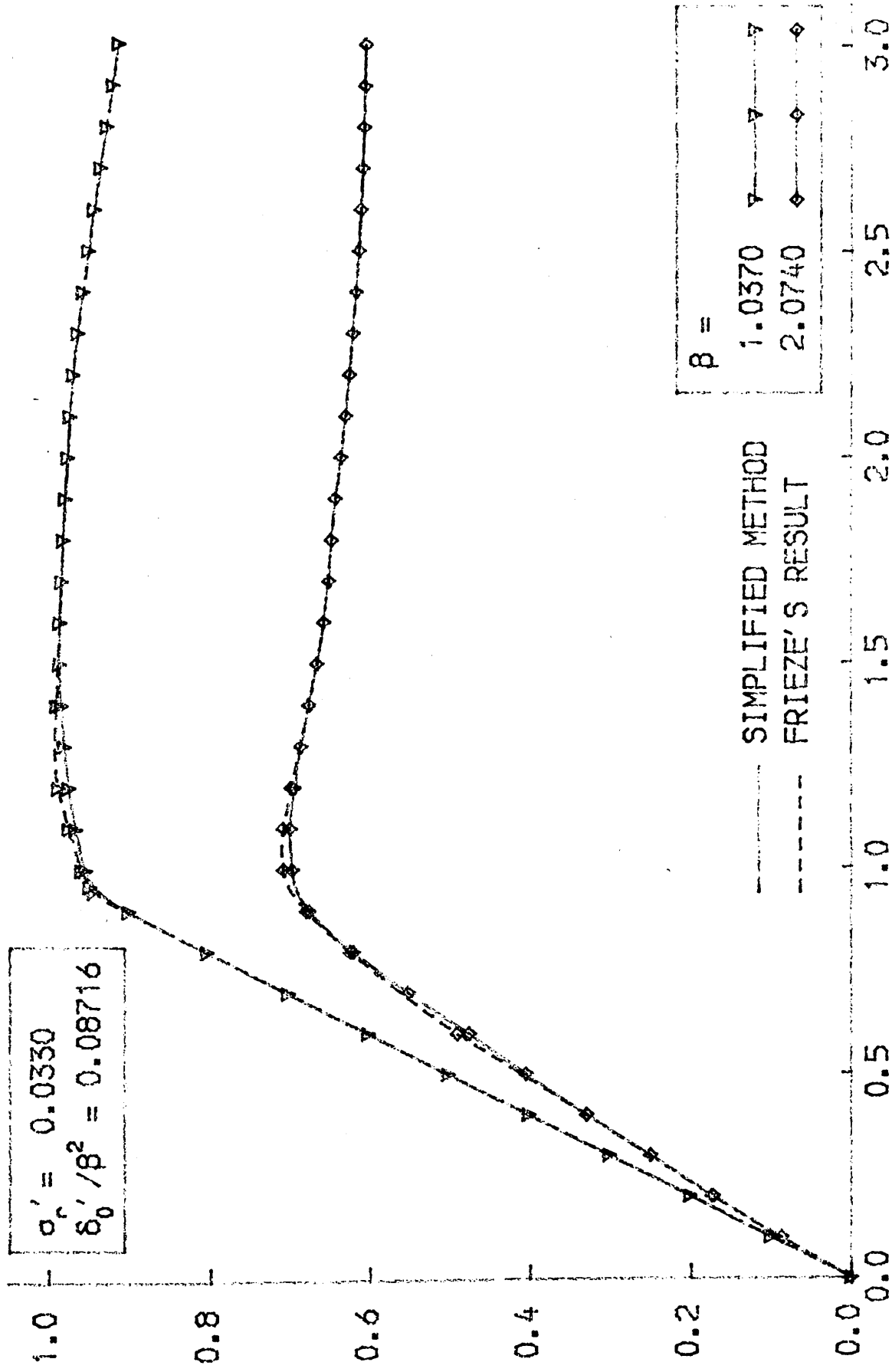

FIG.2-16 AVERAGE STRESS-STRAIN CURVE FOR THE PLATE

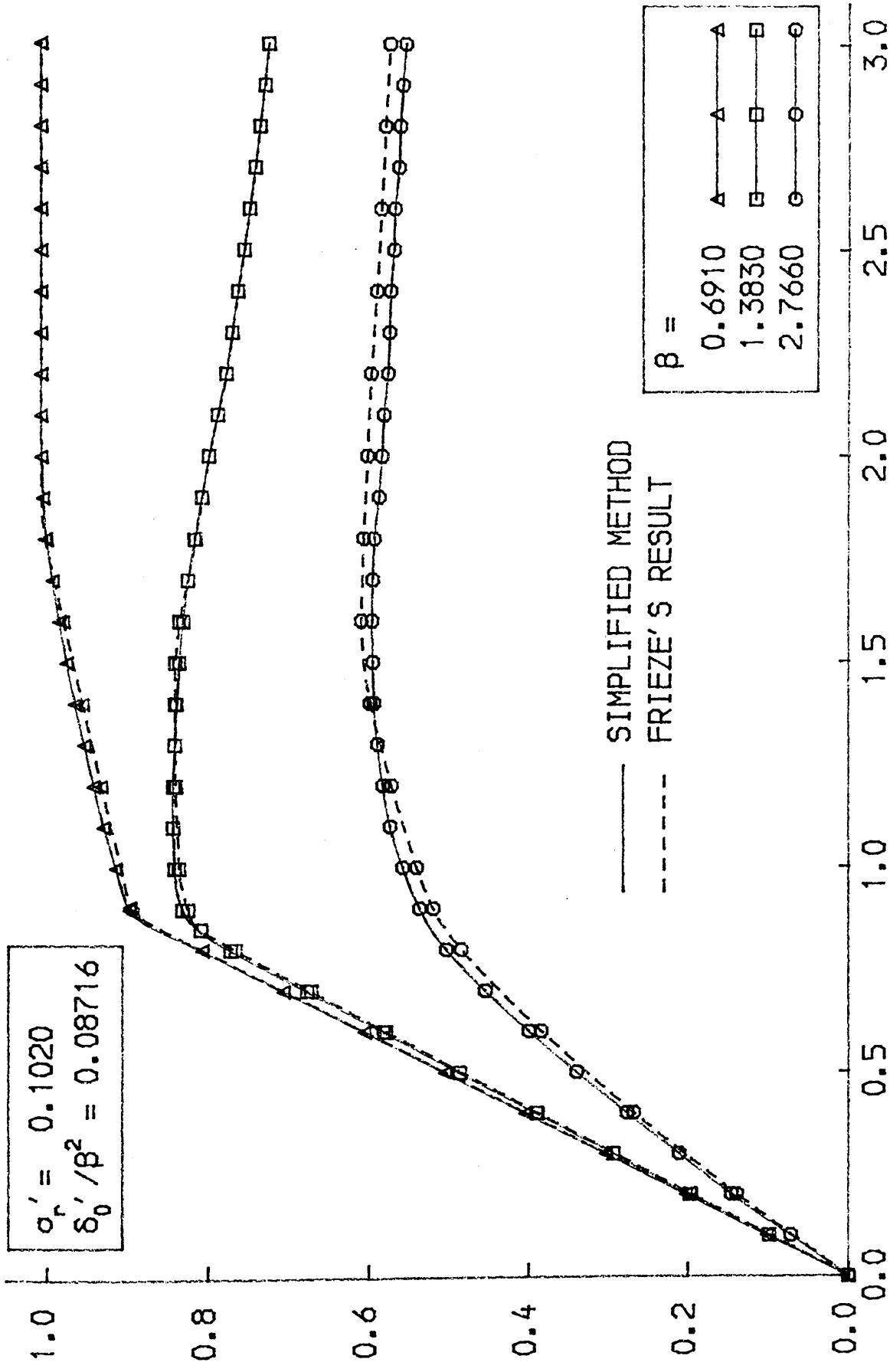

FIG.2-17 AVERAGE STRESS-STRAIN CURVE FOR THE PLATE

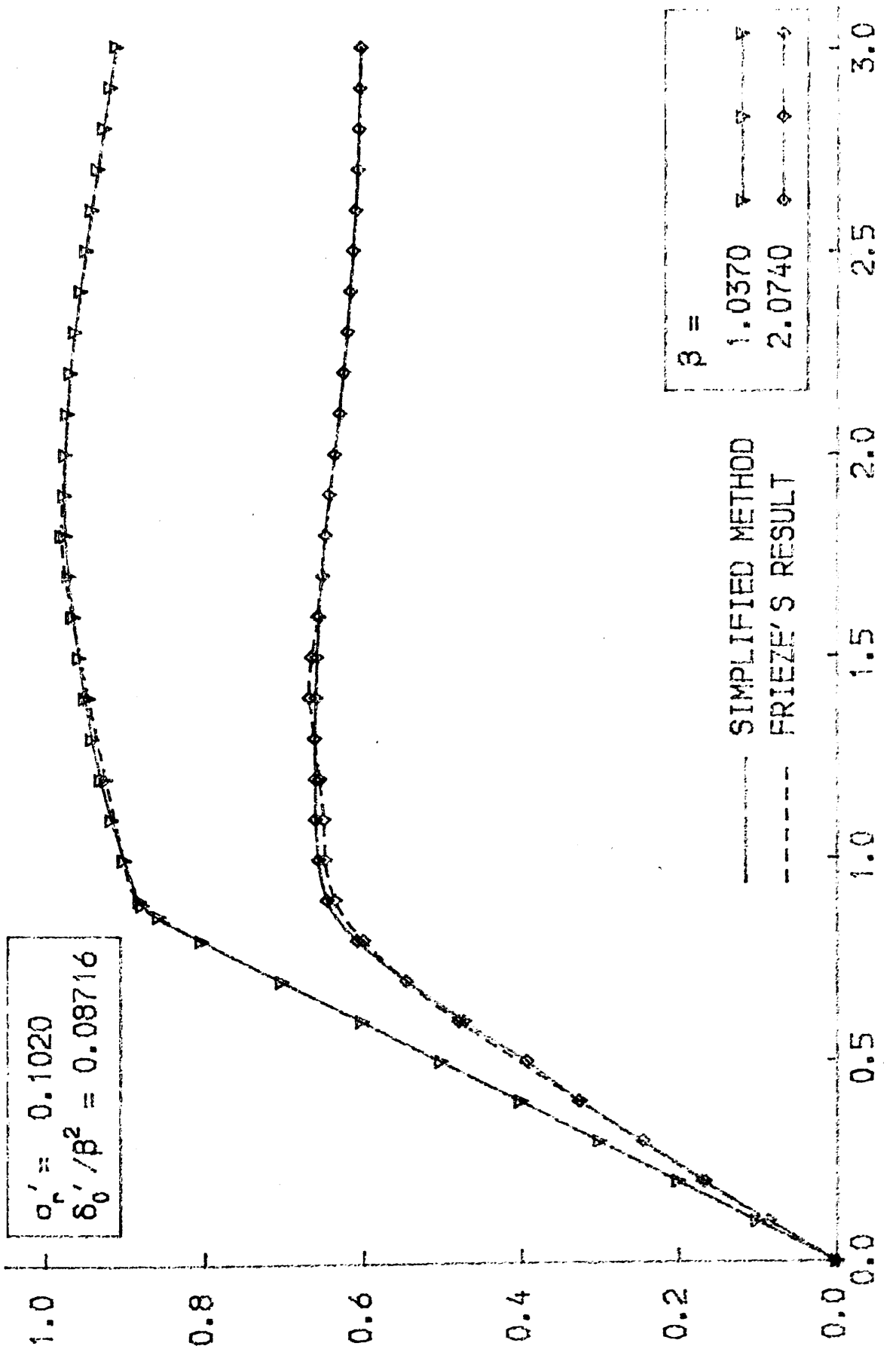

FIG.2-18 AVERAGE STRESS-STRAIN CURVE FOR THE PLATE

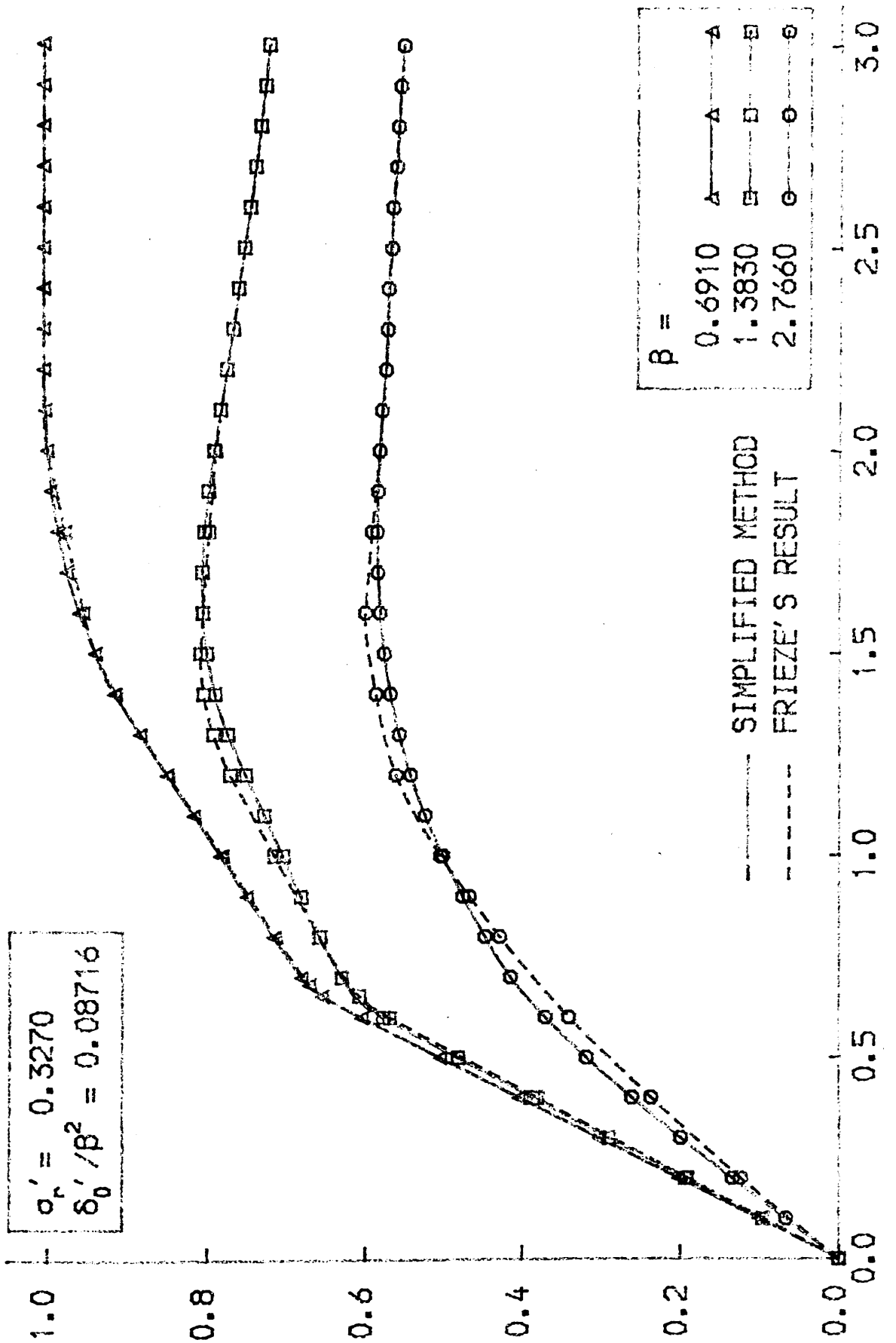

FIG.2-19 AVERAGE STRESS-STRAIN CURVE FOR THE PLATE

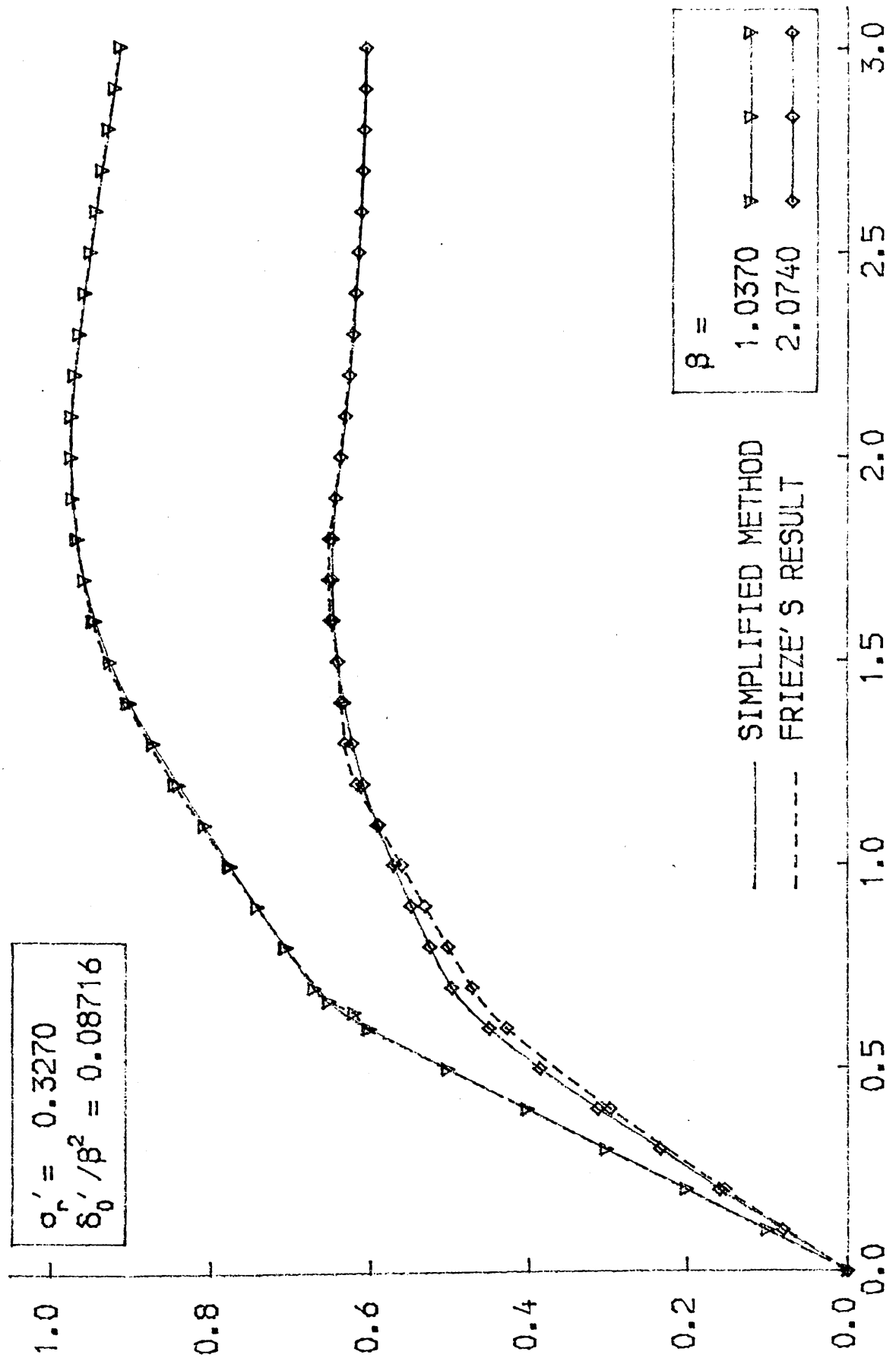

FIG.2-20 AVERAGE STRESS-STRAIN CURVE FOR THE PLATE

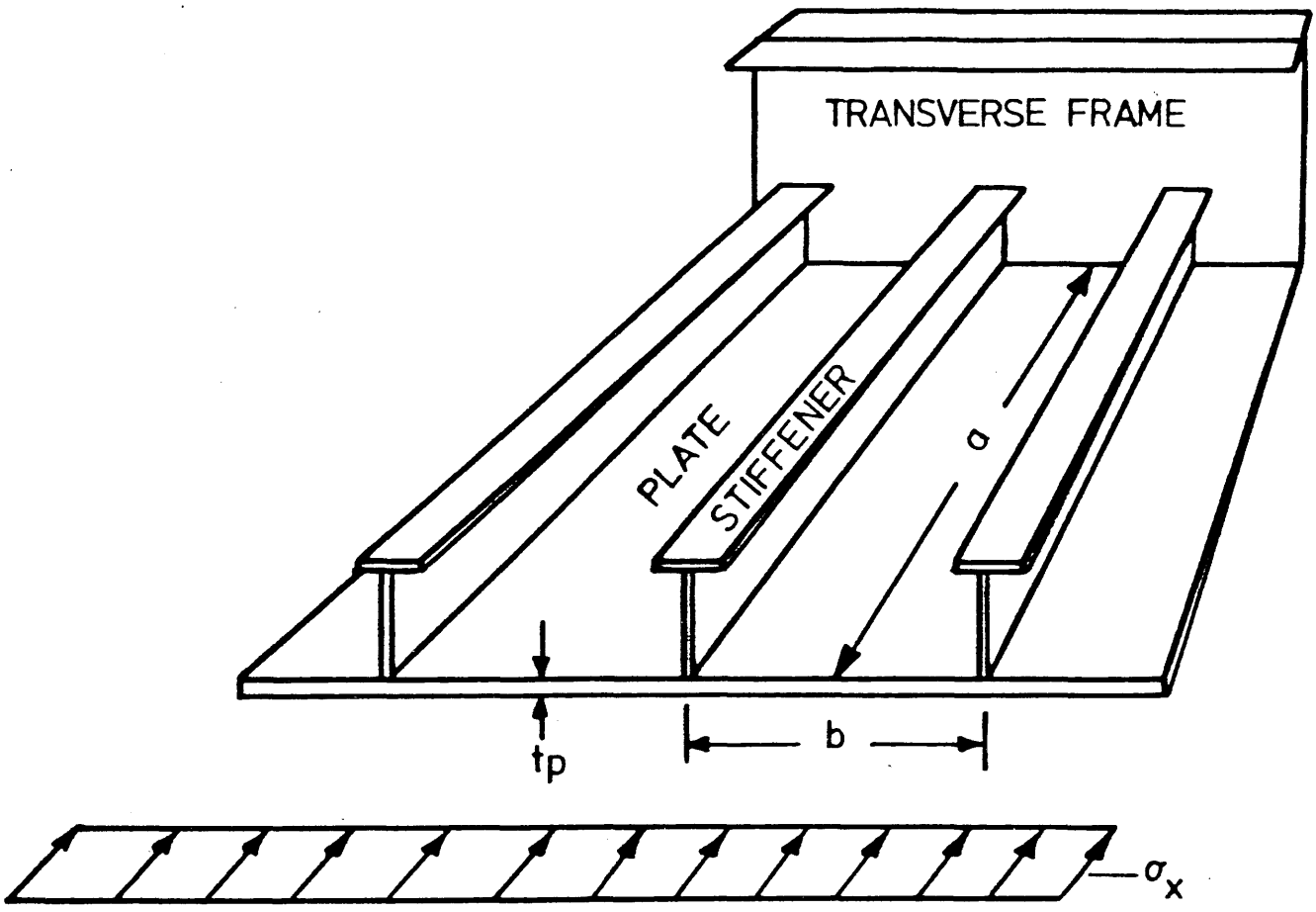

FIG. 3-1 ORTHOGONALLY STIFFENED PANAL

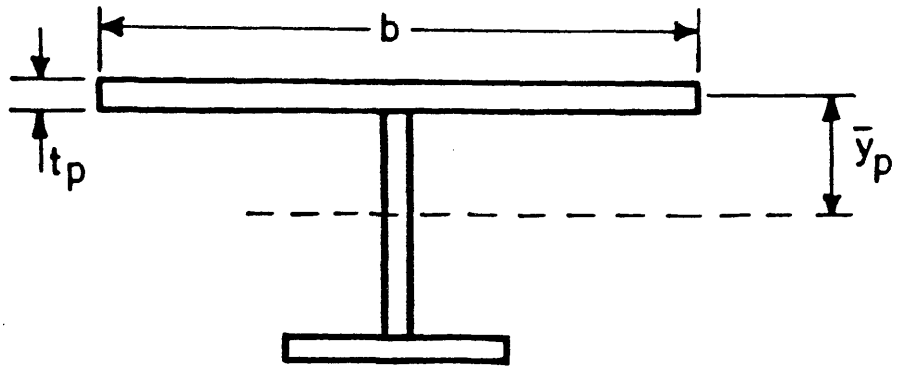

FIG.3-2 BEAM-COLUMN FORMED BY PLATE AND STIFFENER

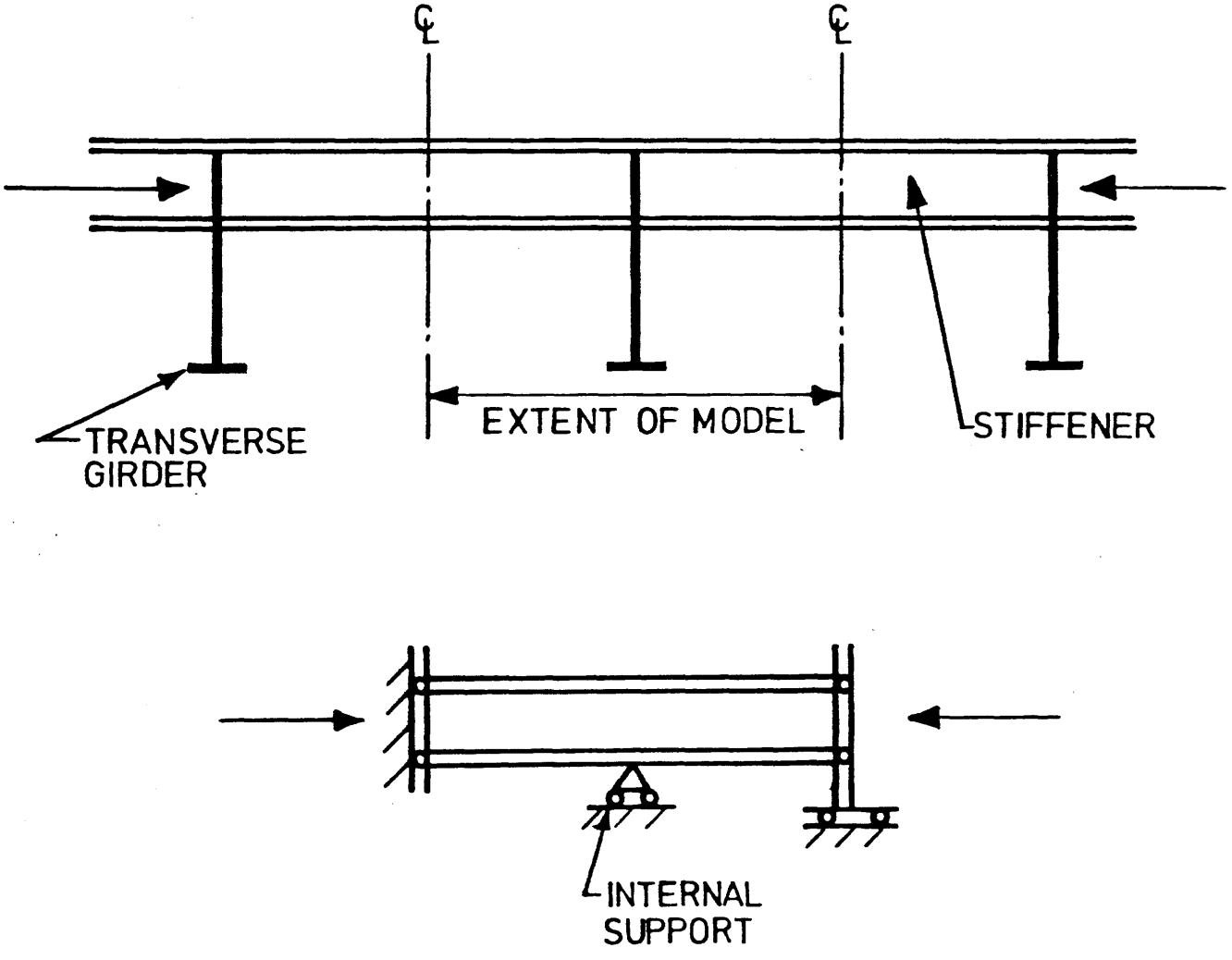

FIG.3-3 BEAM-COLUMN MODEL

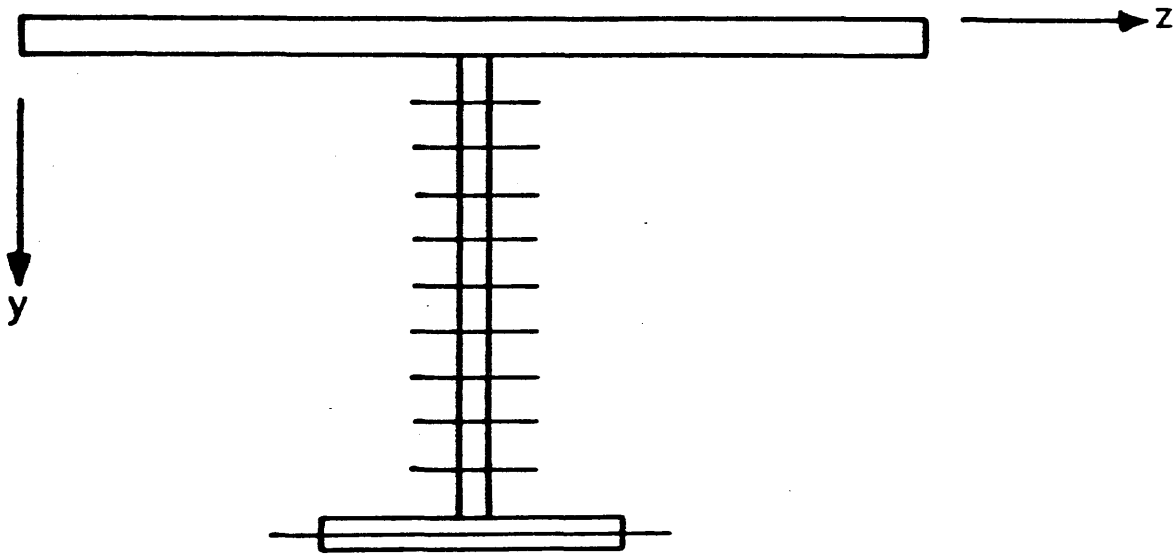

FIG.3-4 DISCRETISATION OF CROSS-SECTION

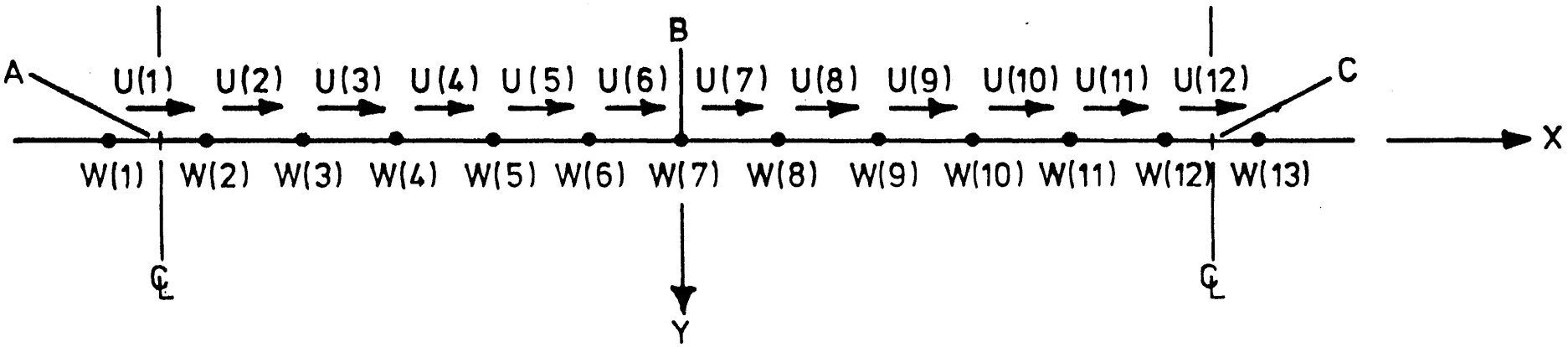

FIG.3-5 INTERLACING MESH for FINITE DIFFERENCE SIMULATION

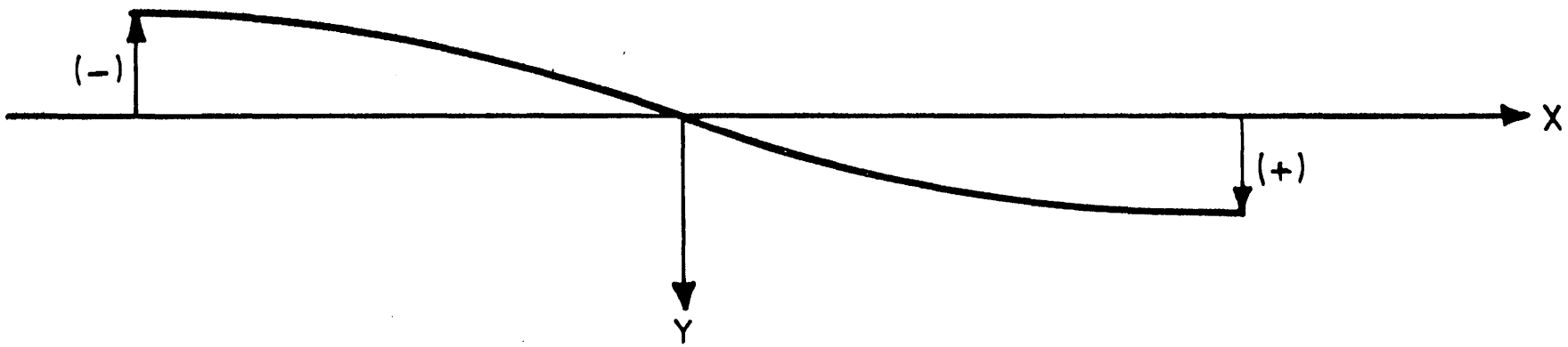

FIG.3-6 INITIAL DEFLECTED SHAPE of BEAM−COLUMN

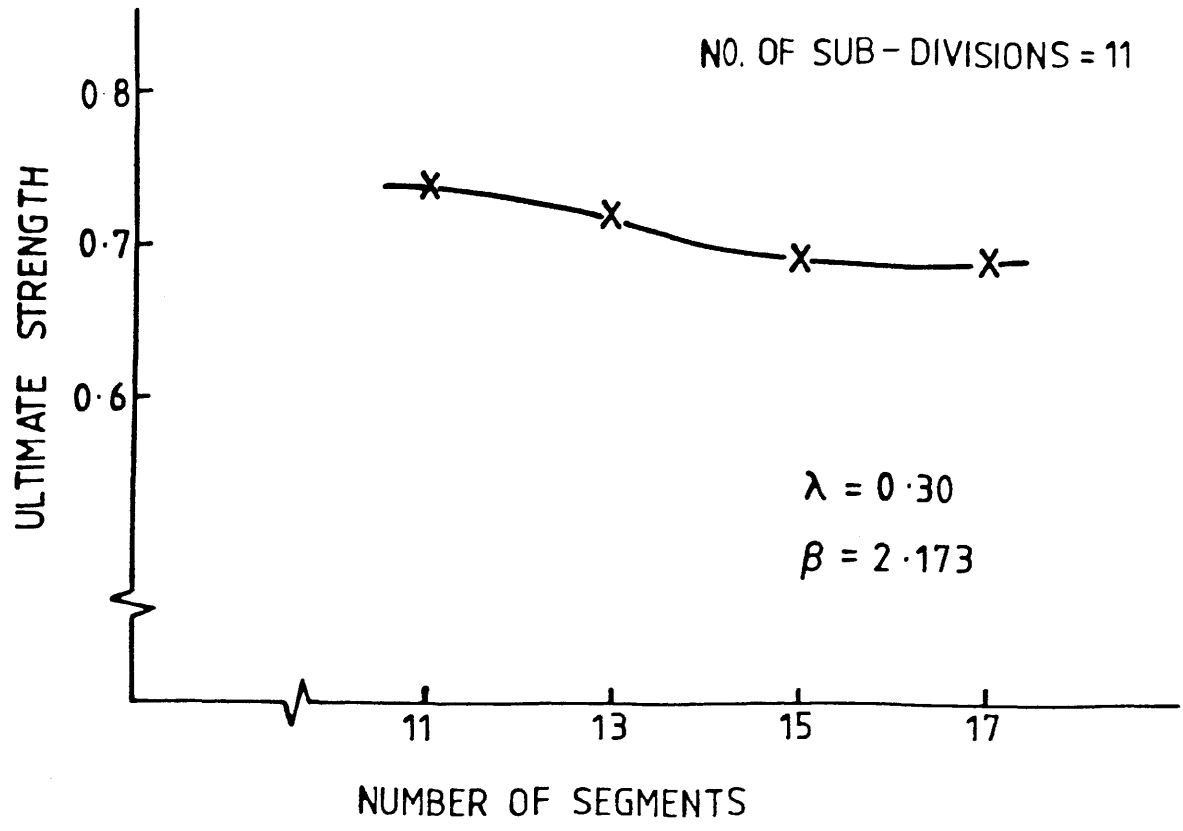

FIG.3-7 VARIATION OF ULTIMATE STRENGTH WITH NUMBER O SEGMENTS.

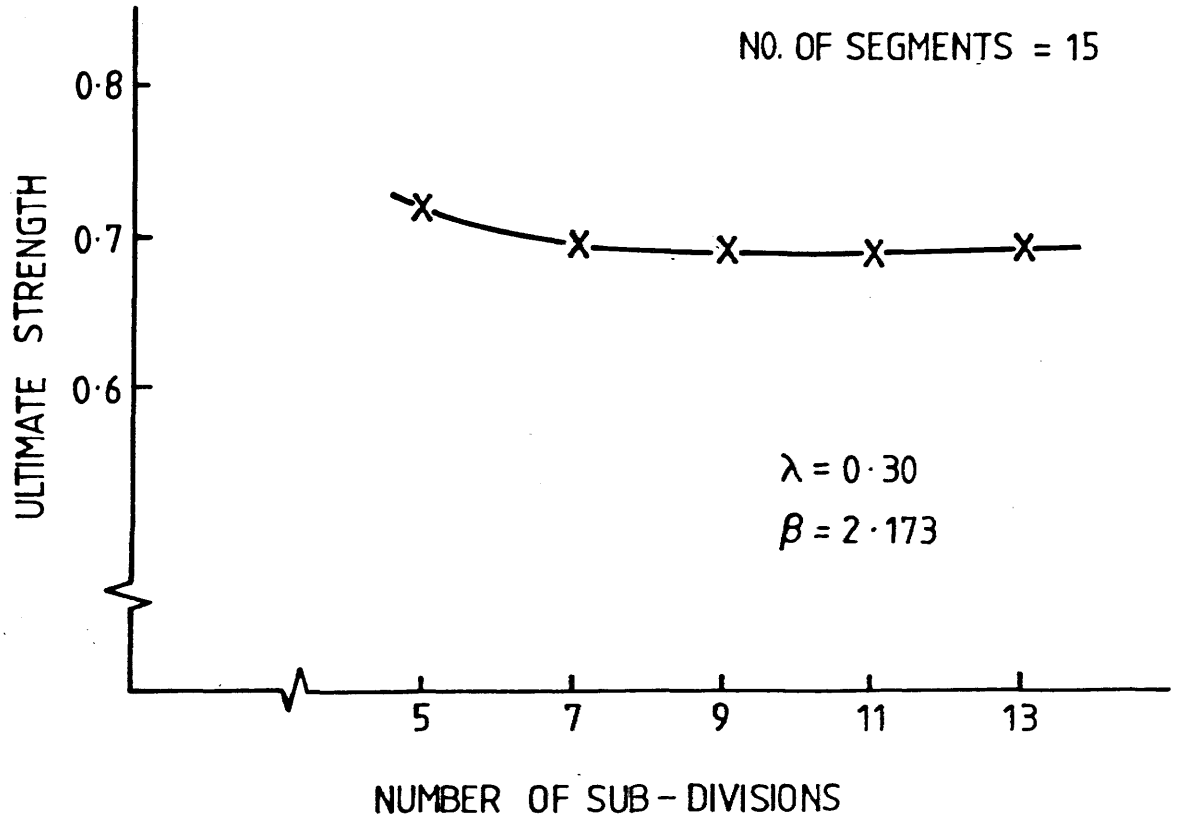

FIG.3-8 VARIATION OF ULTIMATE STRENGTH WITH NUMBER OF SUB-DIVISIONS.

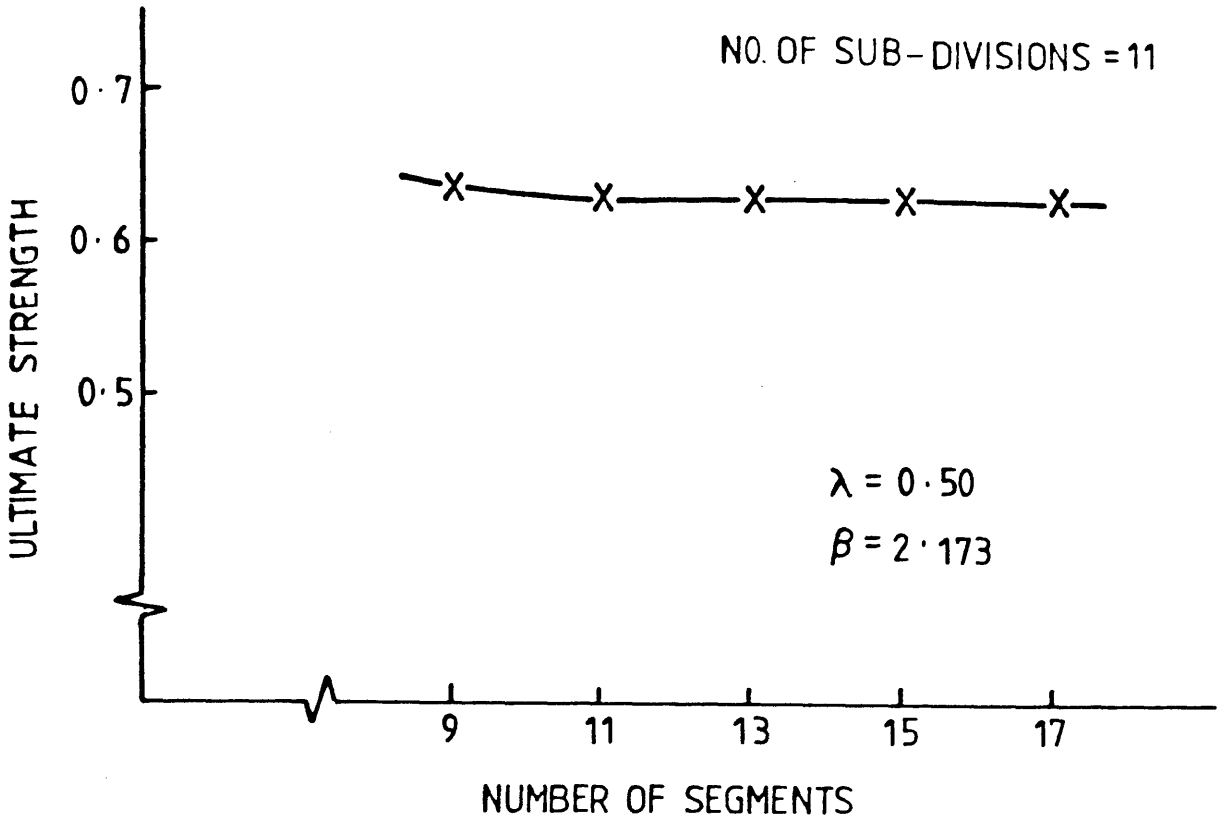

FIG. 3-9 VARIATION OF ULTIMATE STRENGTH WITH NUMBER OF SEGMENTS.

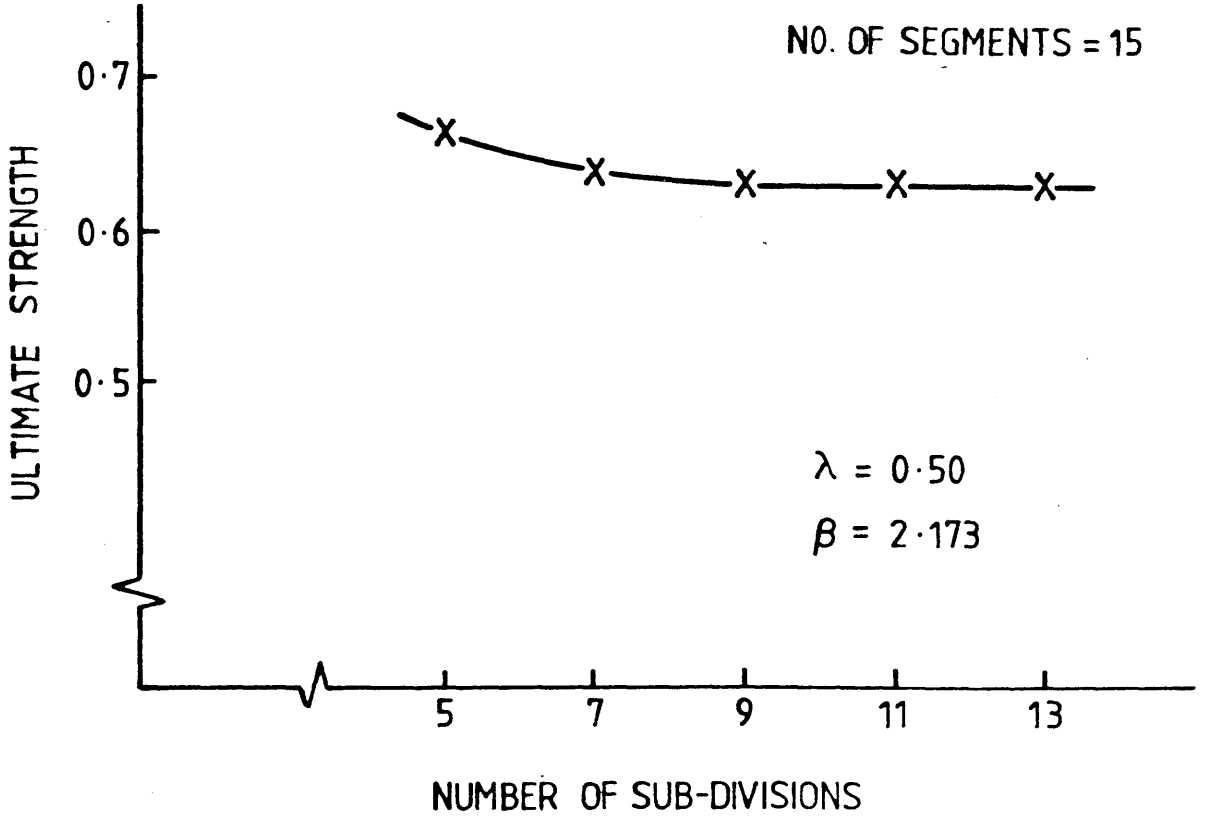

FIG. 3-10 VARIATION OF ULTIMATE STRENGTH WITH NUMBER OF SUB-DIVISIONS.

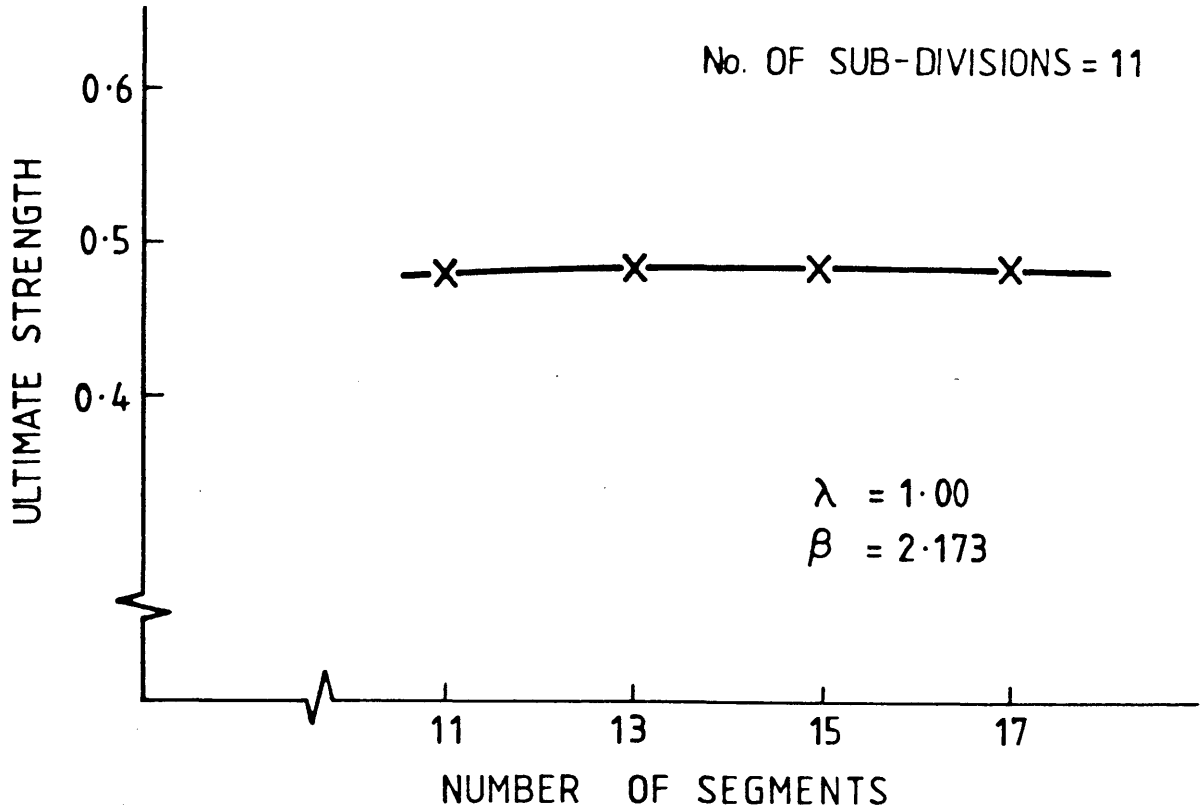

FIG.3-11 VARIATION OF ULTIMATE STRENGTH WITH NUMBER OF SEGMENTS

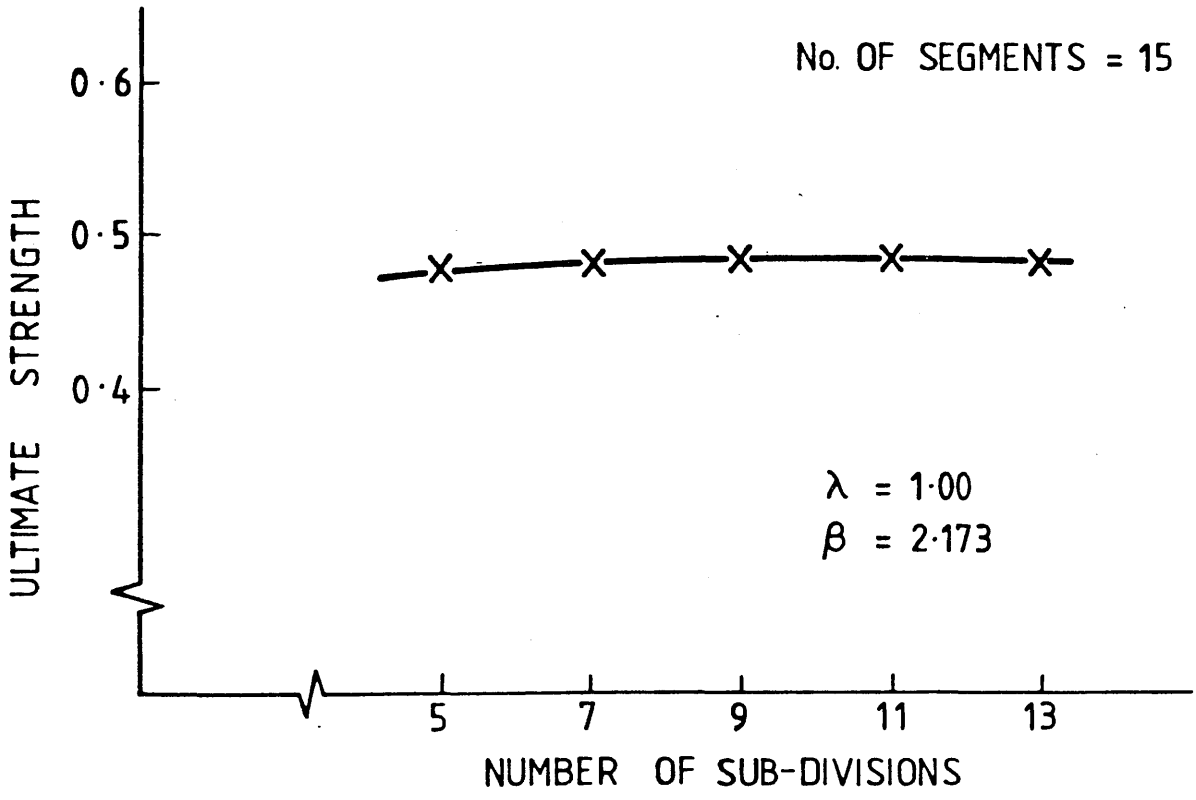

FIG.3-12 VARIATION OF ULTIMATE STRENGTH WITH NUMBER OF SUB-DIVISIONS

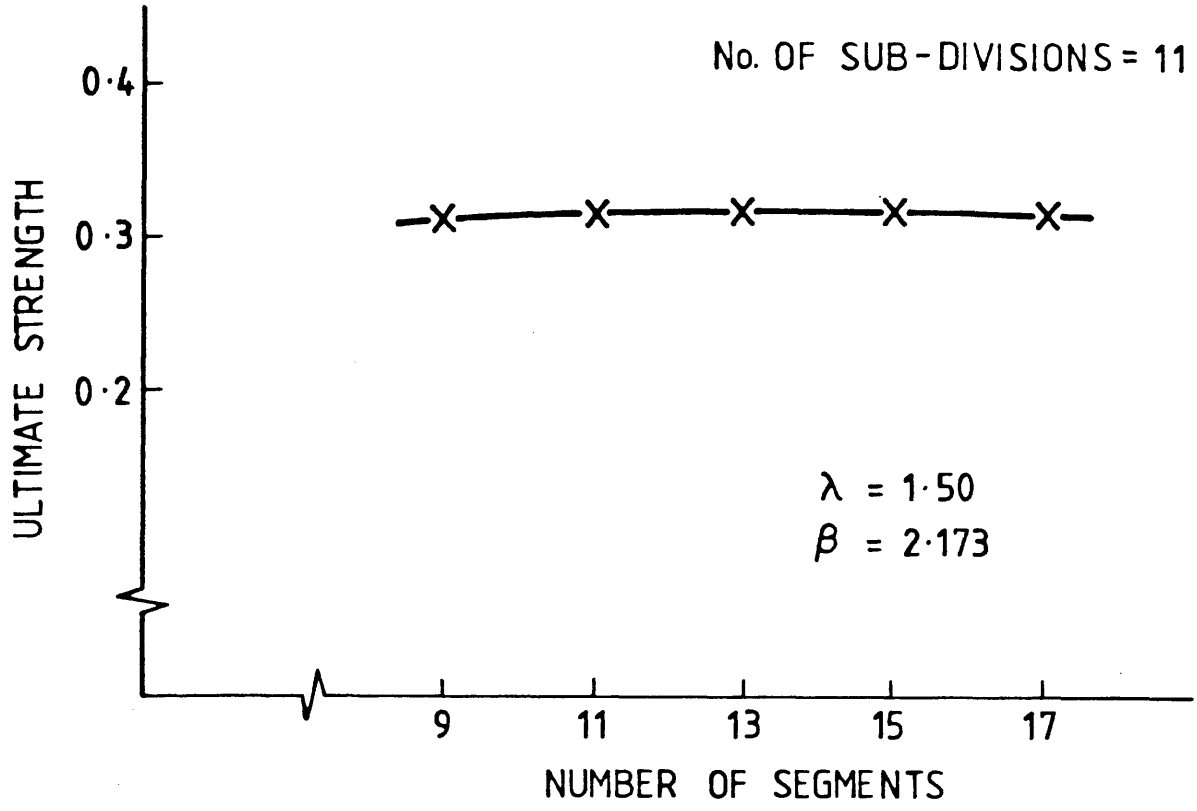

FIG.3-13 VARIATION OF ULTIMATE STRENGTH WITH NUMBER OF SEGMENTS

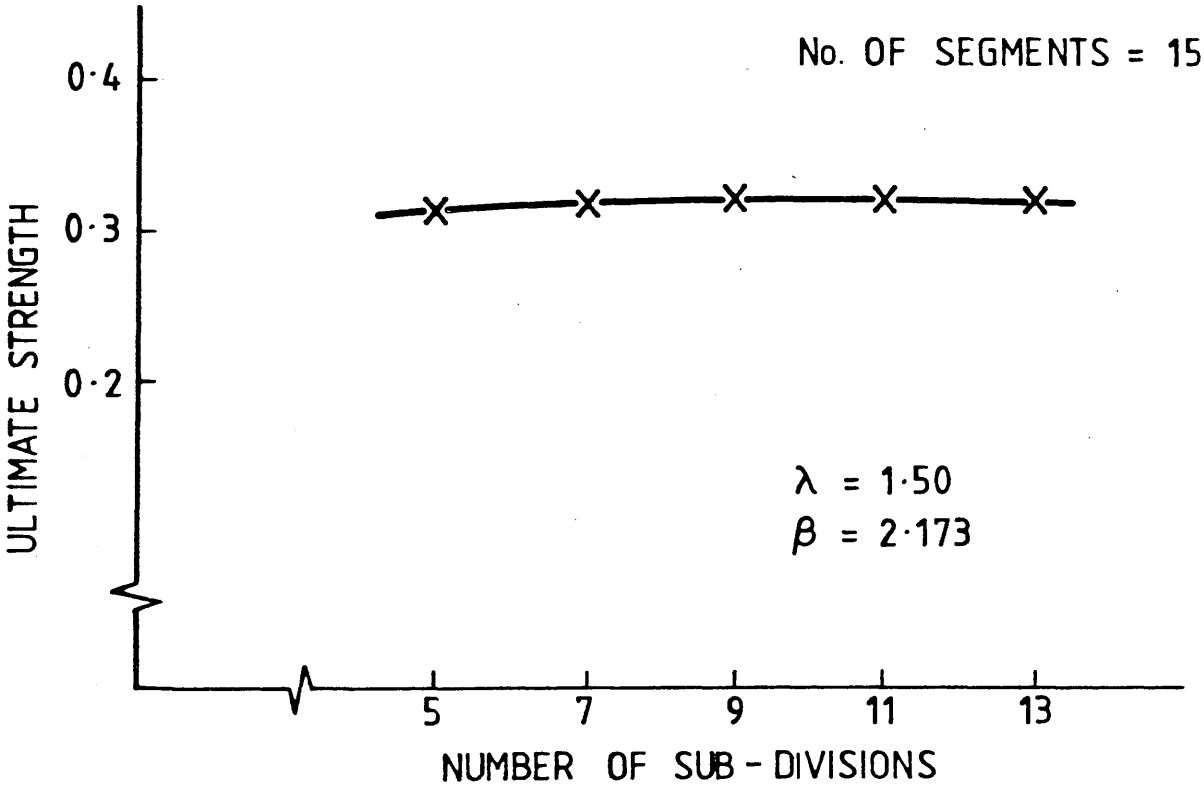

FIG.3-14 VARIATION OF ULTIMATE STRENGTH WITH NUMBER OF SUB-DIVISIONS

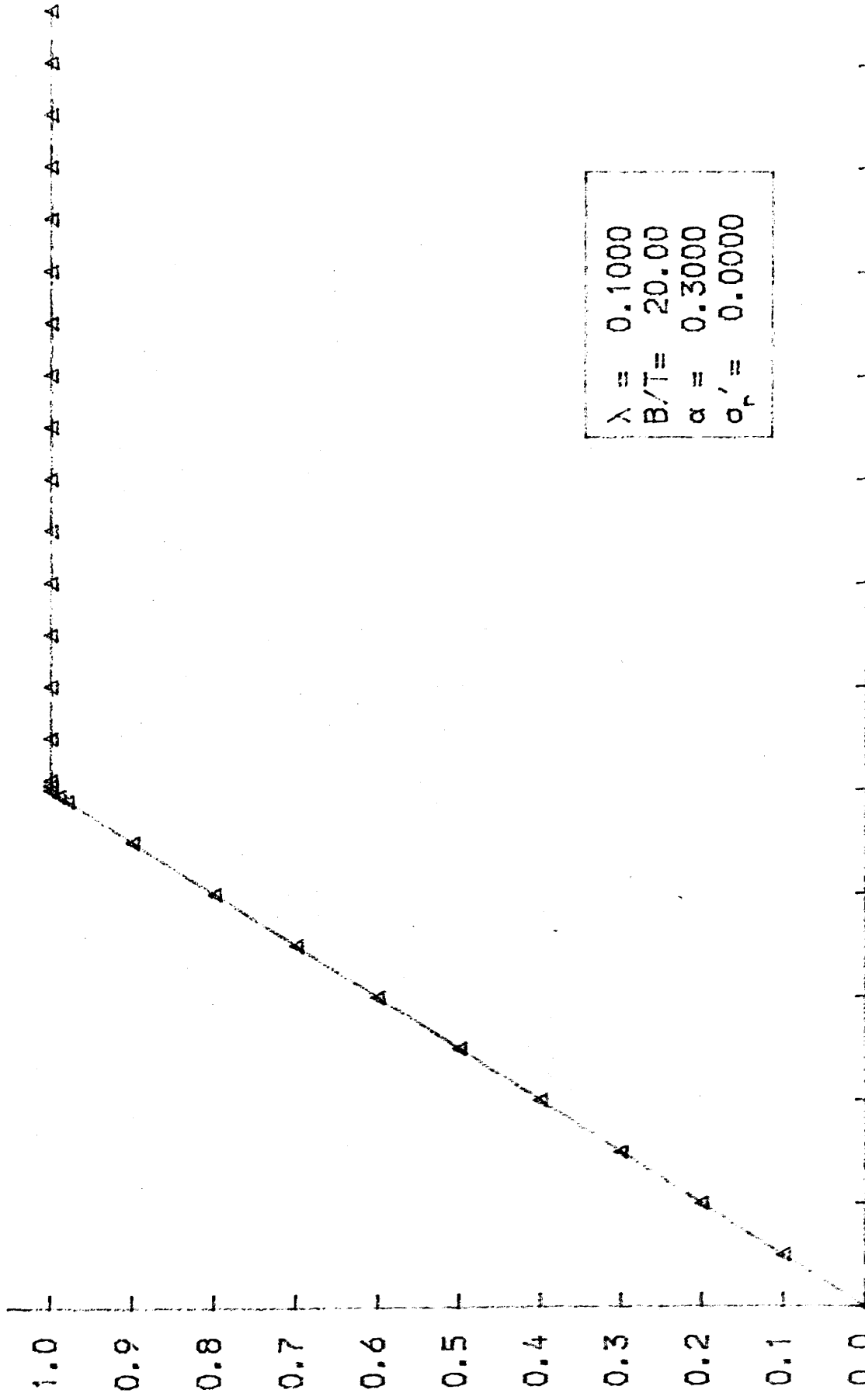

FIG.4-1 LOAD-SHORTENING CURVE FOR THE BEAM-COLUMN

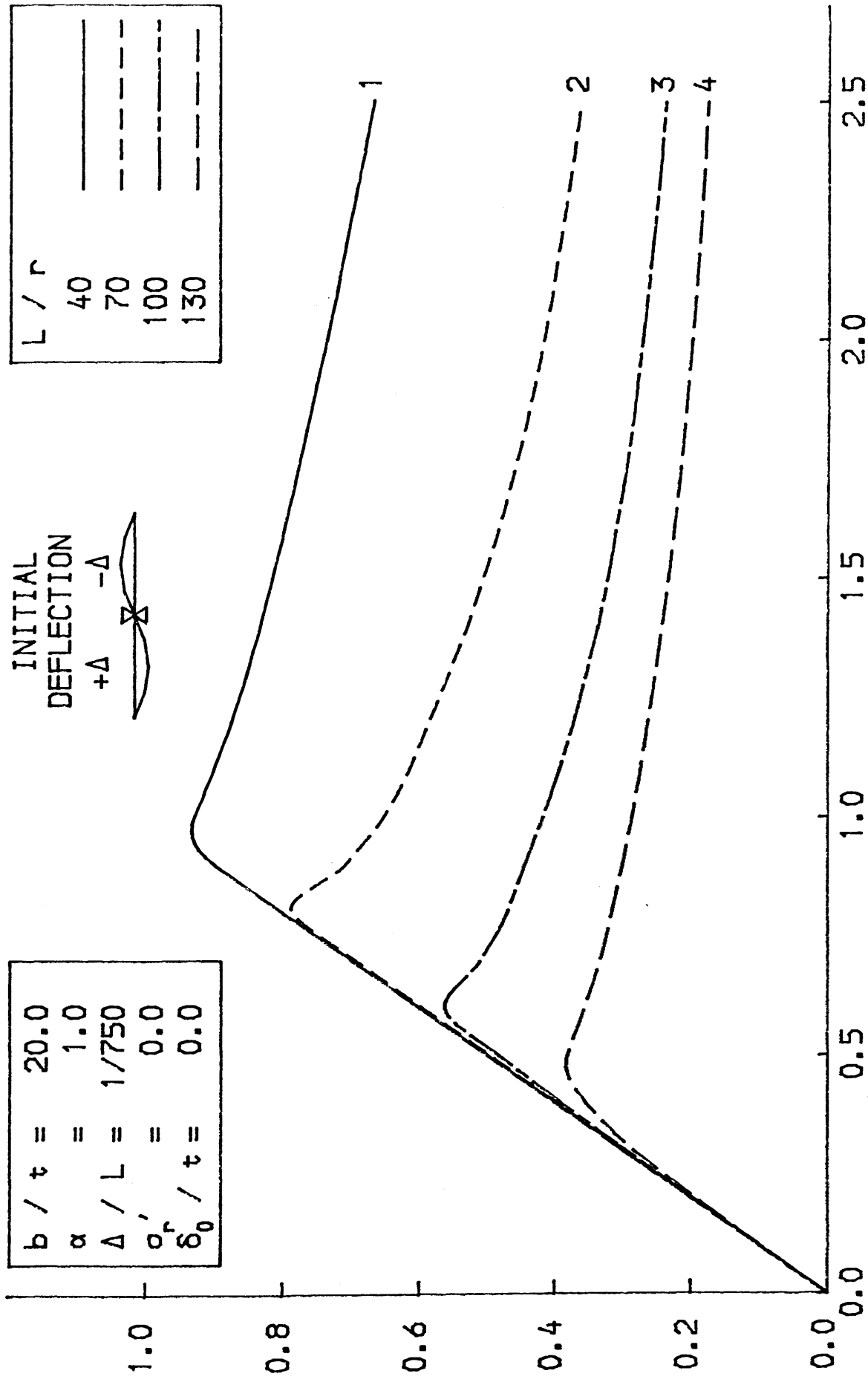

FIG.4-2 LOAD-SHORTENING CURVE FOR THE BEAM-COLUMN

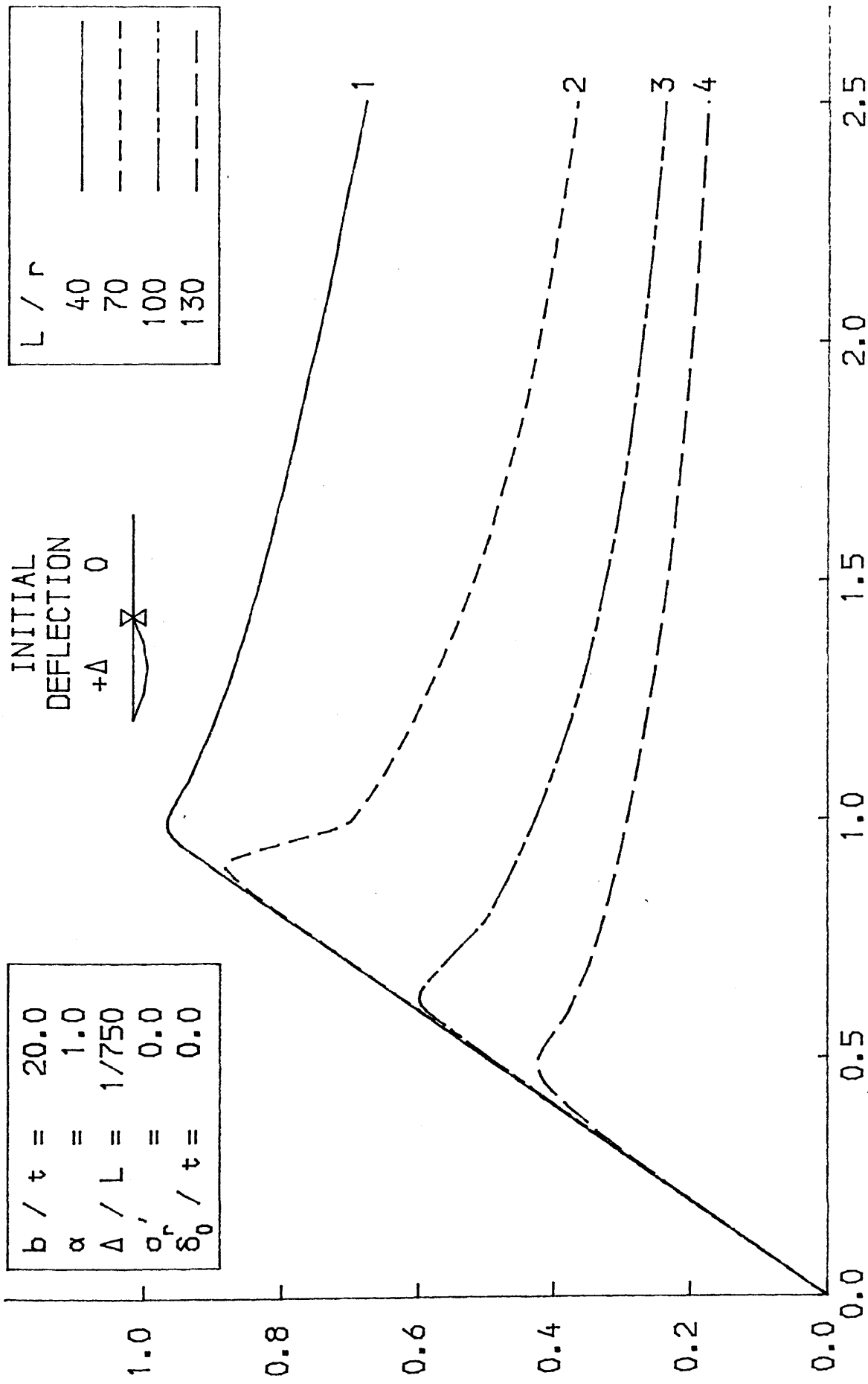

FIG.4-3 LOAD-SHORTENING CURVE FOR THE BEAM-COLUMN

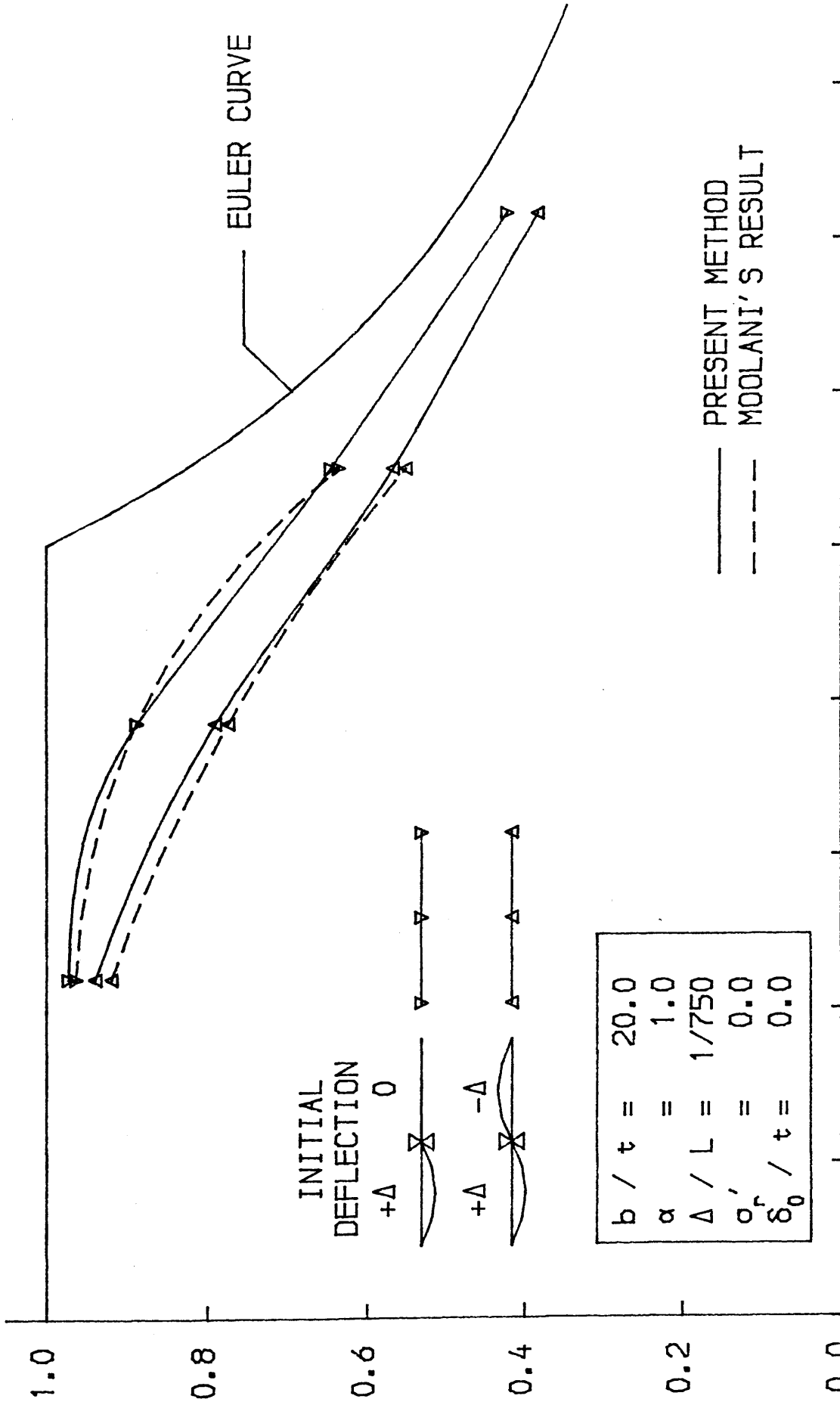

FIG.4-4 ULTIMATE STRENGTH-SLENDERNESS CURVE

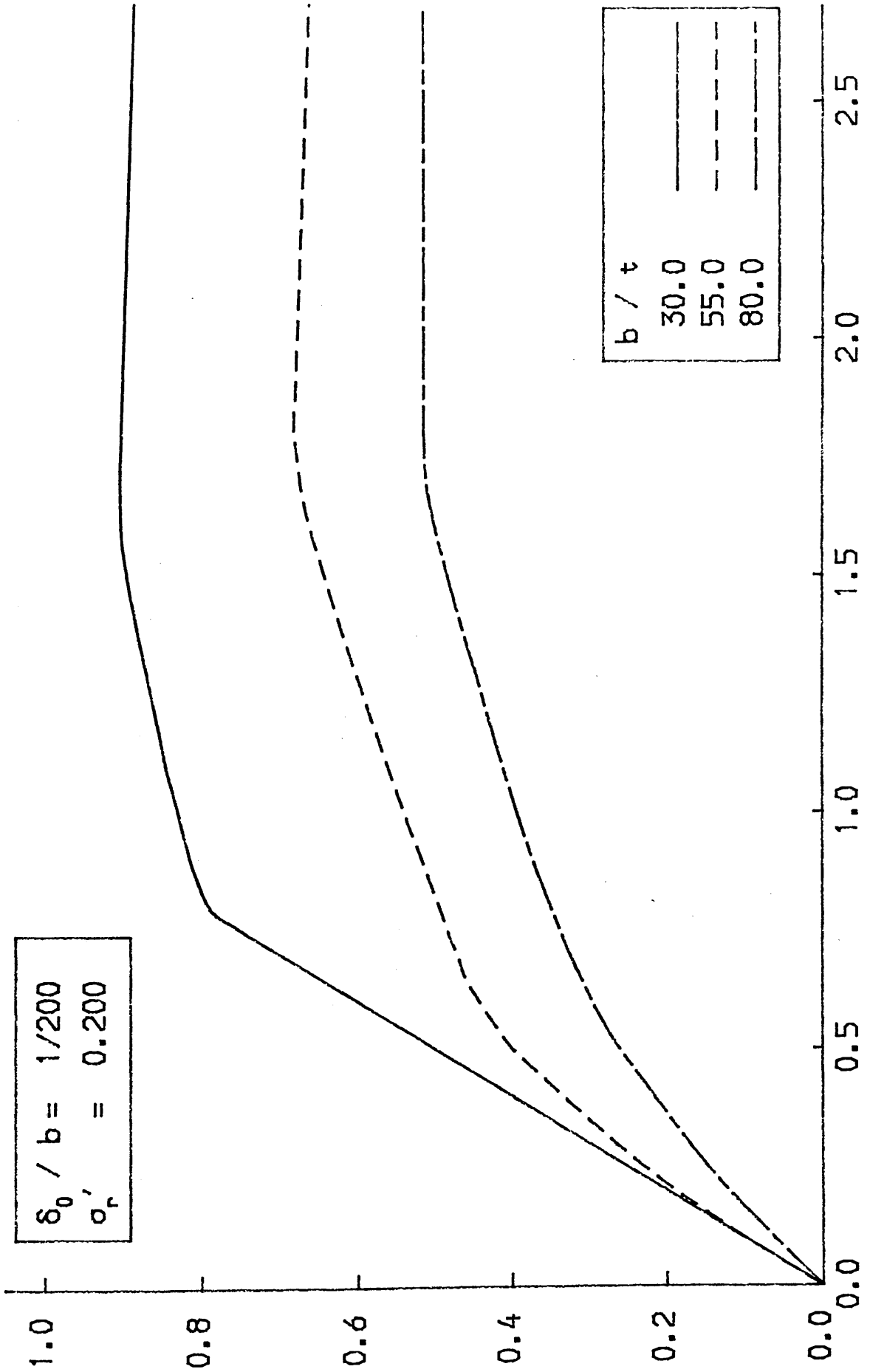

FIG.4-5 AVERAGE STRESS-STRAIN CURVE FOR THE PLATE

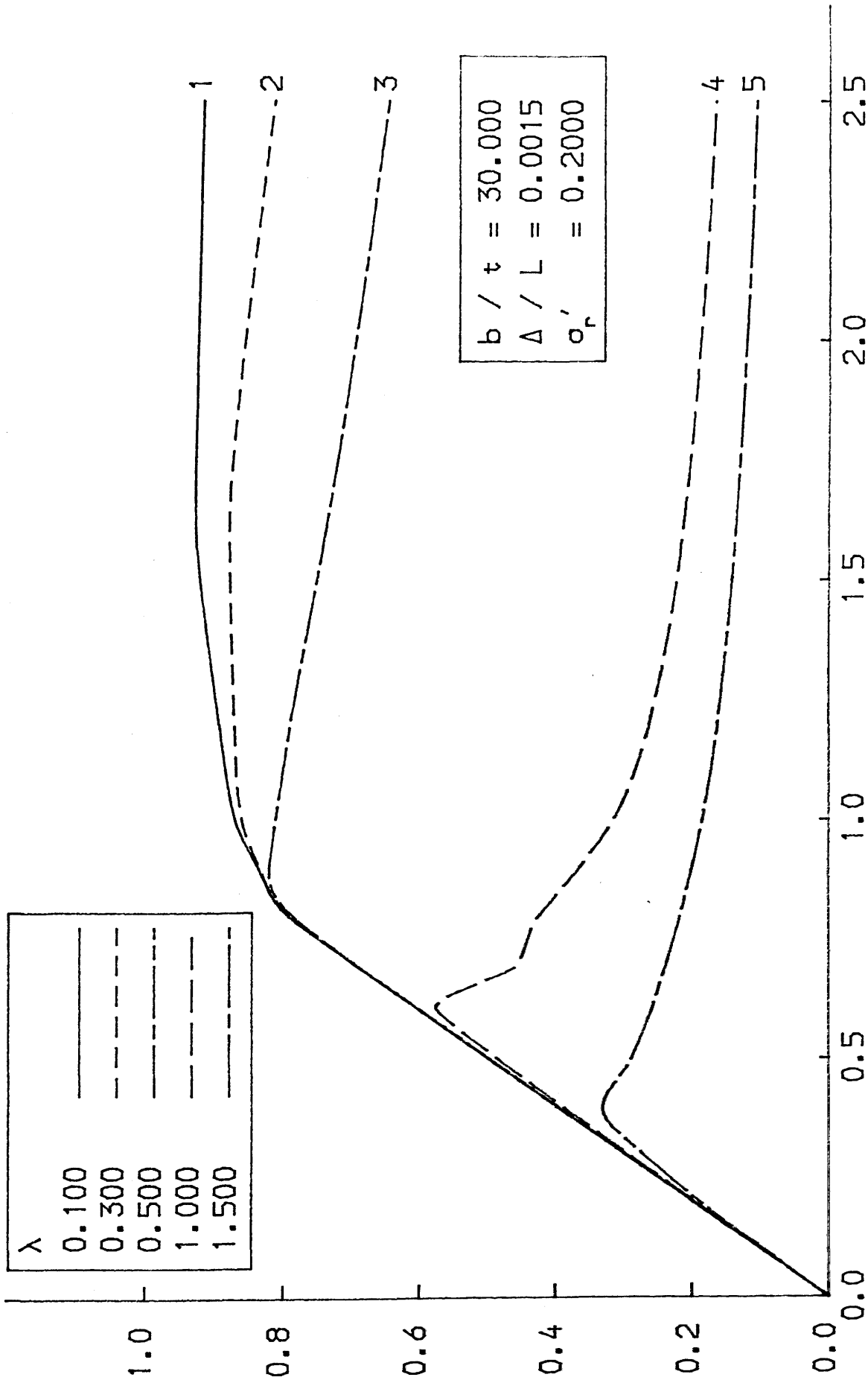

FIG. 4-6 LOAD-SHORTENING CURVE FOR THE BEAM-COLUMN

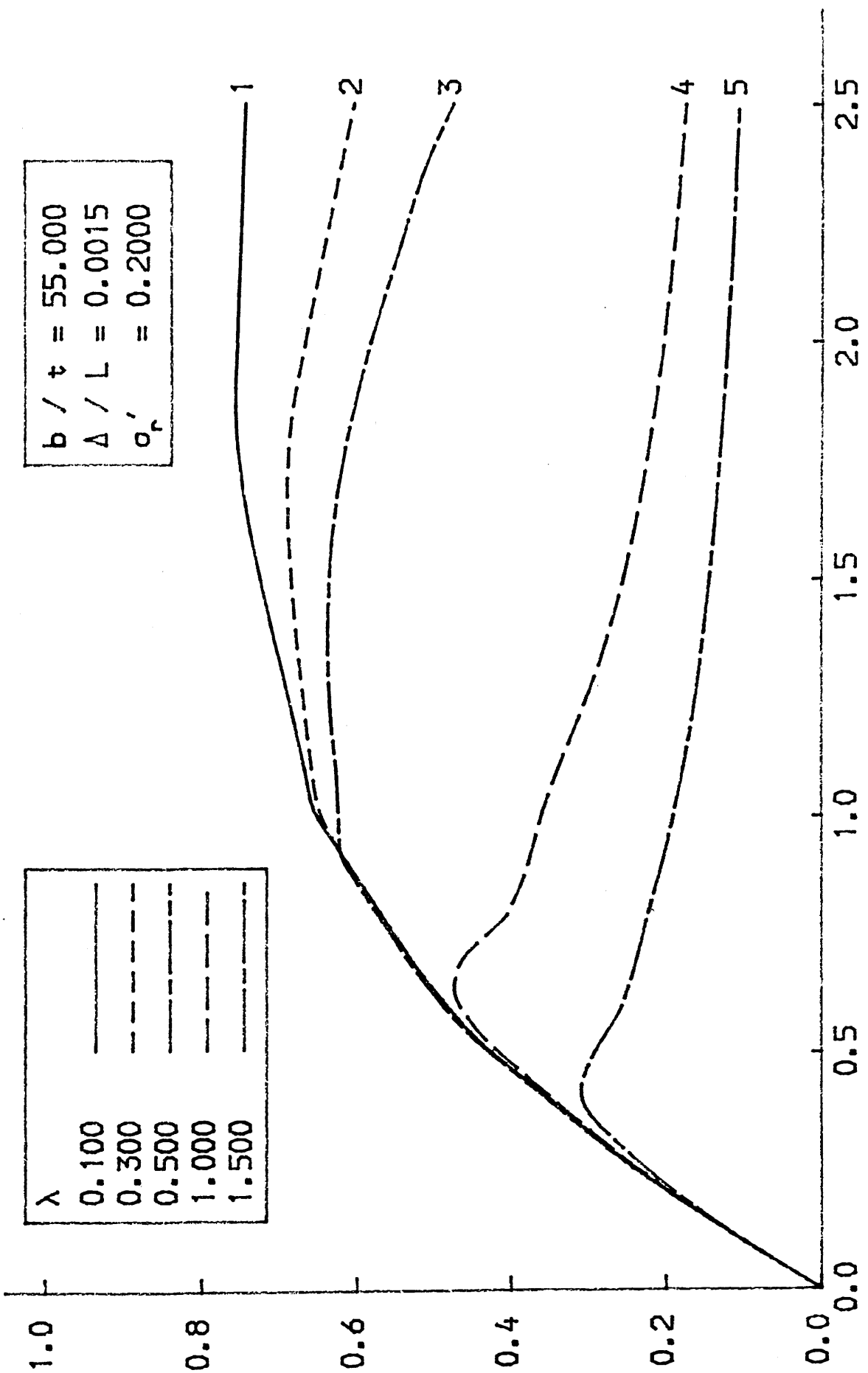

FIG.4-7 LOAD-SHORTENING CURVE FOR THE BEAM-COLUMN

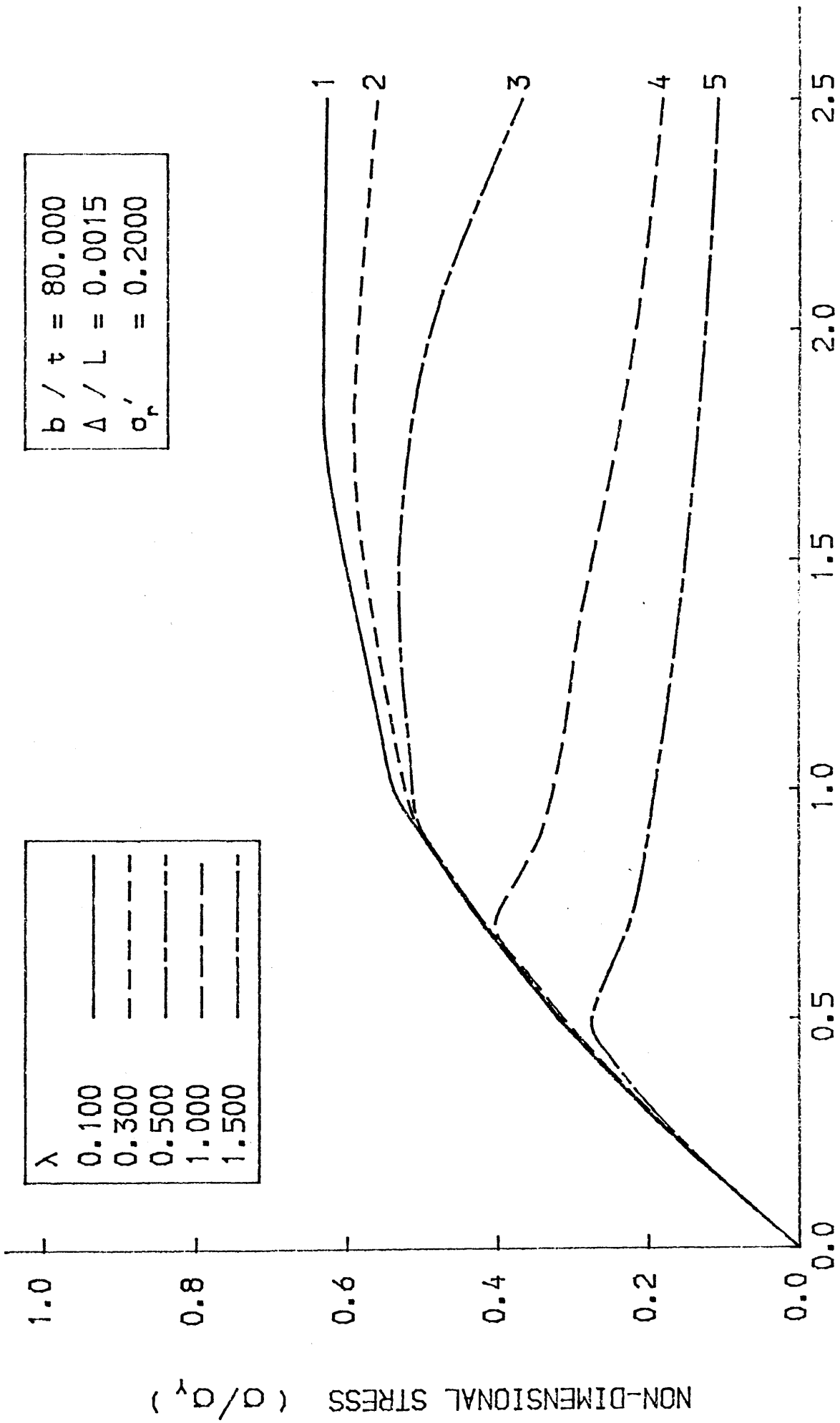

FIG.4-8 LOAD-SHORTENING CURVE FOR THE BEAM-COLUMN

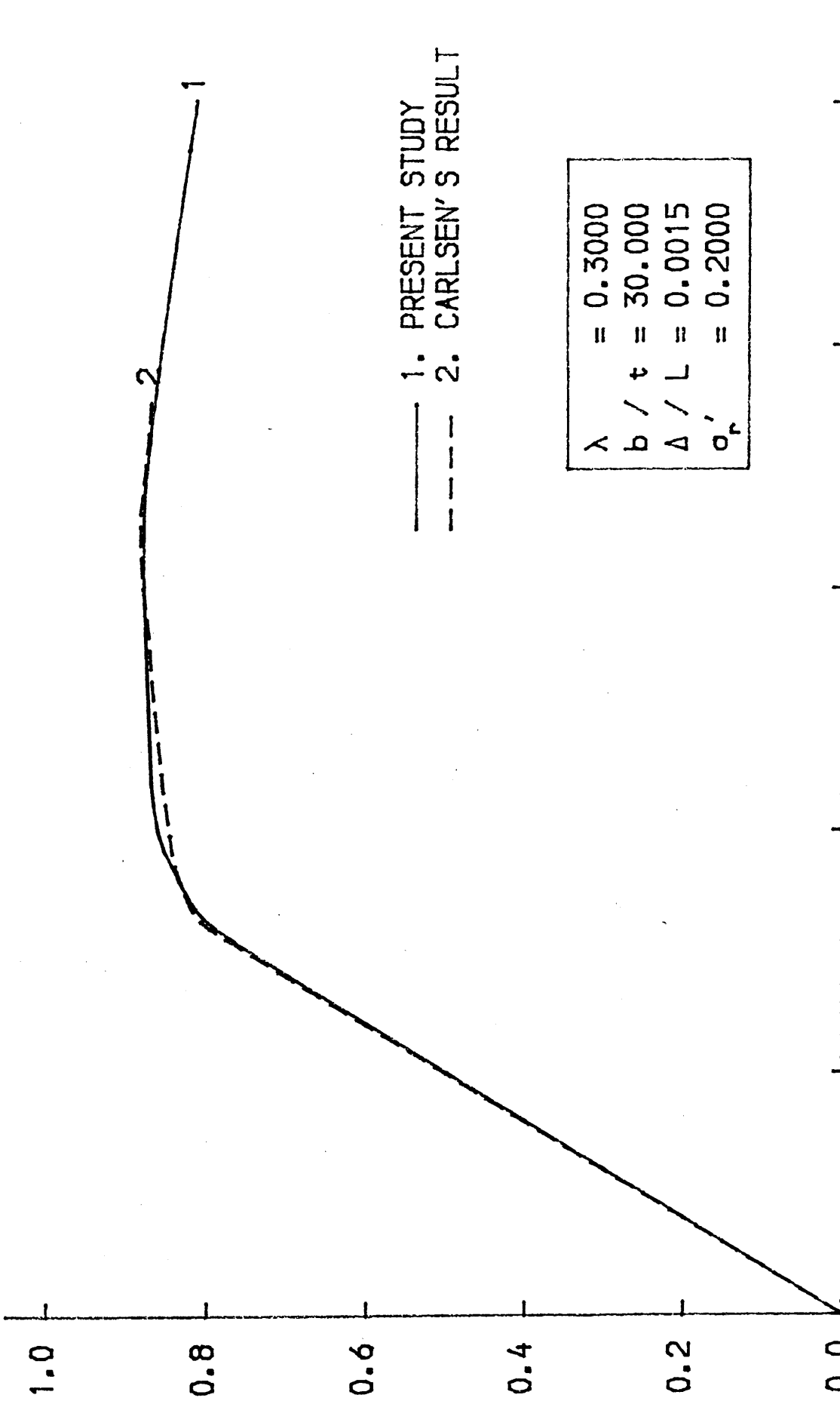

FIG.4-9 LOAD-SHORTENING CURVE FOR THE BEAM-COLUMN

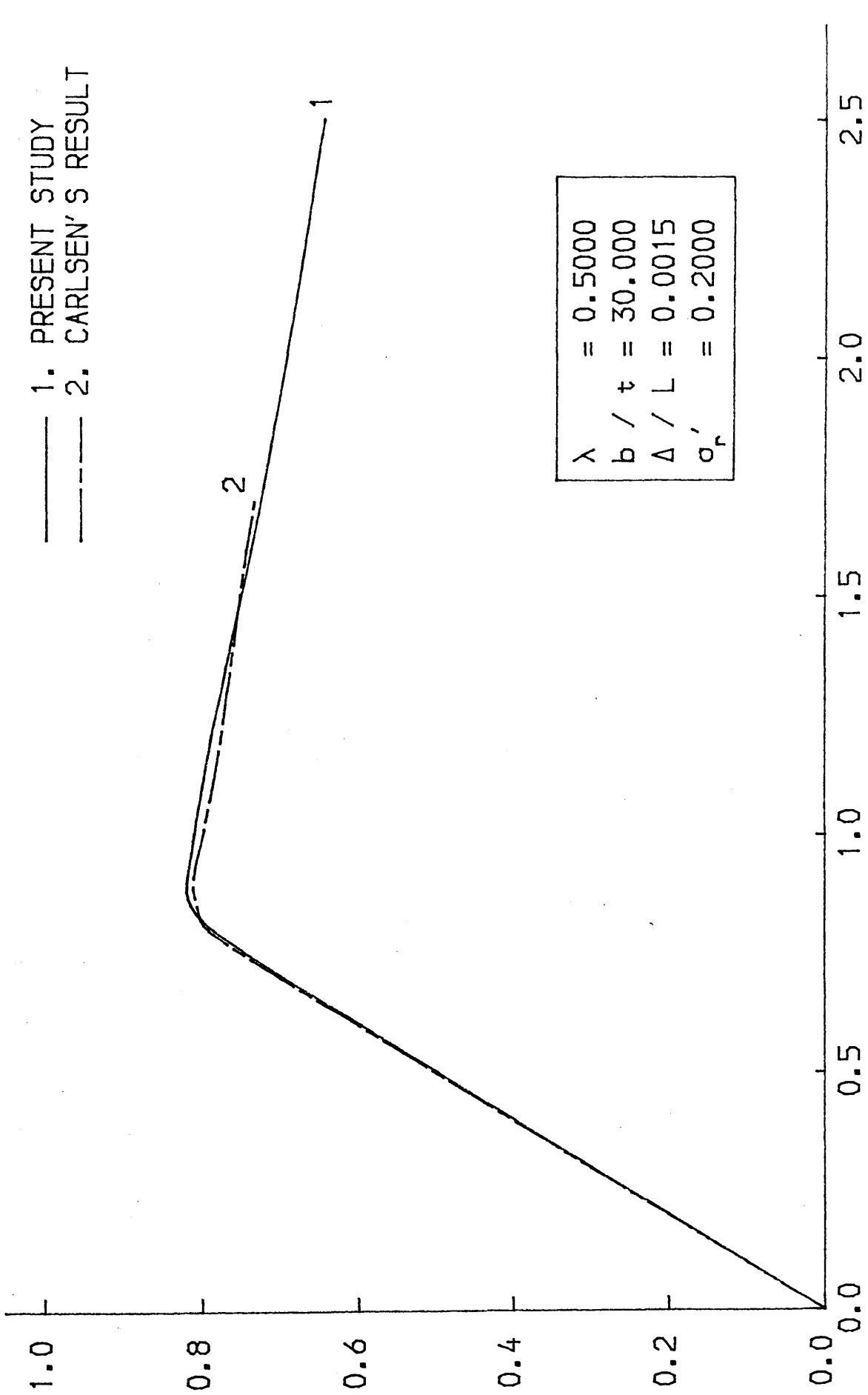

FIG.4-10 LOAD-SHORTENING CURVE FOR THE BEAM-COLUMN

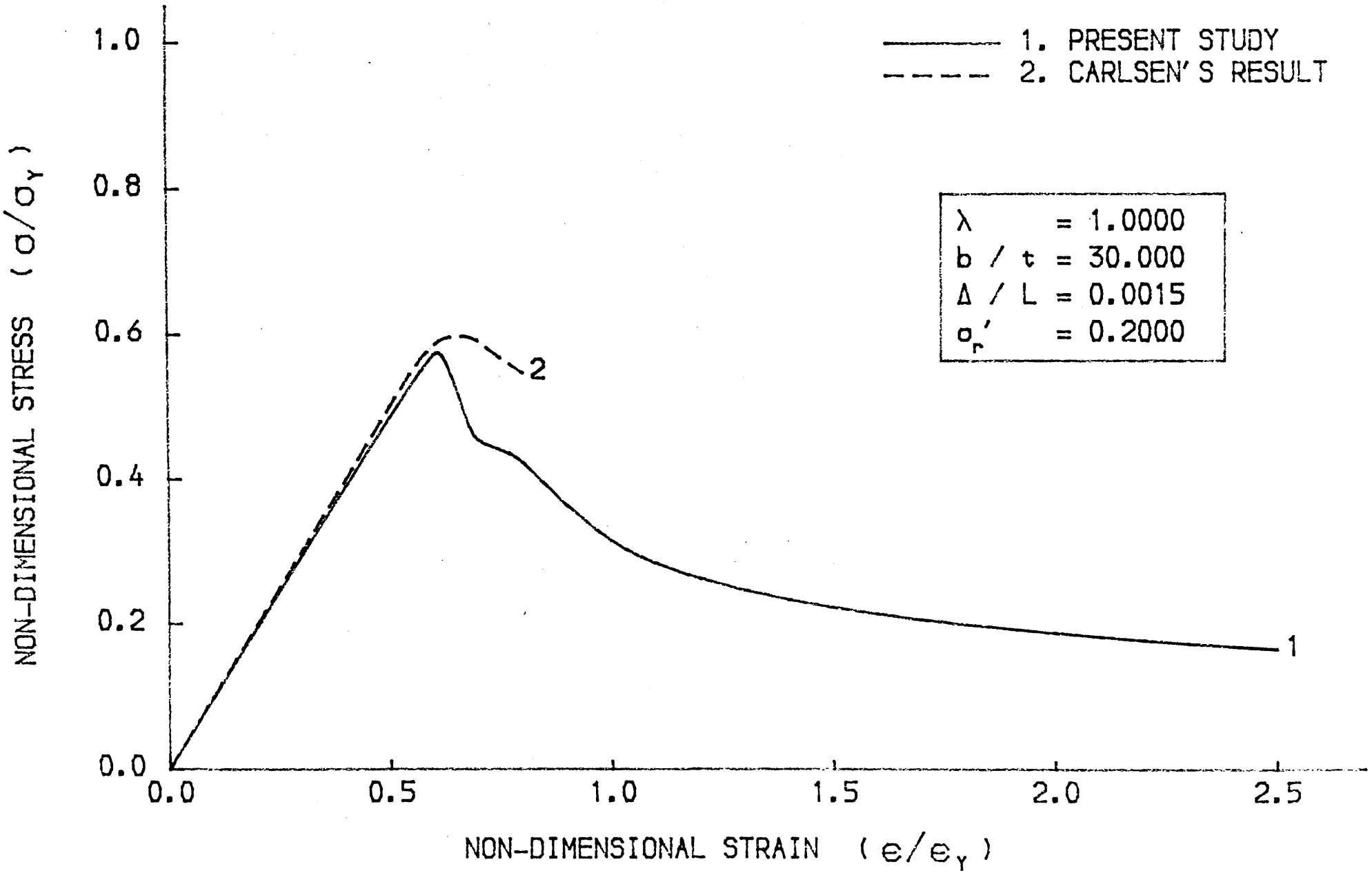

FIG.4-11 LOAD-SHORTENING CURVE FOR THE BEAM-COLUMN

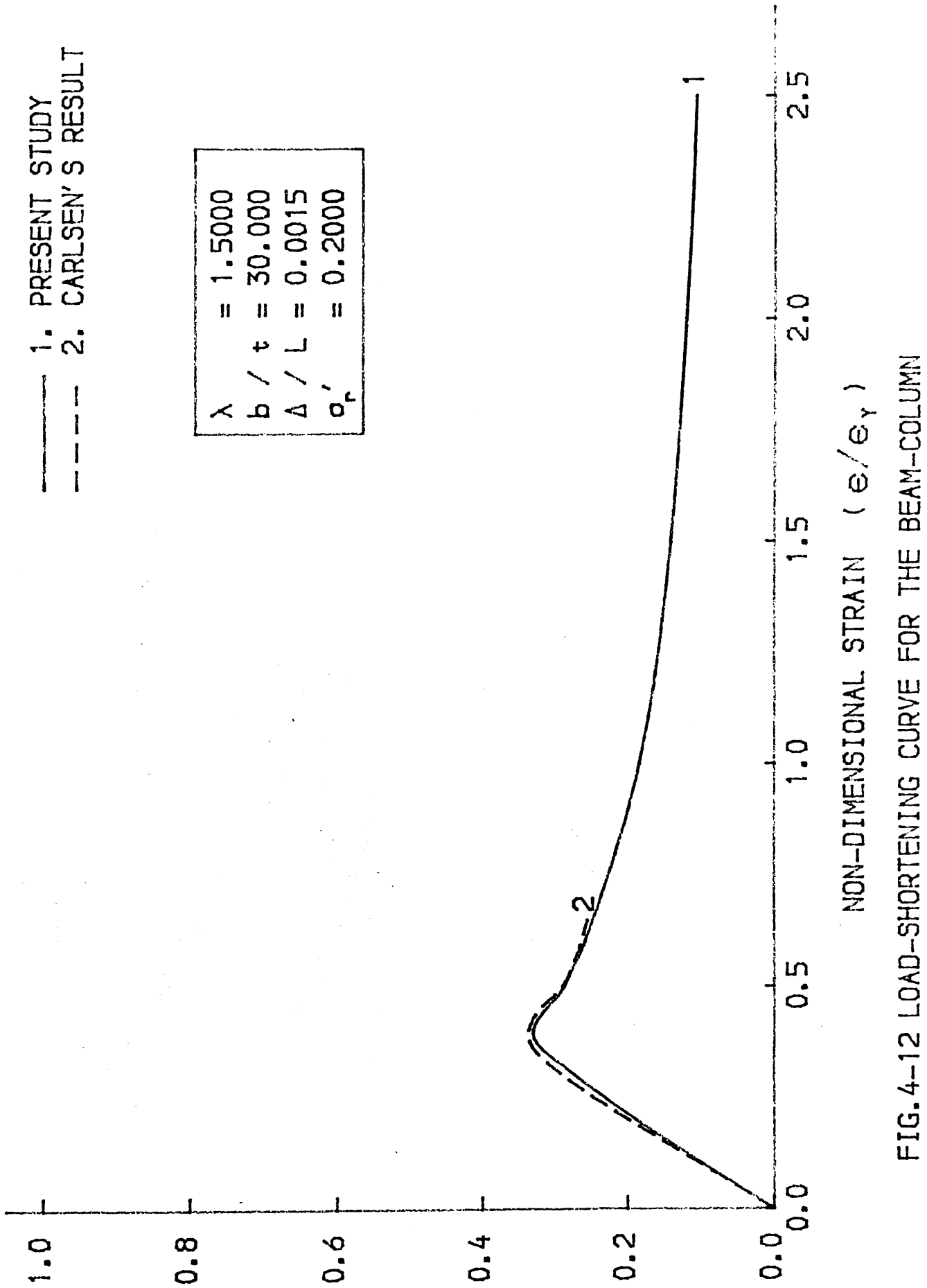

FIG.4-12 LOAD-SHORTENING CURVE FOR THE BEAM-COLUMN

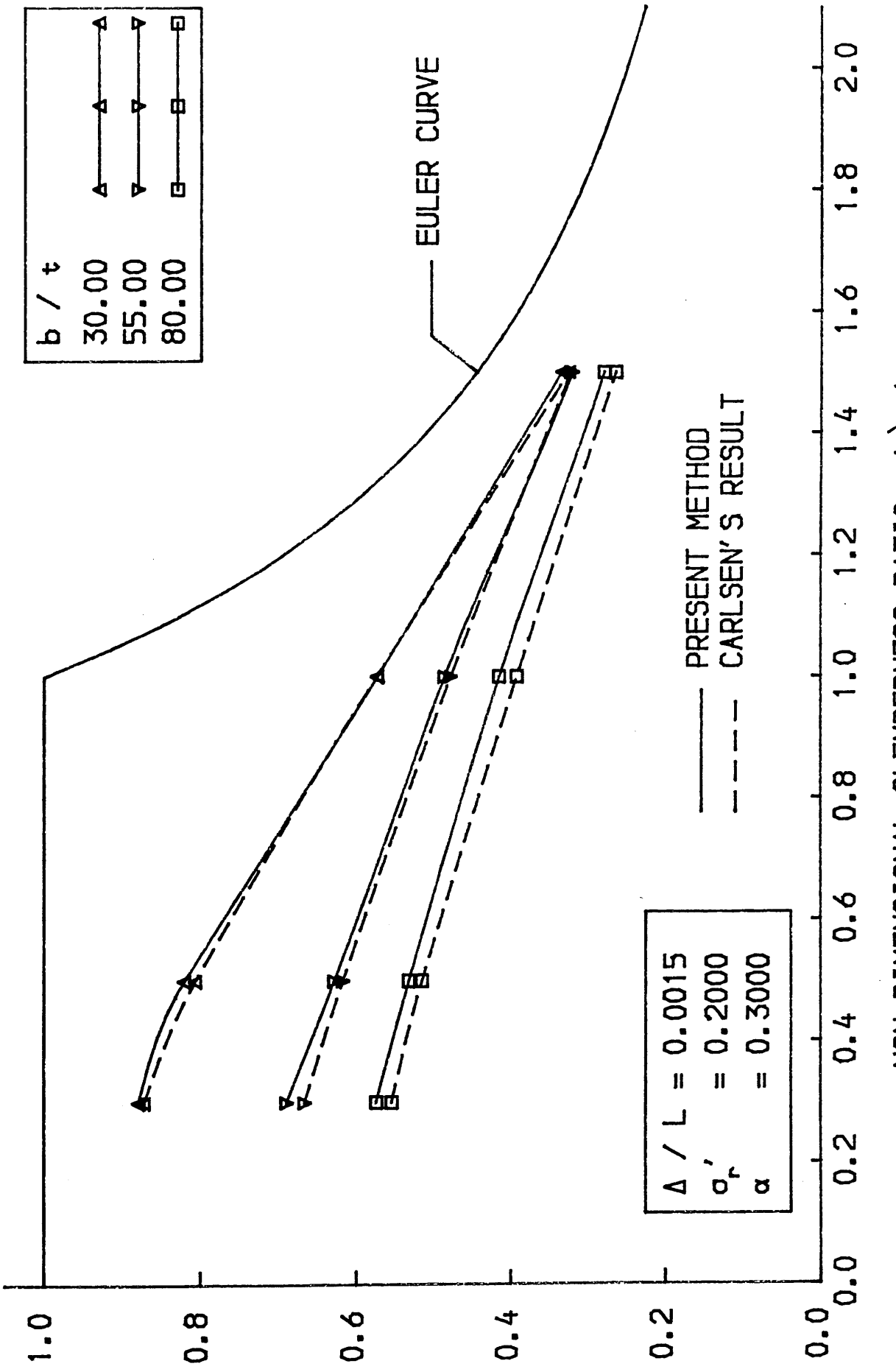

FIG.4-13 ULTIMATE STRENGTH-SLENDERNESS CURVE

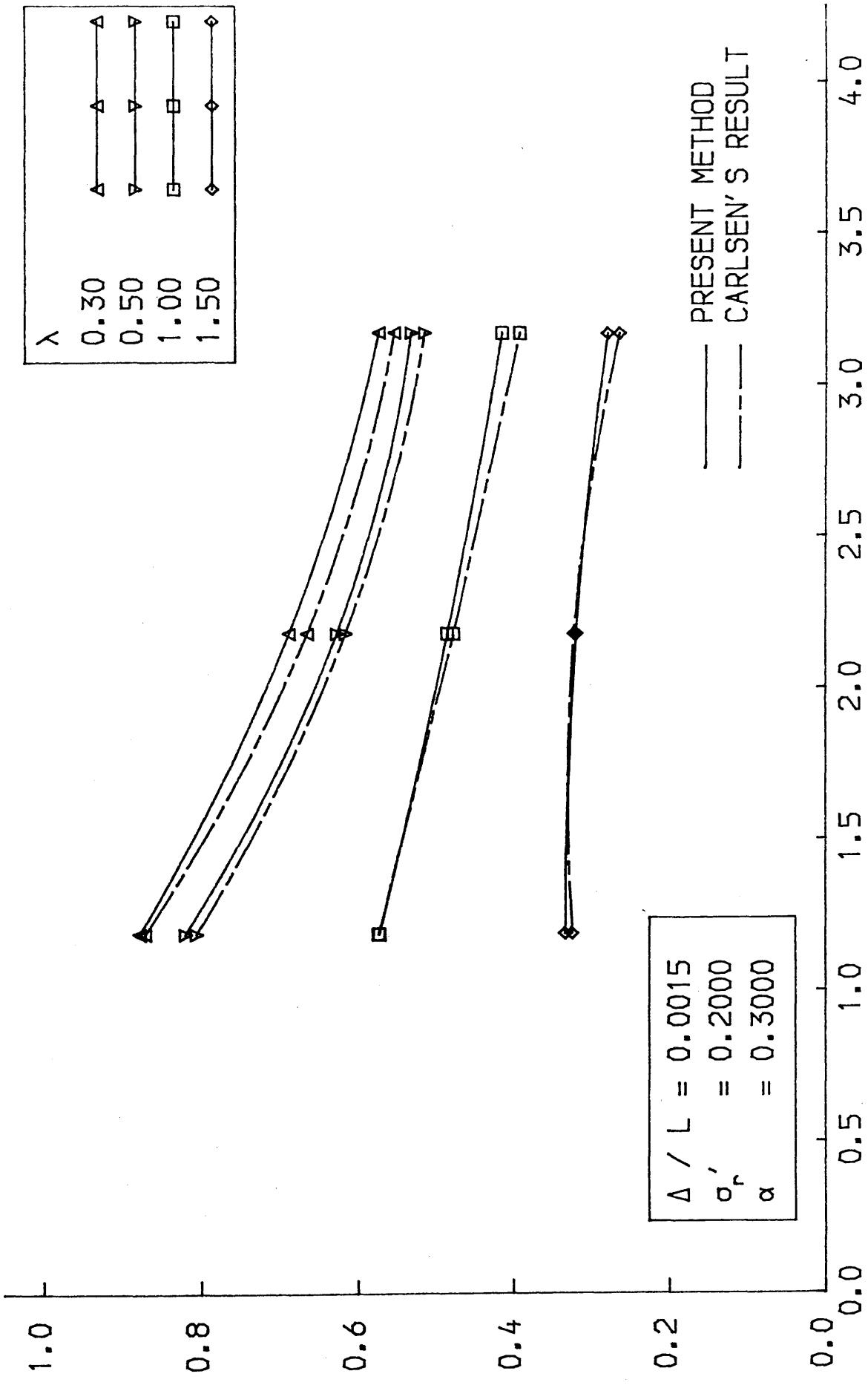

FIG.4-14 ULTIMATE STRENGTH-PLATE SLENDERNESS CURVE

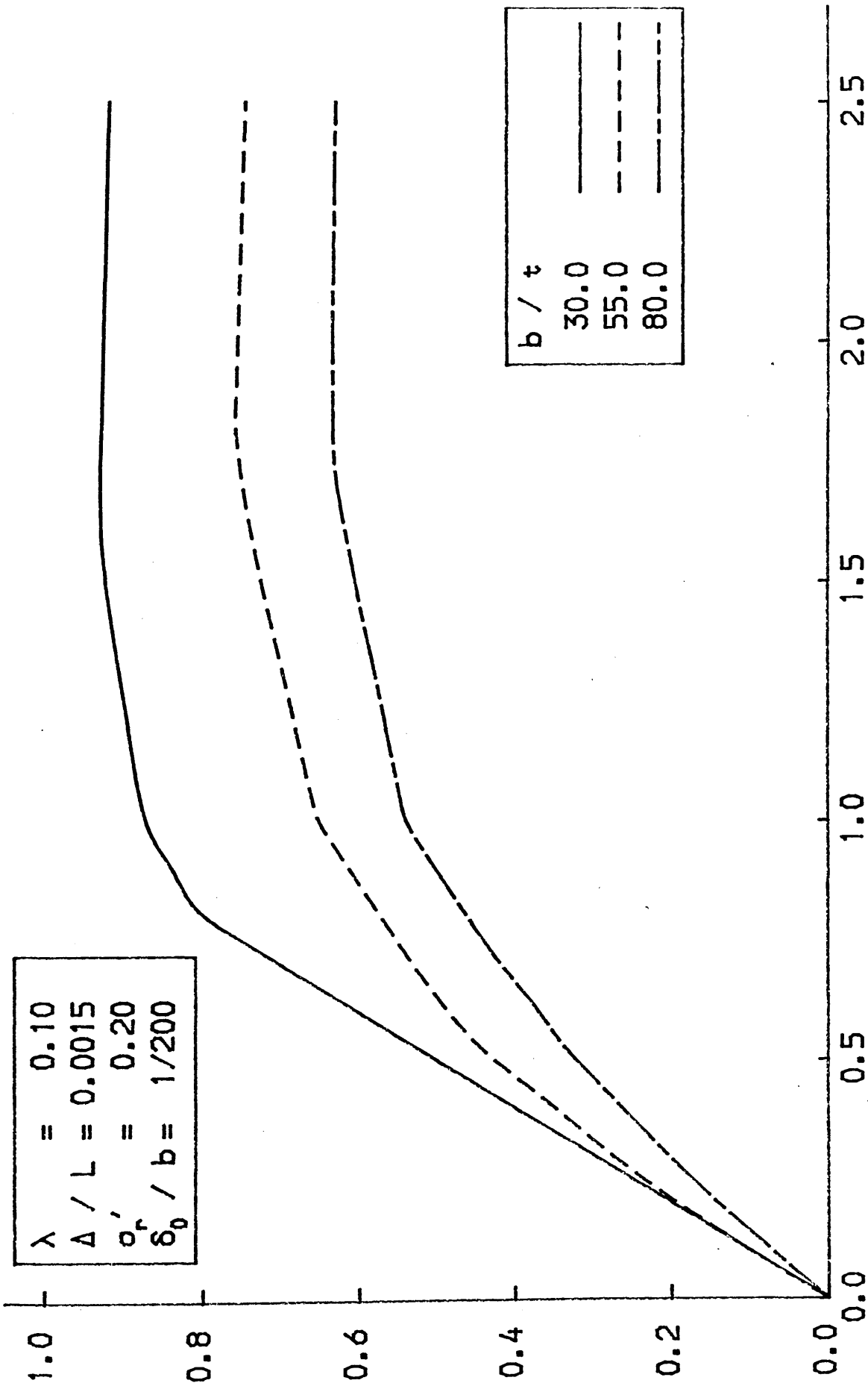

FIG.4-15 LOAD-SHORTENING CURVE FOR THE BEAM-COLUMN

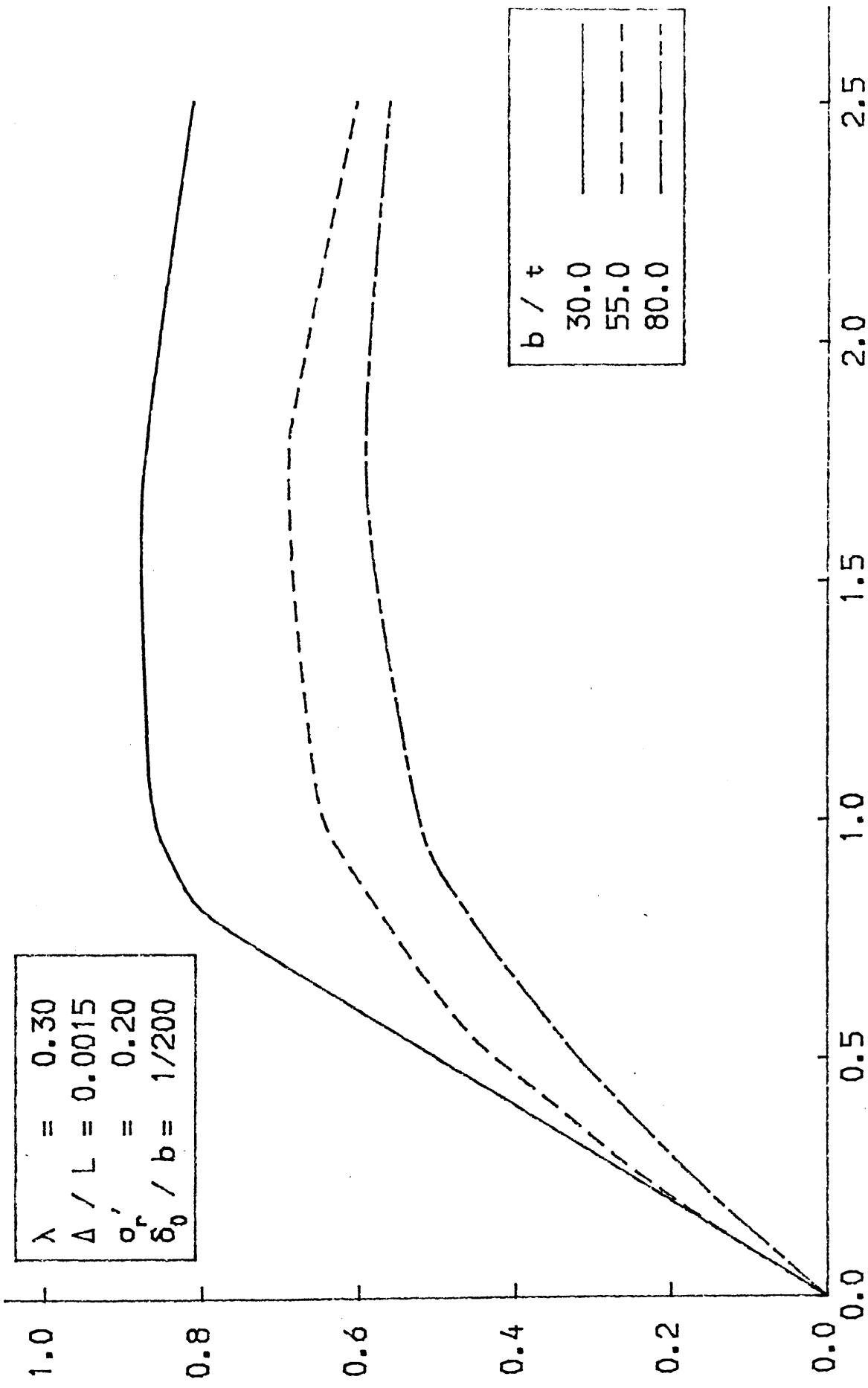

FIG.4-16 LOAD-SHORTENING CURVE FOR THE BEAM-COLUMN

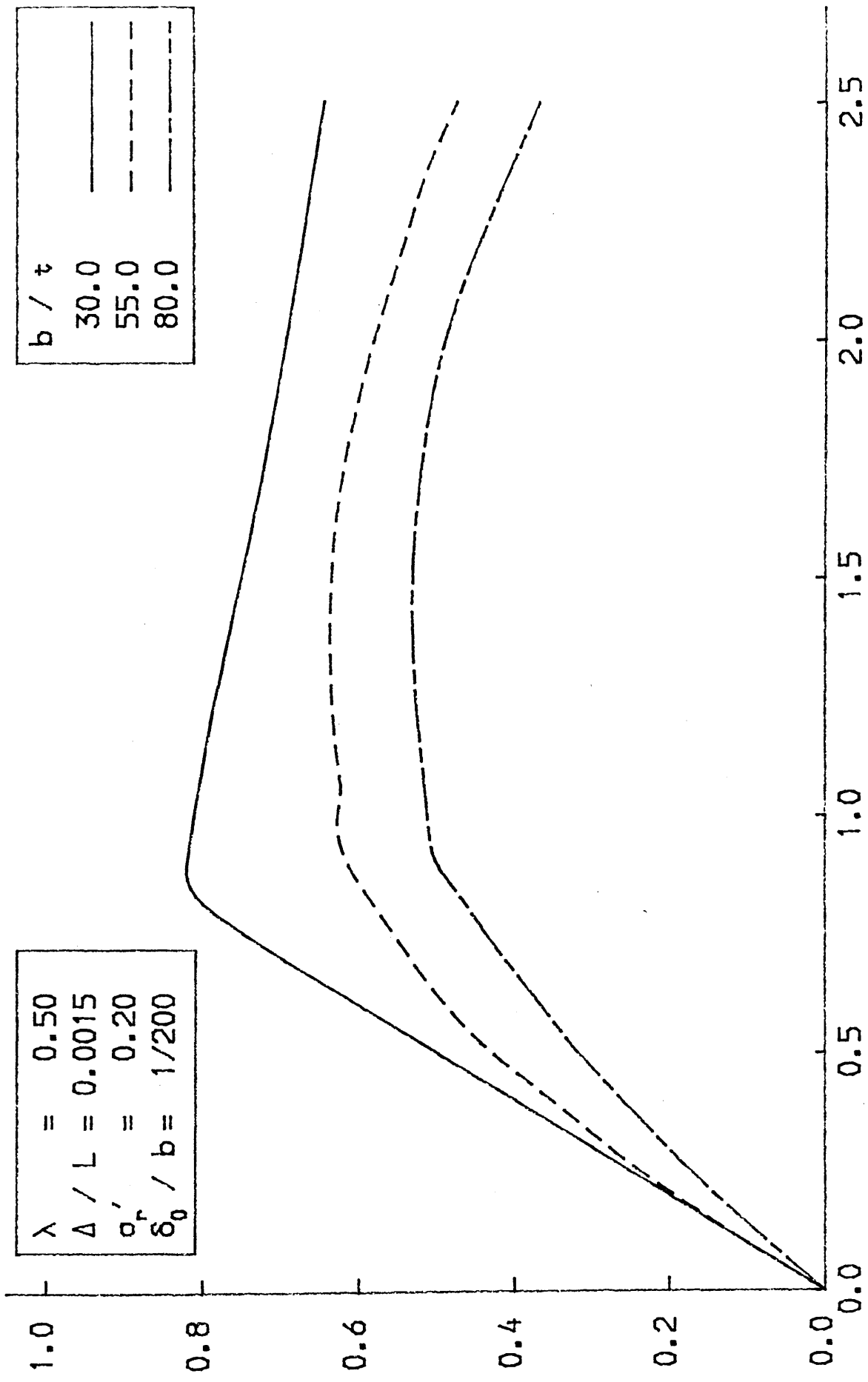

FIG.4-17 LOAD-SHORTENING CURVE FOR THE BEAM-COLUMN

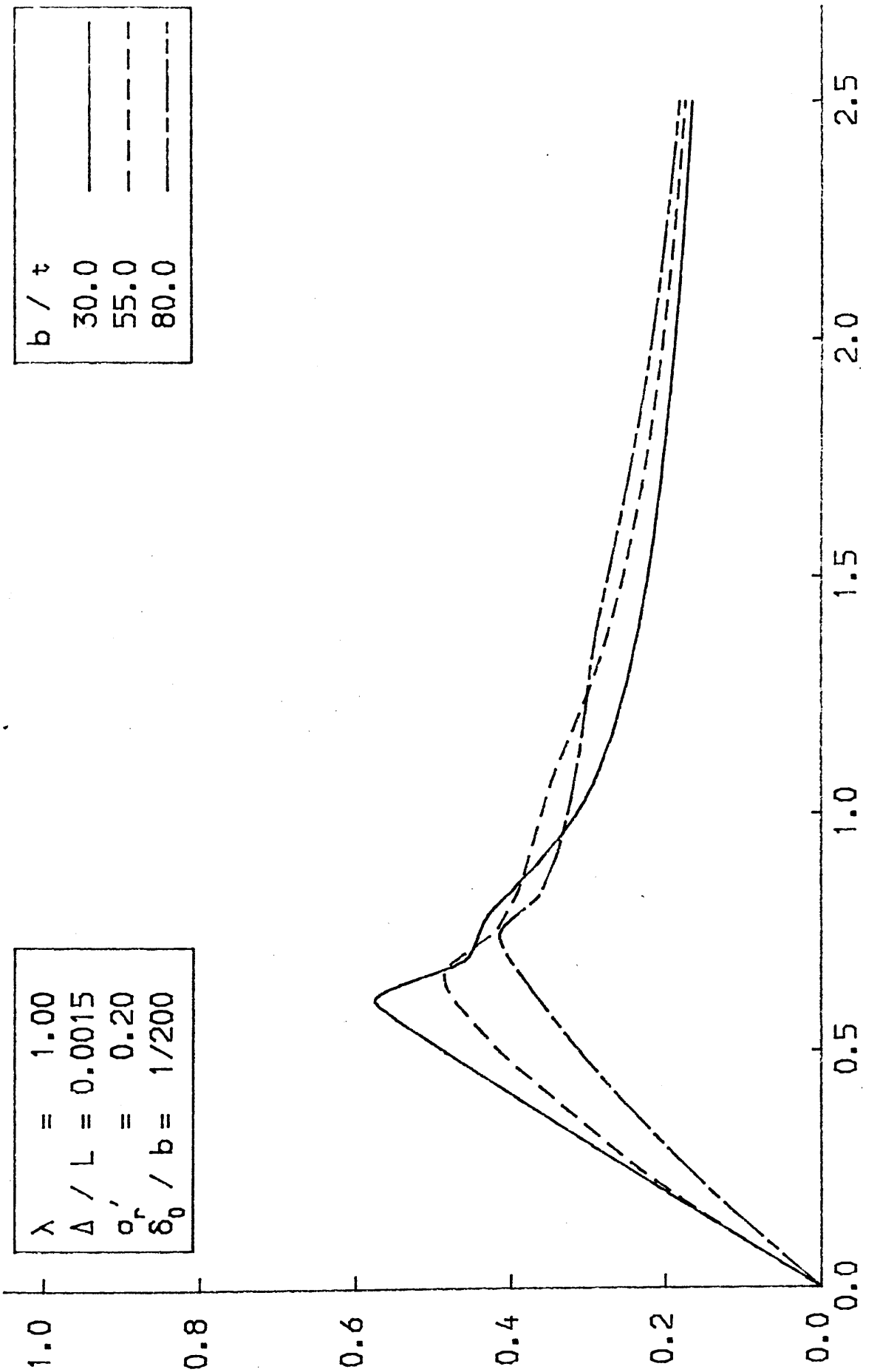

FIG.4-18 LOAD-SHORTENING CURVE FOR THE BEAM-COLUMN

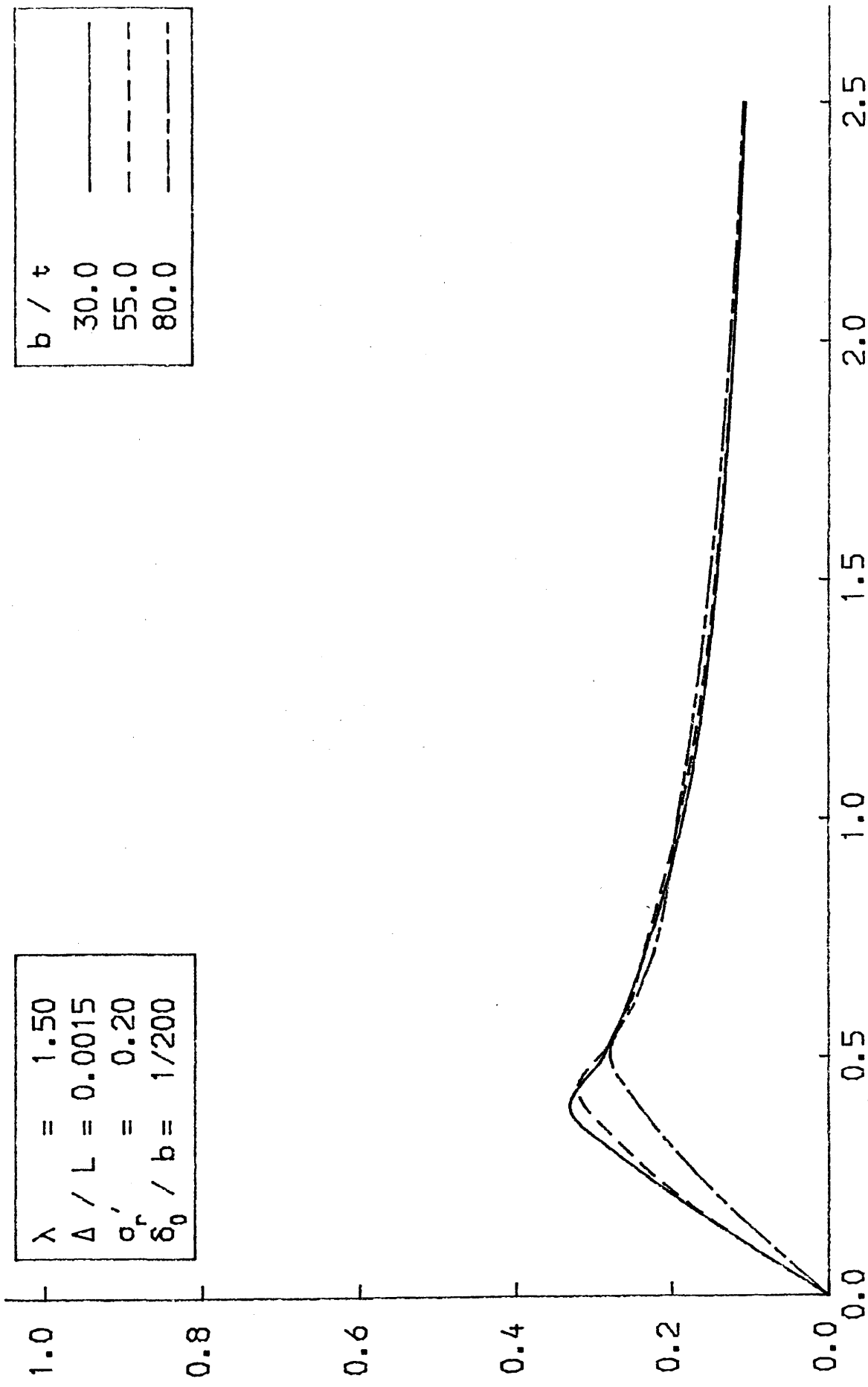

FIG.4-19 LOAD-SHORTENING CURVE FOR THE BEAM-COLUMN

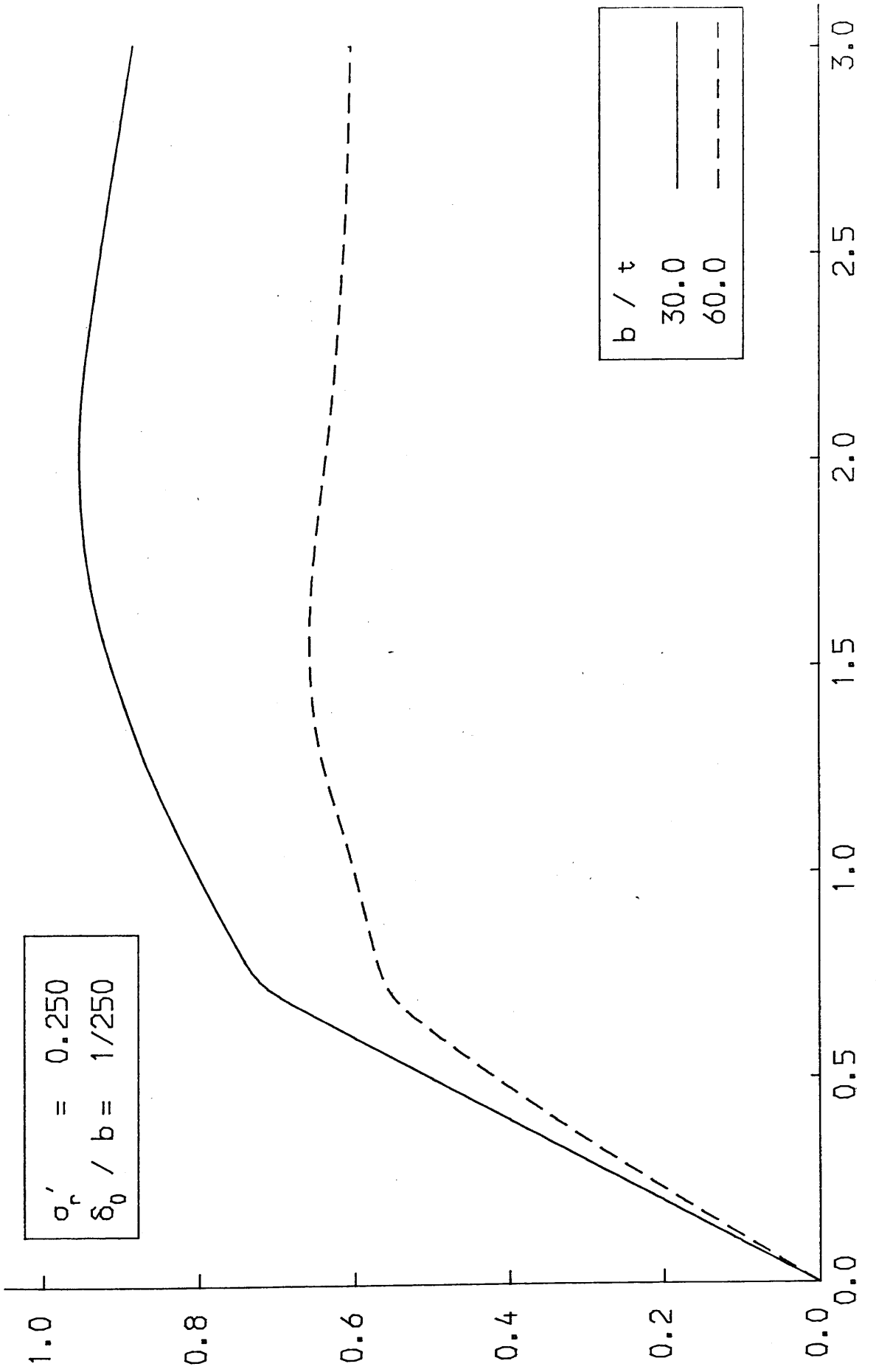

FIG. 4-20 AVERAGE STRESS-STRAIN CURVE FOR THE PLATE

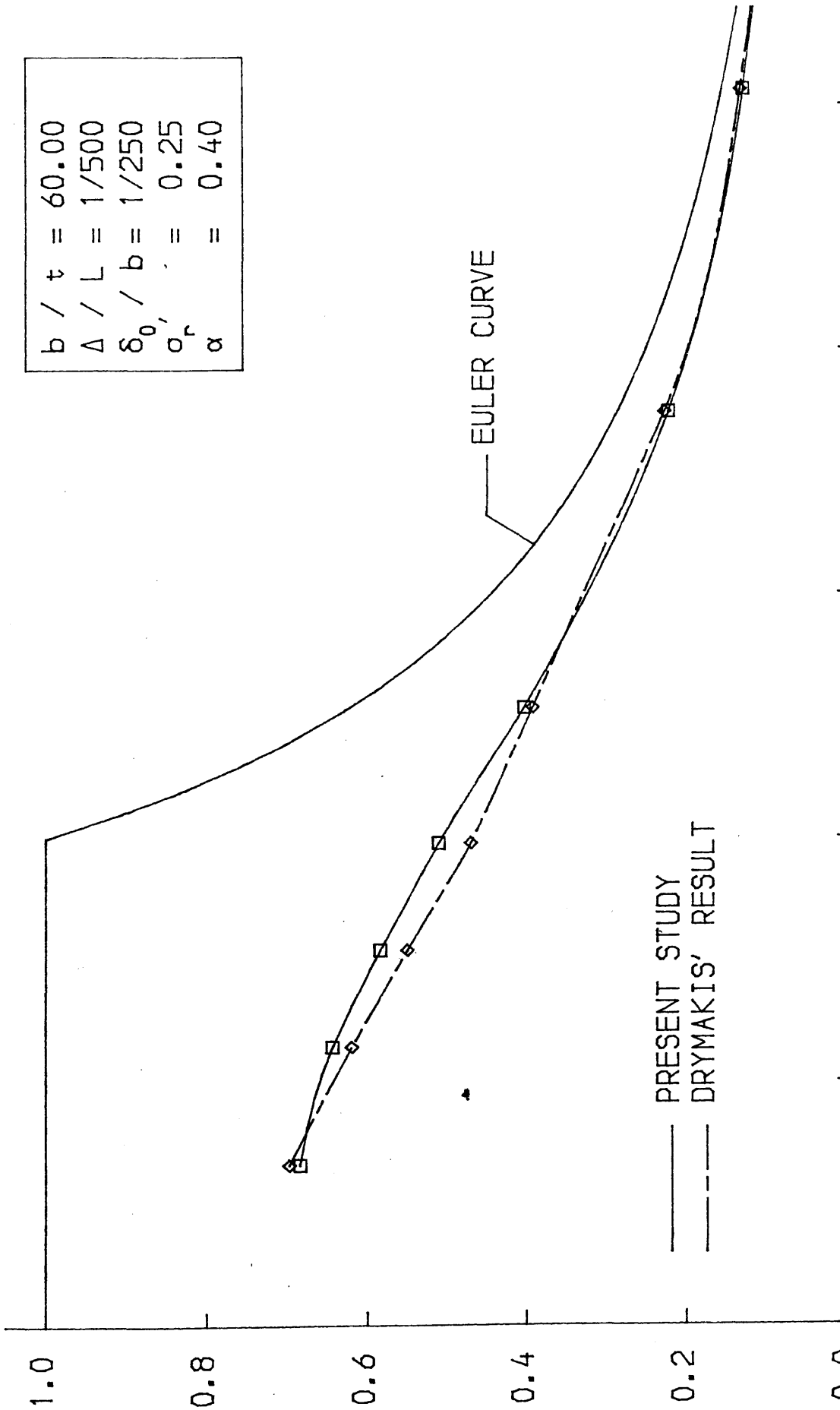

FIG. 4-21 ULTIMATE STRENGTH-SLENDERNESS CURVE

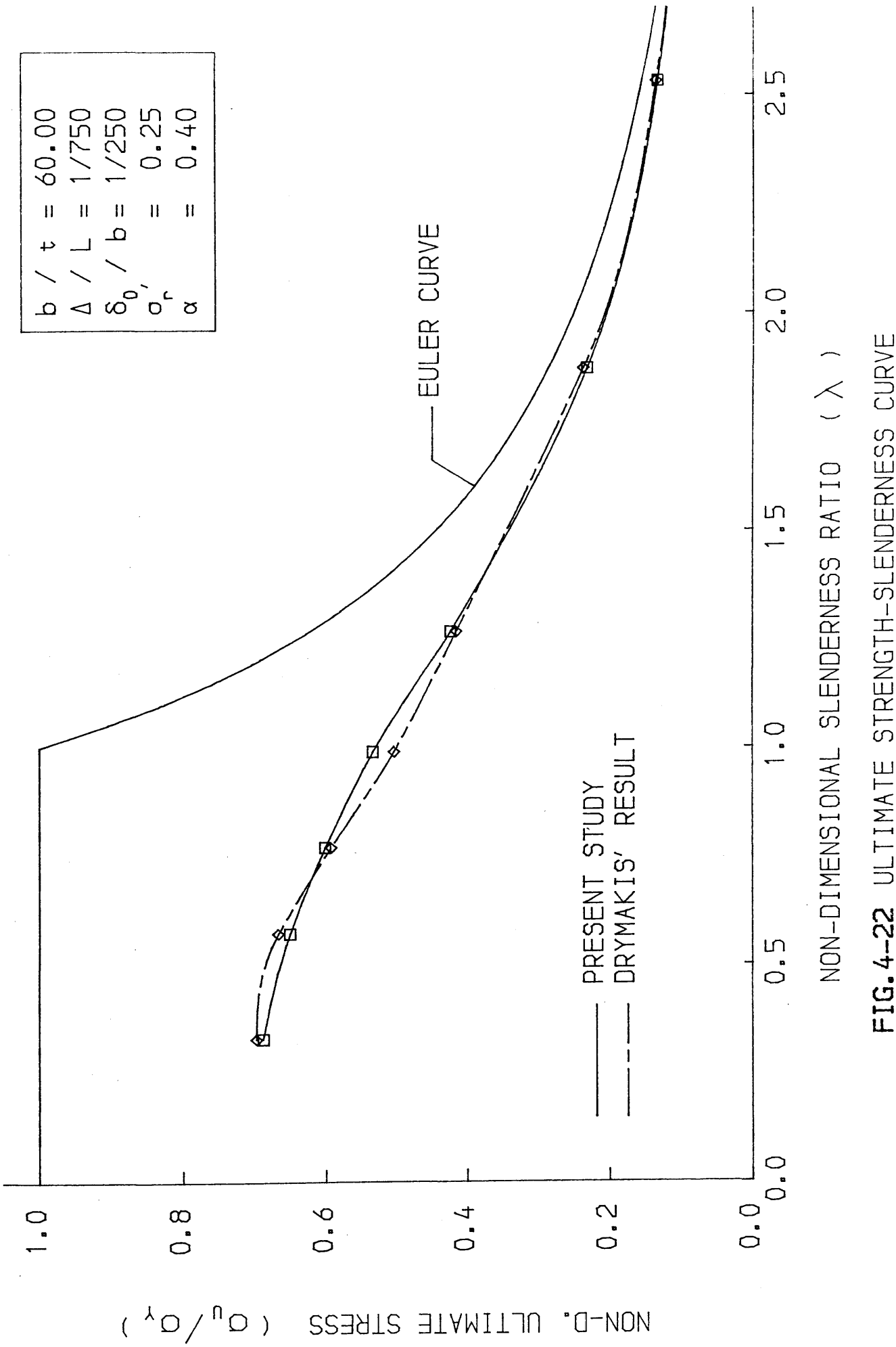

FIG. 4-22 ULTIMATE STRENGTH-SLENDERNESS CURVE

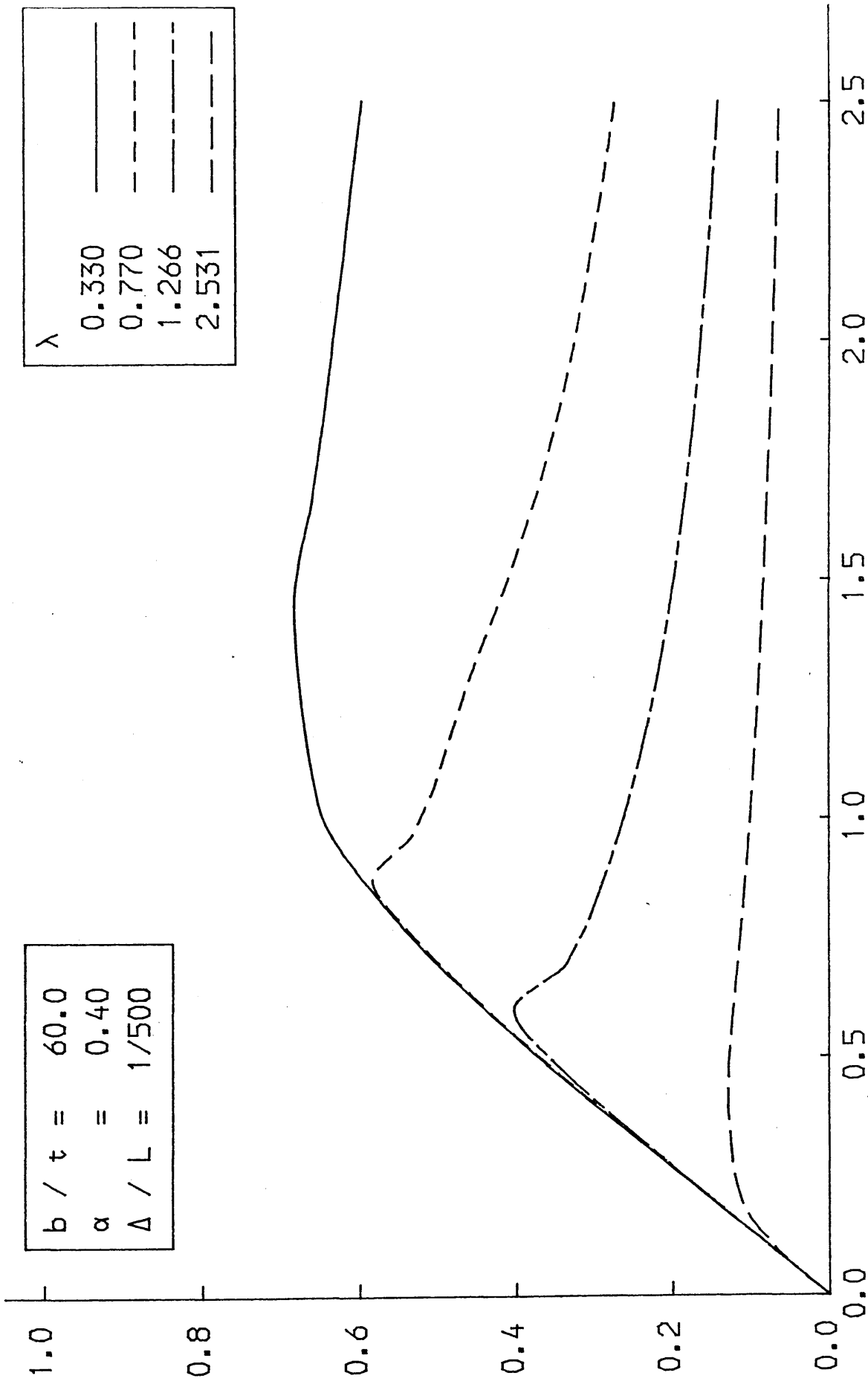

FIG.4-23 LOAD-SHORTENING CURVE FOR THE BEAM-COLUMN

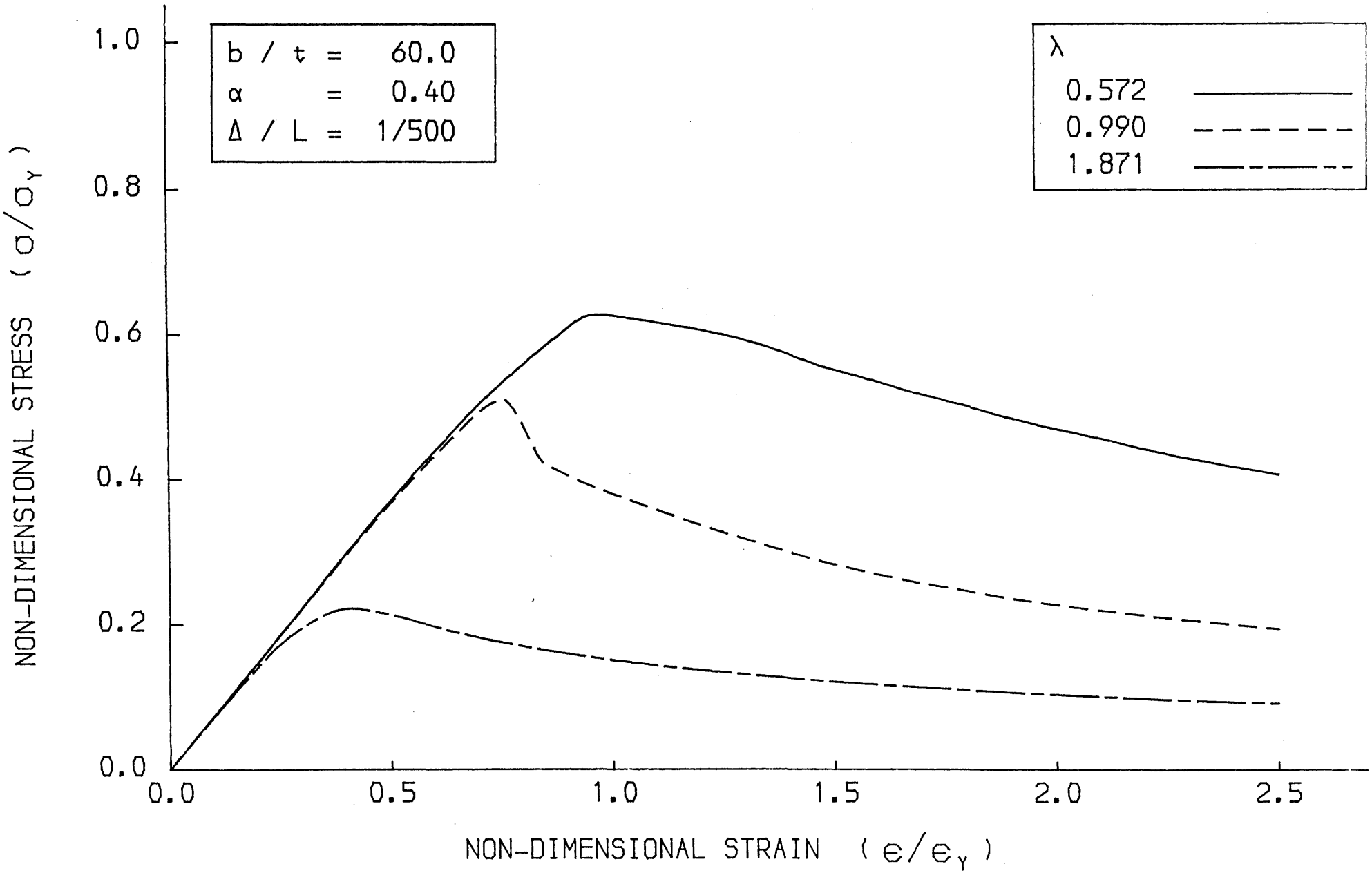

FIG.4-24 LOAD-SHORTENING CURVE FOR THE BEAM-COLUMN

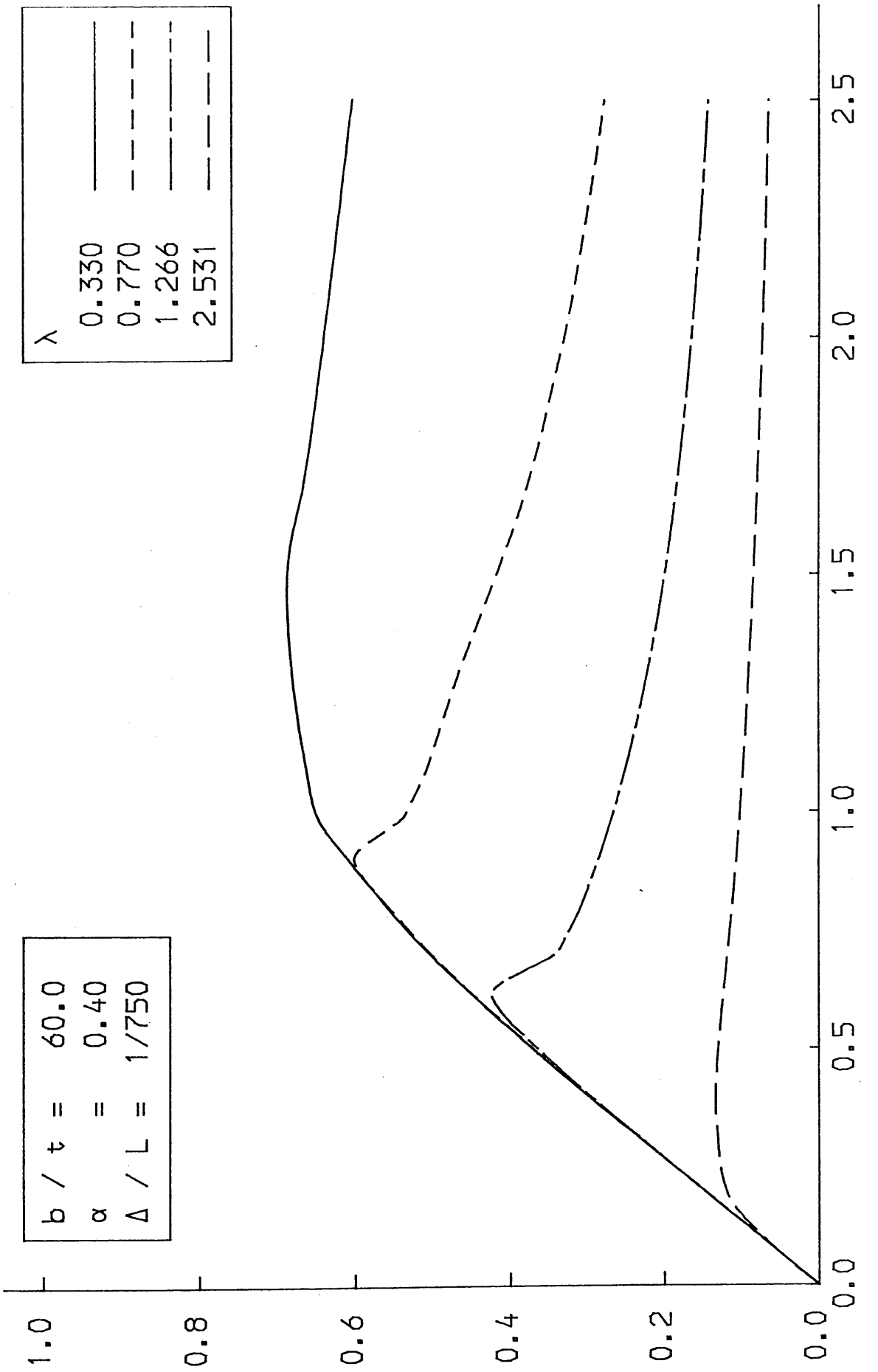

FIG.4-25 LOAD-SHORTENING CURVE FOR THE BEAM-COLUMN

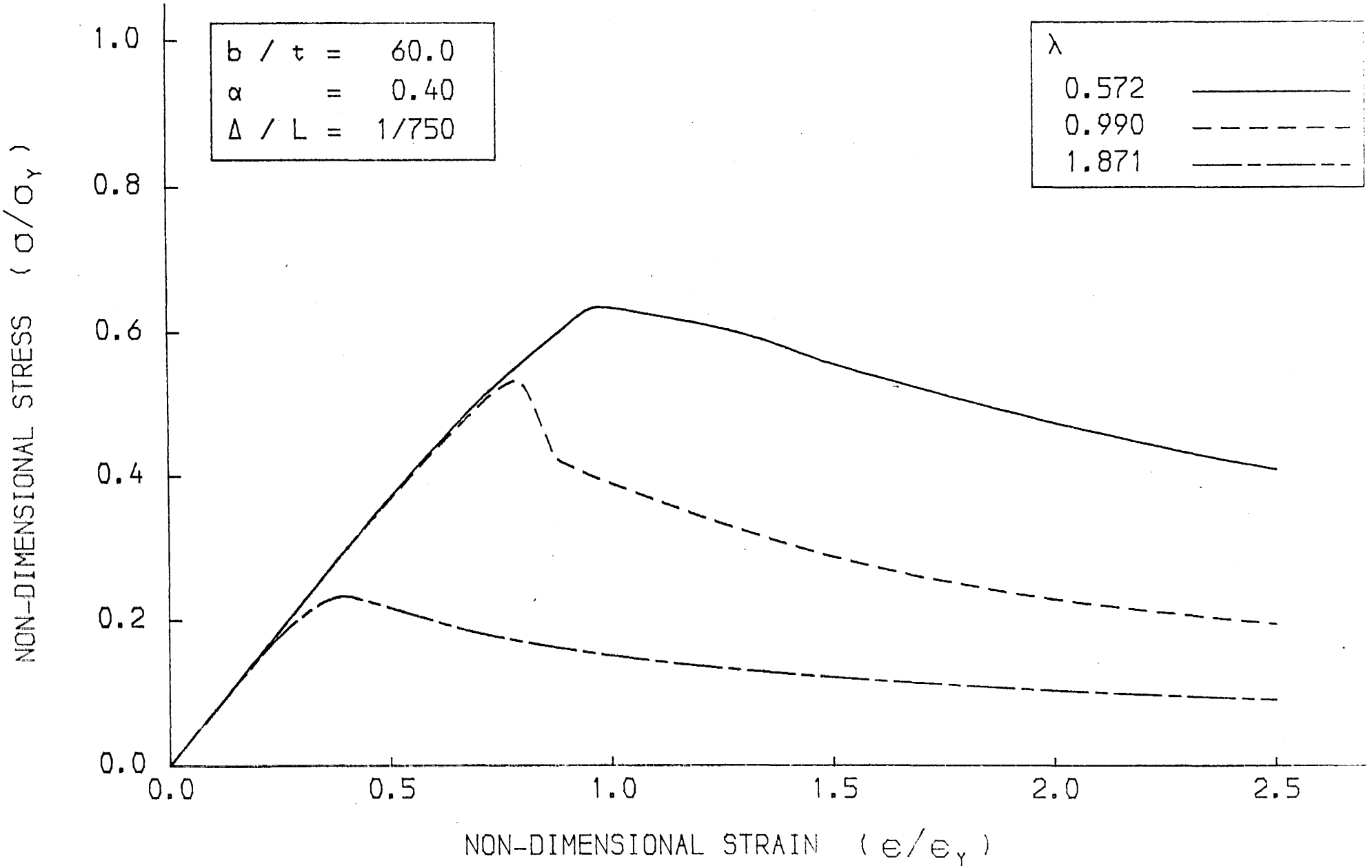

FIG.4-26 LOAD-SHORTENING CURVE FOR THE BEAM-COLUMN

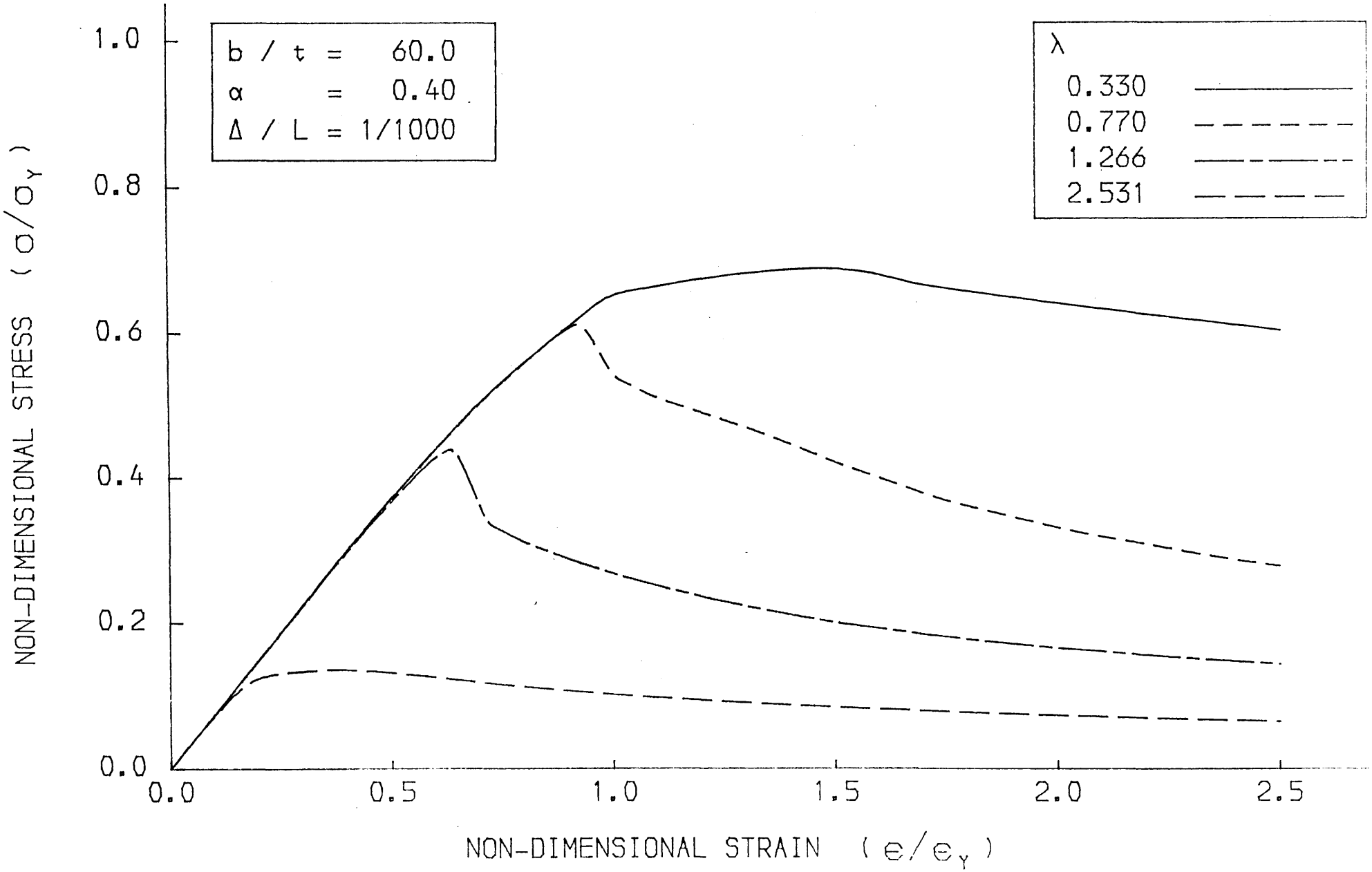

FIG.4-27 LOAD-SHORTENING CURVE FOR THE BEAM-COLUMN

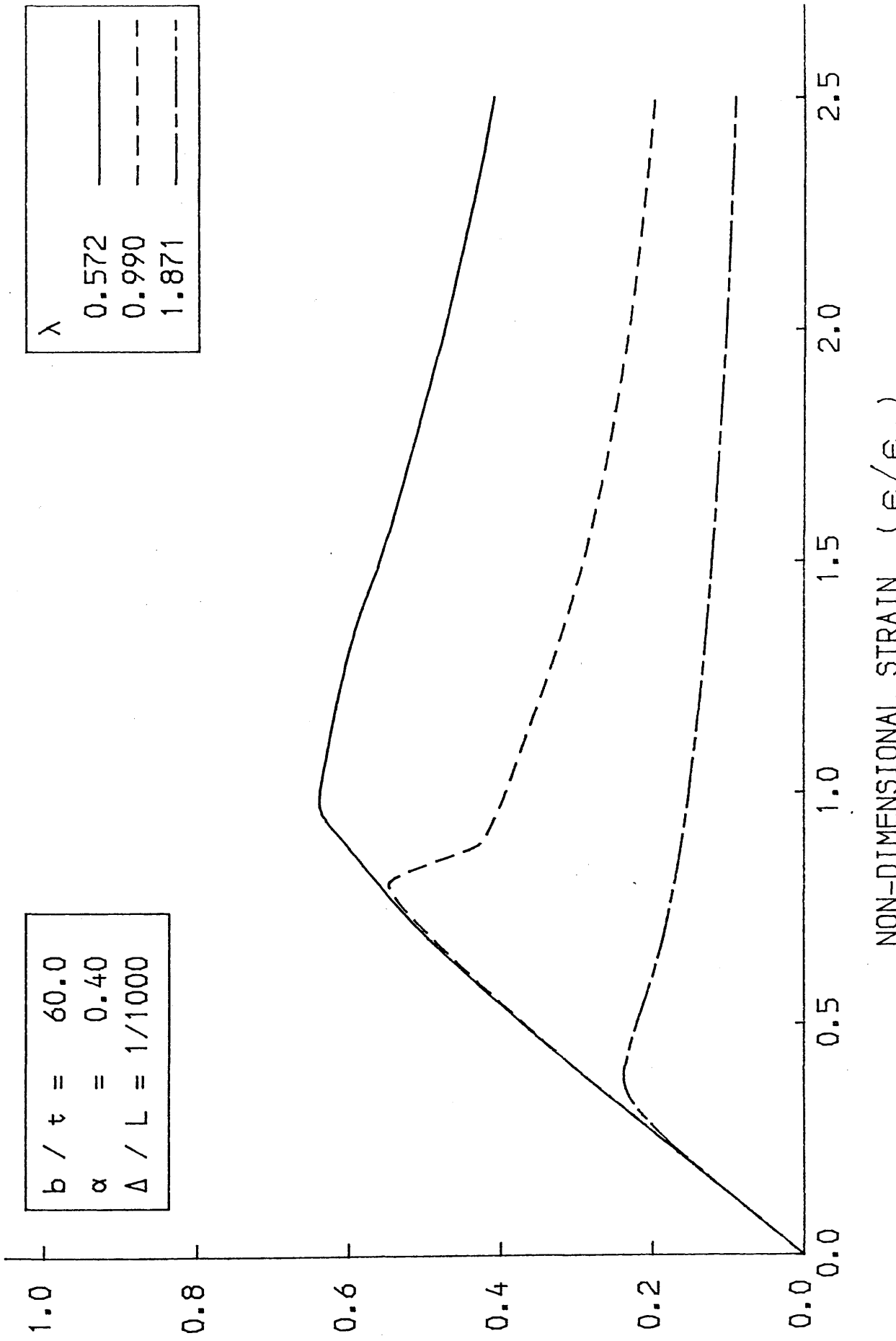

FIG.4-28 LOAD-SHORTENING CURVE FOR THE BEAM-COLUMN

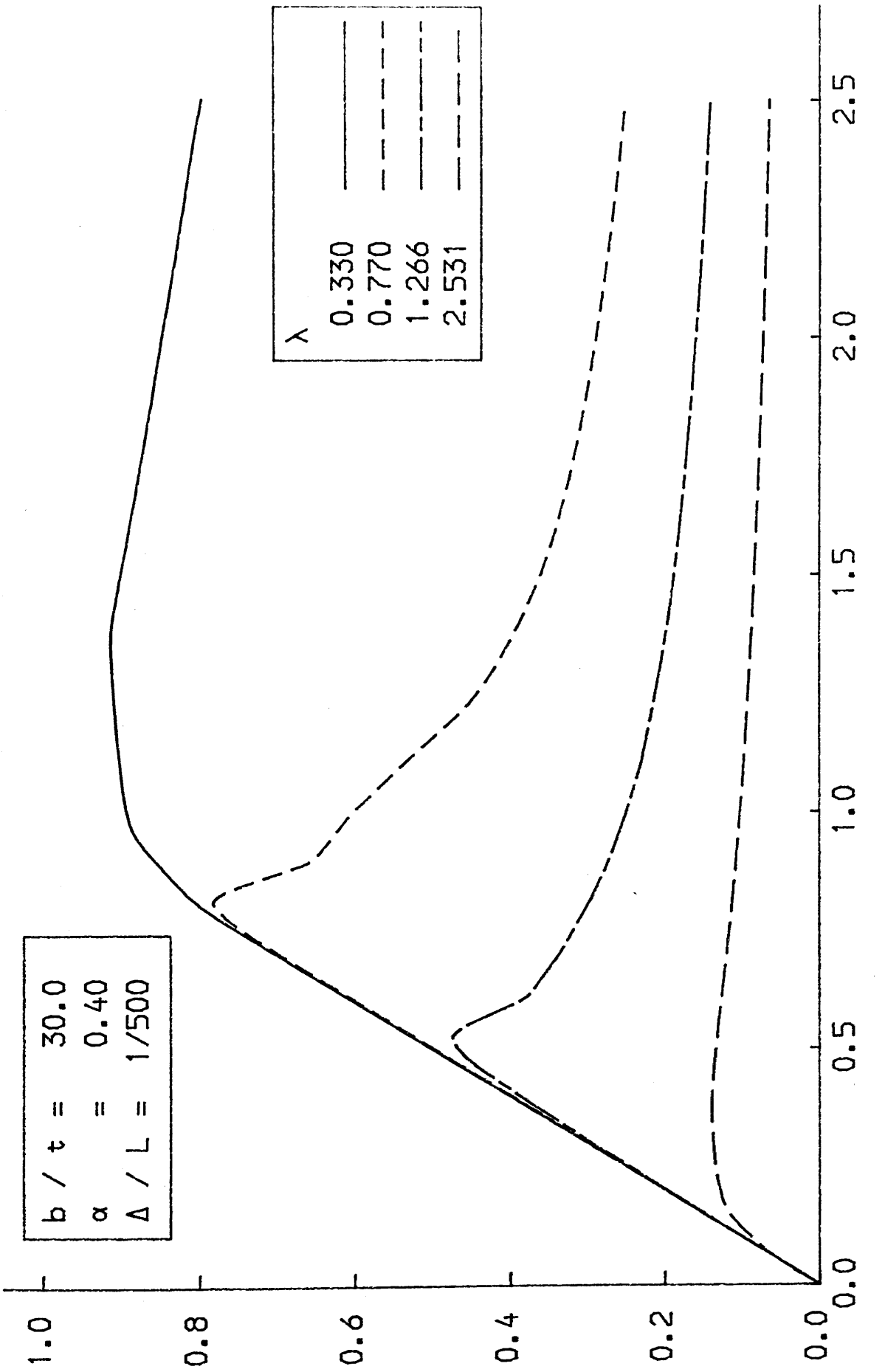

FIG. 4-29 LOAD-SHORTENING CURVE FOR THE BEAM-COLUMN

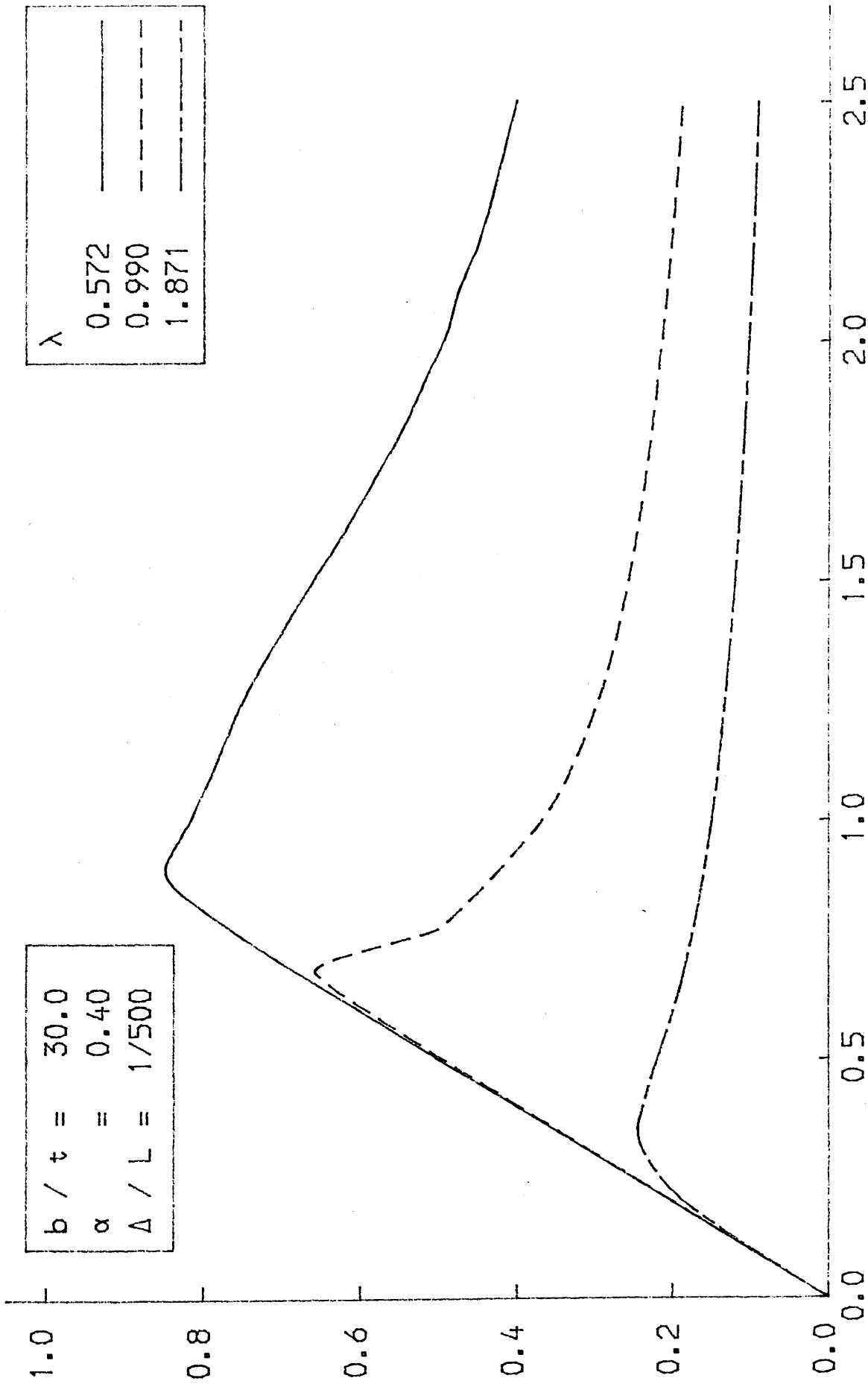

FIG. 4-30 LOAD-SHORTENING CURVE FOR THE BEAM-COLUMN

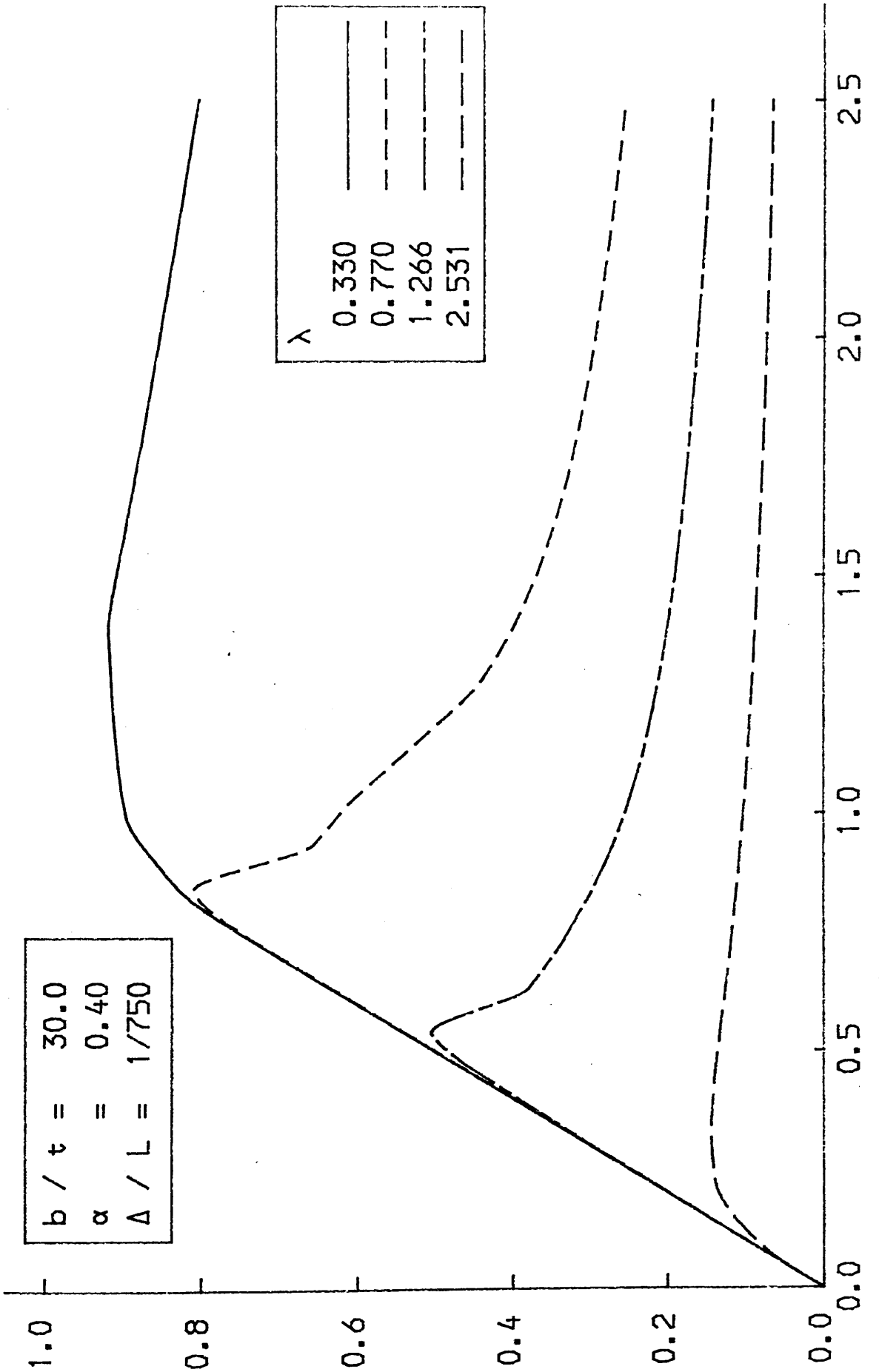

FIG.4-31 LOAD-SHORTENING CURVE FOR THE BEAM-COLUMN

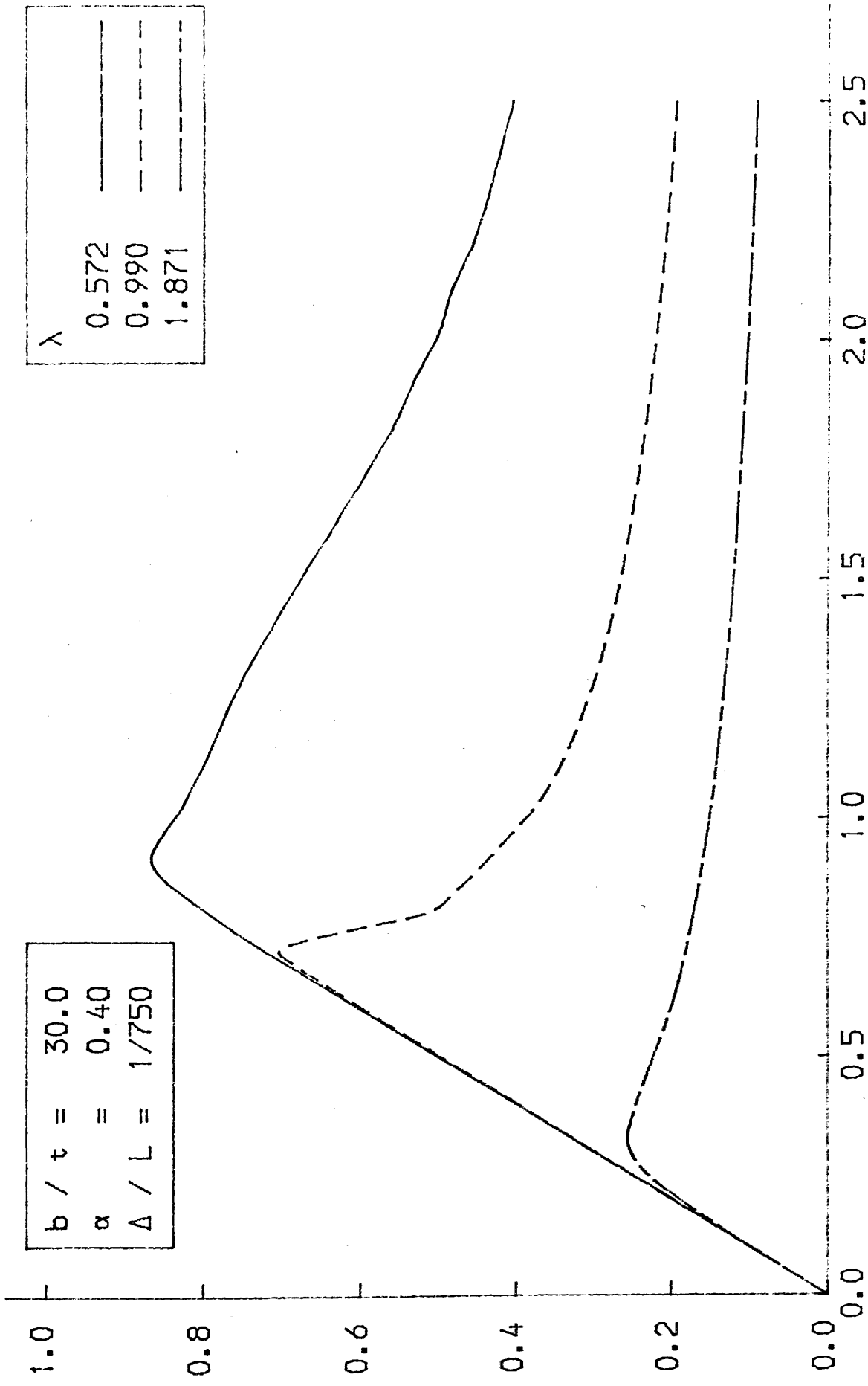

FIG.4-32 LOAD-SHORTENING CURVE FOR THE BEAM-COLUMN

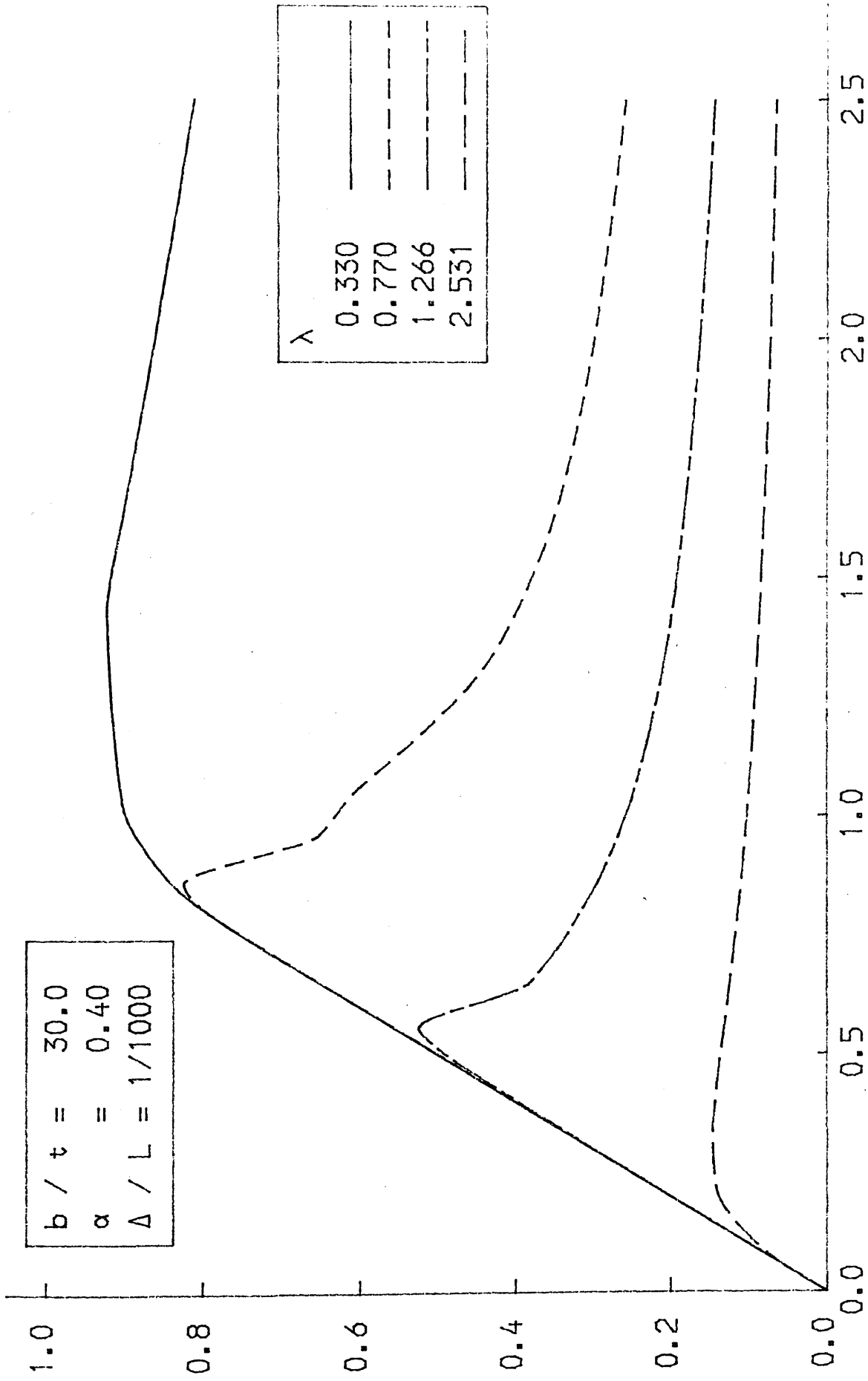

FIG.4-33 LOAD-SHORTENING CURVE FOR THE BEAM-COLUMN

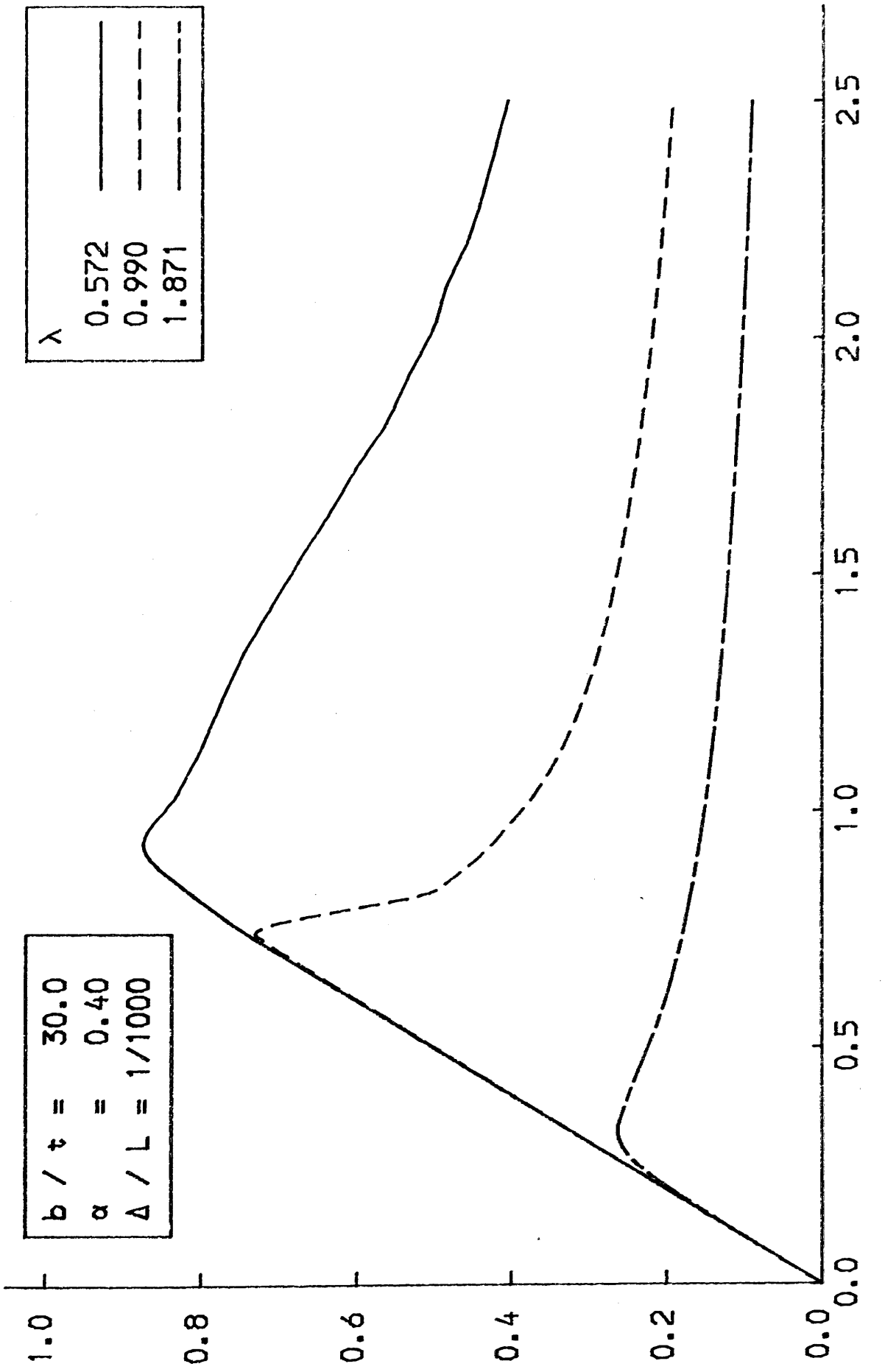

FIG.4-34 LOAD-SHORTENING CURVE FOR THE BEAM-COLUMN

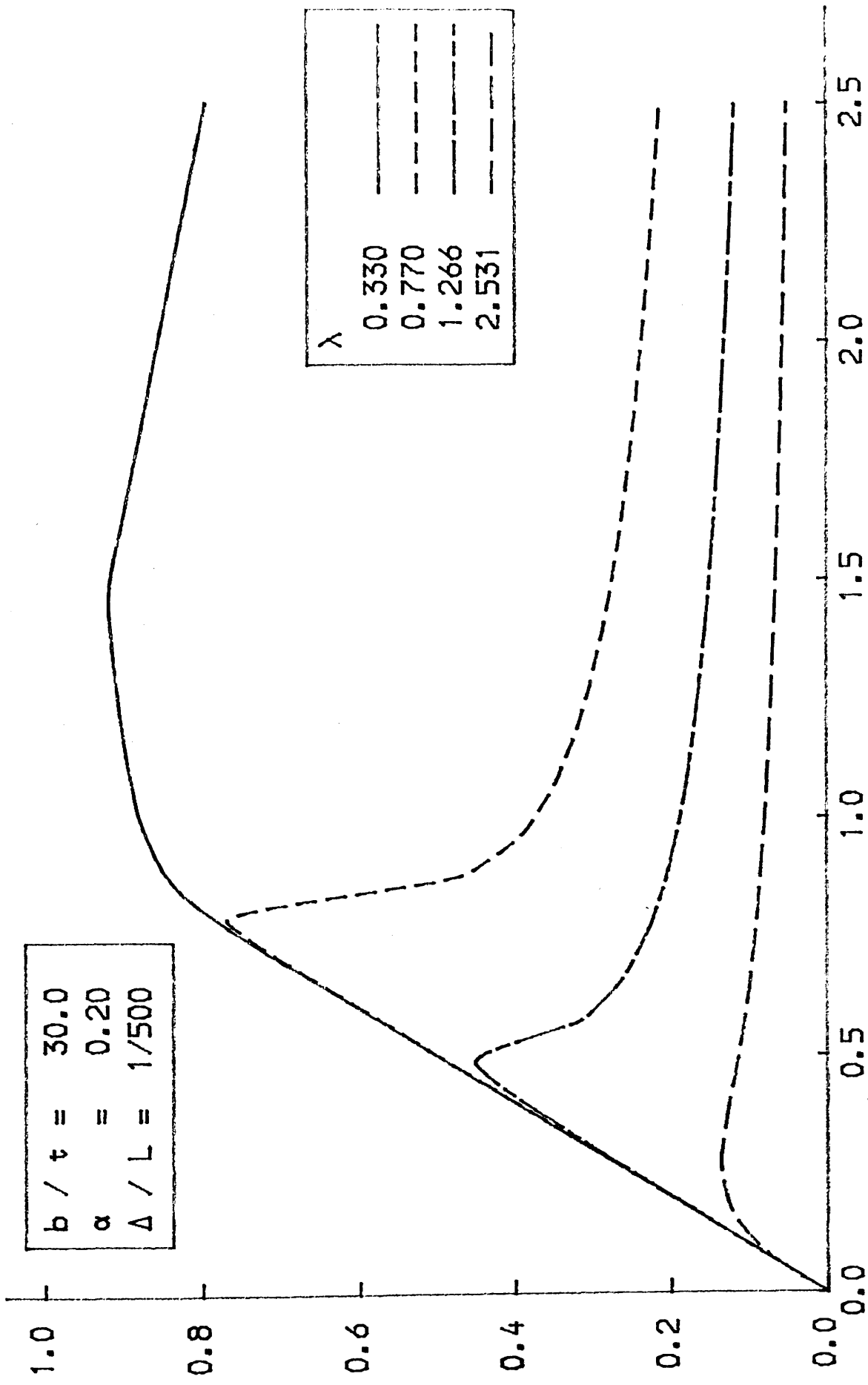

FIG.4-35 LOAD-SHORTENING CURVE FOR THE BEAM-COLUMN

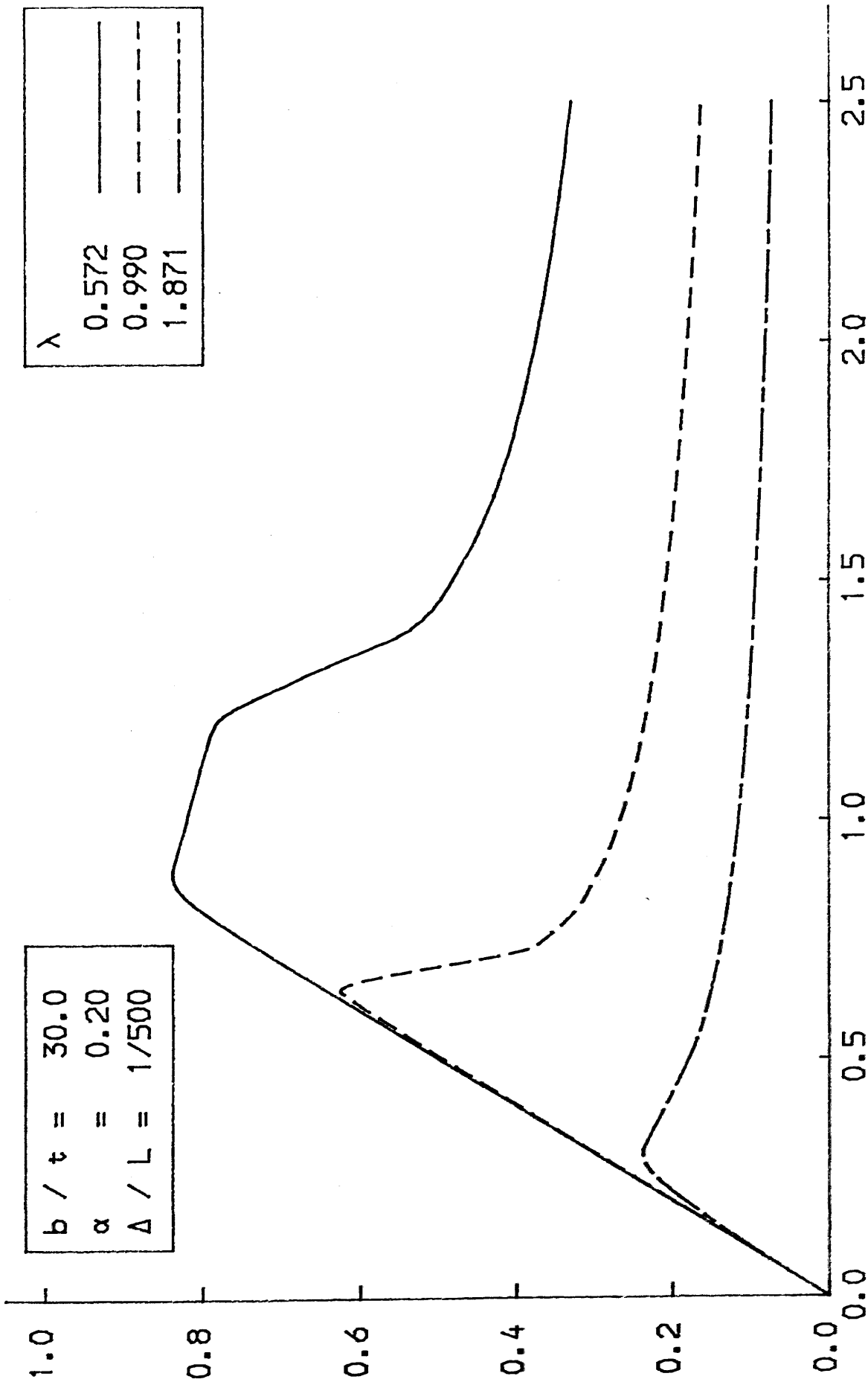

FIG. 4-36 LOAD-SHORTENING CURVE FOR THE BEAM-COLUMN

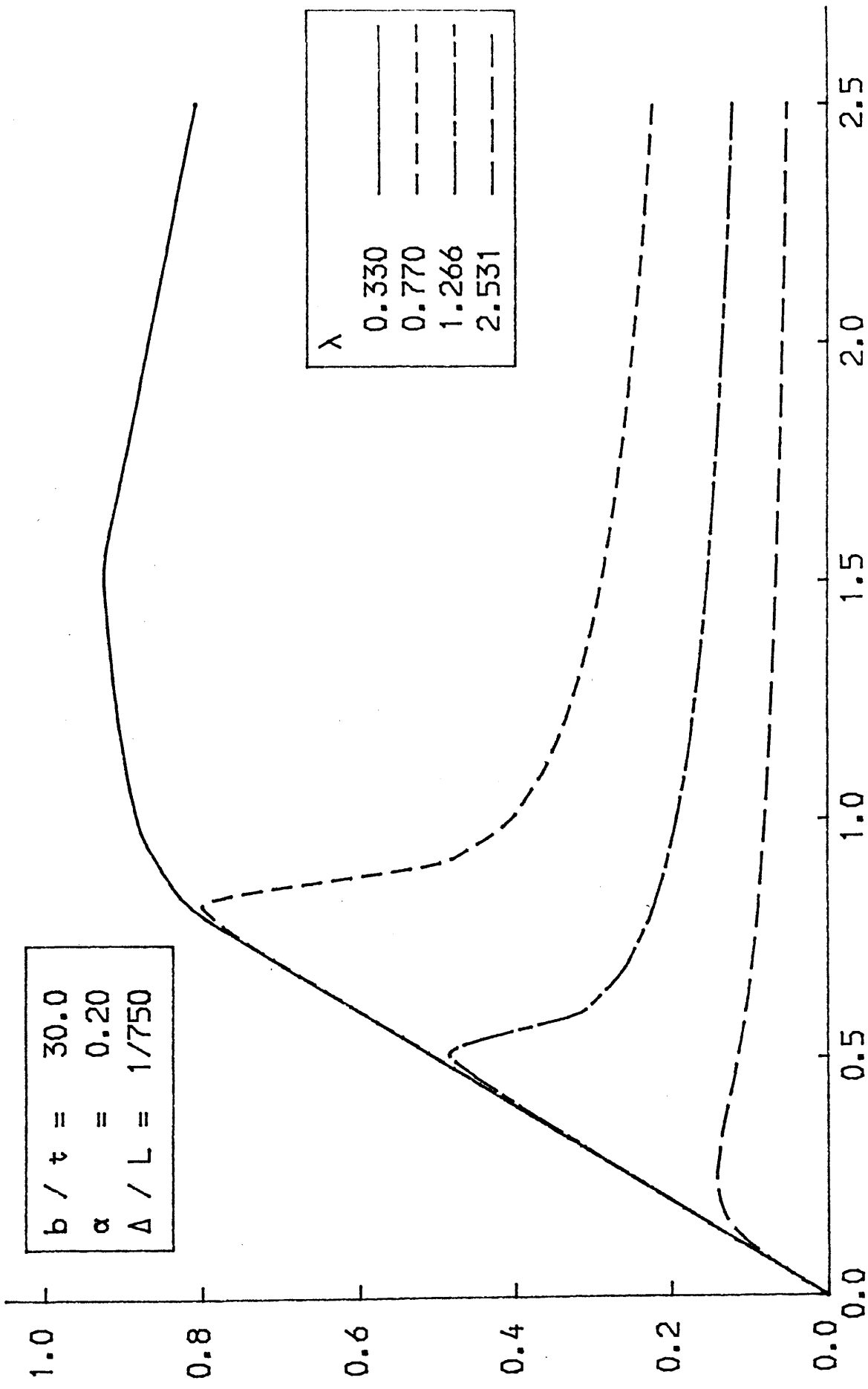

FIG.4-37 LOAD-SHORTENING CURVE FOR THE BEAM-COLUMN

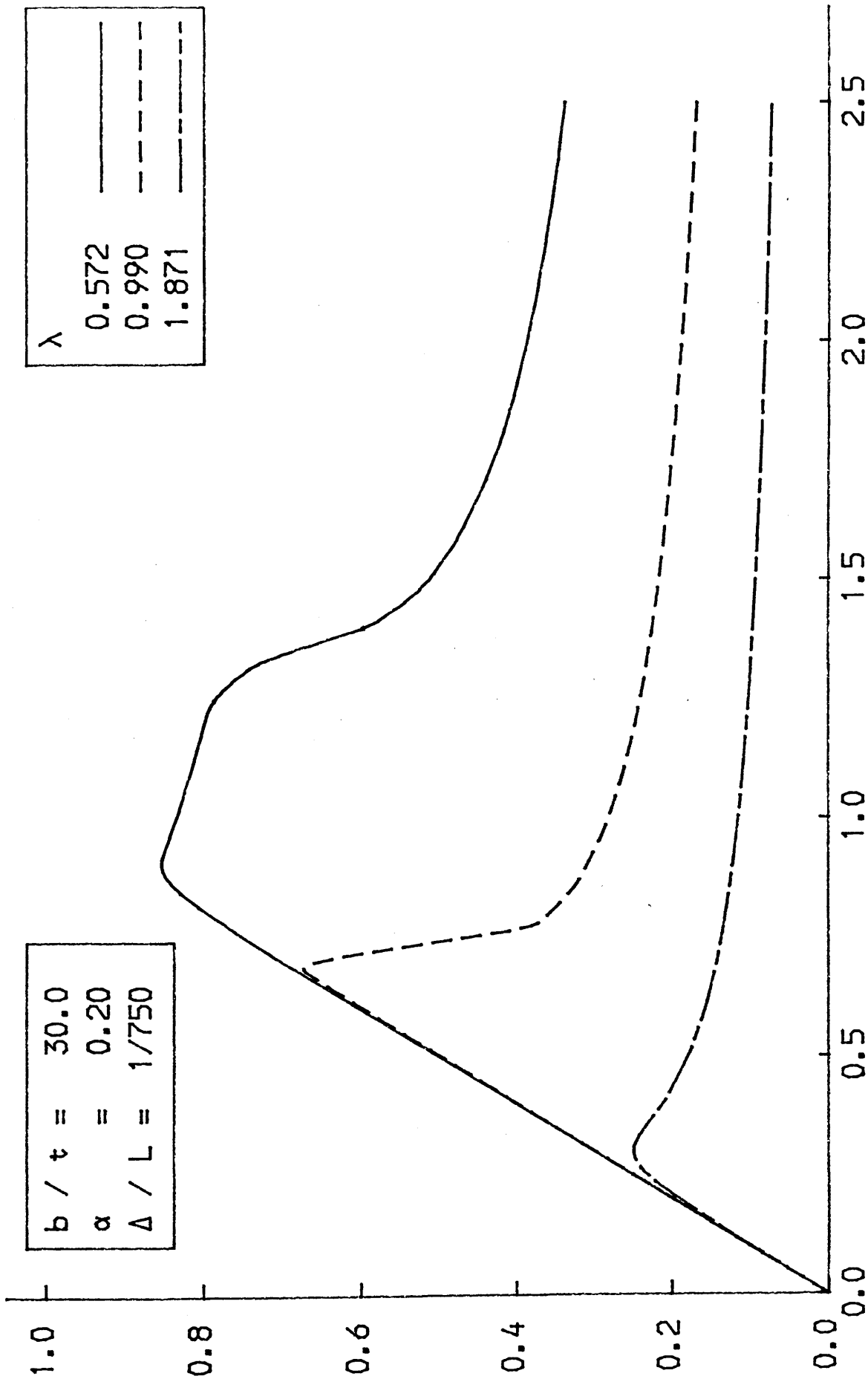

FIG. 4-38 LOAD-SHORTENING CURVE FOR THE BEAM-COLUMN

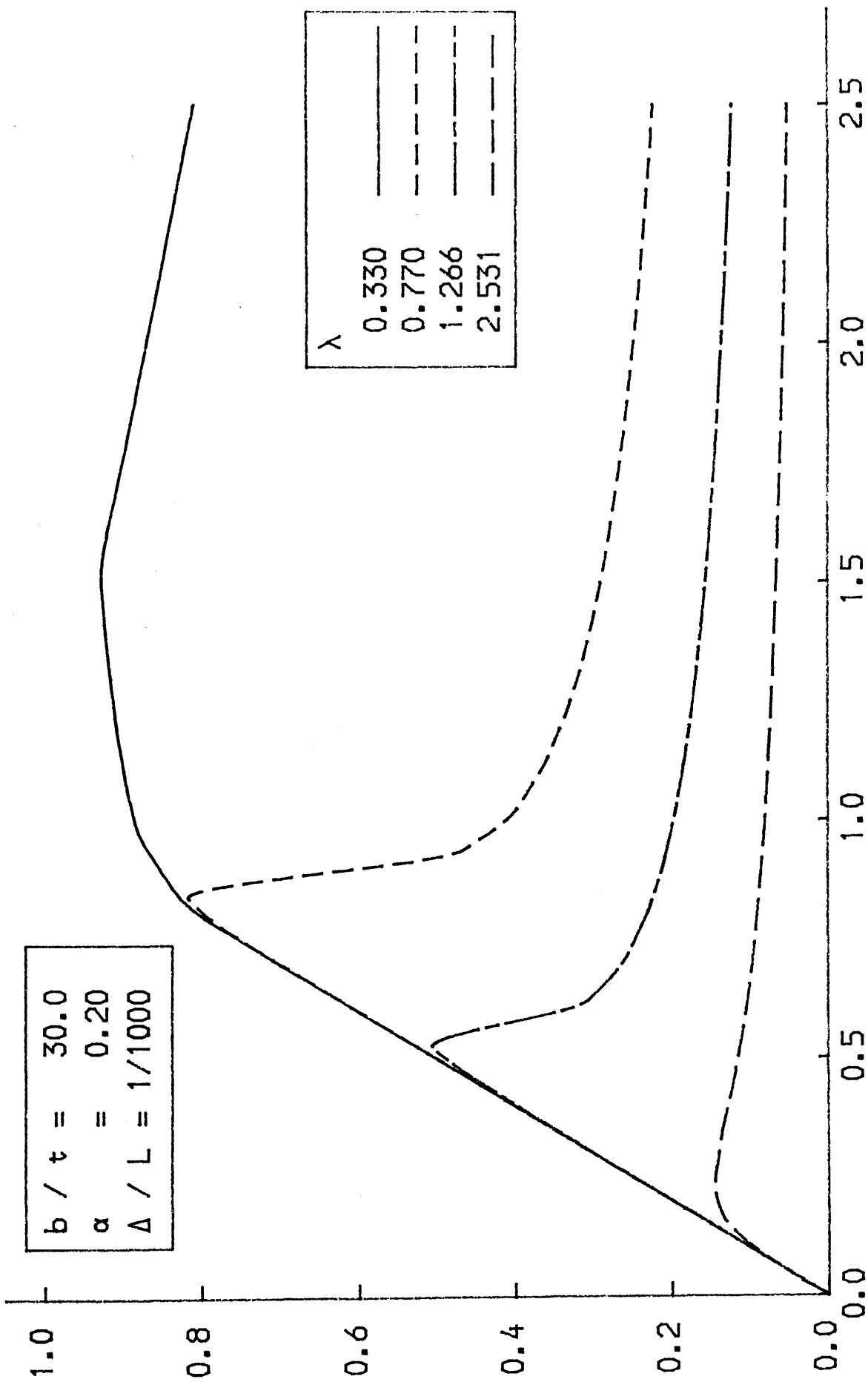

FIG. 4-39 LOAD-SHORTENING CURVE FOR THE BEAM-COLUMN

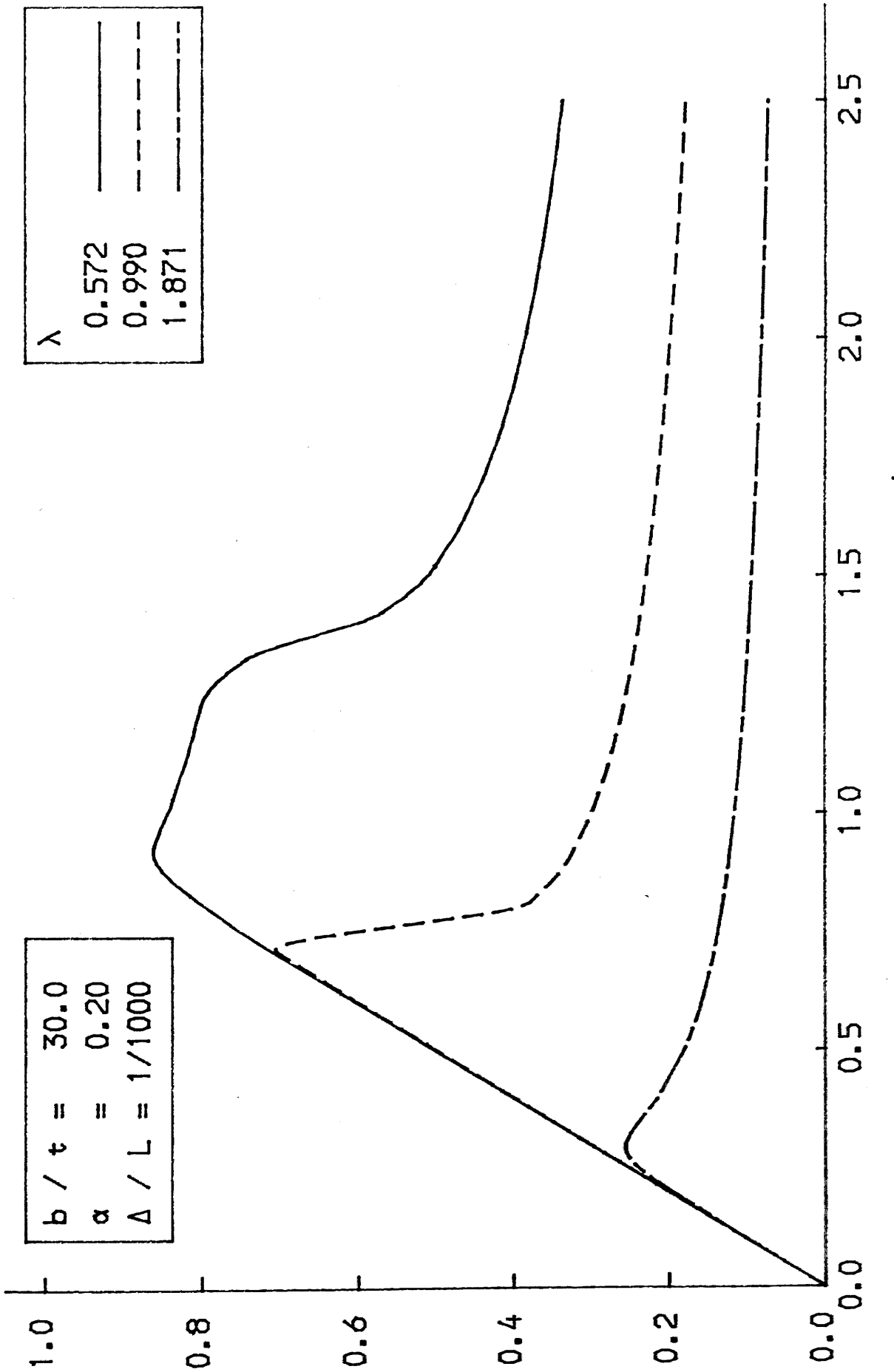

FIG.4-40 LOAD-SHORTENING CURVE FOR THE BEAM-COLUMN

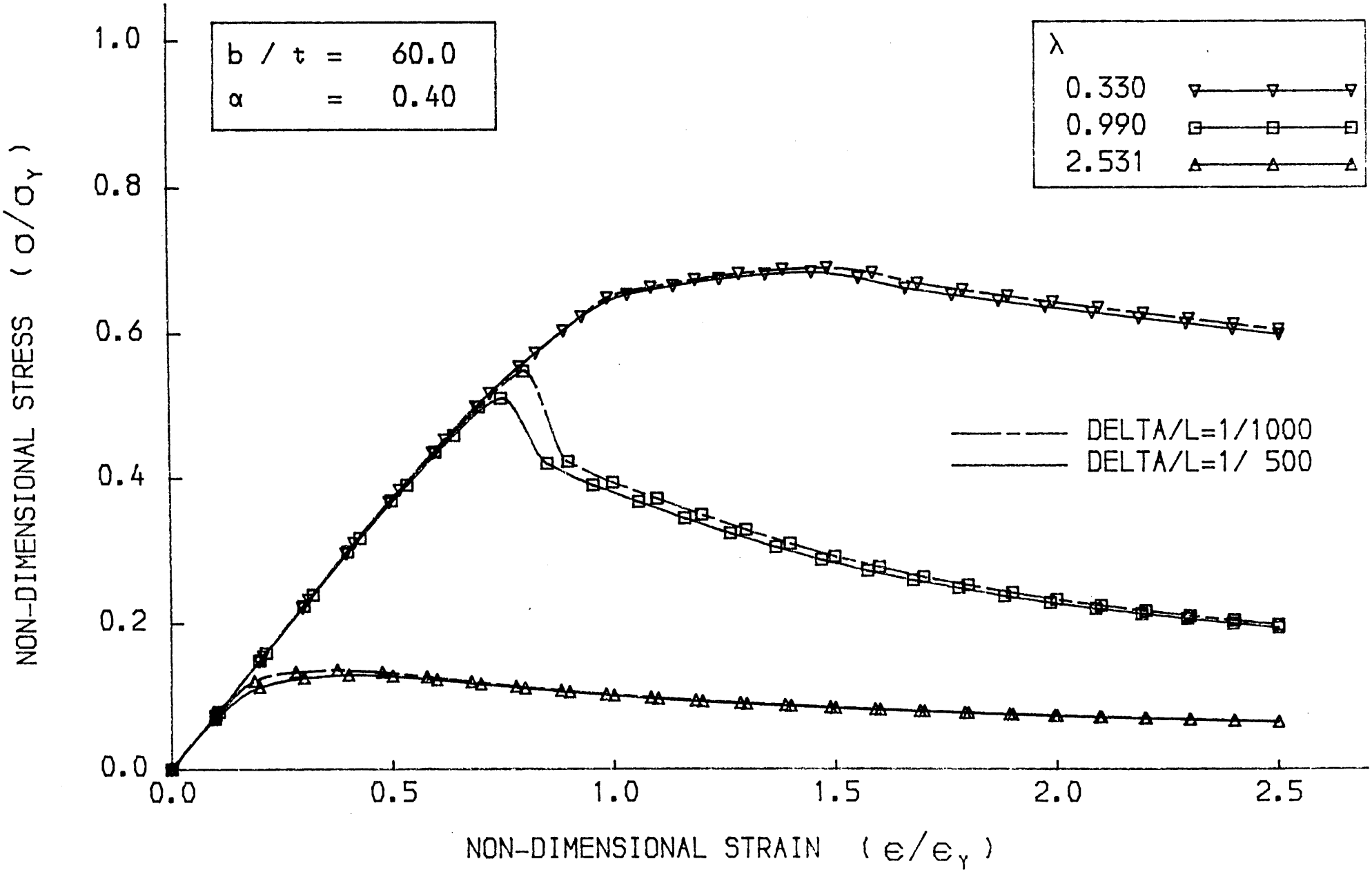

FIG.4-41 LOAD-SHORTENING CURVE FOR THE BEAM-COLUMN

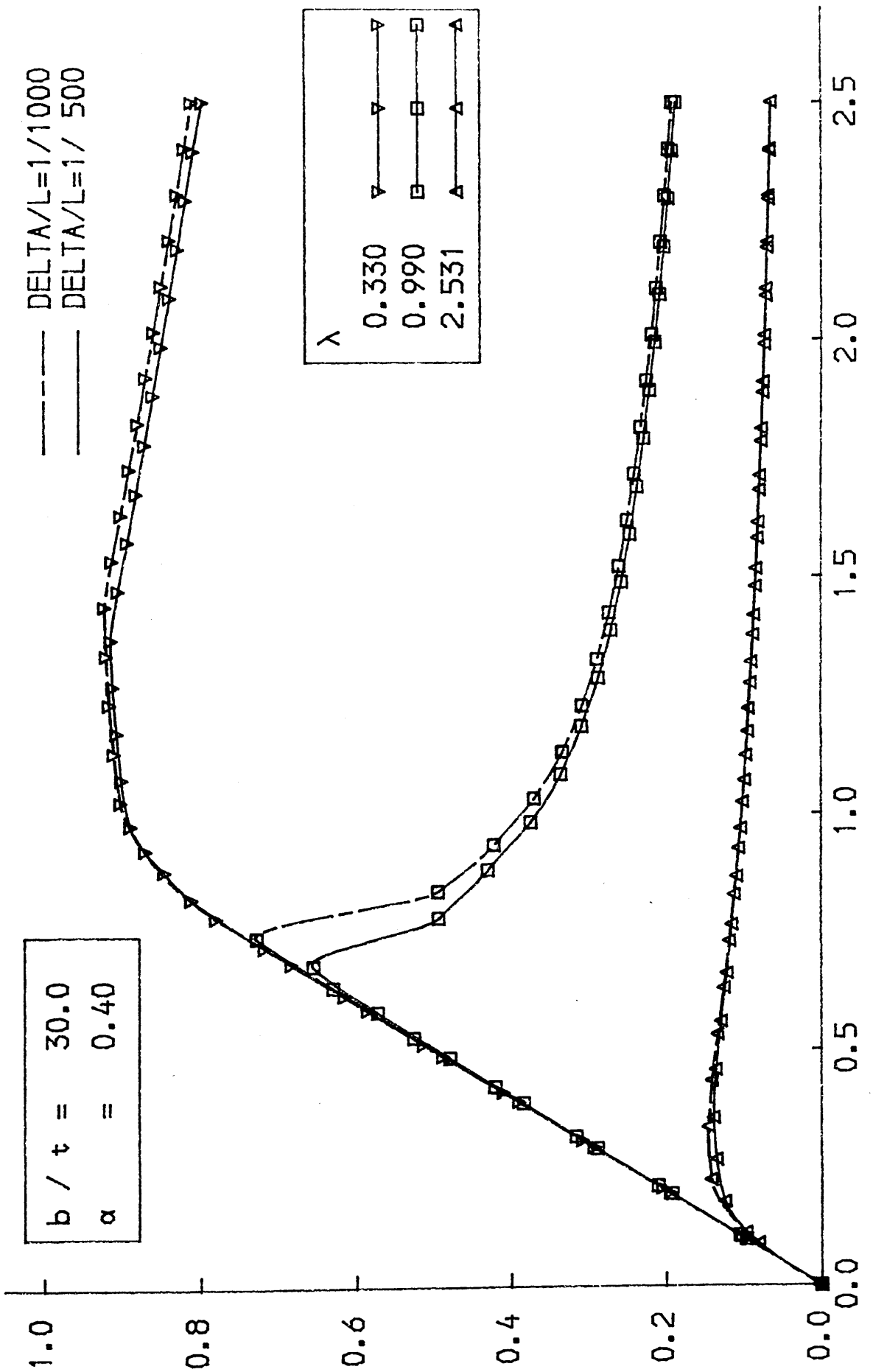

FIG.4-42 LOAD-SHORTENING CURVE FOR THE BEAM-COLUMN

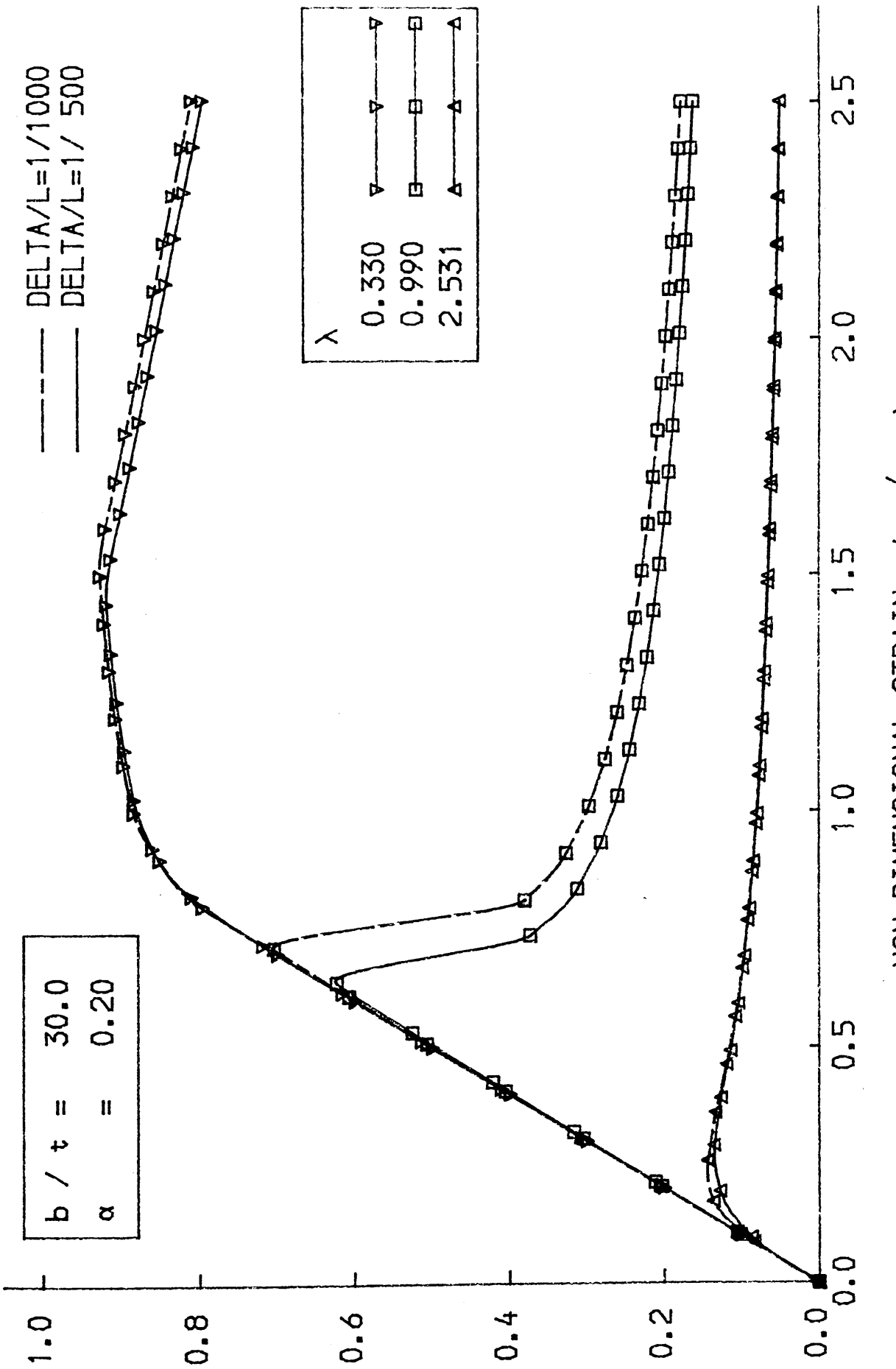

FIG.4-43 LOAD-SHORTENING CURVE FOR THE BEAM-COLUMN

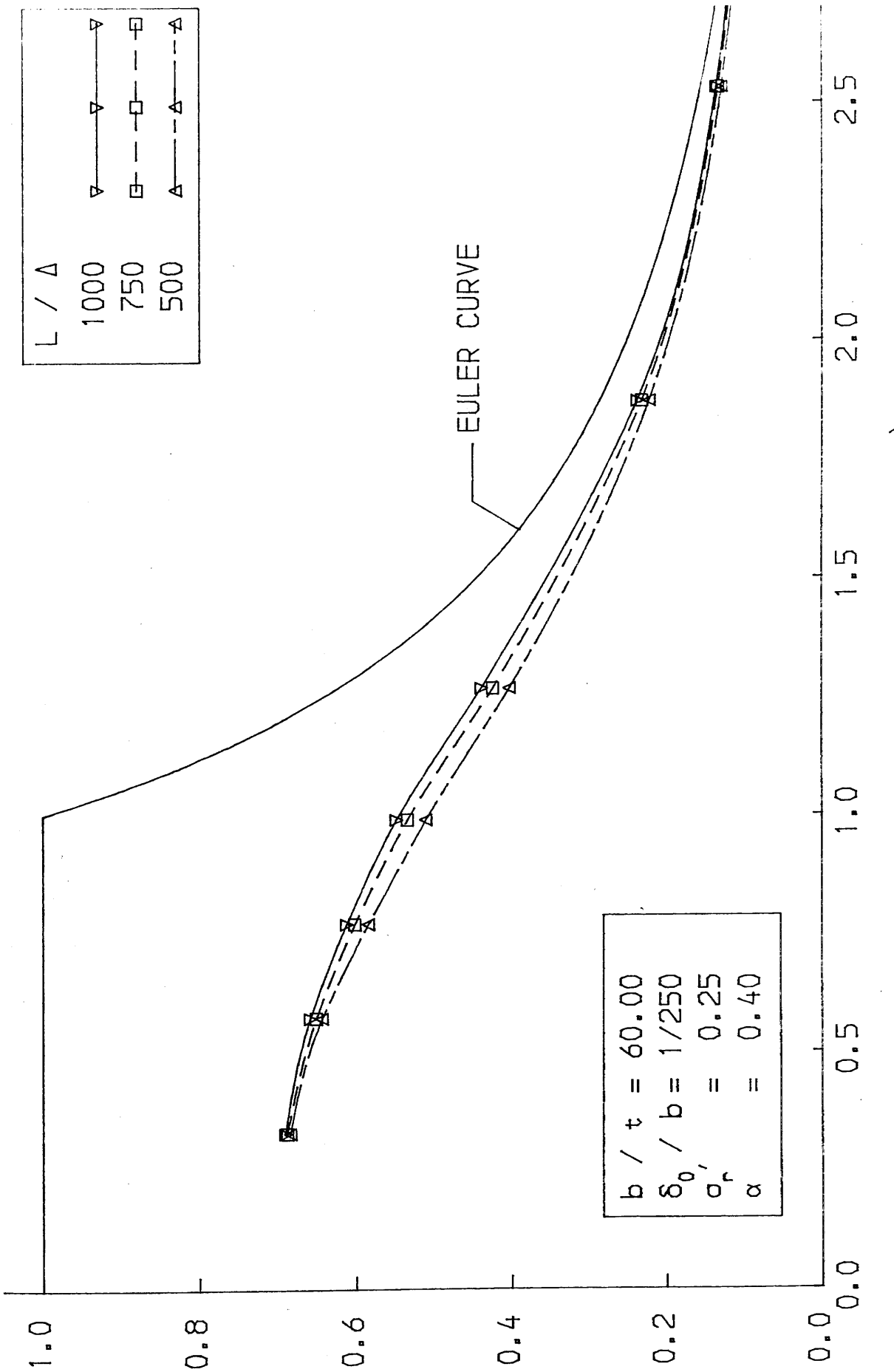

FIG. 4-44 ULTIMATE STRENGTH-SLENDERNESS CURVE

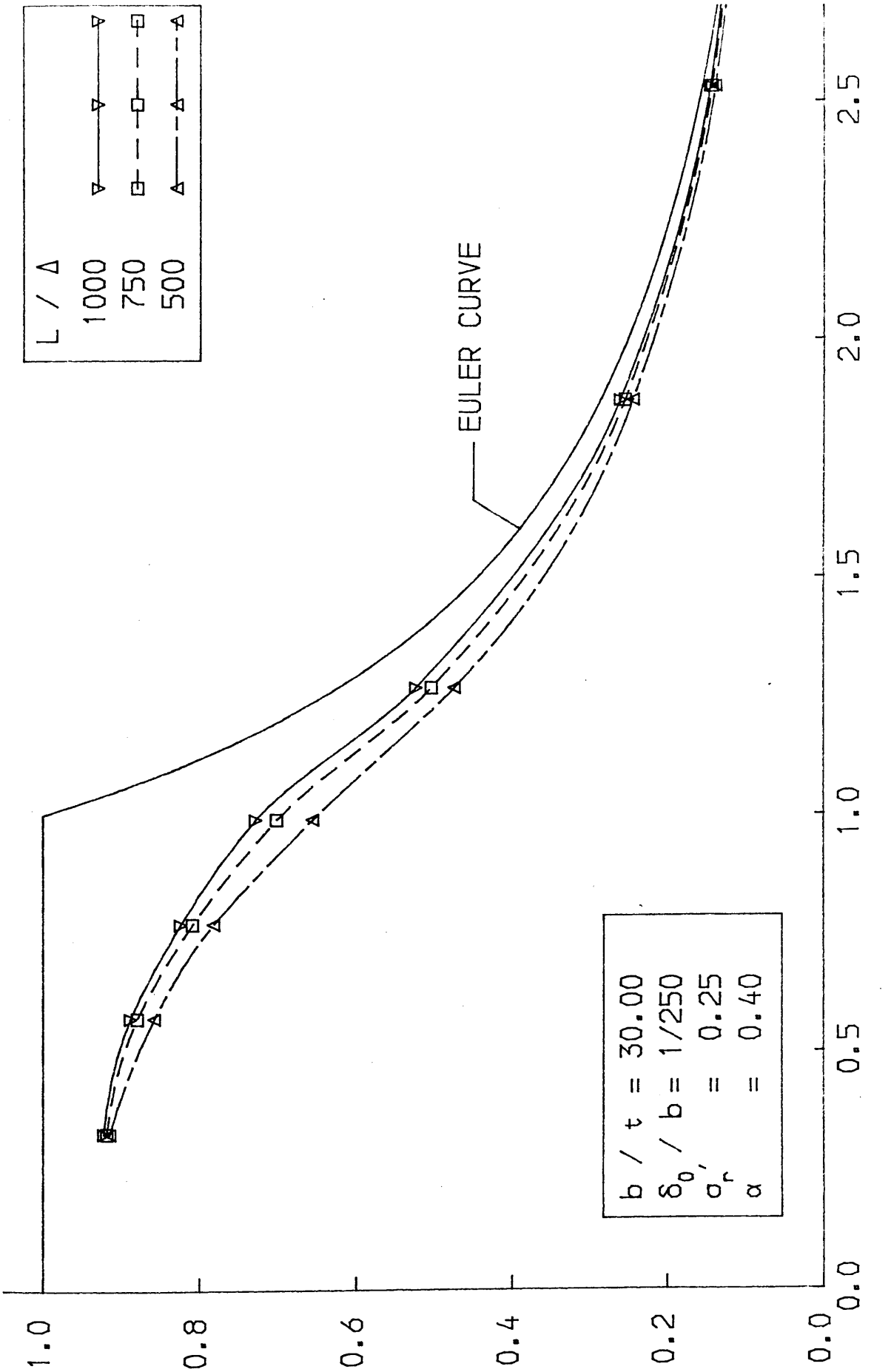

FIG.4-45 ULTIMATE STRENGTH-SLENDERNESS CURVE

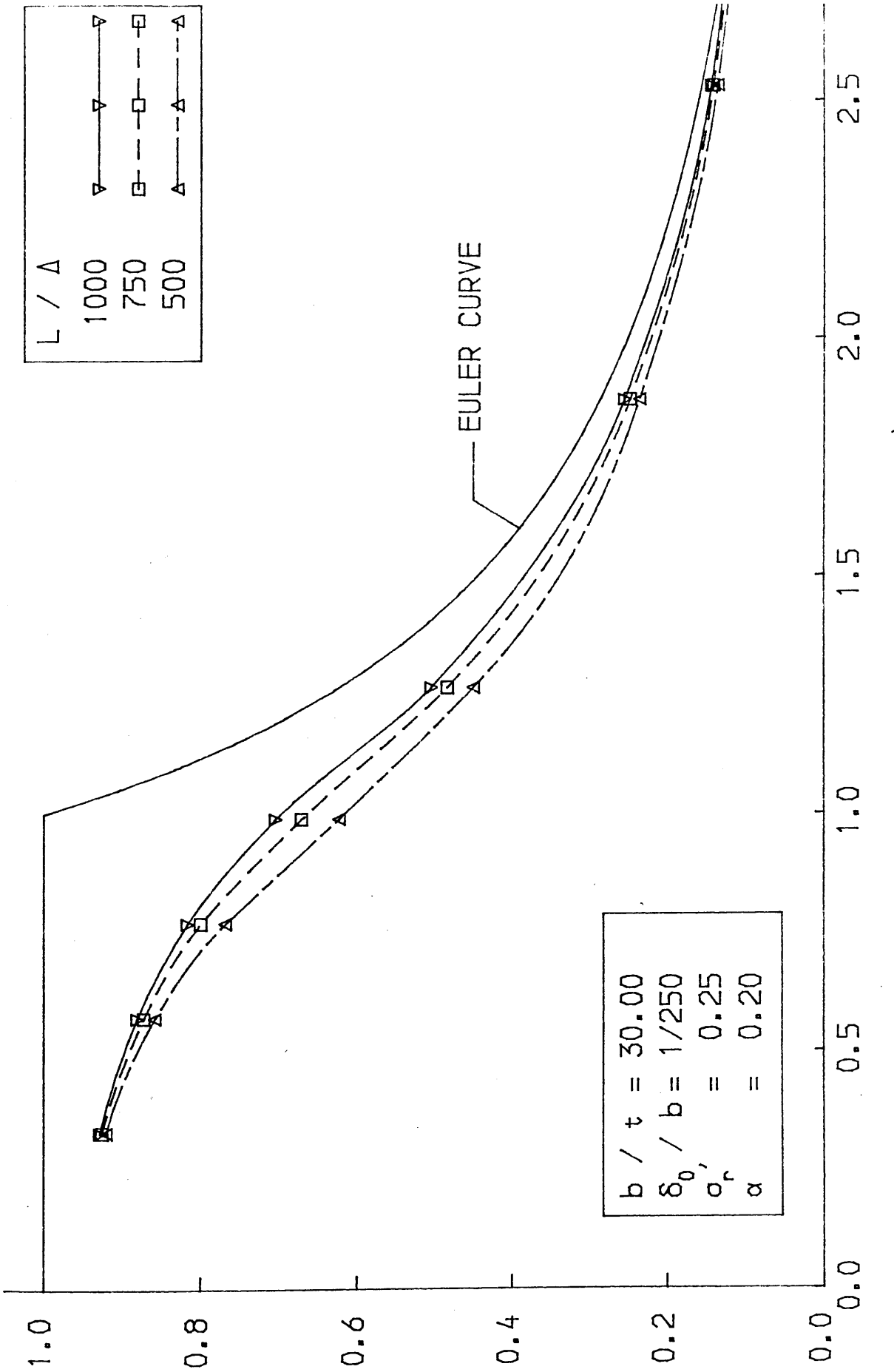

FIG. 4-46 ULTIMATE STRENGTH-SLENDERNESS CURVE

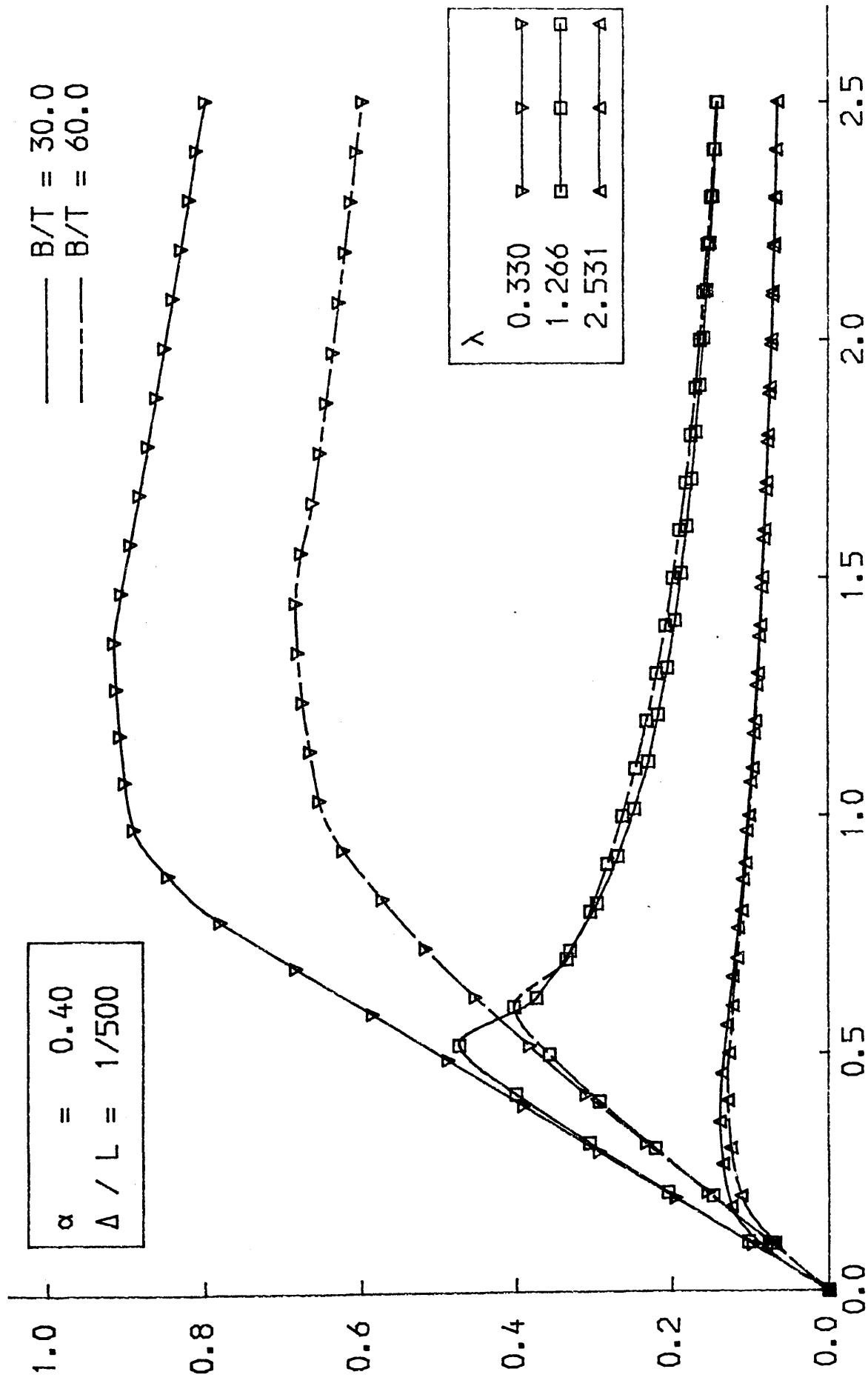

FIG.4-47 LOAD-SHORTENING CURVE FOR THE BEAM-COLUMN

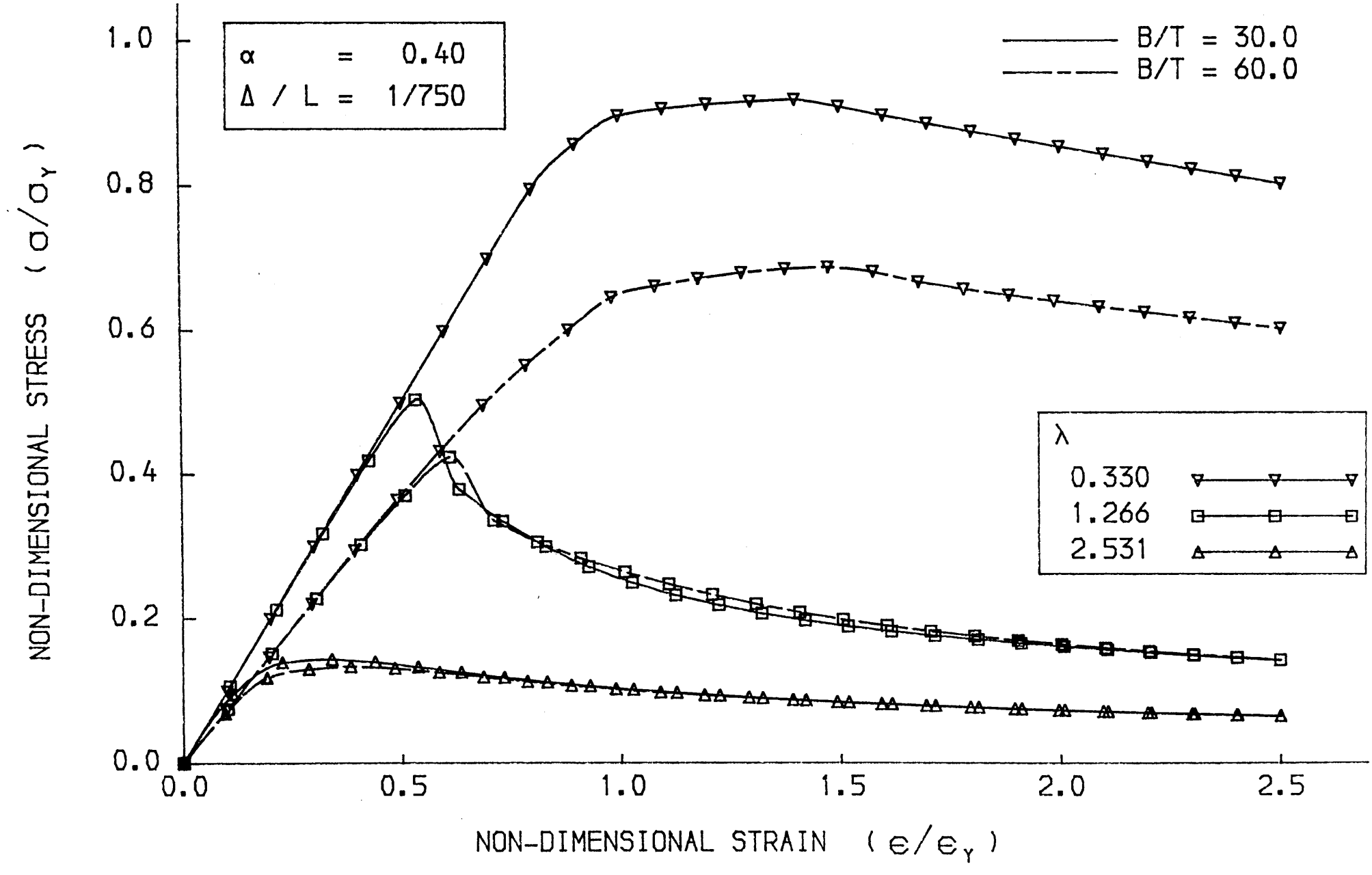

FIG.4-48 LOAD-SHORTENING CURVE FOR THE BEAM-COLUMN

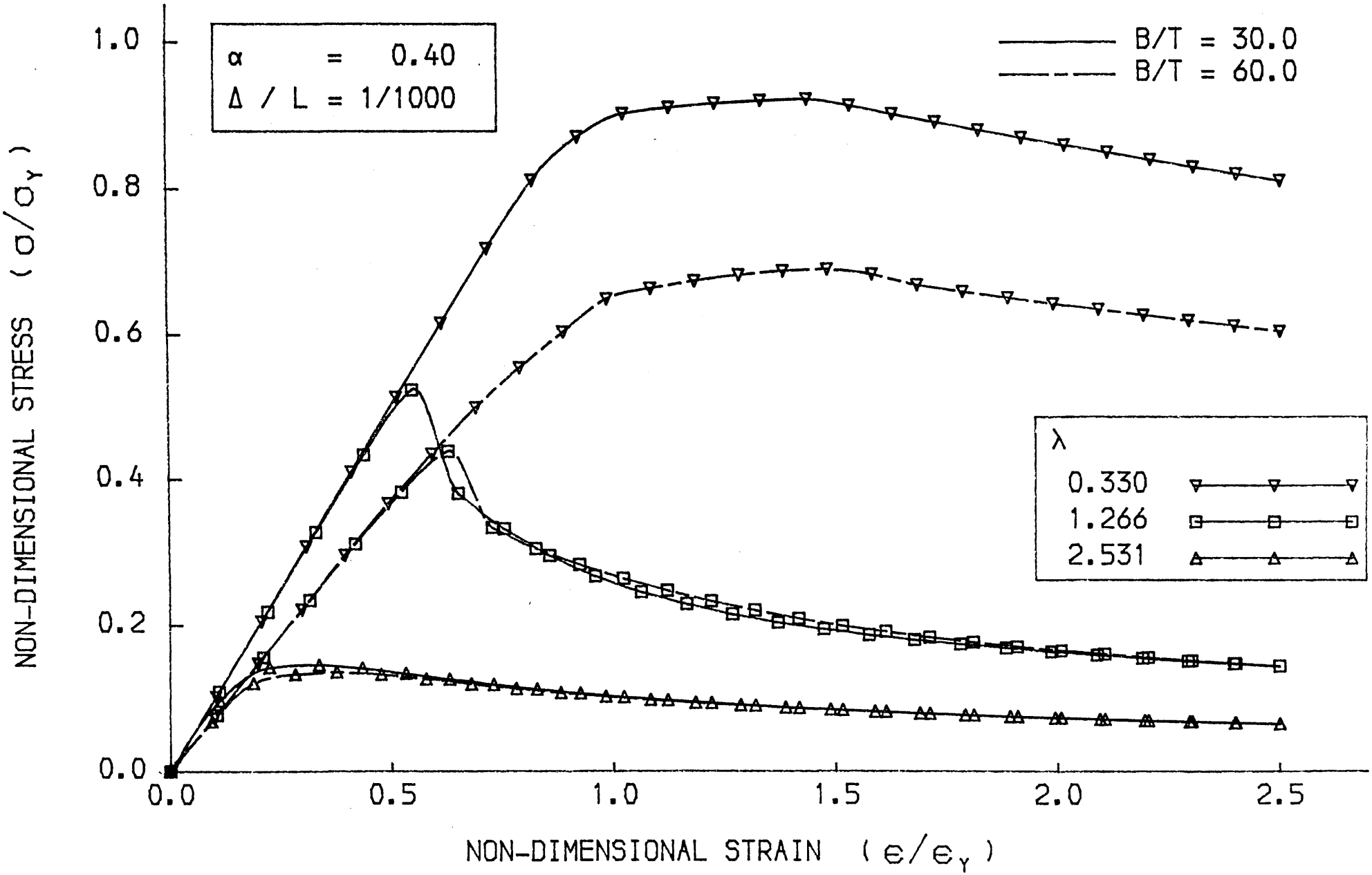

FIG.4-49 LOAD-SHORTENING CURVE FOR THE BEAM-COLUMN

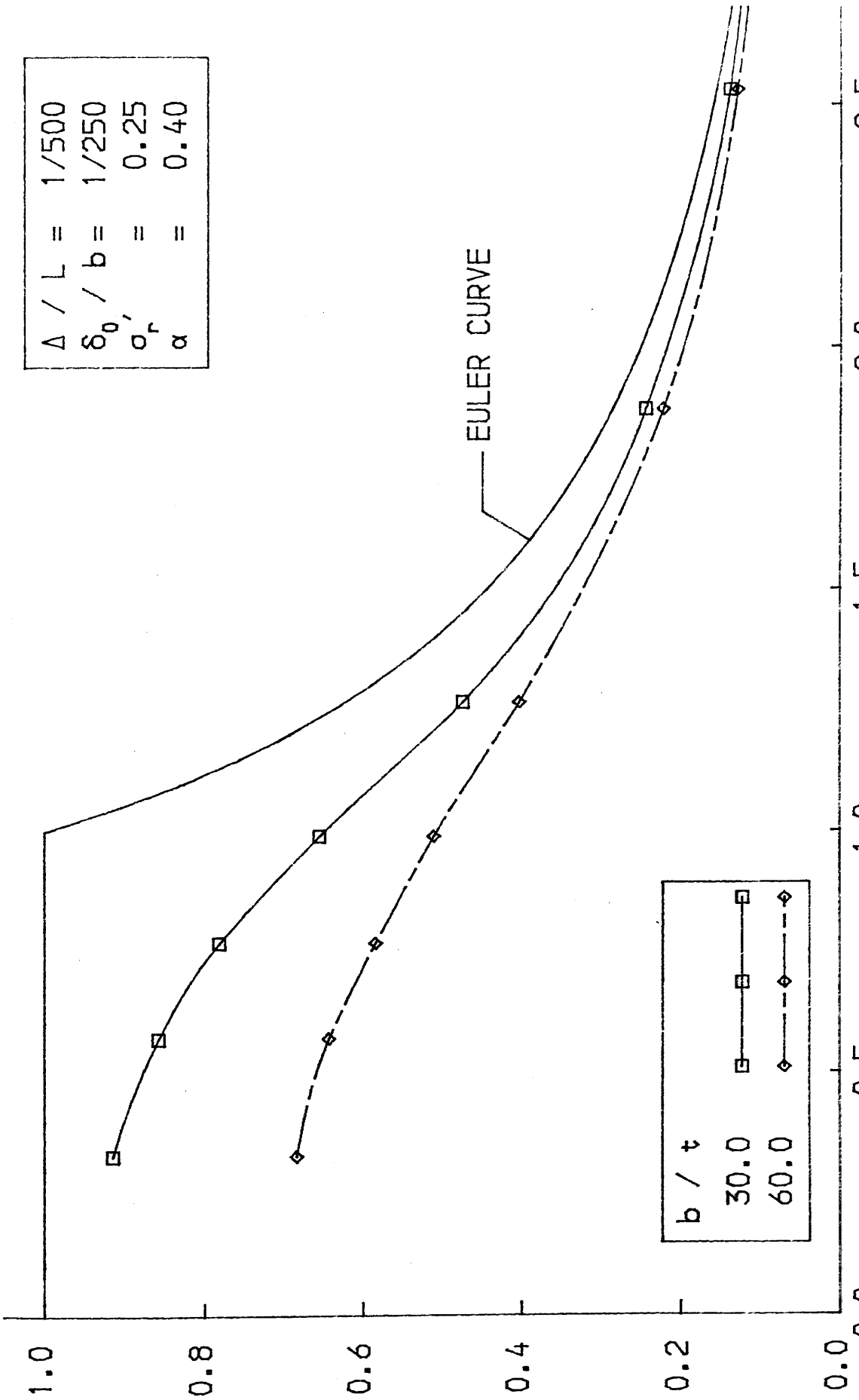

FIG.4-50 ULTIMATE STRENGTH-SLENDERNESS CURVE

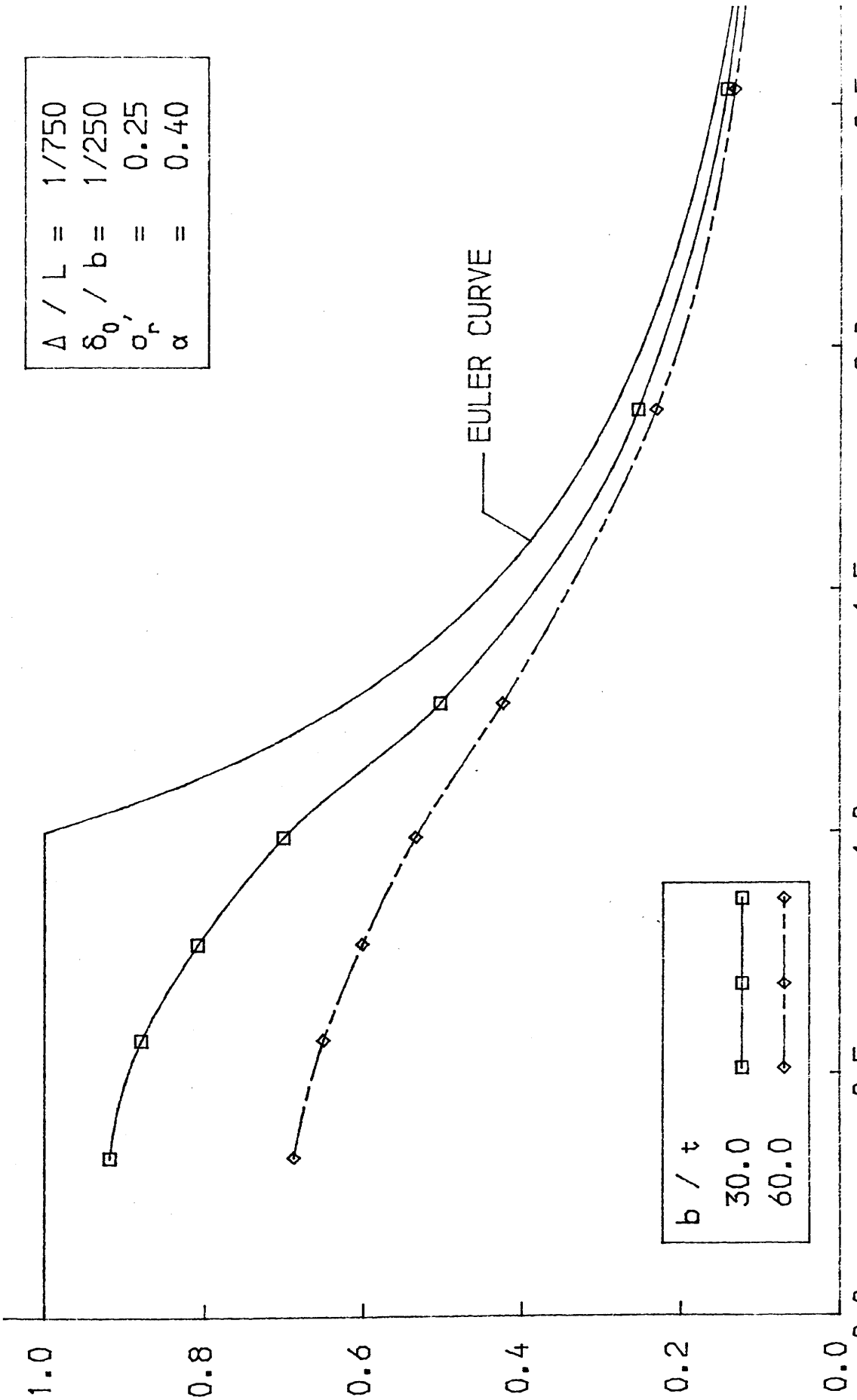

FIG.4-51 ULTIMATE STRENGTH-SLENDERNESS CURVE

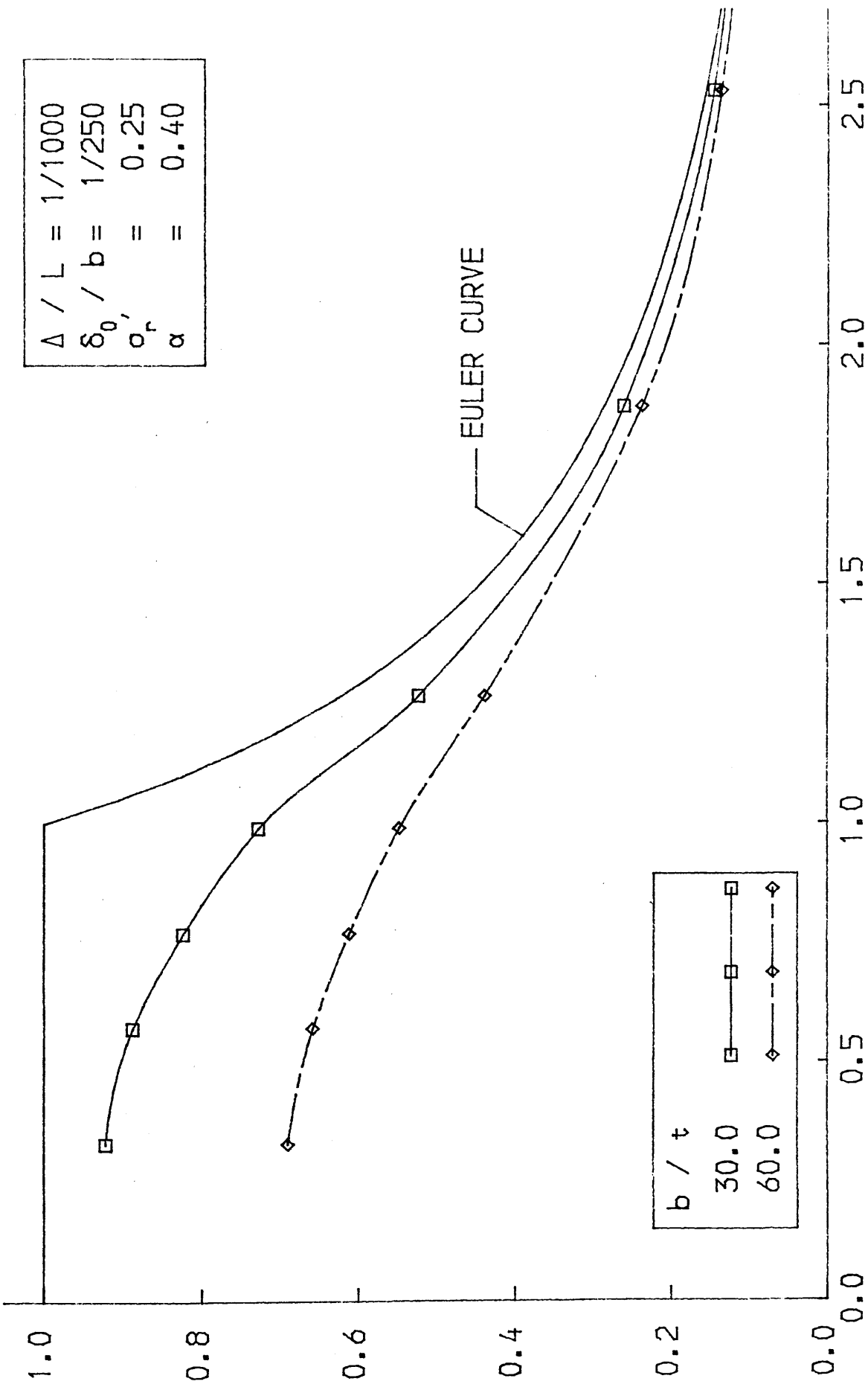

FIG.4-52 ULTIMATE STRENGTH-SLENDERNESS CURVE

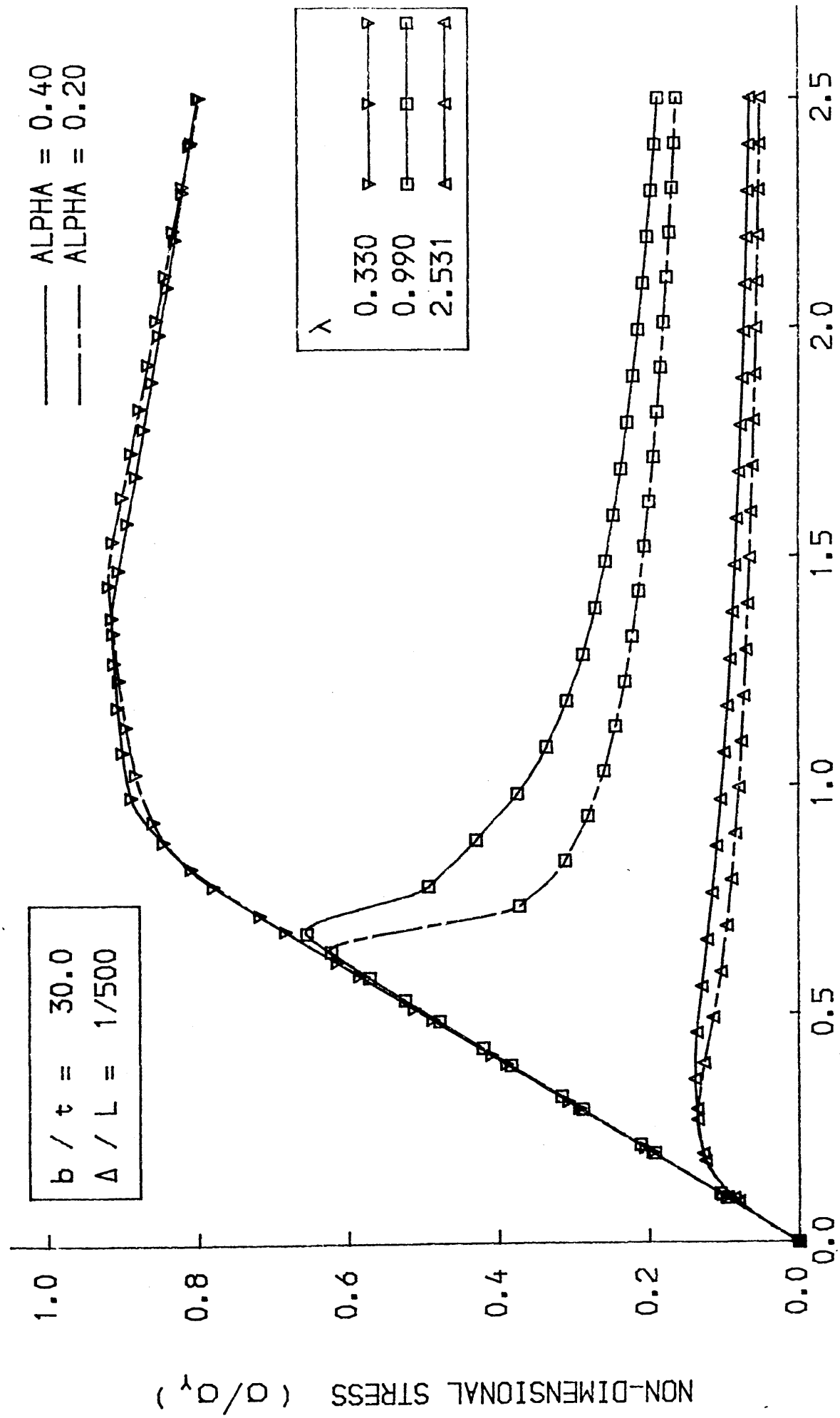

FIG.4-53 LOAD-SHORTENING CURVE FOR THE BEAM-COLUMN

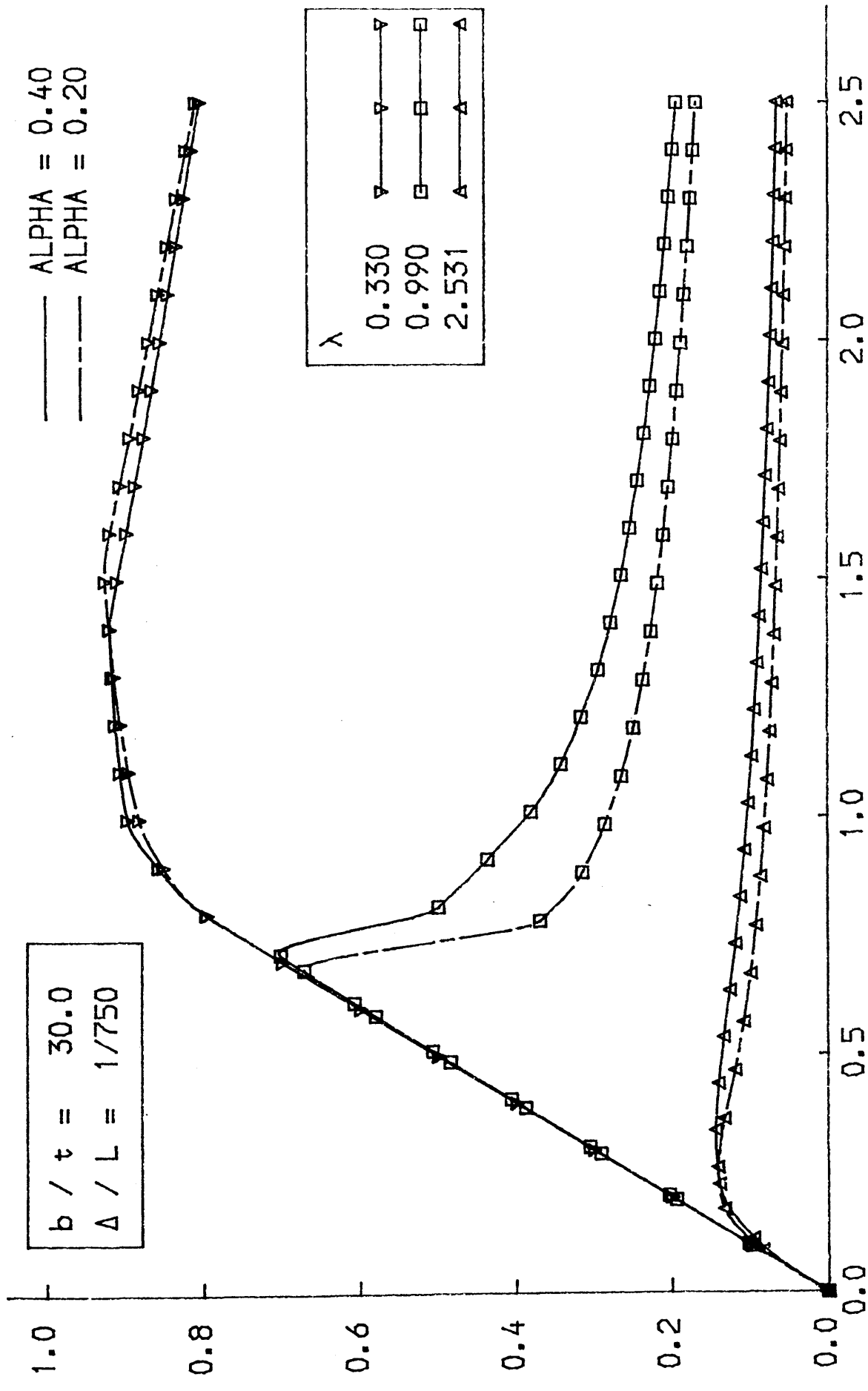

FIG.4-54 LOAD-SHORTENING CURVE FOR THE BEAM-COLUMN

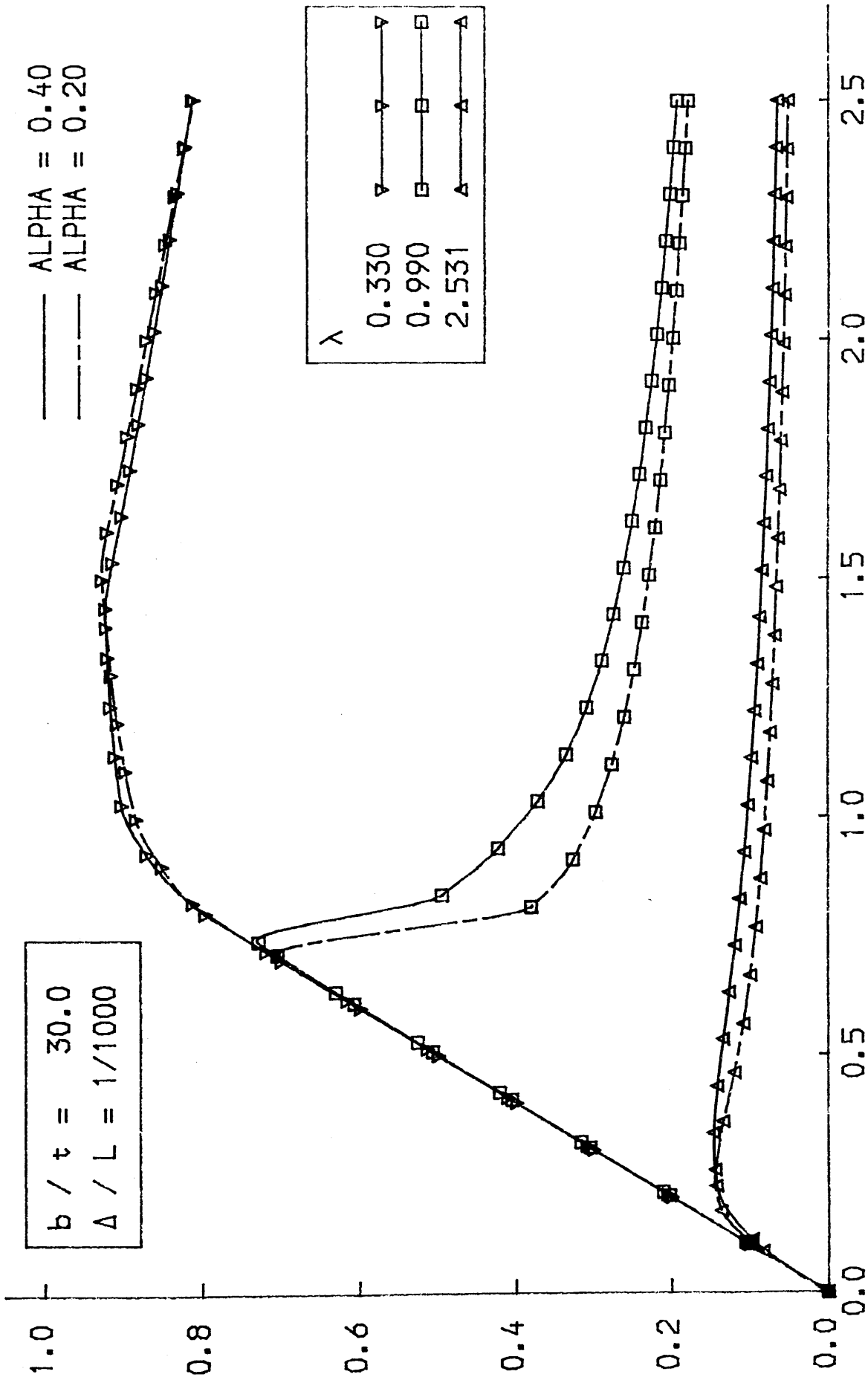

FIG.4-55 LOAD-SHORTENING CURVE FOR THE BEAM-COLUMN

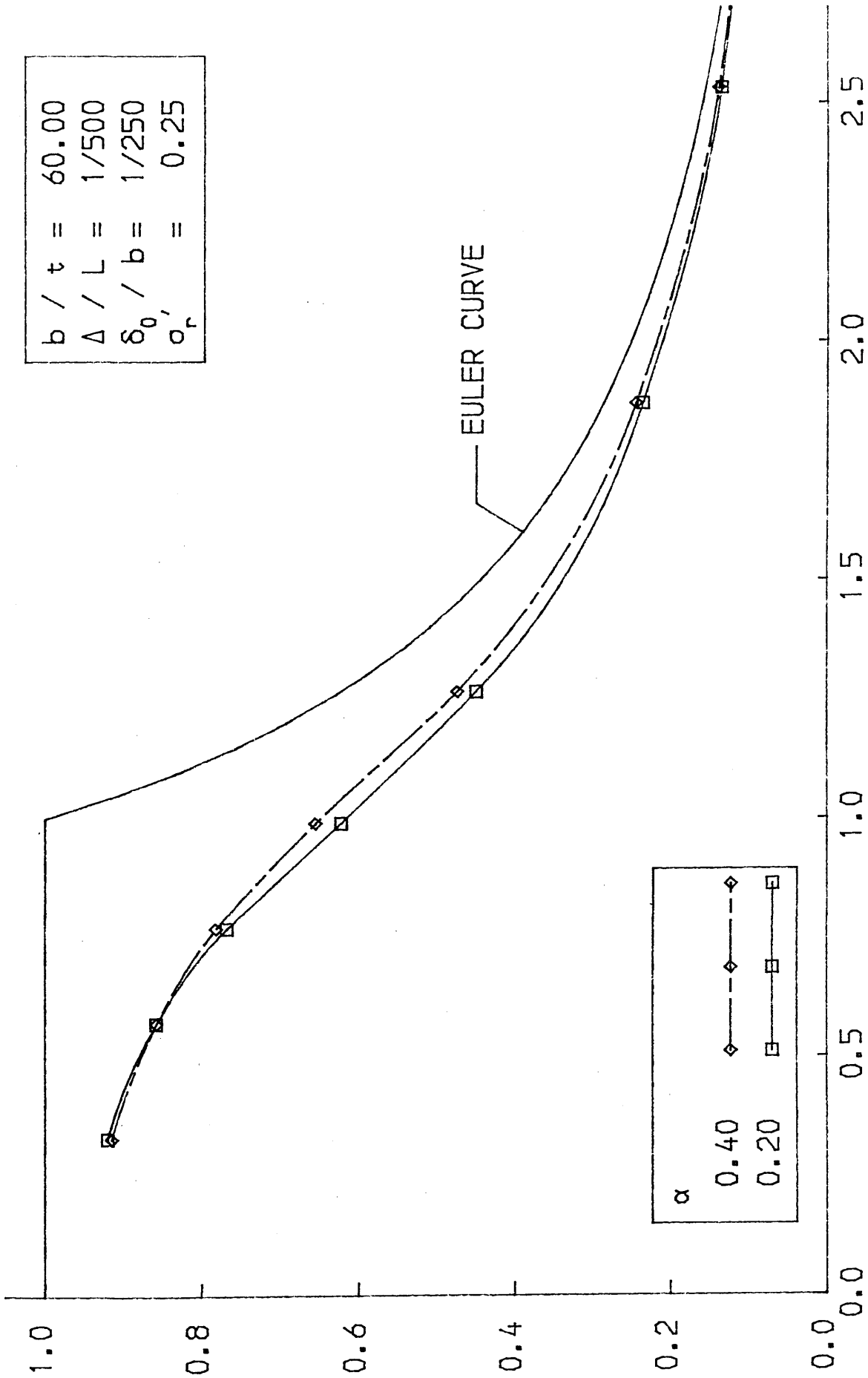

FIG.4-56 ULTIMATE STRENGTH-SLENDERNESS CURVE

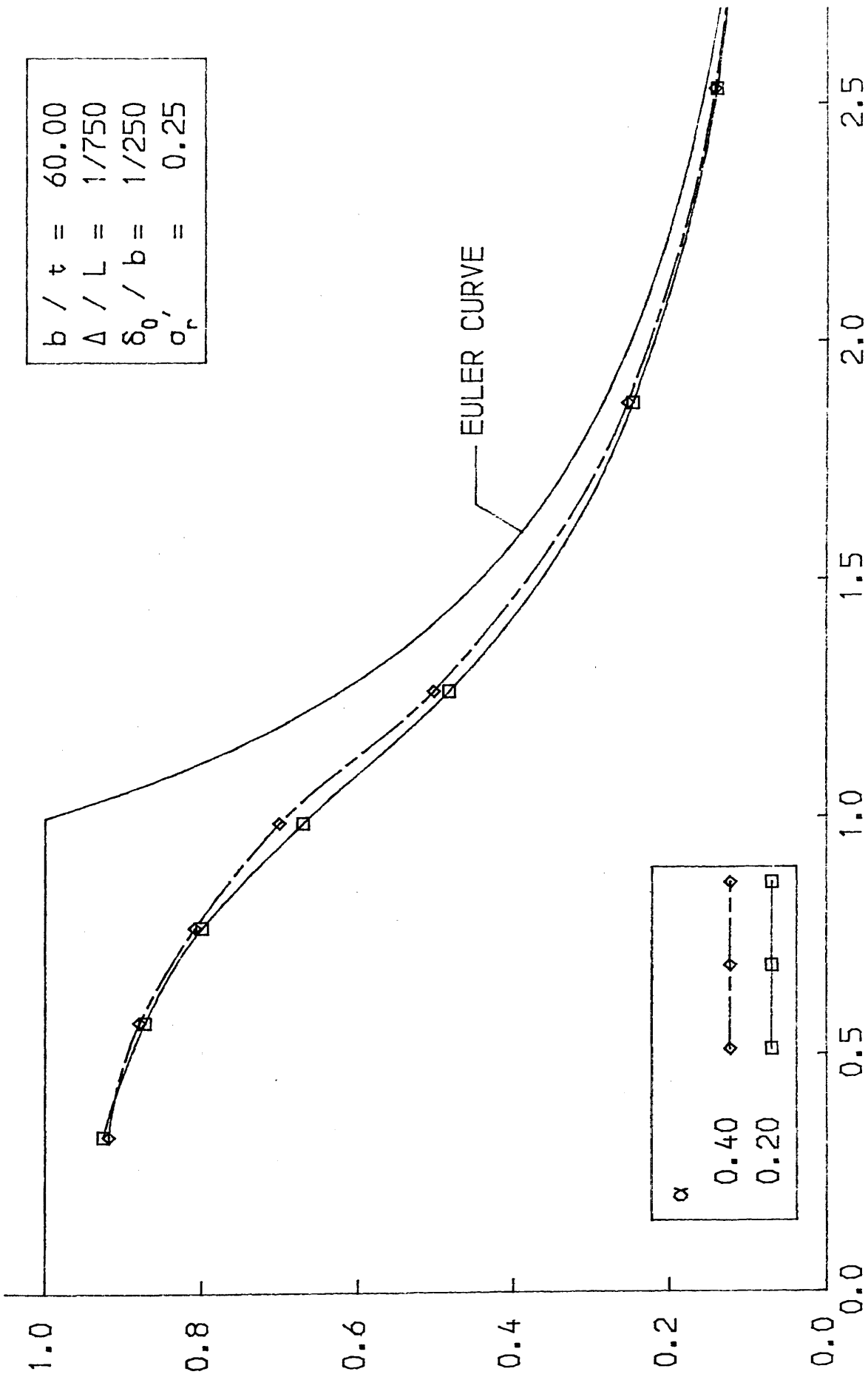

FIG.4-57 ULTIMATE STRENGTH-SLENDERNESS CURVE

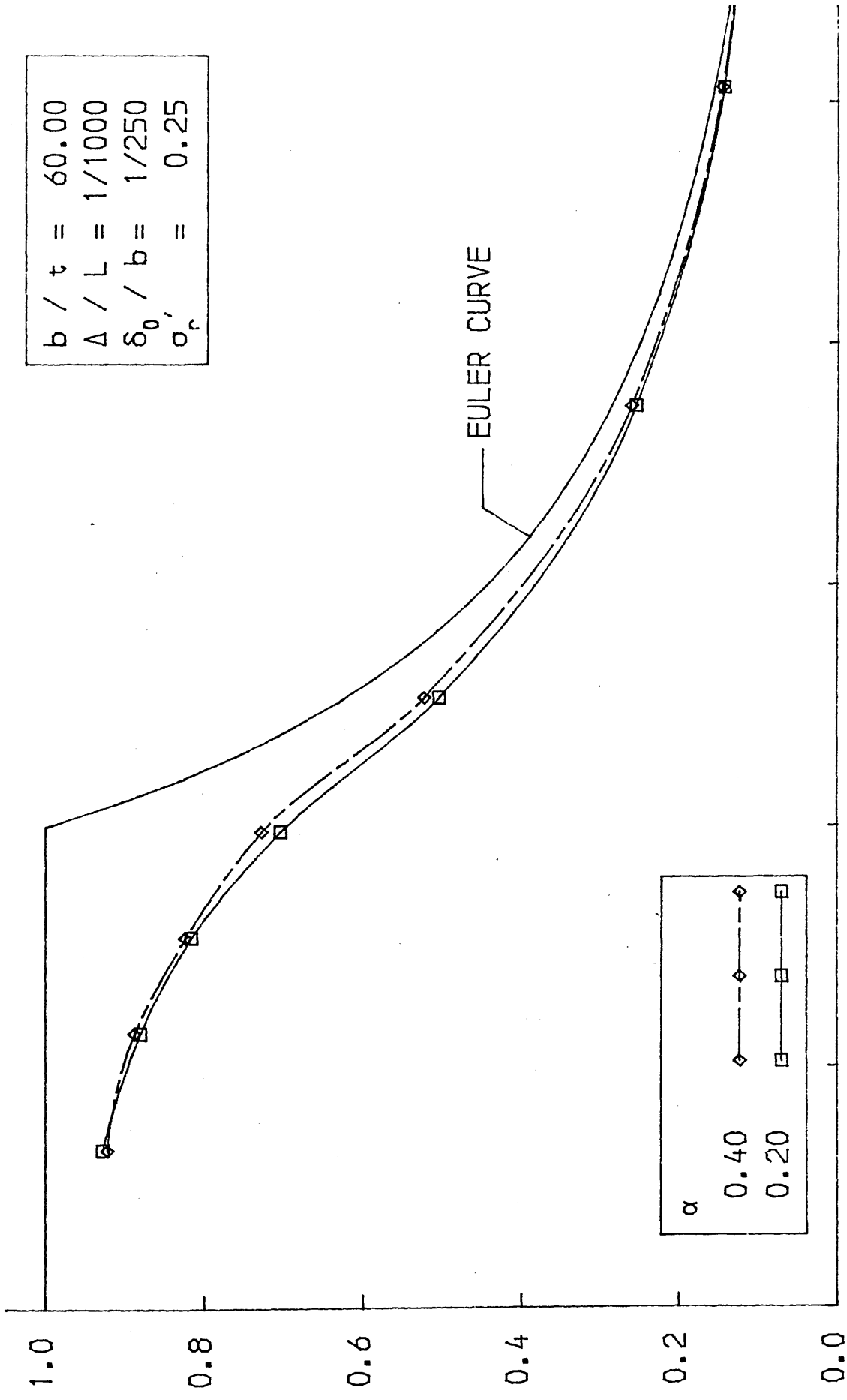

FIG.4-58 ULTIMATE STRENGTH-SLENDERNESS CURVE

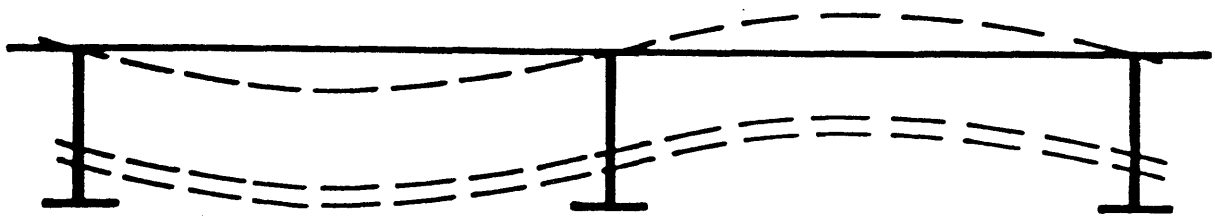

a.) ALTERNATING BUCKLING MODE

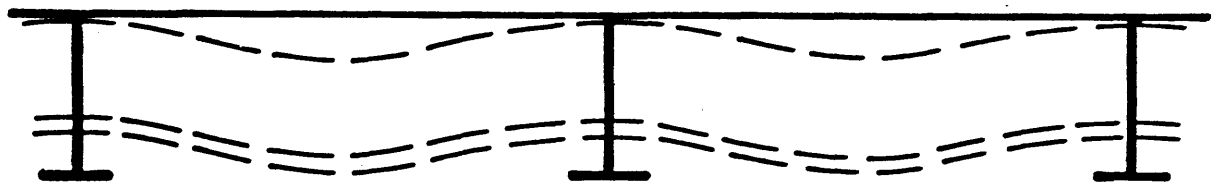

b.) PLATE-INDUCED FAILURE IN BOTH SPANS

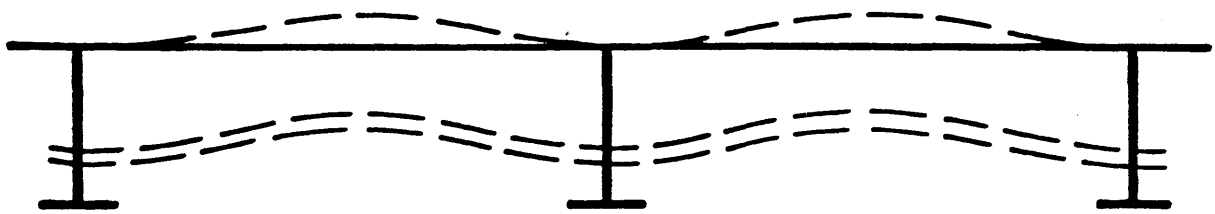

c.) STIFFENER-INDUCED FAILURE IN BOTH SPANS

FIG.5-1 INTERFRAME FLEXURAL BUCKLING MODES

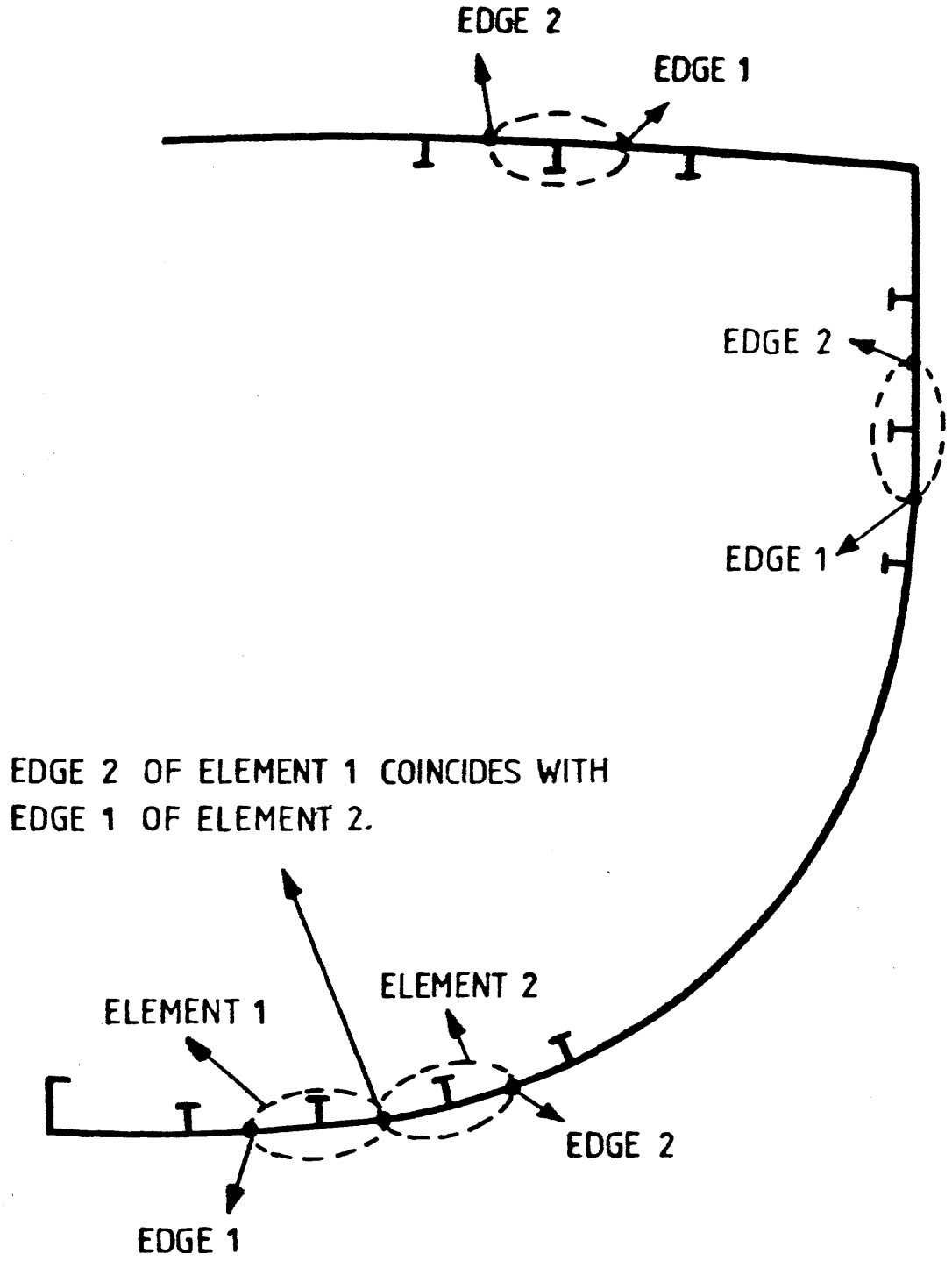

FIG.5-2 COUNTERCLOCKWISE CHOICE FOR EDGE 1 AND EDGE 2 OF PLATE ELEMENTS.

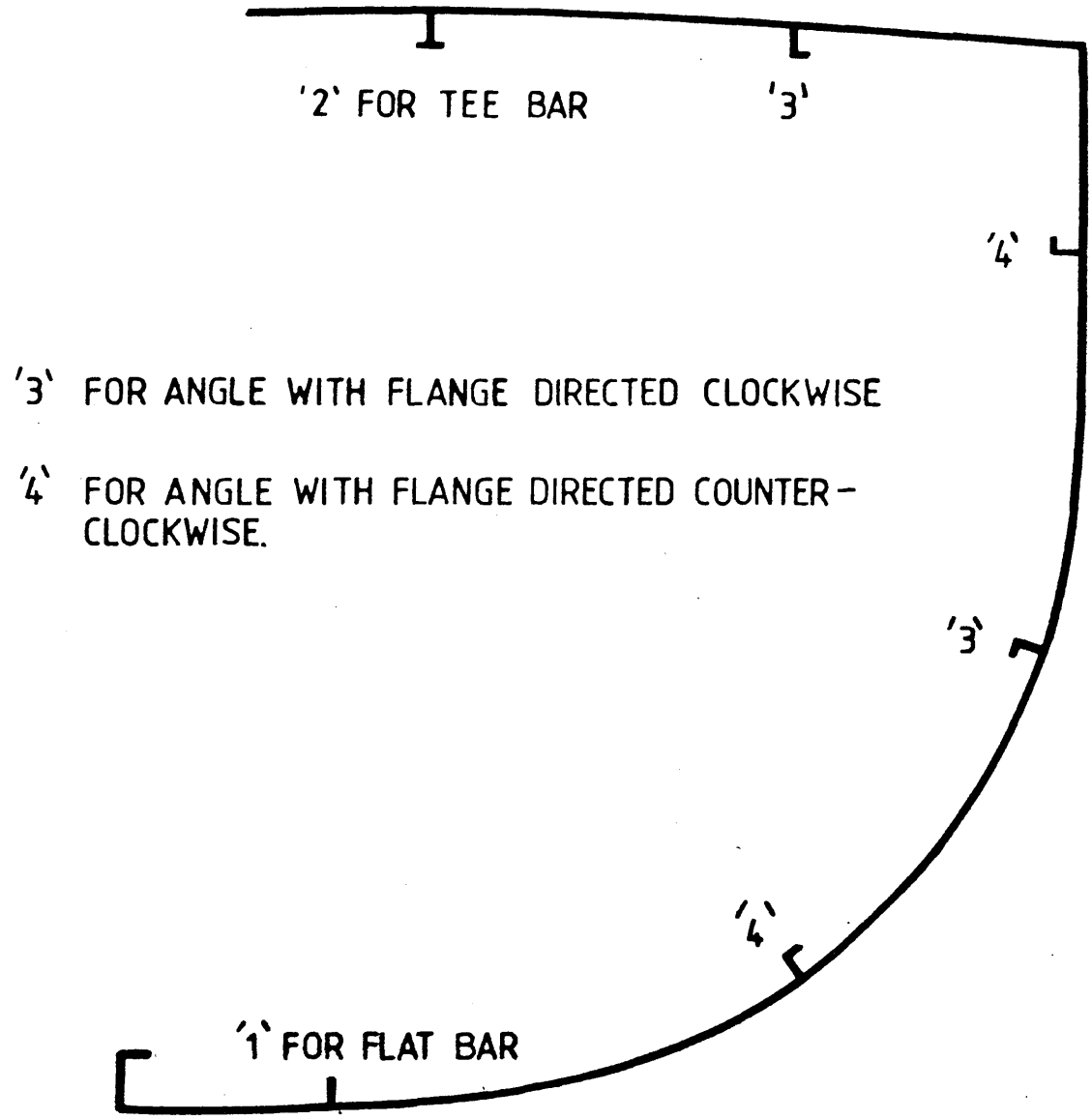

FIG.5-3 CODE NUMBER FOR TYPICAL SHAPES OF STIFFENERS.

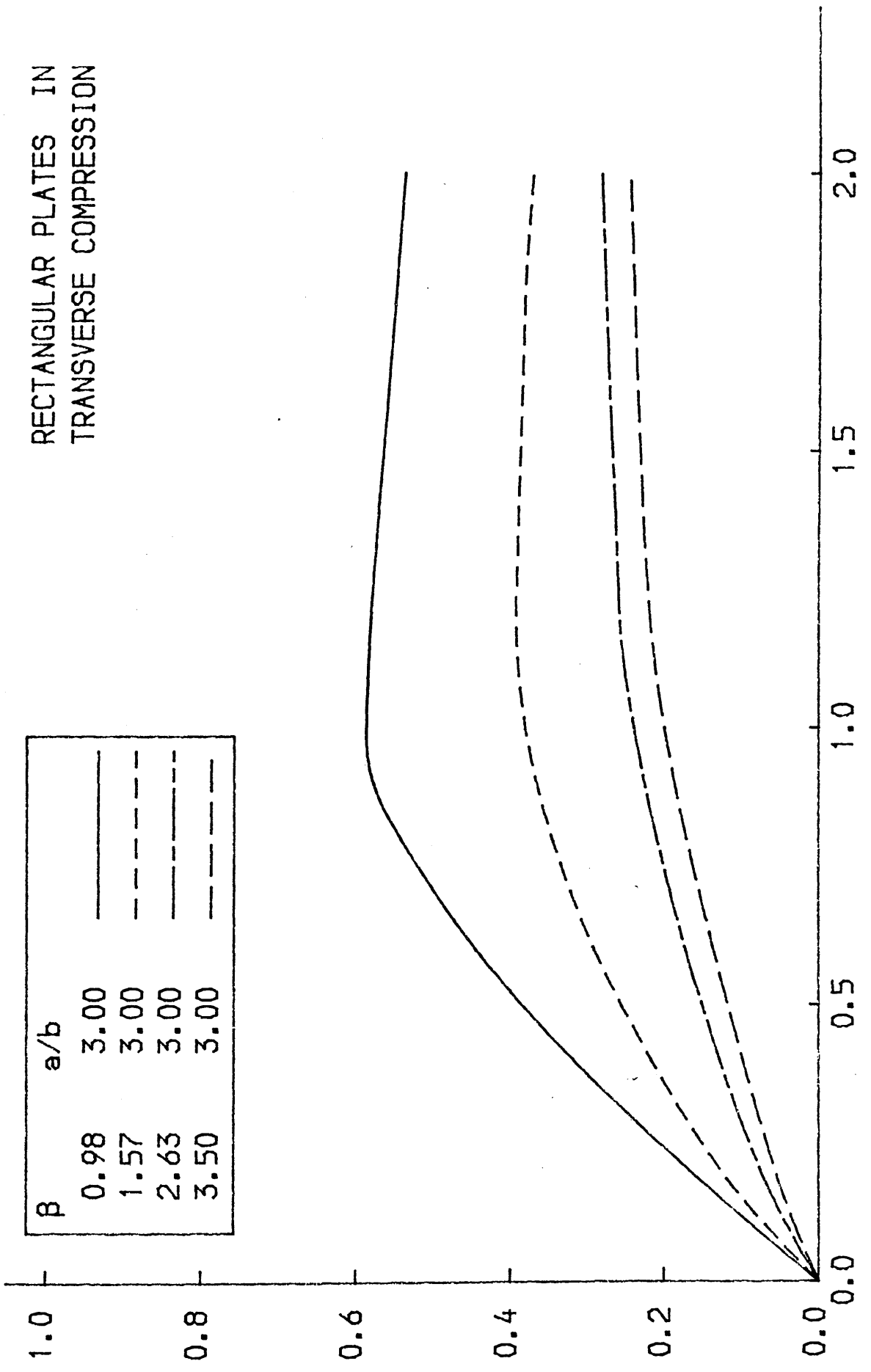

FIG.5-4 AVERAGE STRESS-STRAIN CURVE FOR THE PLATE

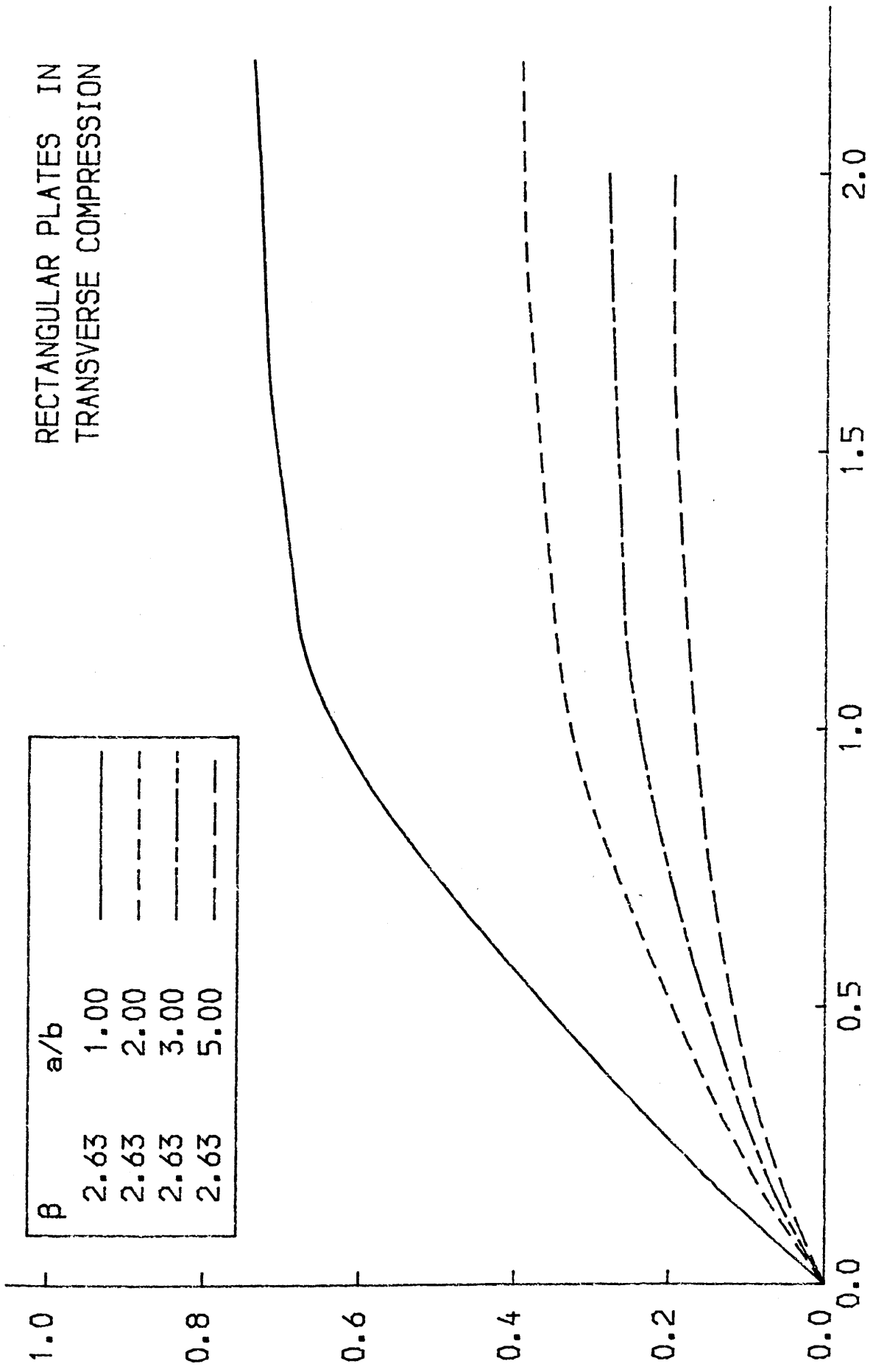

FIG.5-5 AVERAGE STRESS-STRAIN CURVE FOR THE PLATE

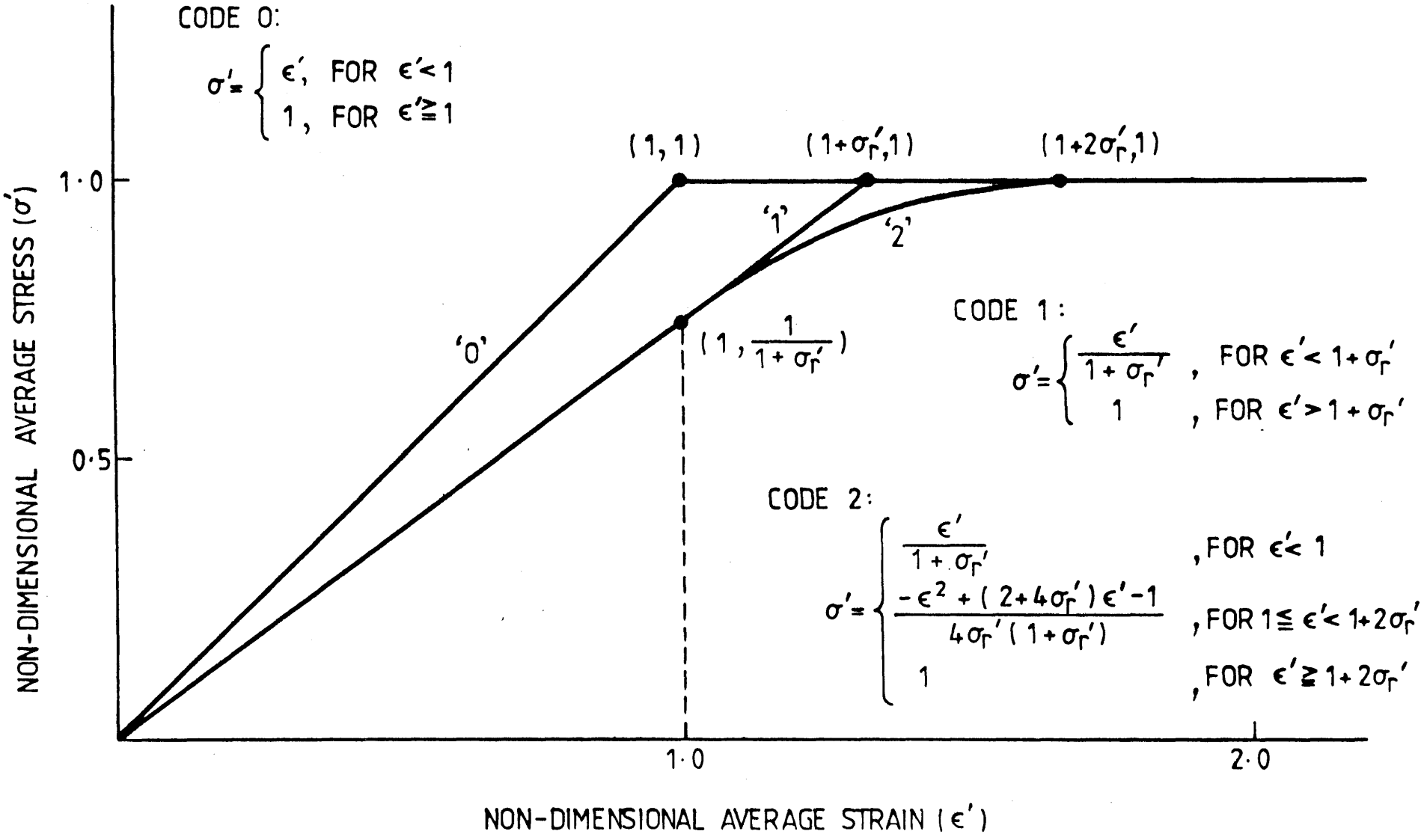

FIG.5-6 REFERENCE CODE FOR AVERAGE STRESS-STRAIN CURVE OF PLATE IN TENSION.

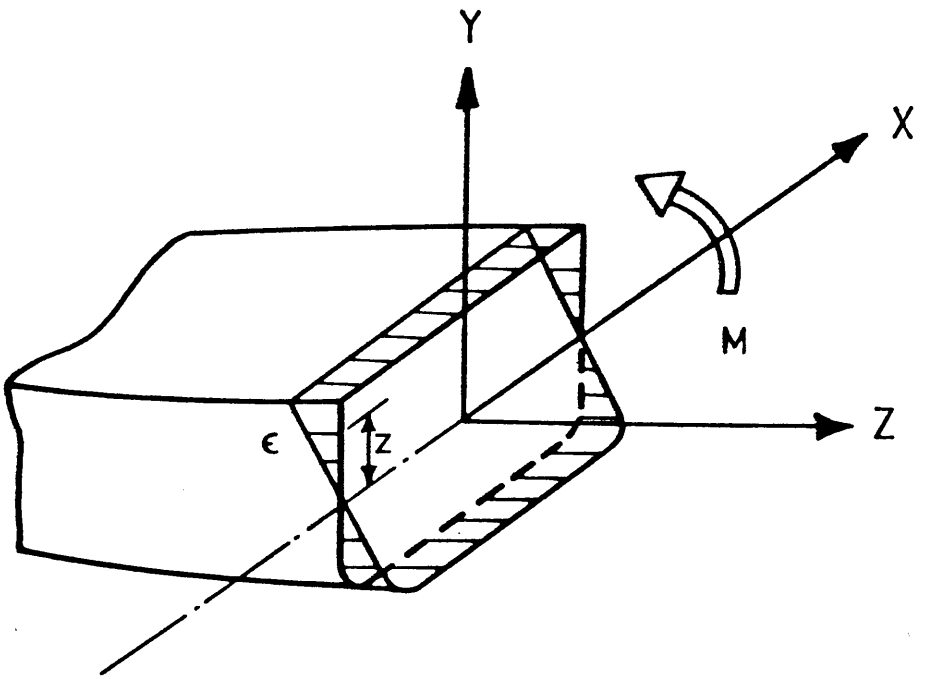

y : HEIGHT ABOVE NEUTRAL AXIS
ϵ : STRAIN

FIG.5-7 LINEAR STRAIN DISTRIBUTION

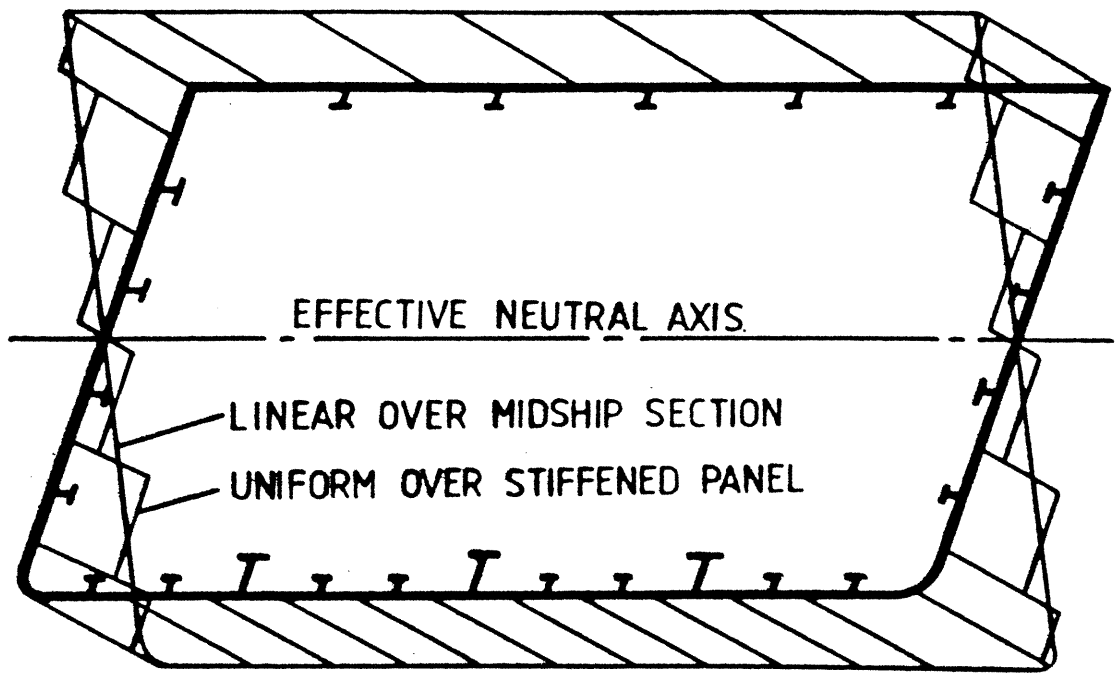

FIG. 5-8 MODIFIED STRAIN DISTRIBUTION.

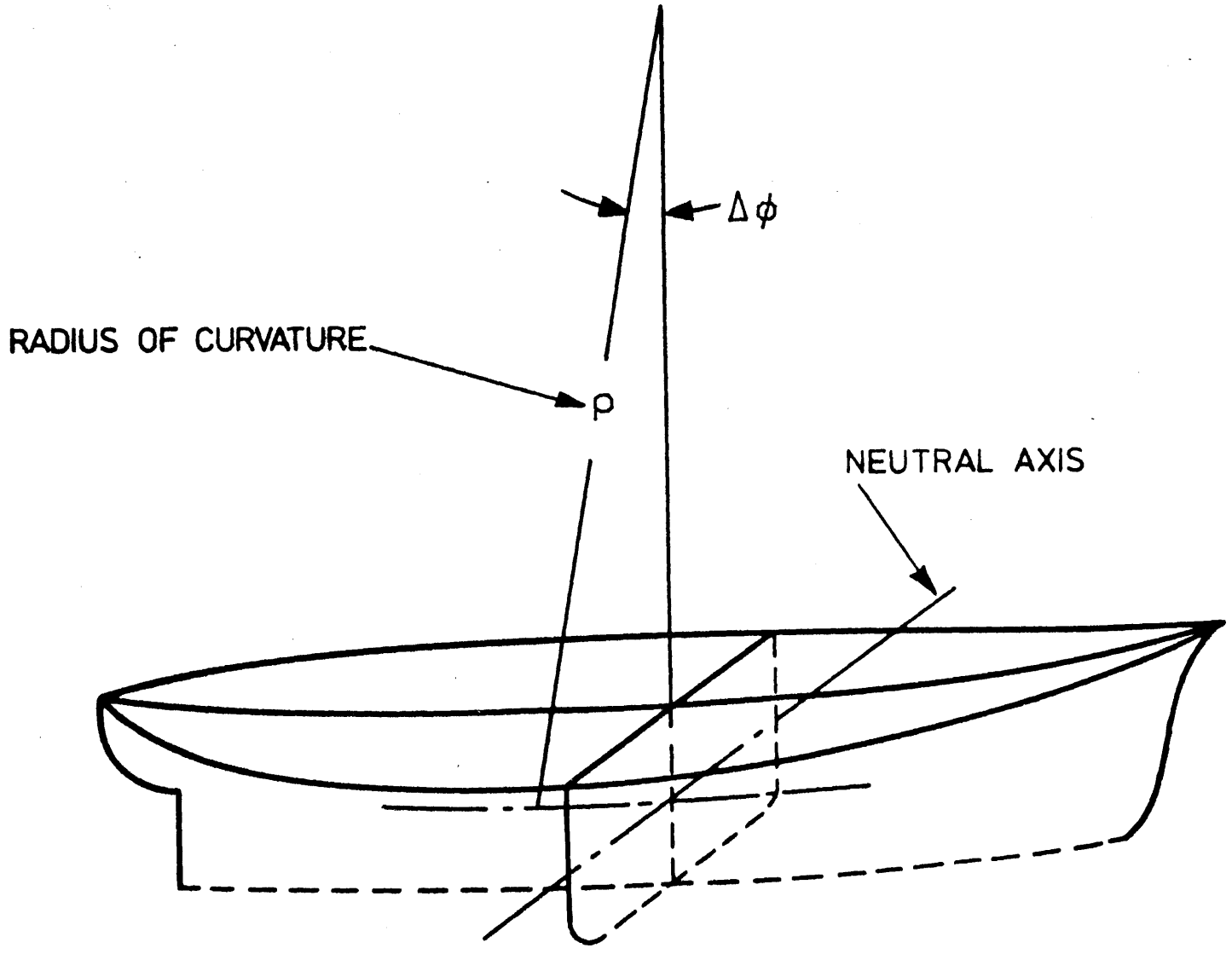

FIG.5-9 HULL GIRDER SUBJECTED TO VERTICAL BENDING MOMENT - SAGGING CONDITION.

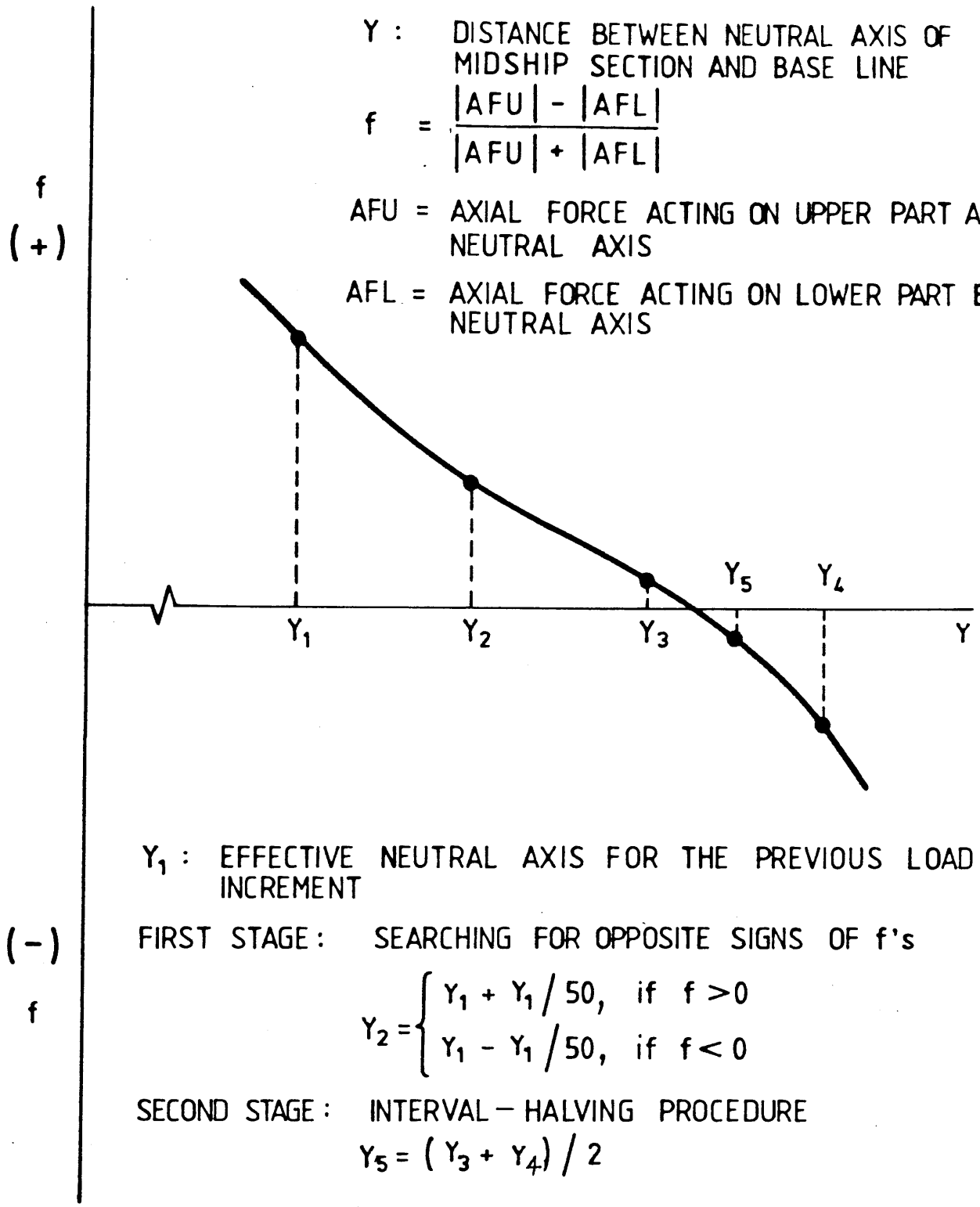

FIG.5-10 ALGORITHM FOR DETERMINING THE EFFECTIVE NEUTRAL AXIS OF MIDSHIP SECTION

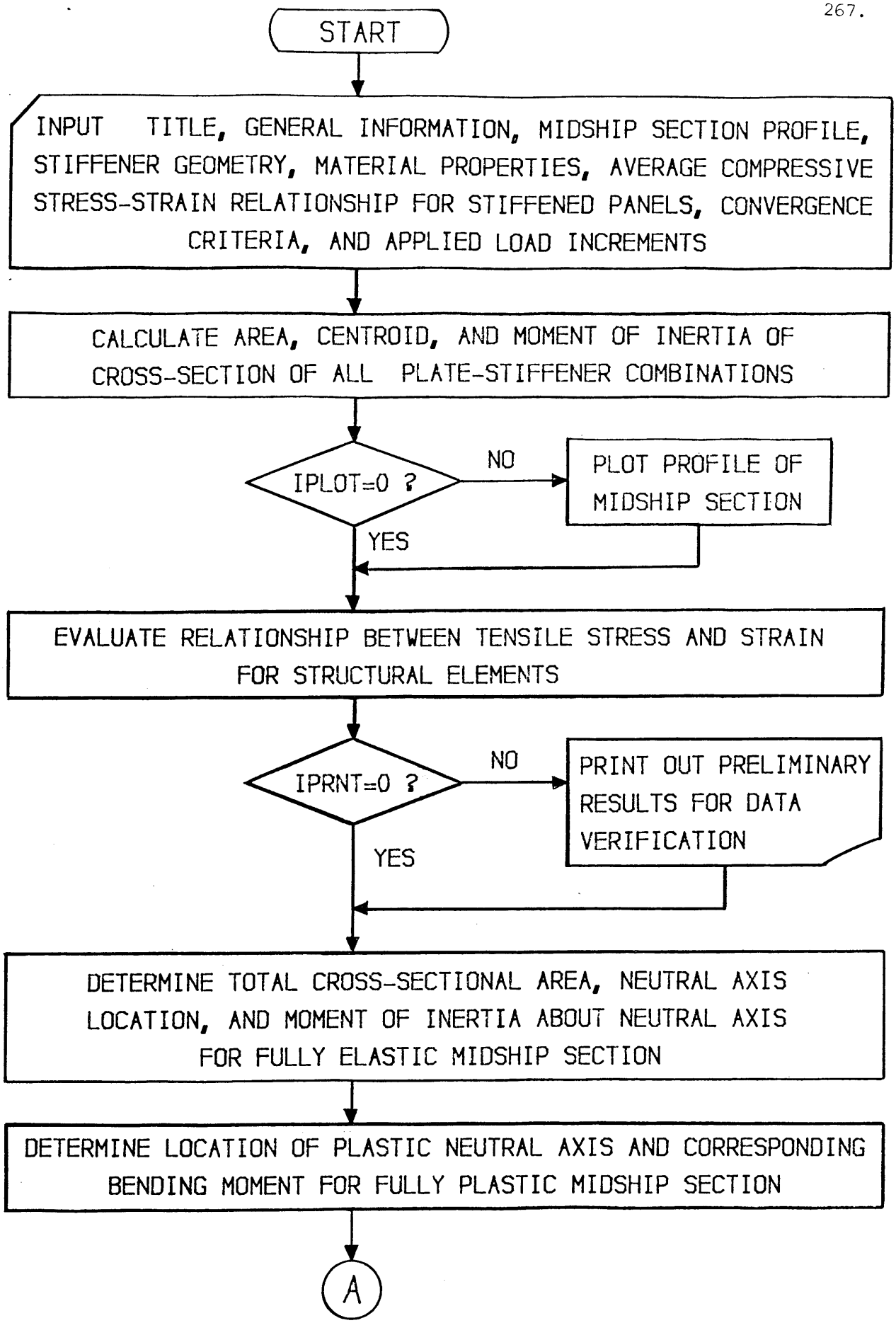

FIG.5-11 FLOW CHART FOR EVALUATION OF BENDING MOMENT-CURVATURE RELATIONSHIP (CONTINUED ON FIG.5-12)

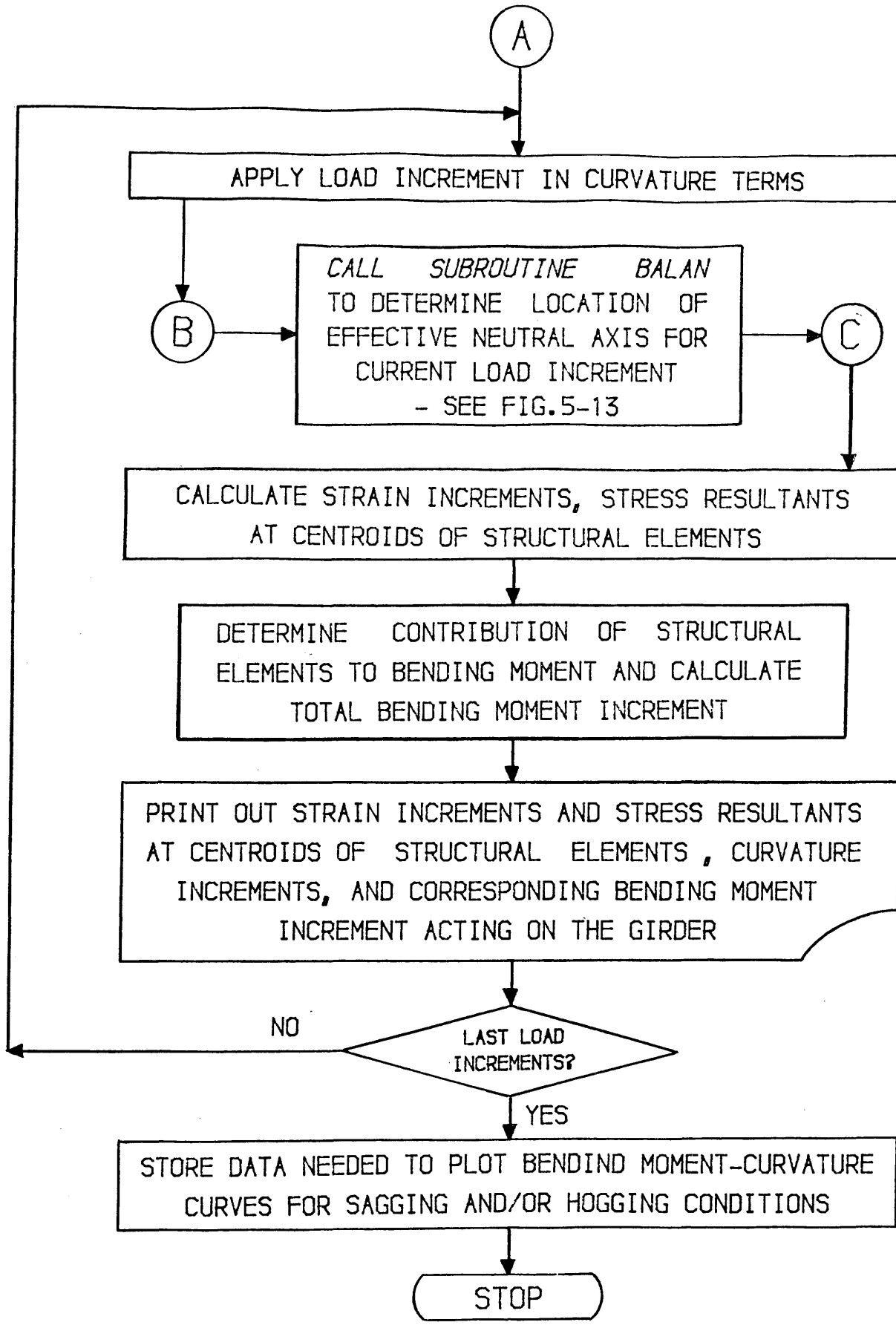

FIG.5-12 FLOW CHART FOR EVALUATION OF BENDING MOMENT-CURVATURE RELATIONSHIP

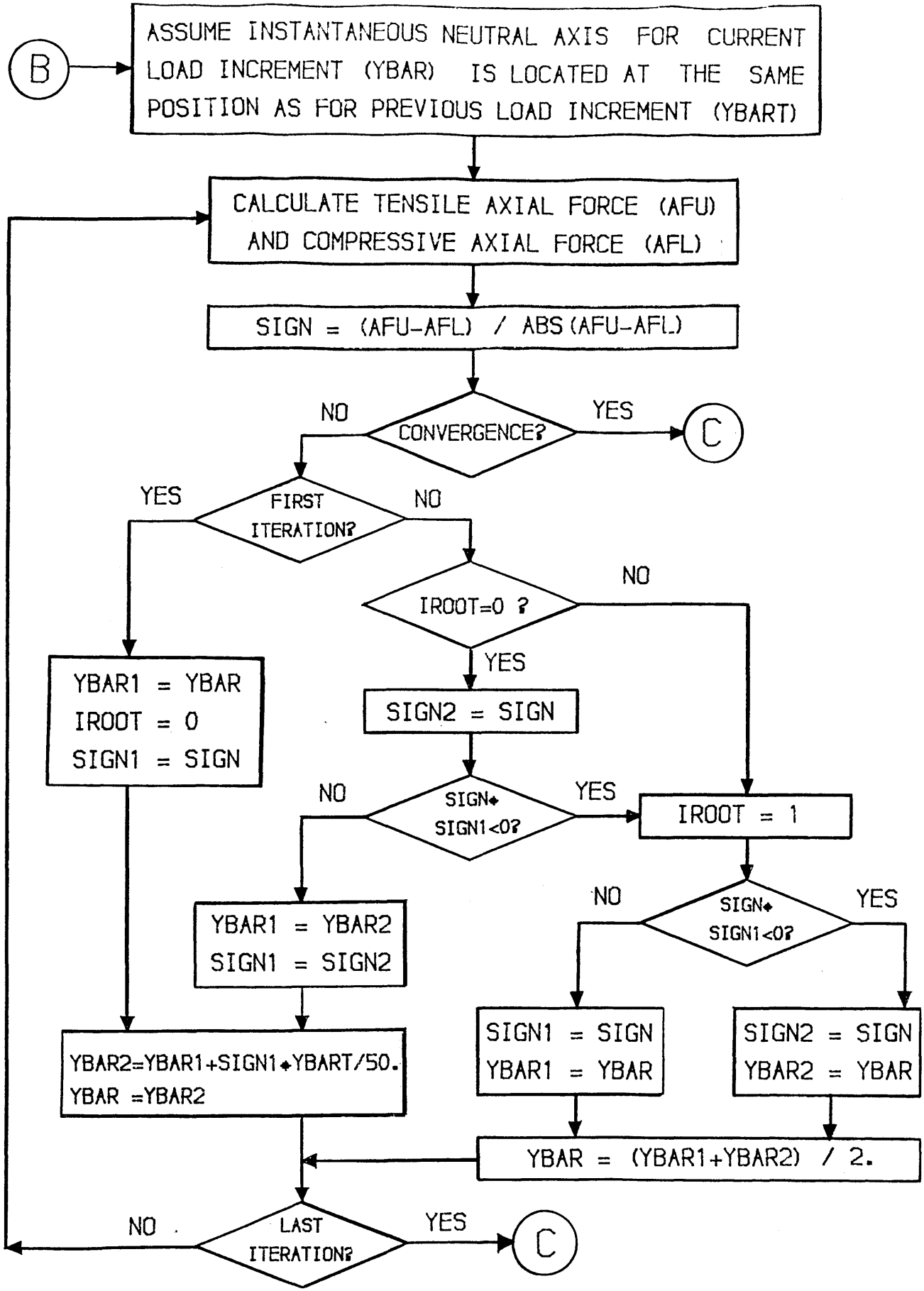

FIG.5-13 FLOW CHART OF ITERATIVE PROCEDURE FOR DETERMINATION OF EFFECTIVE NEUTRAL AXIS

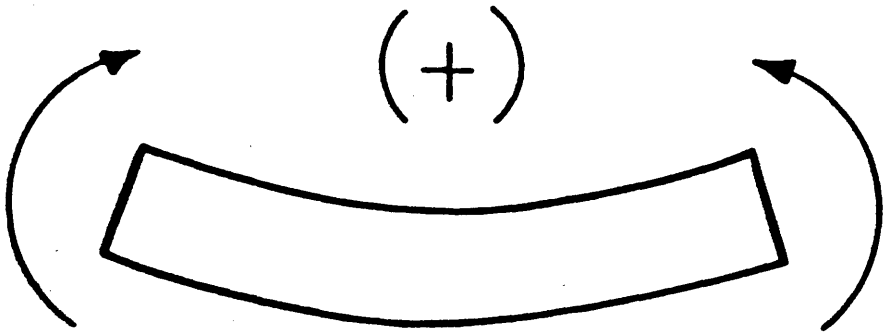

SAGGING CONDITION:

DECK SUBJECTED TO COMPRESSION

BOTTOM SUBJECTED TO TENSION.

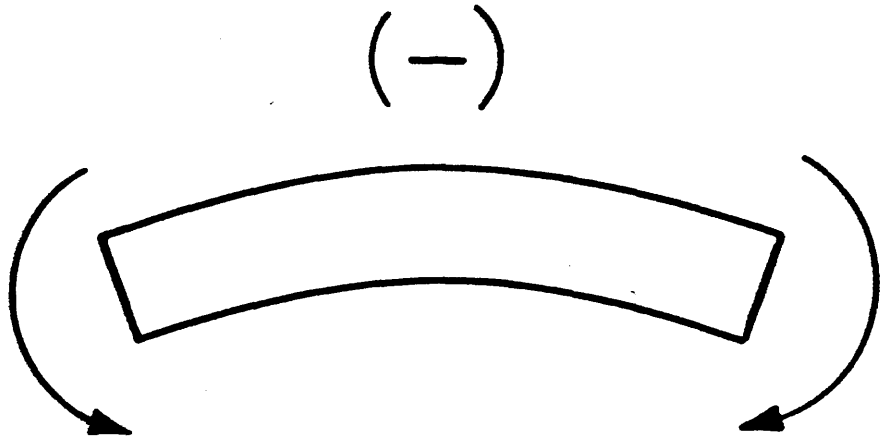

HOGGING CONDITION:

DECK SUBJECTED TO TENSION

BOTTOM SUBJECTED TO COMPRESSION.

FIG.5-14 SIGN CONVENTION FOR VERTICAL BENDING MOMENT.

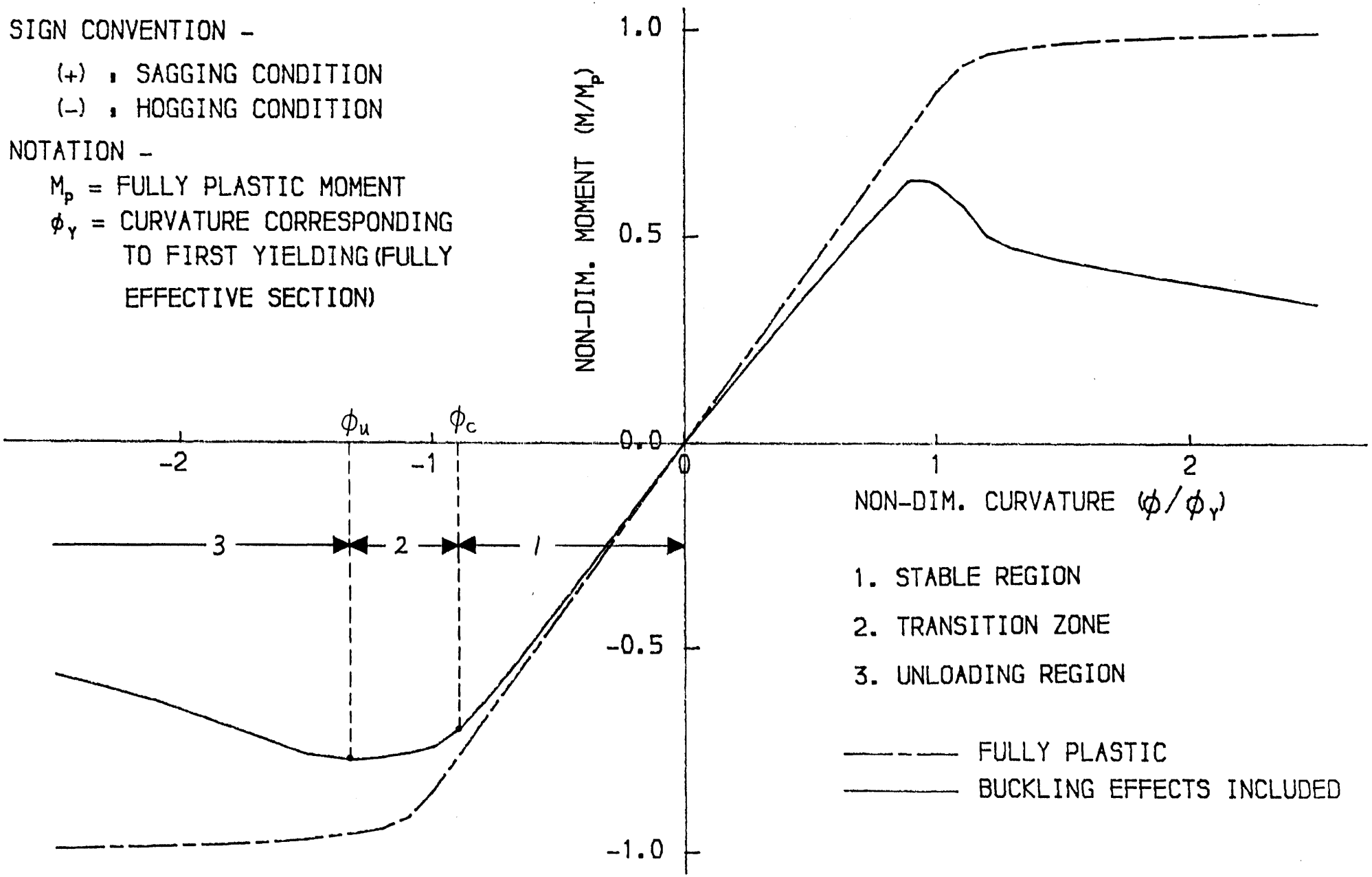

FIG.5-15 TYPICAL BENDING MOMENT-CURVATURE CURVE

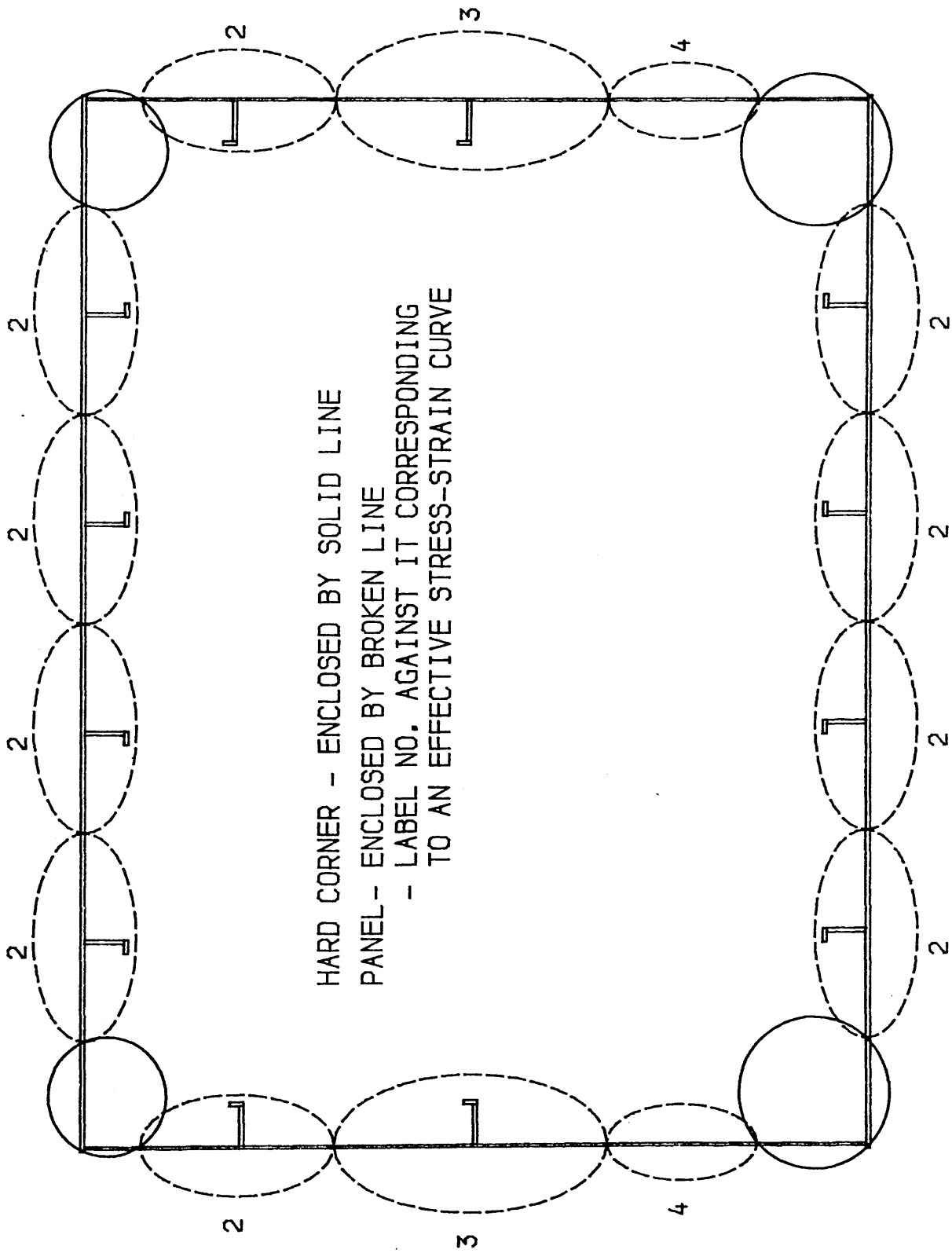

FIG.6-1 DISCRETISATION FOR CROSS-SECTION OF S.B.G. MODEL 2

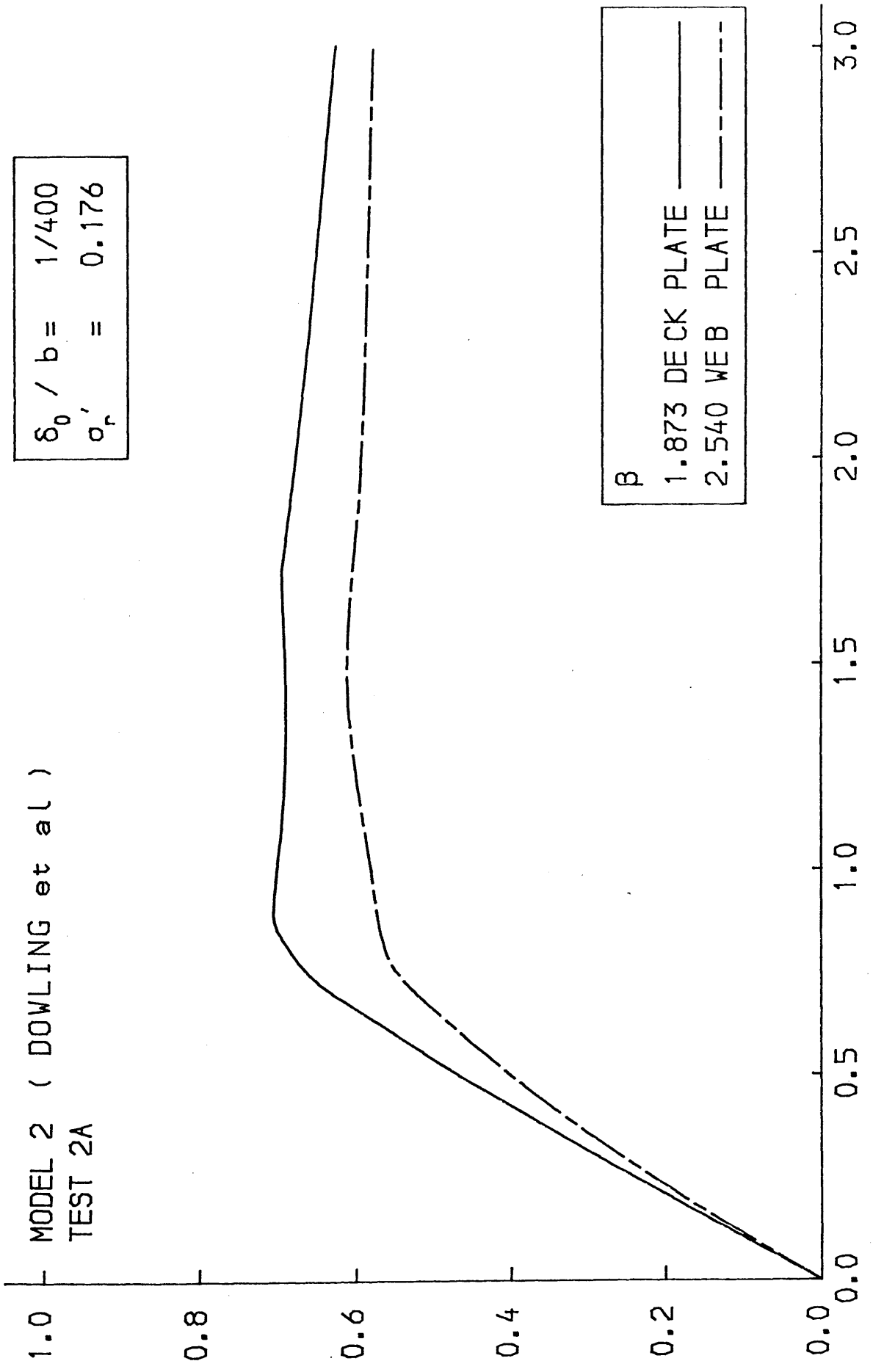

FIG.6-2 AVERAGE STRESS-STRAIN CURVE FOR THE PLATE

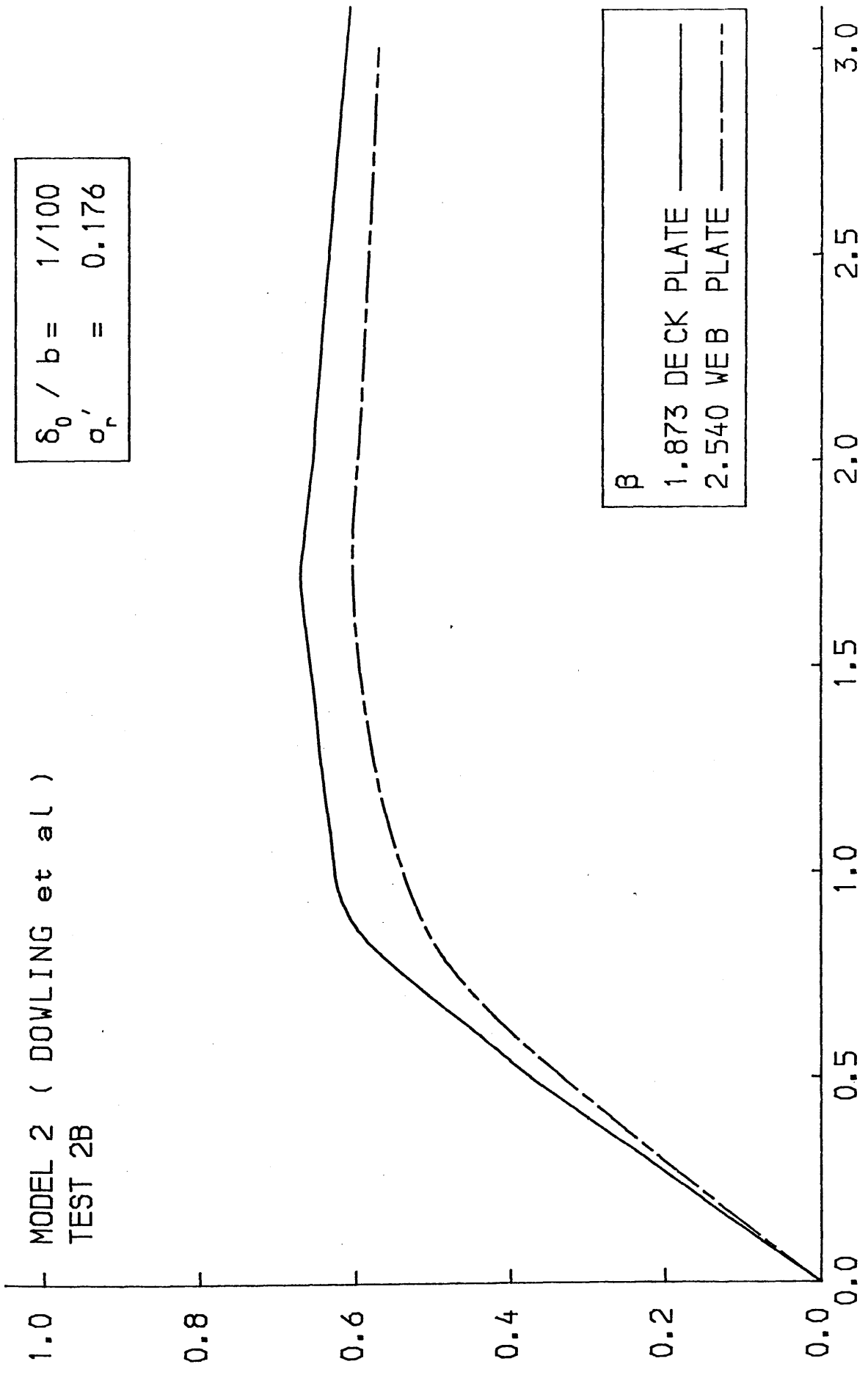

FIG.6-3 AVERAGE STRESS-STRAIN CURVE FOR THE PLATE

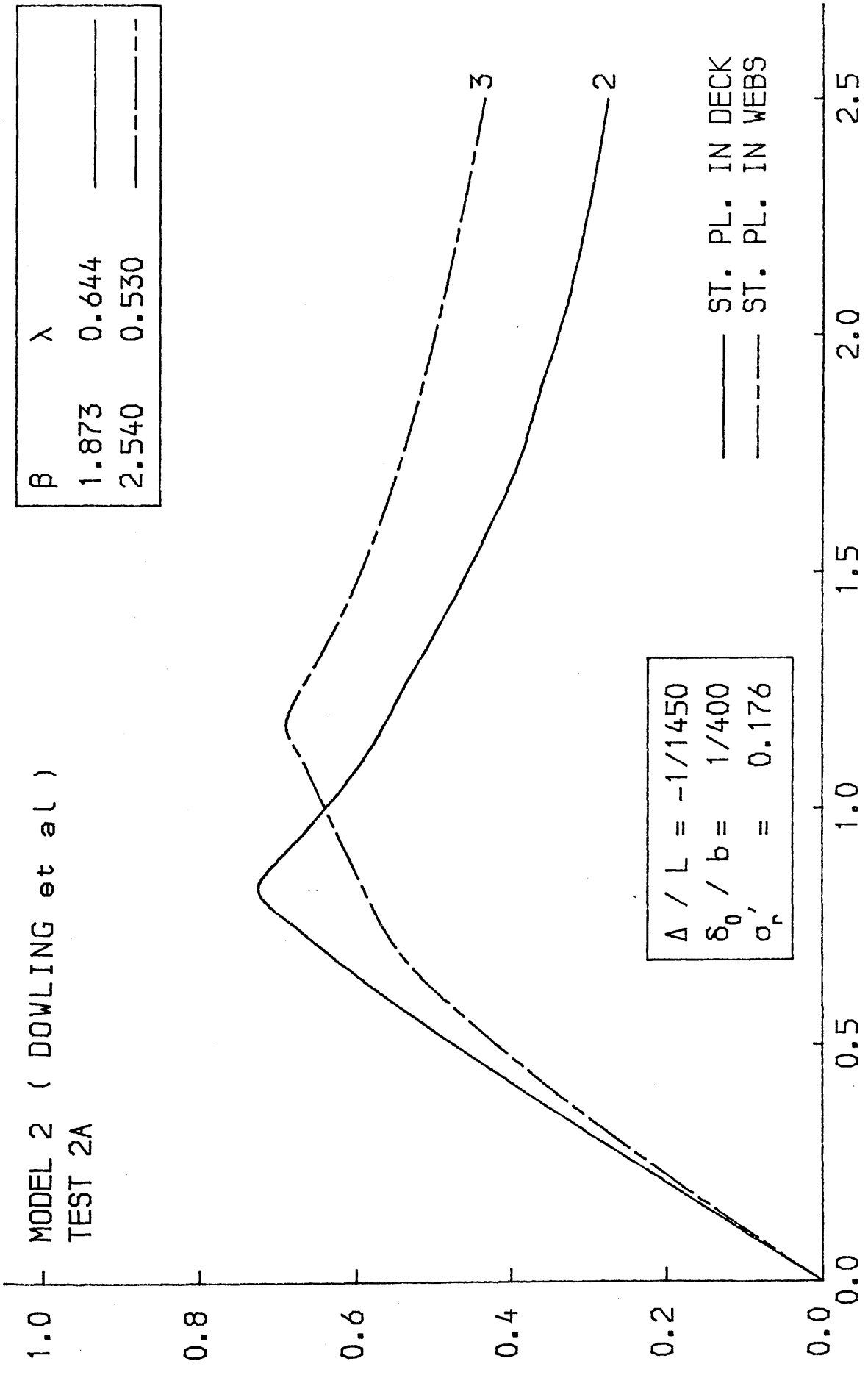

FIG.6-4 LOAD-SHORTENING CURVE FOR THE BEAM-COLUMN

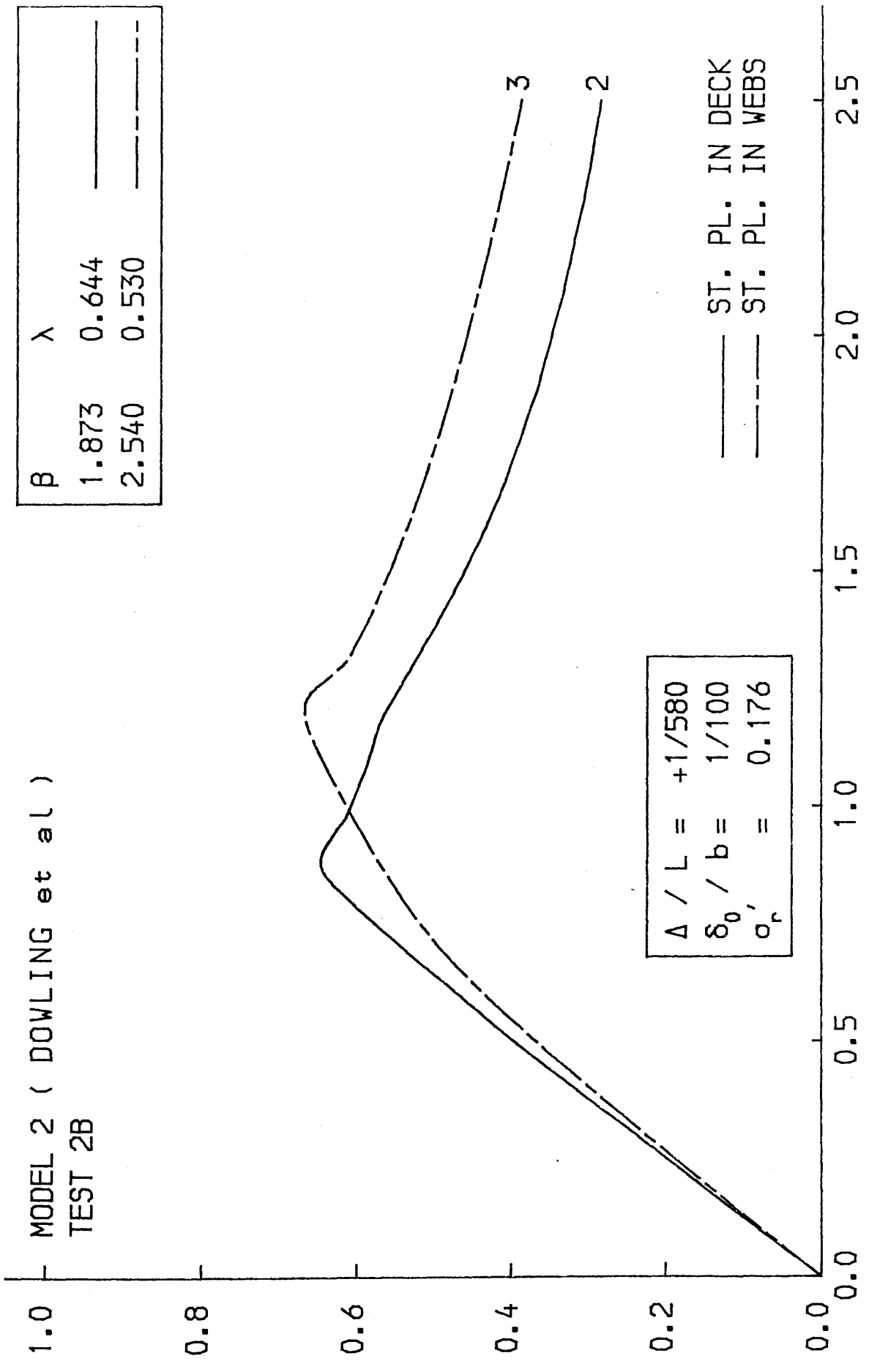

FIG.6-5 LOAD-SHORTENING CURVE FOR THE BEAM-COLUMN

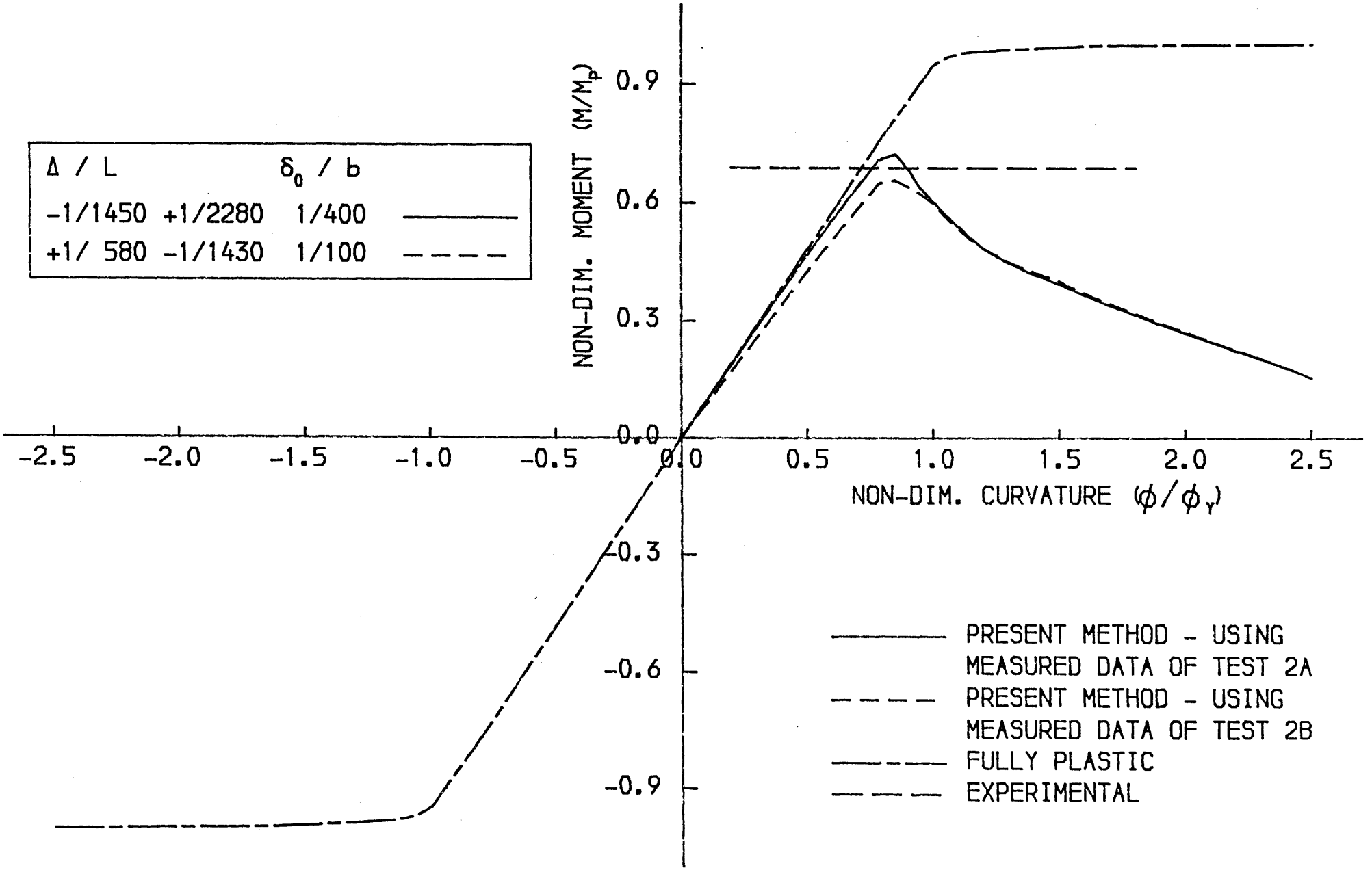

FIG.6-6 BENDING MOMENT-CURVATURE CURVE FOR DOWLING'S MODEL 2

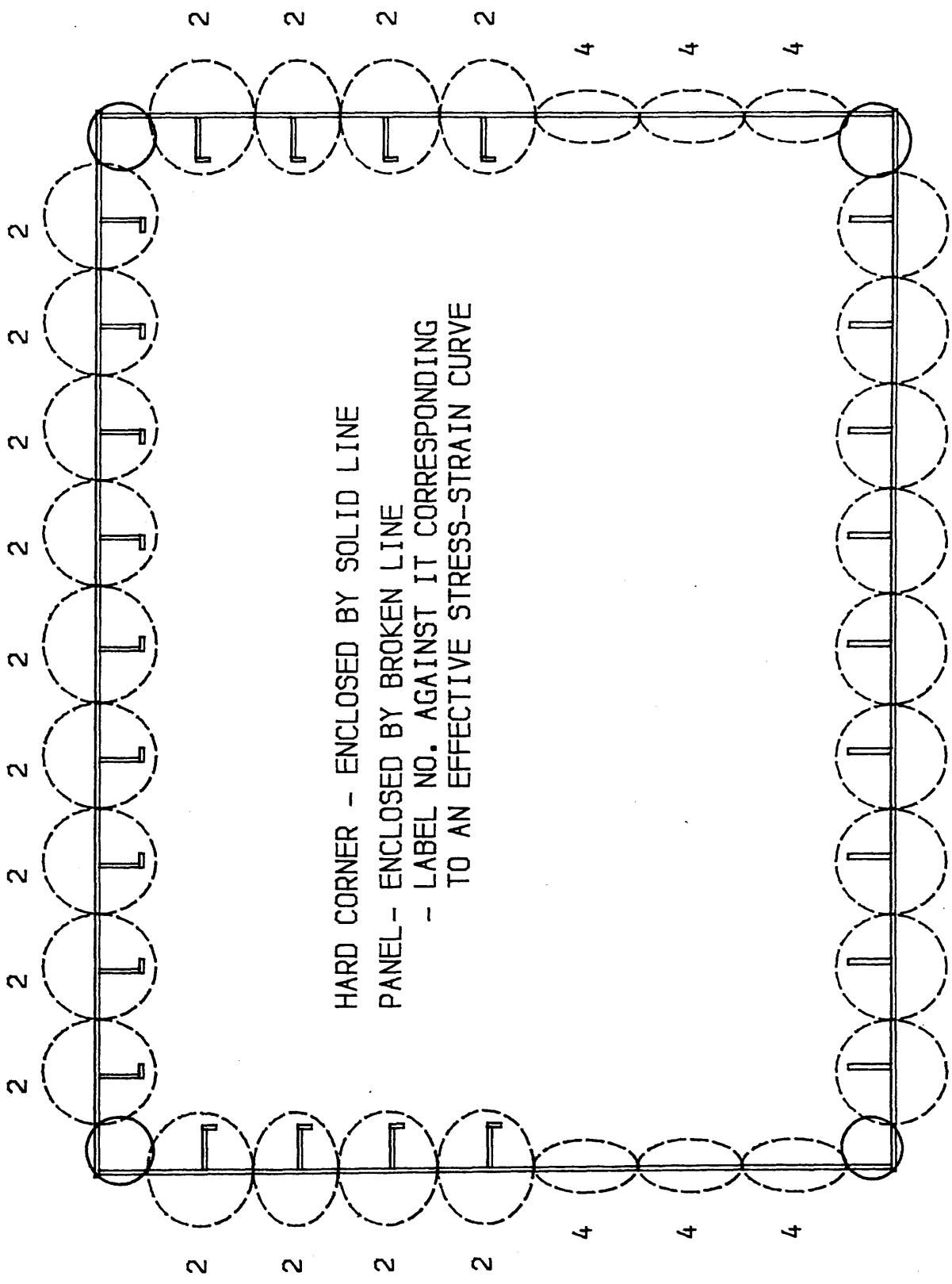

FIG.6-7 DISCRETISATION FOR CROSS-SECTION OF S.B.G. MODEL 4

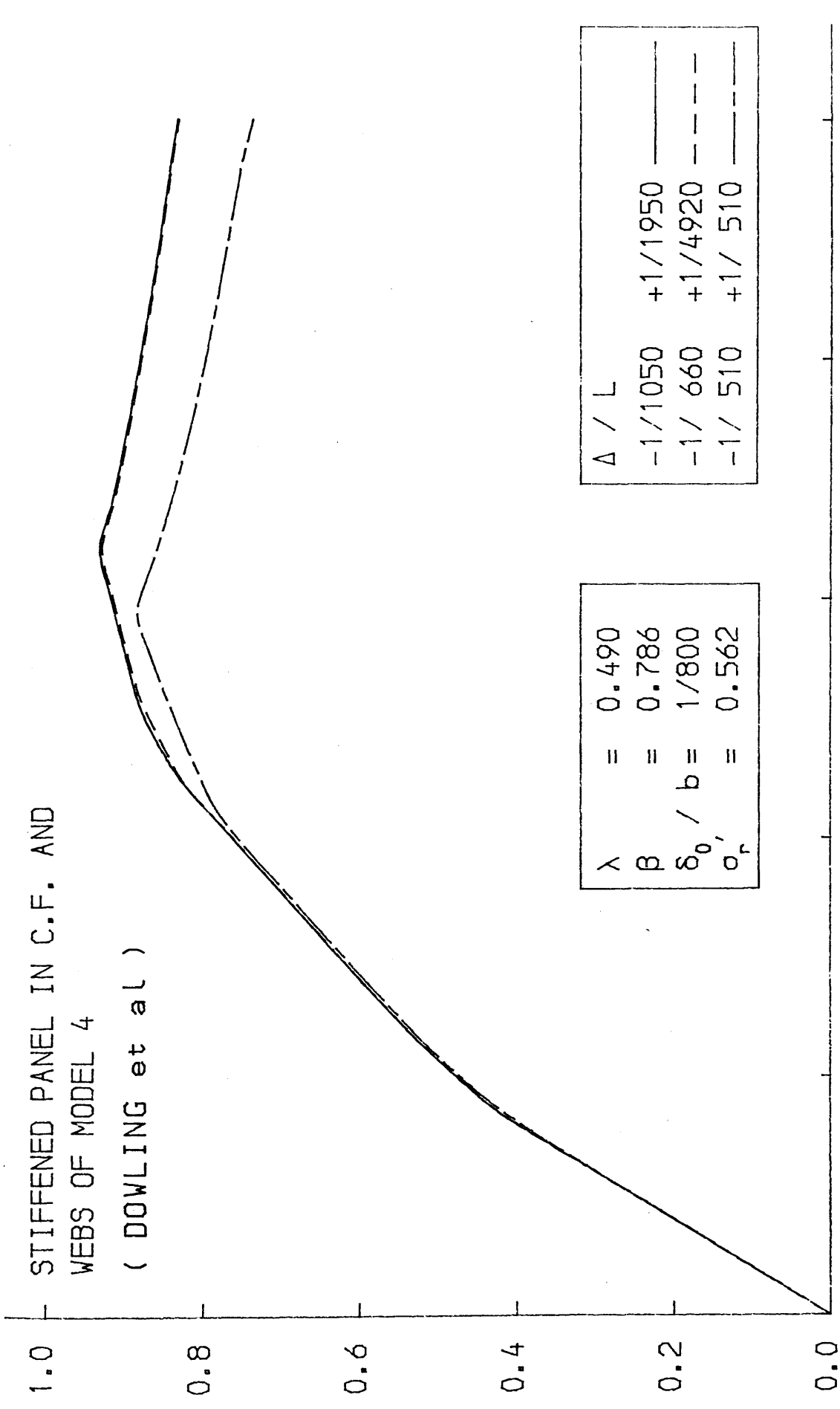

FIG.6-8 LOAD-SHORTENING CURVE FOR THE BEAM-COLUMN

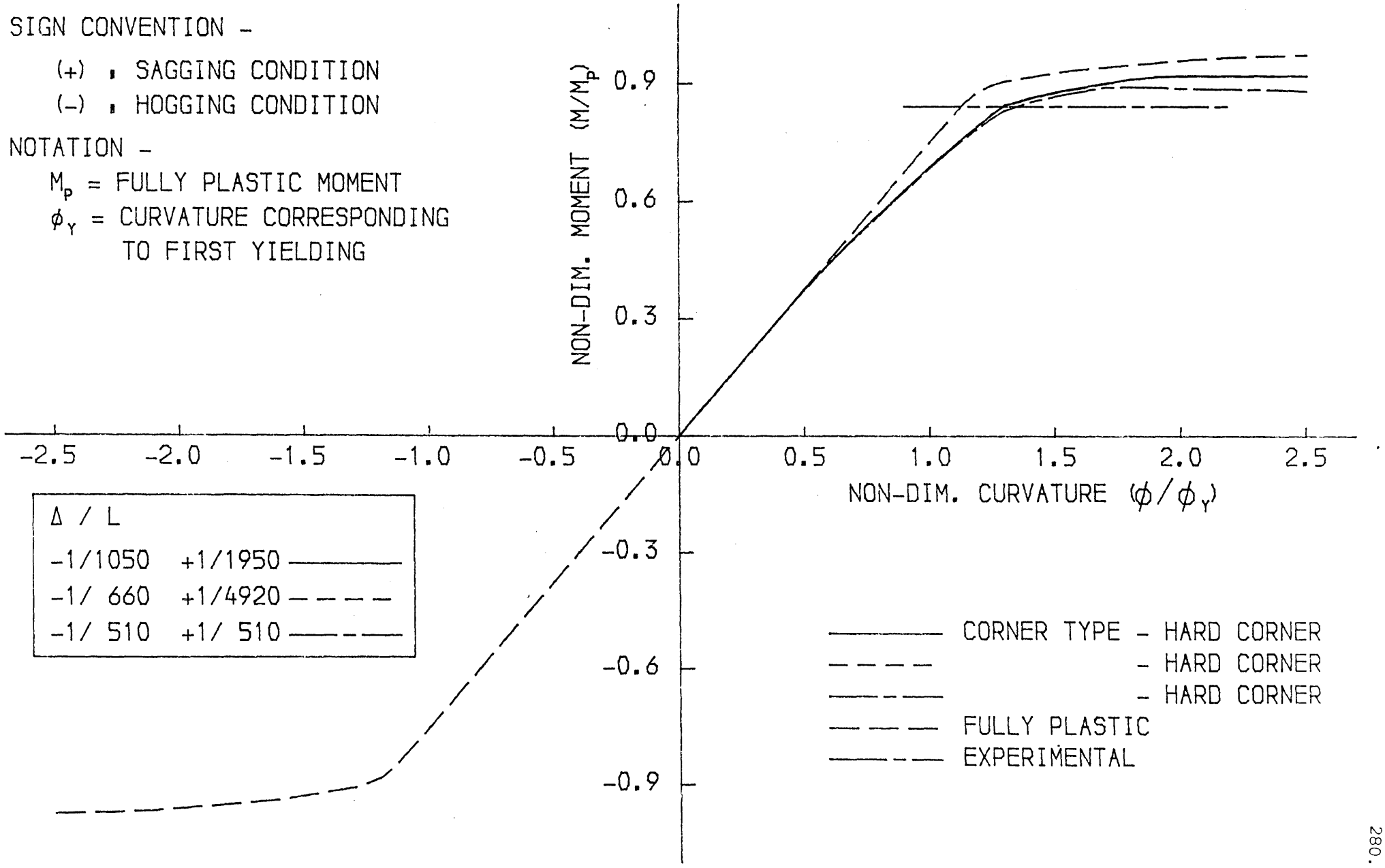

FIG.6-9 BENDING MOMENT-CURVATURE CURVE FOR DOWLING'S MODEL 4

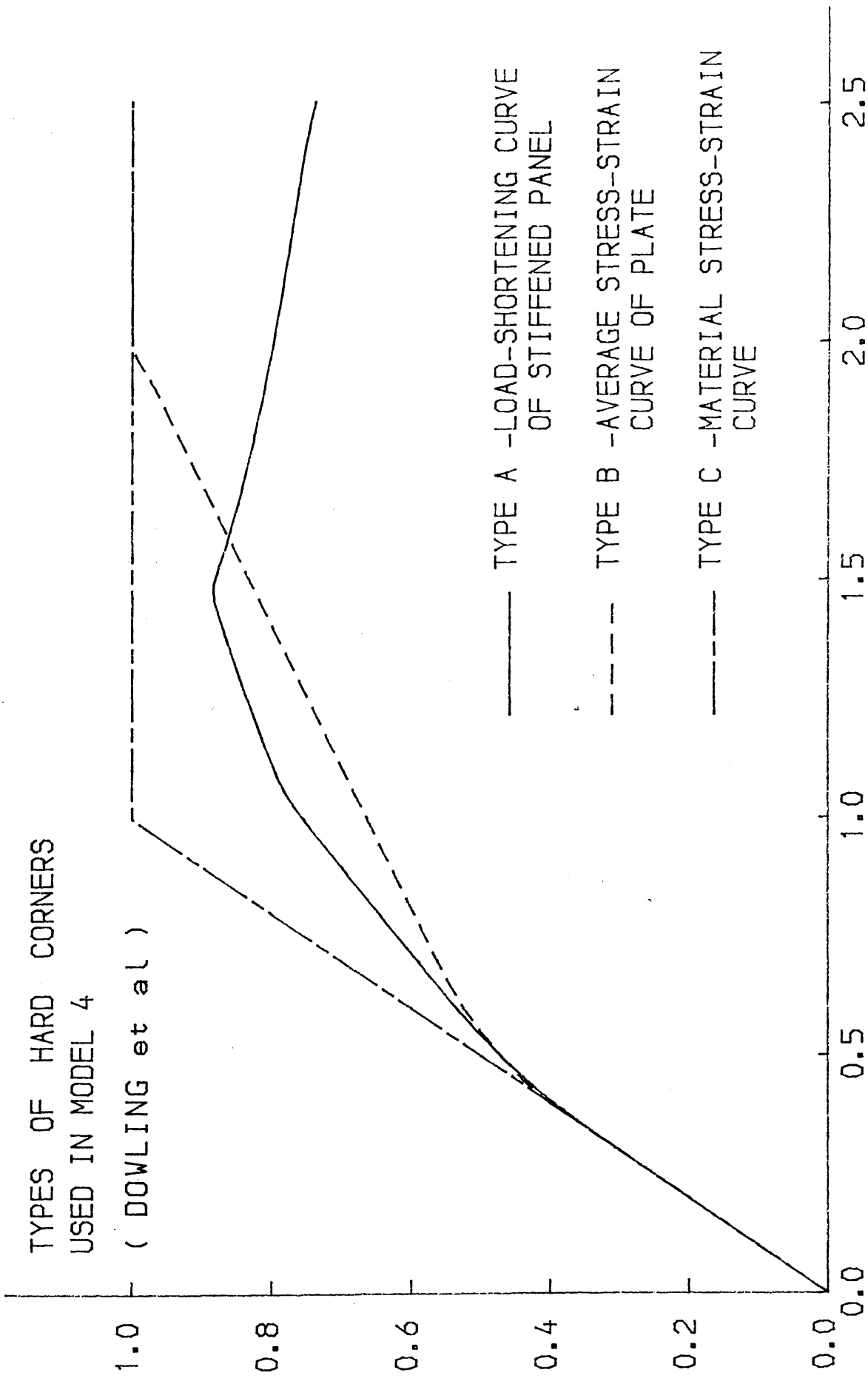

FIG.6-10 AVERAGE STRESS-STRAIN CURVES FOR HARD CORNERS

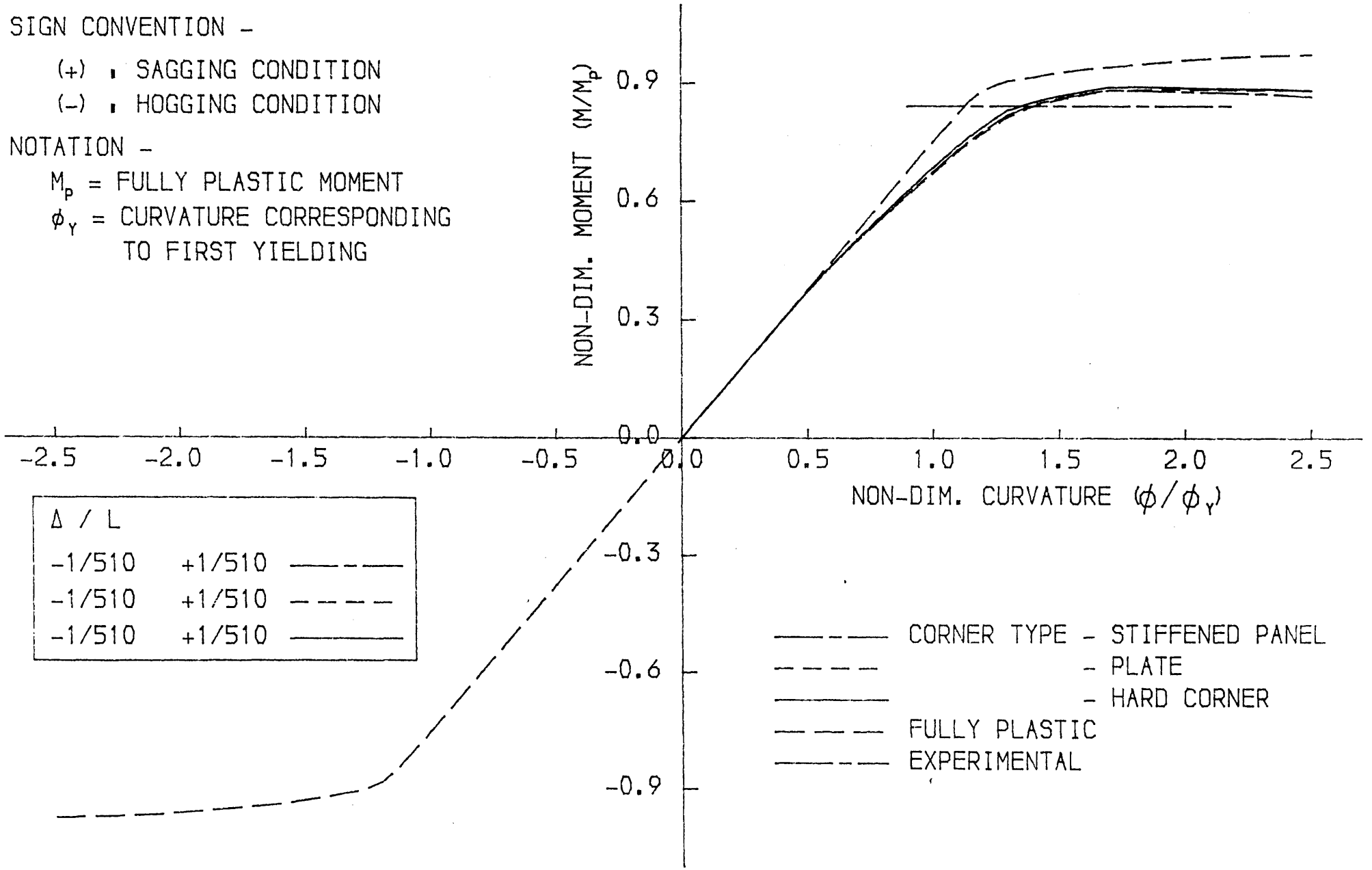

FIG.6-11 BENDING MOMENT-CURVATURE CURVE FOR DOWLING'S MODEL 4

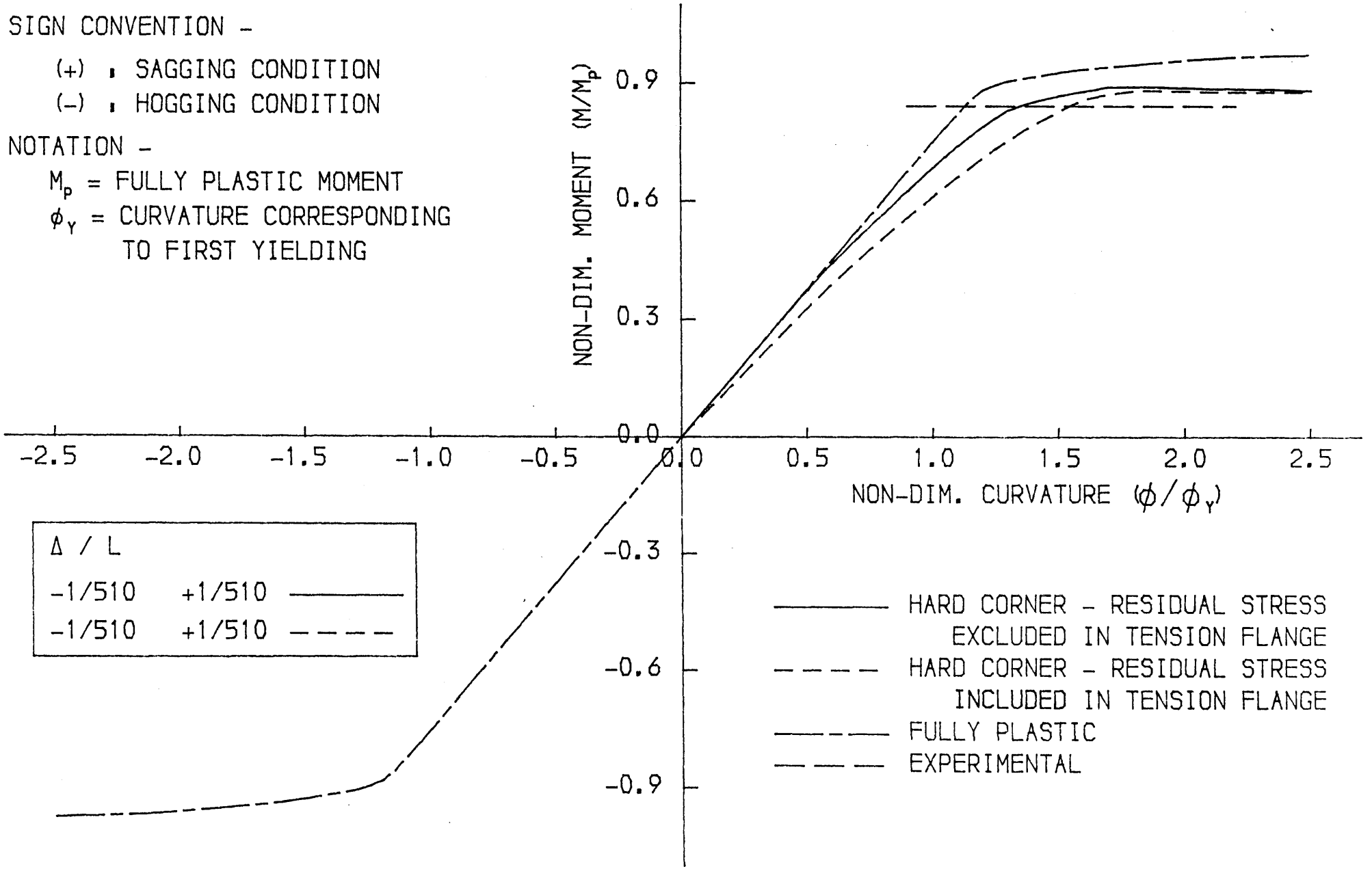

FIG.6-12 BENDING MOMENT-CURVATURE CURVE FOR DOWLING'S MODEL 4

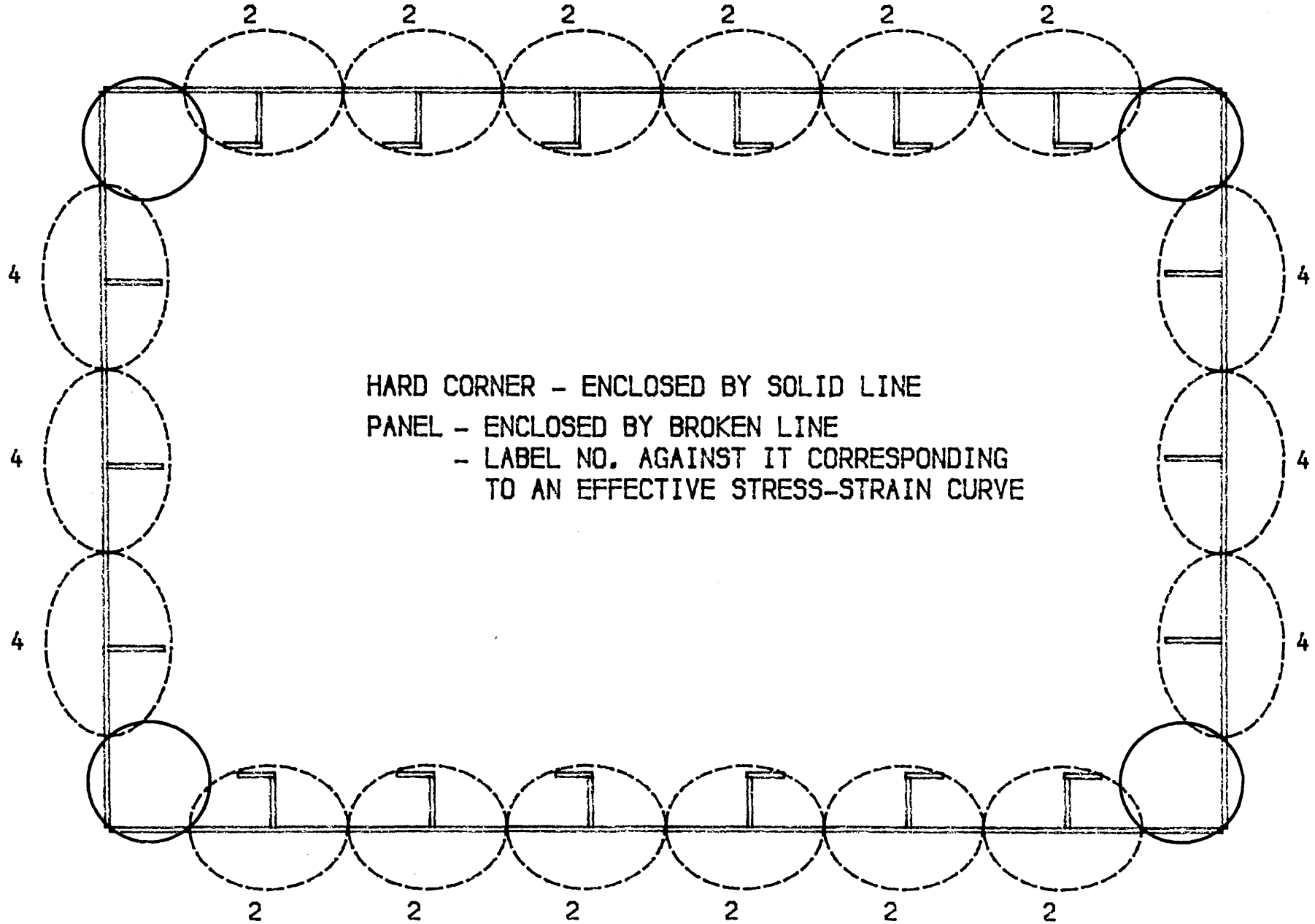

FIG.6-13 DISCRETISATION FOR CROSS-SECTION OF MODEL 23 (RECKLING)

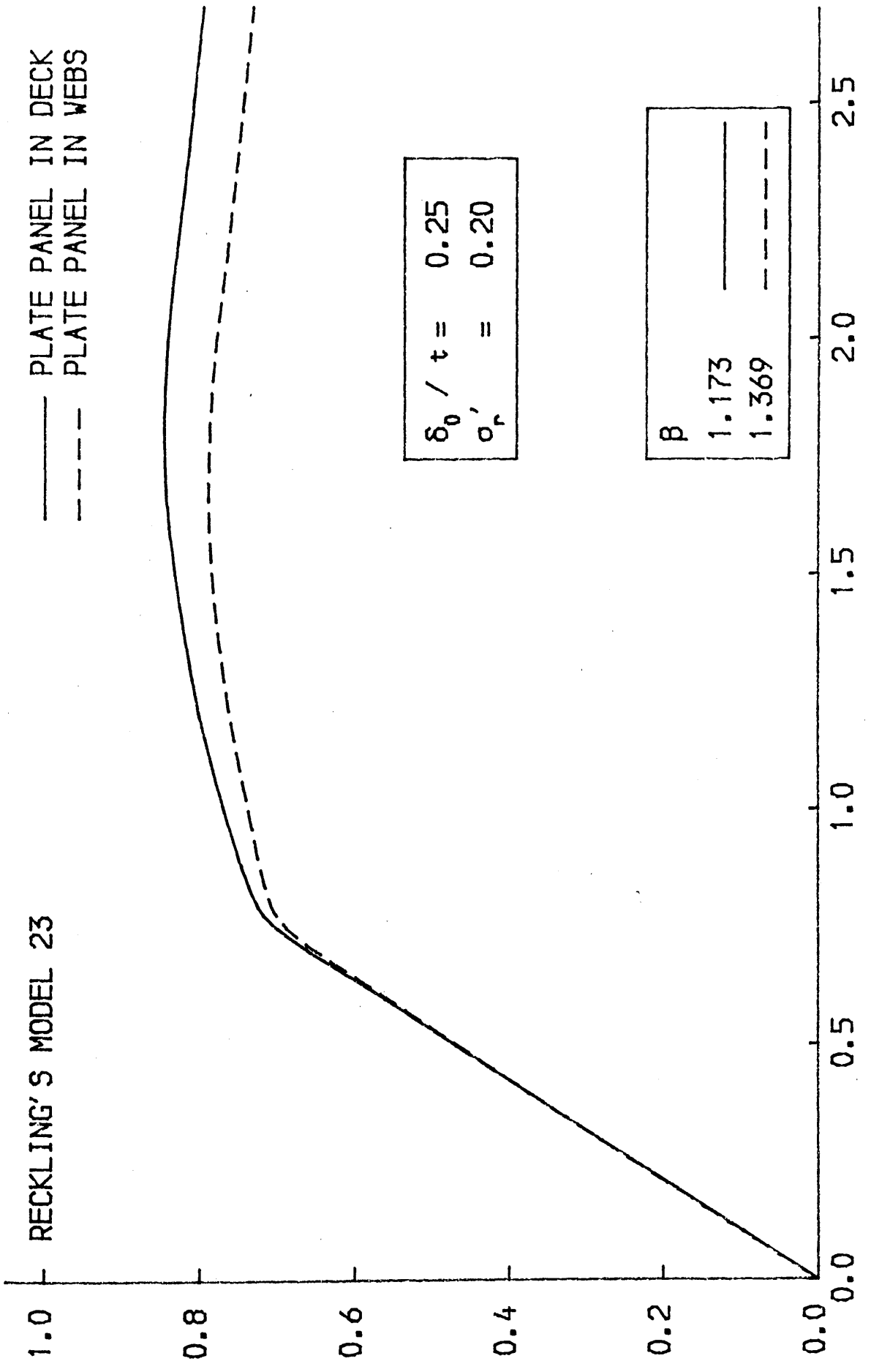

FIG.6-14 AVERAGE STRESS-STRAIN CURVE FOR THE PLATE

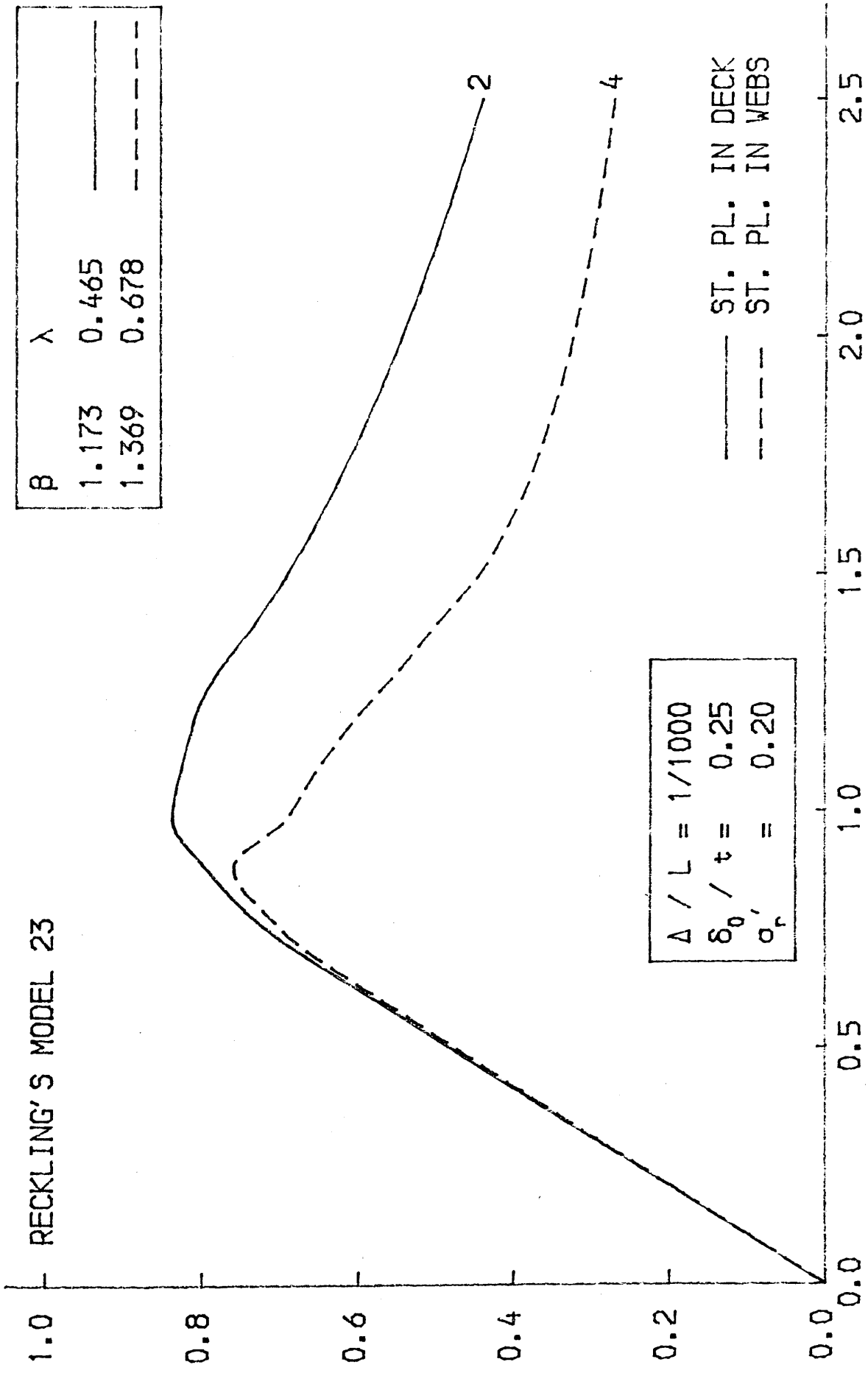

FIG.6-15 LOAD-SHORTENING CURVE FOR THE BEAM-COLUMN

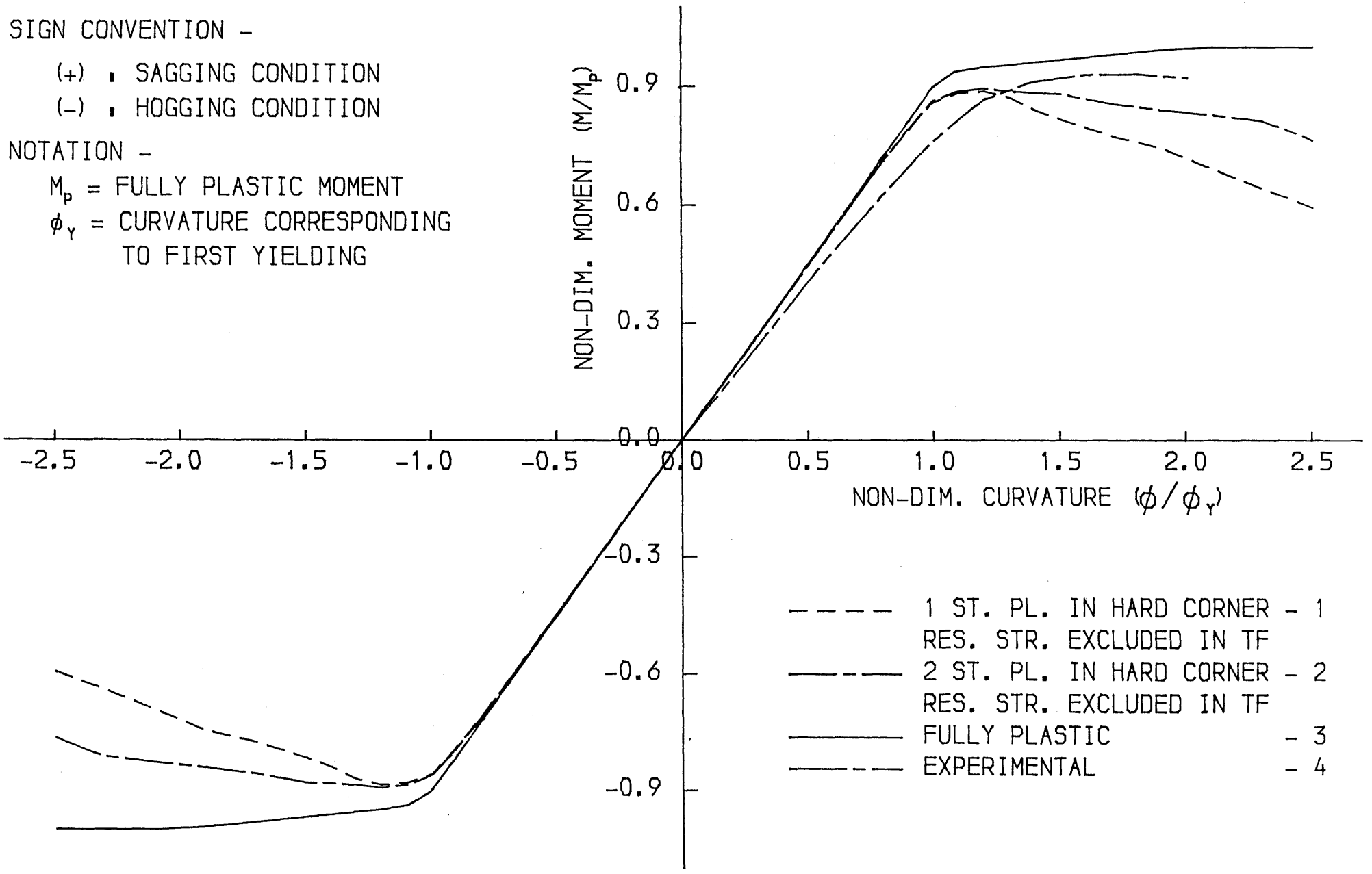

FIG.6-16 BENDING MOMENT-CURVATURE CURVE FOR MODEL 23 (RECKLING)

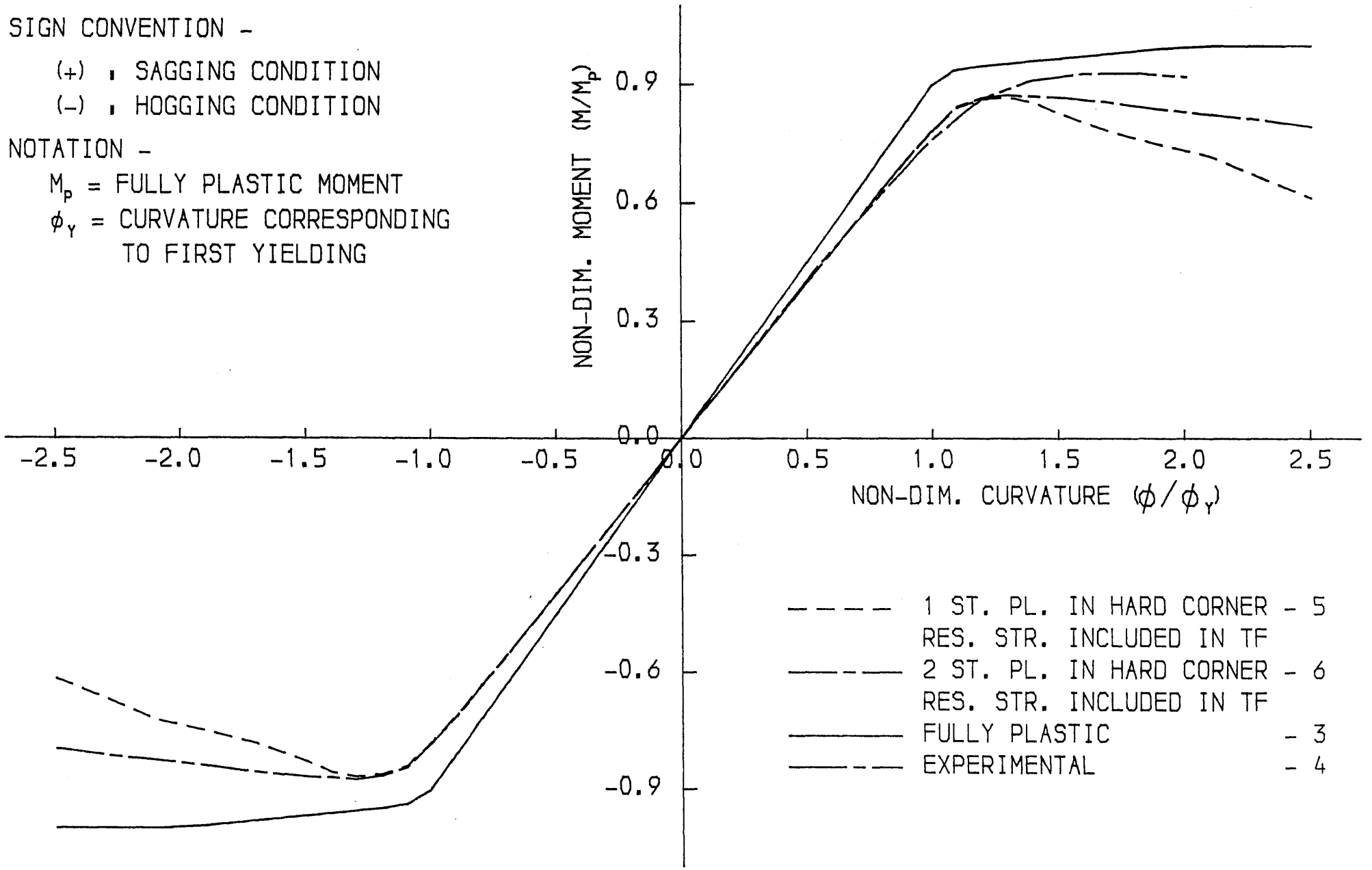

FIG.6-17 BENDING MOMENT-CURVATURE CURVE FOR MODEL 23 (RECKLING)

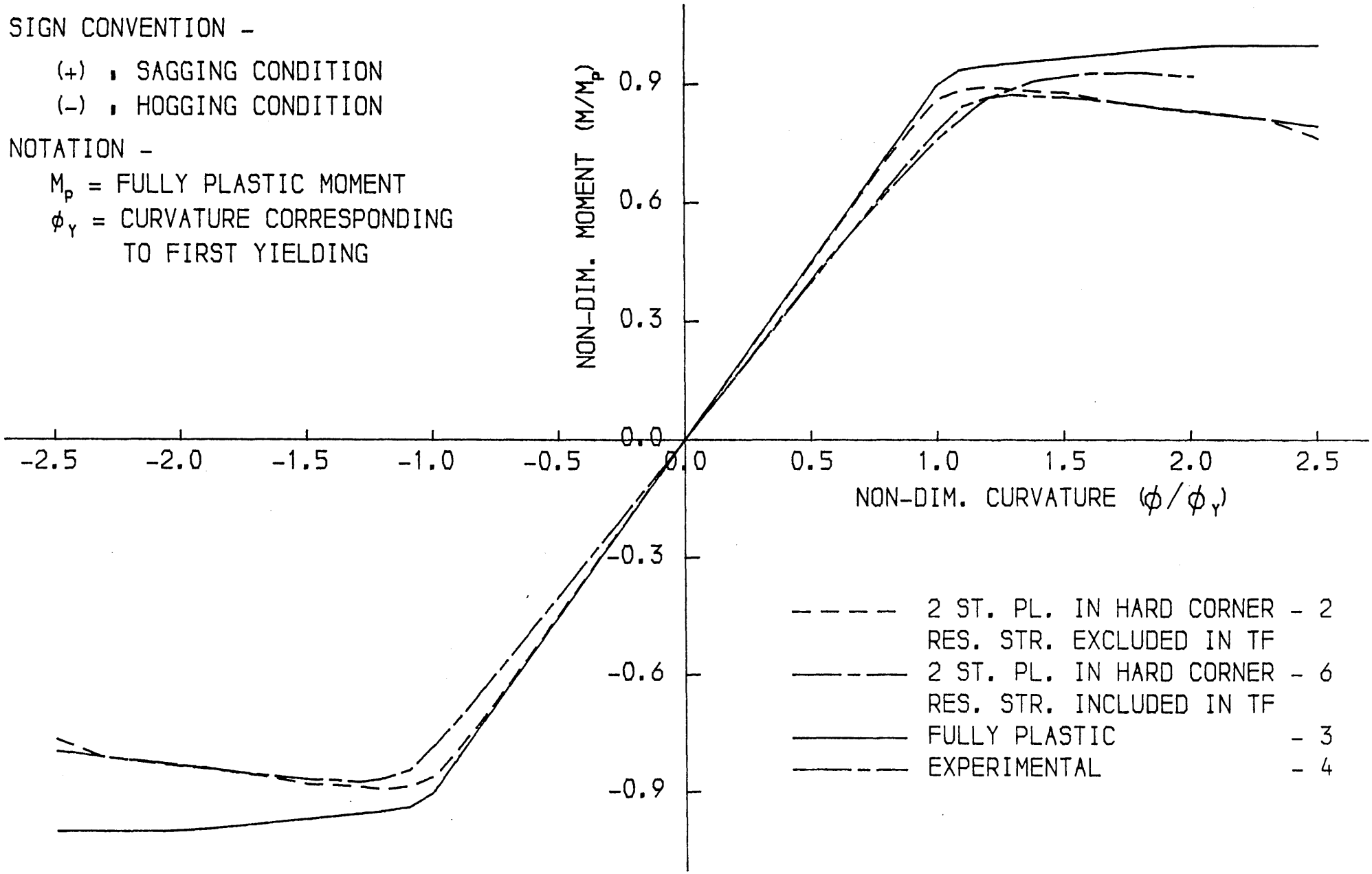

FIG.6-18 BENDING MOMENT-CURVATURE CURVE FOR MODEL 23 (RECKLING)

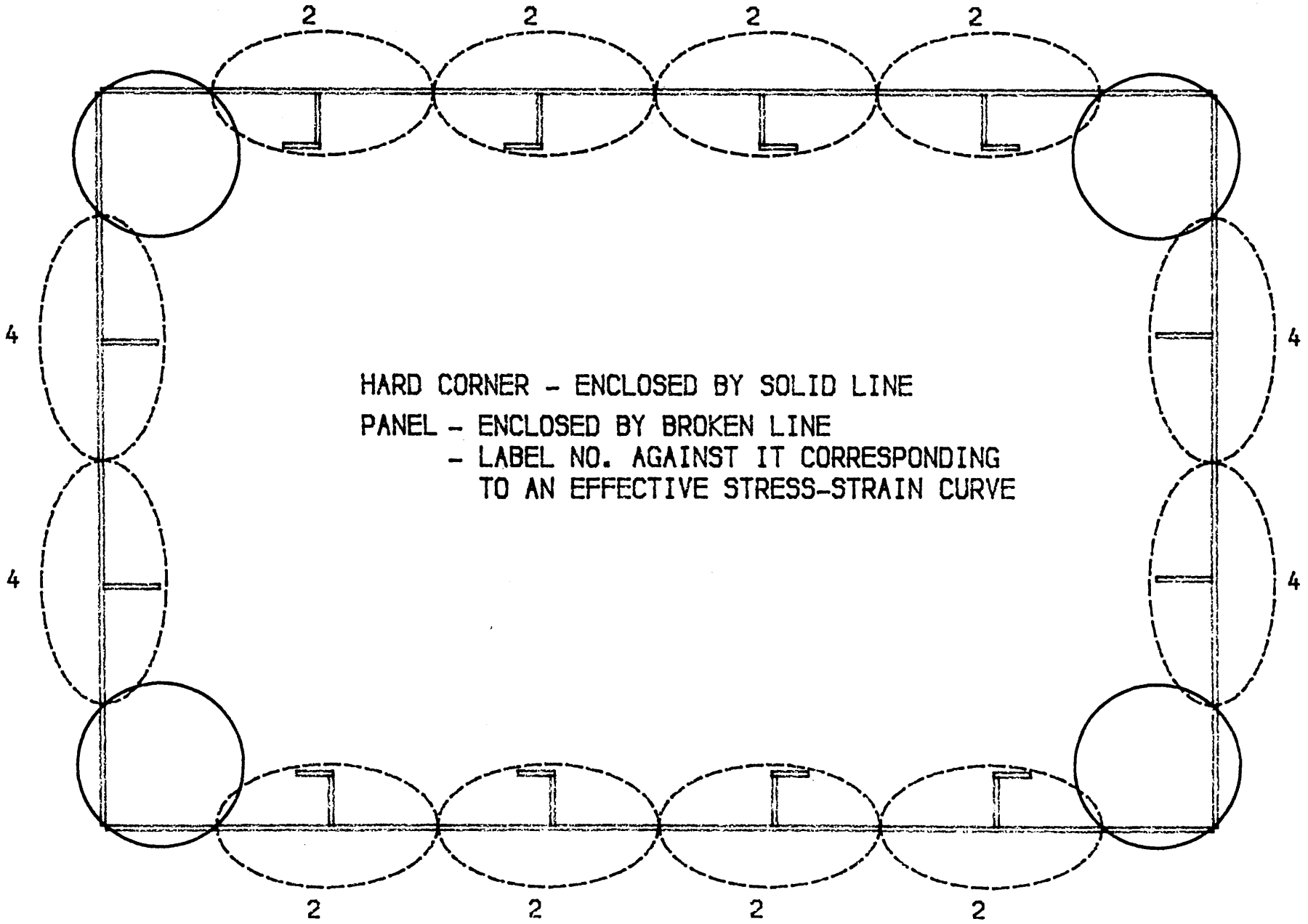

FIG.6-19 DISCRETISATION FOR CROSS-SECTION OF MODEL 31 (RECKLING)

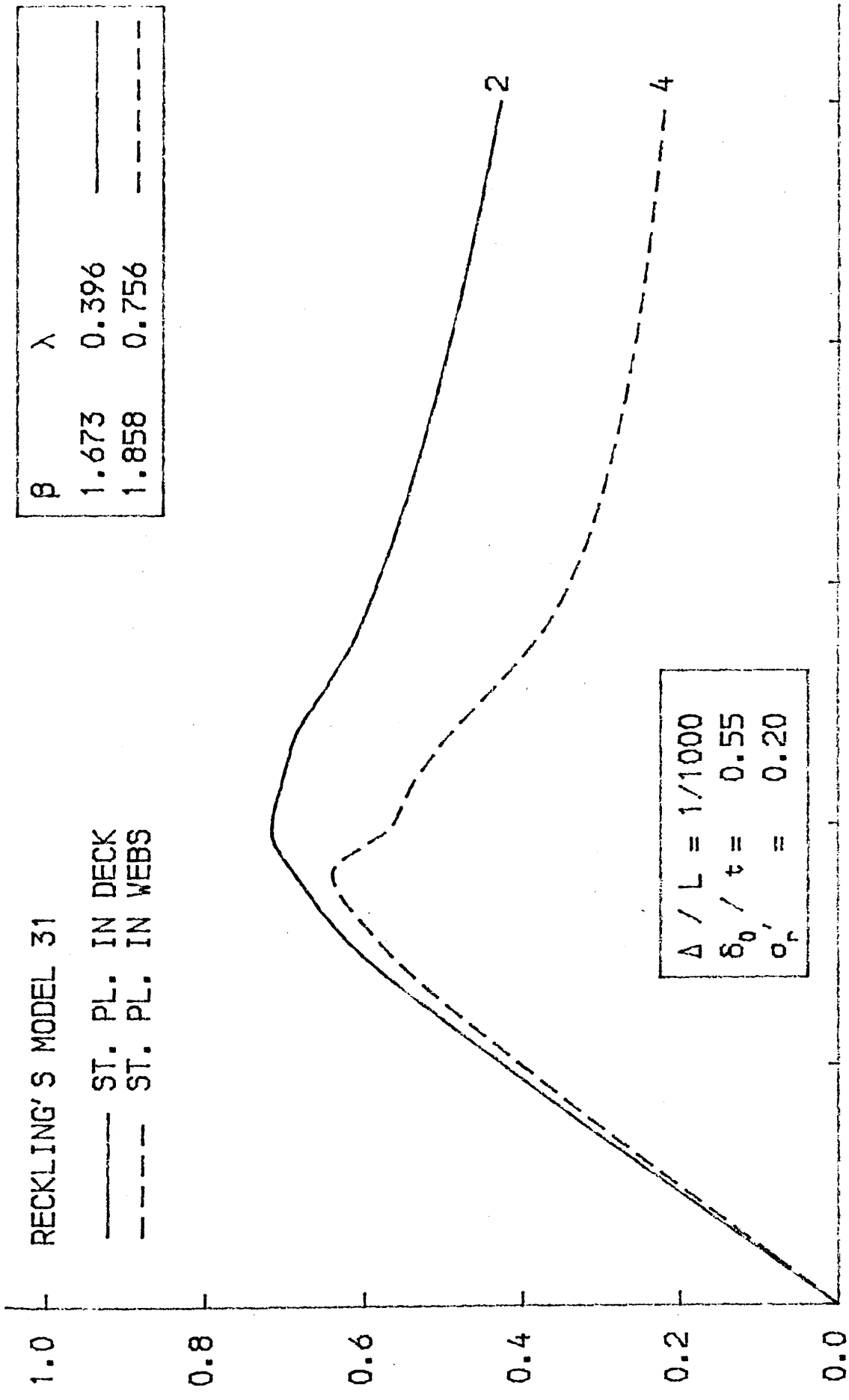

FIG.6-20 LOAD-SHORTENING CURVE FOR THE BEAM-COLUMN

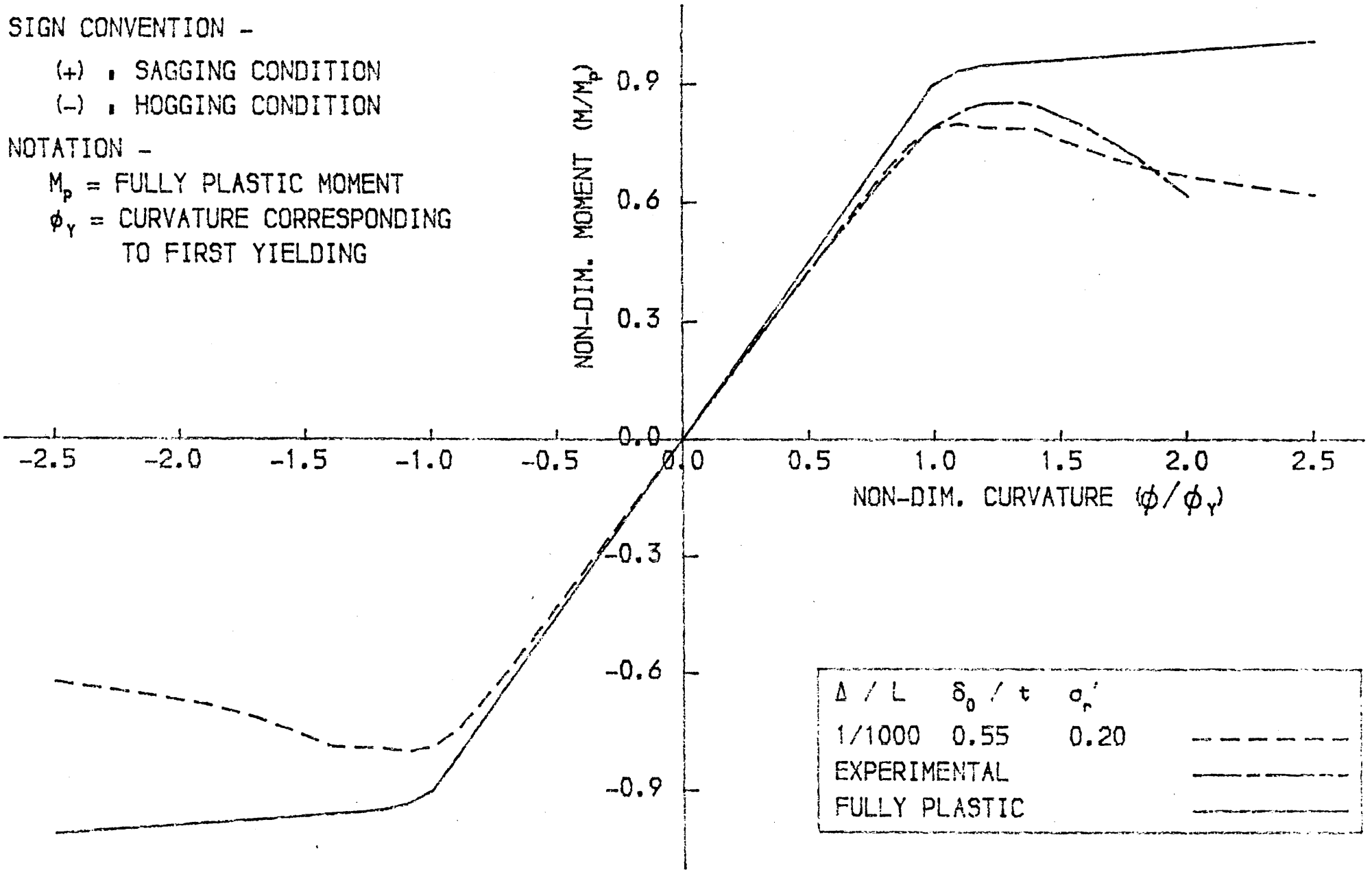

FIG.6-21 BENDING MOMENT-CURVATURE CURVE FOR MODEL 31 (RECKLING)

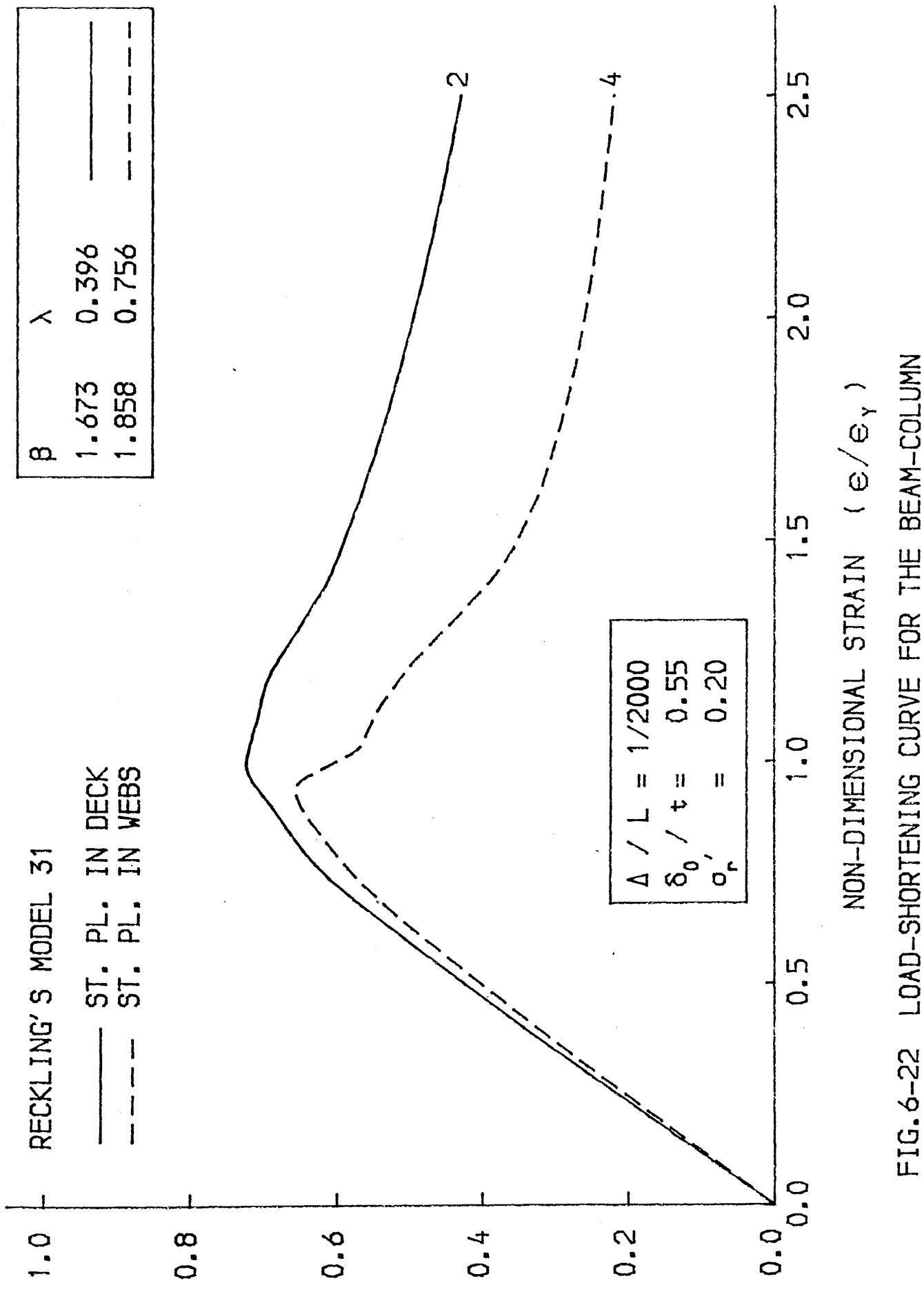

FIG.6-22 LOAD-SHORTENING CURVE FOR THE BEAM-COLUMN

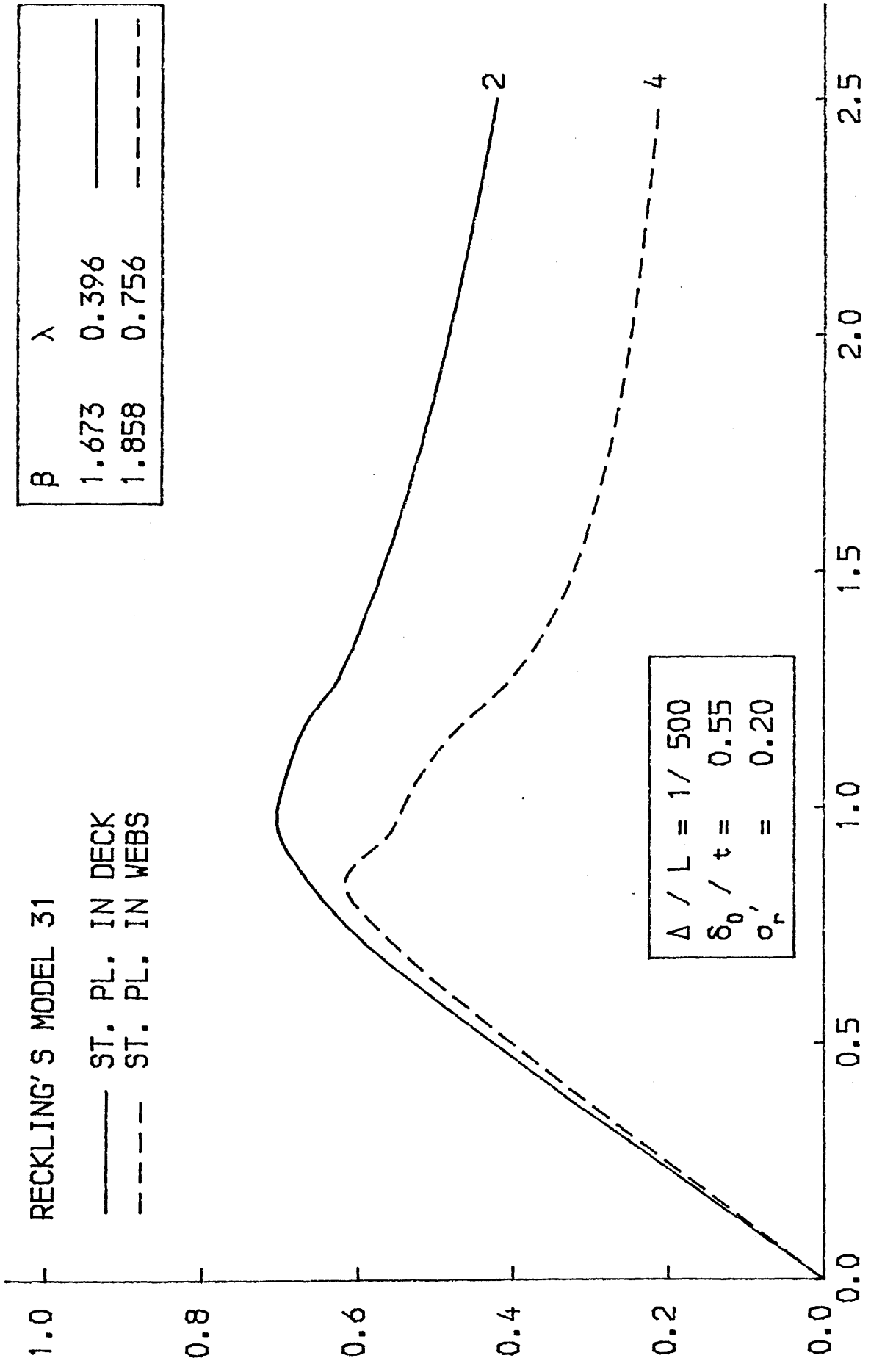

FIG.6-23 LOAD-SHORTENING CURVE FOR THE BEAM-COLUMN

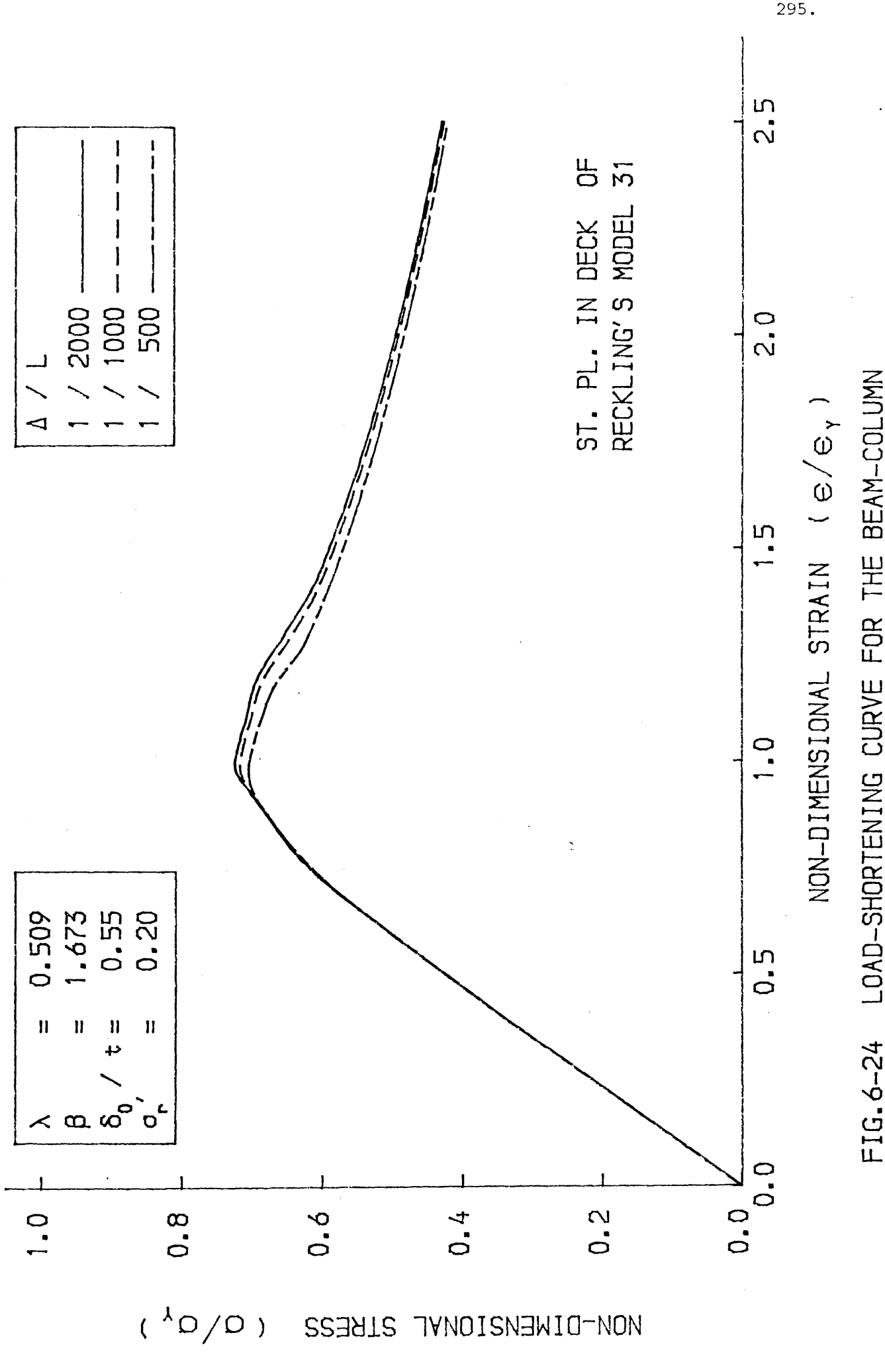

FIG.6-24 LOAD-SHORTENING CURVE FOR THE BEAM-COLUMN

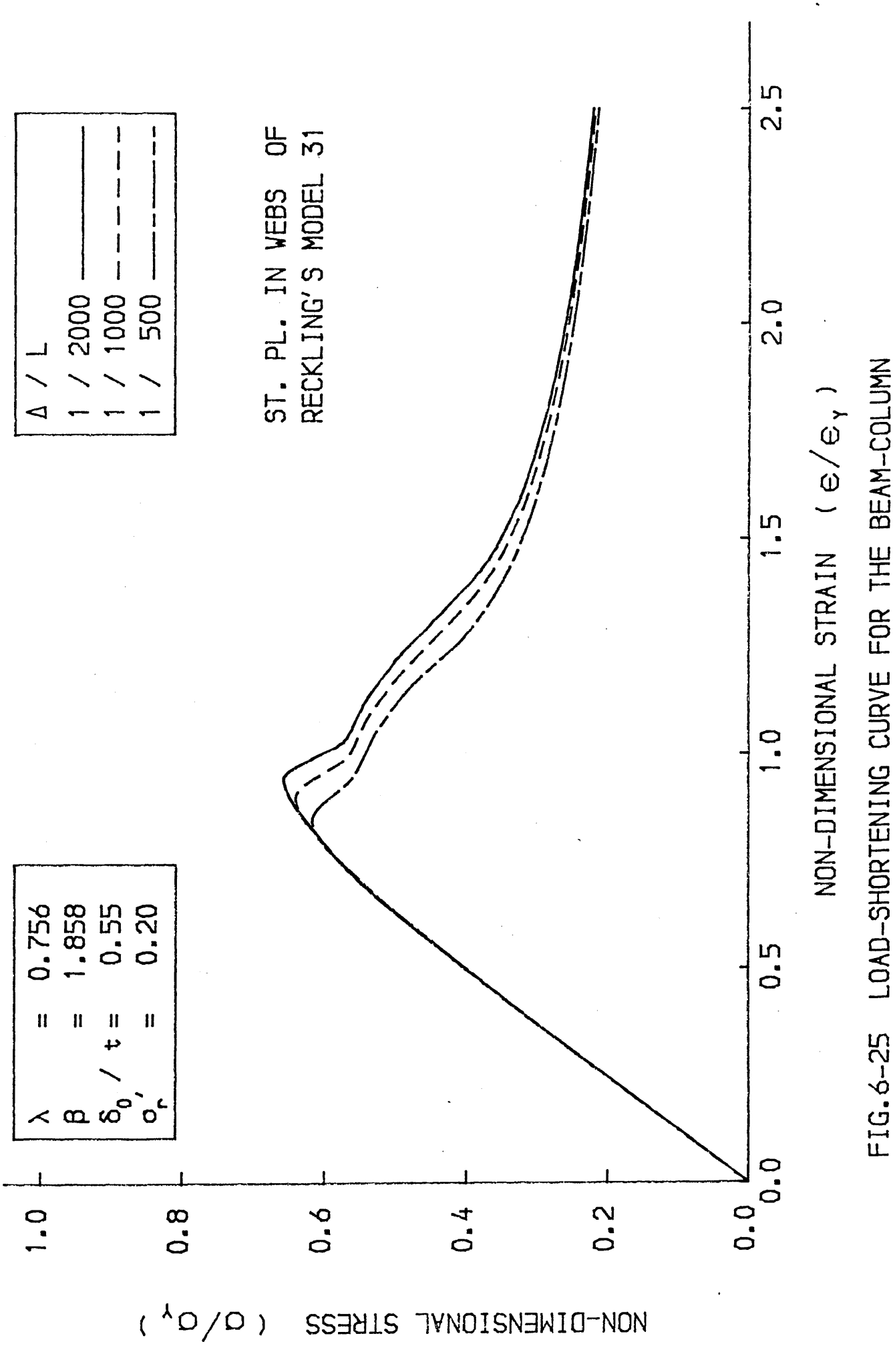

FIG.6-25 LOAD-SHORTENING CURVE FOR THE BEAM-COLUMN

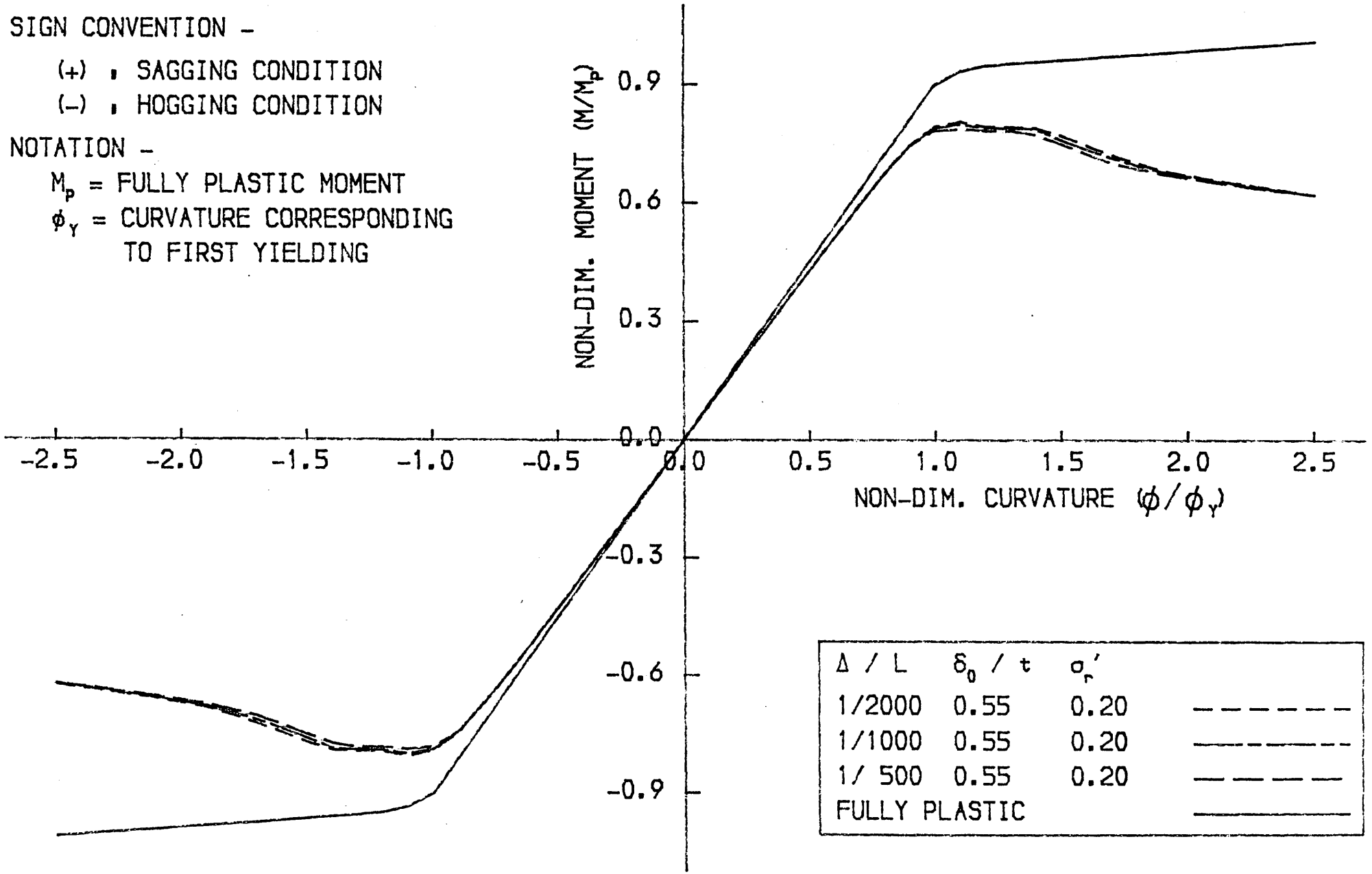

FIG.6-26 BENDING MOMENT-CURVATURE CURVE FOR MODEL 31 (RECKLING)

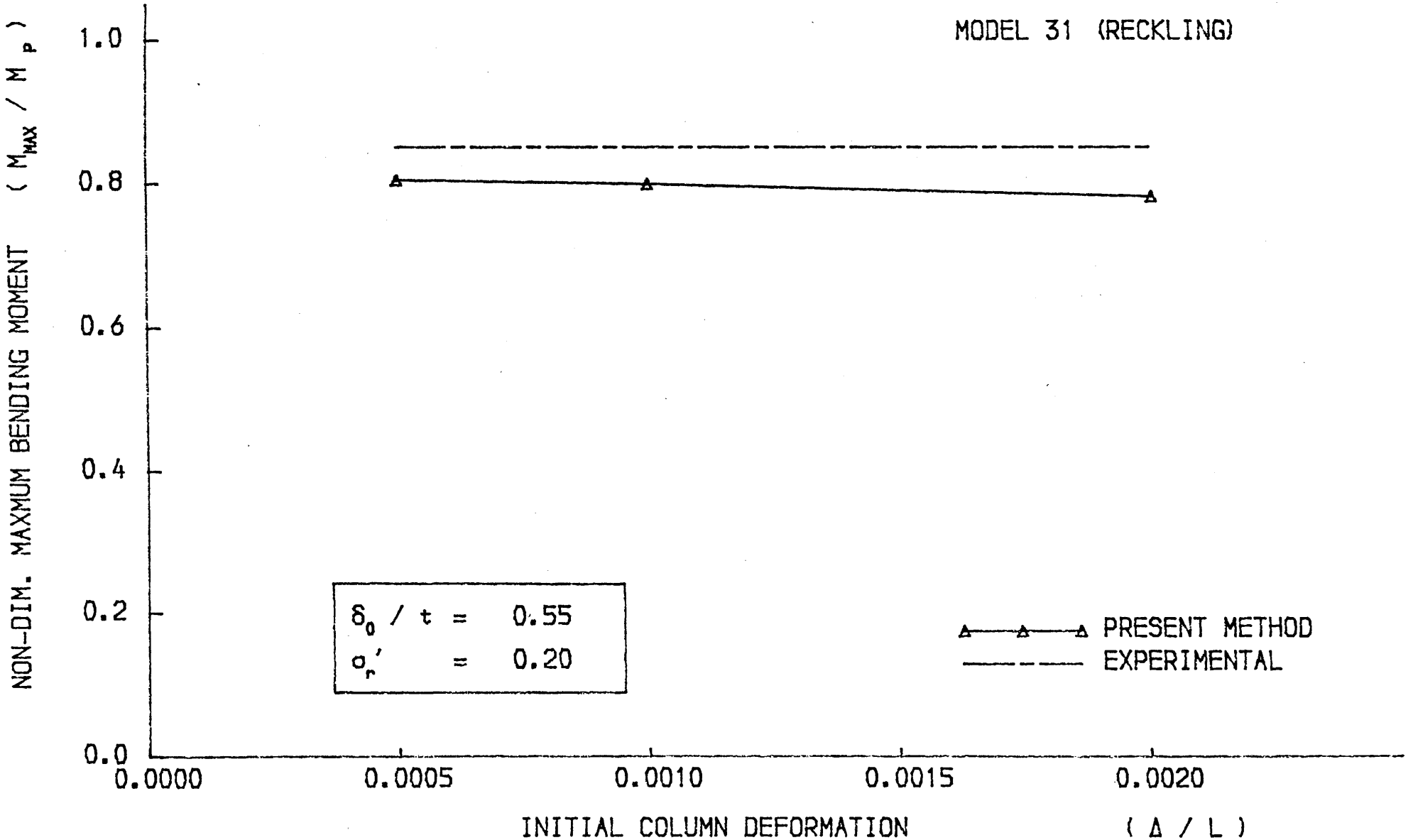

FIG.6-27 VARIATION OF MAXIMUM BENDING MOMENT WITH INITIAL COLUMN DEFORMATION

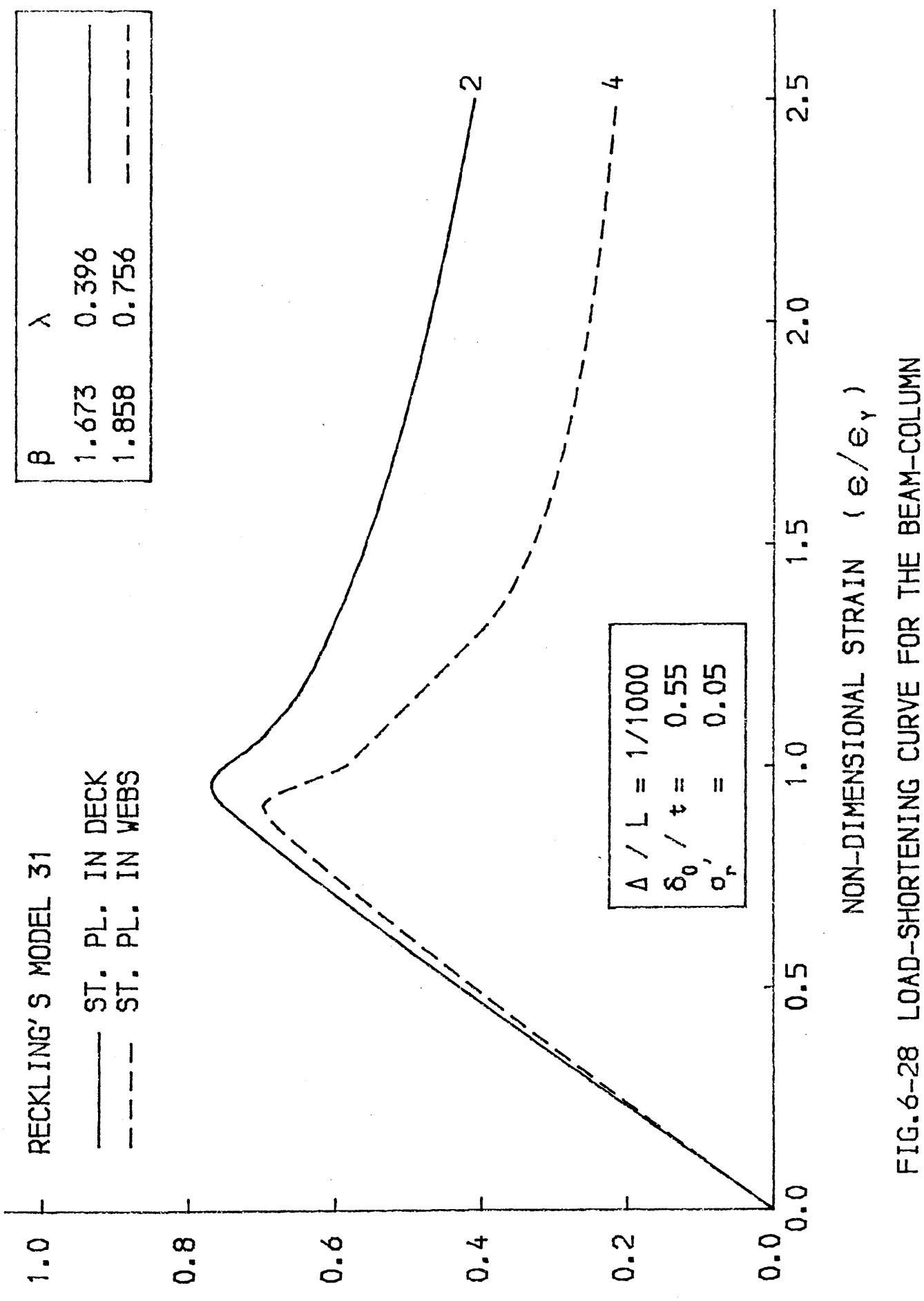

FIG.6-28 LOAD-SHORTENING CURVE FOR THE BEAM-COLUMN

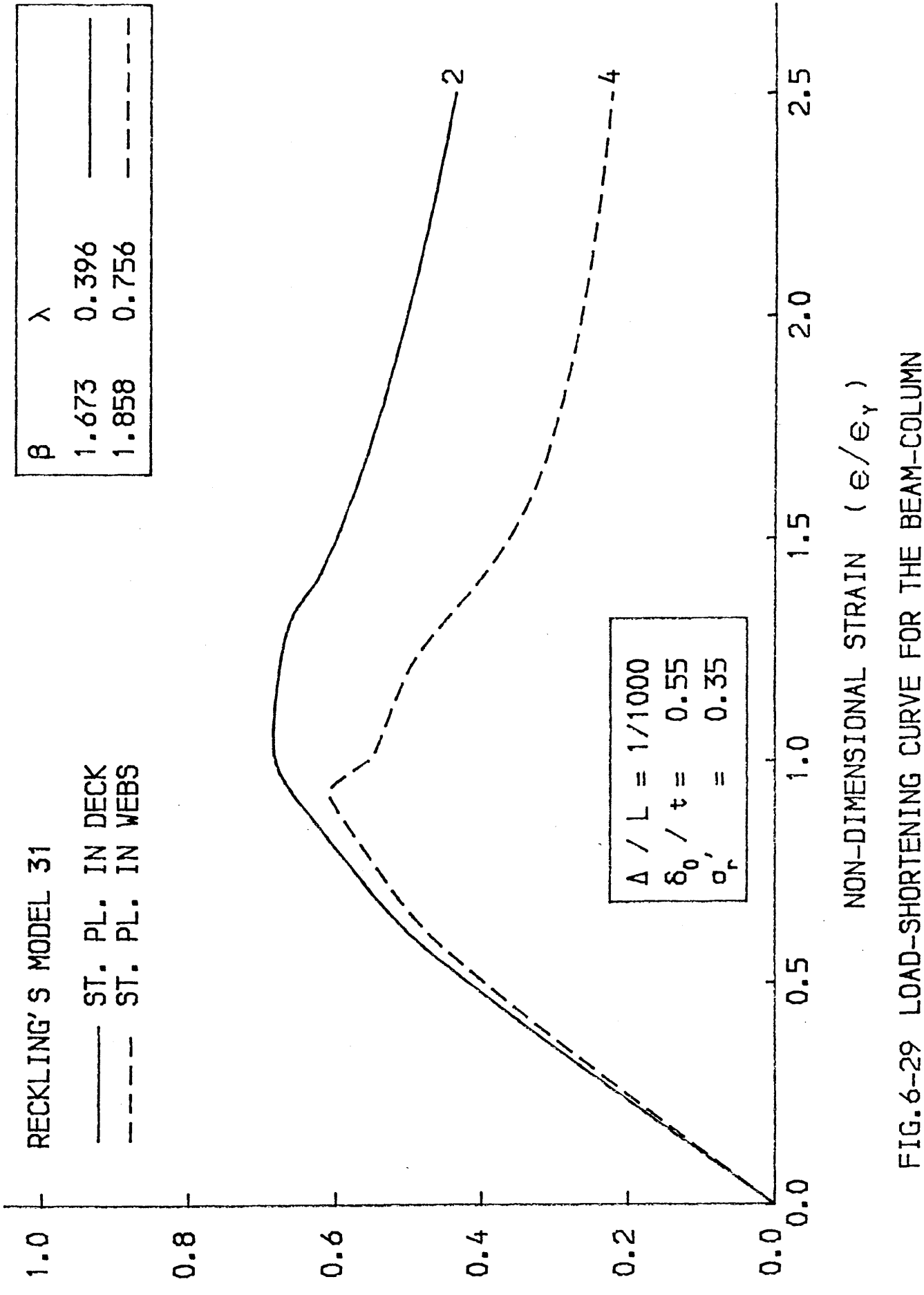

FIG.6-29 LOAD-SHORTENING CURVE FOR THE BEAM-COLUMN

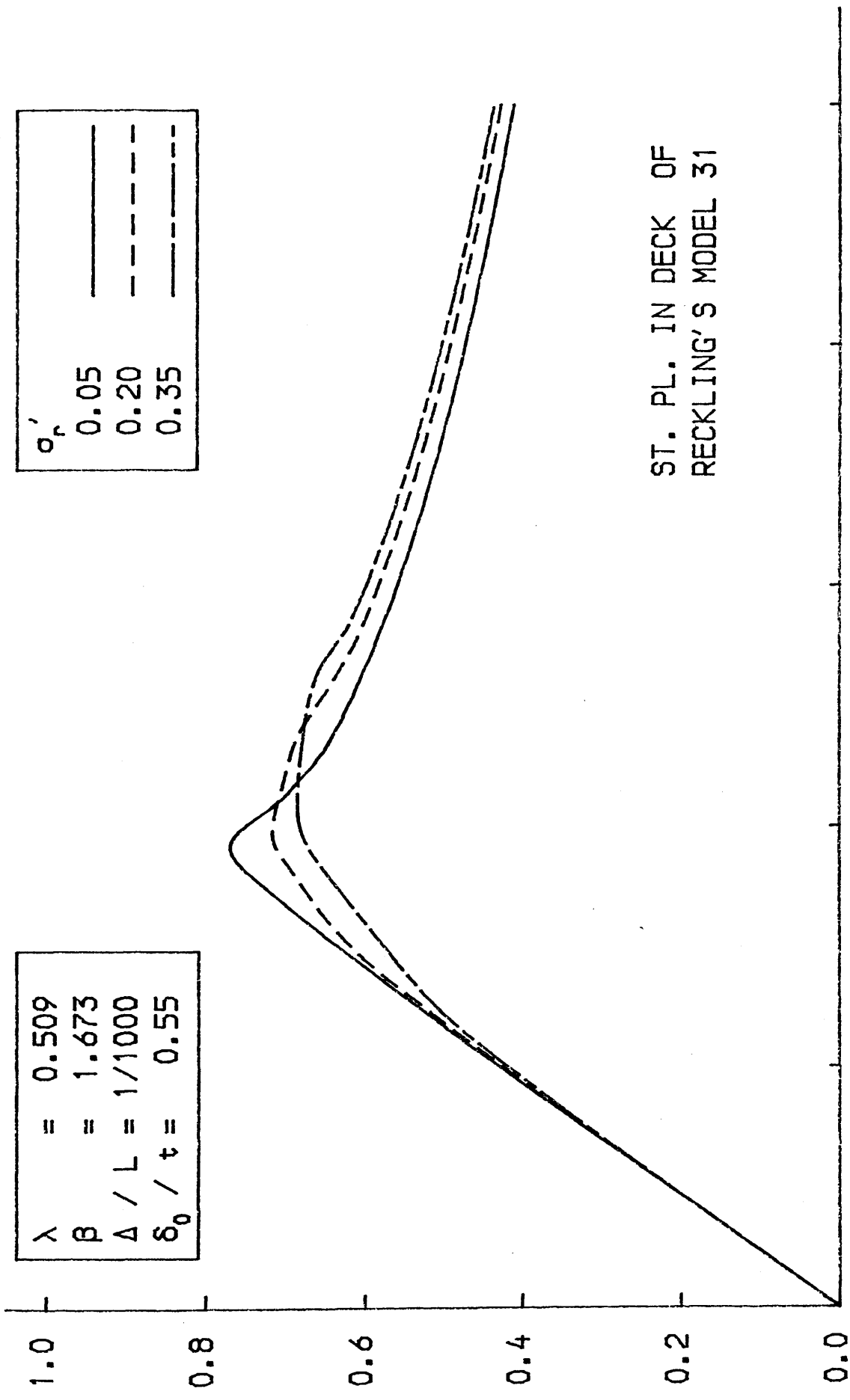

FIG.6-30 LOAD-SHORTENING CURVE FOR THE BEAM-COLUMN

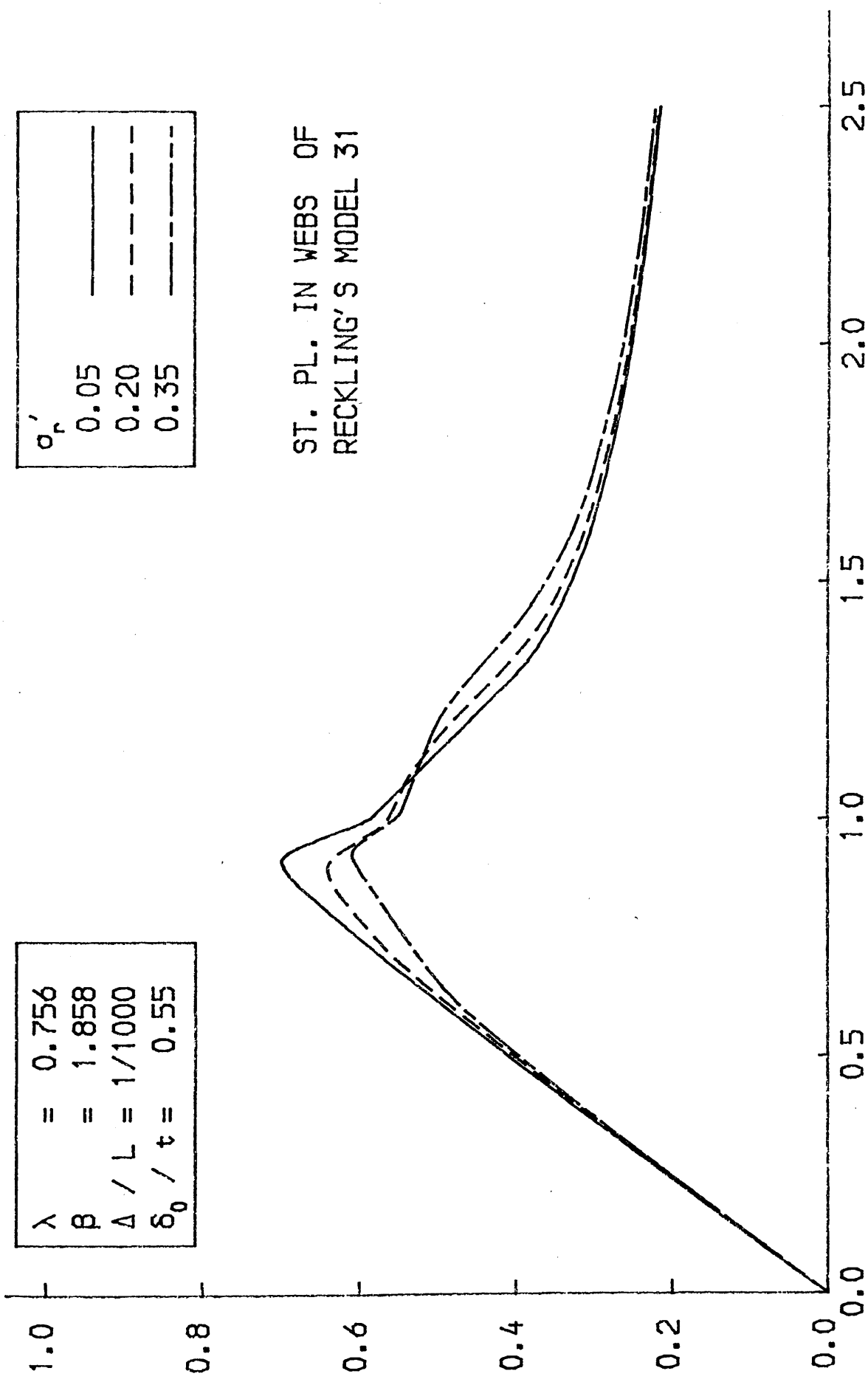

FIG.6-31 LOAD-SHORTENING CURVE FOR THE BEAM-COLUMN

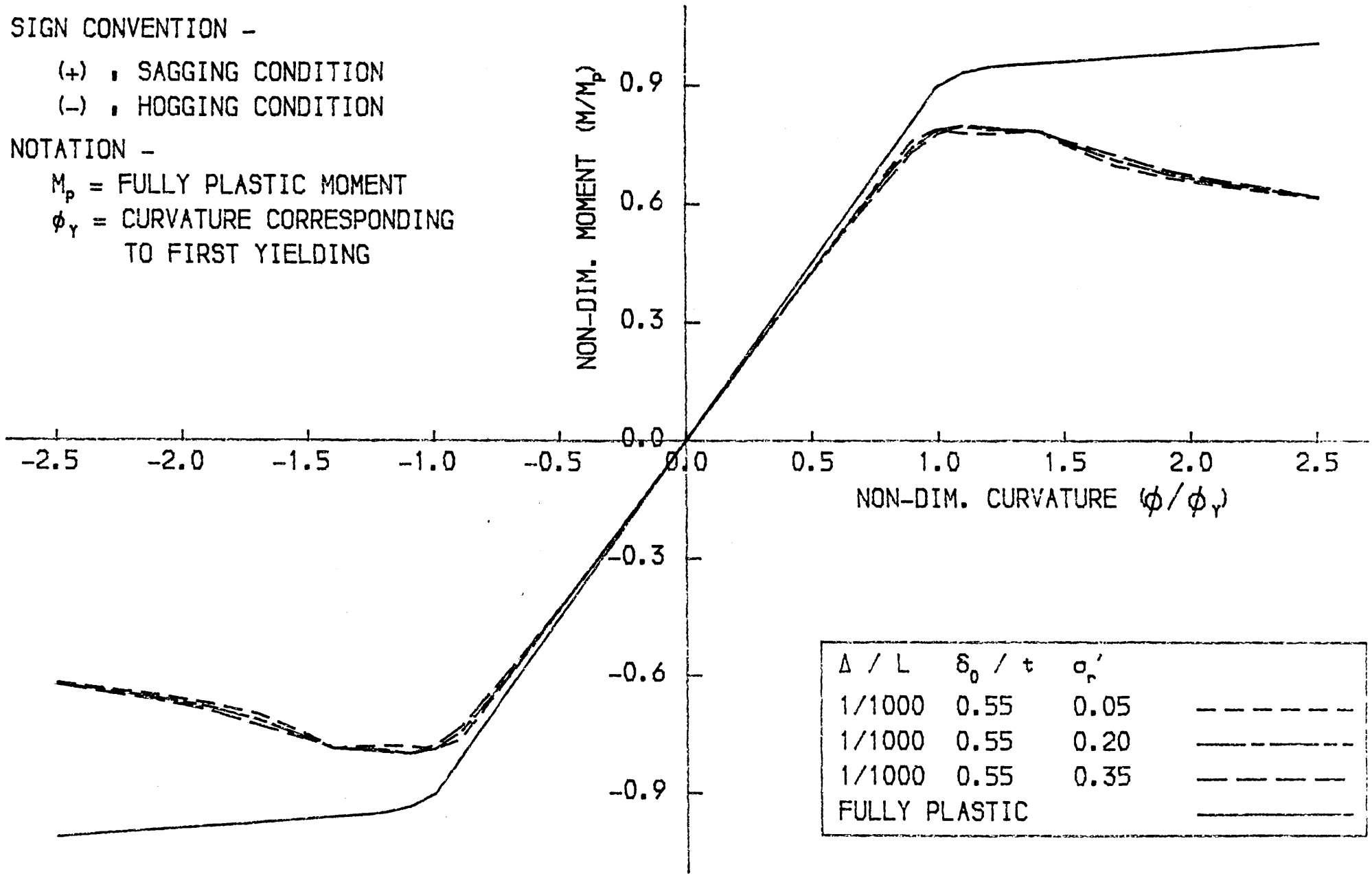

FIG.6-32 BENDING MOMENT-CURVATURE CURVE FOR MODEL 31 (RECKLING)

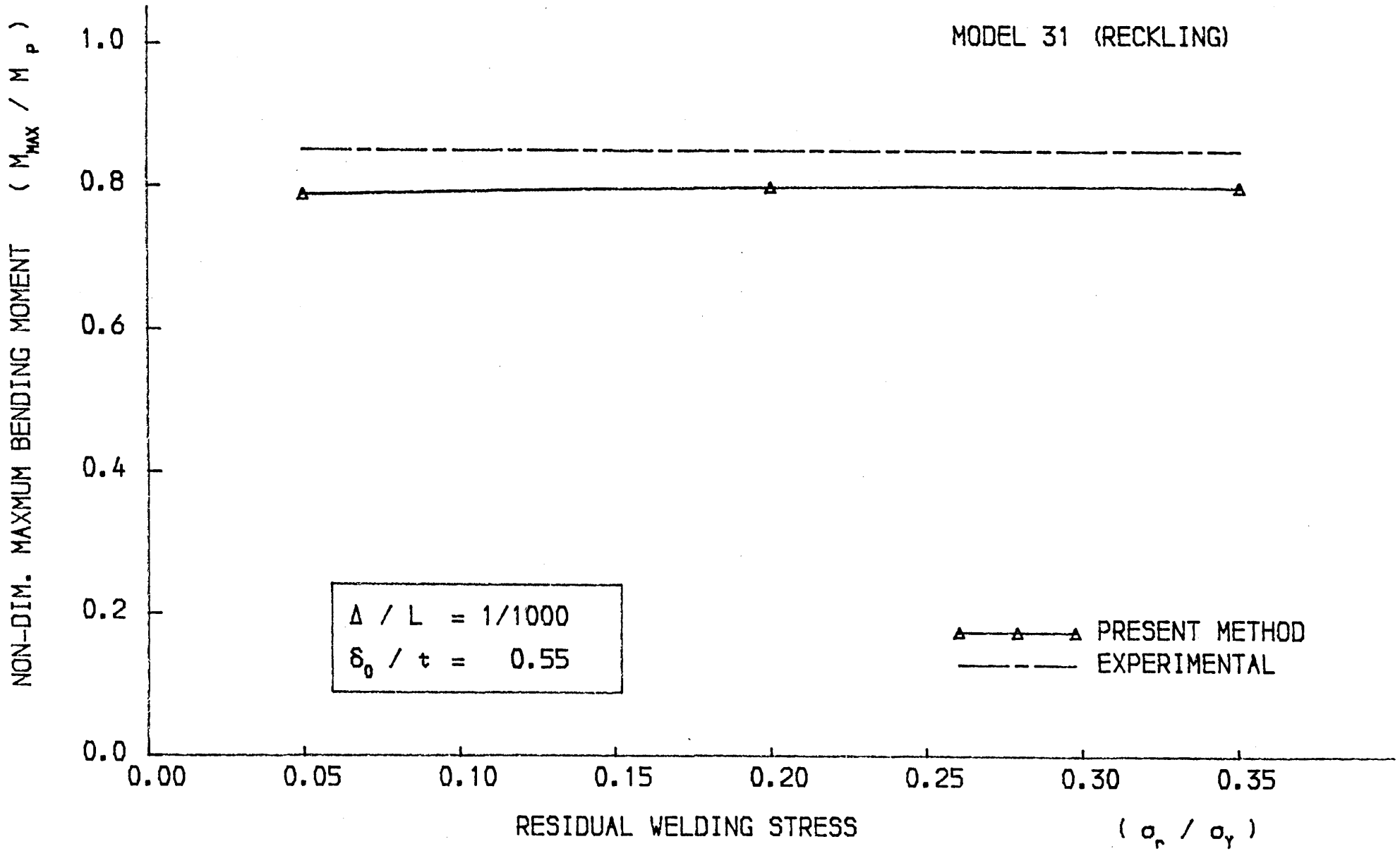

FIG.6-33 VARIATION OF MAXIMUM BENDING MOMENT WITH RESIDUAL WELDING STRESS

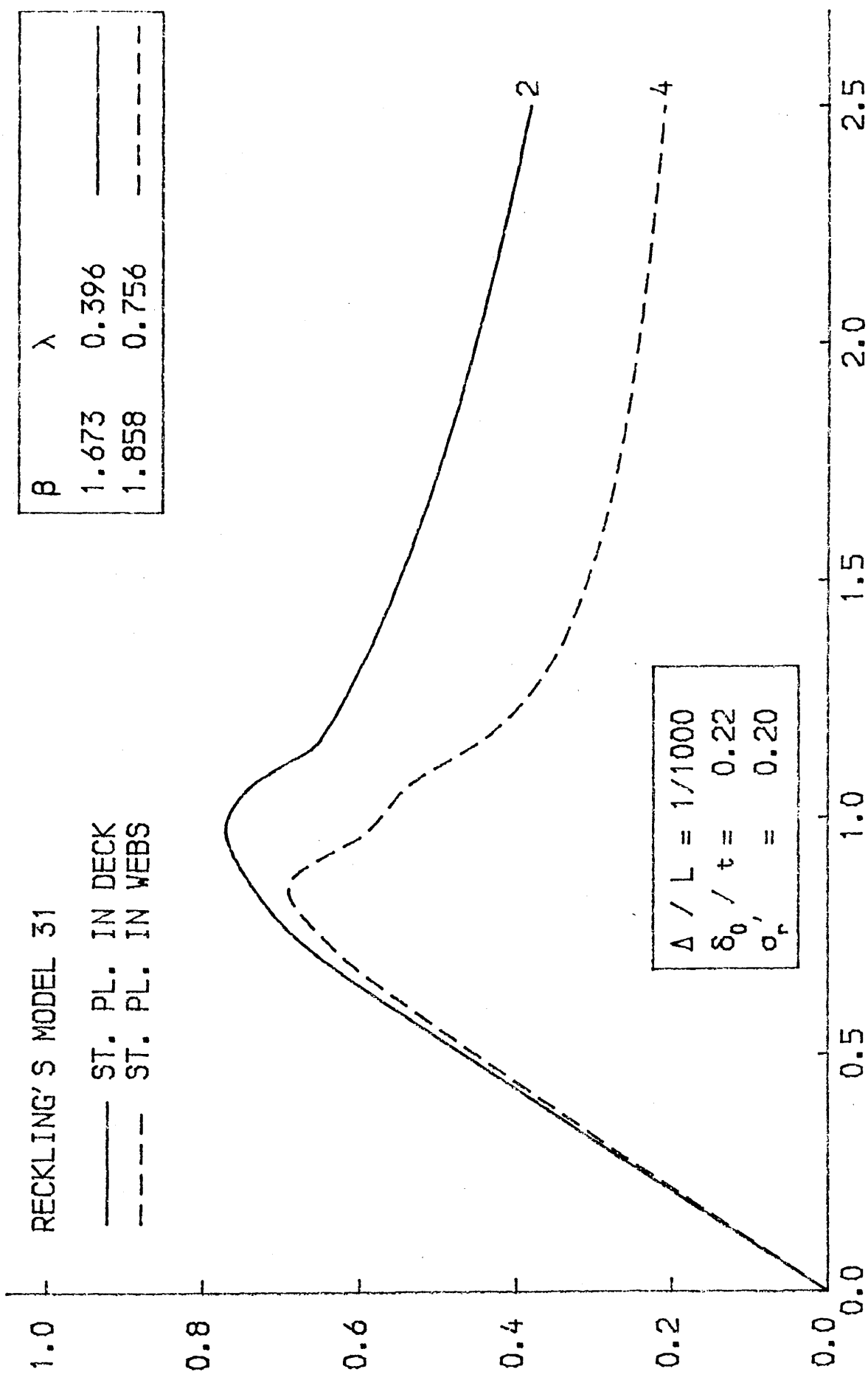

FIG.6-34 LOAD-SHORTENING CURVE FOR THE BEAM-COLUMN

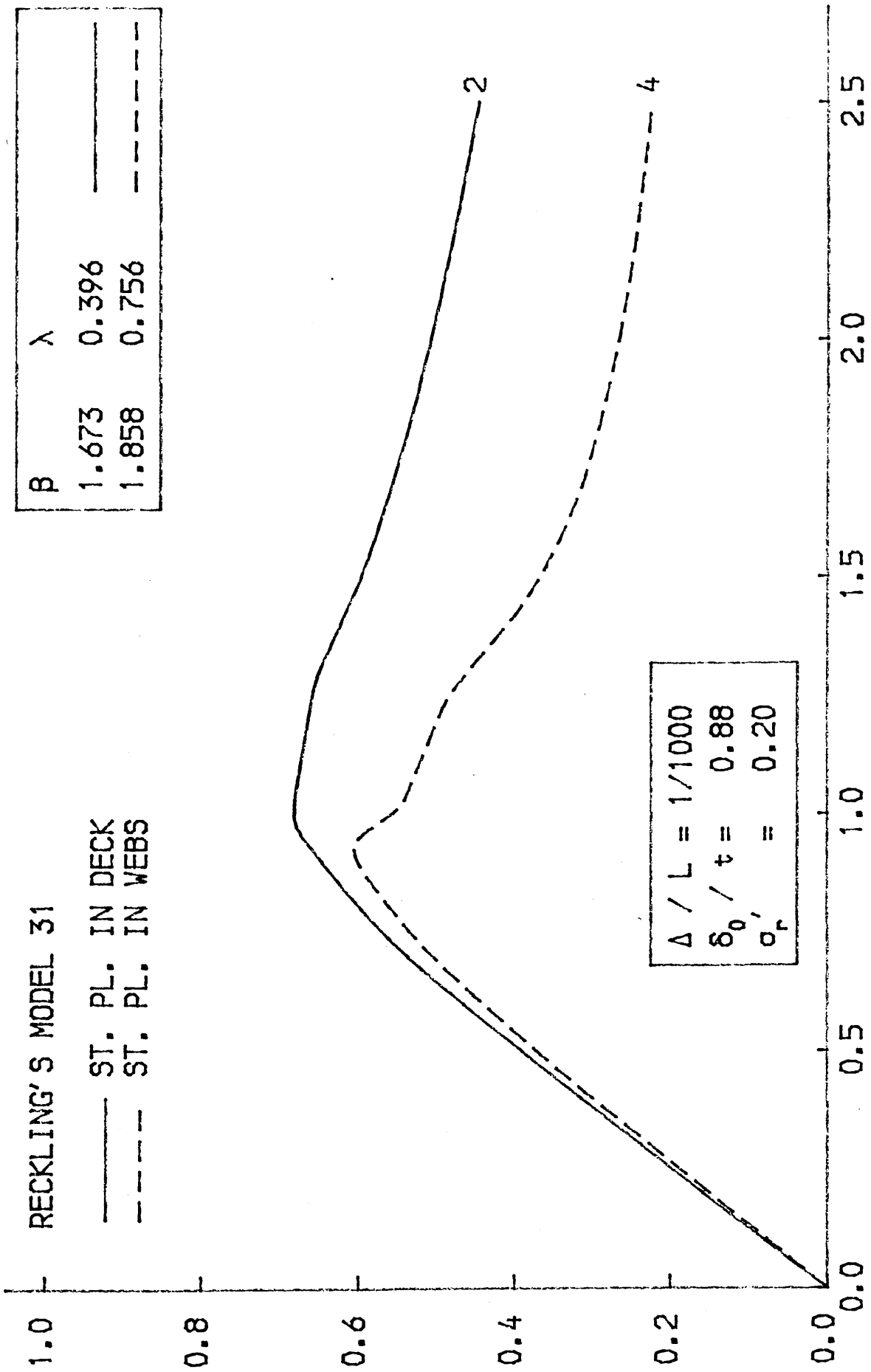

FIG.6-35 LOAD-SHORTENING CURVE FOR THE BEAM-COLUMN

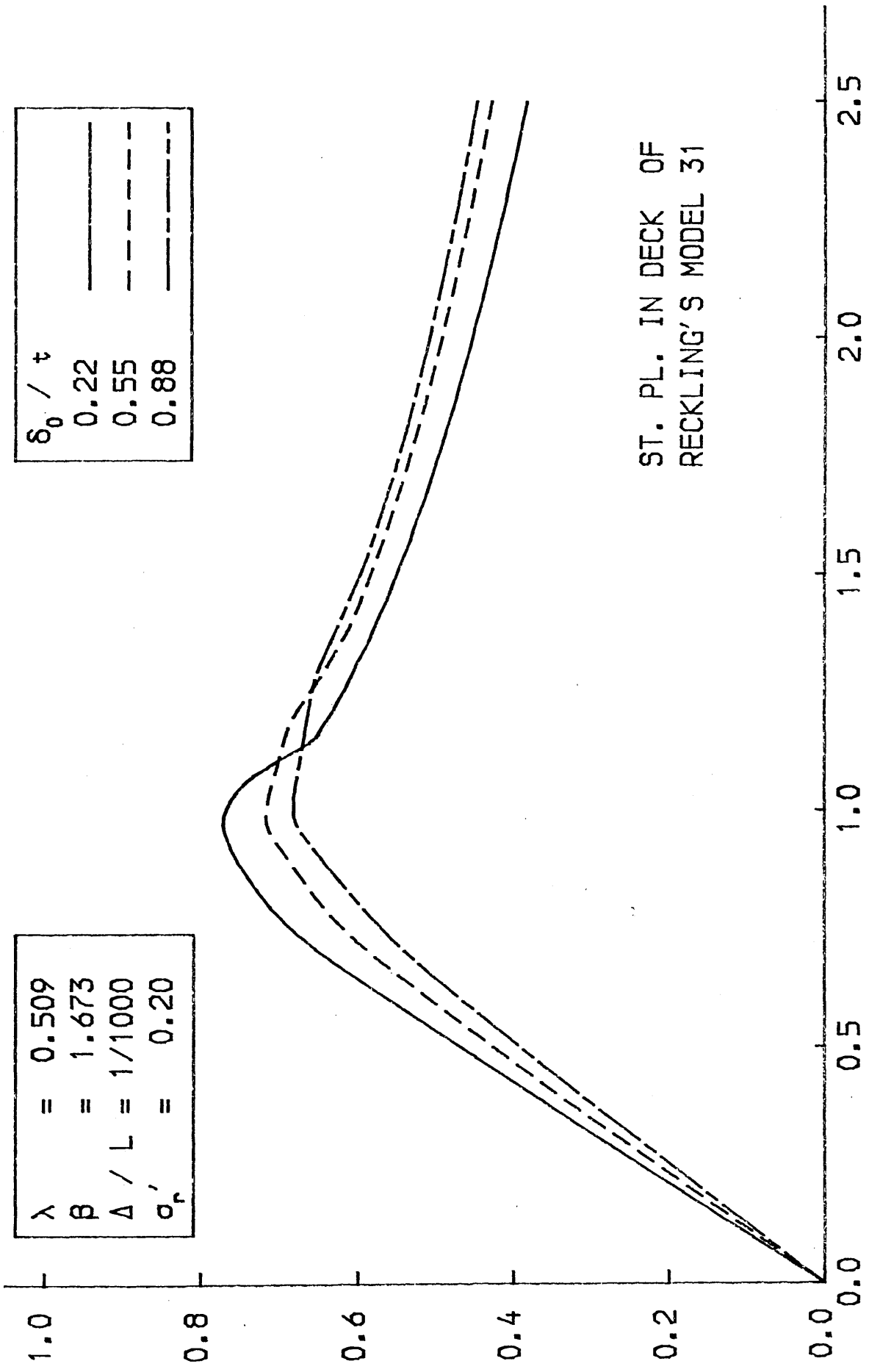

FIG.6-36 LOAD-SHORTENING CURVE FOR THE BEAM-COLUMN

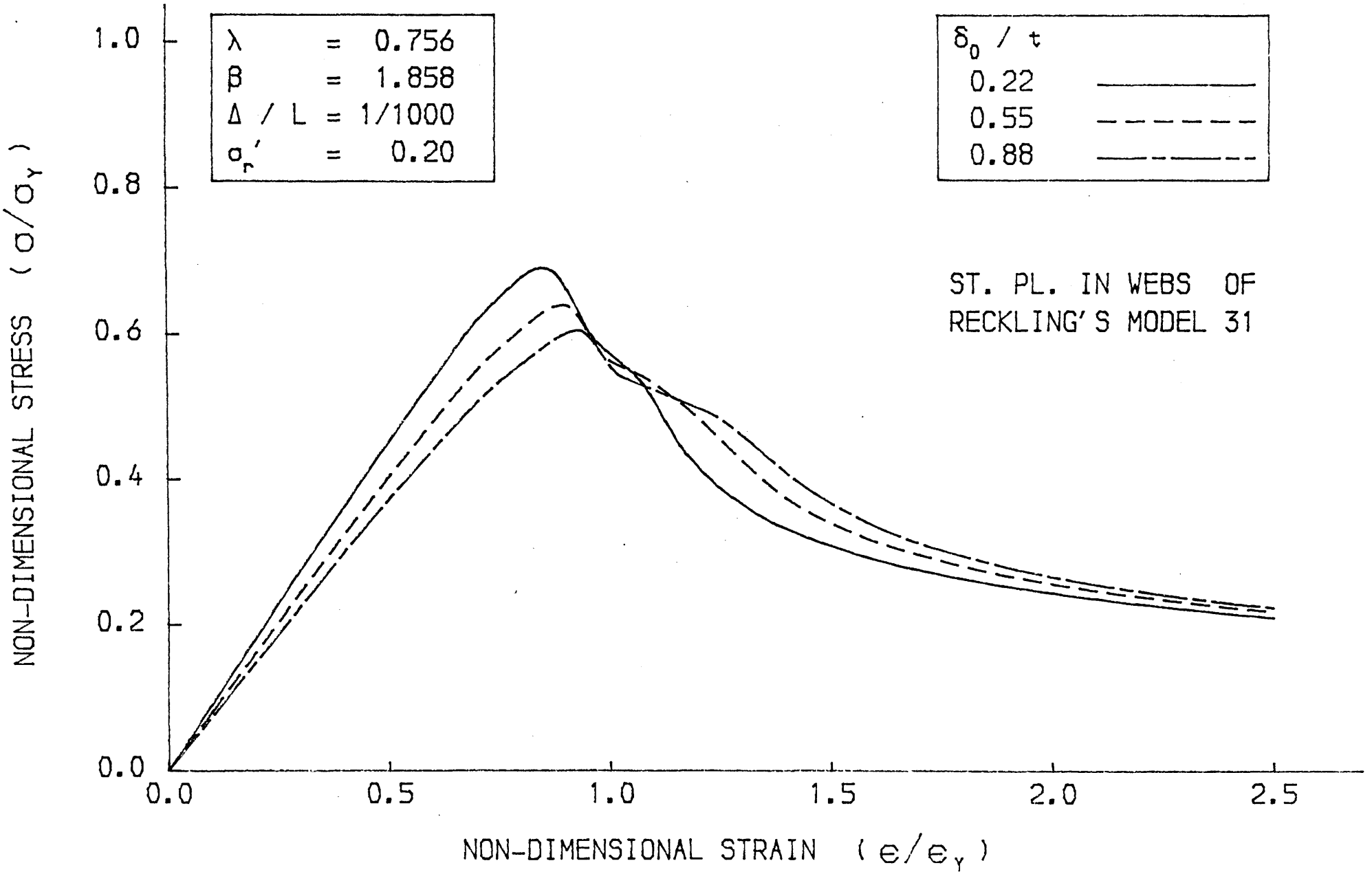

FIG.6-37 LOAD-SHORTENING CURVE FOR THE BEAM-COLUMN

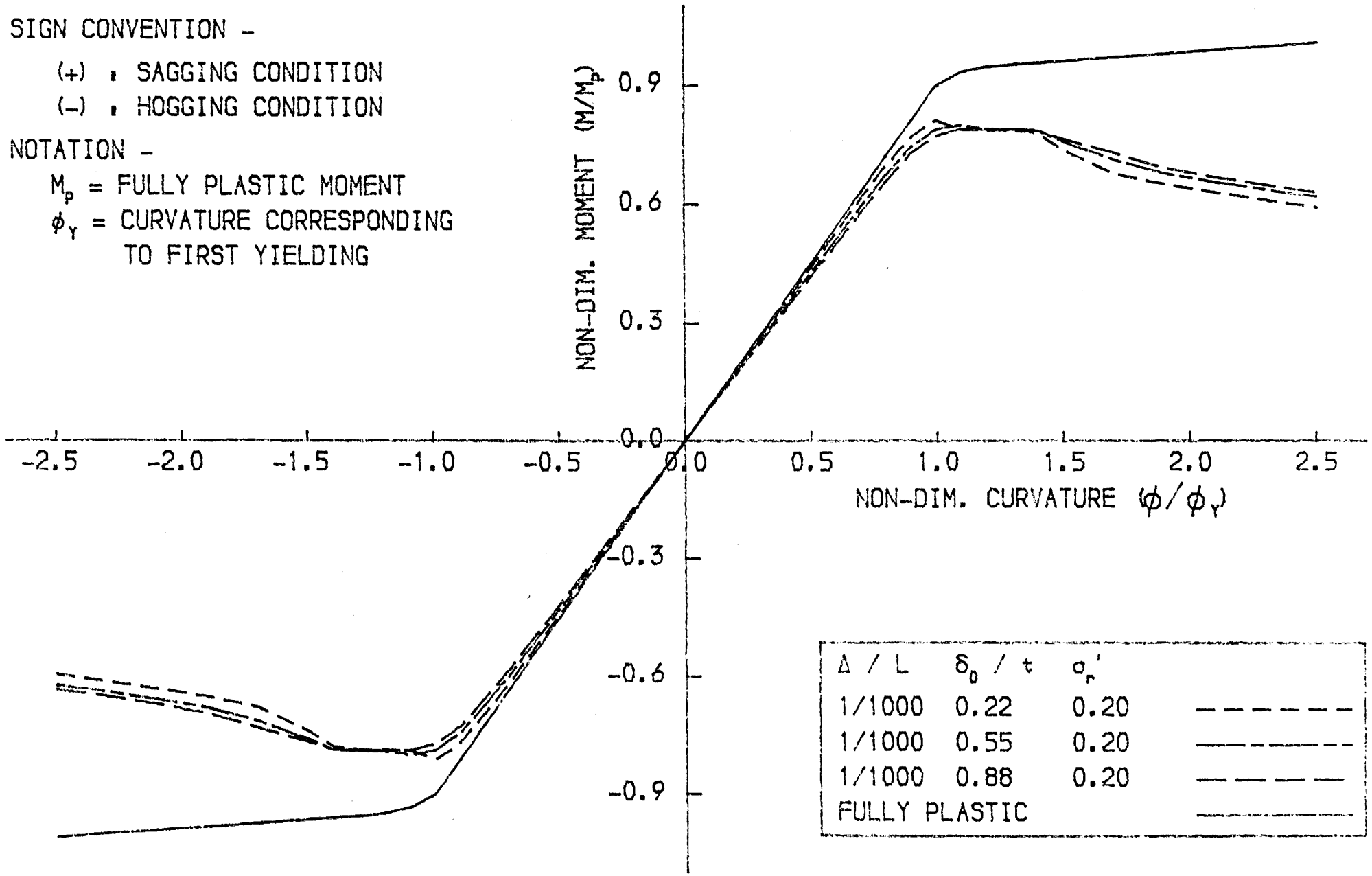

FIG.6-38 BENDING MOMENT-CURVATURE CURVE FOR MODEL 31 (RECKLING)

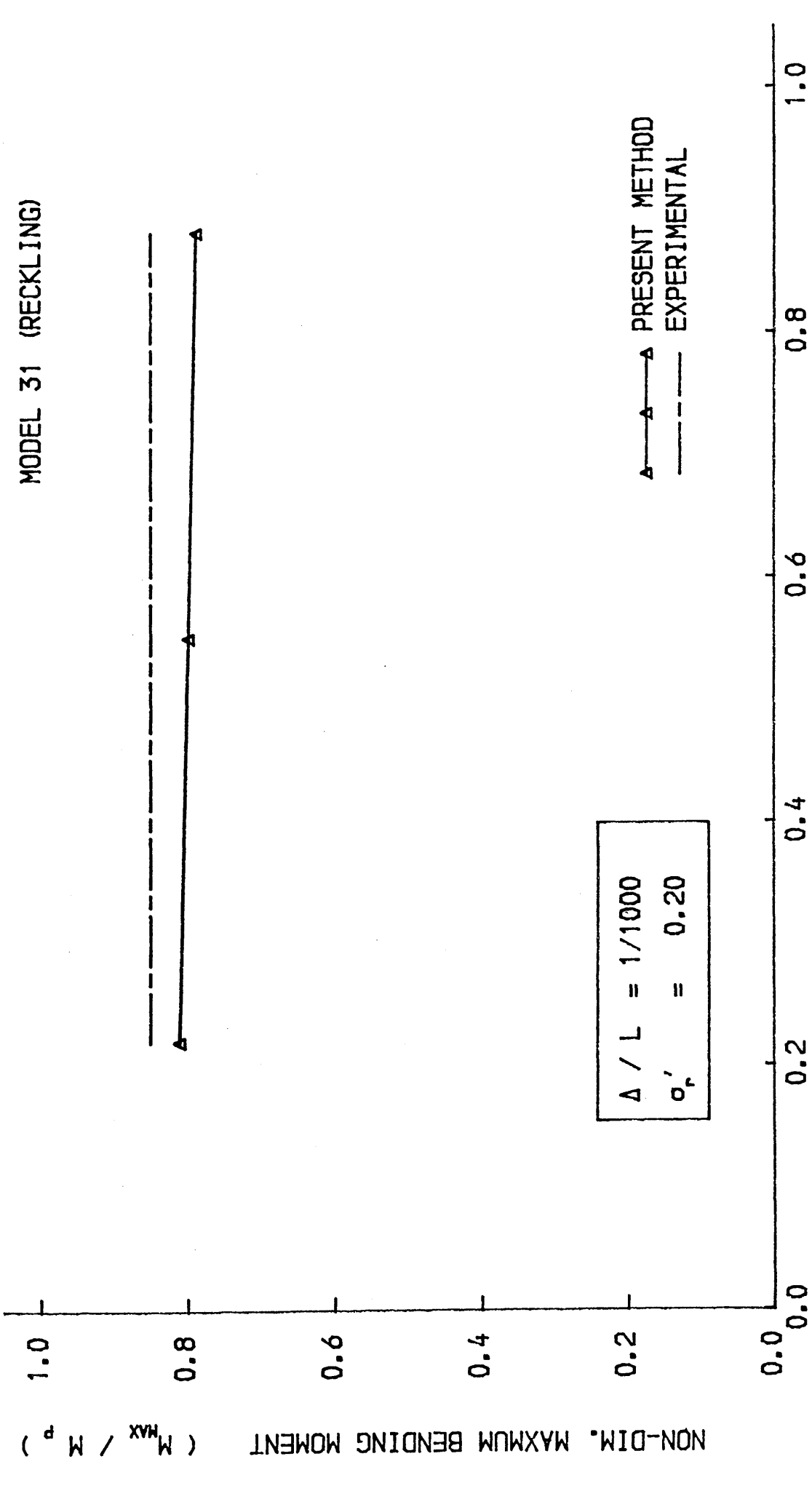

FIG.6-39 VARIATION OF MAXIMUM BENDING MOMENT WITH INITIAL PLATE DEFLECTION

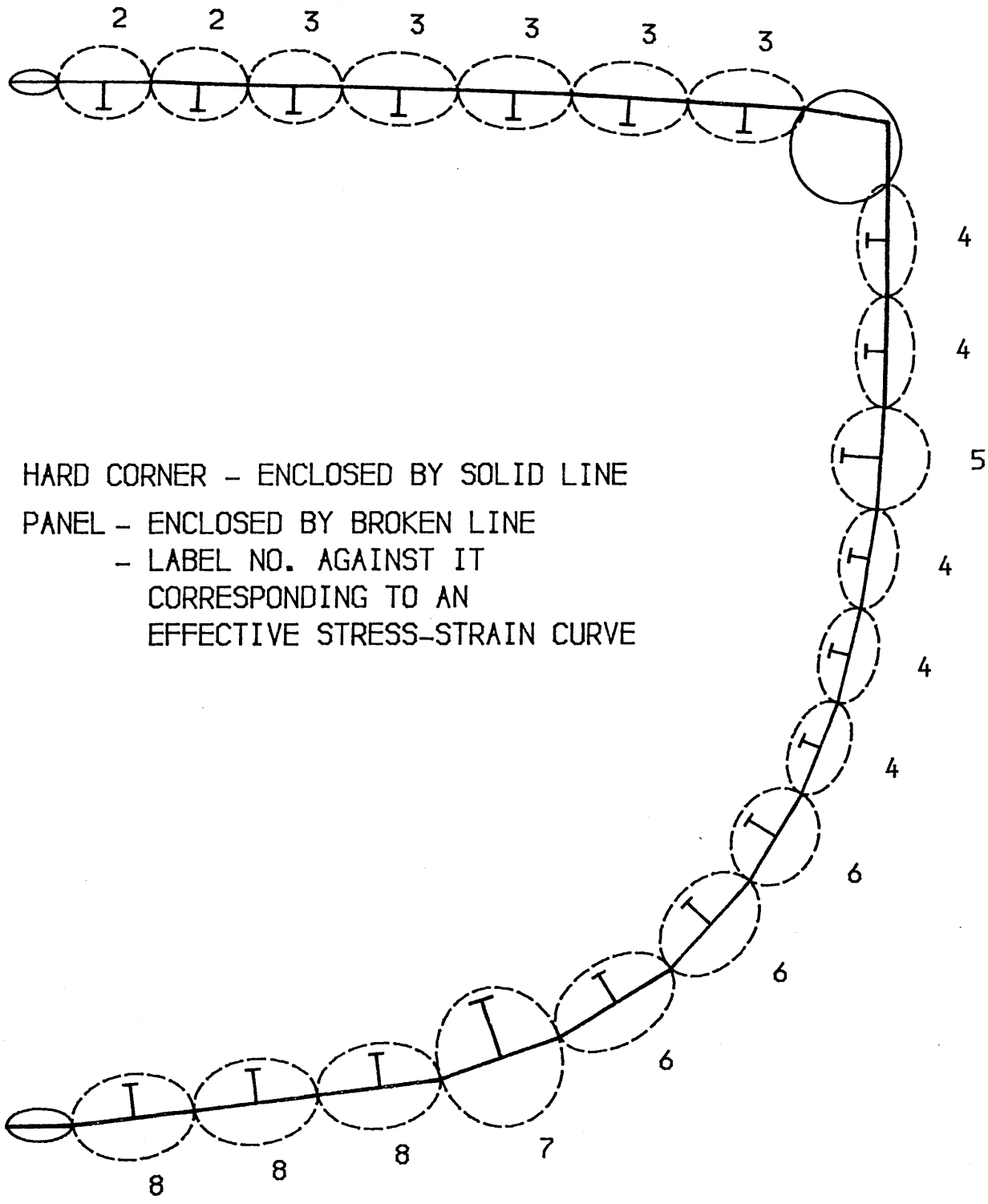

FIG.6-40 DISCRETISATION FOR MIDSHIP SECTION OF HULL A - DTNSRDC-82/076

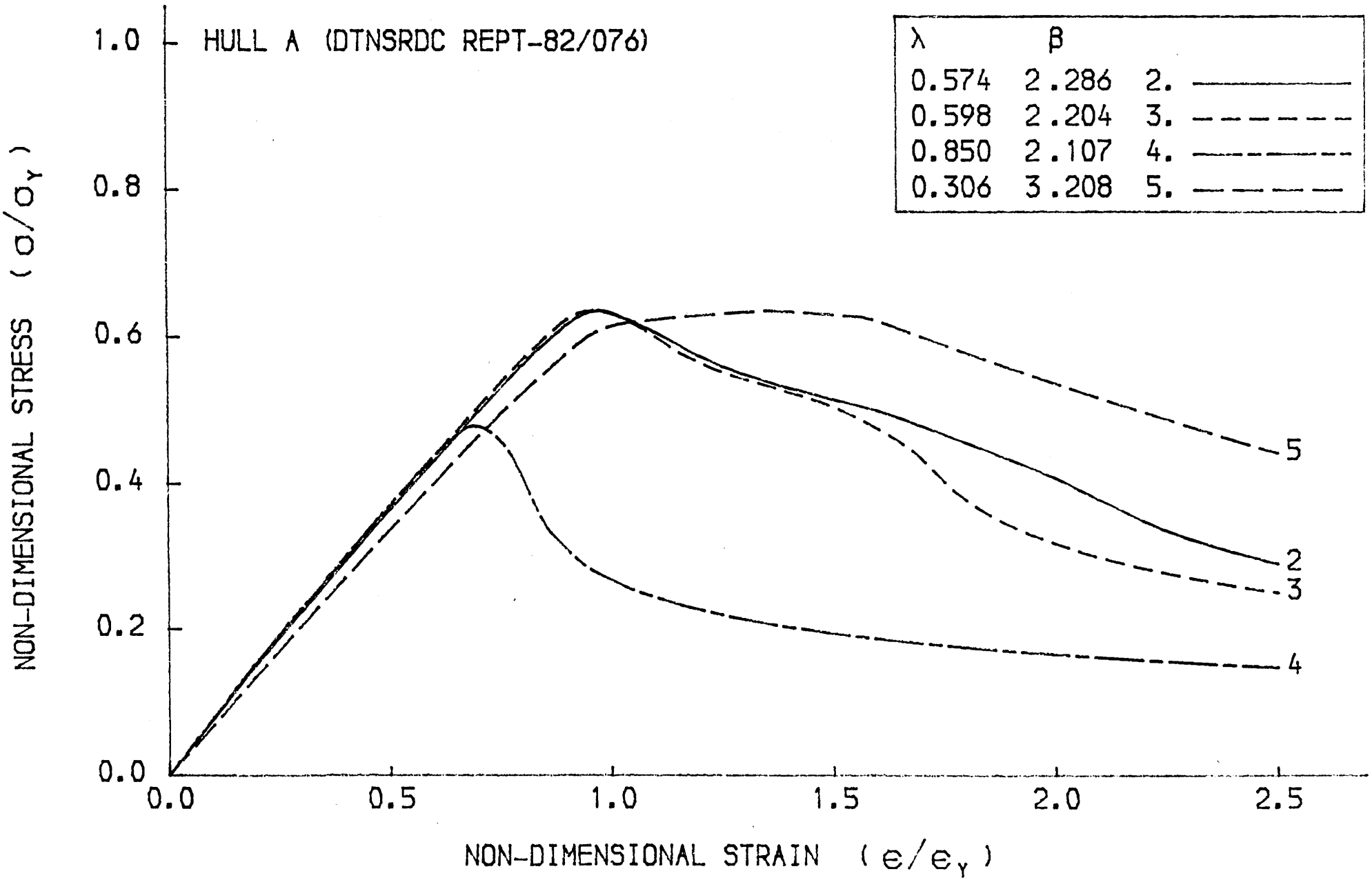

FIG.6-41 LOAD-SHORTENING CURVE FOR THE BEAM-COLUMN

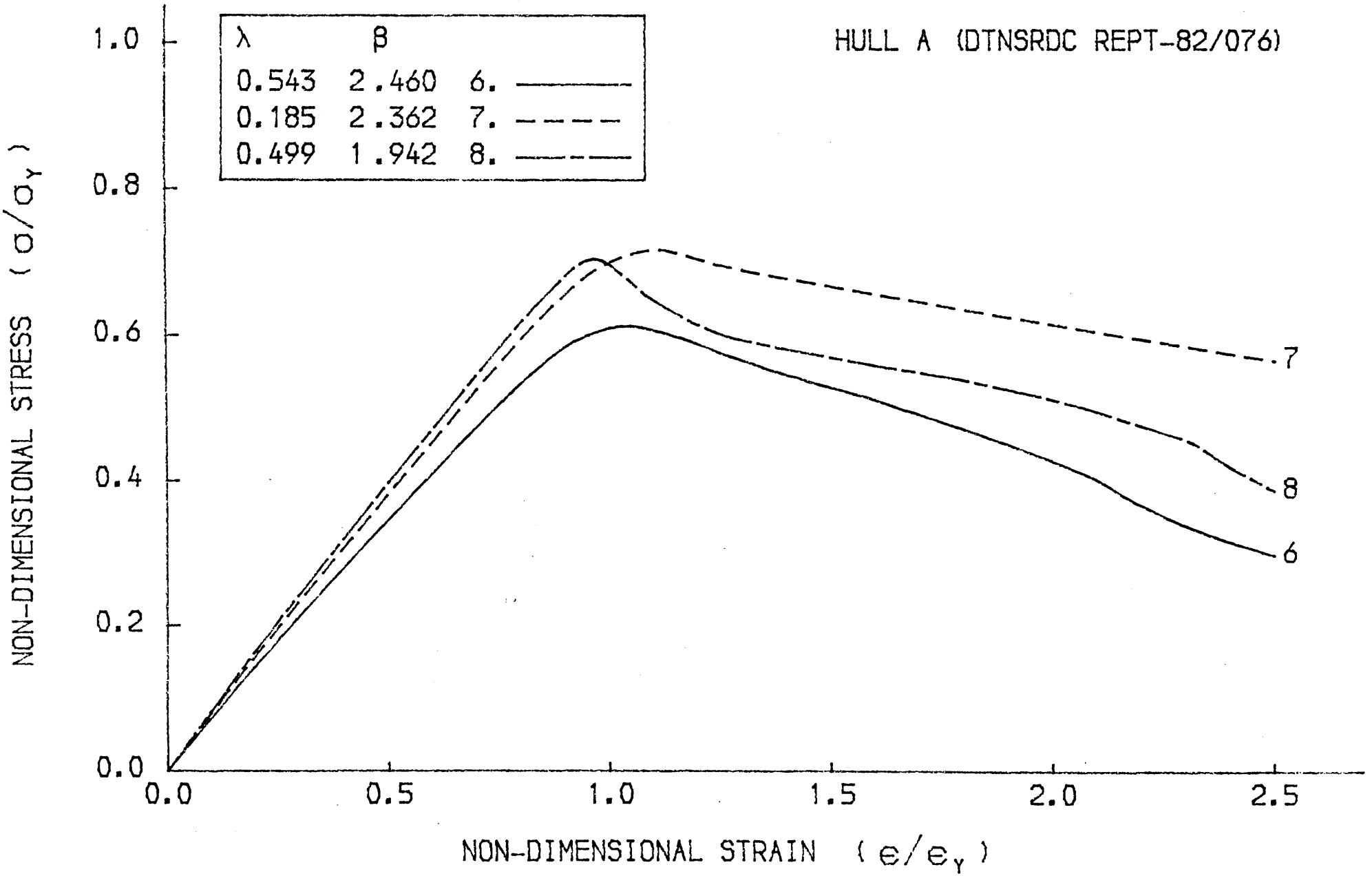

FIG.6-42 LOAD-SHORTENING CURVE FOR THE BEAM-COLUMN

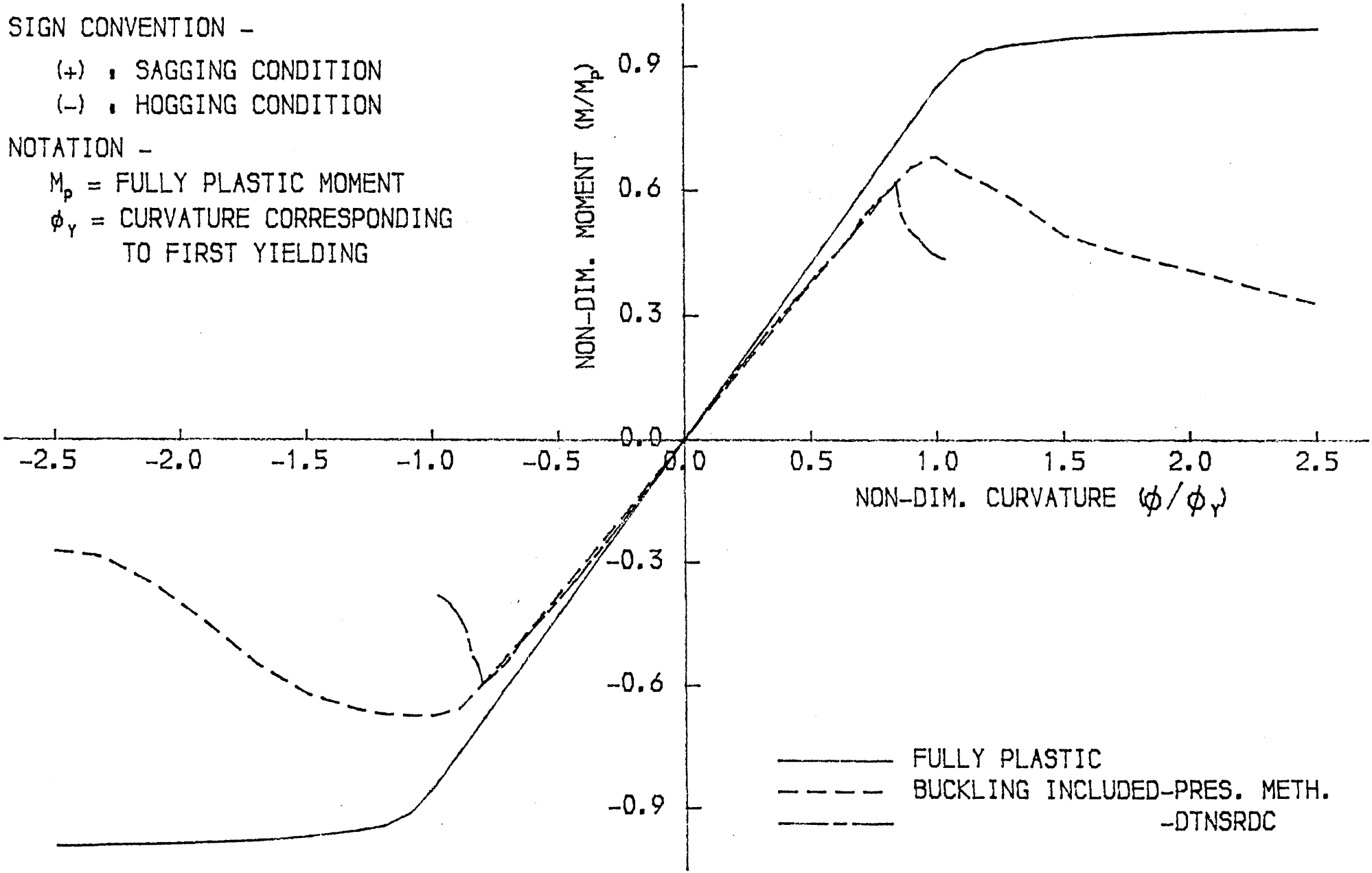

FIG.6-43 BENDING MOMENT-CURVATURE CURVE FOR HULL A (DTNSRDC REPT-82/076)

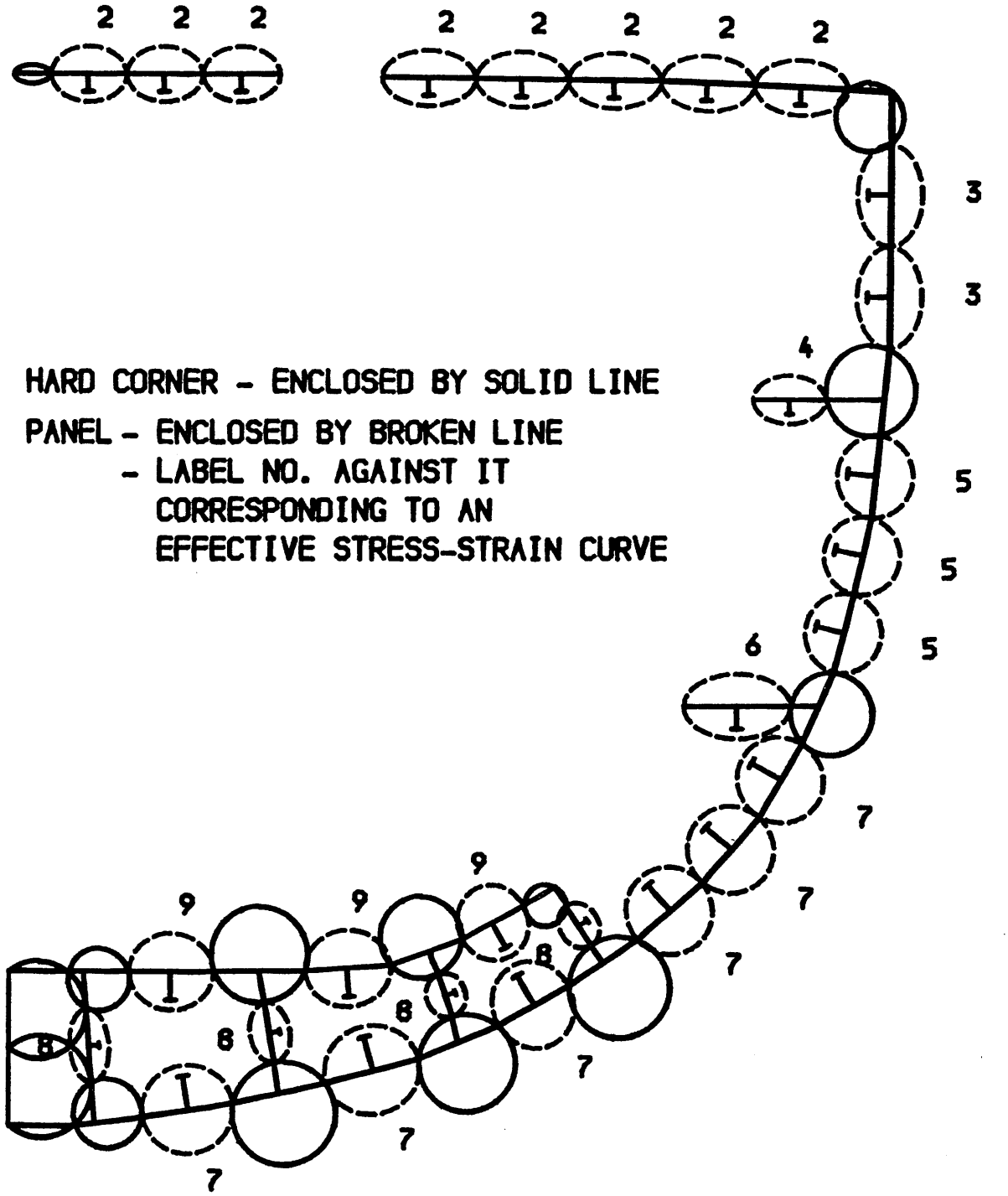

FIG.6-44 DISCRETISATION FOR MIDSHIP SECTION OF HULL B - DTNSRDC-82/076

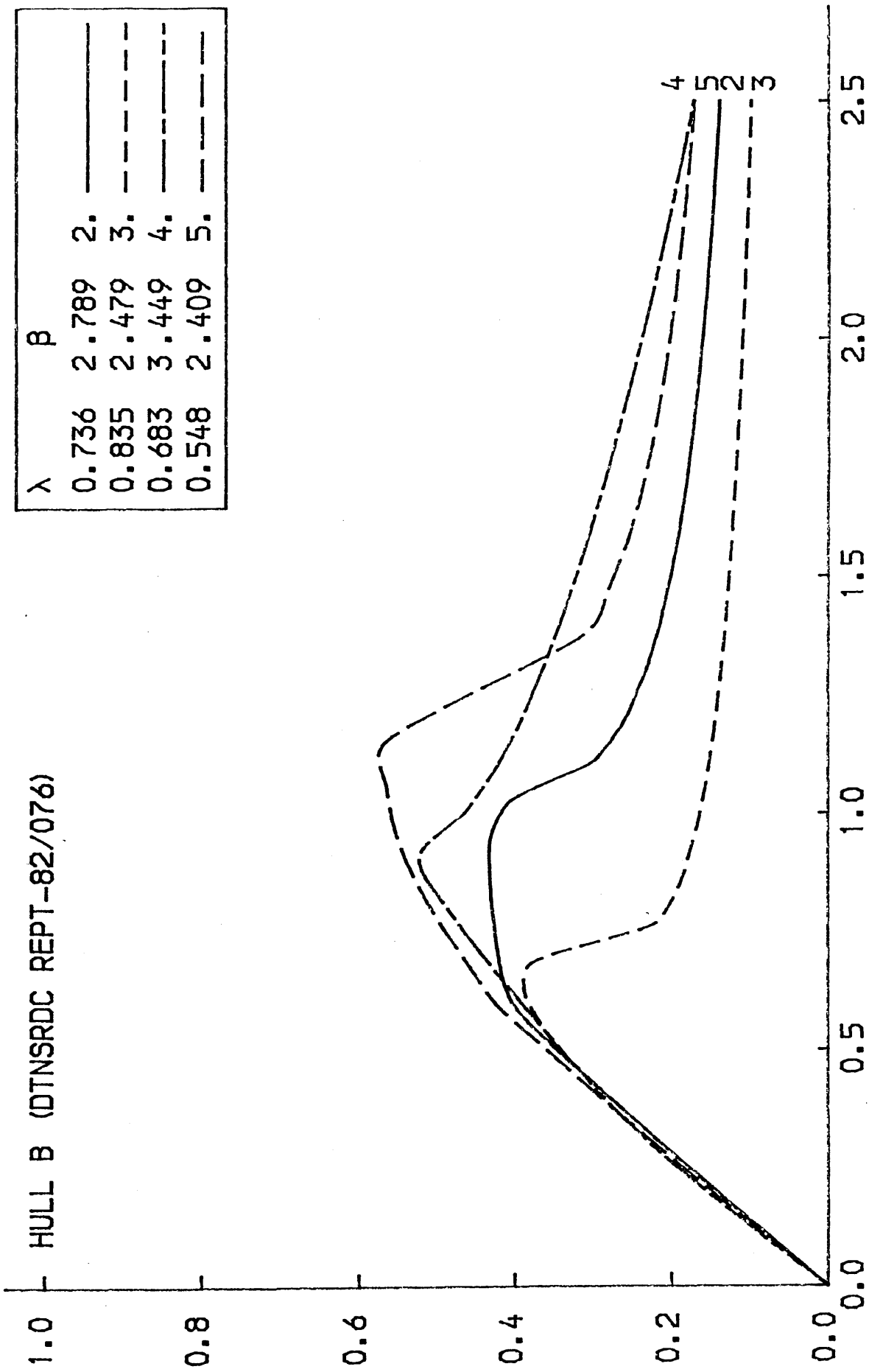

FIG.6-45 LOAD-SHORTENING CURVE FOR THE BEAM-COLUMN

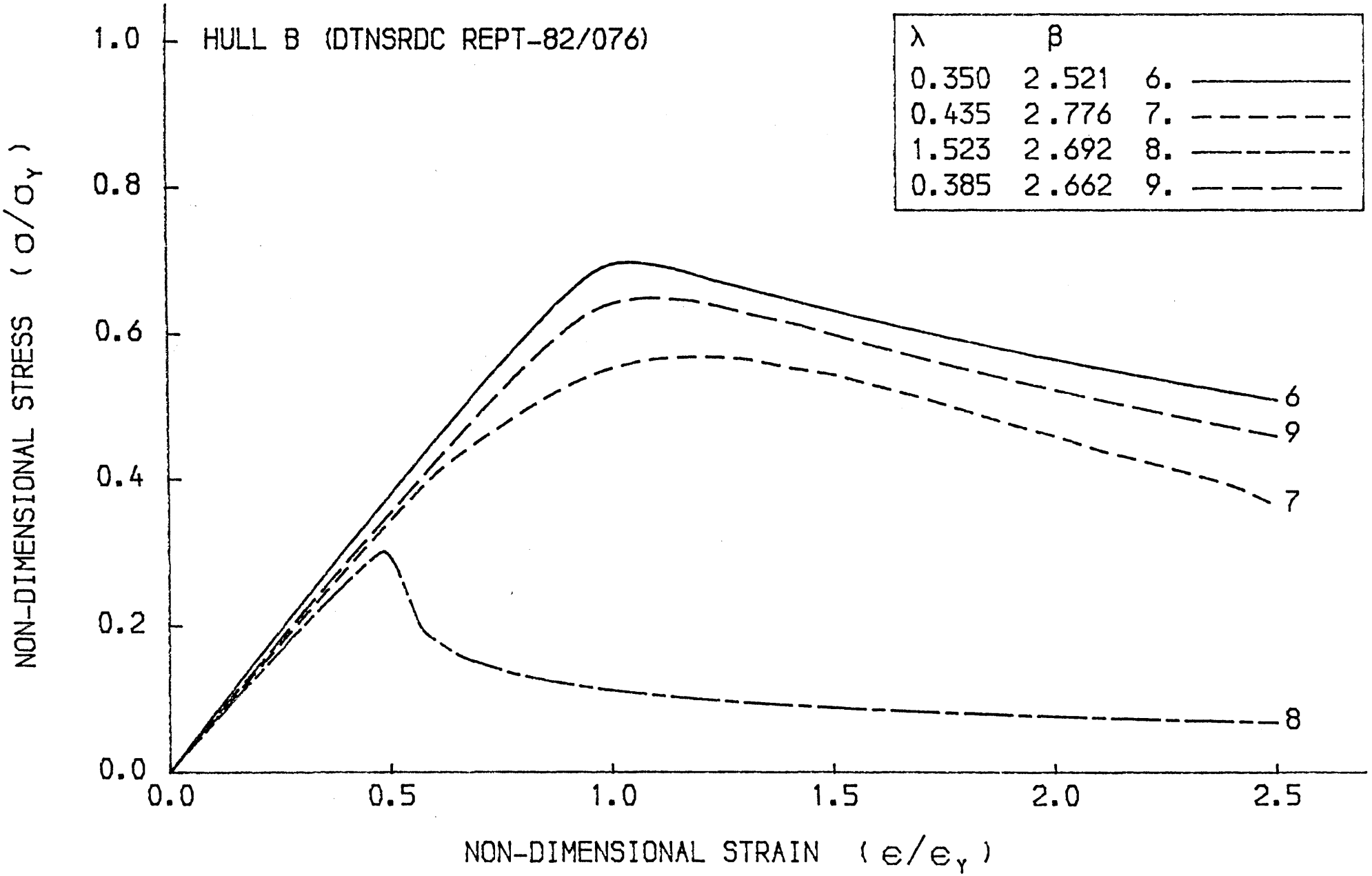

FIG.6-46 LOAD-SHORTENING CURVE FOR THE BEAM-COLUMN

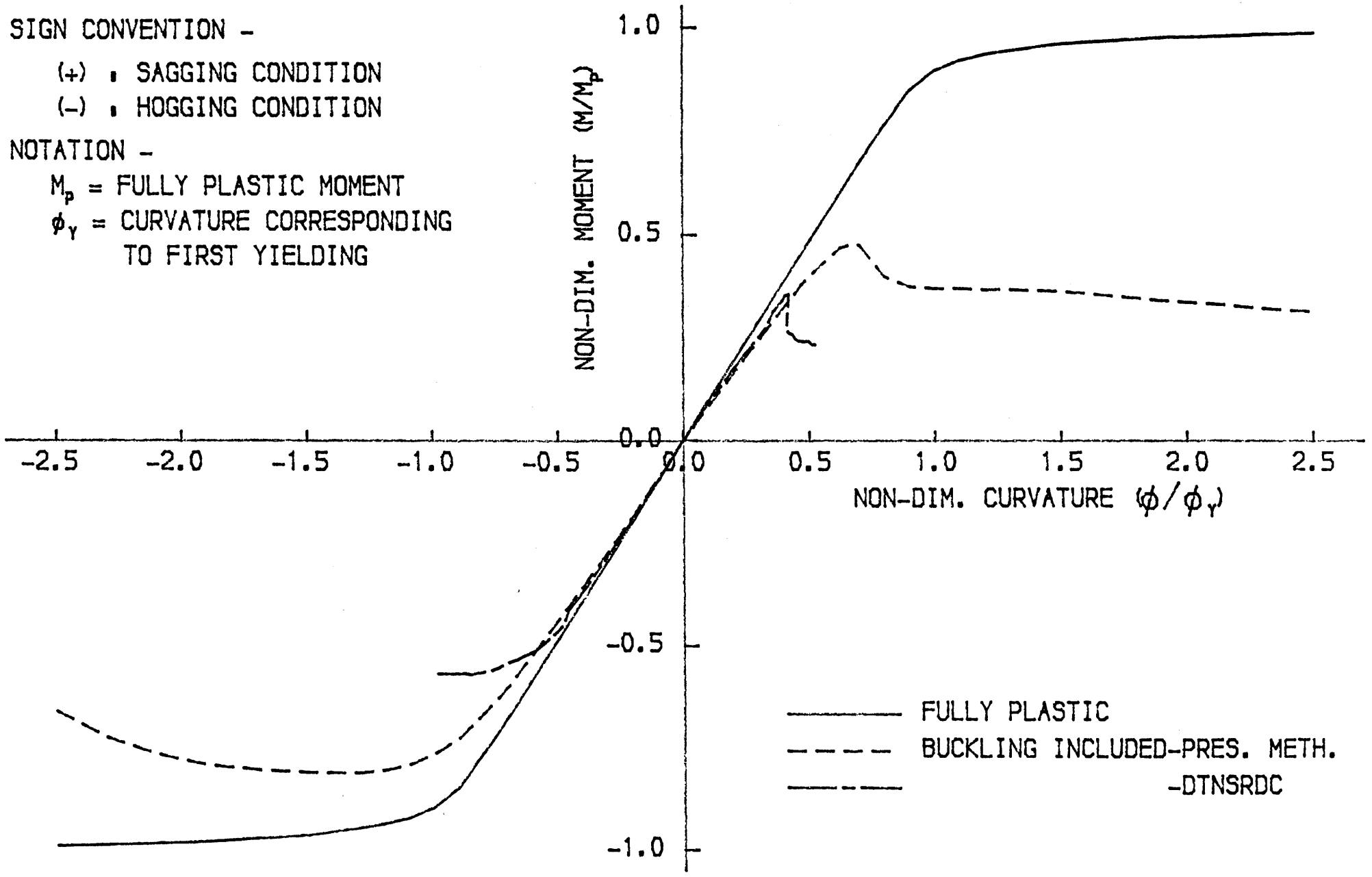

FIG.6-47 BENDING MOMENT-CURVATURE CURVE FOR HULL B (DTNSRDC REPT-82/076)

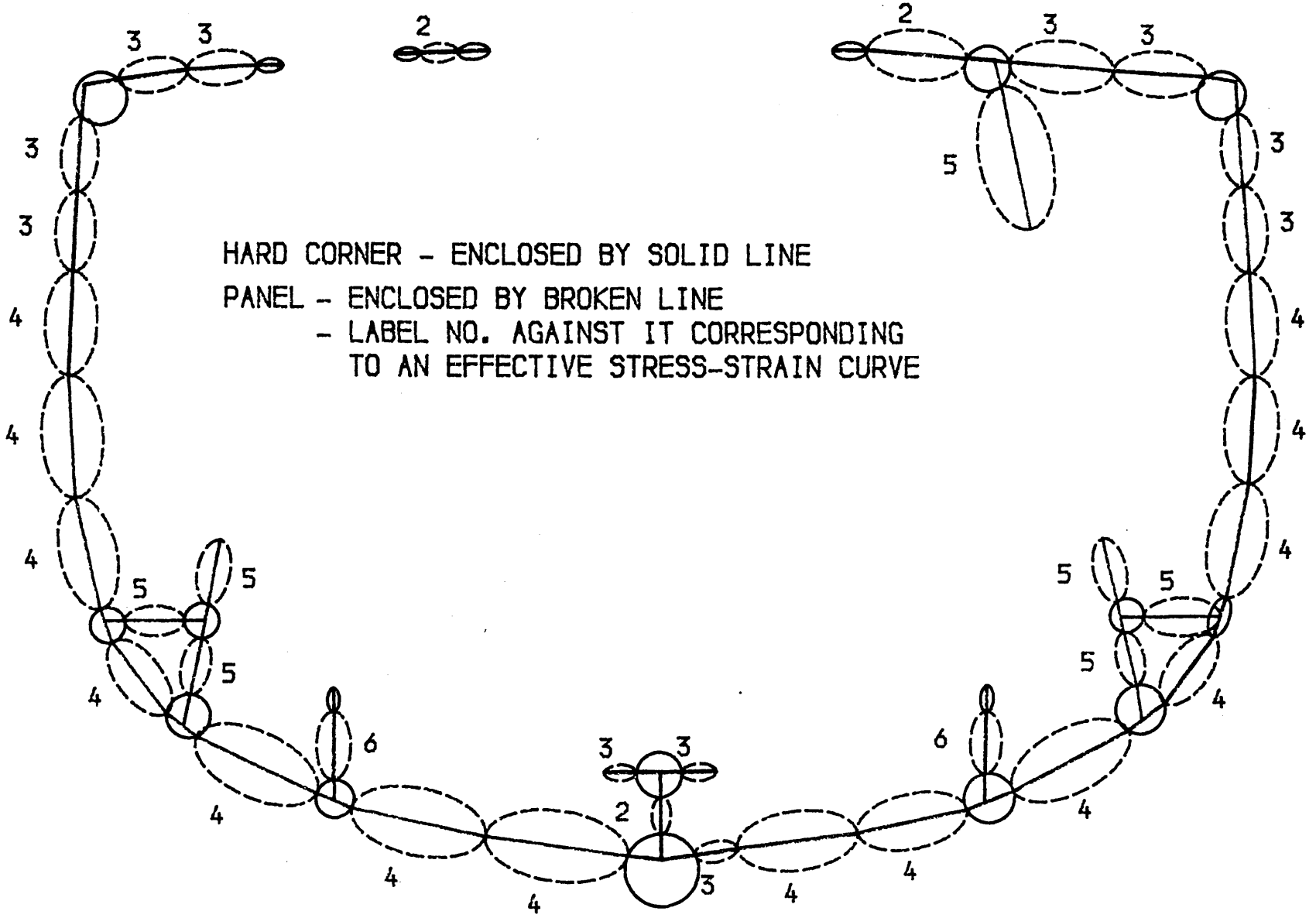

FIG.6-48 DISCRETISATION FOR MIDSHIP SECTION OF "COBRA" T.B. DESTROYER

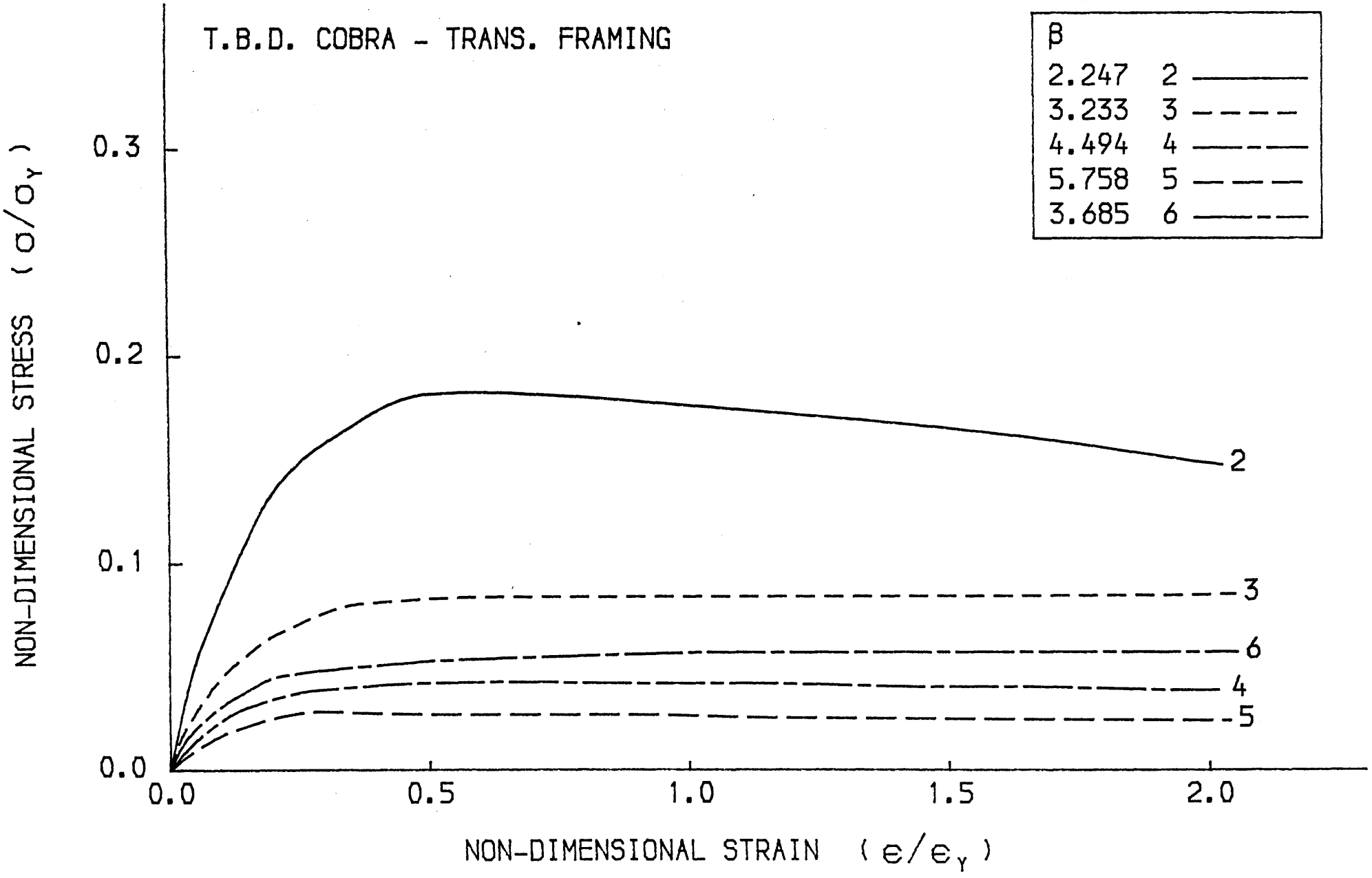

FIG.6-49 AVERAGE STRESS-STRAIN CURVE FOR THE PLATE

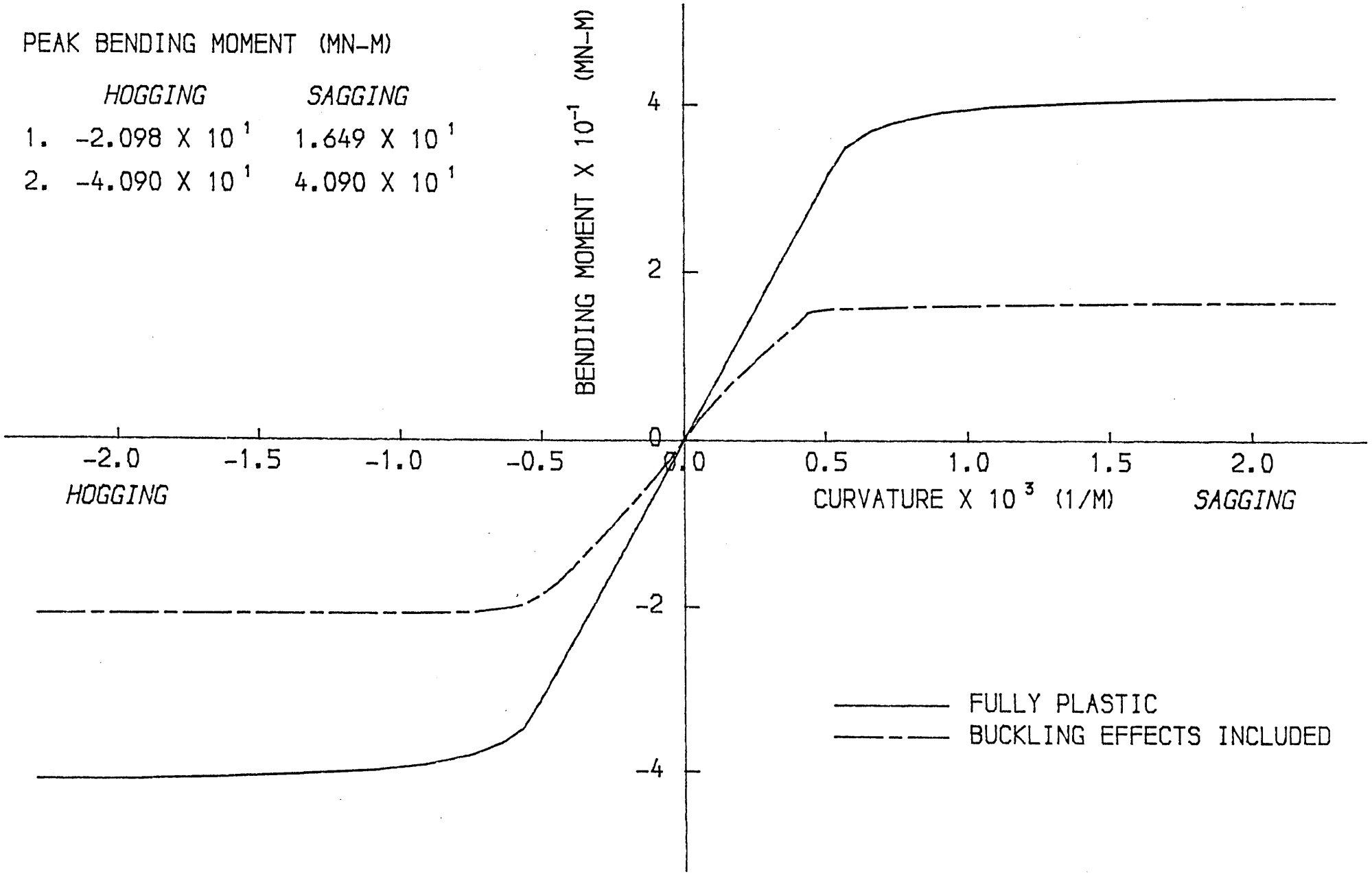

FIG.6-50 BENDING MOMENT-CURVATURE CURVE FOR T.B.D. COBRA (TRANS. FR.)

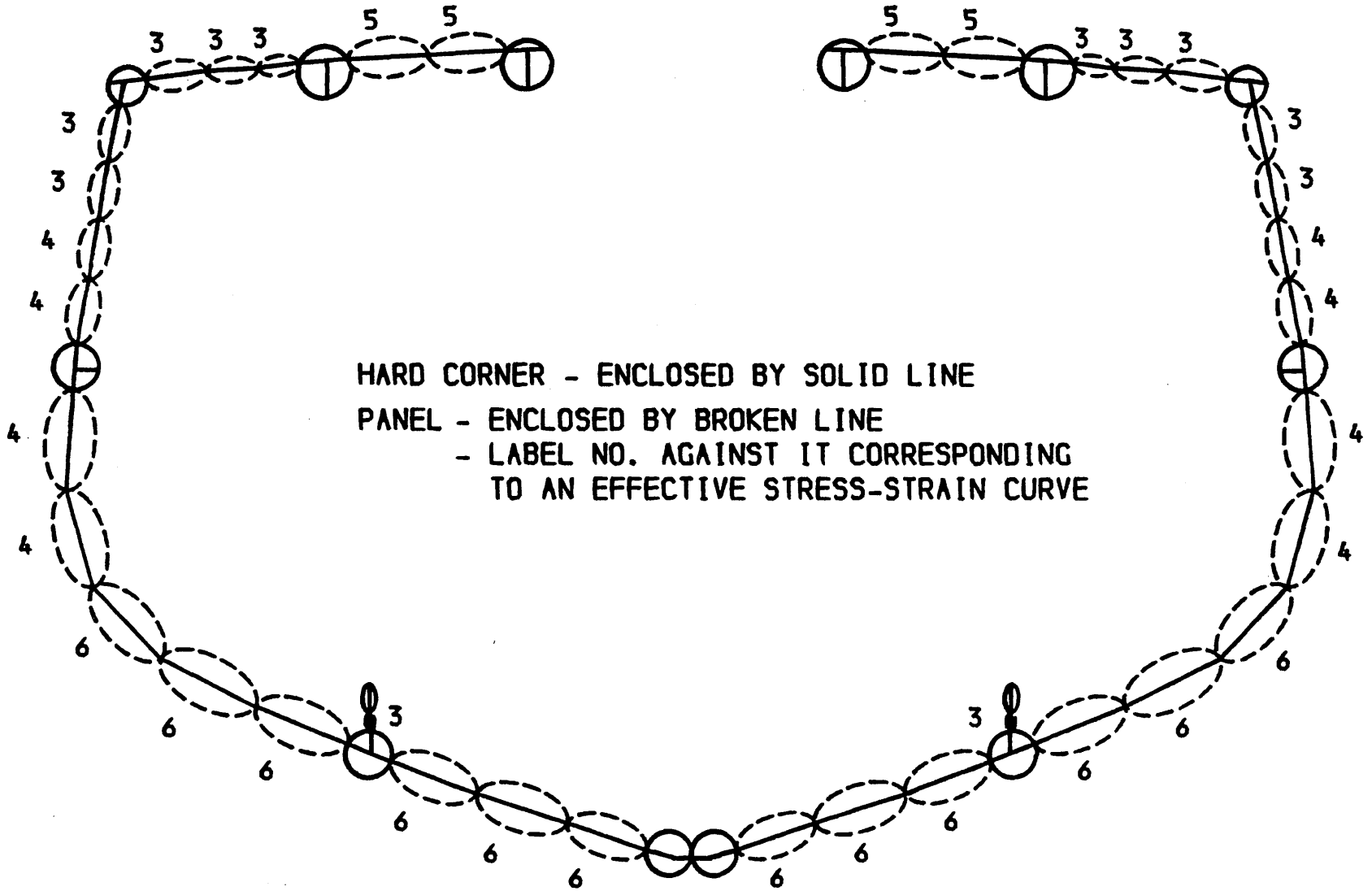

FIG.6-51 DISCRETISATION FOR MIDSHIP SECTION OF HMS WOLF

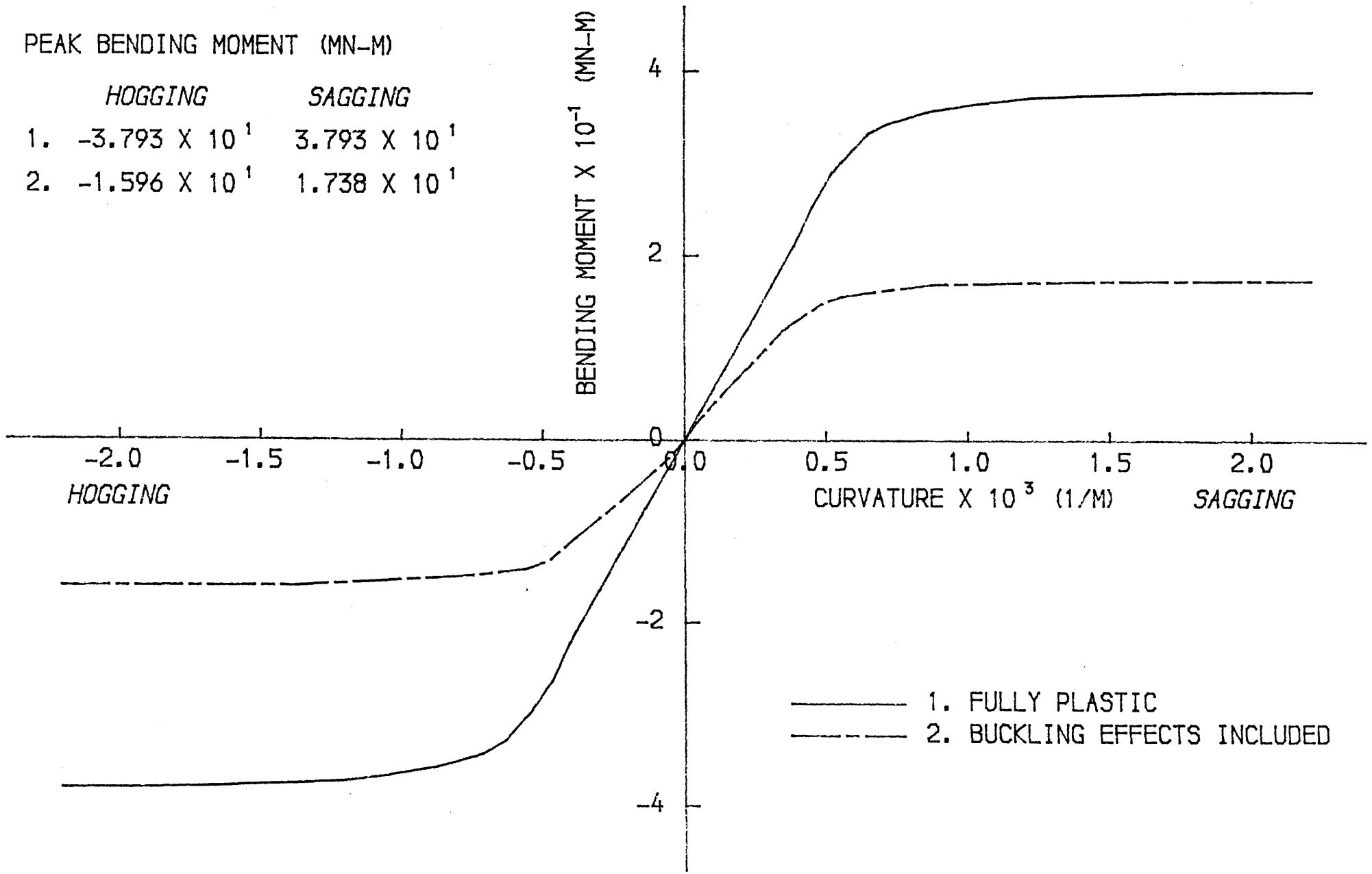

FIG.6-52 BENDING MOMENT-CURVATURE CURVE FOR HMS WOLF (TRANS. FR.)

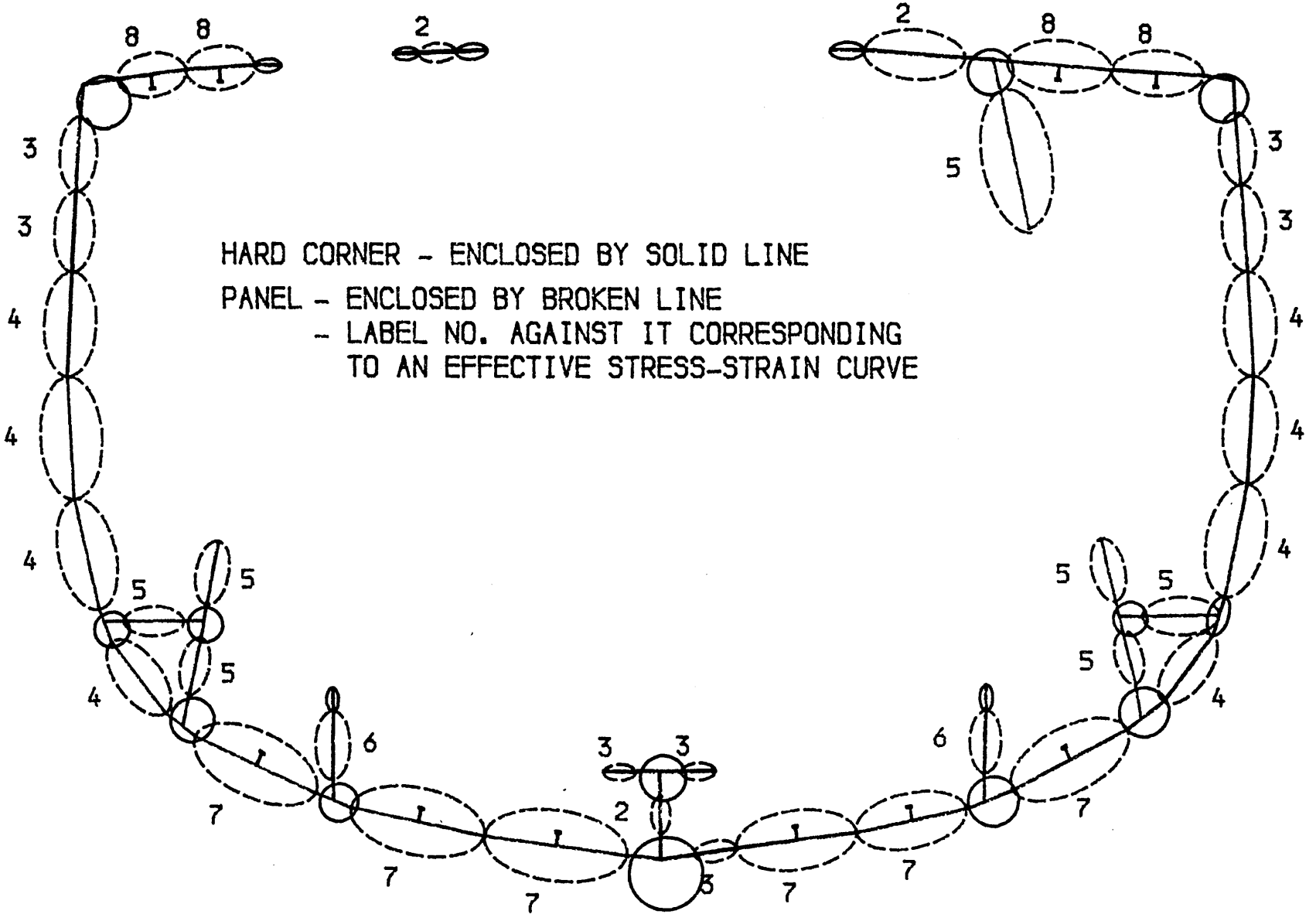

FIG.6-53 DISCRETISATION FOR MIDSHIP SECTION OF "COBRA" T.B.D. (LONG. FR.)

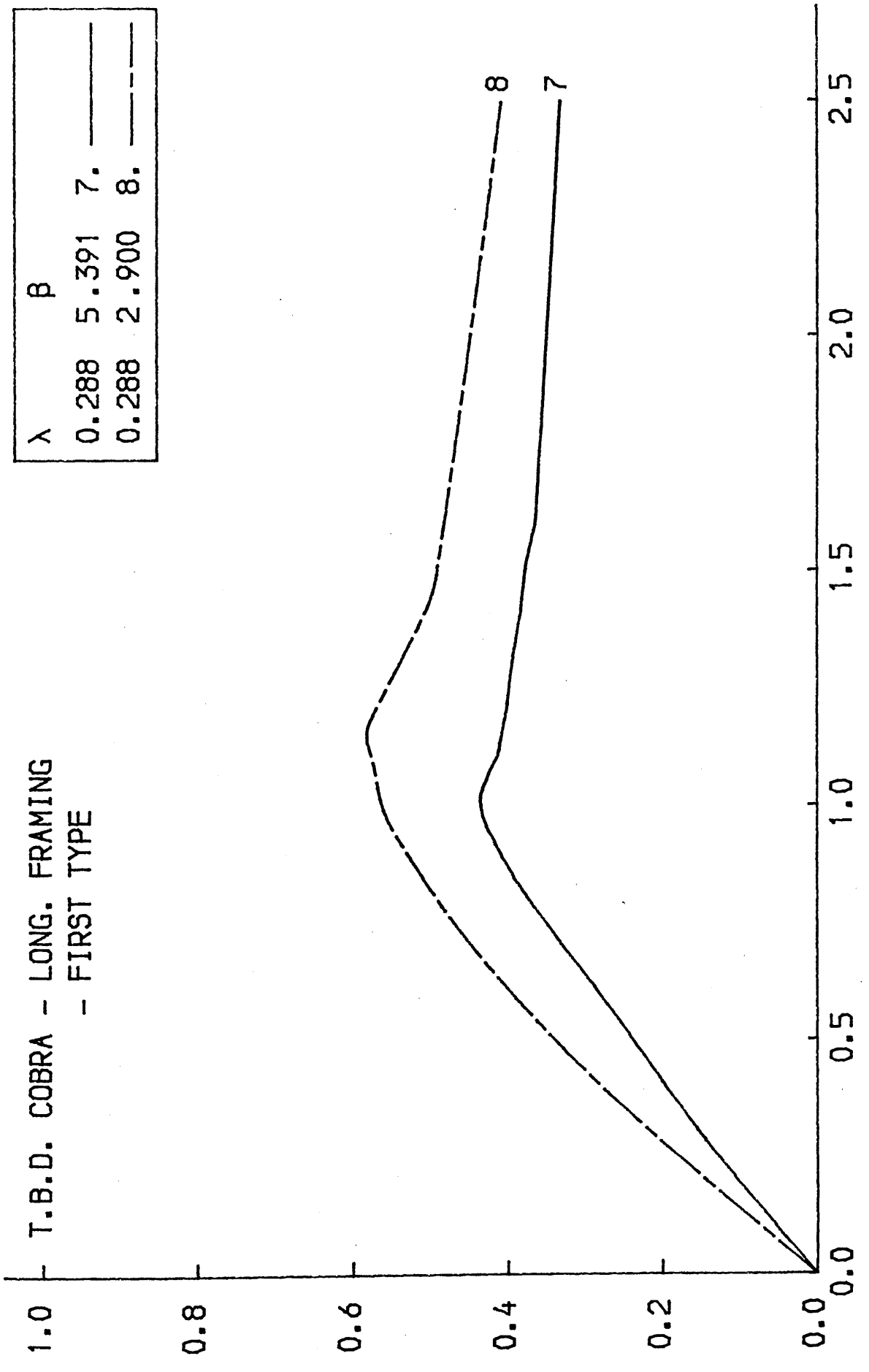

FIG.6-54 LOAD-SHORTENING CURVE FOR THE BEAM-COLUMN

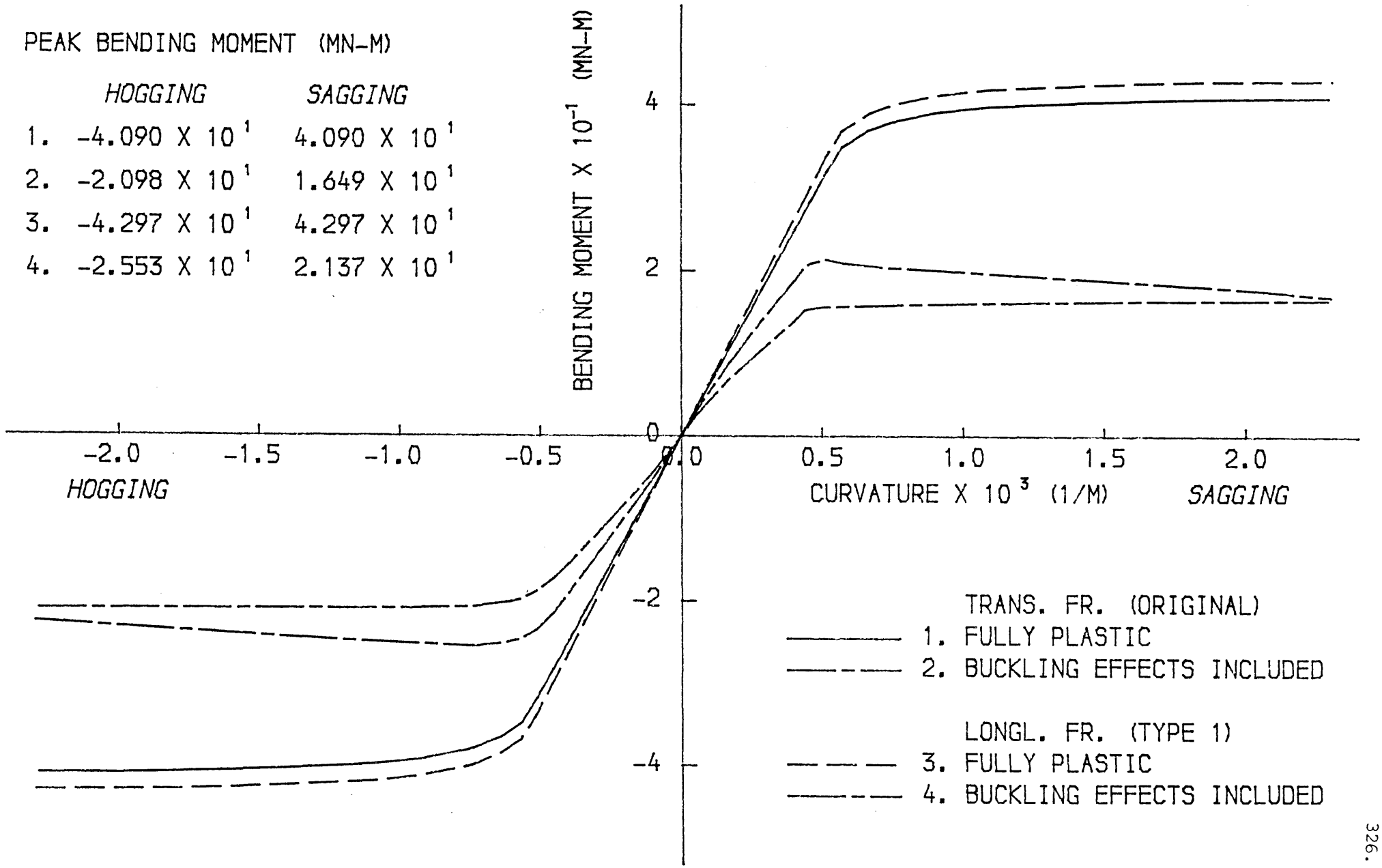

FIG.6-55 BENDING MOMENT-CURVATURE CURVE FOR T.B.D. COBRA

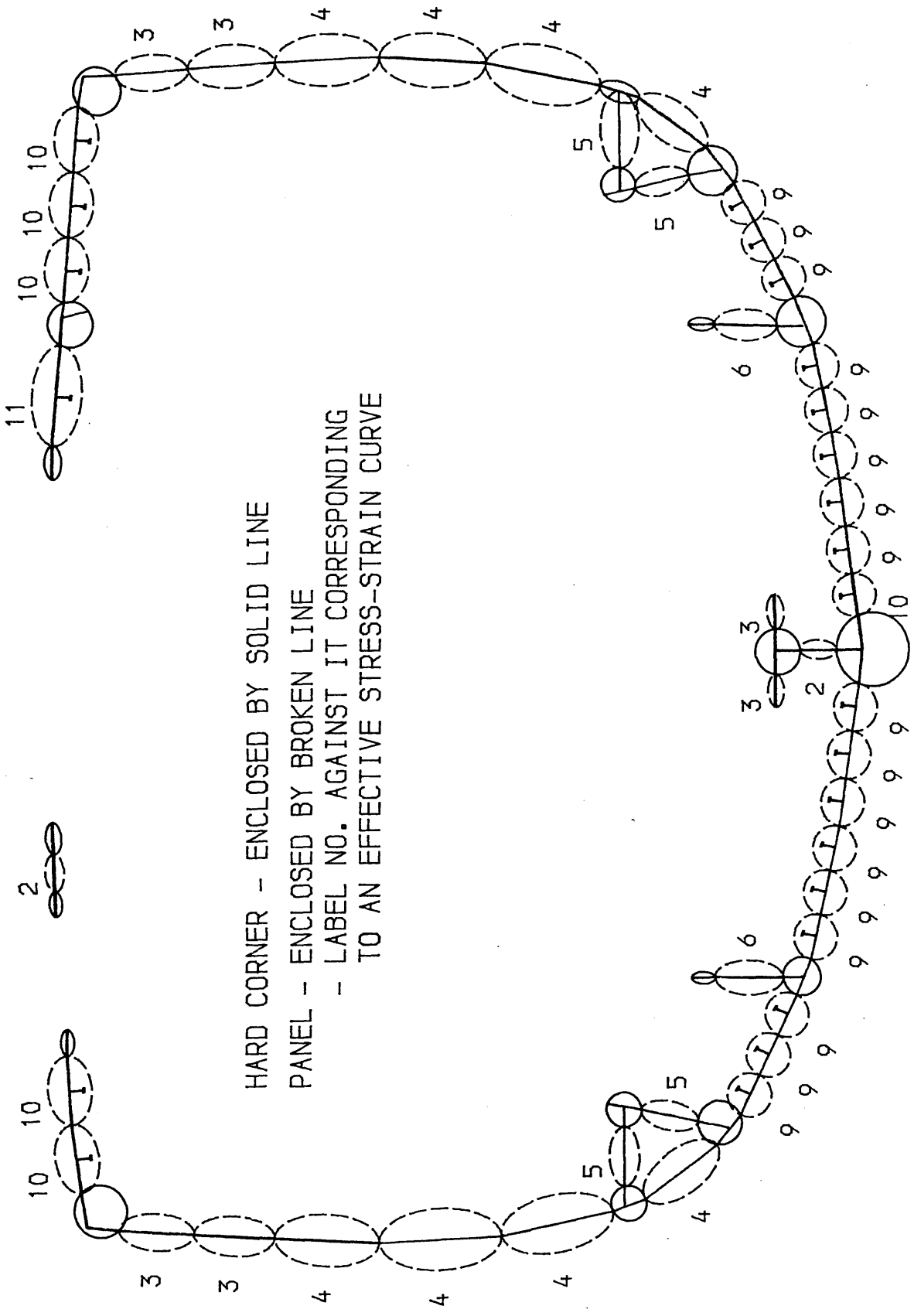

FIG.6-56 DISCRETISATION FOR MIDSHIP SECTION OF "COBRA" T.B.D. (LONG. FR.)

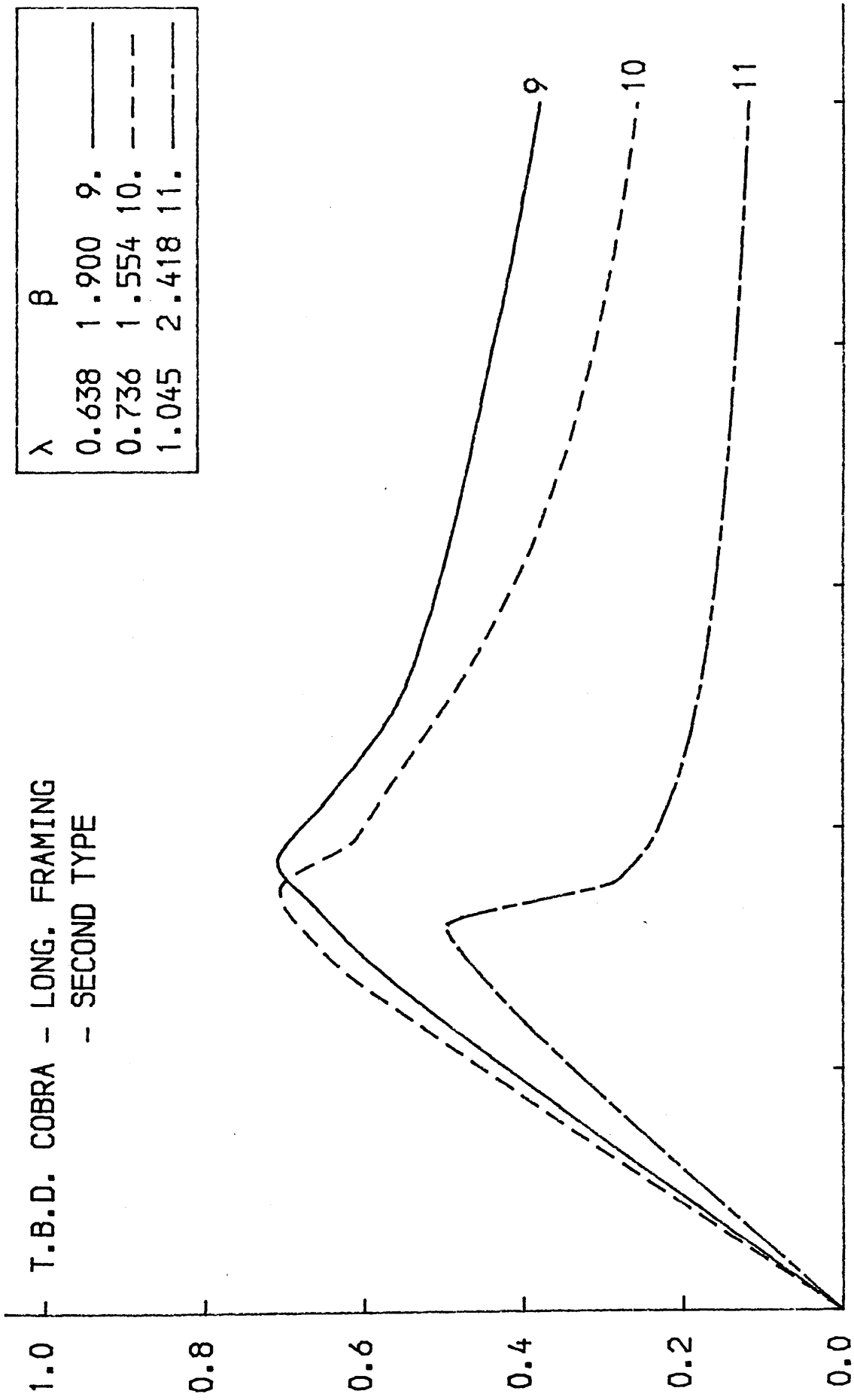

FIG.6-57 LOAD-SHORTENING CURVE FOR THE BEAM-COLUMN

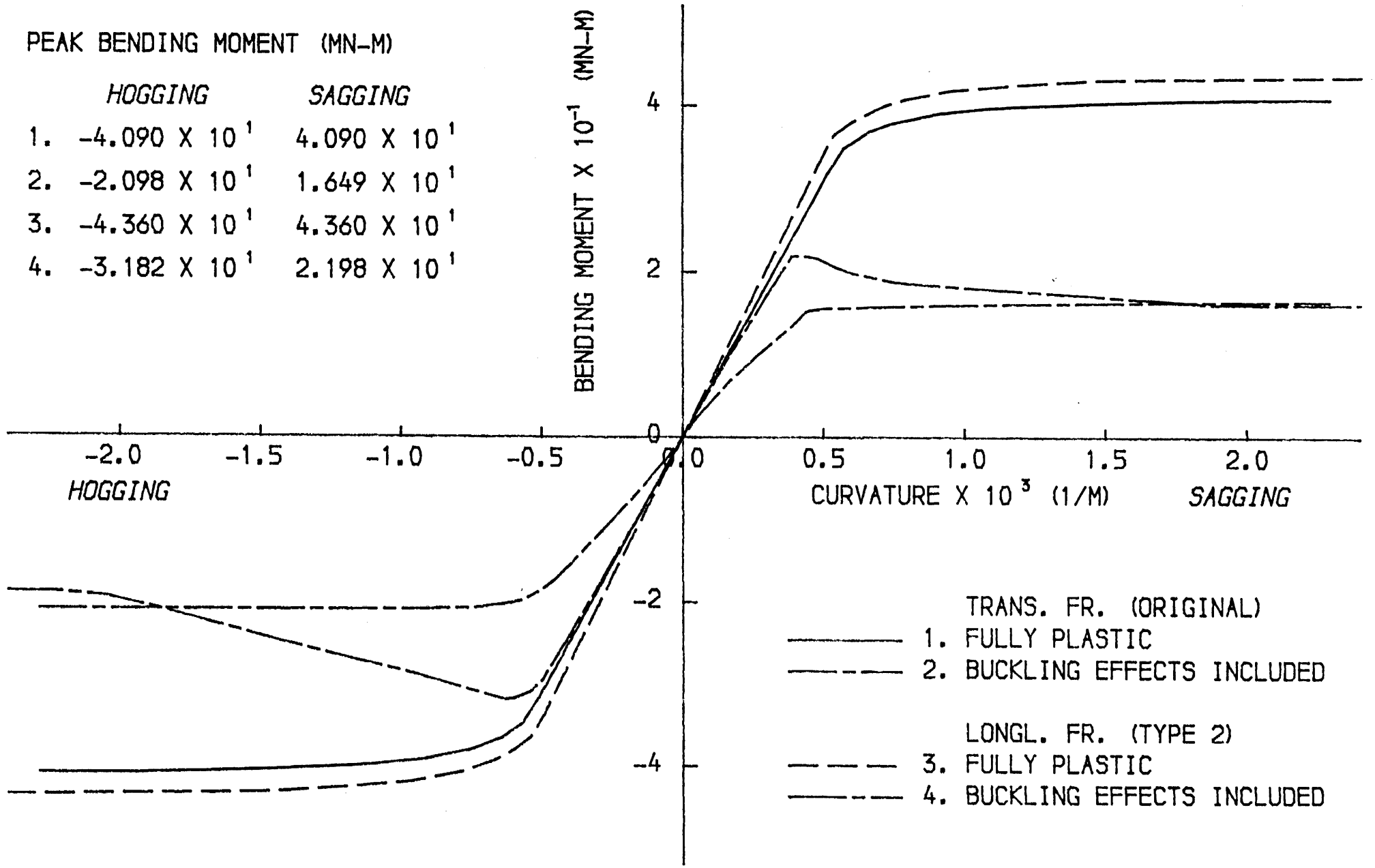

FIG.6-58 BENDING MOMENT-CURVATURE CURVE FOR T.B.D. COBRA

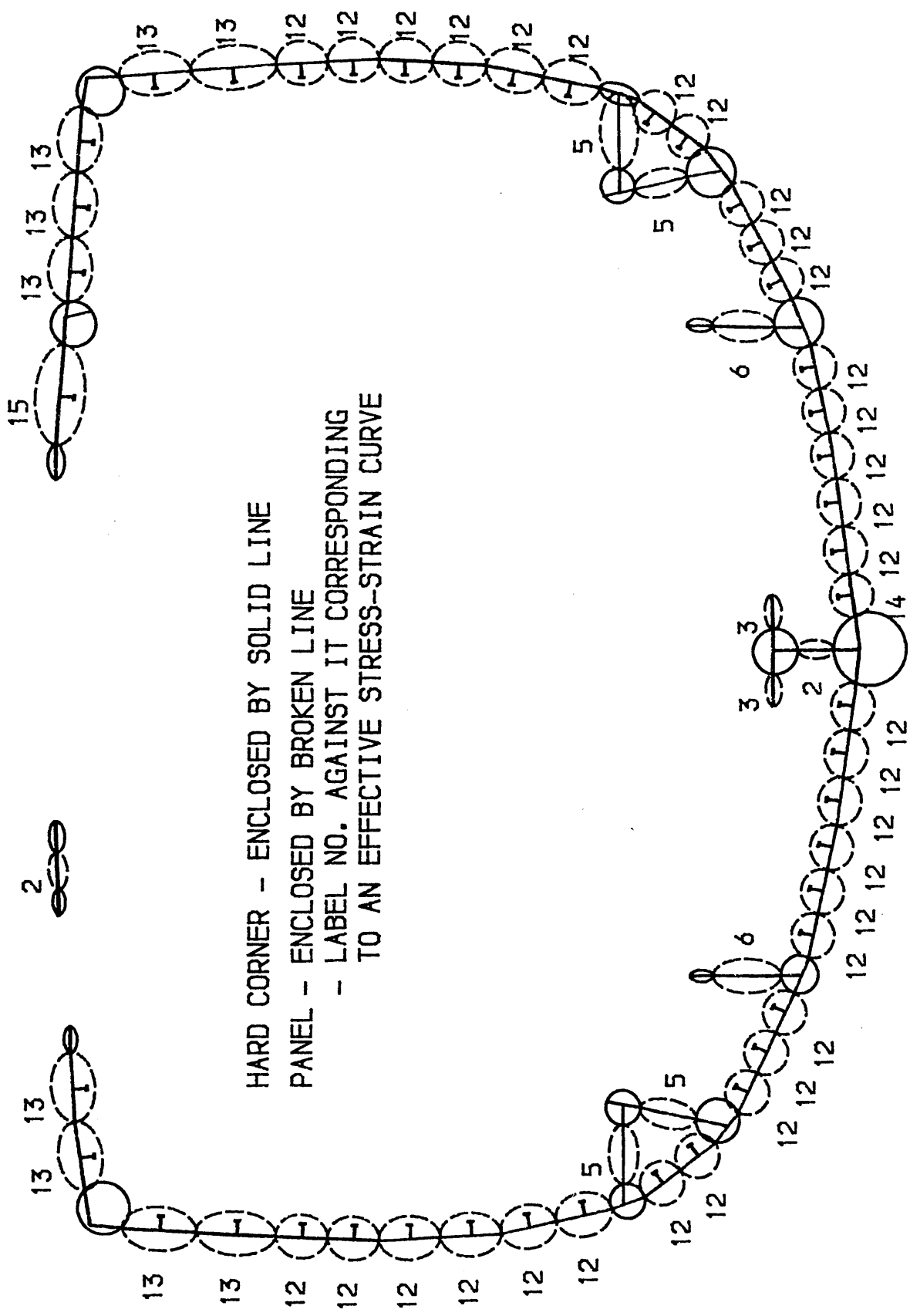

FIG.6-59 DISCRETISATION FOR MIDSHIP SECTION OF "COBRA" T.B.D. (LONG. FR.)

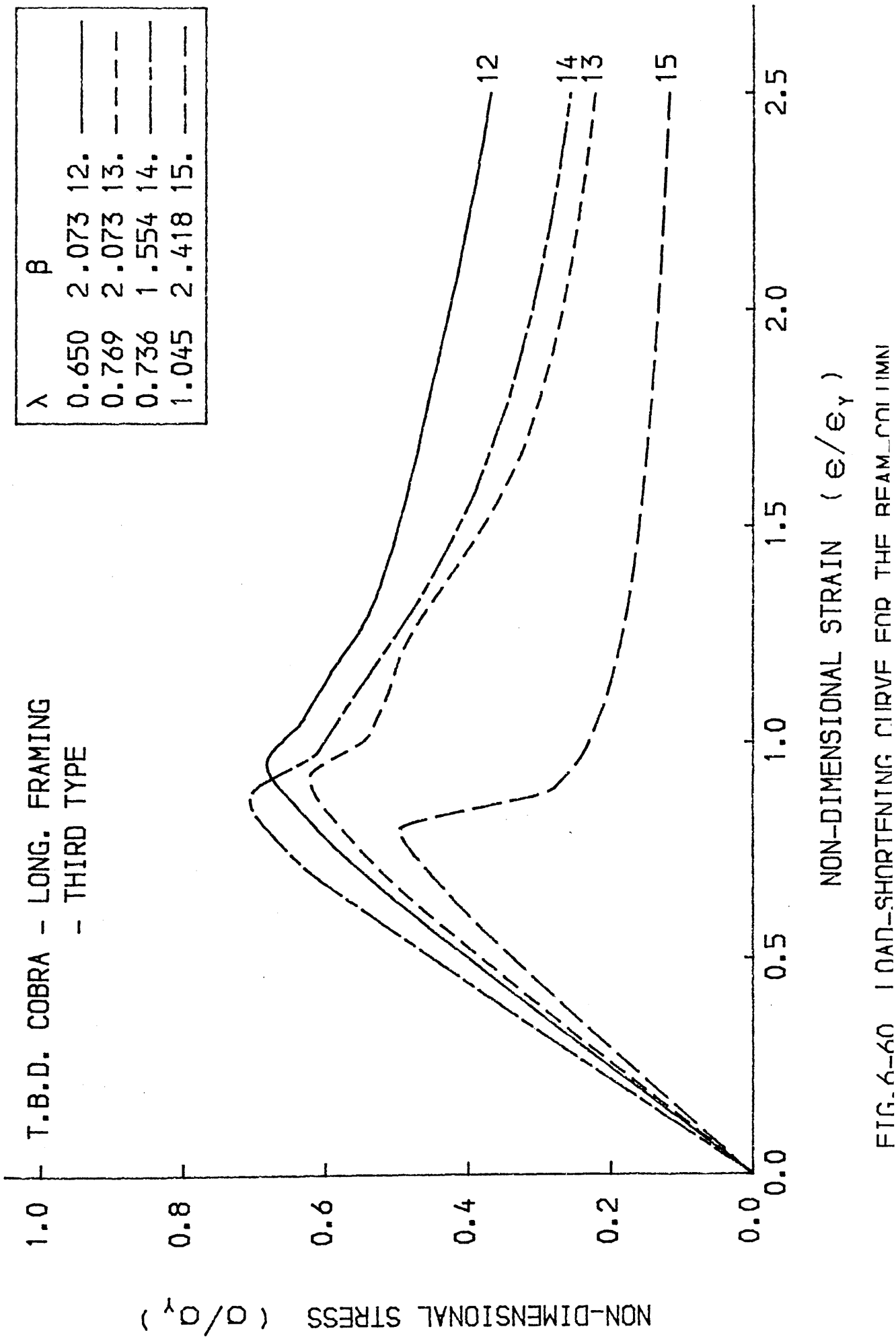

FIG.6-60 LOAD-SHORTENING CURVE FOR THE BEAM-COLUMN

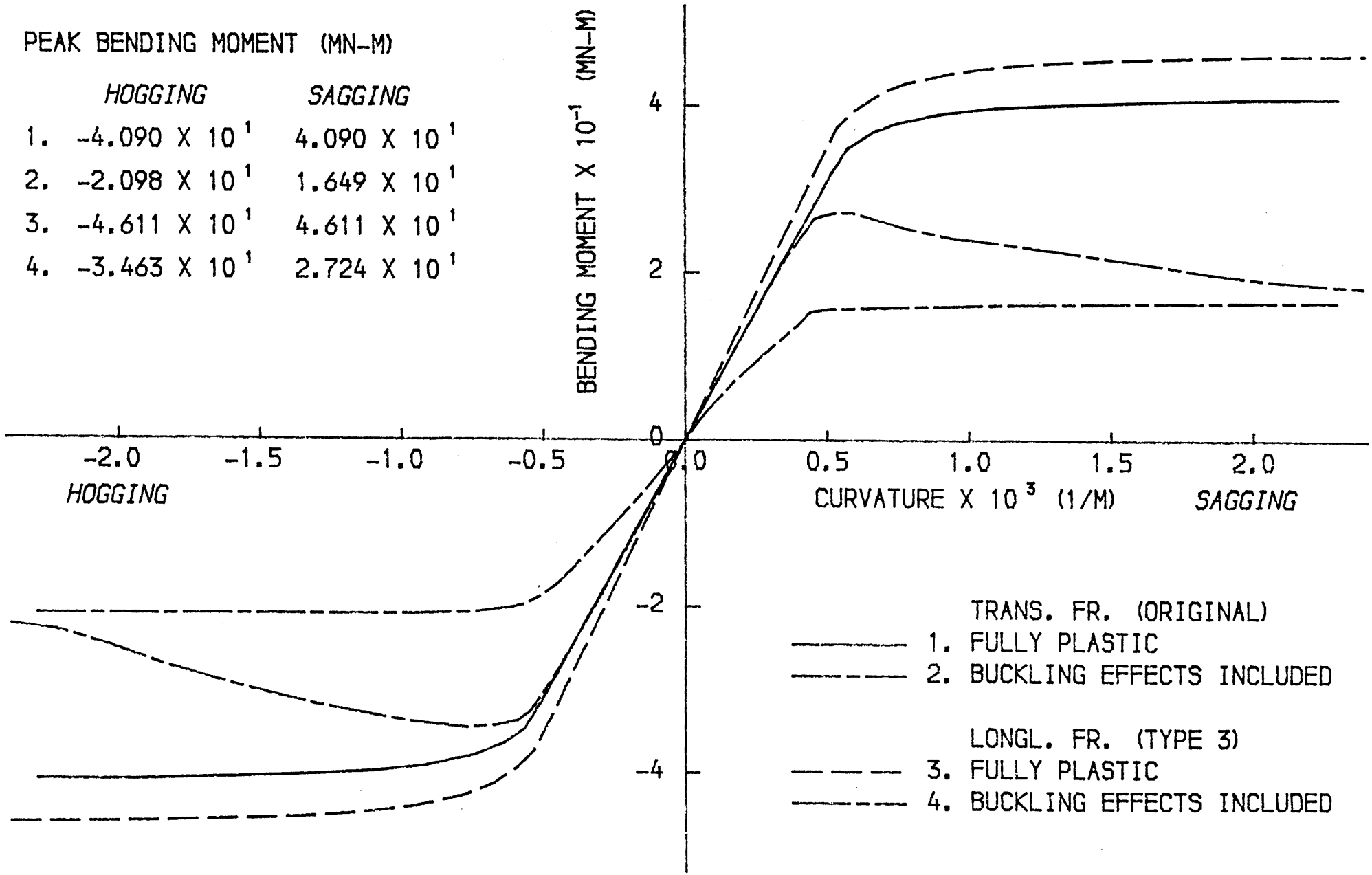

FIG.6-61 BENDING MOMENT-CURVATURE CURVE FOR T.B.D. COBRA

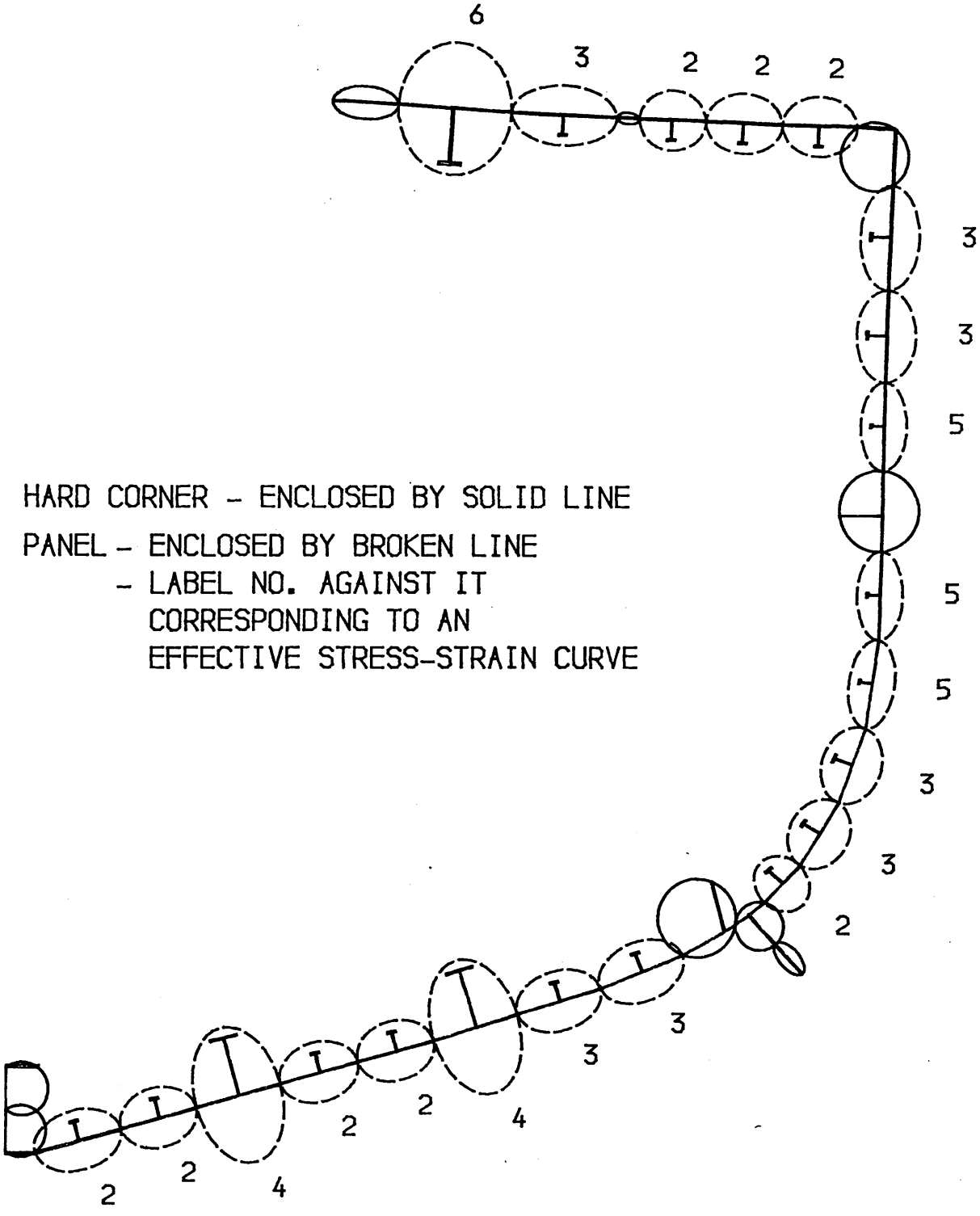

FIG.6-62 DISCRETISATION FOR MIDSHIP SECTION OF TYPE 14 FRIGATE

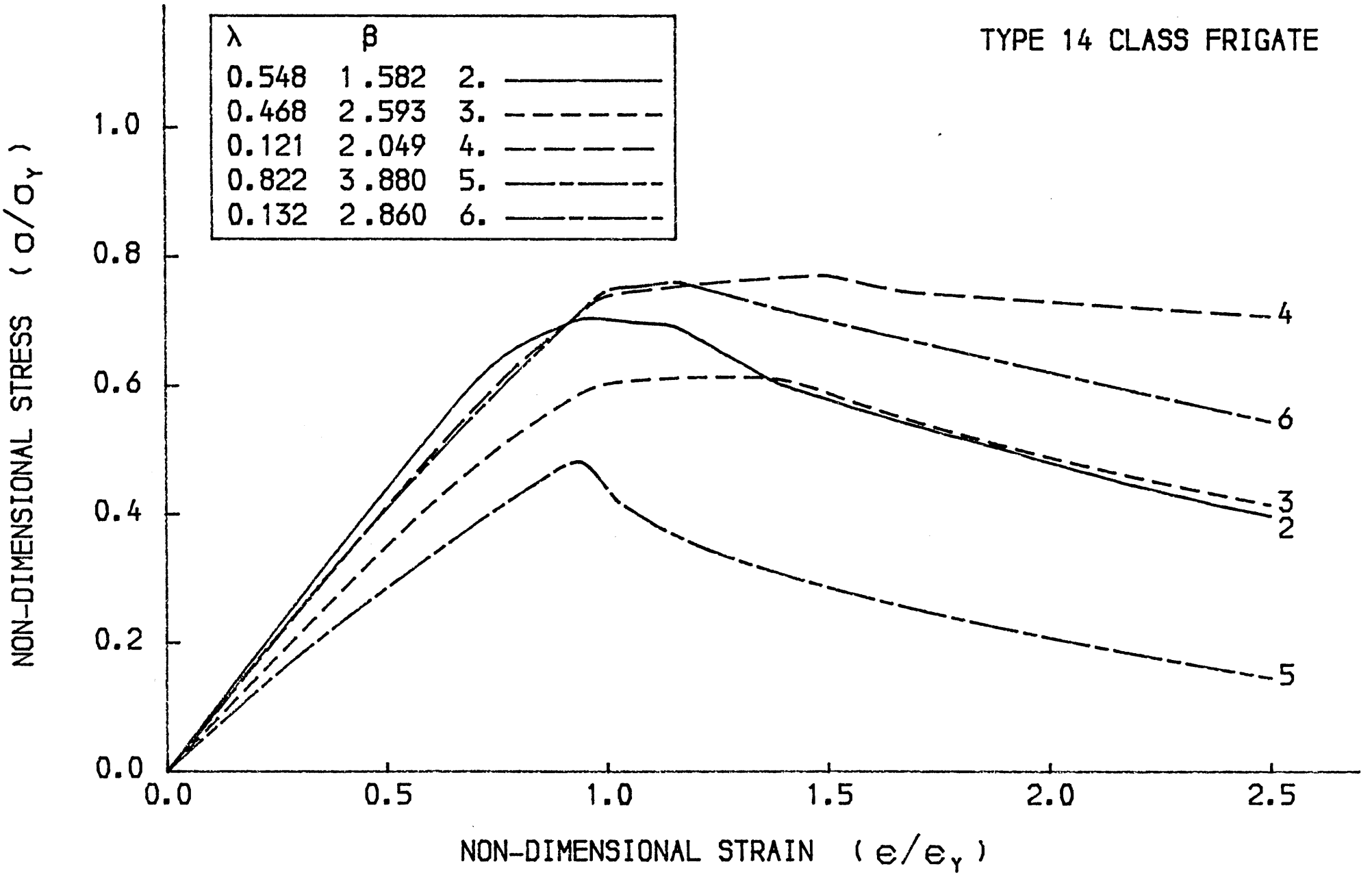

FIG.6-63 LOAD-SHORTENING CURVE FOR THE BEAM-COLUMN

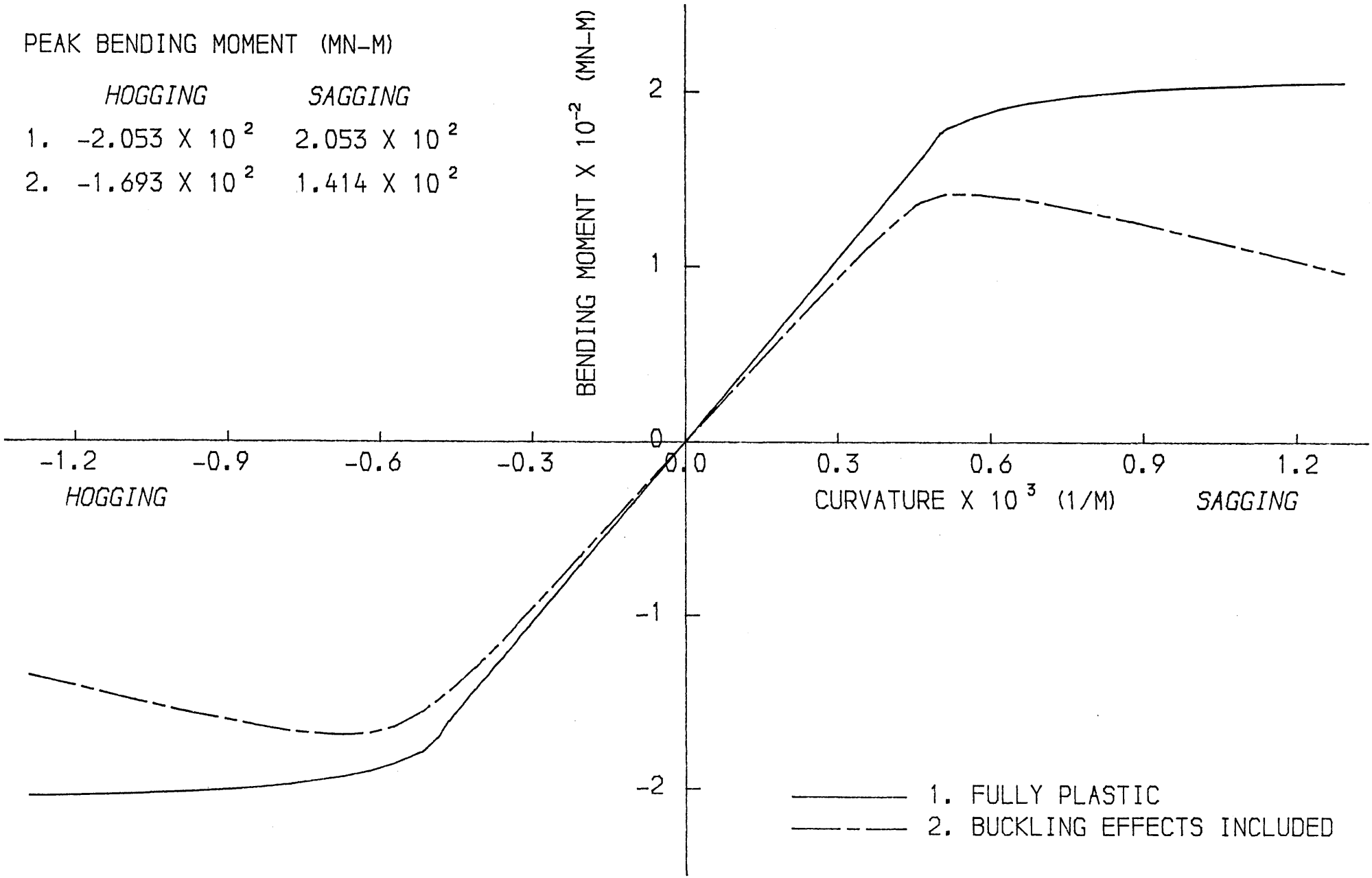

FIG.6-64 BENDING MOMENT-CURVATURE CURVE FOR "TYPE 14" CLASS FRIGATE

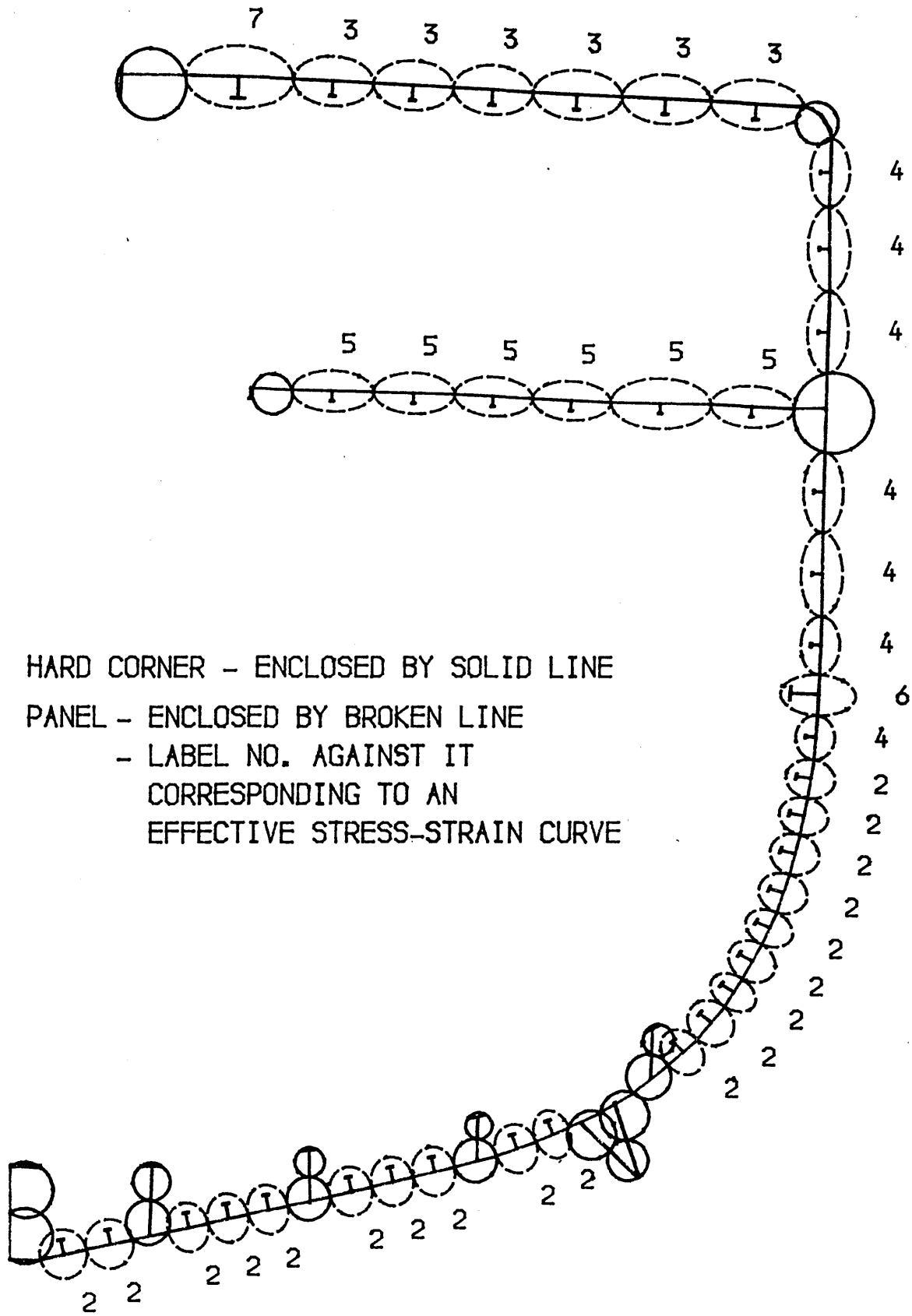

FIG.6-65 DISCRETISATION FOR MIDSHIP SECTION OF "WHITBY" CLASS FRIGATE

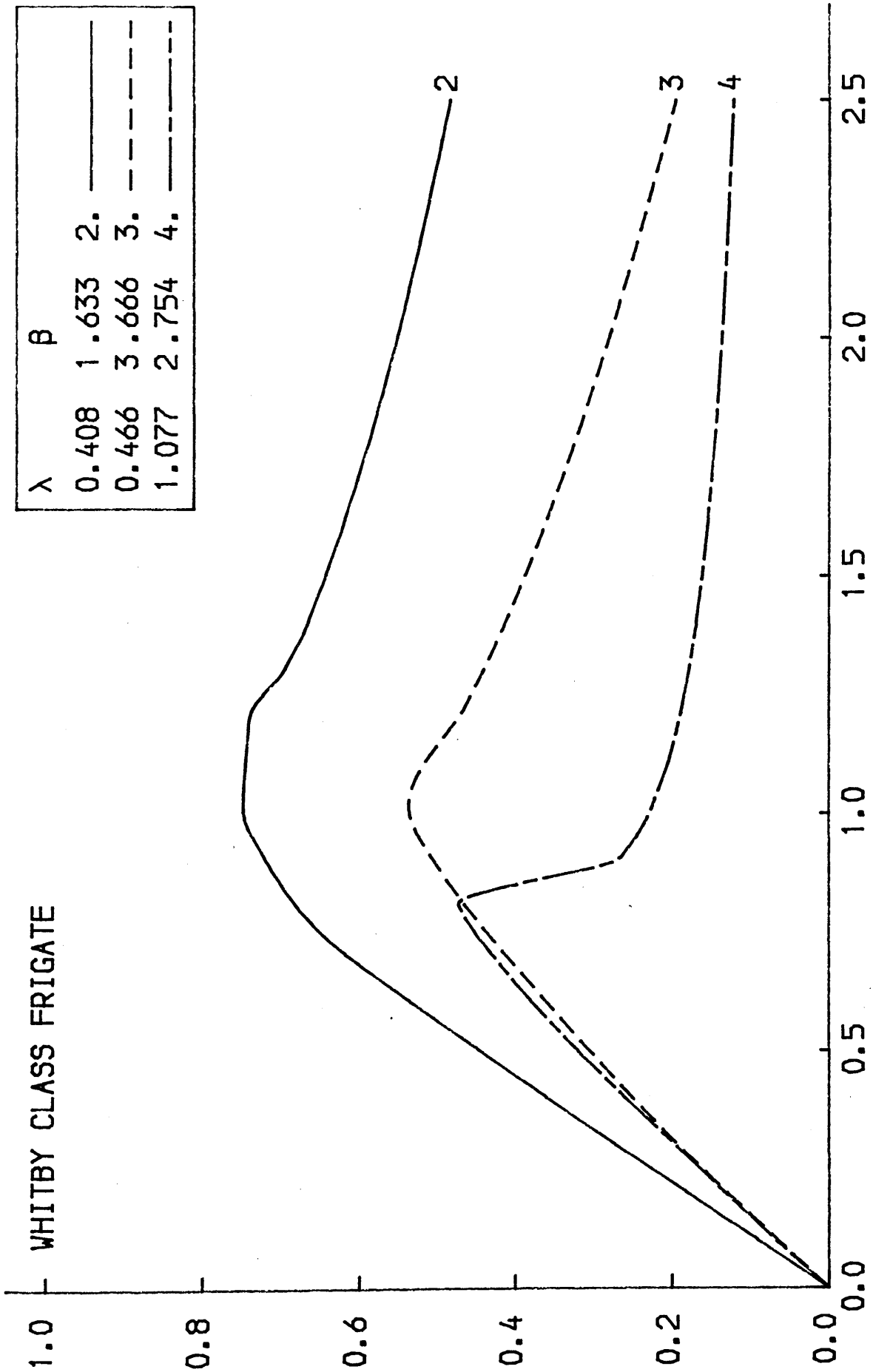

FIG.6-66 LOAD-SHORTENING CURVE FOR THE BEAM-COLUMN

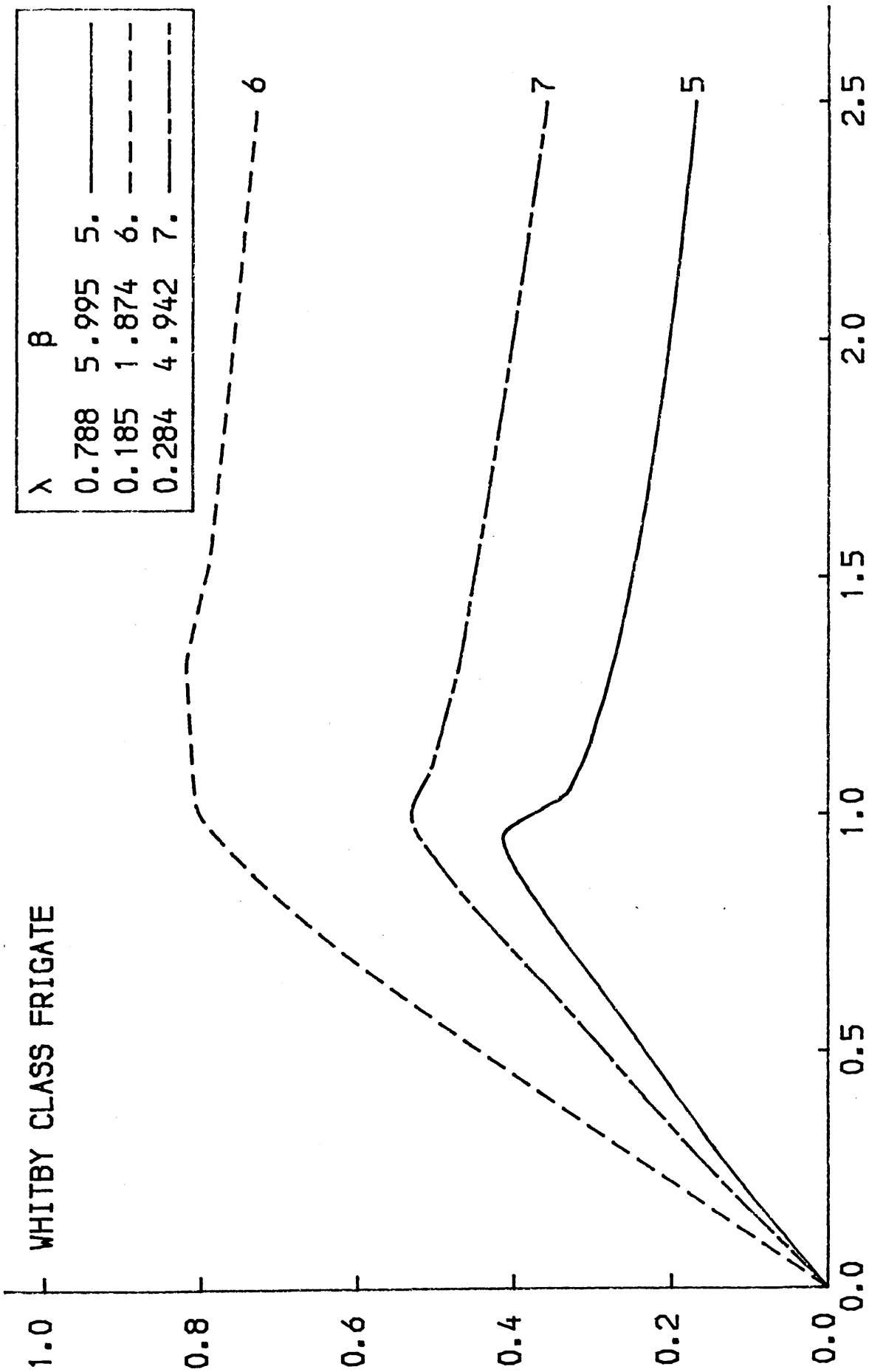

FIG.6-67 LOAD-SHORTENING CURVE FOR THE BEAM-COLUMN

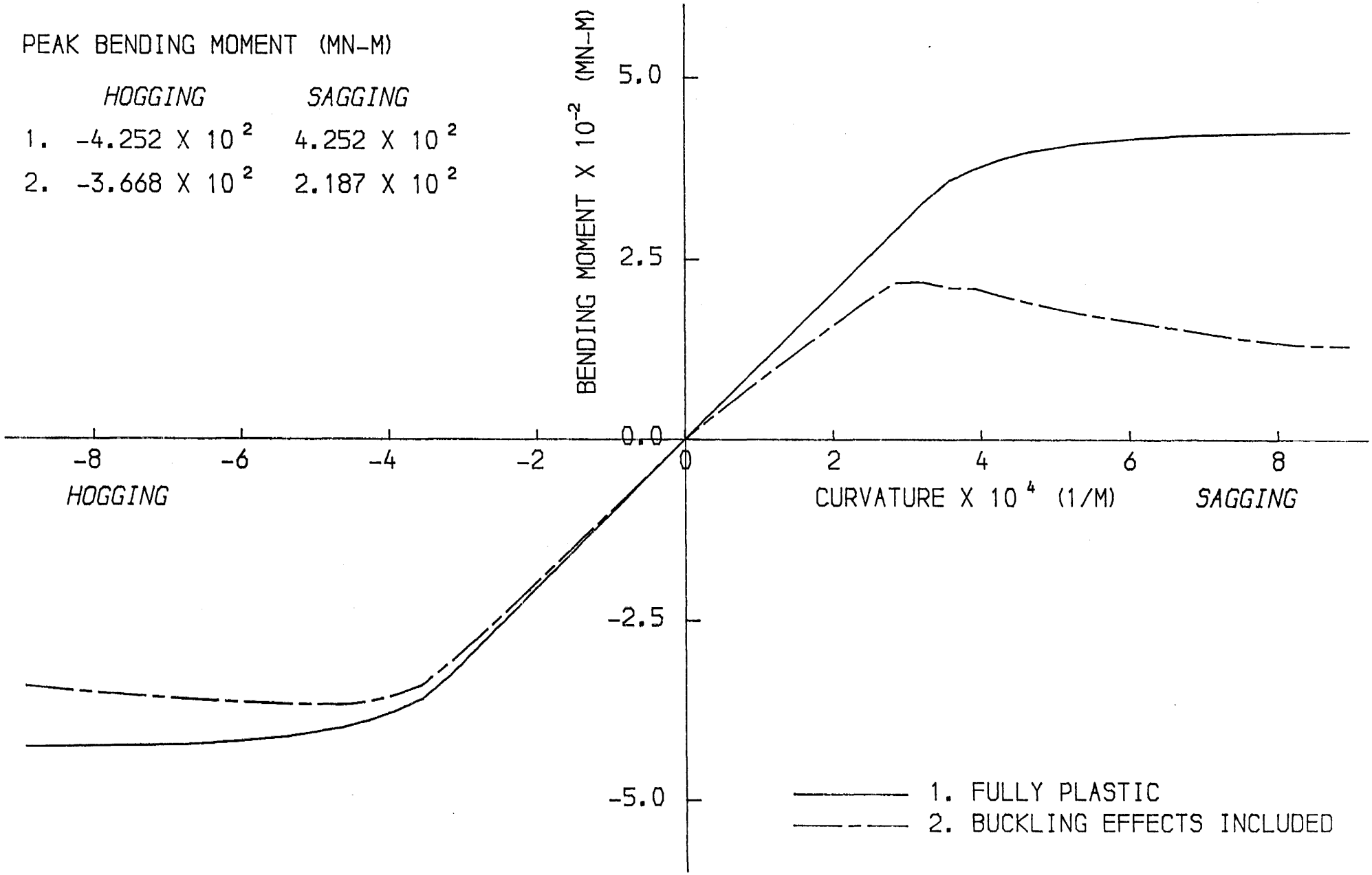

FIG.6-68 BENDING MOMENT-CURVATURE CURVE FOR "WHITBY" CLASS FRIGATE

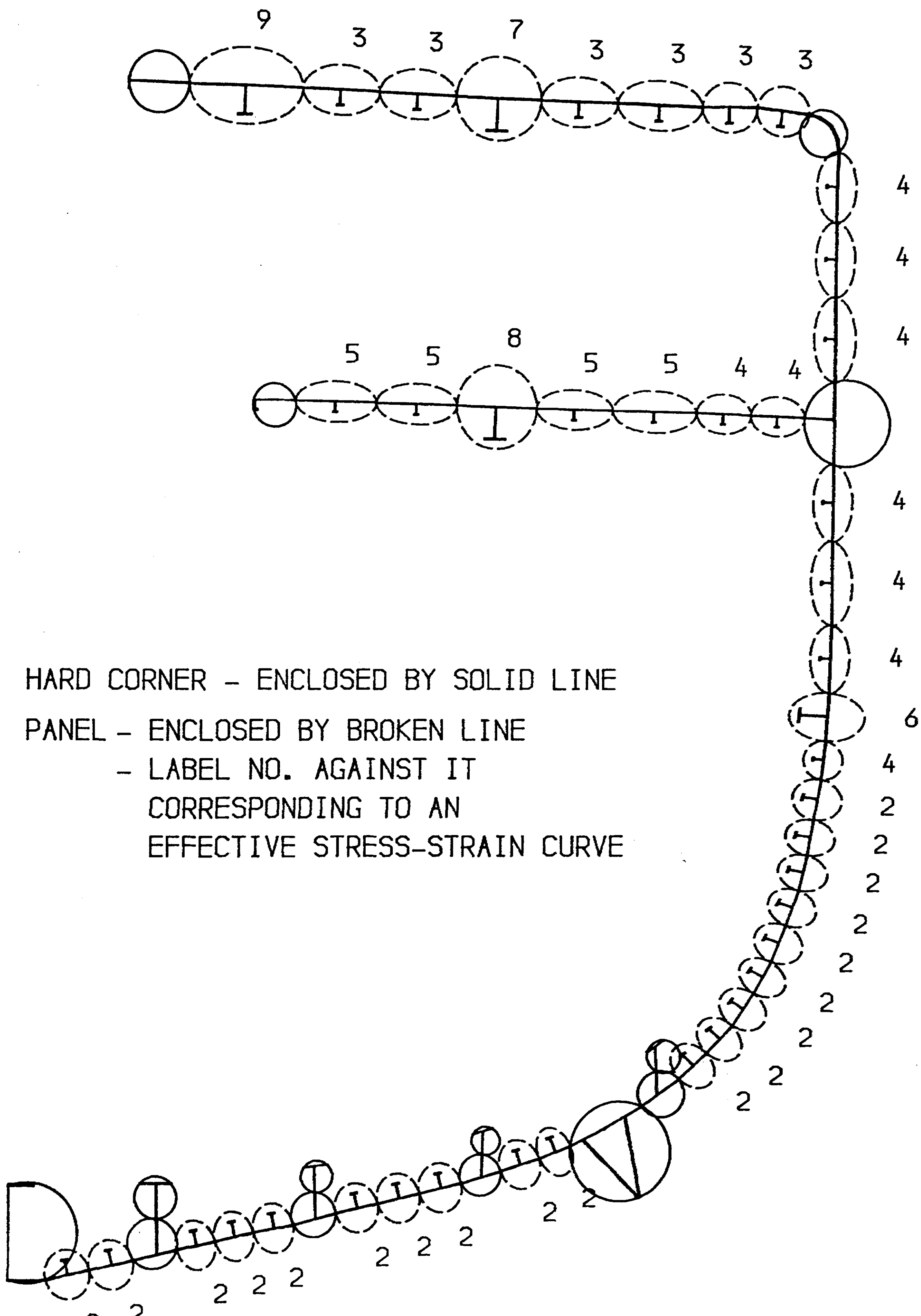

FIG.6-69 DISCRETISATION FOR MIDSHIP SECTION OF "ROTHESAY" CLASS FRIGATE

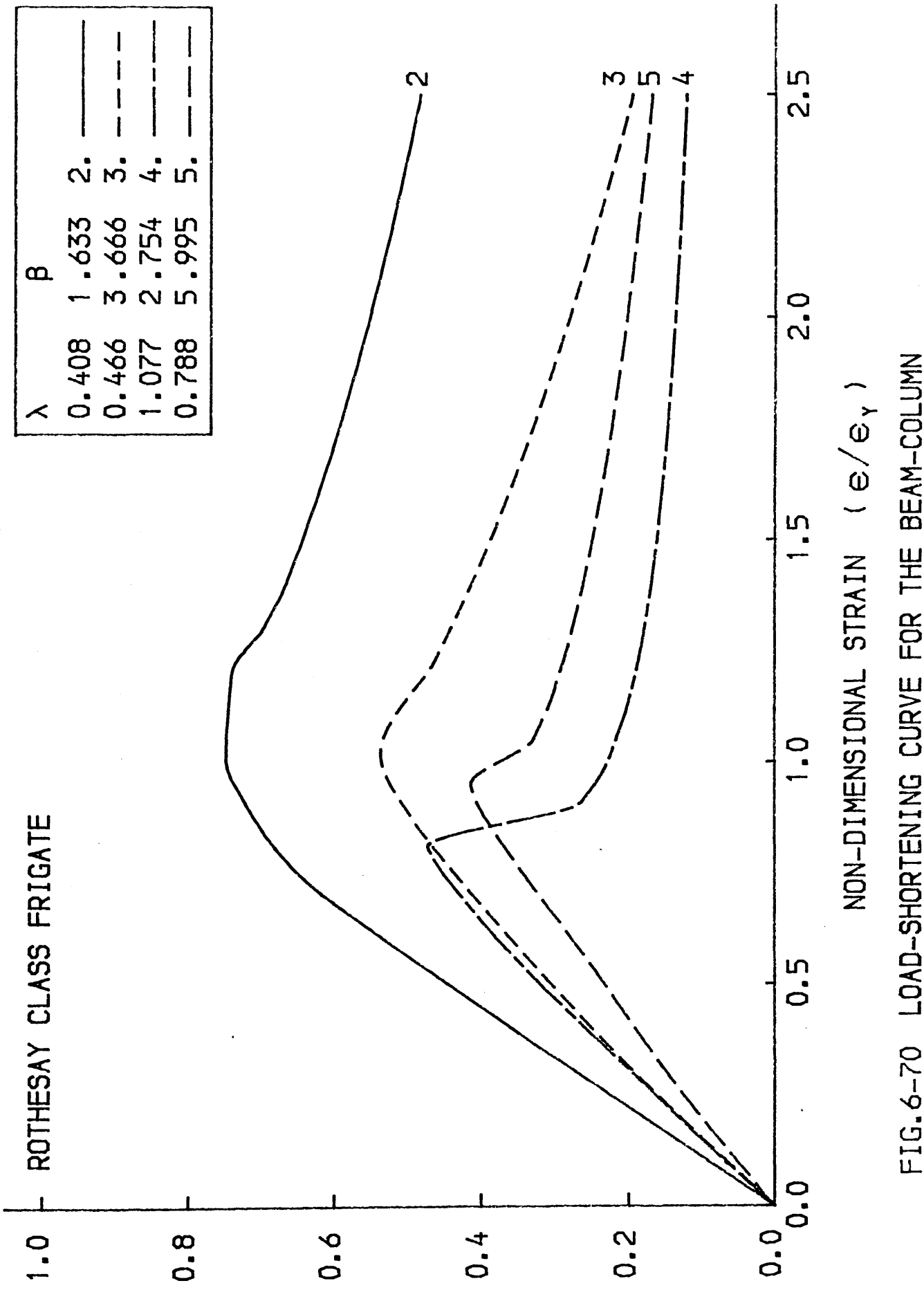

FIG.6-70 LOAD-SHORTENING CURVE FOR THE BEAM-COLUMN

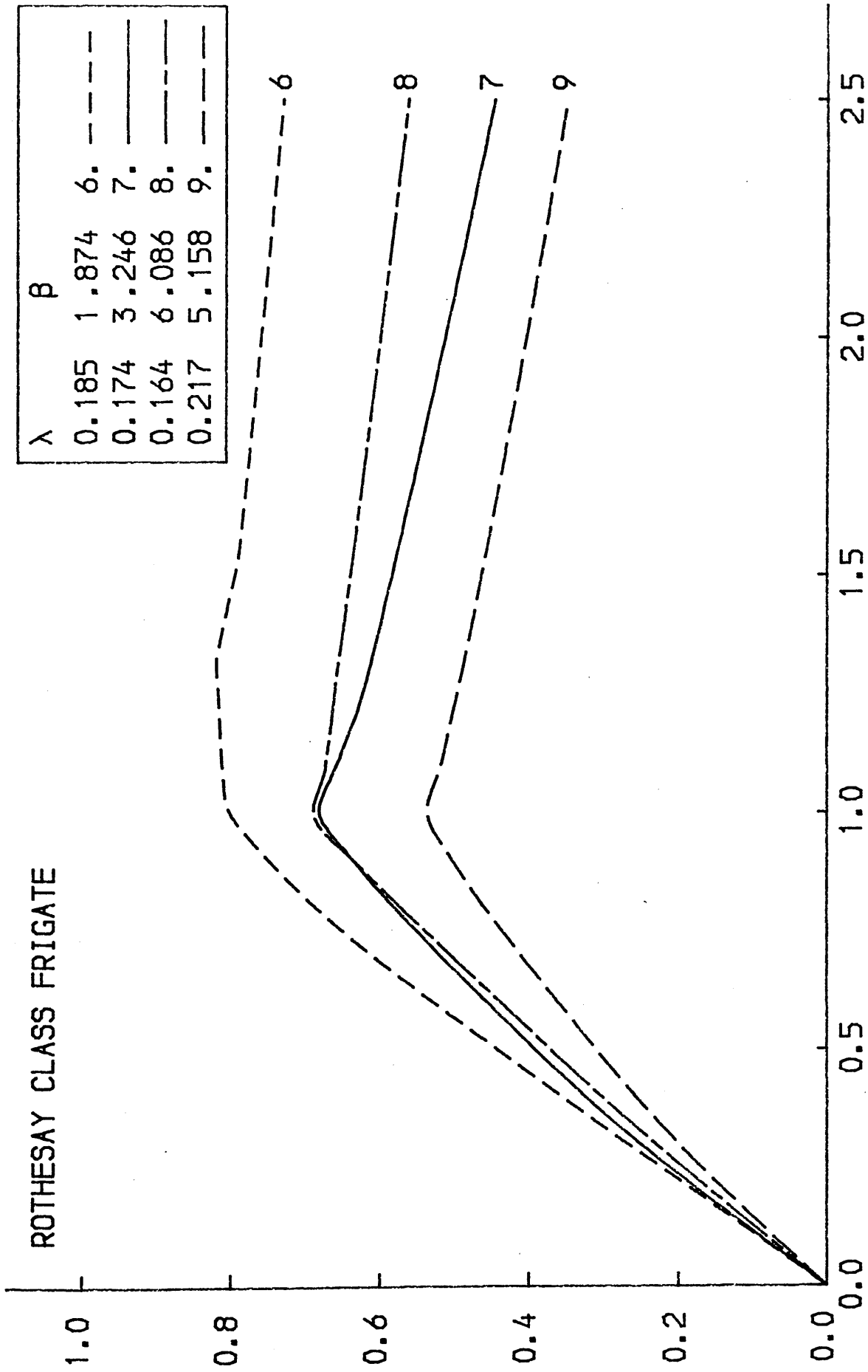

FIG.6-71 LOAD-SHORTENING CURVE FOR THE BEAM-COLUMN

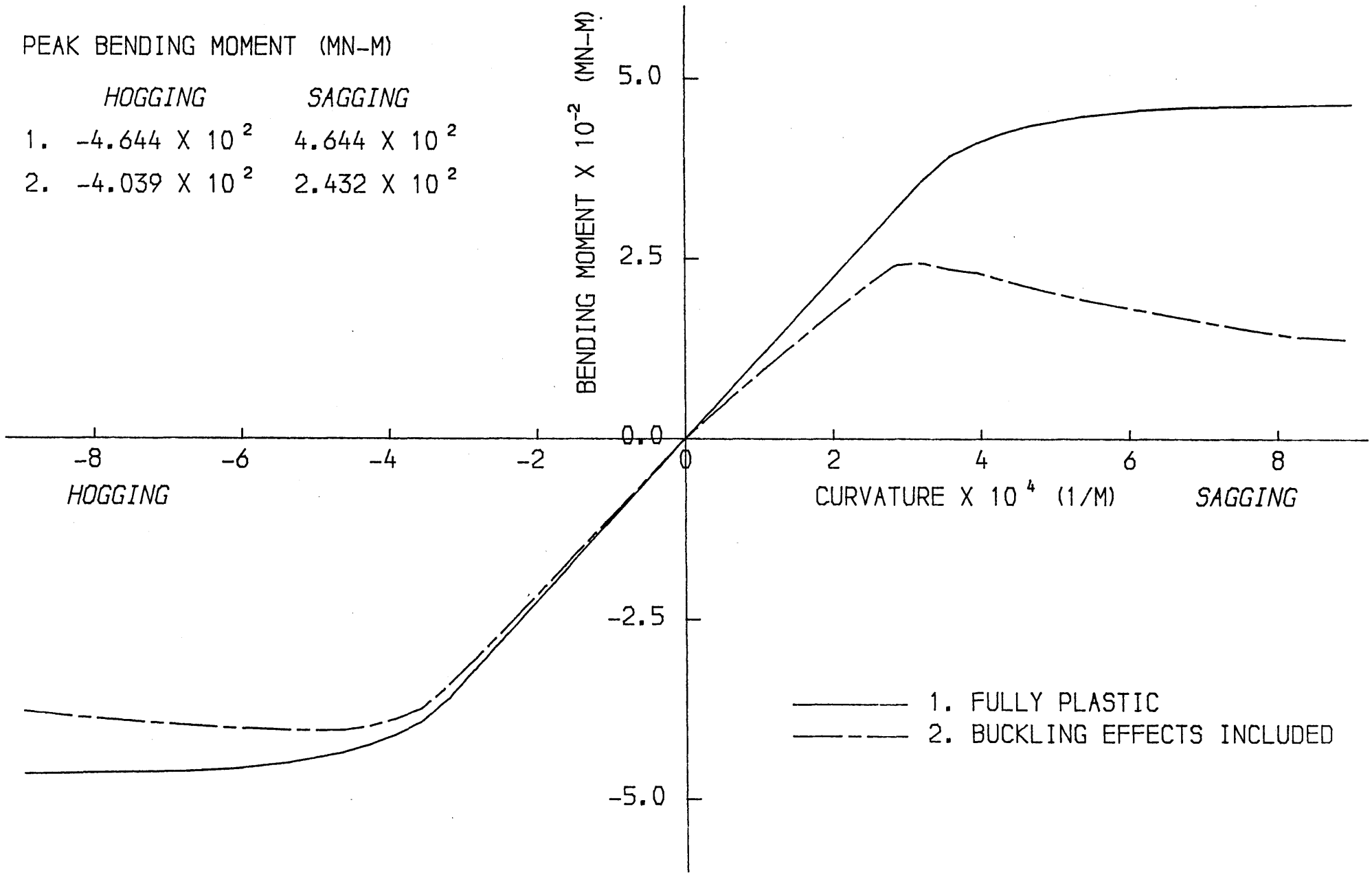

FIG.6-72 BENDING MOMENT-CURVATURE CURVE FOR "ROTHESAY" CLASS FRIGATE

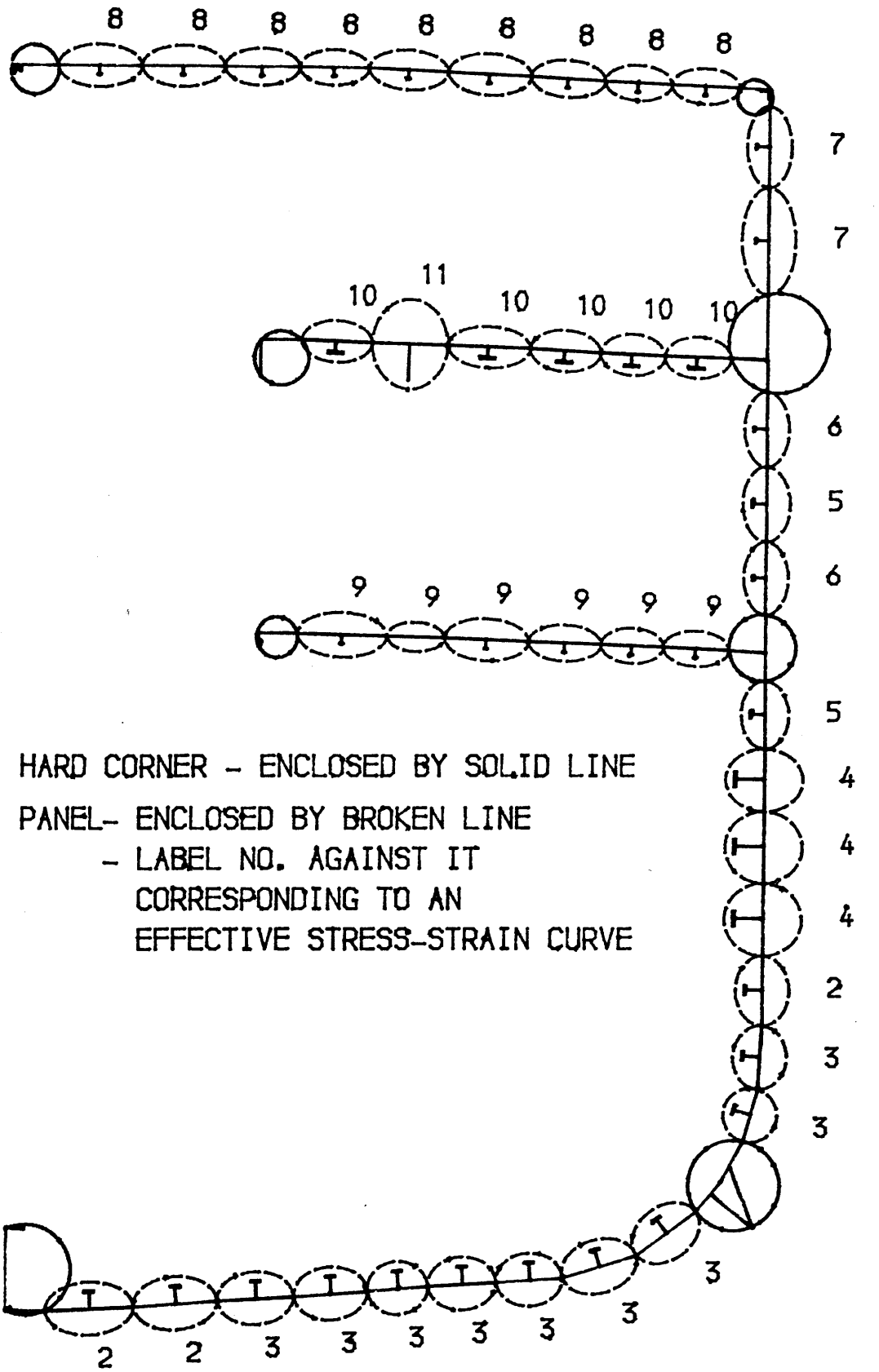

HARD CORNER - ENCLOSED BY SOLID LINE

PANEL- ENCLOSED BY BROKEN LINE
- LABEL NO. AGAINST IT CORRESPONDING TO AN EFFECTIVE STRESS-STRAIN CURVE

FIG.6-73 DISCRETISATION FOR MIDSHIP SECTION OF TYPE 81 FRIGATE

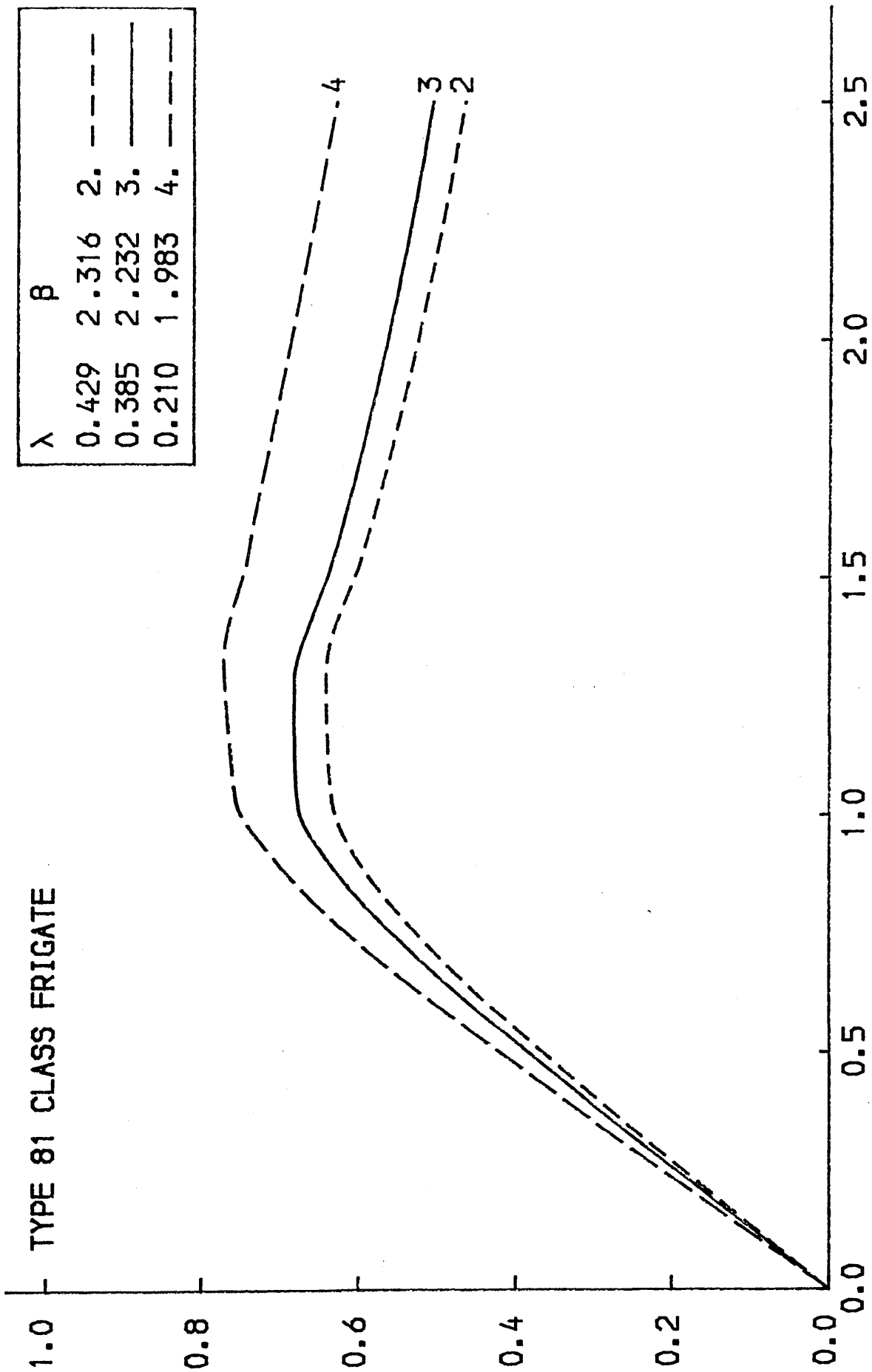

FIG.6-74 LOAD-SHORTENING CURVE FOR THE BEAM-COLUMN

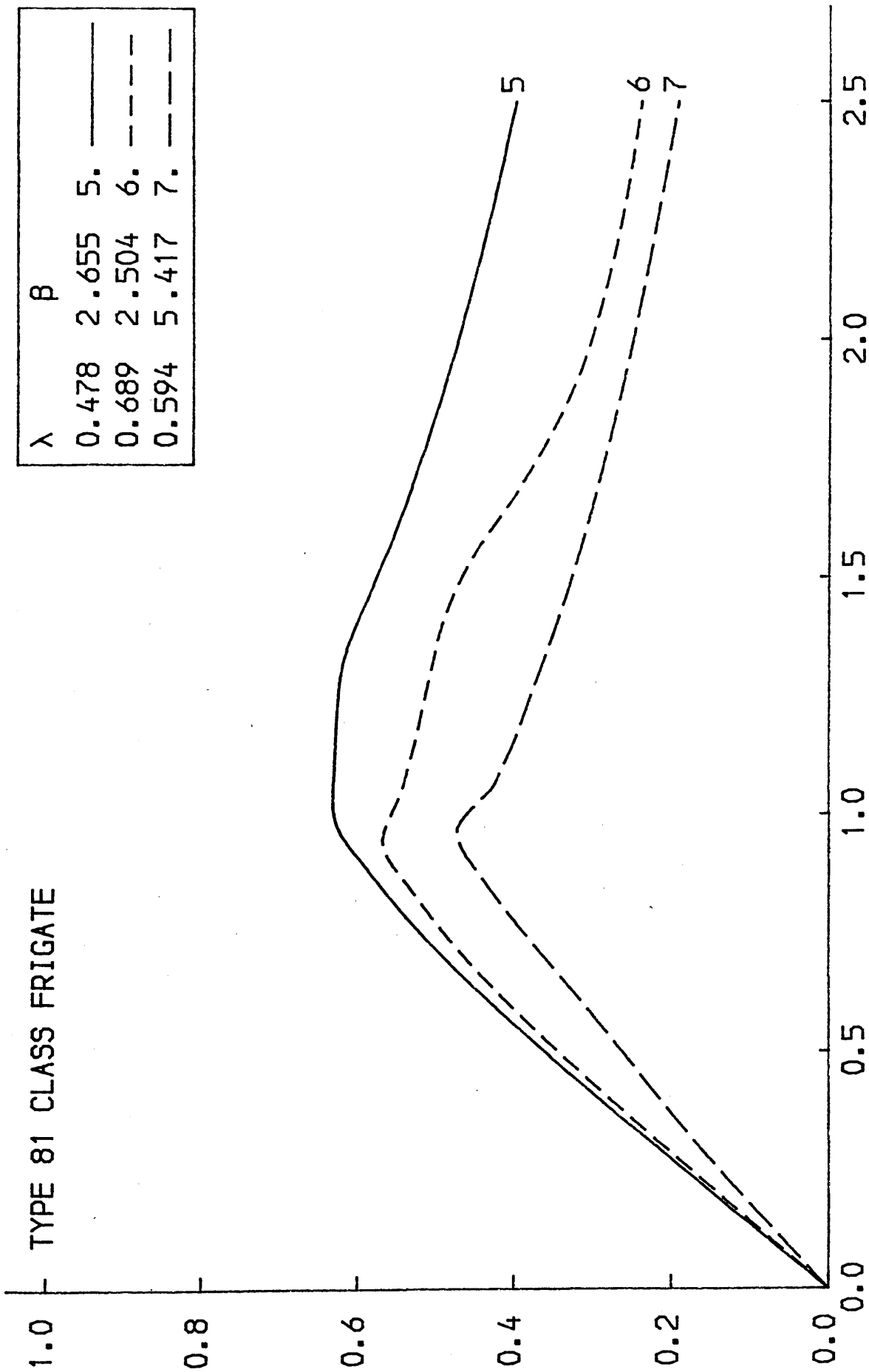

FIG.6-75 LOAD-SHORTENING CURVE FOR THE BEAM-COLUMN

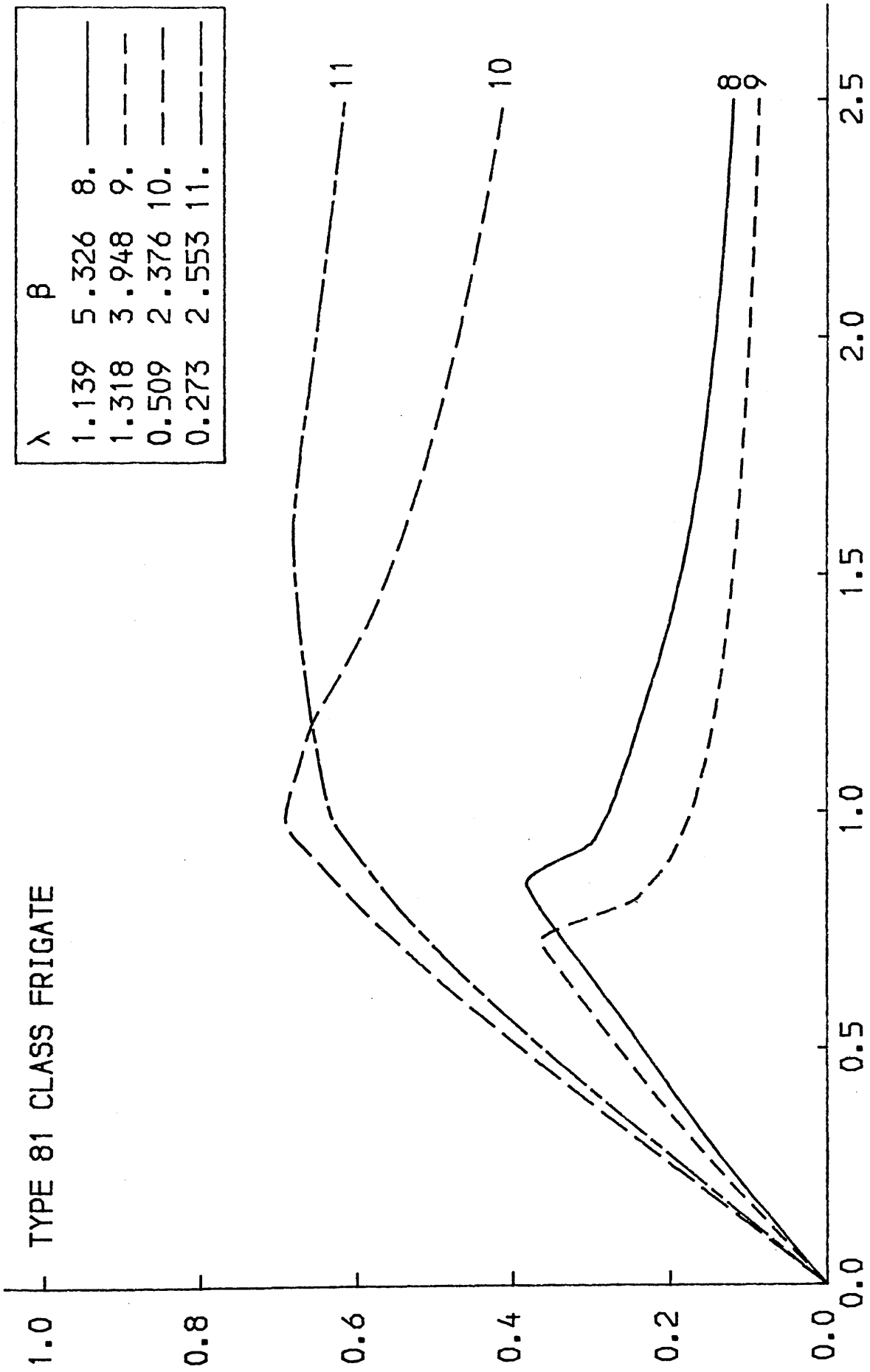

FIG.6-76 LOAD-SHORTENING CURVE FOR THE BEAM-COLUMN

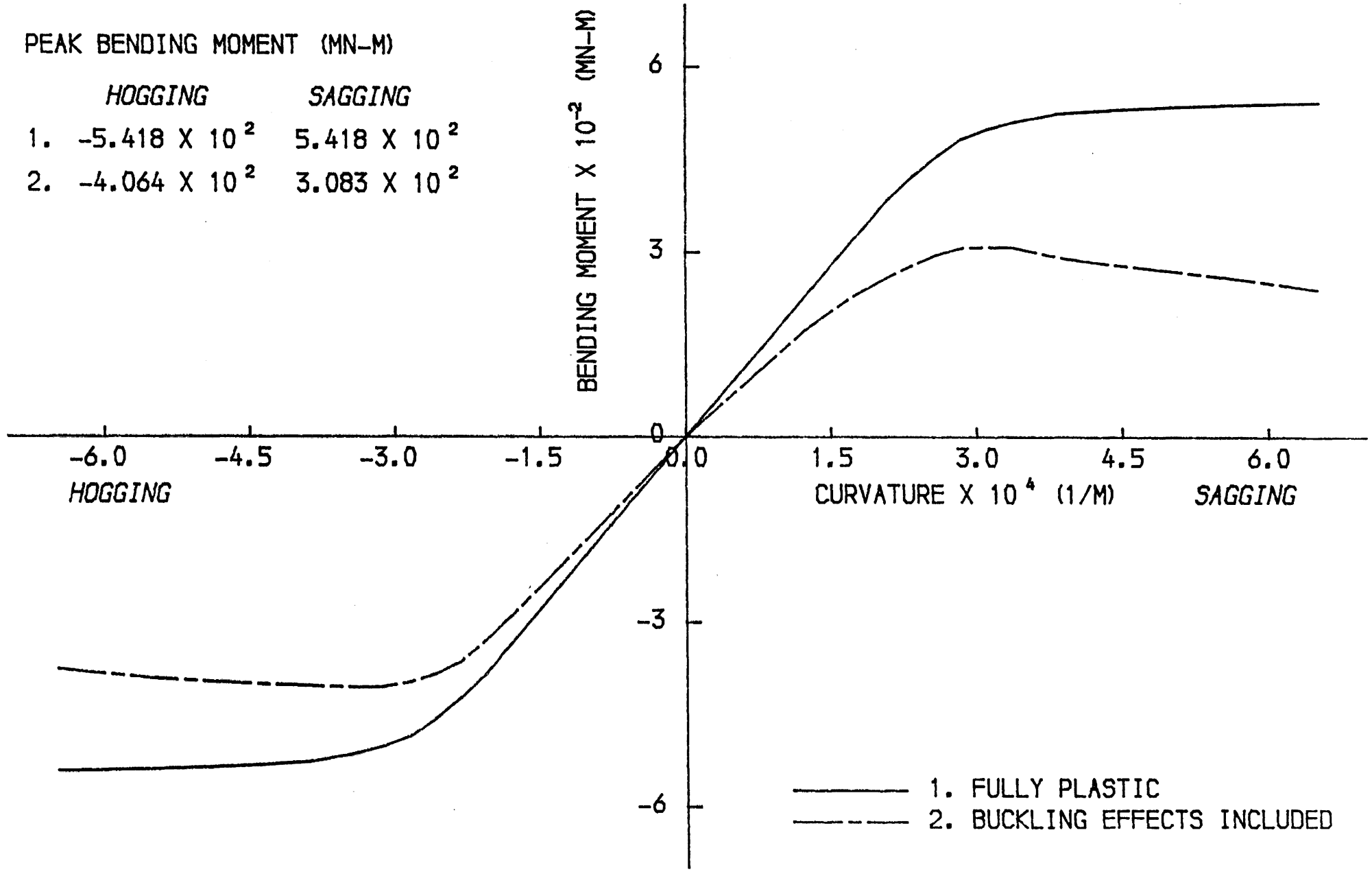

FIG.6-77 BENDING MOMENT-CURVATURE CURVE FOR "TYPE 81" CLASS FRIGATE

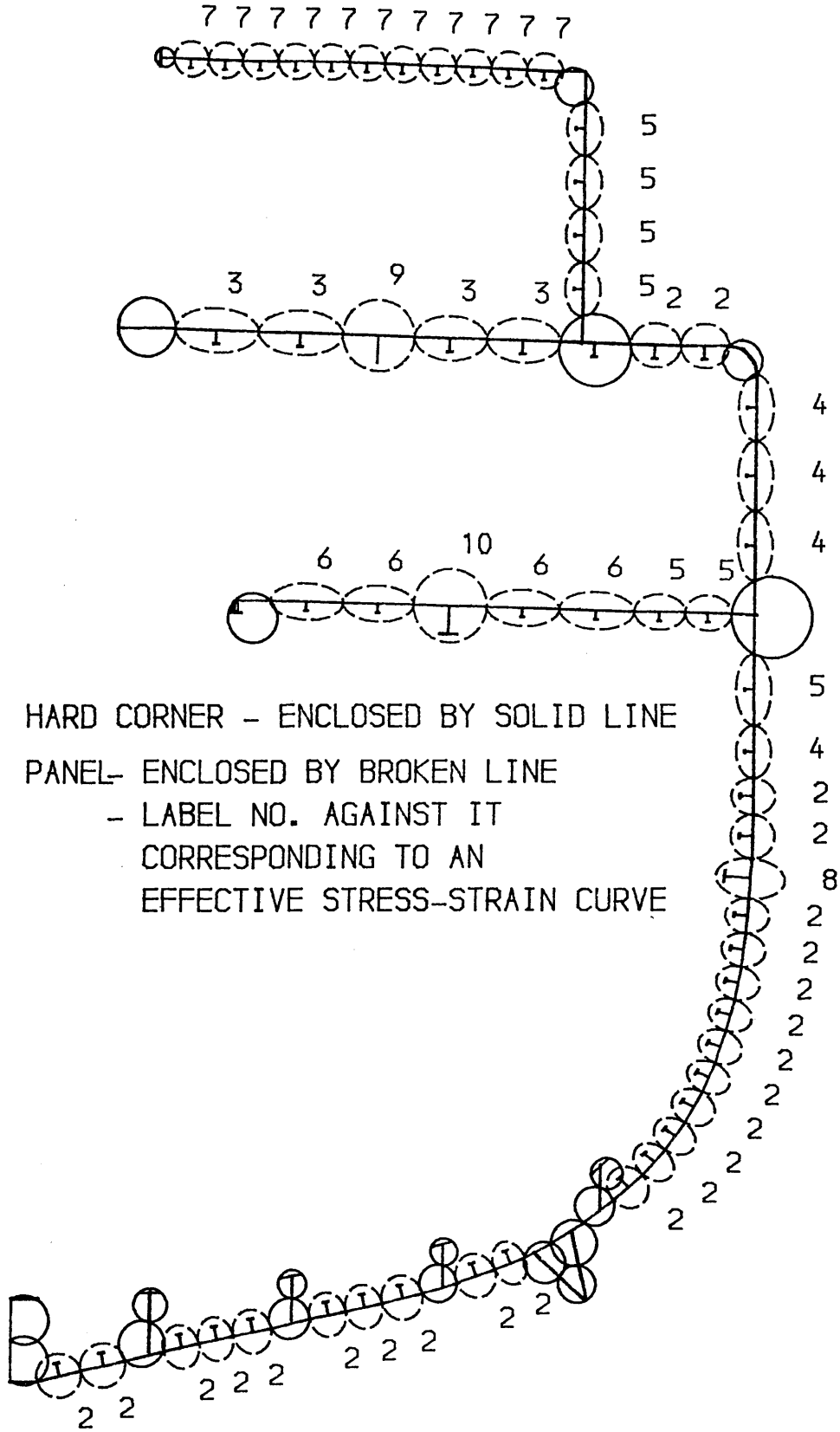

FIG.6-78 DISCRETISATION FOR MIDSHIP SECTION OF LEANDER CLASS FRIGATE

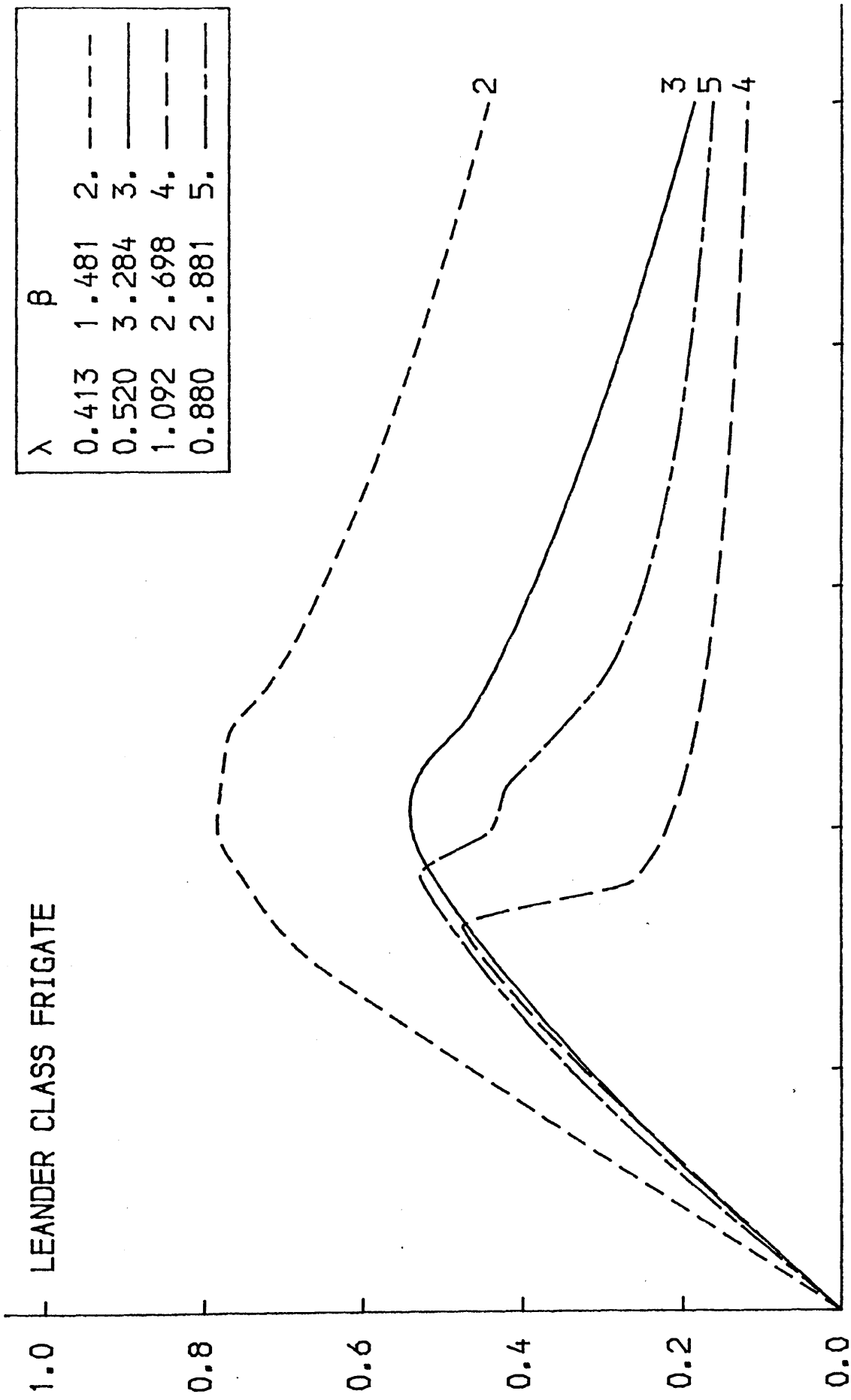

FIG.6-79 LOAD-SHORTENING CURVE FOR THE BEAM-COLUMN

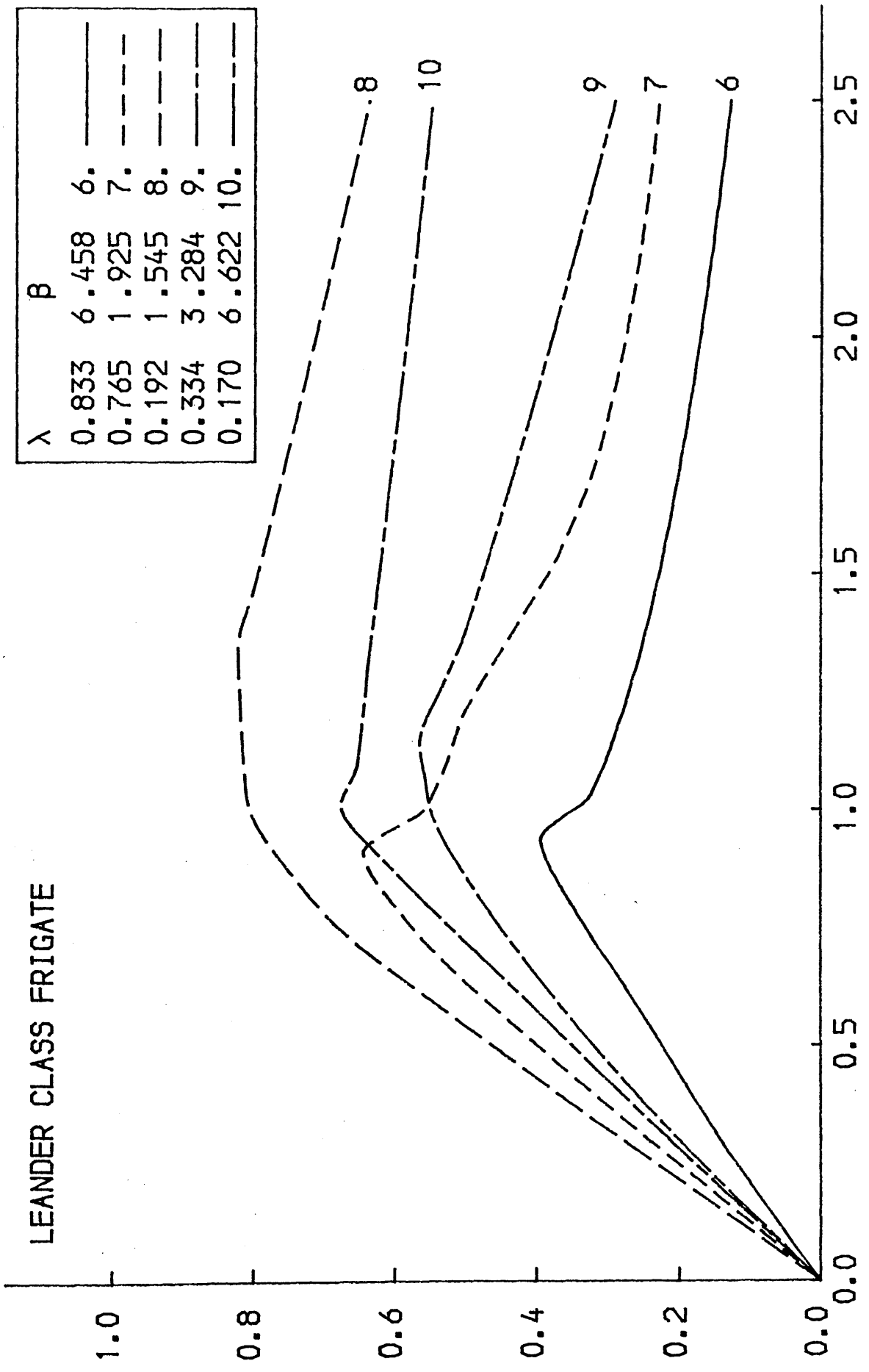

FIG.6-80 LOAD-SHORTENING CURVE FOR THE BEAM-COLUMN

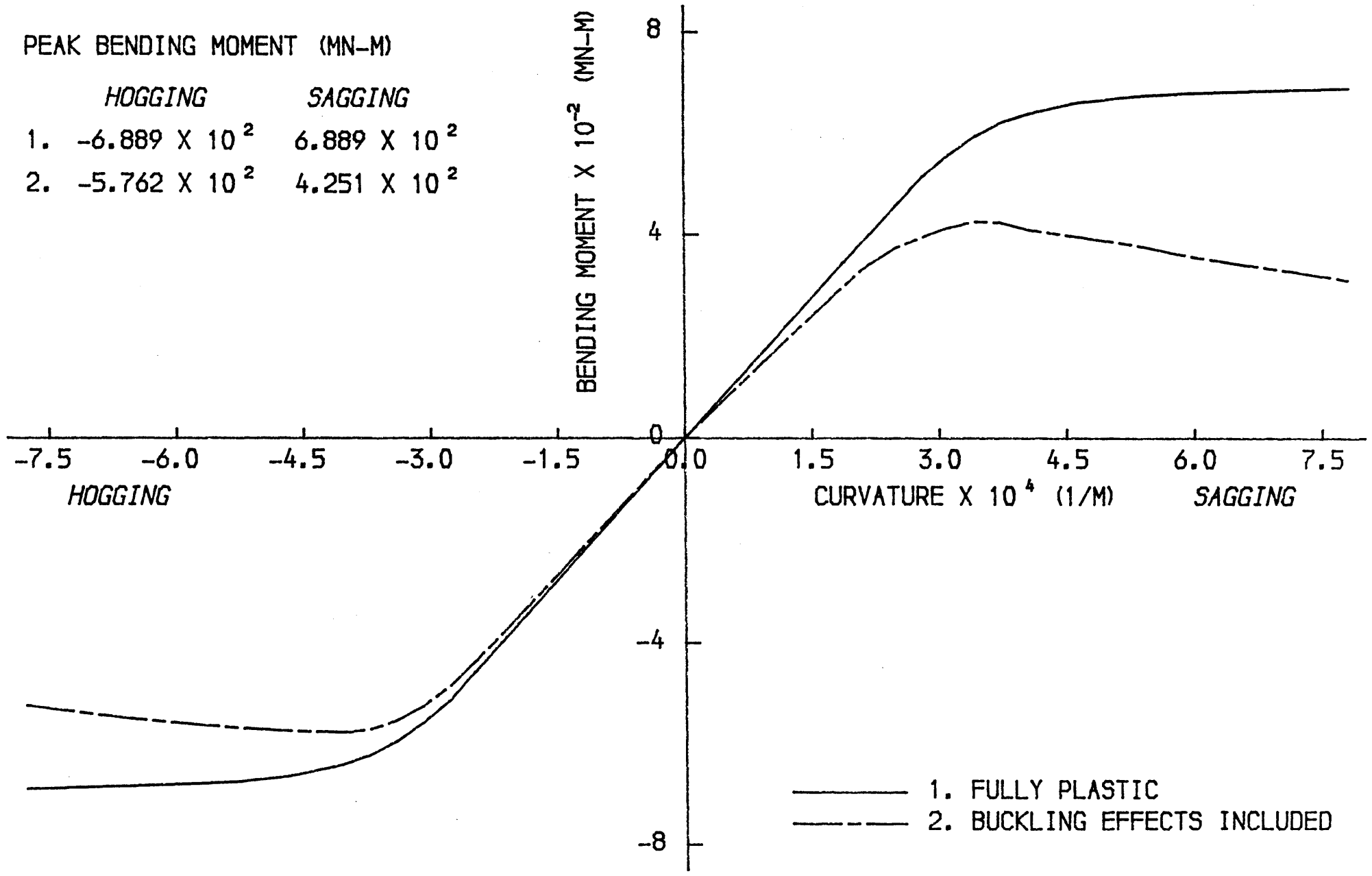

FIG.6-81 BENDING MOMENT-CURVATURE CURVE FOR "LEANDER" CLASS FRIGATE

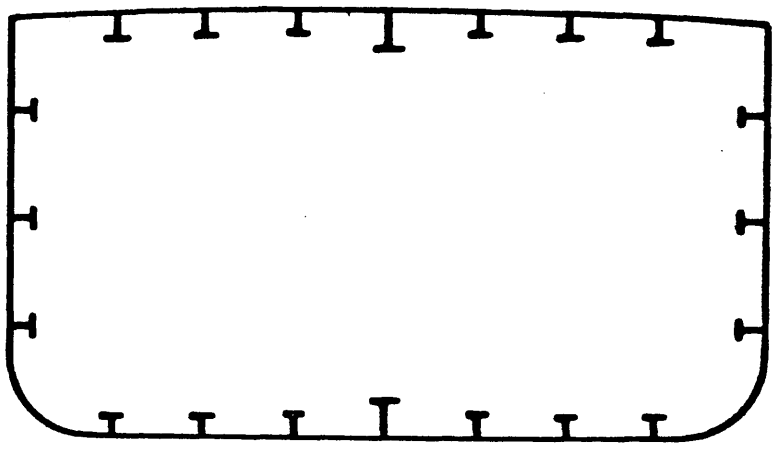

MIDSHIP CROSS-SECTION

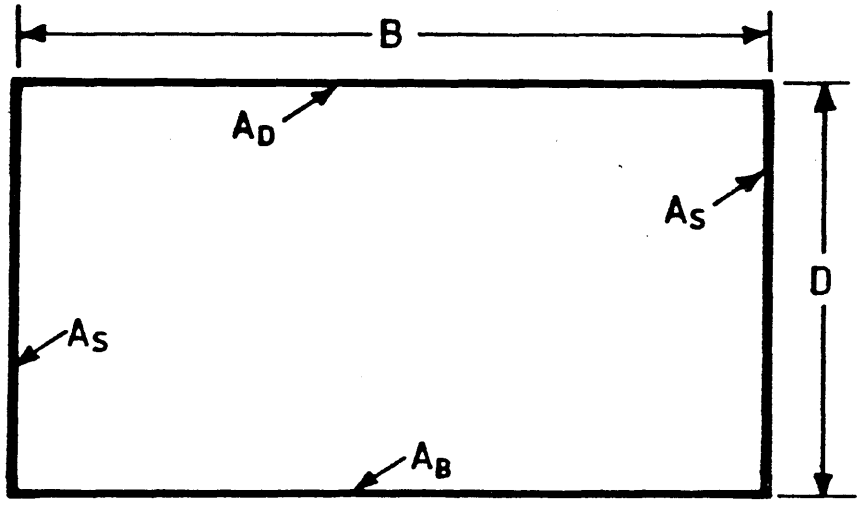

EQUIVALENT CROSS-SECTION

Fig. 7-1. SIMPLIFIED LUMPED AREA FORM of MIDSHIP CROSS-SECTION

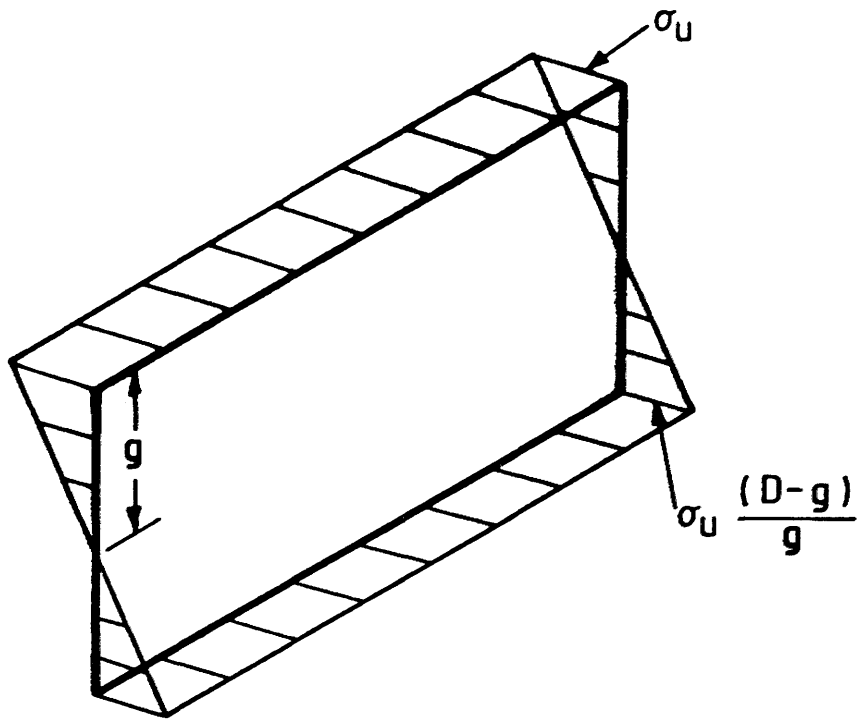

Fig. 7-2. BENDING STRESS DISTRIBUTION — VASTA and ISSC

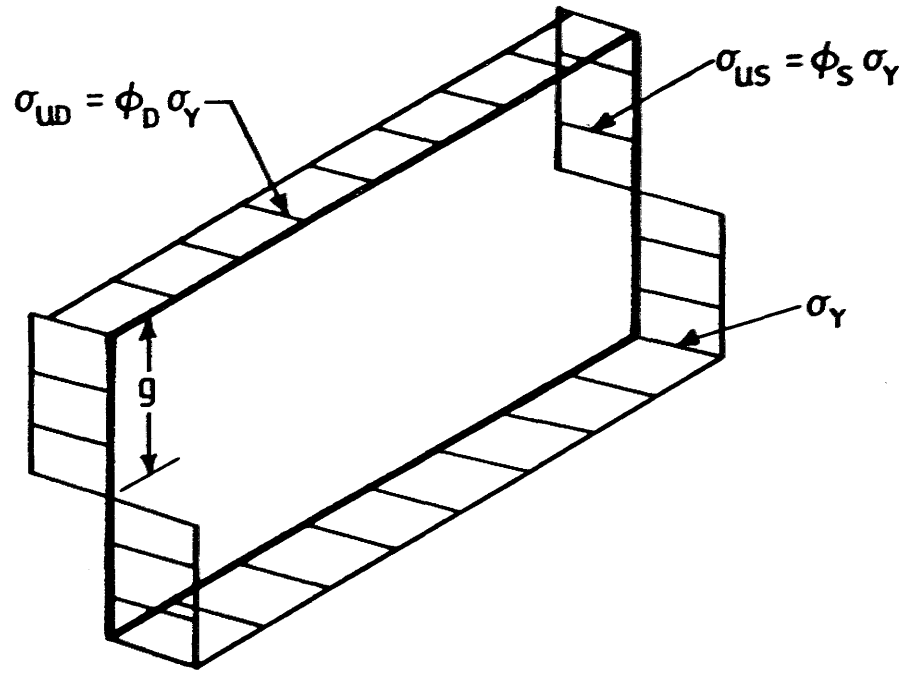

Fig. 7-3. BENDING STRESS DISTRIBUTION — CALDWELL

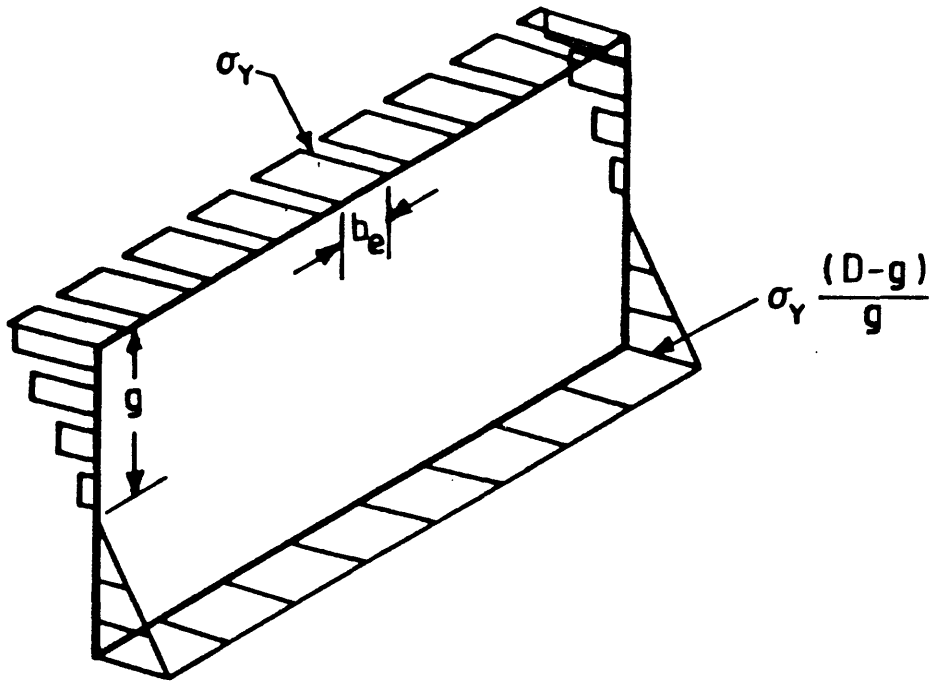

Fig. 7-4. BENDING STRESS DISTRIBUTION — OAKLEY

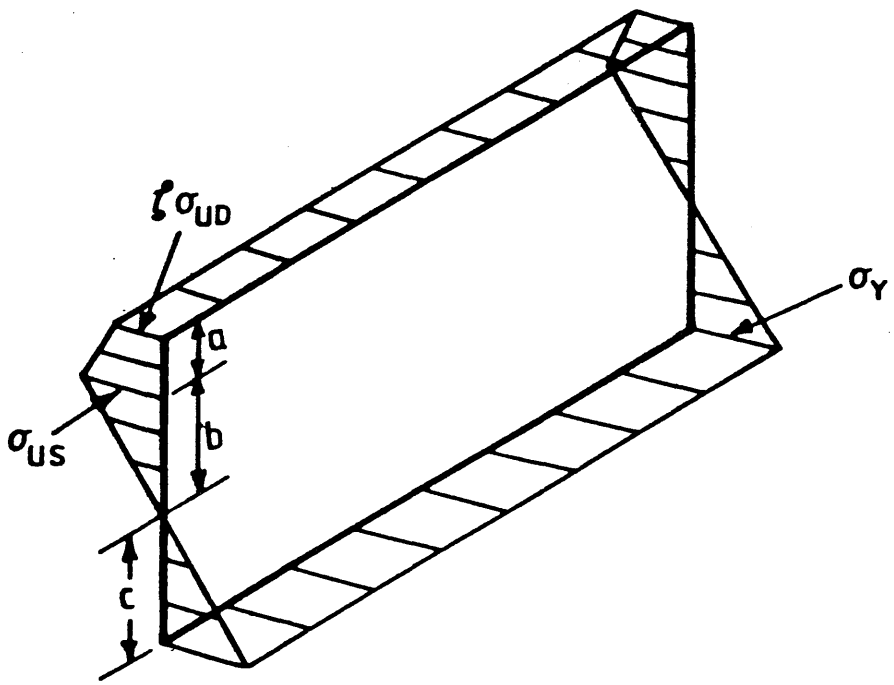

Fig. 7-5. BENDING STRESS DISTRIBUTION — WONG (TYPE 1)

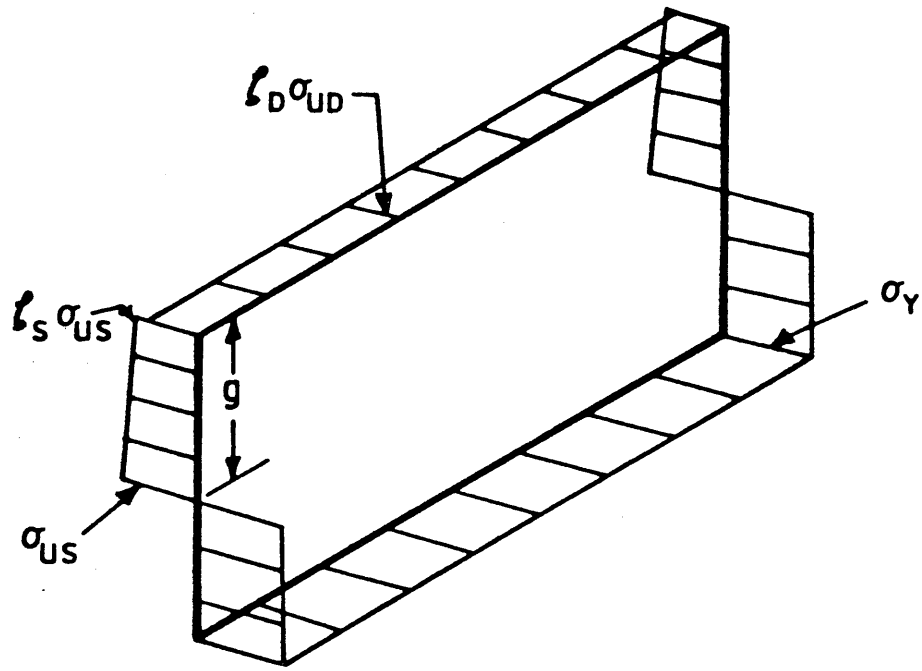

Fig. 7-6. BENDING STRESS DISTRIBUTION —WONG (TYPE 2)

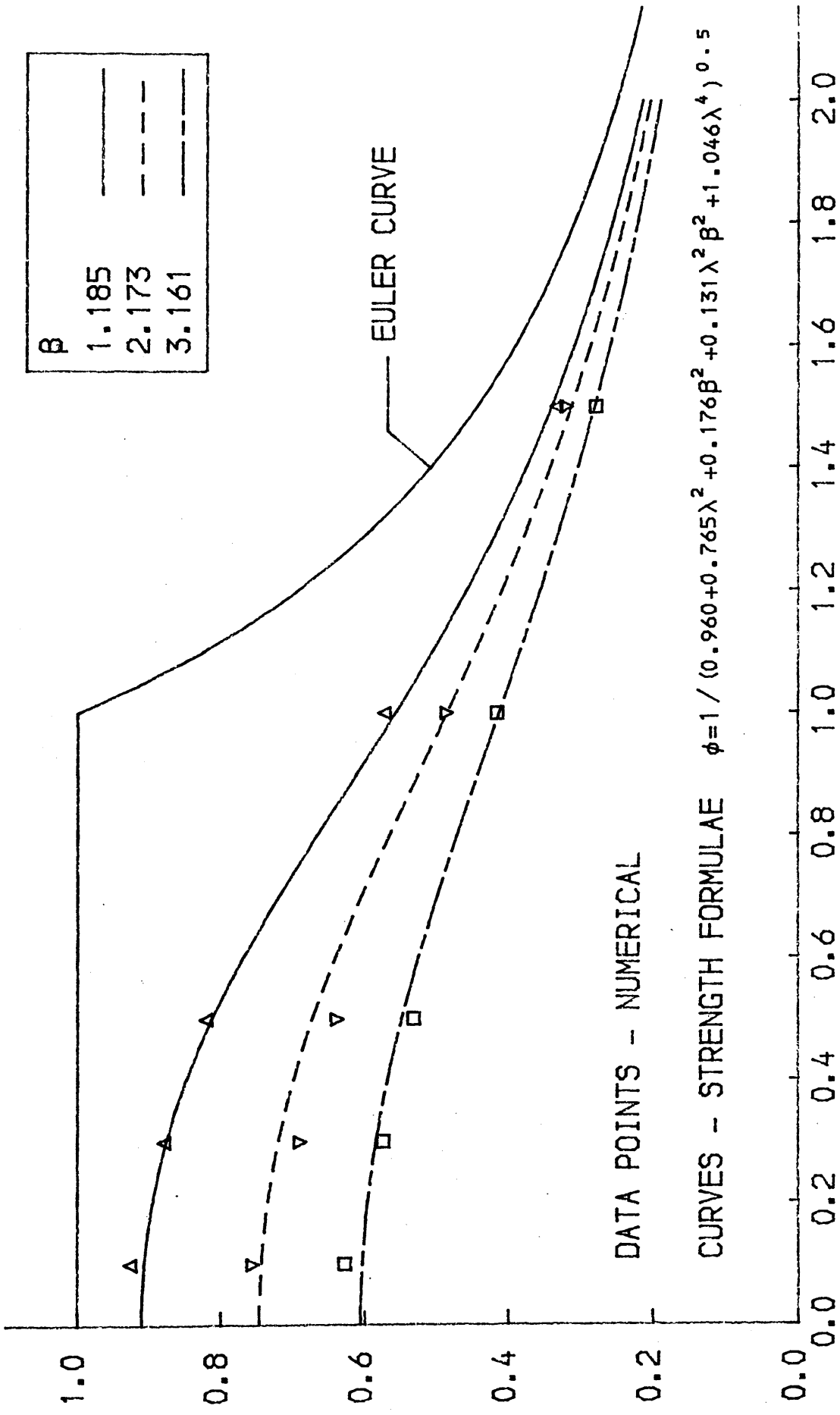

FIG. 7-7 COMPARISON OF SIMPLIFIED STIFFENED PANEL ULTIMATE STRENGTH - SLENDERNESS CURVES WITH NUMERICAL PREDICTIONS

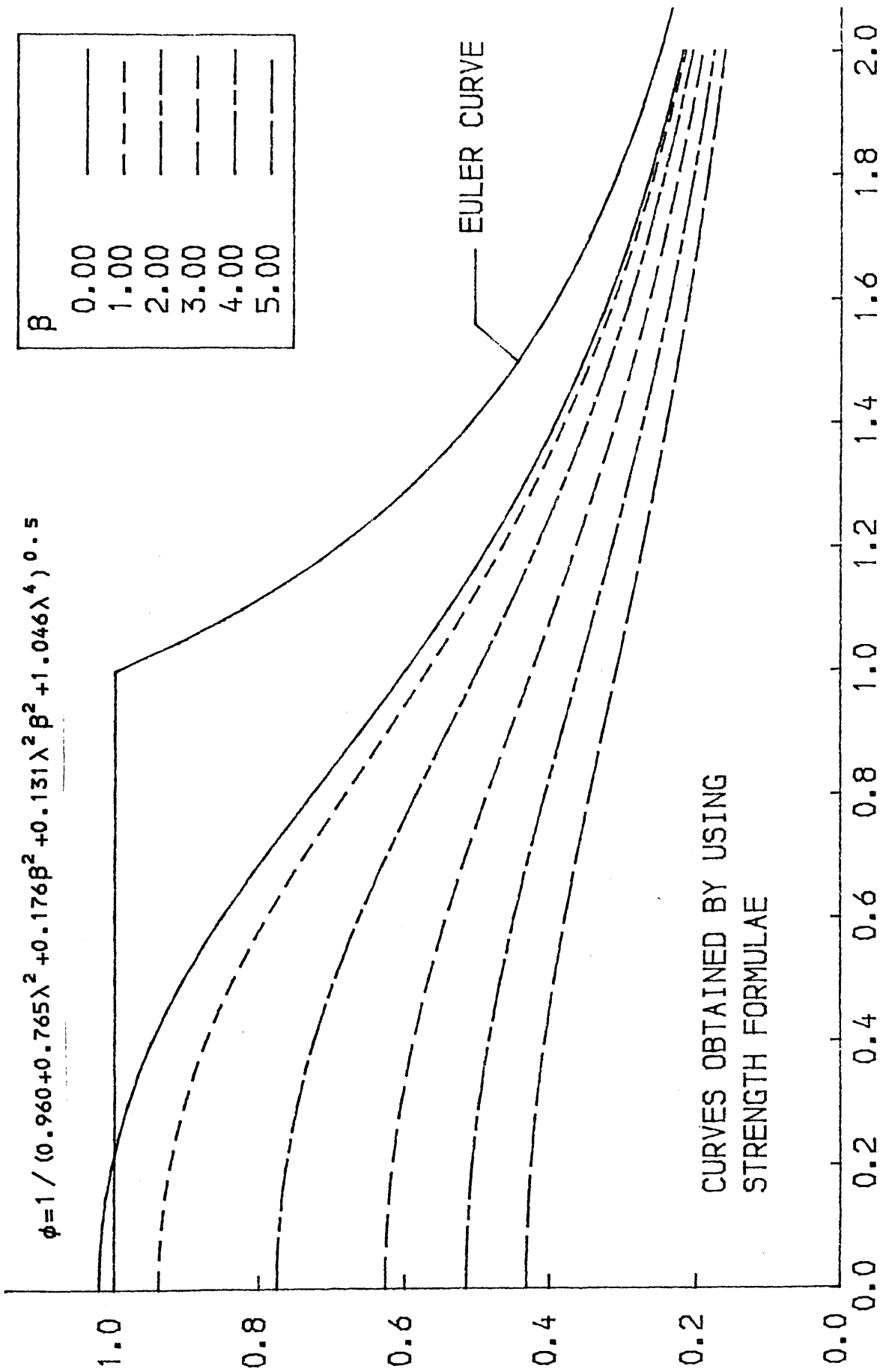

FIG. 7-8 STIFFENED PANEL ULTIMATE STRENGTH-SLENDERNESS CURVES

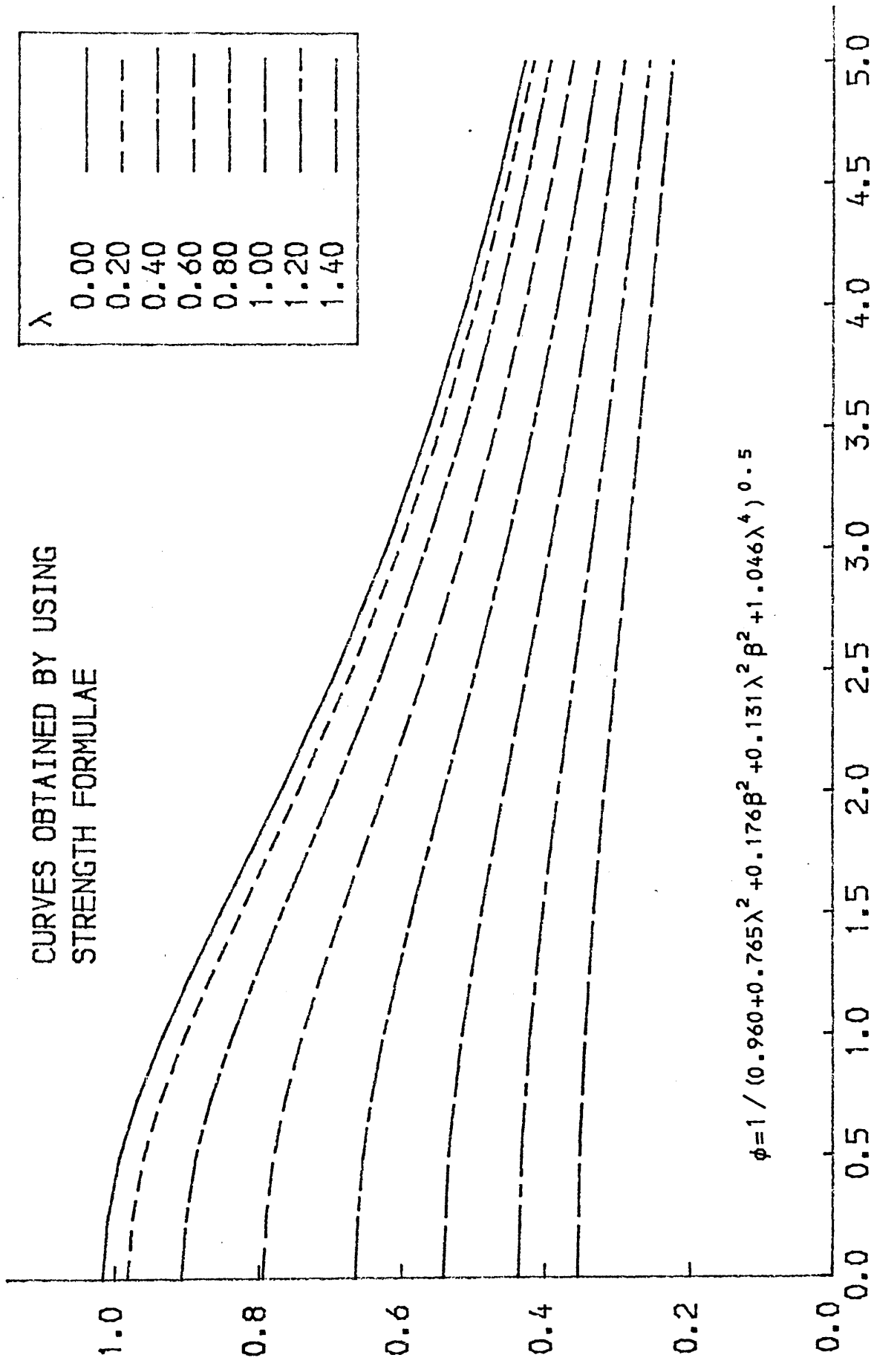

FIG. 7-9 STIFFENED PANEL ULTIMATE STRENGTH-PLATE SLENDERNESS CURVES

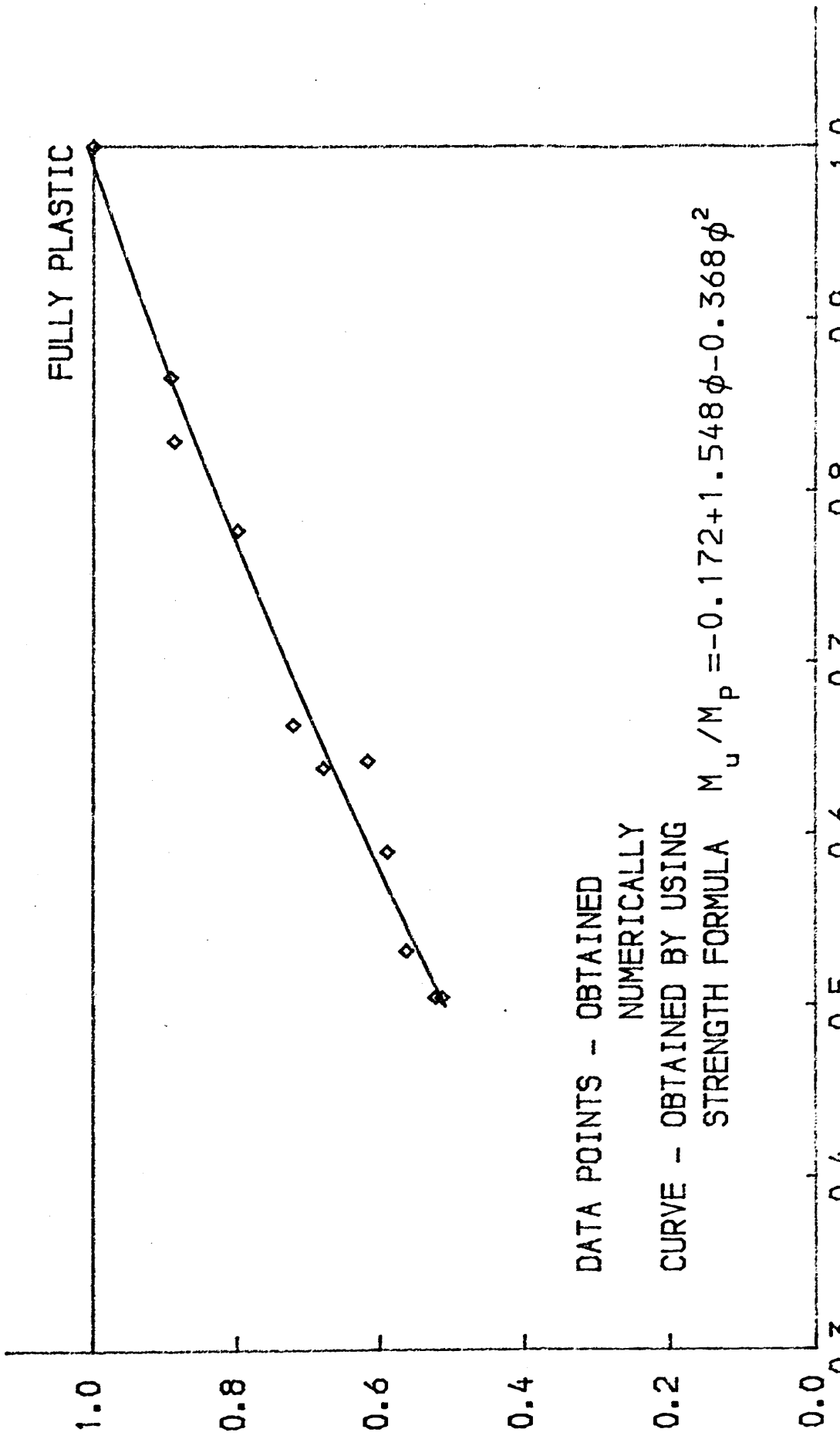

FIG.7-10 RELATIONSHIP BETWEEN ULTIMATE GIRDER MOMENT AND STIFFENED PANEL ULTIMATE STRESS CURVE (SAGGING)

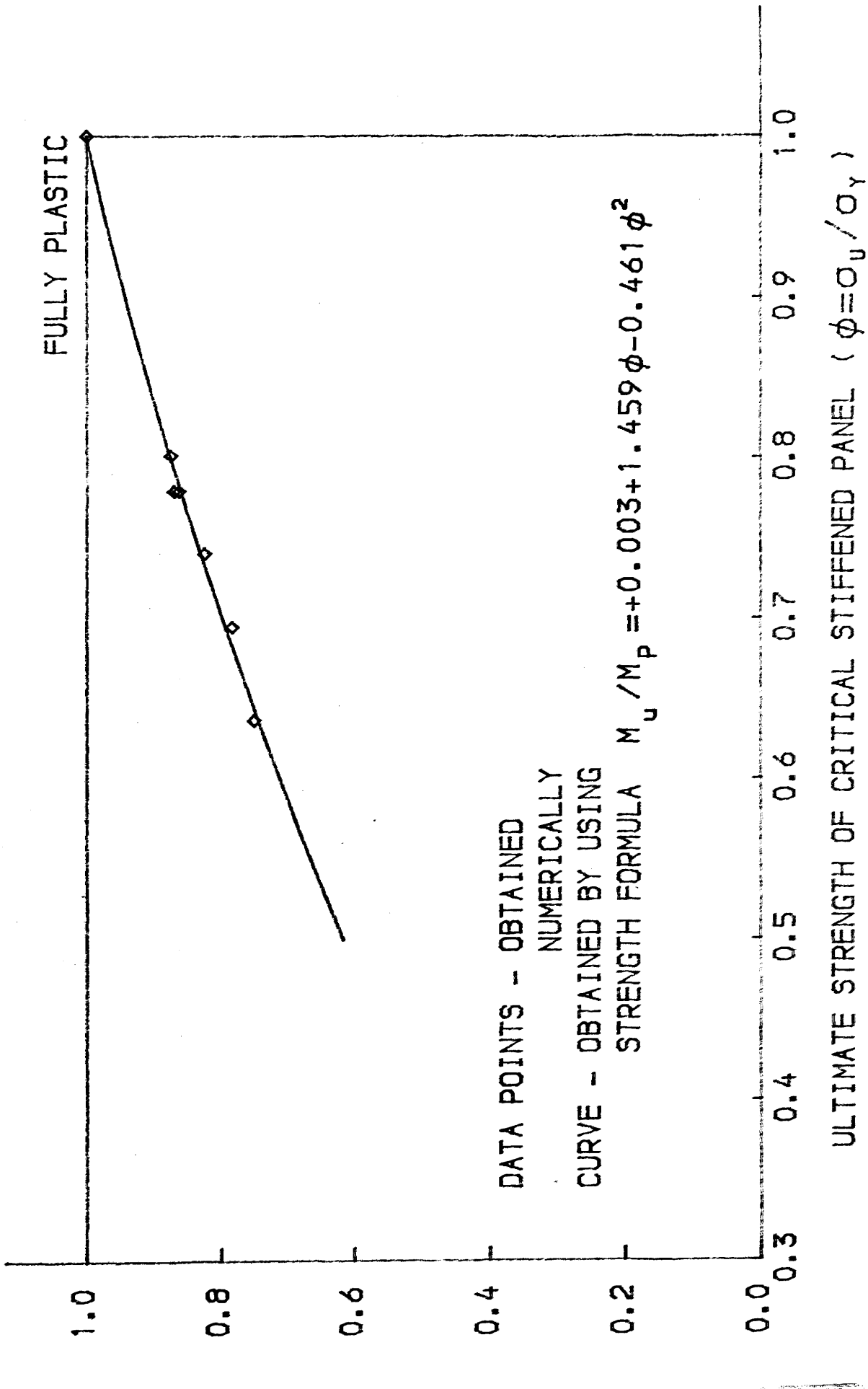

FIG.7-11 RELATIONSHIP BETWEEN ULTIMATE GIRDER MOMENT AND STIFFENED PANEL ULTIMATE STRESS CURVE (HOGGING)